Faculty of Engineering and Science
Department of Civil and Construction Engineering

A Mechanistic Model for Hydraulic Behaviour and Nitrogen Dynamics in a Vertical Flow Constructed Wetland Treating Septage

Tan Yee Yong

This thesis is presented for the Degree of
Doctor of Philosophy
of
Curtin University

November 2016

Declaration

To the best of my knowledge and belief this thesis contains no material previously published by any other person except where due acknowledgment has been made.

This thesis contains no material which has been accepted for the award of any other degree or diploma in any university.

_____

Tan Yee Yong

28 November 2016

Acknowledgement

I would like to acknowledge the Faculty of Engineering and Science, Curtin University Sarawak Malaysia for the scholarship and support to this study. I would like to express my sincere appreciation to my supervisors, Dr. Tang Fu Ee, Dr. Agus Saptoro, and Dr. Khor Ee Huey for their guidance and support throughout my study. I would like to thank the laboratory technicians, George, Denn, Sharinna, and Anthony for their support in the experiment, and the VFCW research students, Ng Chee, Sky, William, Clement, Sunny, Thien, Jason, Brian, and Collin for their help in setting up the experimental rigs and the laboratory experiment. I also want to acknowledge the Dean of Graduated School, Professor Marcus Lee for his suggestion and support to my study. I would like to express my sincere thanks to my family for being supportive throughout the period of study. I would like to acknowledge all my colleagues in the HDR department and friends for the advice and encouragements.

Abstract

Vertical flow constructed wetland (VFCW) is a wastewater treatment system integrated by water, substrate, vegetation, and a variety of microorganism to deliver a series of physical, chemical, and biological process. In this study, a mechanistic model was developed to simulate the hydraulic behaviour and degradation process of nitrogen constituents in the first stage treatment of a two-stage VFCW treating septage. A pilot-scale VFCW-based septage treatment system was constructed using coarse gravel and was loaded in batch with varying hydraulic loading rate (HLR). Its hydraulic performance and nitrogen dynamics were investigated to support the simulations of the system.

The proposed model, VF_Sep, consists of a hydraulic module, transport module and a bio-kinetics module. A transient variably-saturated flow module was employed to describe the hydraulic behaviour, and the effect of evapotranspiration (ET) and sludge accumulation were considered. The transport module was developed using the advection-dispersion equation (ADE). Linear adsorption was implemented to the reactive transport of NH_4^+-N. The bio-kinetics module is a modified activated sludge model that describes the microbial activities in the wastewater treatment. The components involved in the proposed model are DO, alkalinity, four fractions of organic matter, three nitrogenous constituents (NH_4^+-N, NO_3^--N, and dinitrogen), and heterotrophic and autotrophic biomass. The biochemical transformation and degradation processes considered in VF_Sep included hydrolysis, aerobic and anoxic decomposition of organic matter, nitrification, and lysis of heterotrophic and autotrophic biomass.

The laboratory experiments indicated that the influence of HLR and solids load were insignificant to the hydraulic performance. On the other hand, the water recovery and peak effluent flux appeared to be dependent on the thickness of sludge deposit, which is a layer formed by the solids that are retained at the wetland surface. The aeration capacity of the system was excellent. The removal of total solids (TS) and chemical oxygen demand (COD) were approximately 80 %, but the treatment of total nitrogen (TN) and ammonium (NH_4^+-N) were only 69 % and 49 %, respectively. The concentration of nitrate (NO_3^--N) in the effluent increased in the effluent due to the aerobic nitrification. The linear regression analysis between the effluent flux and

nitrogen dynamics demonstrated the dependency of NH_4^+-N removal on hydraulic behaviour, where a slower effluent flux always led to a better treatment efficiency.

The model demonstrated a good match to the measured data of effluent flux. The hydraulic conductivity of sludge deposit layer was found to be the most sensitive parameter towards the peak effluent flux. The mean absolute percentage error (MAE (%)) were generally below 15 %. The poor water recovery was found as the main reason for discrepancies, and thus a correction factor was employed to refine the HLR, which reduced the MAE (%) to approximately 10 %. The influences of ET and sludge accumulation were insignificant in the hydraulic simulation.

As for the nitrogen dynamics, the transport parameters, adsorption coefficient, and biomass concentration were calibrated in advance to deliver a set of prescribed parameters. The bio-kinetics parameters were factorized to the temperature of influent and the DO was assumed to be under a quasi-steady state. The initial concentrations of NH_4^+-N and NO_3^--N were the only parameters to be calibrated to match the measured data. The MAE (%) between the measured and simulated NH_4^+-N concentration were below 10%, while the MAE(%) of NO_3^--N were relatively higher and exceeded 40 % in particular case. Nitrification was found to be the main process in charge of NH_4^+-N removal and then followed by the adsorption and nitrogen consumption in the aerobic decomposition of organic matter. The limitation of the VF_Sep are discussed, and the recommendations for the improvements are proposed.

Publications

1. Tan, Yee Yong, Fu Ee Tang, Valerie Siaw Wee Jong. 2014. "A Conceptual Model for Simulating the Variably-saturated Flow of a Vertical Flow Engineered Wetland – based Septage Treatment System." In *14th International Conference Wetland Systems for Water Pollution Control, Shanghai, People Republic of China*.

2. Tan, Yee Yong, Fu Ee Tang, Agus Saptoro, and Ee Huey Khor. 2015. "Septage Treatment Using Vertical-Flow Engineered Wetland: A Critical Review." In *3rd Postgraduate Colloquium for Environmental Research 2015, Kuching, Malaysia.*

3. Tan, Yee Yong, Fu Ee Tang, Agus Saptoro, and Ee Huey Khor. 2015. "Septage Treatment Using Vertical-Flow Engineered Wetland: A Critical Review." *Chemical Engineering Transaction* 45: 1531-1536. doi: 10.3303/CET1545256

4. Tan, Yee Yong, Fu Ee Tang, Agus Saptoro, and Ee Huey Khor. 2016. "The Interaction between Outflow Dynamics and Removal of NH_4^+-N in a Vertical Flow Constructed Wetlands Treating Septage." In *International Conference on Civil, Architecture and Environmental Engineering, Taipei, Taiwan.*

Table of Contents

Declaration ..... **i**

Acknowledgement ..... **ii**

Abstract ..... **iii**

Publications ..... **v**

Table of Contents ..... **vi**

List of Figures ..... **xii**

List of Tables ..... **xxii**

List of Abbreviations ..... **xxiv**

List of Symbols ..... **xxvi**

Chapter 1 Introduction and Objectives **1**

1.1. Background 1

1.2. Alternative solution: vertical flow constructed wetland (VFCW) 3

1.3. Hydraulic behaviour and nitrogen dynamics in the VFCWs 5

1.4. Identification of problem and research aim 6

1.5. Objectives 7

1.6. Scope and limitation 8

1.7. Thesis outline 10

Chapter 2 Literature Review **12**

2.1. Overview of the VFCWs 12

2.2. Overview of VFCW-based septage treatment system 14

2.2.1. Summary of the VFCW-based septage treatment systems 19

2.3. Treatment of nitrogen in the VFCWs 20

2.3.1. Ammonification 22

2.3.2. Nitrification and denitrification 23

2.3.3. Plant uptake and other mechanisms 24

2.4. Current status of subsurface-flow CW modelling for nitrogen transformation and removal 25

2.4.1. Reactive transport models in saturated conditions 26

2.4.1.1. Wynn and Liehr (2001) 26

2.4.1.2. Liu, Dahad, and Surampali (2005) 28

2.4.1.3. Mayo and Bigambo (2005) 29

2.4.1.4. Wang et al. (2009) 29

2.4.1.5. Rousseau (2005) 30

2.4.1.6. Ojeda et al. (2008) 31

2.4.1.7. Saeed and Sun (2011b) 32

2.4.1.8. BIO_PORE (Samsó and Garcia 2013) 33

2.4.2. Reactive transport models in variably-saturated conditions 34

2.4.2.1. HYDRUS-CW2D (Langergraber and Šimůnek 2005) 35

2.4.2.2. CWM1 (Langergraber, Rousseau, et al. 2009a) 39

2.4.2.3. FITOVERT (Giraldi, de Michieli Vitturi and Iannelli 2010) 40

2.4.2.4. McGechan, Moir, Sym, et al. (2005) 42

2.4.2.5. Ouyang, Luo, and Cui (2011) 43

2.4.2.6. Petitjean et al. (2012) 44

2.4.2.7. Bustillo-Lecompte et al. (2016) 44

2.5. Review summary 45

Chapter 3 Research Methodology I - Laboratory Experimental Setup and Test 53

3.1. Experimental rigs 54

3.1.1. Pre-treatment and storage 54

3.1.2. Raw septage distribution tank 54

3.1.3. First stage wetland bed 56

Figure 3.15: Sludge deposit at the wetland surface 59

Figure 3.16: Wetland bed during acclimatization..... 59

Figure 3.17: Wetland bed after acclimatization..... 59

3.1.4. Percolate storage tank 60

3.2. Operation 60

3.2.1. Assessment of hydraulic behaviour 61

3.2.2. Assessment of raw septage and effluent quality 62

3.2.3. Tracer testing 65

Chapter 4 Research Methodology II - Model Development..... 67

4.1. Hydraulic module 69

4.1.1. Governing equations 69

4.1.1.1. Richards equations 69

4.1.1.2. van Genuchten-Mualem (VGM) model 70

4.1.1.3. Dual-porosity model..... 71

4.1.1.4. Evapotranspiration 72

4.1.1.5. Formation of the sludge deposit layer 75

4.1.2. Numerical implementation 77

4.1.3. Initial and boundary condition 82

4.1.4. Nodal fluxes..... 86

4.1.5. Mass balance conservation 86

4.2. Transport module 87

4.2.1. Governing equations 88

4.2.1.1. Advection-dispersion equation (ADE)..... 88

4.2.1.2. Adsorption..... 89

4.2.1.3. Dual-Porosity transport model with two-site adsorption in mobile phase..... 91

4.2.2. Numerical implementation 93

4.2.3. Initial and boundary conditions 99

4.2.4. Stability constraints 101

4.3. Kinetics module 102

4.3.1. Bio-kinetic module 103

4.3.1.1. Components 104

4.3.1.2. Reactions 107

4.3.1.3. Stoichiometry matrix 110

4.3.2. Surface filtration 113

4.3.3. Nutrient uptake by vegetation 115

4.3.4. Numerical implementation 116

4.4. Summary of program code in MATLAB® 119

Chapter 5 Laboratory Experimental Results 125

5.1. Preliminary experiment 126

5.2. Hydraulic behaviour 131

5.2.1. Water recovery 132

5.2.2. Delay of flow occurrence 132

5.2.3. Peak effluent flux 141

5.2.4. Summary 144

5.3. Treatment performance 145

5.3.1. The quality of raw septage 145

5.3.2. Overall analysis of effluent quality 149

5.3.2.1. Dissolved oxygen (DO) 151

5.3.2.2. pH 152

5.3.2.3. Temperature 152

5.3.2.4. Total solids (TS) 154

5.3.2.5. Total chemical oxygen demand (TCOD) 157

5.3.2.6. Nitrogen dynamics 159

5.3.3. The correlation between hydraulic behaviour and nitrogen dynamic..... 166

5.3.3.1. A direct comparison between 22A (Wetland A) versus 23 B (Wetland B) 167

5.3.3.2. Overall analysis of the influence of hydraulic behaviour on nitrogen dynamic 175

5.3.4. Summary 181

5.4. Tracer experiments 183

Chapter 6 Simulation of Hydraulic Behaviour 187

6.1. Review of the calibration procedure and established hydraulic parameters . 187

6.2. Assumptions 192

6.3. Simulation set-up 193

6.4. Inputs for ET and sludge accumulation 196

6.5. Procedure for calibration of hydraulic parameters to fit measured data 199

6.6. Results and Discussions 202

6.6.1. Simulated results 204

6.6.2. Sensitivity Analysis: ET and Sludge Accumulation 222

6.6.3. Validation with HYDRUS-1D 233

6.7. Summary 235

Chapter 7 Simulation of Nitrogen Dynamics 238

7.1. Simulation setup 239

7.1.1. Fundamental concepts 239

7.1.2. Transport parameters 241

7.1.3. Bio-kinetics parameters 243

7.1.4. Initial conditions and boundary conditions 250

7.1.5. Calibration of transport parameters 251

7.1.6. Summary of Assumptions 253

7.2. Results and Discussions 255

7.2.1. Simulated Results 255

7.2.2. Discussion 263

7.2.2.1. The influence of DO 263

7.2.2.2. Adsorption 265

7.2.2.3. Consumption of NH_4^+-N in the growth of X_H 270

7.3. Summary 274

Chapter 8 Conclusion and Recommendation 277

8.1. Summary of work 277

8.2. Conclusion 277

8.2.1. Laboratory experiment 277

8.2.2. Modelling of the hydraulic behaviour in the VFCW-based septage treatment system 279

8.2.3. Modelling of the nitrogen dynamics in the VFCW-based septage treatment system 281

8.3. Significance of current work 282

8.4. Recommendations for Future Work 283

References 287

Appendices 311

List of Figures

Figure 1.1: Septic tank with excessive sludge 2

Figure 1.2: Desludging process 2

Figure 1.3: Raw septage collected from the domestic area 3

Figure 2.1: A typical VFCW system and its components 13

Figure 2.2: Side view of a pilot-scale, two-stage VFCW-based wetland treatment system (Jong and Tang 2014) 17

Figure 2.3: Conventional nitrogen cycle in CWs 22

Figure 3.1: Plan view of the pilot-scale, two-stage VFCW-based septage treatment system 53

Figure 3.2: 400-gallon and 100-gallon storage tanks 54

Figure 3.3: Primary screening process during unloading 54

Figure 3.4: Secondary screening process in the 100-gallon storage tank before the raw septage was discharged to the feed tank 55

Figure 3.5: Centrifugal pump to transfer raw septage from the storage tank to the feed tank 55

Figure 3.6: 250-gallon distribution tank 55

Figure 3.7: Pipe connection between the distribution tank and the centrifugal pumps 55

Figure 3.8: Cross-sectional view of first stage VFCW 56

Figure 3.9: Ø50 mm drainage layer 57

Figure 3.10: Ø37.5 mm main layer 57

Figure 3.11: Ø10 mm main layer 57

Figure 3.12: Transplantation of common reeds (*Phragmites Karka*) cultivated in a polyethylene bag 57

Figure 3.13: Distribution device during loading 58

Figure 3.14: Drainage device at the bottom of the bed 58

Figure 3.15: Sludge deposit at the wetland surface 59

Figure 3.16: Wetland bed during acclimatization 59

Figure 3.17: Wetland bed after acclimatization 59

Figure 3.18: Percolate storage tank 60

Figure 3.19: Formation of ponding during the loading process 62

Figure 3.20: Sample collection on 1st December 2015 (Case 3A) 63

Figure 3.21: HACH® HQ40d portable multi-parameter meter with specific probes 64

Figure 3.22: HACH DR2800 spectrophotometer and the Test'N Tube ™ vials 64

Figure 3.23: Hach® MM340 radiometer with a bromide ion selective electrode 66

Figure 4.1: Flow chart of model development 68

Figure 4.2: Maximum depth of the root distribution 75

Figure 4.3: Accumulation of sludge deposit 76

Figure 4.4: Heterogenous interface allocated between two nodes 78

Figure 4.5: Variation of Δz_{top} in the simulation due to the sludge accumulation 83

Figure 4.6: Boundary conditions of hydraulic module 83

Figure 4.7: The conceptual relationship between the components 111

Figure 4.8: The procedure to estimate the biochemical reaction rate at node i 117

Figure 4.9: Determination of the total concentration of S_O, S_S, S_I, S_{NO}, S_{N2}, S_{HCO}, X_S, and X_I 118

Figure 4.10: Determination of the total concentration of S_{NH} 118

Figure 4.11: Determination of the total concentration of X_H and X_A 119

Figure 4.12: Flow chart of the VF_Sep 120

Figure 4.13: Flow chart of hydraulic module 122

Figure 4.14: Flow chart of transport module 123

Figure 5.1: The wetland bed before acclimatization 127

Figure 5.2: The wetland bed after acclimatization 127

Figure 5.3: Comparison between raw septage (left 1) and effluent 127

Figure 5.4: Comparison of (a) electrical conductivity (EC), (b) dissolved oxygen (DO) and (c) total suspended solids (TSS) between influent and effluent. The percentages in the diagram indicate the removal efficiency throughout the treatment..... 128

Figure 5.5: Comparison of (a) chemical oxygen demand (COD), (b) ammonia (NH_3) and (c) nitrate (NO_3^-) between influent and effluent. The percentages in the diagram indicate the removal efficiency throughout the treatment..... 129

Figure 5.6: The comparison of total nitrogen (TN) between influent and effluent. The percentages in the diagram indicate the removal efficiency throughout the treatment. 130

Figure 5.7: Water recovery percentage versus hydraulic load 134

Figure 5.8: Water recovery percentage versus solids load..... 134

Figure 5.9: Water recovery percentage versus sludge thickness 134

Figure 5.10: Twenty-five batches of effluent flux measured from the first stage treatment of a pilot-scale VFCW 136

Figure 5.11: “Typical flow” case (case 3A)..... 136

Figure 5.12: "Bypass" case - V-shaped development of effluent flux (Case 9B).... 137

Figure 5.13: “Clogged” case - a low peak flux with rapid reduction (Case 13B).... 137

Figure 5.14: Flow occurring delay versus hydraulic load..... 139

Figure 5.15: Flow occuring delay versus solids load..... 139

Figure 5.16: Flow occurring delay versus sludge thickness 139

Figure 5.17: (Left) The slurry with high water content accumulated on the surface of the wetland bed right after loading. (Center) Some cracks formed on the top surface of sludge deposit layer during resting period. (Right) The large cracks exposed the gravel layer after the extended resting period 140

Figure 5.18: Peak effluent flux versus hydraulic load 142

Figure 5.19: Peak effluent flux versus solid load..... 143

Figure 5.20: Peak effluent flux versus sludge thickness 143

Figure 5.21: Cracks formed via the mechanical vibration of the reed stem caused by the strong wind 144

Figure 5.22: Cracks formed in the controlled bed during resting period 144

Figure 5.23: Sample of raw septage. 145

Figure 5.24: TCOD concentration versus TS concentration 148

Figure 5.25: TN concentration versus TS concentration 148

Figure 5.26: TN concentration versus NH_4^+-N + NO_3^--N concentration 149

Figure 5.27: TN concentration versus Org-N concentration 150

Figure 5.28: TS concentration versus Org-N concentration 150

Figure 5.29: TCOD concentration versus Org-N concentration 150

Figure 5.30: The samples of effluent showed a gradient of cleanliness with regards to time (Case 3A) 151

Figure 5.31: Temporal plots of DO concentration in the effluent for twenty-five batches of treatment 152

Figure 5.32: Temporal plots of pH in the effluent for twenty-five batches of treatment 153

Figure 5.33: Temporal plots of temperature in the effluent for twenty-five batches of treatment 153

Figure 5.34: Temporal plots of TS concentration in the effluent for twenty-four batches of treatment 154

Figure 5.35: Samples of effluent for case 13B (7th January 2016 – clogging) 155

Figure 5.36: Solid loads versus TS removal 155

Figure 5.37: Temporal plots of TCOD concentration in the effluent for twenty-four batches of treatment 157

Figure 5.38: Temporal plots of TN concentration in the effluent for twenty-four batches of treatment 159

Figure 5.39: Temporal plots of NH_4^+-N concentration in the effluent for twenty-five batches of treatment 161

Figure 5.40: Peak effluent flux versus removal efficiency of NH_4^+-N 163

Figure 5.41: Temporal plots of NO_3^--N concentration in the effluent for twenty-five batches of treatment 164

Figure 5.42: Temporal plots of NH_4^+-N + NO_3^--N in the effluent for twenty-five batches of treatment 164

Figure 5.43: (Top) Effluent samples collected in 22A (Wetland A) (Bottom) Effluent samples collected in 23B (Wetland B) 168

Figure 5.44: Effluent flux and cumulative effluent 168

Figure 5.45: Relation between DO and outflow dynamics 169

Figure 5.46: Relation between pH and outflow dynamics 170

Figure 5.47: Relation between TS and outflow dynamics 170

Figure 5.48: Relation between TCOD and outflow dynamics 171

Figure 5.49: Relation between TN and outflow dynamics 173

Figure 5.50: Relation between NH_4^+-N and outflow dynamics 173

Figure 5.51: Relation between NO_3^--N and outflow dynamics 174

Figure 5.52: Relation between NH_4^+-N + NO_3^--N and outflow dynamics 175

Figure 5.53: Relation between outflow dynamics and nitrogen dynamics for “typical flow” cases 177

Figure 5.54: Relation between outflow dynamics and nitrogen dynamic for “bypass” case 178

Figure 5.55: Sample of sludge deposit layer removed from the wetland surface 180

Figure 5.56: Relation between outflow dynamics and nitrogen dynamics for “clogged” cases 182

Figure 5.57: Temporal plots of Br^- concentration in the effluent for twelve batches of treatment 185

Figure 6.1: Constant head test to measure the saturated hydraulic conductivity of porous medium 188

Figure 6.2: Hanging column test to measure the amount of water removed from the saturated porous medium caused by the suction 188

Figure 6.3: Substrate profile in the simulation 194

Figure 6.4: The comparison between a default spatial discretization (1.00 cm) and a finer spatial discretization (0.50 cm). 195

Figure 6.5: Common reeds at the end of experiment 199

Figure 6.6: The root length of common reeds reached up to 30 cm 199

Figure 6.7: Effluent flux of “typical flow” 200

Figure 6.8: Simulated results of case 1A (18-11-2015: 75 l) 204

Figure 6.9: Simulated results of case 3A (1-12-2015: 75 l) 205

Figure 6.10: Simulated results of case 8A (16-12-2015: 100 l) 205

Figure 6.11: Simulated results of case 11A (27-12-2015: 100 l) 206

Figure 6.12: Simulated results of case 19B (24-1-2016: 125 l) 206

Figure 6.13: Simulated results of case 20A (28-1-2016: 150 l) 207

Figure 6.14: Simulated results of case 24B (21-2-2016: 125 l) 207

Figure 6.15: Simulated results of case 25B (27-2-2016: 50 l) 208

Figure 6.16: Simulated results of case 6A (12-12-2015: 75 L) 210

Figure 6.17: Simulated results of case 7B (13-12-2015: 75 L) 211

Figure 6.18: Simulated results of case 17B (21-1-2015: 100 L) 211

Figure 6.19: Simulated results of case 23B (16-2-2016: 50 L) 212

Figure 6.20: Stagnant raw septage at the wetland surface during later stage of treatment 213

Figure 6.21: Simulated effluent flux with and without correction coefficient of case 1A (18-11-2015: 75 L) 215

Figure 6.22: Simulated cumulative effluent with and without correction coefficient of case 1A (18-11-2015: 75 L) 215

Figure 6.23: Simulated effluent flux with and without correction coefficient of case 3A (1-12-2015: 75 L) 216

Figure 6.24: Simulated cumulative effluent with and without correction coefficient of case 3A (1-12-2015: 75 L) 216

Figure 6.25: Simulated effluent flux with and without correction coefficient of case 6A (12-12-2015: 75 L) 217

Figure 6.26: Simulated cumulative effluent with and without correction coefficient of case 6A (12-12-2015: 75 L) 217

Figure 6.27: Simulated effluent flux with and without correction coefficient of case 7B (13-12-2015: 75 L) 218

Figure 6.28: Simulated cumulative effluent with CR of case 7B (13-12-2015: 75 L) 218

Figure 6.29: Simulated effluent flux with and without correction coefficient of case 19B (24-1-2016: 125 L) 219

Figure 6.30: Simulated cumulative effluent with and without correction coefficient of case 19B (24-1-2016: 125 L) 219

Figure 6.31: Simulated effluent flux with and without correction coefficient of case 20A (28-1-2016: 150 L) 220

Figure 6.32: Simulated cumulative effluent with and without correction coefficient of case 20A (28-1-2016: 150 L) 220

Figure 6.33: Simulated effluent flux with and without correction coefficient of case 23B (16-2-2015: 50 l) 221

Figure 6.34: Simulated cumulative effluent with and without correction coefficient of case 23B (16-2-2015: 50 l) 221

Figure 6.35: The growth condition of common reeds during experiment 224

Figure 6.36: Comparison between simulation with- and without evapotranspiration and sludge accumulation for case 1A (18-11-2015: 75 L) 226

Figure 6.37: Comparison between simulation with- and without evapotranspiration and sludge accumulation for case 3A (1-12-2015: 75 L) 227

Figure 6.38: Comparison between simulation with- and without evapotranspiration and sludge accumulation for case 6A (12-12-2015: 75 L) 227

Figure 6.39: Comparison between simulation with- and without evapotranspiration and sludge accumulation for case 7B (13-12-2015: 75 L) 228

Figure 6.40: Comparison between simulation with- and without evapotranspiration and sludge accumulation for case 8A (16-12-2015: 100 L) 228

Figure 6.41: Comparison between simulation with- and without evapotranspiration and sludge accumulation for case 11A (27-12-2015: 100 L) 229

Figure 6.42: Comparison between simulation with- and without evapotranspiration and sludge accumulation for case 17B (21-1-2016: 100 L) 229

Figure 6.43: Comparison between simulation with- and without evapotranspiration and sludge accumulation for case 19B (24-1-2016: 125 L) 230

Figure 6.44: Comparison between simulation with- and without evapotranspiration and sludge accumulation for case 20A (28-1-2016: 150 L) 230

Figure 6.45: Comparison between simulation with- and without evapotranspiration and sludge accumulation for case 23B (16-2-2016: 50 L) 231

Figure 6.46: Comparison between simulation with- and without evapotranspiration and sludge accumulation for case 24B (21-2-2016: 125 L) 231

Figure 6.47: Comparison between simulation with- and without evapotranspiration and sludge accumulation for case 25B (21-2-2016: 50 l) 232

Figure 6.48: Comparison between HYDRUS-1D and VF_Sep for case 1A (18-11-2016: 75 L) 234

Figure 6.49: Comparison between HYDRUS-1D and VF_Sep for case 3A (1-12-2016: 75 L) 234

Figure 6.50: Comparison between HYDRUS-1D and VF_Sep for case 17B (21-1-2015: 100 L) 234

Figure 6.51: Comparison between HYDRUS-1D and VF_Sep for case 19B (24-1-2016: 125 L) 235

Figure 7.1: Simulated results of case 1A (18-11-2015: 75 l) 256

Figure 7.2: Simulated results of case 3A (1-12-2015: 75 l) 256

Figure 7.3: Simulated results of case 8A (16-12-2015: 100 l) 257

Figure 7.4: Simulated results of case 11A (27-12-2015: 100 l) 257

Figure 7.5: Simulated results of case 19B (24-1-2016: 125 l) 258

Figure 7.6: Simulated results of case 20A (28-1-2016: 150 l) 258

Figure 7.7: Simulated results of case 24B (21-2-2016: 125 l) 259

Figure 7.8: Simulated results of case 25B (27-2-2016: 50 l) 259

Figure 7.9: Development of X_A of case 3A (1-12-2015: 75 l) 262

Figure 7.10: Influence of DO on nitrogen dynamics of case 3A (1-12-2015: 75 l). 266

Figure 7.11: Influence of DO on nitrogen dynamics of case 11A (27-12-2015: 100 l) 266

Figure 7.12: Influence of DO on nitrogen dynamics of case 19B (24-1-2016: 125 l) 267

Figure 7.13: Influence of DO on nitrogen dynamics of case 25B (27-2-2016: 50 l)267

Figure 7.14: Influence of adsorption on nitrogen dynamics of case 3A (1-12-2015: 75 l) 268

Figure 7.15: Influence of adsorption on nitrogen dynamics of case 11A (27-12-2015: 100 l) 268

Figure 7.16: Influence of adsorption on nitrogen dynamics of case 19B (24-1-2016: 125 l) 269

Figure 7.17: Influence of adsorption on nitrogen dynamics of case 25B (27-2-2016: 125 l) 269

Figure 7.18: Influence of aerobic respiration on nitrogen dynamics of case 3A (1-12-2015: 75 l) 271

Figure 7.19: Influence of aerobic respiration on nitrogen dynamics of case 11A (27-12-2015: 100 l) 271

Figure 7.20: Influence of aerobic respiration on nitrogen dynamics of case 19B (24-1-2016: 125 l) 272

Figure 7.21: Influence of aerobic respiration on nitrogen dynamics of case 25B (27-2-2016: 50 l) 272

List of Tables

Table 2.1: The optimal solids loading rate (SLR) and removal efficiency of the existing system 18

Table 2.2: Summary of reviewed models 49

Table 2.3: Summary of nitrogen transformation mechanisms in the reviewed models 51

Table 3.1: The probe used to measure the specific water quality parameter 64

Table 4.1: Components in bio-kinetics module 105

Table 4.2: Composition parameters 107

Table 4.3: Kinetic parameters 108

Table 4.4: Stoichiometric parameters 112

Table 4.5: Stoichiometry matrix of bio-kinetics module 114

Table 4.6: Stoichiometry coefficient of alkalinity 115

Table 5.1: Hydraulic loading rate (HLR), sludge thickness, solids loading rate (SLR), collected effluent and water recovery percentage of the experiment 133

Table 5.2: Hydraulic loading rate (HLR), sludge thickness, solids loading rate (SLR), flow occurring delay and peak flow of the experiments 138

Table 5.3: Quality of raw septage for twenty-five batches of treatment 147

Table 5.4: Average concentration of quality parameters in the literature 148

Table 5.5: Removal efficiency of TS 156

Table 5.6: Removal efficiency of TCOD 158

Table 5.7: Removal efficiency of TN 160

Table 5.8: Removal efficiency of NH_4^+-N 162

Table 5.9: Removal efficiency of NH_4^+-N + NO_3^--N 165

Table 5.10: Sludge thickness and influent quality of bed A and bed B 167

Table 5.11: Comparisons of hydraulic performance and treatment efficiency 168

Table 5.12: Coefficient of determination (R^2) of each case 179

Table 5.13: Results of tracer experiment 185

Table 6.1: Laboratory measurement of hydraulic parameters 189

Table 6.2: Hydraulic parameters of gravel used in the literature for hydraulic simulation of VFCW (equilibrium flow) 190

Table 6.3: Hydraulic parameters of gravel used in the literature for hydraulic simulation of VFCW (preferential flow)..... 190

Table 6.4: Hydraulic parameters of sludge deposit used in the literature for hydraulic simulation of VFCW (equilibrium flow) 192

Table 6.5: Standard Hydraulic parameters of loam and silt (equilibrium flow) 192

Table 6.6: The information for geometry, time, and iteration criteria in the hydraulic simulation. 196

Table 6.7: Weather data (Weather Underground 2016)..... 197

Table 6.8: Inputs for ET 198

Table 6.9: Inputs for sludge accumulation..... 199

Table 6.10: The values of hydraulic parameters used in the hydraulic simulation.. 203

Table 6.11: Summary of calibrated parameters and error analysis..... 208

Table 6.12: Summary of calibrated parameters and error analysis..... 212

Table 6.13: MAE (%) and R^2 of the simulated results with and without CR 214

Table 6.14: Summary of calibrated K_s 222

Table 6.15: Potential evapotranspiration rate (PET) in each case 224

Table 6.16: Simulated sludge accumulation in each case 226

Table 7.1: Review on kinetics parameters used in previous studies (20˚C) 245

Table 7.2: Review of stoichiometric parameters used in previous studies (20˚C)... 247

Table 7.3: Review of composition parameters used in previous studies (20˚C)..... 248

Table 7.4: Proposed values for the parameters in bio-kinetics module 249

Table 7.5: Temperature coefficient of bio-kinetics parameters 250

Table 7.6: MAE (%) of NH_4^+-N and NO_3^--N 260

List of Abbreviations

ADE	Advection-dispersion equation
ANNAMOX	Anaerobic ammonium oxidation
BOD	Biological oxygen demand
CO_2	Carbon dioxide
COD	Chemical oxygen demand
CR	Correction factor for hydraulic load
CSTR	Continuous stirred-tank reactor
CW	Constructed wetland
DO	Dissolved oxygen
EC	Electrical conductivity
ET	Evapotranspiration
HFCW	Horizontal flow constructed wetland
HLR	Hydraulic loading rate
HRT	Hydraulic retention time
IST	Individual septic tank
LAI	Leaf area index
NH_3-N	Ammonia nitrogen
NH_4^+-N	Ammonium nitrogen
NO_2^--N	Nitrite nitrogen
NO_3^--N	Nitrate nitrogen
MAE (%)	Mean absolute percentage error
Org-N	Organic nitrogen
ORP	Oxidation-reduction potential
OSS	On-site sanitation system
PET	Potential evapotranspiration
SA	Sludge accumulation
SLR	Solids loading rate
STELLA	Structural Thinking, Experiential Learning Laboratory with Animation
SWCC	Soil water characteristic curve
TCOD	Total oxygen demand
TKN	Total Kjeldahl Nitrogen
TN	Total nitrogen

TS	Total solids
TSS	Total suspended solids
USEPA	United States Environment Protection Agency
VFCW	Vertical flow constructed wetland
VGM	van Genuchen – Mualem
VS2DT	Variably-Saturated 2D Flow and Transport

List of Symbols

Symbol	Description [Dimensional unit]
θ	Volumetric water content [$L^3 L^{-3}$]
h	Hydraulic head [L]
t	Time [T]
z	Vertical coordinate [L]
K	Unsaturated hydraulic conductivity [$L T^{-1}$]
S	Source/sink term [Dimensionless]
θ_r	Residual water content [$L^3 L^{-3}$]
θ_s	Saturated water content [$L^3 L^{-3}$]
α	VGM shape parameters [L^{-1}],
n	VGM shape parameters [Dimensionless]
m	VGM shape parameters [Dimensionless]
K_s	Saturated hydraulic conductivity [$L T^{-1}$],
l	Mualem's pore connectivity parameter [Dimensionless]
θ_{Mobile}	Mobile water content [$L^3 L^{-3}$]
$\theta_{Immobile}$	Immobile water content [$L^3 L^{-3}$]
Γ_w	Water transfer rate [T^{-1}]
$\theta_{r,Immobile}$	Residual water content in immobile region [$L^3 L^{-3}$]
$\theta_{s,Immobile}$	Saturated water content in immobile region [$L^3 L^{-3}$]
Se	Effective saturation [Dimensionless]
Γ_W	First order mass transfer coefficient [T^{-1}]
Se_{Mobile}	Effective saturation in mobile region [Dimensionless]
$Se_{Immobile}$	Effective saturation in immobile region [Dimensionless]
ET_0	Potential evapotranspiration rate [$L T^{-1}$]
λ	Latent heat of vaporization [$L^2 T^{-2}$]
R_n	Net radiation at surface [$M T^{-3}$]
G	Soil heat flux [$M T^{-3}$]
ρ_a	Atmospheric density [$M L^{-3}$]
C_p	Specific heat of moist air [$L^2 T^{-2} Q^{-1}$]
e_s	Saturation vapor pressure at particular temperature [$M L^{-1} T^{-2}$]
e_a	Actual vapor pressure [$M L^{-1} T^{-2}$]
r_c	Crop canopy resistance [$T L^{-1}$]

r_a	Aerodynamic resistance [T L^{-1}]
γ	Psychrometric constant [M L^{-1} T^{-2} Q^{-1}]
Δ	Slope of the vapor pressure curve [M L^{-1} T^{-2} Q^{-1}].
T_0	Potential transpiration rate [L T^{-1}]
E_0	Potential transpiration rate [L T^{-1}]
a_{b1}	Empirical coefficient in Beer-Lambert law [Dimensionless]
ST	Sink term of actual transpiration [L]
z	Depth from top surface [L]
$g(z)$	Non-linear function of root density distribution [Dimensionless]
g_0	root density at z=0 [M L^{-3}]
b	Diminishing coefficient of the root distribution [L^{-1}]
z_R	Maximum root depth [L]
F_{10}	Fraction of root length density in the top 10% of root depth
α_2	Coefficient of water stress distribution [Dimensionless]
θ_{wilt}	Wilting point [Dimensionless]
γ	Functional parameter [Dimensionless]
α_1	Compensation term [Dimensionless]
L_S	Thickness of new-forming sludge deposit layer [L]
ρ_s	Density of solids particles [M L^{-3}]
$\bar{n}$	Average porosity of sludge deposit layer [Dimensionless]
σ	Retention parameter [Dimensionless]
q_p	Input flux rate [L T^{-1}]
K_y	Erosion rate [T^{-1}]
n_s	Porosity of influent [Dimensionless]
ρ_w	Density of water [M L^{-3}]
ρ_s	Density of solid particles [M L^{-3}]
s	Mass fraction of particulates in influent [-]
C	Soil water capacity [L^{-1}]
α_i^j	Coefficient in matrix [Dimensionless]
β_i^j	Coefficient in matrix [Dimensionless]
γ_i^j	Coefficient in matrix [Dimensionless]
R_i^j	Residual term [L]
δ_i^{k+1}	Dependent variable [L]

δ_a	Prescribed tolerance [L]
h_{pond}	h_1 at previous time step (j-1) [L]
q	Nodal flux [L T^{-1}]
c	Solute concentration in aqueous phase [M L^{-3}]
MB	Mass balance
D_T	Hydraulic dispersion coefficient [L^2 T^{-1}]
D_L	Empirical longitudinal dispersivity [L^2 T^{-1}]
D_D	Molecular diffusion coefficient [L^2 T^{-1}]
s_e*	Rate of change of adsorbed solute per unit weight of solid [M M^{-1}]
K_d	First order coefficient [L^3 M^{-1}]
N	Freundlich exponent [Dimensionless]
η_k	Langmuir adsorption constant [Dimensionless]
ρ_b	Bulk density [M L^{-3}]
s_e	Mass of adsorbed compound in equilibrium site [M M^{-1}]
s_k	Mass of adsorbed compound in kinetic site [M M^{-1}]
ω_k	First-order rate constant for the kinetic adsorbed compound [Dimensionless].
f_E	Fractional coefficient [Dimensionless]
c_{Mobile}	Solute concentration in mobile region [M L^{-3}]
$c_{Immobile}$	Solute concentration in immobile region [M L^{-3}]
Γ_s	Exchange rate between the mobile and immobile regions [M L^{-3} T^{-1}]
α_{ph}	Solute transfer coefficient [T^{-1}]
f_{Mobile}	Fraction of adsorption sites exposed to mobile water [Dimensionless]
$s_{e,Mobile}$	Adsorbed concentration in equilibrium in the mobile region [M M^{-3}]
$s_{k,Mobile}$	Adsorbed concentration of the kinetic sites [M M^{-3}]
Φ_{Mobile}	Sink/ source term in the mobile regions [M L^{-3} T^{-1}]
$\Phi_{Immobile}$	Sink/source term in immobile regions [M L^{-3} T^{-1}]
Γ_{s1}	Transfer rate between the mobile and immobile region [$ML^{-3}T^{-1}$]
Γ_{s2}	Mass transfer rate to the kinetic adsorption sites [M L^{-3} T^{-1}]
J	Total flux of solute [M L^{-3} T^{-1}]
k	zero-order kinetic term [T^{-1}]
M	Coefficient in matrix [Dimensionless]
U	Coefficient in matrix [Dimensionless]

L	Coefficient in matrix [Dimensionless]
R	Coefficient in matrix [Dimensionless]
C_0	Influent concentration [M L^{-3}]
Cr	Courant number [Dimensionless]
Pe	Peclet number [Dimensionless]
S_O	Dissolved oxygen [M L^{-3}]
S_S	Readily biodegradable organic matter [M L^{-3}]
S_I	Inert soluble organic matter [M L^{-3}]
S_{NH}	Ammonium plus ammonia nitrogen [M L^{-3}]
S_{N2}	Dinitrogen [M L^{-3}]
S_{NO}	Nitrate nitrogen [M L^{-3}]
S_{HCO}	Alkalinity [mole L^{-3}]
X_S	Slowly biodegradable particulate organic matter [M L^{-3}]
X_I	Inert particulate organic matter [M L^{-3}]
X_H	Heterotrophic biomass [M L^{-3}]
X_A	Autotrophic biomass [M L^{-3}]
i_{NSI}	Nitrogen Content in S_I [M M^{-1}]
i_{NSS}	Nitrogen Content in S_S [M M^{-1}]
i_{NXS}	Nitrogen Content in X_S [M M^{-1}]
i_{NXI}	Nitrogen Content in X_I [M M^{-1}]
i_{NBM}	Nitrogen Content in Biomass [M M^{-1}]
k_H	Hydrolysis rate constant [T^{-1}]
K_X	Saturation coefficient for hydrolysis [M M^{-1}]
μ_H	Maximum growth rate on substrate [T^{-1}]
η_{NO}	Anoxic reduction factor [Dimensionless]
$K_{H,O}$	Saturation/ Inhibition coefficient for DO [M L^{-3}]
$K_{H,S}$	Saturation coefficient for substrate [M L^{-3}]
$K_{H,NO}$	Saturation coefficient for NO_3^--N [M L^{-3}]
$K_{H,NH}$	Saturation coefficient for NH_4^+-N [M L^{-3}]
$K_{H,HCO}$	Saturation coefficient for alkalinity [M L^{-3}]
b_H	Rate constant for lysis [T^{-1}]
μ_A	Maximum growth rate on NH_4^+-N [T^{-1}]
$K_{A,O}$	Saturation/ Inhibition coefficient for DO [M L^{-3}]

$K_{A,NH}$	Saturation coefficient for NH_4^+-N [M L^{-3}]
$K_{A,HCO}$	Saturation coefficient for alkalinity [M L^{-3}]
b_A	Rate constant for lysis [T^{-1}]
f_{SI}	Fraction of S_I in hydrolysis [M M^{-1}]
f_{XI}	Production of X_I in lysis [M M^{-1}]
$Y_{H,O}$	Aerobic Yield of Heterotrophic Biomass [M M^{-1}]
$Y_{H,NO}$	Anoxic Yield of Heterotrophic Biomass [M M^{-1}]
Y_A	Yield of Autotrophic Biomass [M M^{-1}]
$\emptyset_v$	Sink term of passive nutrient uptake [M L^{-2} T^{-1}]
ST	Root water uptake [L T^{-1}]
m	Components in bio-kinetics module [Dimensionless]
n	Processes in bio-kinetics module [Dimensionless]
R_m	Reaction term for component m [M L^{-3} T^{-1}]
$v_{n,m}$	Stoichiometric factor for component m and process n [M M^{-1}]
Pn	Zero-order reaction rate for process n [M L^{-3} T^{-1}]
R^2	Coefficient of determination [Dimensionless]

Chapter 1 Introduction and Objectives

1.1. Background

The installation of on-site sanitation systems (OSSs) has become an attractive solution in developing countries (Strauss 2006). This is a decentralized treatment alternative that engages the storage and primary treatment within a well-protected container at a household level (WHO 2006). In order to reduce the spread of disease caused by the raw sewage, such an improved sanitation facility that links with a feasible storage or treatment system is essential (Langergraber and Muellegger 2005). An individual septic tank (IST) system, which acts as a "combined settling and skimming tank, as an unheated unmixed anaerobic digester, and as a sludge storage tank", is one of the most prevailing OSSs in developing countries (Crites and Tchobanoglous 1998). In Malaysia, there are over 1.50 million ISTs serving approximately a population of 5 million in West Malaysia as of 2006 (AECOM, SANDEC and Eawag 2010) and over 370, 000 ISTs serving approximately a population of 1.90 million in Sarawak as of 2010 (Lau 2012).

Increasing attention has been paid on the massive amounts of septage generated in these septic tanks. These "recalcitrant solids" gradually reduce the space needed for microbial degradation, which eventually leads to the discharge of untreated sewage due to the excessive sludge accumulation within the septic tank (Hamersley et al. 2001), as shown in Figure 1.1. Therefore, scheduled desludging is needed by the septic system in order to maintain its satisfactory operation (Figure 1.2). The management of septage necessitates distinctive tasks which include collection, transportation, treatment, and disposal to reduce its risk to the public health and the environment. Nevertheless, AECOM, SANDEC, and Eawag (2010) revealed that even though efforts have been made to advocate the implementation of ISTs, a proper legal framework for the management of septage is still deficient in most developing countries.

Septage is defined as a semi-liquid mixture of sludge, scum, and liquid removed from the IST that receives domestic sewage only (Crites and Tchobanoglous 1998; Harrison and Moffe 2003). United States Environmental Protection Agency (1999b) describes raw septage as "highly variable and organic, with significant levels of grease, grit, hair, and debris". A sample of septage used in this study with its gross solids is shown in

Figure 1.1: Septic tank with excessive sludge

Figure 1.2: Desludging process

Figure 1.3. Septage is commonly described as having an unpleasant smell, being pathogenic, foam-forming, and reluctant to the treatment processes such as settling and dewatering.

The amount and characteristics of septage depend on various factors such as desludging frequency, tank dimension, water supply pattern, climate, soil condition and disposal of the solid waste or household chemicals to the toilet (AECOM, SANDEC and Eawag 2010; Kone and Strauss 2004), and thus septage characteristics might differ from household to household. In general, septage is concentrated with excessive total solids (TS), chemical oxygen demand (COD) and nutrients (Crites and Tchobanoglous 1998), which could be 10-100 times higher than municipal wastewater

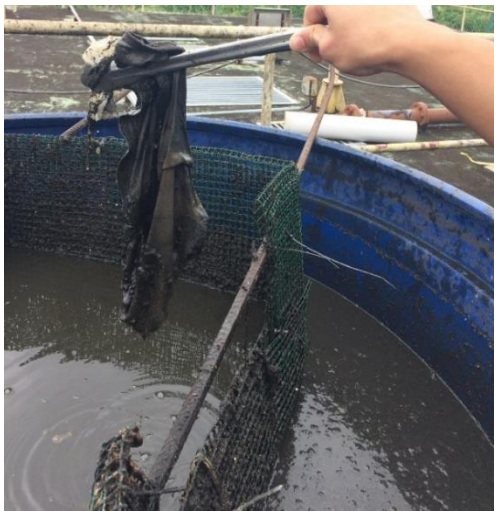

Figure 1.3: Raw septage collected from the domestic area

(Strauss, Larmie and Heinss 1997). The direct disposal of septage into watercourses will lead to immediate oxygen depletion and eutrophication, as well as the spread of waterborne diseases (Centre for Science and Environment New Delhi 2011).

The development of septage management and treatment options are unappreciated compared to sewage treatment (Kone and Strauss 2004), which results in a lack of a safe and sustainable septage disposal plan in many developing countries. Common septage management practices in these countries include land application and co-treatment in sewage treatment systems (Vincent et al. 2011). Land application is still constrained by the health risks posed by disease-causing pathogens and excessive nutrients contained in raw septage (Harrison and Moffe 2003). As for co-treatment, the variation in septage quality and its high solid and nutrient content create challenges for the conventional sewage treatment plant in producing a consistent treatment performance (Harrison and Moffe 2003).

To counter the problems raised by the variable characteristics of septage and the current practices of septage management, a decentralized subsurface wetland system is proposed.

1.2. Alternative solution: vertical flow constructed wetland (VFCW)

The subsurface vertical flow constructed wetland (VFCW) has been introduced as a feasible septage treatment facility for small or medium communities. The constructed wetland (CW) is an artificial water treatment system with controlled conditions and operations to reproduce the water purification processes in natural wetlands to remove

pollutants from wastewater (Kivaisi 2001; Sim 2003; Babatunde et al. 2008; Vymazal 2010a; Zhang, Xu, et al. 2012), as well as septage (Koottatep et al. 2001; Paing and Voisin 2005; Troesch, A. Liénard, et al. 2009; Vincent et al. 2011; Jong 2014). This water treatment technology is integrated by a vegetated wetland bed and a distribution and drainage device to deliver a more consistent treatment capability compared to the natural wetland (Haberl et al. 2003; Kumar and Zhao 2011; Zhang, Xu, et al. 2012). Typically, the treatment processes in CW are stimulated naturally by vegetation and microbial community. The removal of contaminants is a result of biological, chemical and physical processes, including filtration, adsorption, plant uptake, and microbial metabolism (Wynn and Liehr 2001; Kumar and Zhao 2011).

In VFCWs, the raw septage is loaded on the surface of the wetland bed. The wetland bed is a multi-layer porous medium that supports the growth of vegetation and a microbial community, which is also known as substrate. The influent percolates gravitationally through the substrate to conduct physical filtration and biochemical processes. Subsequently, the effluent is collected at the bottom of the bed through a drainage device (Verhoeven and Meuleman 1999; Langergraber, Giraldi, et al. 2009). The vegetation in the system helps in restoring the oxygen content within the wetland bed and stimulates the transpiration process to enhance the dewatering of septage. Since the active biomass develops on the surface of the granular substrate, the VFCWs are generally recognized as an attached growth system.

The VFCW has remarkable aeration capacity, which is not only due to the presence of vegetation but also to loading regime. In an intermittent loading regime, the system is only loaded after the previous batch of influent has been completely drained (Zhang, Tan, et al. 2012), and thus unsaturated conditions are created within the substrate, which allows the oxygen to refill the substrate by convection. The oxygen-rich condition benefits mechanisms such as the aerobic decomposition of organic matter and nitrification within the VFCWs, but the anaerobic process such as denitrification is prohibited.

A pilot-scale, VFCW–based septage treatment system was designed and constructed in Curtin University Sarawak Malaysia to evaluate its performance under a tropical climate (Jong 2014). This septage treatment system consisted of two successive treatments similar to Lienard and Payrastre (1996). In this system, the first stage

wetland bed was designed to filter particle constituents while the second stage wetland bed was designed to remove organic matter and nutrients via biochemical processes.

This study reinforced the capability of using VFCWs to treat septage, as favourable results were obtained, which showed that the operational factors including loading rate and resting period were crucial to achieve the targeted removal performance for TS, COD, and NH_4^+-N. However, the overall nitrogen removal was less desirable, as the concentration of nitrate (NO_3^--N) generally increased in the effluent due to the favourable aerobic condition. In this study, the treatment efficiency of the system was determined by a black-box approach, where the removal rate was evaluated through the comparison between mass-in and mass-out of particular contaminants. The dynamics of the effluent flow rate and treatment performance were not determined in the experiment, and thus a further study is proposed to investigate the correlation between the hydraulic behaviour and nitrogen dynamics in the effluent.

1.3. Hydraulic behaviour and nitrogen dynamics in the VFCWs

The intermittent loading regime resulted in a “continuously varying saturation level” along the substrate profile during the infiltration period (Giraldi and Iannelli 2009). Therefore, the effluent flow rate from the wetland bed fluctuates significantly throughout the operation. As the wetland bed is freely draining, the effluent flow rate represents the retention time of the influent within the bed and controls the contact time between the contaminants and active biomass. Accordingly, the hydraulic behaviour of the wetland, which is described by the effluent flow rate and other factors such as water content along the substrate profile; significantly influences the treatment performance. In fact, the quality of the effluent may be influenced by the variation of hydraulic behaviour, particularly in terms of water recovery and percolation flow rate. However, the correlation between the dynamics of nitrogenous constituents and the associated effluent flow rate in the VFCWs designed for septage treatment has not yet been identified in the literature.

In the wetland-based system, nitrogen removal is a result of complex interactions between physical, chemical and biological processes (Kumar and Zhao 2011). The main nitrogen transformation mechanisms involved in VFCWs are ammonification, nitrification, denitrification, and plant uptake (Vymazal 2007). The rates of these nitrogen transformation processes in VFCWs have been found to be highly related to

influent quality, surrounding environment and operating strategies, including hydraulic retention time, oxygen availability, temperature, pH, carbon-nitrogen ratio, plant species, maturity of the microbial community and others (Lee, Fletcher and Sun 2009). Although the understanding of individual nitrogen transformation and degradation processes are fairly complete in such system, the overall behaviour of nitrogen dynamics is not comprehensively presented in the literature.

Apart from collecting data from the experiments, one of the alternatives to investigate the relation between the hydraulic behaviour and nitrogen dynamics in VFCW is to numerically simulate the treatment mechanism using a mechanistic model. The mechanistic model, which is a process-based model, computes the transport and fate of specific substance individually from the relevant factors within a predefined time frame and it has become the state-of-art in the study of modelling for the wetland-based system. The precision of such models relies upon the coupling of two dominant factors in the VFCW, which are the hydraulic behaviour and the biochemical kinetics (Saeed and Sun 2011b). The mechanistic model provides a platform to reproduce the hydraulic behaviour, solute transport, and the degradation process simultaneously. It is a practical design tool not only to evaluate the treatment performance but also to optimize the configuration and operation under a variety of operating conditions. To date, HYDRUS-CW2D (Langergraber and Šimůnek 2005) and FITOVERT (Giraldi, de Michieli Vitturi and Iannelli 2010) provided the most comprehensive work on the hydraulic behaviour and degradation in the VFCWs.

In order to facilitate the understanding of overall nitrogen removal in the VFCWs designed for septage treatment under a tropical climate, this study aims to investigate the dependency of nitrogen dynamics on the hydraulic behaviour of the VFCW and proposes a mechanistic model to numerically simulate the nitrogen transformation throughout the bed.

1.4. Identification of problem and research aim

As mentioned in section 1.2, the treatment efficiency of a pilot-scale, two-stage VFCW-based septage treatment system was obtained based on a black-box approach. The current literature only provided an analysis of overall water recovery and removal efficiency. However, the dynamics of hydraulic behaviour and treatment, as well as the influence of hydraulic behaviour towards the overall treatment efficiency, were not

clearly identified. This gap increases the difficulty in the optimization of an operating strategy in order to improve the treatment performance, especially to counter the high NO_3^-- N concentration produced in the effluent. Therefore, the first part of the study aims to experimentally identify the relation between hydraulic behaviour and nitrogen dynamics in the first stage wetland bed of the pilot plant.

In addition to the laboratory work, a mechanistic model is proposed to numerically simulate the nitrogen dynamics by combining a hydraulic module, solute transport module, and a reaction kinetics module. Such a reactive transport model provides a platform to interlink these modules to accommodate varying system configurations and operating regimes, which has not been done for septage treatment. A research oriented type of mechanistic model is a useful tool to gain understanding to the black-box in a complex system. However, a comprehensive study is essential to conceptualize the governing factors of treatment mechanism in the VFCWs. Then, an appropriate numerical formulation with adequate equations and solving methods has to be developed to produce the expected outcomes. Besides, laboratory work has to be carried out in order to calibrate and the parameters and validate the feasibility of mechanistic model. As a first step towards the simulation of nitrogen dynamics in the VFCW designed for septage treatment, the scope of the study is only confined to the first stage wetland beds in the system. Hence, the second part of the study aims to simulate the hydraulic behaviour and outflow nitrogen dynamics for a pilot-scale first stage treatment wetland to investigate the influence of hydraulic behaviour on the outflow nitrogen dynamics.

1.5. Objectives

The main objectives and the corresponding research problems and output of this study are stipulated as follows:

I. To develop a mechanistic model to describe the hydraulic behaviour and outflow nitrogen dynamics in a pilot-scale VFCW-based septage treatment system.

The transformation and degradation mechanisms of nitrogenous constituents in VFCWs involve a series of physical, chemical and biological processes, whereas the complexity of the dynamics is further increased due to the correlation to numerous factors such as the system configuration and operating regime. The difference of these

factors typically results in a change of hydraulic behaviour, subsequently varying the overall treatment performance in the system. Currently, the available models in the literature are still inadequate to simulate both the hydraulic behaviour and associated nitrogen dynamics in the VFCW designed for septage treatment. Therefore, a mechanistic model is conceptualized and developed for the first stage treatment in a pilot-scale, two-stage VFCW, which incorporates a hydraulic module, a transport module, and a reaction kinetics.

II. To calibrate the outflow nitrogen dynamics model according to the measured data under the tropical climate.

The proposed model is to be calibrated with the measured data to examine its capability in producing accurate results. A pilot-scale VFCW-based septage treatment system is constructed and operated to obtain the results of the rate of outflow and the associated treatment efficiency. The initial parameters used in the model are obtained from the literature and some simple laboratory experiments.

III. To investigate the influence of hydraulic behaviour upon outflow nitrogen dynamics based on the measured and simulated results

The relation between hydraulic behaviour and nitrogen dynamics is studied according to the outcomes of the numerical simulation and measured data obtained in a pilot-scale system. The existing studies have indicated the impact of operational strategies on the overall water recovery and removal efficiency, but a tracking of hydraulic behaviour and outflow quality is lacking in the literature. The quality of the effluent is compared to identify the influence of hydraulic behaviour on the outflow nitrogen dynamics and overall removal efficiency. It is anticipated that a similar trend will be observed in the results from the pilot-scale system and numerical simulation.

1.6. Scope and limitation

The proposed model, VF_Sep, is an outset of the study for the numerical modelling of a two-stage VFCW-based septage treatment system. This study aims to simulate the outflow nitrogen dynamics from the first stage treatment in the system using a mechanistic approach, which combines the transport module and kinetics module to predict the transport and fate of the nitrogenous constituents. The scope of the study is listed to highlight the expected outcomes from the study:

- VF_Sep is developed using the simulation software MATLAB® to predict the outflow nitrogen dynamic in a pilot-scale system. The outcome focuses on the precision of the simulation, while the discussion of the computational efficiency and mathematical optimization are excluded.
- VF_Sep is conceptualized and developed to compromise between the practicality in handing and complexity of outcomes. The comprehensiveness of the equations and the selection of the numerical approach used in the proposed model are decided according to the versatility, applicability, accuracy, and computation time of the simulation. Comparison between the different equation and numerical approaches is not included in the study.
- VF_Sep is only applied to the first stage treatment of a pilot-scale, two-stage VFCW-based septage treatment system, where the upper and lower boundary conditions are set to be temporal flux-and-pond and free drainage, respectively.
- This study focuses on the development of the mechanistic model and the associated calibration to the measured data in a pilot-scale system. The validation of the model is not conducted to the system with variation in the design configuration and operating regime.
- This study aims to develop a numerical relation between hydraulic behaviour and nitrogen treatment performance. The quantification of oxygen restoration, heat transfer, alkalinity consumption, organic carbon cycle, development of microbial community, and water loss during the resting phase are not included in this study.
- The evaluation of the proposed model is based on the error analysis with regards to the measured data. The proposed model is not compared to the existing models in the literature for its efficiency and accuracy.
- Although VF_sep is able to simulate the transport and fate of the dissolved oxygen, TS, organic carbon, and the development of heterotrophs and autotrophs, the determination of these components is only partially carried out and thus the calibration for these components is excluded from the scope.

- Due to the limitation in the laboratory experiment, the evaluation of the nitrogen removal pathway is only performed with regards to the nitrification-denitrification, adsorption and plant uptake in the numerical form.

1.7. Thesis outline

The objectives of this study are to develop a mechanistic model and conduct laboratory experiment to investigate the transport and fate of nitrogenous constituents and its correlation to the hydraulic behaviour. In **Chapter 2**, an overview of the VFCWs and its application in septage treatment are addressed. A variety of design configurations and operating strategies and the mechanisms of nitrogen removal in this type of systems are discussed. A review of the literature on the existing numerical model for VFCWs is presented, as well as the gaps and significances of research are addressed. **Chapter 3** demonstrates the configurations of the laboratory experimental rigs and the operational regime employed in this study. The sampling and analysis protocols in assessing the hydraulic behaviour and treatment efficiency are also introduced.

Chapter 4 describes the features and theory used in the proposed mechanistic model, VF_Sep. The assumptions and limitations of the model are summarized. The model is subdivided into the hydraulic module, transport module, and kinetics module. The governing equations such as the Richards equation, Penman-Monteith equation, advection-dispersion equation (ADE), activated sludge model (ASM) and etc. are explained. Then, the numerical implementation, initial conditions, and boundary conditions of each module are presented. In addition, the development of the model in the Matlab© is demonstrated in this chapter.

In **Chapter 5**, the hydraulic and treatment performance of the pilot-scale first stage wetland bed are reported. In the first section, the results of the preliminary experiments are presented to highlight the feasibility of VFCW-system treating septage. Then, the measured data obtained from the pilot plant are analysed according to water recovery, delay of flow and peak effluent flux. The influence of hydraulic loading rate (HLR), solids loading rate (SLR) and sludge deposit layer on these parameters are discussed. The characteristic of raw septage used in this study is also reported in this chapter. The dynamics of quality parameters in the effluent including DO, pH, TS, COD, TN, NH_4^+-N, and NO_3^--N and the associated treatment efficiencies are presented. The influence of HLR, SLR and sludge deposit layer on the treatment performance is discussed. In

addition, the analysis of the correlation between hydraulic behaviour and nitrogen dynamics is described in this chapter. Lastly, the results of tracer experiment are presented and discussed.

Chapter 6 presents the results of the hydraulic simulation using VF_Sep. The simulation set-up, assumptions, the procedure of calibration, and input parameters are presented. The error analysis between the simulated results and measured data is discussed. Then, a correction coefficient to improve the simulation performance is introduced. Besides, the discussion of the influence of ET and sludge deposit layer on hydraulic simulation is presented in this chapter.

Chapter 7 shows the simulation of nitrogen dynamics. The simulation set-up, input parameters, calibration method, and assumptions are introduced. The accuracy of the simulated results is analysed and discussed. The contribution of each removal mechanism is evaluated according to the simulated results. The efficiency of VF_Sep is deliberated, and a set of improvement is suggested. **Chapter 8** summarizes the findings from this thesis, and the recommendations for future research are proposed.

Chapter 2 Literature Review

2.1. Overview of the VFCWs

The subsurface-flow (SSF) system is a type of constructed wetland (CW) system where the influent flows beneath a vegetated wetland bed and is ultimately discharged by a drainage system (Verhoeven and Meuleman 1999; Yang, Chang and Huang 2001). This type of CW is further divided into the horizontal flow (HFCW) and vertical flow (VFCW) with regards to the dissimilar system configurations and operating regime, which leads to different flow directions in the system.

Figure 2.1 shows a typical VFCW system. The VFCW is loaded with a large batch of influent that floods the surface, then the influent percolates vertically through the substrate towards the drainage system, in a so-called “fill-and-drain” feeding mode (Zhang, Tan, et al. 2012). Under this feeding mode, the wetland bed might only be partially saturated. Thus, the VFCW is typically recognized as a variably-saturated system (Morvannou et al. 2013b). Meanwhile, the wetland bed is created with a “temporal redox variation” and is re-aerated throughout the dry-wet cycle (Langergraber 2008; Faulwetter et al. 2009; Zurita, De Anda and Belmont 2009; Zhang, Tan, et al. 2012). As a result, the VFCW is well-known for its aerobic behaviour and outstanding performance in removing organic matter and ammonia (NH_3-N) (Saeed and Sun 2011b). Nevertheless, the technical requirement of such a system is higher, where the installation of an inlet structure to regulate the influent volume is essential (Kadlec 2009; Vymazal 2010a). A poor denitrification rate was observed in the VFCW, which eventually led to a high nitrate (NO_3^--N) concentration in the effluent (Koottatep et al. 2004; Kengne et al. 2009; Troesch, A. Liénard, et al. 2009).

In VFCWs, the percolation of influent is driven by th1e gravity and pressure gradients (Haberl et al. 2003). The substrate is defined as a layered porous medium that supports the growth of wetland vegetation and acts as a filter to segregate the solid from the influent (Verhoeven and Meuleman 1999). In addition, the substrate provides attachment surfaces for microbial growth and adsorption sites for ionized contaminants (Saeed and Sun 2011b). The retention time of influent within the wetland bed is the duration for influent passing through the substrate, and thus the retention time

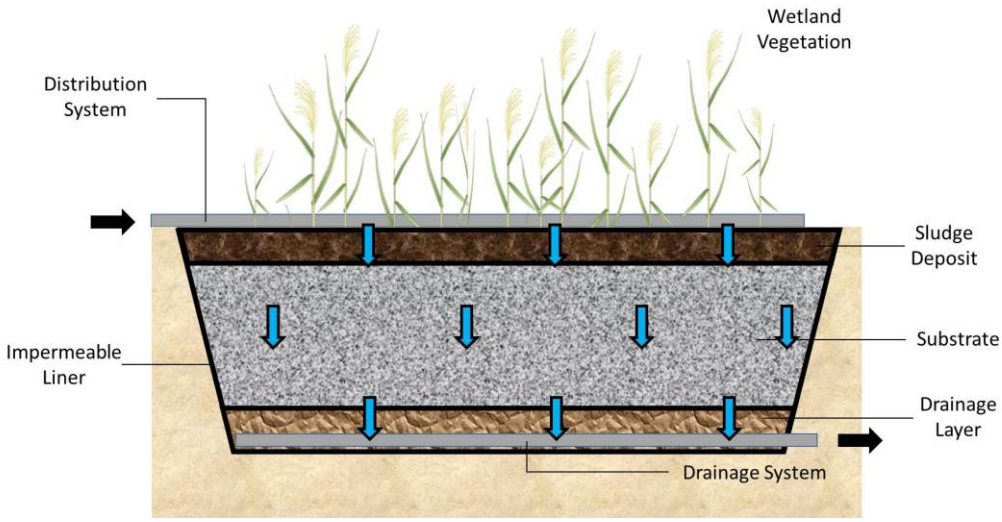

Figure 2.1: A typical VFCW system and its components

significantly relates to the properties of the substrate and the loading regime. The common materials used in the VFCWs are sand and gravel, but the application of industrial and agricultural by-products such as slag and palm kernel shell has also been presented in some studies (Jong and Tang 2015).

Białowiec, Albuquerque, and Randerson (2014) summarized the advantages of vegetation as a source of oxygen and carbon for the microbial activities, as well as the extraction of water and pollutants constituted in the influent. The vegetation in the VFCWs transports a certain amount of oxygen to its roots and creates an aerobic zone around rhizosphere to induce the microbial growth in the wetland bed. Meanwhile, the carbon compound released from its debris could be utilized by the microorganisms in the anaerobic process such as denitrification. The vegetation also uptakes the water and the pollutants such as nutrients (nitrogen and phosphorus) and heavy metals, subsequently enhancing the dewatering and treatment efficiency of the system.

In VFCWs, most of the biodegradable contaminants in wastewater are removed by the attached microorganisms through aerobic and anoxic degradation (Kadlec 2009). Meanwhile, a significant amount of particulate constituents is filtered at the surface of wetland bed, and this forms a deposited layer. Under the typical condition, the restored oxygen in VFCWs facilitates the aerobic process, particularly aerobic respiration, and nitrification to remove chemical oxygen demand (COD), biological oxygen demand (BOD), and NH_3. On the other hand, the efficient restoration of oxygen in the system prohibits the occurrence of the anoxic processes such as denitrification, and thus the

VFCW is commonly incapable of providing a complete route of nitrification-denitrification (Vymazal 2010b).

The combined effect of the evapotranspiration (ET) at the surface water and through the vegetation is one of the main dewatering mechanisms in VFCW. The water loss might lead to an increase in the concentration of dissolved contaminants due to the decreasing of water content, simultaneously enhancing the accumulation of particulate contaminants within the substrate. Moreover, a high ET rate causes a significant reduction in the moisture content of the substrate, which extends the residence time of the influent in the system and eventually improves the treatment performance (Konnerup, Koottatep and Brix 2009). Nevertheless, such studies of water loss were less common, since water losses were extremely sensitive to the system configuration and surrounding environment, including the depth-surface ratio of the wetland bed, the condition of wetland vegetation and the climate condition.

Substrate clogging is the main difficulty in maintaining the operation of VFCWs (Shutes 2001; Cooper 2005; Molle et al. 2005). This phenomenon is the consequence of the accumulation of particle constituents at the upper layer and overgrowth of microorganisms, which significantly reduces the permeability and infiltration capacity. The undesirable infiltration capacity might result in a long duration of surface ponding and eventually leads to system failure (Hua et al. 2010).

2.2. Overview of VFCW-based septage treatment system

VFCWs have been widely applied to treat various types of wastewater, ranging from municipal sewage (Kim et al. 2013) and agricultural wastewater (Herouvim et al. 2011) to leachate (Lavrova and Koumanova 2010) and stormwater (Fournel et al. 2013). However, the application of VFCWs for septage treatment is less common. This section reviews several existing systems, which constituted different features and manipulations to handle septage. The discussion is focused on the corresponding removal efficiency of pollutants on the difference in operating regime.

The first systematic attempt to treat septage using VFCWs was introduced in Lienard and Payrastre (1996). The system consisted of two stages, where the first stage wetland beds were constructed using 0.25 m thick coarse gravel and vegetated with common reeds (*Phragmites australis*). The beds were loaded weekly with a hydraulic load of 1.5 m^3, demonstrating solid loading rate (SLR) approximately 70 kg TSS m^{-2} $year^{-1}$.

This first stage treatment had showed promising removal efficiency with regards to COD, TSS and NH_4^+-N, but the removal of BOD and NH_4^+-N was less efficient. Moreover, the concentration of NO_3^--N increased in the effluent. At the second stage, the wetland bed was topped with a layer of sand to enhance the hydraulic retention time (HRT) and were loaded with the percolate from the first stage treatment at a rate of 1 dose per day. At this stage, the treatment performance was found to be proportional to the thickness of substrate, suggesting a depth of 60 cm could deliver the effluent with low COD and NH_4^+-N. Furthermore, gravel was claimed to be favourable for oxygen renewal due to its large porosity.

This type of two-stage system has been developed into a field study, where Paing and Voisin (2005) evaluated the treatment performance of a full-scale VFCW-based septage treatment system in Beaumont-la-Ronce, France. This system was configured with the same design as in Lienard and Payrastre (1996). The first stage of the system was made up of gravel with a depth of 90 cm and had a surface area of 612 m^2. The raw septage was pre-treated by undergoing a screening process to remove gross solids. Each wetland bed was operated at a SLR of 46 kg TSS m^{-2} $year^{-1}$, where the feeding continued for seven days at a rate of 20 m^3 per day. The feeding was followed by a resting period of five weeks. The physical filtration was the major treatment mechanism and the retention efficiency increased gradually due to the accumulation of sludge deposit. The second stage system was installed with an additional ventilation pipe in the middle of substrate to promote aerobic processes. The final effluent throughout two stages of treatment demonstrated an impressive quality, where the removal of total suspended solids (TSS), BOD, COD and total Kjeldhal nitrogen (TKN) achieved more than 90 %. However, the concentration of NO_3^--N increased in the effluent, implying that denitrification might be absent from the system.

Troesch, Lienard, et al. (2009) built a pilot-scale, single-stage VFCW to treat septage at a SLR of 30 kg TSS m^{-2} $year^{-1}$. The substrates in this system constituted of several layers of graded gravels and two alternative top layers, which were sand and vegetal compost. All wetland beds were planted with common reed (*Phragmites australis*). The raw septage was loaded in two alternatives; one was applied directly and the other was mixed with aerated sludge before application. Both handling regimes can eliminate more than 80 % of SS, COD and TKN, but the overall performance of NH_4^+-N and NO_3^--N were still less desirable. The study observed that the mixing method

enhanced the dewaterability of septage due to the "flocculation" of aerated sludge. The sludge deposit at the wetland surface accumulated at a rate of 11.50 cm year^{-1}. Substrate clogging was not observed throughout the experiment, which was mainly attributed to the low applied SLR and appropriate resting period. Vincent et al. (2011) further elaborated an operating strategy, which suggested a 5-day feeding period and 24-day resting period with a SLR of 50 kg TSS m^{-2} year^{-1} to effectively reduce the possibility of substrate clogging.

Koottatep et al. (2001) designed and built a single-stage pilot VFCW to treat septage in Thailand, which was referred as the first attempt of wetland-based septage treatment in the tropical region. Three wetland beds were constructed, each with a surface area of 25 m^2 and a depth of 65 cm. The substrate was mainly built by gravel and sand, and the wetland bed was vegetated with narrow-leaf cattails (*Typha augustifolia*) at a density of 10-15 shoots m^{-2}. A network of aerated pipes was constructed to secure the growth of vegetation. Since the microbial activities are favourable under the tropical climate (Diemont 2006), the SLR in this study was up to 250 kg TS m^{-2}year^{-1}. This system removed more than 80% of TS, COD, TKN, and NH_4^+-N, while NO_3^--N increased significantly after treatment. The problems of shock loading and water deficiency were detected throughout the experiment, causing the wilting and even death of vegetation. Accordingly, the wetland vegetation was suggested to be acclimatized in the system for a certain period. In addition, the attempt of "percolate impounding", where the wetland bed was impounded by the influent for 6 days instead of free drainage, was seen to be a solution for the water deficiency.

An updated operational guideline with regards to the treatment performance was established in Koottatep et al. (2004) after seven years of operation. Due to the high variation in solids concentrations of raw septage, maintaining a constant HLR is more practical than operating at a constant SLR. A longer impounding period ultimately improved the removal of total nitrogen (TN), but no obvious impact was observed for the removal of SS, BOD and COD. Such circumstance promoted the occurrence of anoxic denitrification due to the long ponding period. Furthermore, the growth rate of cattails accelerated rapidly after acclimatization, and thus regular harvesting was necessary.

By using the similar principles of system layout and operating regime, Kengne et al. (2009) specified that a SLR range of 100 – 200 kg TS m^{-2} $year^{-1}$ delivered promising treatment performance for SS, COD, TKN and NH_4^+-N, and effectively reduce the risk of clogging. Besides, an alternative wetland vegetation of antelope grass (*E. pyramidalis*) demonstrated a good sustainability in dewatering and stabilizing faecal sludge collected in African countries (Kengne et al. 2008). In the meantime, approximately 100 – 150 tons $hectare^{-1}$ of dry plants were produced. This study also indicated that the accumulated nutrient-rich bio-solids might potentially be reused under proper management, which will increase the advantages in terms of cost-efficiency.

A pilot-scale, two-stage VFCW-based septage treatment system (Figure 2.2), was designed and constructed in Curtin University Sarawak Malaysia (Jong and Tang 2013, 2014). The stage one wetland was aimed to remove excessive solids and organic matter through physical filtration and sedimentation to minimize the risk of clogging in the following treatment. At this stage, three wetland beds had been built and each bed had a surface area of 2.20 m^2 and a total depth of 0.80 m. The substrate was built by various layers of graded crushed stone, and the surface of wetland beds was vegetated with the common reeds (*Phragmites karka*). Three SLRs have been tested, which were 100 kg TS m^{-2} yr^{-1}, 250 kg TS m^{-2} $yr^{-1}$and 350 kg TS m^{-2} yr^{-1}. The wetland beds were operated with a feed-rest ratio of 1:6 days, indicating that the bed was operated once a week and followed by a 6-day resting period. This stage of VFCW was set to be freely drained, and the percolate was collected in a tank for twenty-four hours. At this stage, the removals of TS, COD and NH_4^+-N were excellent.

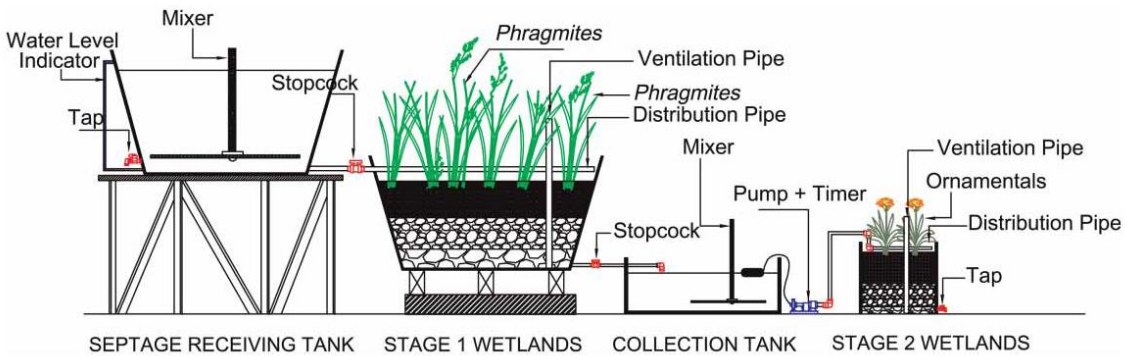

Figure 2.2: Side view of a pilot-scale, two-stage VFCW-based wetland treatment system (Jong and Tang 2014)

The percolates collected from the stage one wetlands were stored, and then it was applied to the second stage wetlands after mixing and stirring. Stage two consisted of four wetland beds; each has a surface area and a depth of 0.24 m^2 and 0.80 m, respectively. The substrate is a combination of gravel, palm kernel shell (PKS) and sand. The PKS has been found to be a carbon source to stimulate denitrification. Two beds were planted with common reed and two were planted with ornamental (*Costus Woodsonij*). Two HLRs had been conducted at stage two, which were 8.75 cm/day and 17.50 cm/day. The beds were loaded intermittently with the dosing frequencies of 4 times or 8 times per day. The percolates were impounded within the substrate for two alternative regimes, which were 1-day and 3-day. Overall, this system obtained a desirable efficiency in removing TSS, NH_4^+ and COD. However, the removal efficiency of NO_3^- was insignificant. In summary, the VFCW is a feasible treatment method to remove the solid content and organic matter in the raw septage. However, the removal of nitrogen especially NO_3^--N were relatively poor. The capability of the VFCW in treating raw septage with regards to the system configuration and operational strategies has been reviewed and described comprehensively. The treatment performance of these systems is summarized in Table 2.1.

Table 2.1: The optimal solids loading rate (SLR) and removal efficiency of the existing system

Case Study	Optimal SLR (kg TS m^{-2} yr^{-1})	COD	BOD	TKN	TS	NH_4^+-N	NO_3^--N
Lienard and Payrastre (1996) – First Stage	70	>78%	58%	>71%	>84%	>59%	Increased
Lienard and Payrastre (1996) – Second Stage	-	60%	-	-	60%	85%	45%
Koottatep et al. (2001)	250	>80 %	-	>80 %	>80 %	>80 %	Increased
Paing and Voisin (2005)	46	98.5%	98.5%	94%	99%	-	Increased
Troesch, Lienard, et al. (2009)	50	>89%	-	>82%	>92%	<50%	Increased
Kengne et al. (2009)	<200	95%	-	90%	86%	77%	Increased
Jong and Tang (2013)- First Stage	250	96%	-	-	97%	87%	Increased
Jong and Tang (2013) - Second Stage	-	96%	-	-	98%	99%	Increased

2.2.1. Summary of the VFCW-based septage treatment systems

To date, current studies have given useful insights in terms of the design configurations and operation strategies of the VFCW-based septage treatment systems towards the variation in environmental condition. The analysis of such septage treatment system is still at a "black-box" level, where the treatment performance is evaluated based on the difference between the influent and effluent quality. There is no comprehensive study with regards to its hydraulic behaviour and the associated treatment efficiency, and thus the optimization of the system mainly focused on the substrate design and the selection of SLR and resting period.

The lack of knowledge in the relationship between hydraulic performance and treatment process hinders a systematic design standard guideline to be established for VFCW-based septage system. Currently, the scale and capacity of the treatment are decided using rules-of-thumb and its operational strategies are determined empirically based on the experiments. A practical design tool such as mathematical modelling is then proposed to facilitate the fundamental understandings of nitrogen removal in the VFCWs designed for septage treatment.

A mechanistic model is appropriate since it is a more comprehensive approach to understand the complex interactive processes under a variety of circumstances. It has become a state-of-art in the modelling and design of CW systems. Up until now, some integrated models such as HYDRUS-CW2D (Langergraber and Šimůnek 2005) has been developed to simulate the hydraulic flow and treatment kinetics of the VFCW. However, these existing models are limited to the application of municipal wastewater treatment. There is no specific model for septage-based treatment to the author's knowledge. In order to achieve this, an analysis of the impact factors, including system-related and operation-related features towards the efficiency and sustainability of the VFCWsystem, is essential in the conceptualization of the numerical model.

The high solids load in the septage treatment highlights the importance of the design of substrate to ensure a robust treatment capacity in the VFCW. The existing evidence has shown that a thicker substrate prolonged the hydraulic retention time (HRT), subsequently improving the overall treatment efficiency of the VFCW (Torrens et al. 2009). The substrate generally was constructed by coarse gravel to avoid substrate clogging. In some system, the wetland bed was topped with sand to prolong the HRT

of the influent (Troesch, A. Liénard, et al. 2009; Jong and Tang 2014). The presence of wetland vegetation enhances the dewatering efficiency, oxygen restoration, filtration capability, as well as protecting the substrate from erosion (Lee and Scholz 2007; Gagnon et al. 2012). The other benefit of vegetation is to prevent the substrate clogging by creating a bypass in the sludge deposit via the mechanical effect of the reed stalk (Lee and Scholz 2007; Molle et al. 2006).

The applied loading rate and feeding frequency are of great importance to the treatment capability and durability of the VFCWs. It is observed that almost all the existing VFCW-based septage treatment systems were managed with regards to solid loading rate (SLR) instead of hydraulic loading rate (HLR). This approach is to control the high solids content in septage and its fluctuating characteristics between each batch of the collection. Currently, the optimum SLR for VFCW-based septage treatment system has not been extensively determined in the literature. The SLRs ranged from 30 to 70 TSS m^{-2} $year^{-1}$ in the temperate region (Troesch, Lienard, et al. 2009; Vincent et al. 2011) and could be up to 250 kg TS m^{-2} $year^{-1}$ in the tropical region (Koottatep et al. 2004).

The VFCW is operated in batch, where the system is rested for a certain period after it has been experienced a treatment cycle. This feeding-resting regime is important to the oxygen renewal, microbial growth, and mineralization of sludge deposit. From the perspective of hydraulic load, a higher frequency of batch loading is beneficial to control the retention time of influent, but the short resting period limited the re-aeration efficiency of the system as well as drying of the accumulated sludge deposit (Molle et al. 2006). In order to provide a complete nitrogen removal, the influent could be impounded in the system for a certain period of time instead of being freely discharged to stimulate denitrification at the saturated region of the substrate. Nevertheless, the longer impounding duration apparently limits the overall productivity of the system. As a result, some systems implemented a multi-stage treatment to carry out further microbial degradation of NO_3^--N at the subsequent stage of treatment.

2.3. Treatment of nitrogen in the VFCWs

In a wetland ecosystem, nitrogen is regarded as one of the essential nutrients for plant growth, but excessive amounts of nitrogen in the watercourses have become a principal concern because of its severe consequences including eutrophication, hypoxia, and

toxicity, which eventually causes losses of biodiversity and habitats (Baker 1998). Nitrogen is an indispensable component of life and presents in many forms among the soil community (Robertson and Groffman 2007). The nitrogen compound within municipal wastewater and septage exist in the forms such as organic nitrogen (Org-N) and ammoniacal nitrogen (NH_3-N and NH_4^+-N), while the portion of oxidized nitrogen such as nitrite-nitrogen (NO_2^--N) and nitrate nitrogen (NO_3^--N) are minor. It should be noted that the fraction of these nitrogenous constituents in septage is dominated by origin and level of pre-treatment (Faulwetter et al. 2009).

The treatment mechanisms in the VFCWs comprise an enormous number of processes that involve complex interactions between air, water, substrate and microorganisms (Kumar and Zhao 2011), which is a combination of physical, biological and chemical mechanisms. The physical mechanism, which mainly refers to the physical filtration, is important to the removal of particulate contaminants. The wetland bed is a deep porous medium that traps the solid particles in the influent at the top surface. This mechanism has been found to be the main contributor of excellent performance in removing total solids in the septage treatment (Liénard, Duchène and Gorini 1995). The solid particles filtered on the wetland surface forms a layer of sludge deposit, which potentially reduces the overall hydraulic performance of the system due to its low permeability.

Biochemical mechanisms remove organic and nitrogenous pollutants from influent through the carbon and nitrogen cycles with the presence of microorganisms in the system (Grady Jr et al. 2011). The VFCW is an attached growth bioreactor, where the microbial communities are provided with the porous medium as a surface media for growth. Generally, these microorganisms might be categorized into heterotrophs and autotrophs, where the former digests organic carbon to obtain energy and carbon while the latter demands carbon dioxide and inorganic matter to grow. The nitrogenous compounds are consumed in these microbial activities as complementary components in the cell synthesis, oxidation and electron transfer.

The overall nitrogen removal in VFCWs, in general, is still undesirable as the amount of NO_3^--N were revealed to be high in the effluent (Liénard, Duchène and Gorini 1995; Paing and Voisin 2005; Vymazal 2007; Kengne et al. 2009; Troesch, A. Liénard, et al. 2009). The noticeable nitrogen transformation processes found in the literature include

NH_3-N volatilization, ammonification, nitrification, denitrification, nitrogen fixation, plant and microbial uptake, anaerobic NH_4^+ oxidation, heterotrophic nitrification, sorption, desorption, etc. (United States Environmental Protection Agency 1999a; Vymazal 2007; Wallace and Austin 2008). Among the known nitrogen-cycling mechanisms, the sequential anoxic ammonification, aerobic nitrification and anoxic denitrification are recognized as the major nitrogen removal mechanism in CWs (Gersberg, Elkins and Goldman 1983; Bowmer 1987; Verhoeven and Meuleman 1999; Kuschk et al. 2003; Siracusa and La Rosa 2006; Vymazal 2007). Figure 2.3 illustrates a conventional nitrogen cycle within a CW system. The descriptions of these processes are summarized in the following section.

2.3.1. Ammonification

Ammonification occurs under both aerobic and anoxic conditions, and hence the removal of Org-N is always satisfactory in VFCWs (Vymazal 2010a). This biodegradation process releases the amino groups from organic compounds, subsequently converting into NH_4^+-N to the medium (Grady Jr et al. 2011). Ammonification is a rapid process compared to nitrification and the rate is higher in the aerobic environment (Kadlec and Wallace 2008). In most of the cases, the Org-N

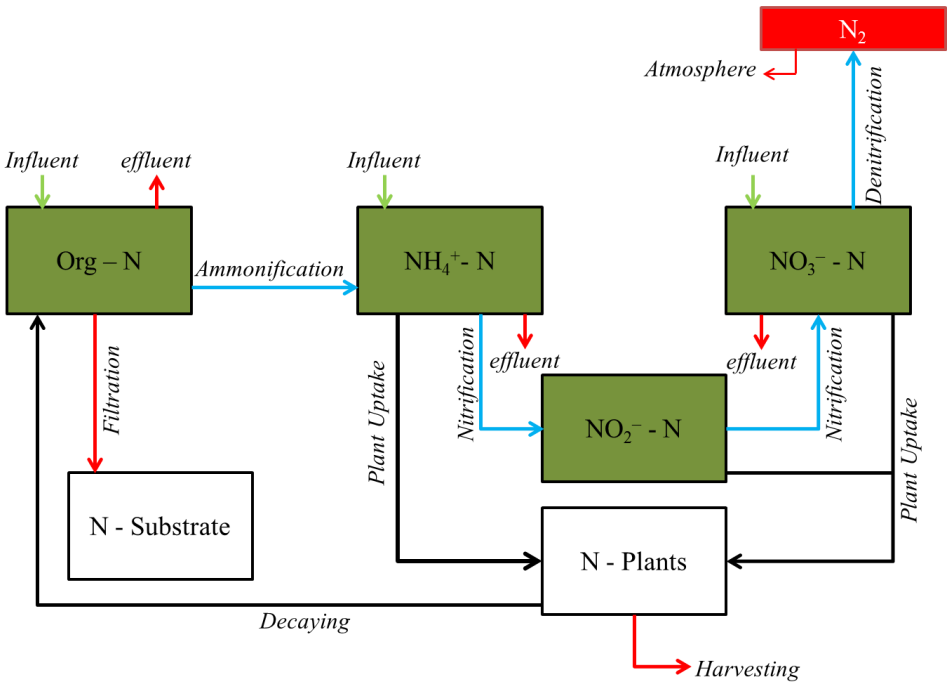

Figure 2.3: Conventional nitrogen cycle in CWs

is readily biodegradable. The temperature, pH, C/N ratio, oxidizing state and available nutrients are the main influencing factors of ammonification (Martin and Reddy 1997).

2.3.2. Nitrification and denitrification

The reduced form of nitrogen generally exhibits in free ammonia (NH_3-N) or ionized ammonium (NH_4^+-N). The portion of NH_3-N proportionally increases with pH, but NH_4^+-N is still the majority in the most cases (Gerardi 2003). The removal of can NH_4^+-N is simply achieved through an oxidation process, so-called nitrification. This process is believed to be one of the most important biological processes in the wetland system.

The biological nitrification occurs by the means of nitrifiers such as *Nitrosomonas* and *Nitrobacter* (Gersberg, Elkins and Goldman 1983) to oxidize NH_4^+-N to NO_3^--N as NO_2^--N as an intermediate product. Nitrification is typically recognized as a chemoautotrophic process, but recent studies have highlighted the participation of heterotrophic bacteria in this process (Grady Jr et al. 2011). Nitrification is favourable in VFCWs with intermittent loading due to its predominantly aerated condition. The common representation of overall nitrification is using two equations to describe this sequential biological process:

$$NH_4^+ + 1.5O_2 \rightarrow NO_2^- + H_2O + 2H^+ \tag{2.1}$$

$$NO_2^- + 0.5O_2 \rightarrow NO_3^- \tag{2.2}$$

where the first step is always assumed to be governed by the *Nitrosomonas* and the second step by *Nitrobacter*. The performance of this biological process is dependent on the level of aeration in the system. Furthermore, Zhao, Sun, and Allen (2004) indicated that the competition between the degradation of organic matter for DO also inhibit the performance of NH_4^+-N oxidation as the heterotrophs are characterized with a higher respiration rate, using more oxygen in the decomposition of organic matter. Therefore, significant nitrification is only observed after a substantial amount of organic matter has been removed.

In addition to the oxygen status, the alkalinity is a complementary inorganic carbon source in this process. By using the conventional half equation analysis, Grady Jr et al. (2011) showed that 8.64 mg of HCO_3^- alkalinity are consumed when per mg of NH_4^+-

N is oxidized. Even though the amount of alkalinity might be sufficient for the nitrification, the rapid consumption will subsequently lead to a drop in the pH, where a depressed pH level eventually inhibits the nitrification process. Besides, the temperature and moisture content influences the rate of nitrification as well but is relatively minor compared to the effect of oxygen content and alkalinity (Vymazal 2007).

Denitrification is a heterotrophic process, where the heterotrophs decompose the organic compounds to obtain energy and carbon under anoxic conditions and NO_3^--N acts as the terminal electron acceptors while the DO is limited in the system (Vymazal 2007):

$$6CH_2O + 4NO_3^- \leftrightarrow 6CO_2 + 2N_2 + 6H_2O \qquad (2.3)$$

Dinitrogen gas is released as the final product of the reaction. The community of denitrifying bacteria consists of diverse organisms, while the chemo-heterotrophs is regarded as the majority in wastewater treatment (Vymazal 2007). In general, the lack of anoxic conditions in VFCW-based systems limits the occurrence of denitrification, subsequently reducing the efficiency of nitrogen removal (Platzer 1999; Liu, Dahad and Surampali 2005; Yalcuk and Ugurlu 2009).

The influencing factors to denitrification include temperature, pH, microbial community, available organic carbon source and moisture content (Lee, Fletcher and Sun 2009). Saeed and Sun (2011a) highlighted that the overall nitrogen removal via denitrification showed a dependency on the properties of the substrate, where the substrate constructed by organic material performed better in the nitrogen removal. It is due to the leaching of organic carbon that recharges the carbon ratio to enhance the denitrification rate. The different requirement in terms of the oxygen availability between nitrification and denitrification is the main challenge in achieving a high removal rate of nitrogen in specific CW system (Vymazal 2007).

2.3.3. Plant uptake and other mechanisms

Plant uptake plays a remarkable role in nitrogen removal (Brix 1997; Liu, Dahad and Surampali 2005; Mayo and Bigambo 2005). The plants uptake of NH_4^+-N and NO_3^--N as nutrients and subsequently convert into organic nitrogen for cell formation at different rates ranging from 2-88 gN m^{-2} yr^{-1} (Vymazal 2007). However, according to

Stottmeister et al. (2003), Langergraber (2005) and Vymazal (2007), it was indicated that the contribution of plant uptake towards overall nitrogen removal was insignificant in VFCW compared to the microbial processes. A complete nitrogen removal through plant uptake has to be accompanied with annual harvesting to avoid the return of organic nitrogen to the wetland due to the decomposition of plant material and litter.

The adsorption of ionized NH_4^+-N is prevailing while sufficient hydraulic retention time and suitable substrate media are provided, especially when the organic matter is a presence in the wetland bed (Fetter and Fetter Jr 1999). The detail of this mechanism is elaborated in section 4.2.1. The processes such as anaerobic NH_4^+-N oxidation, heterotrophic nitrification, and ANNAMOX have been found to be a potential nitrogen removal mechanism in CWs. However, the studies of this mechanisms are still limited (Lee, Fletcher and Sun 2009).

In summary, the rates of the biological nitrogen removal mechanisms depend on numerous environmental factors (climate), influent characteristic (concentration of nitrogenous constituents, carbon/ nitrogen ratio, pH), system-related factors (substrate profile, biomass storage, vegetation maturity) and operation-related factors (HLR, retention time, feeding regime), which increase the complexity of the modelling of nitrogen transformation and removal mechanisms in the VFCW-based septage treatment system (Lee, Fletcher and Sun 2009).

2.4. Current status of subsurface-flow CW modelling for nitrogen transformation and removal

The VFCW is a complex bioreactor that is sensitive to the surrounding environment, resulting in more difficulties in the prediction of its treatment performance compared to other types of wastewater treatment method such as trickling filter and activated sludge system (Kadlec and Wallace 2008). The fundamental simulation of the processes in VFCW can be achieved by means of a first-order kinetics model (Haberl et al. 2003; Langergraber 2008; Kumar and Zhao 2011), which is a series of analytical equations derived empirically from the relationship between the influent and effluent concentration of the particular contaminants. This method assumes that the hydraulic behaviour and all parameters remain constant throughout the operation, and thus it only consist of two components, which are first-order removal rate constants (k) and

background concentration (C^*) (Martin and Reddy 1997; Gerke, Baker and Xu 2001). Such an approach is used to predict the effluent concentration for design purposes (EPA 1999, 63; Kumar and Zhao 2011, 400). Nevertheless, the first-order kinetics model is considered at a "lumped" level due to the lack of process quantification, and thus it is incapable of providing a reliable result when the flow and parameters are varied during operation (Kadlec 2000). This drawback is significant in the modelling of VFCWs due to its variably-saturated flow. In addition, the hydraulic behaviour of the wetland bed is actually a function of time.

As a result, a mechanistic model is an adequate approach to describe the complex interactive processes within VFCWs (Langergraber 2011). In the early 21st century, the development of mechanistic modelling for subsurface-flow CWs was remarkable (Langergraber, Giraldi, et al. 2009). This approach successfully delivers a better prediction on the treatment performance, as the VFCW is always conceptualized as an accumulated system, which allows for time-varying conditions caused by the substrate, vegetation, and biomass capacity along the operating period.

As this type of model always incorporates a hydraulic module and associated reaction kinetics, it is capable of describing comprehensive interactions between influent and wetland ecosystems during treatment. In this review, several existing mechanistic models for subsurface-flow CWs are presented. The reviewed models must be capable of modelling the reactive transport of nitrogenous constituents, while the models which excluded the simulation of nitrogen processes such as Rajabzadeh, Legge, and Weber (2015) are not included.

2.4.1. Reactive transport models in saturated conditions

2.4.1.1. Wynn and Liehr (2001)

Wynn and Liehr (2001) introduced a mechanistic model that incorporated six interacted modules to simulate the treatment behaviour in an HFCW. The authors conceptualized the model by taking the CW as "a series of continuously stirred tank reactors (CSTRs)", and the model was programmed using a simulation software called STELLA II. This model aimed to reproduce the dynamics of carbonaceous and nitrogenous constituents by considering the microbial processes, associated water budget and oxygen status within the system.

The flow in the wetland bed was modelled using Darcy's equation, where the hydraulic gradient was determined by the bed slope. Precipitation and ET were taken into account in the hydraulic module. The vegetation and organic carbon in the wetland bed were included in the carbon cycle. In addition, six nitrogen compounds were considered, including dissolved Org-N, particulate Org-N, NH_4^+-N, NO_3^--N, immobilized nitrogen and nitrogen content in accumulated sludge.

In this model, the transformation mechanisms involved in the nitrogen cycle were ammonification, immobilization, nitrification, denitrification, sludge accumulation and plant uptake. The dissolved nitrogen was assumed to be absorbed by heterotrophic or autotrophic bacteria as complementary compounds in nitrification-denitrification and assimilated by the vegetation as a nutrient. Therefore, the reaction rates of nitrification and denitrification were governed by the microbial growth. The microbial transformations were correlated to the oxygen availability. The assimilation rate of nitrogen within vegetation was a function of plant growth and nutrient content (C/N ratio).

The microbial activities were divided into autotrophic and heterotrophic processes, where the previous represents the nitrification and the later indicates metabolism of organic carbon and denitrification. Monod dual-substrate limitation kinetics was utilized to estimate the microbial growth. The limited substrates of the Monod kinetics in autotrophic and heterotrophic dynamics were NH_4^+-N and total organic carbon (TOC), respectively. The microbial growth demand DO in the process, where its source was dependent on inherent oxygen and vegetation transport in the wetland bed. The temperature and pH were also included as the factors that influence the growth rate.

On the other hand, the particulate organic carbon and nitrogen were assumed to be accumulated on the wetland surface at a constant rate, which was modelled as the forming of sludge deposit layer. Then, the excessive dissolved constituent was discharged or retained in sludge deposit. This model considered that the particulate constituents were completely trapped within the wetland bed.

The simulated results were calibrated using a working HFCW. In general, this mechanistic model yielded satisfactory results towards the effluent concentrations of organic matter and nitrogenous constituents with regards to seasonal trends, which

validated that the interactions between sub-models were reasonably simulated. However, the model was unable to cope with the variation of individual parameters because of its complex network of transformation mechanisms. Furthermore, the simulated results were generally governed by the microbial development and the associated limited constituents. In order to establish a practical design tool for HFCWs, the authors suggested that further studies should be conducted to identify the effect of hydraulic behaviour on treatment performance and microbial growth, as well as the impact of NH_4^+-N adsorption, the adequacy of the simplified carbon cycle and the oxygen transfer module.

2.4.1.2. Liu, Dahad, and Surampali (2005)

Liu, Dahad, and Surampali (2005) applied a compartmental analysis to develop a sequential nitrogen transformation model for SSF CWs. The model was calibrated based on a set of performance data obtained at a full-scale HFCW system and was conceptualized as a series of CSTRs that exhibited a sequential nitrogen transformation network. Ordinary differential equations were utilized to determine the associated exchange rate of constituents between the compartments, where the solutions were obtained using the Levenberg-Marquardt nonlinear optimization method. The total mass in each compartment was then estimated as a result of mass conservation law, first-order rate constant and the rate of exchange.

In this model, Org-N and NH_4^+-N were assumed to be the major nitrogen form in the influent, while the influence of NO_2^--N and NO_3^--N were relatively minor. The mechanisms involved in the nitrogen cycle encompassed ammonification, nitrification, denitrification and plant uptake. The reaction rates of ammonification, nitrification and denitrification were implemented in terms of first-order kinetics, while plant uptake is described using zero-order approach.

The simulated results of the averaged effluent concentrations for Org-N, NH_4^+-N, and NO_3^--N were fair, but the model was undesirable in obtaining peak concentration. It was suggested that the model can be improved by implementing a more comprehensive series of CSTR. This study concluded that 1/3 of influent nitrogen was removed through sequential nitrification and denitrification, while 1/3 was assimilated by plants, and the remaining was discharged in the effluent.

2.4.1.3. Mayo and Bigambo (2005)

Mayo and Bigambo (2005) proposed a numerical model that covered the activities of both suspended and attached microbes to predict the nitrogen removal in HFCWs. The model was developed using STELLA II while a field-scale HFCW were used to calibrate the model and validate the results. The most significant achievement of this model was incorporating the activities of both suspended biomass in the water and biofilm attached to the substrate and plant roots. The nitrogenous compounds involved were particulate Org-N, dissolved ON, NH_4^+-N and NO_3^--N, and each was modelled using a mass balance approach to predict the substance entered in the system and removed from the system.

Monod kinetics equations were implemented to describe the growth of suspended and attached microbes. Then, these microbial behaviours were further used to compute the reaction rate in terms of first order kinetics. In summary, the input required by the nitrogen dynamics were temperature, substrate characteristics, oxygen status, loading rate, pH, roots surface area, influent characteristics and biofilm conditions. According to the simulated results, it was concluded that the principle nitrogen removal mechanisms were denitrification (29.9%), plant uptake (10.2%) and sedimentation (8.2%) in an HFCW. In a further study, Bigambo and Mayo (2005) elaborated the role of biofilm in the nitrogen transformation with HFCWs. The investigation found that the biofilm was vital to the efficiency of nitrification and denitrification, but it impacted less upon the removal of Org-N.

2.4.1.4. Wang et al. (2009)

Wang et al. (2009) applied a similar approach in Mayo and Bigambo (2005) to numerically investigate the nitrogen cycle in a VFCWs. The model was developed using the simulation program MAPLE 5.1 with a four-dimensional numerical approach. Four nitrogenous constituents including Org-N, NH_4^+-N, NO_3^--N, and assimilated nitrogen within vegetation were modelled with regards to the retention time within the substrate. Five transformation mechanisms were taken into account, which was ammonification, nitrification, denitrification, plant uptake, and ammonia volatilization. The Monod kinetics equations were utilized to simulate the biological processes, where the temperature and pH were considered as the main influencing factors in microbial development. The model was then validated by comparing to an

existing system that had operated for three years. The simulated results of overall nitrogen removal were fair compared to the measured data.

2.4.1.5. Rousseau (2005)

Rousseau (2005) proposed a mechanistic model that incorporated the carbon and nitrogen cycles, microbial and vegetative-mediated processes for HFCWs. The author aimed to implement the existing conventional wastewater treatment model Activated Sludge Model 1 (ASM1) (Henze et al. 2000) to develop a multi-component reactive transport model. In order to give an insight into the long-term performance of the system, the influence of clogging processes and associated climatic data were assessed in this model too.

This mechanistic model simulated the flow condition using the CSTR approach. The Darcy's equation was used to predict the steady-state flow in the porous substrate. The microbial-mediated processes were conceptualized based on the ASM1 with the addition of several mechanisms obtained from the later version of ASM (Henze et al. 2000). ASM is a simple numerical model that describes the biological conversion within a single suspended microbes-based treatment reactor carrying out respiratory degradation, nitrification, and denitrification. In this model, the behaviour of microbial processes was governed by the oxygen distribution along the substrate. The anaerobic removal mechanisms apparently dominated the overall treatment due to the limited oxygen transfer in HFCWs.

As for physical mechanisms, it was assumed that the HFCWs most likely filtered all the suspended solids at the inlet zone, whereby the discharge of solids might occur at a high loading rate. On the other hand, the aging biofilm was postulated to be retained within the porous medium, simultaneously undergoing metabolism until it was discharged by a peak flow. The growth and decay of vegetation were determined by means of nutrient availability. Lastly, the oxygen consumption and restoration were predicted based on the interactive processes mentioned above. In summary, this model consisted of twenty-six state variables and twenty-six mass balances due to the complexity of the conceptual mechanisms network.

The simulated results of this mechanistic model were validated by a pilot-scale HFCW (55 m^2) and an experimental system (0.55 m^2). The drawbacks had been found on the uncertainties of wastewater characteristics and insufficient experimental

measurements of the loading dynamic, as well as the non-calibrated parameter used in the simulation; however, this mechanistic model yielded fair results in terms of treatment performance and effluent quality.

The author indicated that this model was not yet a practical design tool at the time of writing, mainly attributed to its excessive input of parameters. However, with this model, a guideline was established on the complex interactive mechanisms within HFCWs. Emphasis was also placed on the consideration of adequate influent characteristics. Further investigation is required for the physical oxygen transport mechanisms and the subsequent effect caused by the particulate substances retained in the porous medium.

2.4.1.6. Ojeda et al. (2008)

Ojeda et al. (2008) developed a two-dimensional numerical model based on the code RetrasoCodeBright to reproduce the biochemical degradation processes involved in the HFCW system that received urban wastewater. The main aim of the model was to estimate the relative contribution of different microbial mechanisms in removing organic matter, as well as the nitrogen transformation processes including nitrification and denitrification. The authors utilized this model to investigate the impact of organic loading rate on both the overall removal efficiency and the microbial processes.

RetrasoCodeBright is composed of the reactive transport model Retraso (Saaltink et al. 2004) and multiphase flow and heat code CodeBright (Olivella et al. 1996), which is capable of describing the movement of dissolved and gaseous constituents under non-isothermal saturated or unsaturated condition in the finite element method (Saaltink et al. 2003). This reactive transport model consists of fourteen reaction processes incorporating eight equilibrium laws and six kinetics equations. The reaction kinetics used in this model was a model established by Van Cappellen and Gaillard (1996), which involved a range of aerobic, anoxic and anaerobic processes that took place simultaneously. The noteworthy microbial-mediated processes included are hydrolysis, aerobic respiration, nitrification, denitrification, sulphate reduction and methanogenesis. These processes were implemented using first-order kinetics with multiplicative Monod-type expressions.

A set of experimental results were obtained from two HFCWs with a total surface area of 55 m^2 to calibrate and validate the efficiency of the model. According to the

simulated results, anaerobic reactions dominated the organics removal in HFCWs, and variation in the HLR affected the removal efficiency significantly. This model fairly predicted the concentration of NH_4^+-N and NO_3^--N in the effluent and compared favourably with the experimental measurements. Due to the lack of aerobic condition in the system, the occurrence of nitrification was limited, resulting in a relatively high concentration of NH_4^+-N observed in both measured and simulated results.

2.4.1.7. Saeed and Sun (2011b)

Saeed and Sun (2011b) compared the availability of three kinetics models, including first order kinetics, single Monod and multiple Monod kinetics in predicting the biodegradation of nitrogen and the removal of organic matter in a subsurface VFCW and HFCW. This study proposed a simplified design tool by linking the effluent water quality to the influent condition, which effectively reduced the number of empirical parameters required in the mechanistic model.

The hydraulic behaviour of the VF system was described using a CSTR flow approach while the HF system was based on ideal plug flow pattern. The water quality parameters involved in the kinetics modelling are NH_4^+-N, NO_3^--N, BOD_5, and COD. Accordingly, nitrification and denitrification are the processes in-charge of NH_4-N and NO_3-N removal, respectively. Both BOD_5 and COD removal are achieved by heterotrophic degradation. This review focuses on the simulation of the VF system only.

The kinetics dynamics in CSTR flow pattern is estimated by hydraulic retention time, which is calculated based on inlet discharge, and dimension and porosity of wetland bed. In terms of first order kinetics, the expression of dynamics can be correlated to influent and effluent concentration and loading rate. Then, the single Monod kinetics includes a maximum removal rate and limiting substrate in the equation. This approach can be enhanced to comprise multiple limiting substrates.

In this model, the limiting substrate of Monod kinetics was NH_4-N and dissolved oxygen for nitrification, while denitrification was restricted by NO_3-N and COD. In addition to this, the denitrification only occurs under anoxic conditions, and thus an inhibitory oxygen constant is implemented in the kinetics expression. The heterotrophic degradation of BOD and COD take the concentration of organic matter and dissolved oxygen as a substrate in the process.

The simulated results were compared to the measured data obtained from eight laboratory-scale VFCW columns. The multiple Monod kinetics model with CSTR flow pattern demonstrated the best match with measured data for denitrification and heterotrophic degradation of organic matter, while the single Monod kinetics model predicted the most accurate effluent concentration of NH_4-N. In summary, the Monod kinetics with CSTR model is a practical and adequate method for simulating the performance of subsurface VFCW. Nevertheless, such an approach is limited by the assumption of steady-state hydraulic conditions, as well as the removal of nitrogen components which are completely attributed to biological degradation. The effect of vegetation and the influence of clogging were omitted in this study.

2.4.1.8. BIO_PORE (Samsó and Garcia 2013)

Samsó and Garcia (2013) established a two-dimensional mechanistic model, BIO_PORE, which merged a variety of physical and biological mechanisms to predict the long-term performance of an HFCW. This model was developed using the finite element simulation software COMSOL Multiphysics™ by incorporating a general bio-kinetics model, Constructed Wetland Model number 1 (CWM1) (Langergraber, Rousseau, et al. 2009a). This review focuses on the innovative biofilm sub-model, which gave an insight into the limited biomass growth and the associated clogging phenomenon in HFCW. The bio-kinetics simulated by CWM1 will be introduced in the following section.

BIO_PORE applied Darcy's equation to describe the 2D longitudinal saturated flow in the wetland bed. The microbial activity of dissolved components is constrained in the aqueous phase, which utilized the advection-dispersion equation (ADE) to model the solute transport through the wetland bed. A first-order attachment-detachment process was adjoined to the microorganism to describe the mechanism of biofilm. The oxygen distribution and nutrient uptake via plant were considered in this model.

BIO_PORE adapted a limitation of microbial growth in terms of substrate and space availability in order to minimize the overestimation of treatment efficiency. Primarily, the microbial growth is limited by the available substrate in the influent, and the space constraint is mainly attributed to the reduction of pore volume within the wetland bed due to the accumulated inert solids. The hydraulic performance was independent of

the reduction of porosity due to the accumulation of particulate constituents in the porous medium.

A pilot-scale HFCW with the length of 10.30 m and width of 5.30 m was used to calibrate and validate the BIO_PORE model. The inlet zone was located at the first 0.30 m length of the bed, which also acted as the mixing zone in this model. The depth of the bed at the inlet was about 0.60 m and at the outlet was 0.70 m. The results showed that BIO_PORE successfully estimated the hydraulic behaviour of the pilot system and gave fairly accurate predictions on COD and NH_4-N concentrations in the effluent. Water temperature was found to be an important parameter to improve the accuracy of the simulation, but the effect of oxygen transport and nutrient uptake via vegetation in BIO_PORE were insignificant compared to the measured results. In addition to this, the influence of microbial growth and associated accumulation of inert particulate constituents were further investigated in a long-term scenario, subsequently leading to the introduction of "the Cartridge Theory" that described the interaction between microorganisms and accumulated particulate constituents to illustrate the phenomenon of progressive clogging throughout operational duration of a HFCW (Samsó and García 2014).

2.4.2. Reactive transport models in variably-saturated conditions

In contrast to the continuous feeding mode in HFCWs, the intermittent loading regime in VFCWs causes pores in the substrate to be partially filled during infiltration, resulting in a "continuously varying saturation level" along the wetland bed (Giraldi and Iannelli 2009). Simulation methods such as the CSTR approach, and the flow models using Darcy's equation might be inappropriate for modelling treatment mechanisms of VFCWs with such a loading regime. As a result, a transient variable-saturated flow module is required for the development of mechanistic models (Langergraber and Šimůnek 2005; Giraldi, de Michieli Vitturi and Iannelli 2010). The development of the variably-saturated numerical flow model is complex since it is constituted by time-varying parameters and is often governed by gravitation and capillary action. Due to the complexity and uncertainty of the variably-saturated flow, such simulation is highly dynamic and always considered as a "black-box" (Langergraber, Giraldi, et al. 2009; Morvannou et al. 2013b). In this section, several mechanistic models developed for nitrogen dynamics under variably-saturated

conditions are introduced, either simulating the flow statistically or numerically. The HYDRUS-CW2D (Langergraber and Šimůnek 2005) and FITOVERT (Giraldi, de Michieli Vitturi and Iannelli 2010) are considered as the landmarks in the field of mechanistic modelling of VFCWs, and thus these models are reviewed in detail in this section.

2.4.2.1. HYDRUS-CW2D (Langergraber and Šimůnek 2005)

HYDRUS-CW2D (Langergraber and Šimůnek 2005) is a multi-component reactive transport model for a VFCW. In this model, the hydraulic behaviour is quantitatively described using a variably-saturated water flow and solute transport software, HYDRUS-2D (Šejna and Šimůnek 2007). HYDRUS-2D simulates the two-dimensional, variably-saturated flow using Richards equation (Richards 1931) with the van Genuchten-Mualem soil parameters (Mualem 1976; van Genuchten 1980). The effect of transpiration was considered as a sink term in the simulation. Richards equation (Richards 1931) is a common equation to reproduce the variably-saturated flow, which is presented as:

$$\frac{\partial \theta}{\partial t} = \frac{\partial}{\partial z}\left[K(\theta)\frac{\partial h}{\partial z}\right] + \frac{\partial K(\theta)}{\partial z} - S \tag{2.4}$$

where θ denotes the volumetric water content [$L^3 L^{-3}$], h indicates the hydraulic head [L], t denotes the time [T], z represents the vertical coordinate (positive upwards) [L], K is the unsaturated hydraulic conductivity [$L\ T^{-1}$], and S represents the source/sink term. The source/sink term is used to represent the additional water due to precipitation or water loss via ET.

The simulation of hydraulic behaviour depends on the hydraulic properties of the porous medium, which is always represented as unsaturated hydraulic conductivity K. The determination of K is always challenging, where a set of empirical parameters that are hard to obtain is required (Maier et al. 2009). Direct field measurement of K is time-consuming and costly, and thus an indirect estimation is always adapted to theoretically compute K from a soil-water characteristic curve (SWCC). The SWCC is a non-linear function describing the relationship between volumetric water content and the pressure potential. This study implements the analytical model proposed by van Genuchten (1980), which predict the unsaturated hydraulic conductivity by

coupling the concept of empirical pore-size distribution simulation established by Mualem (1976):

$$\theta = \theta_r + \frac{(\theta_s - \theta_r)}{[1 + (\alpha|\varphi|)^n]^m} \tag{2.5}$$

$$K = K_s(\frac{\theta - \theta_r}{\theta_s - \theta_r})^l \left[1 - \left(1 - \left(\frac{\theta - \theta_r}{\theta_s - \theta_r}\right)^{\frac{1}{m}}\right)^m\right]^2 \tag{2.6}$$

where θ_r is the residual water content [L^3L^{-3}], θ_s is the saturated water content [L^3L^{-3}], α [L^{-1}], n [-], and m (=1-1/n) [-] are the empirical van Genuchten's shape parameters of the SWCC, K_s is the saturated hydraulic conductivity [LT^{-1}], and l is Mualem's pore connectivity parameter (=0.50) [-]. This van Genuchten – Mualem (VGM) model has been widely applied in simulating the variably-saturated flow processes in VFCW (Langergraber and Šimůnek 2005; Wanko et al. 2006; Maier et al. 2009; Giraldi, de Michieli Vitturi and Iannelli 2010).

In HYDRUS-2D, a preferential flow theorem has been used, which considered the mobile-immobile liquid phase with potential water exchange between the phases (Langergraber 2003). Then, the solute transport is theoretically described by using the advection-dispersion concept in the liquid phase, gaseous phase and a transition phase between solid and liquid phases. HYDRUS-2D can be used under a variety of boundary condition including surface ponding and reduction of peak flow.

In HYDRUS-2D, the macroscopic reactive transport of component (subscript i) was simulated using the ADE with the consideration of sorption and decay, which governs the solute movements taking place within the solid, liquid and gaseous phases:

$$\frac{\partial \theta c_i}{\partial t} + \frac{\partial \rho s_i}{\partial t} = \nabla(\theta D_i \nabla c_i) - \nabla(q \nabla c_i) + Sc_{s,i} + r_i \tag{2.7}$$

where i is the number of components (=1… N), c_i is the concentration in the aqueous phase [ML^{-3}], s_i is the concentration in the solid phase [$M\ M^{-1}$], θ is the volumetric water content [$L^3\ L^{-3}$], ρ is the soil bulk density [$M\ L^{-3}$], D_i is the effective dispersion tensor [$L^2\ T^{-1}$], q is the volumetric flux density [$L^3\ L^{-2}\ T^{-1}$], s is the source-sink term

[$L^3 L^{-3} T^{-1}$], $c_{s,i}$ is the concentration of the source-sink [$M L^{-3}$], and r_i is the reaction term [$M L^{-3} T^{-1}$].

The advection describes the solute movement due to the fluid flow, while dispersion indicates the displacement of the dissolved substances spread out from the expected flow path in a porous medium (Kresic 2006). In equation 2.10, the advection is represented by the second term in RHS, where the transport is proportional to the flux intensity. A dispersion tensor is used to reproduce the degree of dispersion, which is a combined coefficient of mechanical dispersion and diffusion. The source-sink term reproduces the adsorption and desorption of dissolved substances between the liquid and solid phases. Lastly, the reaction term is the decay or reproduction along the transport process. This type of ADE model is widely applied in modelling the treatment performance of VFCWs and similar systems (Wanko et al. 2006; Giraldi, de Michieli Vitturi and Iannelli 2010), including the modelling of oxygen distribution in the gaseous phase.

HYDRUS-CW2D consists of twelve components, including dissolved oxygen, NH_4^+, NO_2^-, NO_3^-, N_2, inorganic phosphorus, organic matter (subdivided into readily-biodegradable, slowly biodegradable and inert organic matter), heterotrophic bacteria and two species of autotrophic bacteria. It should be noted that organic nitrogen and organic phosphorus are included under organic matter. Simultaneously, nine processes are considered, which consist of hydrolysis, mineralization of organic matter, nitrification (two-stage process), denitrification and lysis of microorganisms. The heterotrophic bacteria were set to be responsible for hydrolysis, mineralization, and denitrification, whereas the autotrophic bacteria carried out the nitrification.

The population of microorganisms was postulated to be uniformly distributed along the bed while the physical effect of biofilm was omitted. The sorption-desorption process was considered to describe the growth of biofilm that attaches on the porous medium. The Activated Sludge Model (ASM) (Henze et al. 2000) was applied as the basic concept of the numerical computation of microbial growth and transformation by means of stoichiometry matrix. The transformation and degradation processes were expressed using the first-order Monod-type equation and the rate constant was dependent on temperature. The simulation of nutrient uptake by plants has been found

to be effective under a specific condition. (Langergraber 2005). On the other hand, oxygen release via roots was encompassed as a re-aeration process in CW2D.

Comparisons of the simulated water flows with the experimental measurements (flow rate measurements and tracer tests) have validated the reliability of CW2D in estimating the effluent volume (Langergraber and Šimůnek 2005), as well as the effect of temperature (Langergraber 2007) and vegetation (Langergraber and Šimůnek 2012) to the efficiency of simulation. The model has been successfully applied to one-stage and two-stage VFCW treating domestic wastewater (Langergraber and Šimůnek 2005; Morvannou et al. 2014), a two-stage, pilot-scale hybrid system treating domestic wastewater (HF and VFCW) (Toscano et al. 2009) and a system designed for combined sewer overflow (CSO) treatment (Dittmer, Meyer and Langergraber 2005). Langergraber and Šimůnek (2005) suggested several improvements needed for CW2D including the investigation of the hydraulic performance in field-scale CWs, estimation of substrate clogging and the optimization of the experimental methods to obtain parameters used in the model.

In order to elaborate the capability of HYDRUS-CW2D, an example of simulating nitrogen removal is introduced. Morvannou et al. (2014) modelled the nitrogen removal in a VFCW treating domestic wastewater using the HYDRUS-CW2D. The characterization of the hydraulic properties of the system is described in Morvannou et al. (2013a), where the direct laboratory methods and the inverse modelling from in situ measurements were used. The results showed that the direct laboratory measurements failed to reproduce the water content obtained from the laboratory experiments, while the inverse modelling showed a better reliability in the simulation.

The inherent concentration and the maximum growth rate of autotrophic biomass are determined by a solid respirometric technique (Morvannou et al. 2011). The calibrated parameters reasonably simulated the residual COD, NH_4^+-N, and NO_3^-- N in the effluent, as well as the DO and biomass in the wetland bed. The oxygen re-aeration rate and the adsorption coefficient of is the most sensitive parameters in optimizing the simulated results. The adsorption of NH_4^+-N delivered a significant contribution to the overall nitrogen removal, and the nitrification occurred during the resting period caused a higher NO_3^--N concentration in the early effluent of the subsequent loading. The study also highlighted that further research should be conducted to include the

influence of sludge layer in the hydraulic simulation. In addition, the determination of oxygen transfer and the application of the non-equilibrium model in the hydraulic simulation was required to be investigated.

2.4.2.2. CWM1 (Langergraber, Rousseau, et al. 2009a)

CWM1 (Langergraber, Rousseau, et al. 2009a) was introduced as an advanced version of CW2D. The motivation for proposing this bio-kinetics model was to obtain an insight into the biochemical transformation and removal mechanisms of organic matter and nitrogenous compounds in subsurface-flow CWs with a minimum number of processes. Compared to CW2D, anaerobic microbial processes such as fermentation, methanogenesis, and sulphate reduction were taken into account in CWM1. Therefore, it is also an appropriate tool to model an HFCW system (Langergraber and Šimůnek 2012). In addition, the reactive transport in gaseous phases was excluded in this model, as well as the consideration of phosphorus constituents due to its minor influence to the overall simulation. CWM1 encompassed sixteen components and seventeen processes. Eight dissolved components and eight particulate components were considered and are summarized as follows.

- Soluble components: (a) dissolved oxygen, (b) fermentable, readily biodegradable soluble COD, (c) fermentation products as acetate, (d) inert soluble COD, (e) NH_4^+-N/ NH_3-N, (f) NO_2^--N / NO_3^--N, (g) sulphate sulphur, (h) dihydrogensulphide sulphur.
- Particulate components : (a) slowly biodegradable particulate COD, (b) inert particulate COD, (c) heterotrophic bacteria, (d) autotrophic nitrifying bacteria, (e) fermenting bacteria, (f) Acetotrophic methanogenic bacteria, (g) Acetotrophic sulphate reducing bacteria, (h) sulphide oxidizing bacteria.

The processes involved in this model are hydrolysis, the aerobic growth of microorganisms, the anoxic growth of microorganisms, and lysis of microorganisms. The reaction kinetics was described as a stoichiometry matrix, which was based on the ASM approach mentioned previously. The author indicated that the consideration of variably-saturated flow in the porous wetland bed, effect of vegetation, transport of particulate constituents and substrate clogging, physical re-aeration and adsorption-desorption process were important to develop a reliable mechanistic model for subsurface-flow constructed wetlands. CWM1 has been successfully applied with

various hydraulic and reactive transport simulation software including HYDRUS-2D (Langergraber and Šimůnek 2012), RetrasoCodeBright (Llorens, Saaltink and García 2011) and AQUASIM (Mburu et al. 2012) to simulate the treatment behaviour of different CW systems.

2.4.2.3. FITOVERT (Giraldi, de Michieli Vitturi and Iannelli 2010)

Giraldi, de Michieli Vitturi, and Iannelli (2010) developed a mono-dimensional dynamic multi-component reactive transport model FITOVERT for VFCW using the simulation software MATLAB®. In summary, this model comprehensively reproduced the variably-saturated flow in a multi-layered wetland bed that took the ET, the biochemical transformation and removal of organic matter and nitrogen, the transport of solute and particulate components, as well as the oxygen recharging into account. Moreover, the most noteworthy achievement of FITOVERT was its capability to estimate the clogging problem from the accumulation of particulate compounds and biofilm growth above the wetland bed and within the upper layer of the wetland bed.

FITOVERT subdivided the vertical-flow wetland bed into a self-decided number of homogeneous horizontal layers. Each layer can be input with different hydraulic characteristics and initial conditions. Then, the flux was assumed to be “time-varying hydraulic and organic loads” applied on the surface of wetland bed, and the boundary condition might be altered automatically due to the surface ponding that occurs when the applied load exceeds the infiltration capacity of the top layer of wetland bed. On the other hand, the bottom of the wetland bed was modelled as a “valve”, where the percolate can be either assumed to be discharged freely or impounded within the wetland bed. The water flow was simulated according to Richards equation, which was solved by using a general mass-conservative numerical solution in the form of modified Picard iterative method (Huang, Mohanty and van Genuchten 1996). The van Genuchten – Mualem theory was applied to determine the unsaturated hydraulic characteristics. The water balance considered the water loss via evaporation and plant uptake individually, which were implemented in separated approaches but not a combination of potential ET.

In FITOVERT, the biochemical kinetics was directly based on the Activated Sludge Model No. 1 (ASM1) (Henze et al. 2000). This biochemical kinetics module

considered seven dissolved components and six particulate components. The microbial-mediated processes consisted of eight first-order Monod-type equations, which was presented using a stoichiometry matrix with proper mass balance parameters. In VFCW, the development of the microbial community generally happens by attachment onto the surface of porous medium and plant's rhizosphere, which is different from the assumption in ASM1 in which microorganisms were modelled as suspended biomass within the system. In addition to this, FITOVERT involved "kinetics of diffusion" to describe the reaction between dissolved components and microorganism. Neither the nutrient nor metal uptake by the vegetation was considered, as well as the phenomenon of adsorption of phosphorus.

The solute transport in the liquid phase was simulated with regards to the ADE proposed by Bresler (1973) and the transport of particulate components was based on the concept developed by Iwasaki, Slade, and Stanley (1937). The implementation of the transport of dissolved oxygen was the same as solute transport for the microbial processes. Besides, the diffusive exchange of oxygen in the gaseous phase was included in this model. Fick's law was utilized to compute the conversion between dissolved oxygen and gaseous oxygen.

As mentioned previously, FITOVERT gave an insight into the accumulation of microorganisms and particulate components within the porous medium, subsequently providing a useful prediction on the occurrence of substrate clogging. The reduction of pore size was estimated through the volumetric specific deposit, and this parameter was used in the Kozeny-Carman equation (Boller and Kavanaugh 1995) to describe the reduction of hydraulic conductivity in the simulation, which was presented as:

$$K = \frac{K_0}{\left[\left(1 + p\frac{D_{vtot}}{\varepsilon_0}\right)^x \left(1 - \frac{D_{vtot}}{\varepsilon_o}\right)^y\right]} \tag{2.8}$$

where K_0 is the hydraulic conductivity for the clean filter [L T^{-1}], ε_0 is the porosity of the clean filter [L^3 L^{-3}], *p*, *x*, and *y* are the empirical parameters [-].

A good agreement of hydraulic simulation of FITOVERT and measured data was obtained (Giraldi and Iannelli 2009). This model incorporated the ET and clogging processes, which ensures a more accurate water balance from the influence of vegetation and porosity reduction due to the accumulation of particulate constituents

and biomass. Nevertheless, the overall performance of reactive transport simulation had not been calibrated and validated.

2.4.2.4. McGechan, Moir, Sym, et al. (2005)

McGechan, Moir, Sym, et al. (2005) simulated the transformation of both organic and inorganic nitrogen in subsurface CWs based on the concept of reed beds. The model was applicable to both HFCWs and VFCWs, and their simulation was distinguished based on the hydrology and aeration status. In VFCWs, the water flow was simulated as the time needed by the influent to percolate through the wetland bed and a flooded layer at the wetland surface was taken into account.

The nitrogen cycle in this model was modified from a soil nitrogen transformation model, where Org-N, NH_4^+-N, NO_2^--N and NO_3^--N were taken into account. Nitrification and denitrification were expressed as two-stage processes, where the NO_2^--N acted as an intermittent compartment. Microbial-mediated processes were presented using first-order Monod kinetics equations. In this model, the relative contribution of different processes was dominated by the aeration status (aerobic, anaerobic and facultative).

The model has been calibrated and verified with a hybrid CW system. This model reproduced reliable results by using calibrated rate constants obtained from the experimental system. The model was further upgraded by implementing a simplified oxygen transport module to reproduce the influence of oxygen recharge via convection and diffusion, as well as the oxygen release via vegetation to the biofilm attached to roots and rhizomes (McGechan, Moir, Castle, et al. 2005). The rate of diffusion was estimated using a diffusion coefficient D for oxygen in water (=1.76×10^{-4} m^2 d^{-1} at 20°C), whereas the oxygen transport through convection was estimated using the O'Connor and Dobbins (1958)'s concept, which was presented as:

$$K = \sqrt{\frac{DU}{h}} \tag{2.9}$$

where U is the water speed [L T^{-1}] and h is the water depth [L]. This attempt improved the accuracy of the model in simulating the aerobic processes such as nitrification due to the presence of additional oxygen availability.

2.4.2.5. Ouyang, Luo, and Cui (2011)

Ouyang, Luo, and Cui (2011) developed a nitrogen transformation model for VFCWs that included the consideration of variably-saturated flow, substrate clogging, surface ponding, ET and plant uptake using STELLA. This model subdivided the VFCW into multiple horizontal homogeneous layers. The detail of the hydraulic modules used in this model is described in Ouyang et al. (2010), where Darcy's law was used to describe the water flow with regards to the hydraulic head difference in the wetland bed. The flow rate under unsaturated conditions was determined by means of the volumetric water content within the individual layer. The substrate clogging was estimated with regards to the fraction of effluent volume and influent volume, which was presented as:

$$F_{clogging} = \frac{l}{l_o} = e^{-7\times10^{-5*}t} \tag{2.10}$$

where l is the average rate of wastewater discharged [L^3 T^{-1}] and l_o is the average rate of wastewater recharged [L^3 T^{-1}]. The parameters such as drainage rate, substrate clogging factor, and ET rate coefficient need to be calibrated from the extensive field data, subsequently restricting its application for design purposes.

The nitrogen compounds considered in this model comprised particulate Org-N, dissolved Org-N and NH_4^+-N and NO_3^--N. The mechanisms included in the nitrogen cycle were the transport of particulate Org-N, NH_3-N volatilization, nitrification, and denitrification. The leaching rate was estimated according to hydraulic flow rate and concentration of the constituents. The transformation and degradation processes such as volatilization, adsorption, mineralization, nitrification, and denitrification were implemented based on the first-order kinetics expression. In addition, the nitrogen uptake by vegetation was described in three compartments which are root, stem, and leaf.

This nitrogen dynamic model has been calibrated with a VFCW planted with *Cyperus alternifolius* that operated with a feeding-resting period of 1:3 days. The simulated results revealed that increasing bed depth might improve the degradation of NH_4^+-N and NO_3^--N, and a reduction of NO_3^- in the effluent was observed in the case of longer retention periods. Furthermore, this model indicated that denitrification is the main

removal mechanism of total nitrogen in VFCW, but the amounts of nitrogenous components were still very high in the effluent.

2.4.2.6. Petitjean et al. (2012)

Petitjean et al. (2012) developed a multi-component transport module using a biphasic theorem for VFCWs. A one-dimensional "transient spatial boundary condition" was adopted to describe the flow and oxygen transport by incorporating the mass balance equations with Darcy equations for both liquid and air phases (Forquet et al. 2009). The flow under the unsaturated condition is described using basic soil properties such as porosity, density, and degree of saturation. This attempt showed a better performance in predicting the dynamic of oxygen restoration such as air convection.

The transport module was numerically implemented using a local, discontinuous Galerkin method and the CWM1 (Langergraber, Rousseau, et al. 2009a) was used as the basis of the bio-kinetics module. The number of components was reduced to six, which were oxygen, dissolved readily degradable COD, particulate slowly degradable COD, NH_4^+-N, heterotrophic biomass, and autotrophic biomass. Meanwhile, the hydrolysis, aerobic growth of heterotrophic bacteria, nitrification and lysis of bacteria were considered as the four main processes in the bio-kinetics.

The proposed model was calibrated and verified with existing measured data in terms of oxygen transport. In summary, this study provided a simplified kinetics module to model the aerobic biodegradation in VFCWs. Besides, it had an excellent capability in demonstrating the dynamics of oxygen renewal and consumption, subsequently giving important insights into the correlation between aeration status and treatment efficiency.

2.4.2.7. Bustillo-Lecompte et al. (2016)

Bustillo-Lecompte et al. (2016) developed a two-dimensional numerical model integrated ADE and first-order decay kinetics to predict the treatment efficiency of BOD and TN in the VFCWs treating domestic wastewater. The hydraulic behaviour and solute transport in the wetland bed were computed using the software Variably-Saturated 2D Flow and Transport (VS2DT), where the flow pattern and transport mechanism in the porous medium were simulated based on the Richards equation and ADE. The effect of ET and linear adsorption isotherm was included in the proposed model. The model was formulated using the finite difference approach.

As for the process simulation, the proposed model considered the removal of organic matter and nitrogen as lumped parameters, which were BOD_5 and TN respectively. The mass balance of BOD_5 and TN includes the initial solute within the bed, influent, effluent, and losses due to ET, degradation, and adsorption. The model was calibrated with regards to the effluent concentration of BOD_5 and TN in a laboratory scale VFCW, where the substrate was composed of three different layers including a 0.12 m top organic soil layer, a 0.4 m main gravel layer and a 0.2 m drainage layer.

The calibrated results showed a good match with the measured data with a coefficient of determination (R^2) of 0.99 for both BOD_5 and TN. The simulated results indicated that the removal of organic matter and nitrogen was not significantly affected by the vegetation. The overall performance was excellent, where the removal efficiency reached 88.33 and 91.95 % for BOD_5 and TN, respectively. As for the validation, the residual analysis showed a more random pattern but was still acceptable in practice. The biochemical processes were the main mechanisms in removing nitrogen and were represented by the degradation in the mass balance. A further determination regarding the parameters in the experiment and a more comprehensive monitoring of flow rate and solute level were essential in improving the model.

2.5. Review summary

The literature has evidently shown that the VFCW has become a feasible alternative for septage treatment because of its outstanding capability in removing solids content and organic matter (Koottatep et al. 2004; Paing and Voisin 2005; Kengne et al. 2009; Troesch, A. Liénard, et al. 2009; Jong 2014). However, its overall treatment efficiency of nitrogen is less desirable. The removal of NO_3^--N in most of the VFCW-based septage treatment system reviewed from the literature were insignificant compared to TS, organic matter and NH_4^+-N (Lienard and Payrastre 1996; Koottatep et al. 2001; Troesch, Lienard, et al. 2009; Jong and Tang 2013). The literature have provided a list of design configurations and operating regimes for VFCW-based septage treatment system. Nevertheless, the design of such a system still remains at a “black-box” level, where the rules-of-thumb and overall removal efficiency were commonly used to determine the capacity and operational strategies of the wetland beds (Kumar and Zhao 2011). As a result, a mathematical model is proposed to facilitate the fundamental understanding of nitrogen dynamics in the VFCW designed for septage treatment.

In the VFCW with intermittent loading, the hydraulic flow through the substrate is variably-saturated and is highly dynamic (Morvannou et al. 2013b). The nitrogen transformation in this treatment system is by means of biochemical and physical processes, which is a dynamics interacted by influent quality, microbial community, availability of oxygen and environmental factors (Vymazal and Kröpfelová 2009). Therefore, a first-order kinetics model, which predicts the concentration of particular contaminants based on the influent concentration, is insufficient to model the nitrogen dynamics within the VFCW due to the time-varying scenario during operation (Kadlec 2000). A mechanistic model is proposed in this study to simulate the nitrogen dynamics in the VFCW-based septage treatment system. This approach delivers a comprehensive analysis towards the hydraulic behaviour and process kinetics in the wetland bed, which has been regarded as the state-of-art in the aspect of design and modelling of CW system.

The accuracy of the hydraulic simulation is crucial in determining the retention time of influent within the wetland bed, eventually governing the prediction of process dynamics (Langergraber and Šimůnek 2005). Therefore, the models implemented with the steady-state flow module are incapable of providing a reliable simulation for the VFCW under intermittent loading. In addition, the models relying on the empirical approach such as McGechan, Moir, Sym, et al. (2005) and Ouyang, Luo, and Cui (2011) are impractical to describe the varying operational strategies and hydraulic properties in the system. For those models developed with the transient flow module, only HYDRUS-CW2D (Langergraber and Šimůnek 2005), FITOVERT (Giraldi, de Michieli Vitturi and Iannelli 2010), and Bustillo-Lecompte et al. (2016) provided a numerical approach to adapt to the boundary condition of ponding and included an analytical equation to estimate ET rate, while the others were dependent on the empirical method. The substrate clogging in the VFCW treating septage is provoked due to the high solids load in the influent. To date, only FITOVERT (Giraldi, de Michieli Vitturi and Iannelli 2010) and model described in Ouyang, Luo, and Cui (2011) included a clogging module to account for the variation of hydraulic conductivity in the wetland bed, but the overall influence of sludge deposit layer was not clearly explained.

In terms of the nitrogen dynamics, most of the models provided a basic nitrogen cycle including the components of Org-N, NH_4^+-N and NO_3^--N, while NO_2^--N is always

lumped in NO_3^--N or even neglected in some models due to its minor contribution to the overall nitrogen balance (Wynn and Liehr 2001; Mayo and Bigambo 2005; Ojeda et al. 2008; Langergraber, Rousseau, et al. 2009a; Giraldi, de Michieli Vitturi and Iannelli 2010; Ouyang, Luo and Cui 2011). The presence of oxygen is essential for aerobic nitrification, while the denitrification is prohibited by excessive oxygen content. Therefore, an oxygen transport module is required to deliver a reliable simulation, which was found in most existing mechanistic models.

It should be noted that many models were developed to simultaneously simulate the transport and fate of organic matter and nitrogenous constituents (Langergraber and Šimůnek 2005; Langergraber, Rousseau, et al. 2009b; Petitjean et al. 2012; Bustillo-Lecompte et al. 2016). From the perspective of nitrogen dynamics, the decomposition of organic matter consumed of NH_4^+-N in the growth of the microorganism and denitrified NO_3^--N under anoxic condition. Monod kinetic has been validated as the feasible approach to describe the bio-kinetics in both HFCWs and VFCWs (Langergraber and Šimůnek 2005; Toscano et al. 2009; Saeed and Sun 2011b, 2011a; Langergraber and Šimůnek 2012; Morvannou et al. 2014). This approach includes a term of limiting components such as oxygen content, concentration of microorganism, carbon supply, and nutrient source in the estimation of reaction rate, subsequently avoiding the treatment performance to be overestimated.

In the CW systems, the main removal pathway of the nitrogen is the sequential ammonification-nitrification-denitrification process, which was included in all the reviewed models. The other mechanisms such as plant uptake, adsorption, sludge assimilation and ammonia volatilization were considered in particular model. The reaction kinetics module requires a platform to integrate the fate of organic matter, nitrogenous constituents, and microbial community. Therefore, Activated Sludge Model (ASM) (Henze et al. 2000) was generally applied. This stoichiometry concept has been widely used in the literature including Rousseau (2005), HYDRUS-CW2D (Langergraber and Šimůnek 2005), CWM1 (Langergraber, Rousseau, et al. 2009a) and FITOVERT (Giraldi, de Michieli Vitturi and Iannelli 2010). The concept of ASM is to incorporate the Monod-based bio-kinetic processes, which include the growth and decay of heterotrophs and autotrophs under either aerobic or anoxic condition, with the stoichiometric coefficient and kinetic parameters to predict the fate of particular components throughout the biological treatment.

Fifteen existing mechanistic models that include the simulation of nitrogen dynamics have been reviewed. The components and mechanisms included in these mechanistic models are summarized in Table 2.2 and the processes included in each model are listed in Table 2.3.

According to the author's best knowledge, five main gaps from the literature are summarized as follows:

- A mechanistic approach to model septage treatment using a VFCW-based system is lacking in literature;
- The understanding of the hydraulic behaviour and nitrogen dynamics in the first stage treatment of a pilot-scale, two-stage VFCW-based septage treatment still remained unclear;
- A transient variably-saturated flow module, which describes the operational strategies of the proposed VFCW-based septage treatment system and includes the influence of ET and sludge accumulation, is lacking in literature;
- A reaction kinetics module, which describes the nitrogen dynamics by incorporating ammonification, nitrification, adsorption and plant uptake in the VFCWs designed for septage treatment, is absent in the literature.
- The influence of sludge deposit layer in the VFCW-based septage treatment system towards the overall performance is lacking in the literature.

In order to facilitate the understanding of the influence of hydraulic behaviour upon nitrogen removal, the hydraulic and treatment performance in the first stage treatment of a pilot-scale, two-stage VFCW designed for septage treatment are observed and analysed. Then, the transport and fate of nitrogenous constituents throughout the wetland bed are simulated by a proposed mechanistic model, which is integrated into a transient flow and a stoichiometry reaction kinetics and is calibrated with the measured data obtained from the pilot plant.

Table 2.2: Summary of reviewed models

Model	Flow	Dimen-sion	Nitrogen Cycle				Microbial Dynamics	Oxygen Transport	Organic Carbon Cycle	Particle Transport	Clogging	ET
			Org-N	N-NH_3	N-NO_2^-	N-NO_3^-						
Wynn and Liehr (2001)	Steady-state	1-D	√	√	X	√	√	√	√	X	X	√
Liu, Dahad, and Surampali (2005)	Steady-state	1-D	√	√	√	√	X	X	X	X	X	X
Mayo and Bigambo (2005)	Steady-state	1-D	√	√	X	√	√	√	X	X	X	X
Wang et al. (2009)	Steady-state	1-D	√	√	X	√	√	X	X	X	X	X
Rousseau (2005)	Steady-state	1-D	√	√	X	√	√	√	√	X	√	√
Ojeda et al. (2008)	Steady-state	2-D	X	√	X	√	√	√	X	X	X	X
Saeed and Sun (2011)	Steady-state	-	X	√	X	√	X	X	√	X	X	X
BIO_PORE (Samsó and Garcia 2013)	Steady-state	2-D	√	√	X	√	√	√	√	√	√	X
McGechan, Moir, Sym, et al. (2005)	Transient	1-D	√	√	X	√	√	√	√	X	X	X

Table 2.2: Summary of reviewed models (continue)

Model	Flow	Dimen-sion	Nitrogen Cycle				Microbial Community	Oxygen Transport	Organic Carbon Cycle	Particle Transport	Clogging	ET
			Org-N	NH_3-N	NO_2^--N	NO_3^--N						
HYDRUS-CW2D (Langergraber and Šimůnek 2005)	Transi ent	2-D	√	√	√	√	√	√	√	X	X	√
CWM1 (Langergraber, Rousseau, et al. 2009)	Transi ent	2-D	√	√	X	√	√	√	√	X	X	√
FITOVERT (Giraldi, de Michieli Vitturi and Iannelli 2010)	Transi ent	1-D	√	√	X	√	√	√	√	√	√	√
Ouyang, Luo, and Cui (2011)	Transi ent	1-D	√	√	X	√	√	√	X	X	√	√
Petitjean et al. (2012)	Transi ent	1-D	√	√	X	X	√	√	√	X	X	X
Bustillo-Lecompte et al. (2016)	Transi ent	2-D	√	X*	X*	X*	X	X	√	X	X	√

*lumped as TN

Table 2.3: Summary of nitrogen transformation mechanisms in the reviewed models

Model	Ammonification	Nitrification	Denitrification	Plant Uptake	Sludge Assimilation	Adsorption	Ammonia Volatilization
Wynn and Liehr (2001)	√	√	√	√	√	X	X
Liu, Dahad, and Surampali (2005)	√	√	√	√	X	X	X
Mayo and Bigambo (2005)	√	√	√	√	√	X	X
Wang et al. (2009)	√	√	√	√	X	X	√
Rousseau (2005)	√	√	√	√	√	√	√
Ojeda et al. (2008)	X	√	√	X	X	X	X
Saeed and Sun (2011)	X	√	√	X	X	X	X
BIO_PORE (Samsó and Garcia 2013)	√	√	√	X	√	X	X
McGechan, Moir, Sym, et al. (2005)	√	√	√	√	X	X	√
HYDRUS-CW2D (Langergraber and Šimůnek 2005)	√	√	√	X	X	X	X

Table 2.3: Summary of nitrogen transformation mechanisms in the reviewed models (continue)

Model	Ammonification	Nitrification	Denitrification	Plant Uptake	Sludge Assimilation	Adsorption	Ammonia Volatilization
CWM1 (Langergraber, Rousseau, et al. 2009)	√	√	√	X	X	X	X
FITOVERT (Giraldi, de Michieli Vitturi and Iannelli 2010)	√	√	√	X	X	X	X
Ouyang, Luo, and Cui (2011)	√	√	√	√	X	√	√
Petitjean et al. (2012)	√	√	X	X	X	X	X
Bustillo-Lecompte et al. (2016)	X*	X*	X	X	X	√	X

*lumped as degradation

Chapter 3 Research Methodology I - Laboratory Experimental Setup and Test

A pilot-scale, two-stage VFCW-based septage treatment system has been constructed according to the design recommendation established in (Jong 2014). Figure 3.1 illustrates the plan view of the pilot-scale VFCW-based septage treatment system. The raw-septage feed tank, first stage wetlands, percolate storage tank, and second stage wetlands were sheltered from the rain. The system is a sequential treatment combined with pre-screened, storage, primary treatment and secondary treatment. It should be noted that the experiment carried out and data collected from the pilot-scale VFCW-based system is aimed at providing data to give an insight to the correlation between the hydraulic behaviour and nitrogen dynamics, as well as for the calibration of the proposed model, VF_Sep.

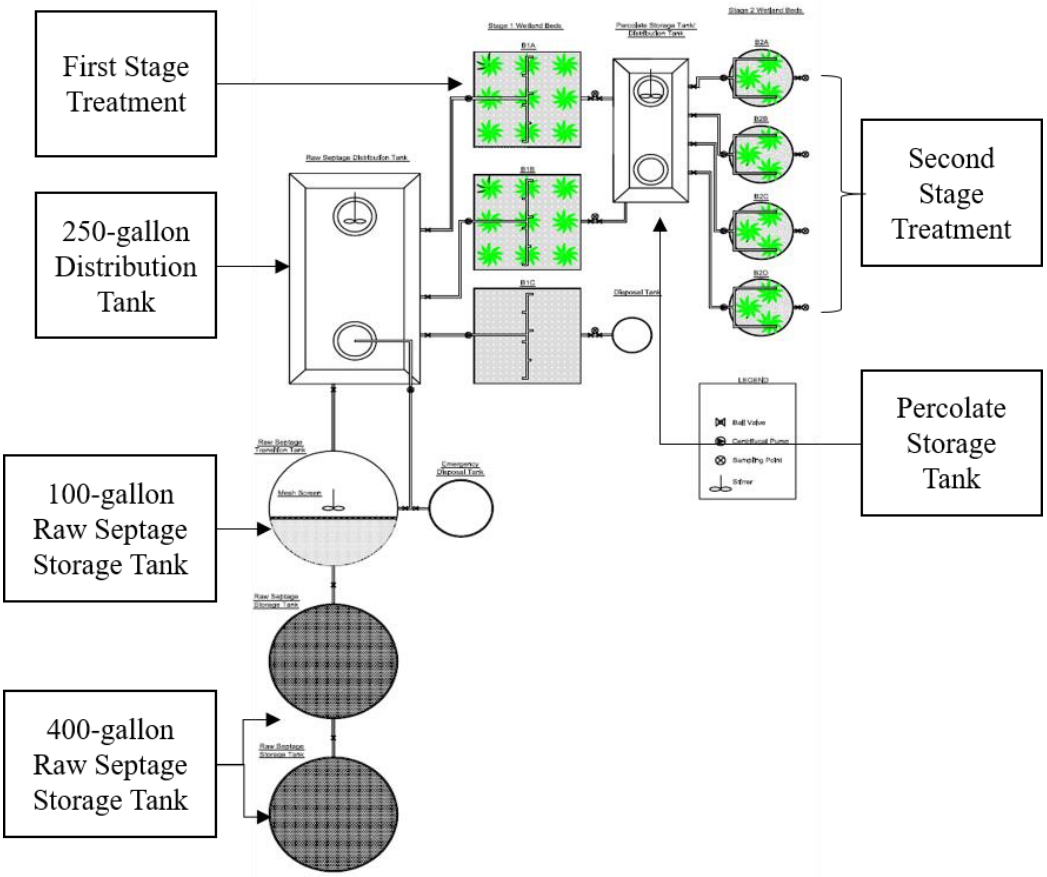

Figure 3.1: Plan view of the pilot-scale, two-stage VFCW-based septage treatment system

3.1. Experimental rigs

3.1.1. Pre-treatment and storage

Two connected 400-gallon (1816 l) polyethylene tanks and a 100-gallon (454 l) polyethylene tank were used to store the raw septage collected from domestic sources, which is as shown in Figure 3.2 The raw septage was screened by a plastic flat mesh during unloading into the 400-gallon polyethylene tank. The screening was to remove the gross solids such as sticks, rags and other debris (Figure 3.3). Then, the screened raw septage was discharged into the 100-gallon polyethylene tanks and was screened again using a layer of welded wire mesh (Figure 3.4) to eliminate the residual debris, especially finer contaminants such as hair that potentially clogs the centrifugal pumps in the following treatment process.

3.1.2. Raw septage distribution tank

A 250-gallon (1100-liter) polyethylene tank was utilized as the distribution tank to homogenize the raw septage and measure the specific volume of raw septage loaded to the first stage wetland bed. A centrifugal pump (0.50 HP) was installed to transfer the raw septage from the 100-gallon storage tank to the distribution tank, as shown in Figure 3.5. Then, three centrifugal pumps connected to the ball valve and distribution system was used to load the raw septage to the wetland beds in the first stage (Figure 3.6 and Figure 3.7).

Figure 3.2: 400-gallon and 100-gallon storage tanks

Figure 3.3: Primary screening process during unloading

Figure 3.4: Secondary screening process in the 100-gallon storage tank before the raw septage was discharged to the feed tank

Figure 3.5: Centrifugal pump to transfer raw septage from the storage tank to the feed tank

Figure 3.6: 250-gallon distribution tank

Figure 3.7: Pipe connection between the distribution tank and the centrifugal pumps

3.1.3. First stage wetland bed

The first-stage treatment encompassed three wetland beds, two beds (1A and 1B) were vegetated with common reeds (*Phragmites karka*) and the remaining one was unplanted (1C). Each wetland bed was accommodated in a 1 m^3 square polyethylene water tank (surface area = 1.10 m^2) and the substrate was a multi-layered granular bed built by crushed limestone. Crushed limestone is chosen as the material due to its cheaper cost and availability in the local area compared to other porous mediums (Jong 2014). The substrate profile is demonstrated in Figure 3.8, which consists of (from bottom to top) a 0.20 m coarse gravel layer (Ø 50 – 60 mm) as drainage layer (Figure 3.9), a 0.27 m layer medium size gravel layer (Ø 30 – 45 mm) (Figure 3.10) and a 0.27 m layer small size gravel (Ø 9.75 – 12 mm) as main layer (Figure 3.11). All gravel materials were sieved and washed before filling the water tank to minimize the clogging risk caused by clay. The substrate was adequately compacted during construction. Eighteen common reeds plants were cultivated in polyethylene bags and were watered with diluted septage before being transplanted to the bed, as shown in Figure 3.12. There were nine common reeds plants planted in each bed.

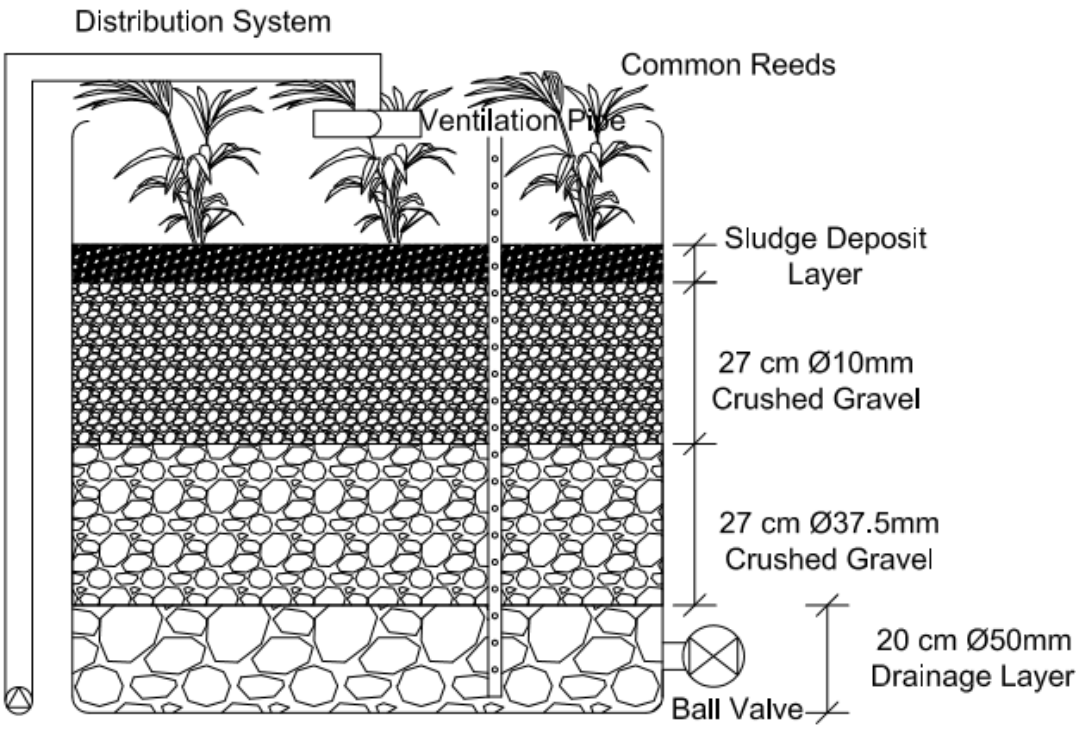

Figure 3.8: Cross-sectional view of first stage VFCW

Figure 3.9: ∅50 mm drainage layer

Figure 3.10: ∅37.5 mm main layer

Figure 3.11: ∅10 mm main layer

Figure 3.12: Transplantation of common reeds (*Phragmites Karka*) cultivated in a polyethylene bag

In each bed, two perforated PVC pipes with a diameter of 30 mm were installed along the substrate as a ventilation channel that allows the recharge of air into the substrate. The distribution device was powered by a centrifugal pump (0.50 HP). The distribution system was designed as six outlets that discharge the raw septage on the wetland bed. Figure 3.13 displayed the distribution device in operation. At the bottom of the tank, a built-in ball valve served as a discharge point, which was connected to two ball valves as shown in Figure 3.14, where one functioned to collect samples of effluent and the other functioned to transfer the excessive effluent to the percolate storage tank.

In order to stimulate the growth of biomass in the substrate and to ensure the growth of macrophytes, the wetland bed was acclimatized for two months before preliminary tests took place. The wetland beds were initially ponded with diluted raw septage, which increased to undiluted raw septage towards the end of the acclimatization period. A layer of sludge deposit was formed by the trapped solid particles at the top surface during the acclimatization, which is as shown in Figure 3.15.

Figure 3.17 show the wetland bed during and after acclimatization, respectively. The acclimatization period was ended when a significant reduction of contaminant concentration in the effluent was accomplished. The excessive sludge deposit on the surface was removed to prevent clogging in the following experiment.

Figure 3.13: Distribution device during loading

Figure 3.14: Drainage device at the bottom of the bed

Figure 3.15: Sludge deposit at the wetland surface

Figure 3.16: Wetland bed during acclimatization

Figure 3.17: Wetland bed after acclimatization

3.1.4. Percolate storage tank

A 100-gallon rectangular polyethylene tank was installed at the downstream of the first stage wetland beds to collect the percolate (Figure 3.18). In fact, the percolate storage tank functioned as the raw septage feed tank, but it collected the percolate and transported it to the second stage wetland bed for further purification by means of centrifugal pumps. It should be noted that the second stage treatment is excluded in this study and thus its configuration, operation, and treatment performance are not discussed in the thesis.

3.2. Operation

The raw septage was collected from the households near the Curtin University Sarawak Campus using a septic truck provided by a local sewerage company. The raw septage underwent two stages of screening during the transferring to the distribution tank. In subchapter 2.3.2, the advantages of operation based on solid loading rate (SLR) were highlighted. Solids control has been claimed to be better in clogging prevention and influent quality regulation, but this operation regime requires the amount of total solids (TS) to be quantified in the influent before loading. The standard method to measure TS, which is the oven-drying method, requires a day to sample and obtain the results, subsequently increasing the workload in the operation. The other concern with

Figure 3.18: Percolate storage tank

solids control is the varying solids content in the raw septage, where the low solids content results in high hydraulic load, and vice versa for raw septage with high solids content. The hydraulic load might exceed the system capacity, or be too low to produce effluent for the critical cases. In addition to this, one of the purposes of conducting the experiment is to obtain data for calibraiton of the proposed model, which was developed based on a flux-controlled boundary condition. As a result, the hydraulic-based operation with hydraulic loading rate (HLR) was carried out for this study, instead of SLR.

In order to investigate the impact of HLR on treatment performance, the wetland beds were operated with the HLR of 50 l, 75 l, 100 l, 125 l and 150 l for every loading. Before loading, the thickness of sludge deposit was measured using a ruler. The sediments were always observed in the bottom of the distribution tank due to the high solid content in the raw septage, and thus it was manually homogenized by stirring for at least five minutes. The volume of raw septage loaded to the bed was measured according to the water level in distribution tank, where 1 cm of water level in the distribution tank was equivalent to 15 l of septage. The loading rate can be controlled by the ball valve installed between the distribution tank and centrifugal pump. The raw septage was loaded at a constant rate throughout the loading.

During loading, temporary ponding was observed due to the low permeable sludge deposit layer. The associated depth can be regarded as the hydraulic load in terms of the head (Figure 3.19). The ball valve at the bottom of the tank was opened permanently to allow the effluent to be freely drained. The details of sample collection and analysis are introduced in the following sections. After loading, the bed was rested for at least three days to ensure complete drainage and mineralization of organic matter, which is of great importance to the growth of microorganisms and clogging prevention.

3.2.1. Assessment of hydraulic behaviour

Before starting the experiment, the sludge thickness was measured using a ruler. After a significant effluent flow has formed (> 20 mL in five minutes), the volume of effluent was measured using a 1000 ml measuring tube (minimum scale = 5 ml) and recorded continuously. The measurement was conducted frequently at the beginning of flow occurrence (five to ten minutes once), and the time interval increased to thirty minutes or one hour due to the slower effluent flow. It should be noted that the duration of

Figure 3.19: Formation of ponding during the loading process

the hydraulic assessment was limited to be 10 hours due to the technical and safety reasons.

The conversion of HLR to per-unit area (cm d^{-1}) is required and the calculation is as follows:

$$Head - based\ HLR = \frac{Hydraulic\ loading\ rate\ (cm^3 d^{-1})}{Surface\ area\ (cm^2)} \tag{3.1}$$

The effluent flow rate is calculated similarly but the time unit is changed to minute:

$$Effluent\ flux = \frac{Collected\ volume\ (cm^3)}{Surface\ area\ (cm^2)\ \times\ time\ interval\ (\text{min})} \tag{3.2}$$

The analysis of the hydraulic behaviour includes the assessment of peak flow rate and water recovery. The water recovery is the volumetric ratio between collected effluent (l) and the loading (l), which is expressed as:

$$Water\ recovery\ \% = \frac{Total\ volume\ of\ effluent\ (l)}{Volume\ of\ influent\ (l)}\ \times 100\% \tag{3.3}$$

3.2.2. Assessment of raw septage and effluent quality

The water quality parameters of the raw septage and its effluent are monitored. The raw septage sample was taken at the downstream of the distribution device and the

effluent was sampled simultaneously with the assessment of hydraulic performance. Nevertheless, when a long time interval (30 minutes to 1 hour) was used, the sampling of effluent for water quality test was conducted individually to obtain a more accurate effluent quality. The samples were collected in a 300 ml disposable BOD bottle with a plastic cap, as shown in Figure 3.20.

The concentration of dissolved oxygen (DO), ammonium nitrogen (NH_4^+-N) and nitrate nitrogen (NO_3^--N) and the physical properties including pH and temperature were identified instantaneously at the site using the HACH® HQ40d portable multi-parameter meter with specific probes (Figure 3.21), which is listed in Table 3.1. The samples were stored in a low-temperature refrigerated incubator in the temperature of 4˚C and were analysed for TS, COD, and TN for maximally twenty four hours.

The concentration of TS is determined according to the gravimetric method (Method 8163 2012) standardized by United States Environmental Protection Agency (USEPA) with a drying oven and an analytical balance. The measurement of COD and TN concentration were conducted using the USEPA Reactor Digestion Method (Method 8000) and Persulfate Digestion Method (Method 10072, Test'N Tube ™ Vials), respectively, with a HACH DR2800 spectrophotometer (Figure 3.22).

The typical analysis of the removal efficiency for a particular contaminant is performed by comparing the volume and concentration of the influent to the volume and quality of the effluent, which is expressed as (Liu et al. 2013):

$$E = \frac{C_0V_0 - C_eV_e}{C_0V_0} \times 100\% \tag{3.4}$$

Figure 3.20: Sample collection on 1st December 2015 (Case 3A)

Table 3.1: The probe used to measure the specific water quality parameter

Parameter	Probe
Dissolved Oxygen	IntelliCAL™ LDO101 Standard Luminescent/ Optical Dissolved Oxygen (LDO) probe
Ammonium	IntelliCAL™ ISENH4181 Ammonium Ion Selective Electrode (ISE)
Nitrate	IntelliCAL™ ISENO3181 Nitrate Ion Selective Electrode (ISE)
pH	IntelliCAL™ PHC101 Standard Gel Filled pH Electrode

Figure 3.21: HACH® HQ40d portable multi-parameter meter with specific probes

Figure 3.22: HACH DR2800 spectrophotometer and the Test'N Tube ™ vials

where C_i and C_e are the concentration of influent and effluent [M L^{-3}], respectively. The V_i and V_e denote the volume of influent and effluent [L^3], respectively. However, this analysis is only practical when all effluent is collected and mixed properly in an undisturbed tank to obtain the volume and concentration. This is not possible for this study since it is difficult to completely empty the percolate storage tank in every operation. Therefore, a modified equation to accommodate the temporal volume and concentration of the effluent was used, which is expressed as:

$$E = \frac{C_i V_i - \sum_{i=1}^{N} C_e V_e}{C_i V_i} \times 100\% \tag{3.5}$$

This approach provided a precise estimation for the total mass recovery of the contaminants in the effluent. However, the modified equation might lead to overestimated efficiency when the influent does not completely infiltrate into the wetland bed. Therefore, a conservative approach is conducted to avoid such overestimation, where the volume of the influent is replaced by the total volume of effluent:

$$E = \frac{C_i \sum_{i=1}^{N} V_e - \sum_{i=1}^{N} C_e V_e}{C_i \sum_{i=o}^{N} V_e} \times 100\% \tag{3.6}$$

This equation is applied to evaluate the removal efficiency of TS, TCOD, TN, and NH_4^+-N. The concentration of DO and NO_3^--N usually increased in the effluent, and hence these parameters are not involved in the analysis of treatment efficiency.

3.2.3. Tracer testing

In order to investigate the solute transport capability of the first-stage wetland beds, 12 sets of quantitative tracer studies was conducted simultaneously with the hydraulic assessment by feeding the wetland bed with raw septage that had been mixed with the diluted tracer to monitor the solute movement over a specified time frame. The tracer test aims to reproduce the mean travel duration of solute transport through a concentration-time plot.

Bromide (Br^-) is recognized as a reliable tracer due to its positive characteristics such as its ease of use, its high solubility, its non-biodegradable and non-toxic nature and its absence in septage and soil system (Levy and Chambers 1987). The procedure to

conduct the tracer tests in this study is modified from the standard field monitoring (Meiri 1989) and similar experiments carried out in VFCWs (Giraldi et al. 2009; Panuvatvanich, Koottatep and Koné 2009).

Before the experiment, the raw septage was sampled and tested for the background concentration of Br^- using Hach® MM340 radiometer with a bromide ion selective electrode as shown in Figure 3.23. As the pilot-scale VFCW is loaded in batches, the bromide tracer in the form of potassium bromide (KBr), was premixed with the raw septage at a specific volume. The influent concentration was designed to be 0.001 mole l^{-1} and the amount of KBr required was calculated as follows:

$$V_1 = \frac{M_2 V_2}{M_1} \tag{3.7}$$

where V_1 is the volume of tracer required (L), M_2 is the designed concentration (=0.001 mole l^{-1}), V_2 is the volume of influent (L) and M_1 is the concentration of tracer (=1 mole l^{-1}).

As this test was carried out simultaneously with the hydraulic assessment, the sampling schedule was as same as described in the previous section. The mass recovery of the tracer was analysed to evaluate the conservation of solute transport in the wetland bed, where the equation used is same as equation 3.6.

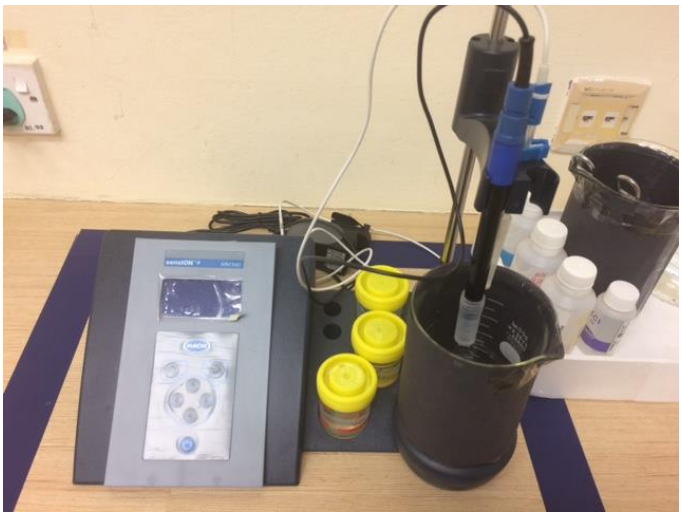

Figure 3.23: Hach® MM340 radiometer with a bromide ion selective electrode

Chapter 4 Research Methodology II - Model Development

The proposed model aims to simulate the transport and fate of nitrogenous constituents in one-dimension within a heterogeneous substrate profile. Neither water movement nor contaminant transport in the horizontal direction was considered in the model. A set of essential features is summarized as follows:

- A simple approach should be adopted since a highly complex model has been found to be inefficient due to the challenge in obtaining the required parameters (Marsili-Libelli and Checchi 2005);
- A variably-saturated flow module is essential to describe the hydraulic behaviour of VFCW with intermittent feeding mode (Langergraber and Šimůnek 2005; Maier et al. 2009; Giraldi, de Michieli Vitturi and Iannelli 2010; Morvannou et al. 2013b);
- The model should incorporate various boundary conditions including loading, surface ponding, and free drainage,
- The accumulation of sludge deposit on the surface of wetland bed and the associated impact on the hydraulic behaviour should be considered;
- The influence of evapotranspiration (ET) should be included in the water balance;
- The transport of both dissolved and particulate constituents in liquid and solid phases should be taken into account;
- The filtration of particulate constituents should be included;
- The bio-kinetics module is required to incorporate a set of biochemical degradation processes and biomass growth.

Figure 4.1 presents the flow chart for the model development in this study. The conceptual model was inspired by the observation in the preliminary test, and the governing equations were obtained from the literature. The proposed model, which is named as VF_Sep, was numerically implemented in the simulation software MATLAB®. VF_Sep was then calibrated by matching the simulated data to the measured data of a pilot-scale VFCW-based septage treatment system. The unit of the variable is self-defined in VF_Sep, and thus the dimensional unit is used instead of SI unit to explain the model development.

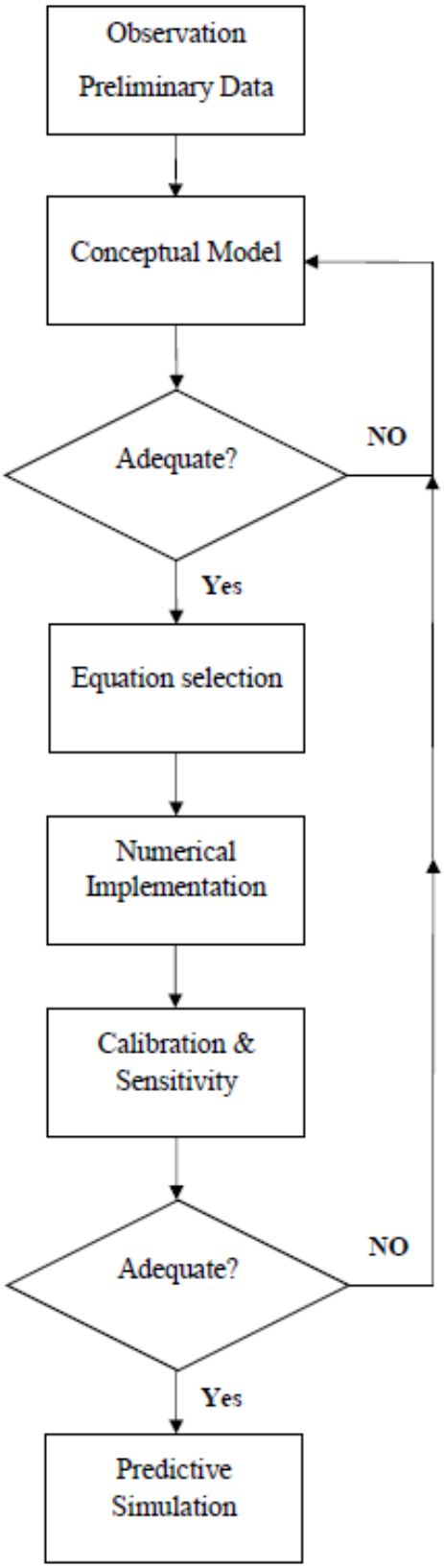

Figure 4.1: Flow chart of model development

4.1. Hydraulic module

The hydraulic module is fundamental to the simulation of the transport and fate for nitrogenous constituents through the wetland bed. Due to the intermittent loading regime and the heterogeneous hydraulic properties within a multi-layer substrate, the wetland bed is partially saturated and results in a continuously varying saturation level (Giraldi et al. 2009). Therefore, a transient variably-saturated flow model was developed to describe the infiltration flow in the VFCW with regards to the hydraulic properties of substrate materials, which include grain size, pore size distribution.

4.1.1. Governing equations

4.1.1.1. Richards equations

According to the literature review, Richards equation (Richards 1931) is widely used to describe the variably-saturated flow in the VFCW (Langergraber 2008). It is a partial differential equation that comprises the effect of gravity and water pressure to relate the variation of volumetric water content within a partially saturated porous medium. The mixed-form Richards equation, where the equation is expressed in water content and pressure head, is presented as:

$$\frac{\partial \theta}{\partial t} = \frac{\partial}{\partial z}\left[K(\theta)\frac{\partial h}{\partial z}\right] - \frac{\partial K(\theta)}{\partial z} - S \tag{4.1}$$

where θ denotes the volumetric water content [$L^3\ L^{-3}$], h denotes the hydraulic head [L], t denotes the time [T], z denotes the vertical coordinate (assumed positive upwards) [L], K denotes the unsaturated hydraulic conductivity [$L\ T^{-1}$], and S denotes the source/sink term. The source/ sink term is used to represent the additional water due to precipitation or water loss via ET.

This approach postulates that the effect of the gas phase is insignificant compared to the water phase in the liquid flow process, thereby the air content within the porous medium is easily displaced by water with negligible resistance due to its high mobility and low viscosity (1% of the viscosity of water) (Bear and Braester 1972). Furthermore, the volumetric variation caused by the fluid compressibility is presumed to be negligible in the Richards equation and the density of influent is assumed to be constant along the simulation (Nielsen, Th. Van Genuchten and Biggar 1986). This equation computes the water movement in a porous medium based on the hydraulic

head difference between two observed points and the associated hydraulic conductivity. The hydraulic conductivity under the unsaturated condition is a function of pressure head and water content. In this study, an analytical van Genuchten-Mualem model (Mualem 1976; van Genuchten 1980) was applied to estimate the hydraulic conductivity.

The Richards equation has been widely used in modelling the hydraulic performance of VFCW (Langergraber and Šimůnek 2005; Wanko et al. 2006; Giraldi, de Michieli Vitturi and Iannelli 2010). Nevertheless, the behaviour of nonlinearity in the equation limits the application of the analytical solution to specific presumed conditions. As a result, a numerical approach using finite difference or finite element method is always recommended to solve the Richards equation.

4.1.1.2. van Genuchten-Mualem (VGM) model

In VF_Sep, the unsaturated hydraulic conductivity was determined using the van Genuchten-Mualem (VGM) model (Mualem 1976; van Genuchten 1980), which is the most common approaches to describe the hydraulic properties in the VFCW (Langergraber and Šimůnek 2005; Giraldi et al. 2009; Toscano et al. 2009). Fundamentally, the VGM model includes two equations, where the first equation is to estimate the water content based on the given variables including pressure head, VGM parameters, and saturated and residual water content. This equation is expressed as:

$$\theta = \theta_r + \frac{(\theta_s - \theta_r)}{[1 + (\alpha|h|)^n]^m} \tag{4.2}$$

Then, the second equation is to determine the unsaturated hydraulic conductivity from the VGM parameters, saturated hydraulic conductivity, and the water content obtained in the first equation. This equation is expressed as:

$$K = K_s \left(\frac{\theta - \theta_r}{\theta_s - \theta_r}\right)^l \left[1 - \left(1 - \left(\frac{\theta - \theta_r}{\theta_s - \theta_r}\right)^{\frac{1}{m}}\right)^m\right]^2 \tag{4.3}$$

where θ_r is the residual water content [$L^3 L^{-3}$], θ_s is the saturated water content [$L^3 L^{-3}$], α [L^{-1}], n [-], and m (=1-1/n) [-] are the empirical VGM shape parameters of the SWCC, K_s is the saturated hydraulic conductivity [$L\ T^{-1}$], and l is Mualem's pore

connectivity parameter (= 0.50) [-]. The reliability of the numerical flow simulation highly has been found to rely upon the precision of the VGM parameters, which is normally calibrated from the measured data.

4.1.1.3. Dual-porosity model

Typically, the Richards equation describes the variably-saturated flow in a uniform flow pattern, so-called equilibrium flow (Simunek, Van Genuchten and Sejna 2005). Nevertheless, the granular substrate used in the VFCW consists of disordered pore spaces due to the accumulated sludge deposit, vegetation and trapped organic matter, consequently leading to an inconsistency with the actual flow pattern. Giraldi et al. (2009) highlighted that the dead zones in the substrate contributed a significant amount of stagnant water, subsequently disturbing the consequent flow. Moreover, Morvannou et al. (2013b) indicated that the water flow might preferentially the macro-pores and partial water might be retained in the stagnant regions caused by the irregularity of pore size and trapped organic matter in the substrate. On the other hand, the cracks in the sludge deposit layer and the presence of vegetation potentially creates a predominant pathway for the influent (Molle 2014). This phenomenon is known as preferential flow, where the concept is to split the pore spaces into two or more domains, thereby the pressure head is under a non-equilibrium condition. Currently, the existing preferential flow models included a variety of concepts such as single porosity, dual-porosity and dual permeability (Šimůnek and van Genuchten 2008).

The dual-porosity model (Šimůnek and van Genuchten 2008) has been verified as an adequate hydraulic model for the VFCW. This concept separates the pore spaces to mobile and immobile regions and a mass transfer interrelates between two regions (Gerke and Genuchten 1993). The water flow only takes place in the mobile regions while the water content in immobile regions is stagnant. As a result, the total water content, θ [L^3 L^{-3}] is the combination of mobile water content, θ_{Mobile} [L^3 L^{-3}] and immobile water content, $\theta_{Immobile}$ [L^3 L^{-3}], which is expressed as:

$$\theta \quad = \theta_{Mobile} + \theta_{Mobile} \tag{4.4}$$

The flow in the mobile region was solved based on the Richards equation. A transfer rate of water exchange between mobile and immobile region was added to the equation. Therefore the equation is given as (Šimůnek et al. 2003):

$$\frac{\partial \theta_{Mobile}}{\partial t} = \frac{\partial}{\partial z}\left[K(\theta_{Mobile})\frac{\partial h_{Mobile}}{\partial z}\right] - \frac{\partial K(\theta_{Mobile})}{\partial z} - S_{Mobile} - \Gamma_w \qquad (4.5)$$

where Γ_w [T^{-1}] is the water transfer rate. Then, the stagnant water in the immobile region is described using a mass balance equation as:

$$\frac{\partial \theta_{Immobile}}{\partial t} = -S_{Immobile} + \Gamma_w \qquad (4.6)$$

The mass transfer is generally obtained based on the difference of effective saturation or pressure head gradient between the mobile and immobile regions (Šimůnek et al. 2003). In this study, the difference of effective saturation was used to estimate the transfer rate due to its simplicity. The additional hydraulic parameters required in the approximation of the mass transfer rate are residual water content $\theta_{r,Immobile}$ [L^3 L^{-3}] and saturated water content $\theta_{s,Immobile}$ [L^3 L^{-3}] of the immobile region, and a first-order mass transfer coefficient ω [T^{-1}]. The equation is demonstrated as:

$$\Gamma_w = \omega\,(Se_{Mobile} - Se_{Immobile}) \qquad (4.7)$$

where the Se_{Mobile} [-] and $Se_{Immobile}$ [-] is the effective saturation in the mobile and immobile region, respectively. This equation assumed that the mass transfer rate is proportional to the difference between effective water content. The effective saturation was obtained from the water content, residual water content and saturated water content, which is expressed as:

$$S_e = \frac{\theta - \theta_r}{\theta_s - \theta_r} \qquad (4.8)$$

When the Γ_w is positive, the water tends to transfer from mobile region to immobile, while if Γ_w is negative, the water transfer in an opposite direction.

4.1.1.4. Evapotranspiration

In VF_Sep, the potential evapotranspiration (PET) was estimated using the FAO-56 Penman-Monteith combination equation (Zotarelli et al. 2010). It is an approach that combines both radiation and aerodynamics to predict the overall water loss to the atmosphere. It should be noted that the ET_0 is only practical under the standard condition, where the study site should have a significant coverage of well-grown

vegetation with sufficient water supply, as well as a desirable soil water condition. It was assumed that the system configuration and operating regime satisfied the standard condition. The Penman-Monteith equation is as follows:

$$ET_o = ET_{rad} + ET_{aero} = \frac{1}{\lambda}\left[\frac{\Delta(R_n - G) + \rho_a C_p \frac{(e_s - e_a)}{r_a}}{\Delta + \gamma\left(1 + \frac{r_c}{r_a}\right)}\right] \quad (4.9)$$

where ET_o is the PET rate [L T^{-1}], ET_{rad} is the radiation term [L T^{-1}], ET_{aero} is the aerodynamic term [L T^{-1}]. In the combined equation, λ denotes the latent heat of vaporization [L^2 T^{-2}] , R_n denotes the net radiation at surface [M T^{-3}], G denotes the soil heat flux [M T^{-3}] , ρ_a is the atmospheric density [M L^{-3}], C_p denotes the specific heat of moist air [L^2 T^{-2} Q^{-1}], e_s is the saturation vapor pressure at temperature [M L^{-1} T^{-2}] , e_a is the actual vapor pressure [M L^{-1} T^{-2}], r_c is the crop canopy resistance [T L^{-1}] , r_a is the aerodynamic resistance [T L^{-1}], γ is the psychrometric constant [M L^{-1} T^{-2} Q^{-1}] and Δ is the slope of the vapor pressure curve [M L^{-1} T^{-2} Q^{-1}]. The detailed calculation of PET using Penman-Monteith equation is presented in Appendix A.

The estimation of PET provides a simple attempt to give an insight into the overall water loss from the surface evaporation and plant transpiration. However, the ET not only occurs at the wetland surface, while the water extraction can reach a certain depth from the surface due to the root distribution of macrophytes. Therefore, the implementation of PET in the numerical model could be problematic and an approach of separation in terms of evaporation and transpiration is necessary. A Beer-Lambert law, which separates PET into potential evaporation and potential transpiration using the leaf area index (*LAI*), was employed in the proposed model (Varado, Braud and Ross 2006):

$$T_0 = ET_o\,[1 - \exp(-a_{b1}LAI)] \quad (4.10)$$

$$E_0 = ET_o\,[\exp(-a_{b1}LAI)] \quad (4.11)$$

where the T_0 and E_0 are the potential transpiration rate and potential evaporation rate, respectively [L T^{-1}]. *LAI* denotes the leaf area index [-], which quantify the plant canopies from the fraction of leaf area to the unit surface area. The a_{b1} is an empirical coefficient [-], where a classical value of 0.50 was used.

In terms of the numerical implementation, the sink term of evaporation was allocated at the top surface and the water balance can be analysed directly from the water content. On the other hand, the water loss by the transpiration is a function of root distribution along the surface profile. The root water uptake is estimated by means of the equation developed by Li, Boisvert, and Jong (1999) and Lai and Katul (2000), where the equation was formulated by taking the root-density distribution, water stress distribution and water compensation into account (Varado, Braud and Ross 2006):

$$ST(z,t) = \alpha_1(\theta,z)\alpha_2(\theta,z)g(z)T_0 \tag{4.12}$$

where *ST(z,t)* is the sink term of actual transpiration [L T^{-1}], *z* is the depth from the top surface [L] and t is the time [T]. The term *g(z)* [-] denotes a non-linear function of root density distribution [M L^{-3}] (Li, Boisvert and Jong 1999):

$$g(z) = g_0 \frac{(e^{-bz})\left[1.5 + 0.5\, e^{-bz}\right]}{1 + e^{-bz}} \tag{4.13}$$

where g_0 is the root density at $z=0$ [M L^{-3}] and *b* is a diminishing coefficient of the root distribution [L^{-1}]. The coefficient *b* is derived from an analytical approach depending on measurable input:

$$b = \frac{24.66(F_{10})^{1.59}}{z_R} \tag{4.14}$$

where z_R is the maximum root depth [L] (as shown in Figure 4.2) and F_{10} is the fraction of root length density in the top 10 % of root depth [-].

The coefficient of water stress distribution was derived using the theory established by Lai and Katul (2000), where the stress was estimated based on the difference between potential water content and wilting point (θ_{wilt}) :

$$\alpha_2(\theta,z) = \left(\frac{\theta(z,t) - \theta_{wilt}}{\theta_s}\right)^{\frac{\gamma}{\theta(z,t)-\theta_{wilt}}} \tag{4.15}$$

where γ is a functional parameter [-].

The compensation term describes the mechanism of water extraction in deeper layers when the upper layer becomes too dry. This term was estimated by determining the

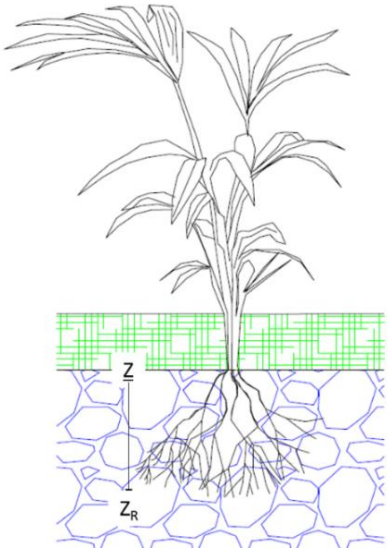

Figure 4.2: Maximum depth of the root distribution

maximum between local ratio and the water storage up to maximum root depth, which is expressed as:

$$\alpha_1(\theta, z) = MAX\left(\frac{\theta(z,t)}{\theta_s - \theta_{wilt}}, \frac{\int_0^z \theta(y,t)dy}{\int_0^R \theta(y,t)dy}\right) \tag{4.16}$$

4.1.1.5. Formation of the sludge deposit layer

The removal of the solid particles in the VFCW-based septage treatment system mainly depends on the surface filtration (Tan et al. 2015). The accumulated solids from the filtration form a layer of particle aggregation and destabilized flocs on the surface of wetland bed, which is commonly known as the sludge deposit layer (Molle 2014). In general, the modelling of instantaneous sludge formation is based on the accumulation rate of the sludge cake, which typically depends on the properties of the suspended particles and the grain size of the top surface layer. In order to improve the accuracy, the additional parameters such as the applied pressure, the porosity, and compressibility of the sludge cake are required, which increases the difficulty in the simulation (Abboud 1993).

The literature has shown that the formation of this low permeable layer significantly reduces the hydraulic efficiency of the wetland bed and eventually leads to the clogging phenomenon (Hua et al. 2010). The traditional approach analyses the formation of the sludge cake into the initial and transient stage. The initial stage

hypothesises the porous medium as a "clean filter", where the filter rate is estimated from the hydraulic properties of the wetland bed. After a certain amount of suspended particles has accumulated on the wetland surface, the remaining filtration shows a dependency on the permeability of accumulated sludge cake, which is known as the transient stage of solid filtration.

After acclimatization, a certain thickness of sludge deposit layer was observed in the pilot-scale VFCW. This layer served as an efficient filter septum in removing the solids and a flow regulator that prolongs the retention time of the influent in the wetland bed, subsequently improving the treatment performance. In the simulation, a sludge deposit layer was modelled as an inherent layer in the initial substrate profile and thus the filtration is described as the transient stage, which is as shown in Figure 4.3.

Abboud and Corapcioglu (1993) proposed a numerical model for cake filtration to determine the thickness of the solid accumulation using an instantaneous mass balance between the TS concentration in the influent and effluent. This macroscopic analysis was used and simplified to estimate the continuous increment of the sludge deposit layer in VF_Sep, which assumed that the permeability of the new-forming solid accumulation was same as the existing sludge layer. Then, a flow resistance was imposed based on the increment of the sludge thickness, subsequently, the consequent flow delay was calculated.

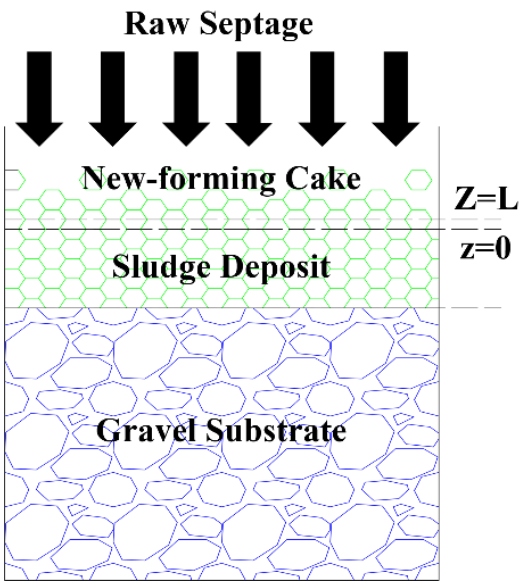

Figure 4.3: Accumulation of sludge deposit

The increment of the sludge deposit thickness was obtained from the amount of solid particles entering the wetland bed with an empirical retention coefficient, which is an equation that is modified from a mass conservative equation proposed by Abboud (1993):

$$\rho_s(1-\bar{n})\frac{dL}{dt} = \sigma\rho_s\frac{q_p}{n_s} - K_y\rho_s(1-\bar{n})L \tag{4.17}$$

where L is the thickness of new-forming sludge deposit layer, ρ_s is the density of solids particles [M L^{-3}], $\bar{n}$ is the dimensionless average porosity of sludge deposit layer [-], σ is the retention parameter [-], q_p is the input flux rate [L T^{-1}], K_y is the erosion rate [T^{-1}] and n_s is the porosity of influent [-]. The n_s can be estimated from the density of water (ρ_w) and solid particles (ρ_s) [M L^{-3}] and the associated dimensionless mass fraction of particulates in influent s [-]:

$$n_s = \frac{1}{1+\left(\frac{s}{1-s}\frac{\rho_w}{\rho_s}\right)} \tag{4.18}$$

This approach assumed that the porosity of the accumulated sludge deposit remains constant during the loading period due to the incompressible property. The delay of flow to the wetland bed was then estimated using Darcy's law to determine the flow rate through the new-forming sludge layer. It was presumed that the accumulation of new-forming sludge deposit occurs under saturated condition. The effect of sedimentation was neglected at this stage.

4.1.2. Numerical implementation

The numerical method solves the differential equation by "subdividing the time and spatial coordinates into smaller pieces and reformulating the continuous form of governing partial differential equations in terms of a system of algebraic equations" (Šimůnek 2005), which is known as space-time discretization. In this study, the one-dimensional variably-saturated hydraulic model was developed using the finite difference method, which has been verified as a feasible approach compared to the finite element scheme in numerically solving the Richards equation in a mono direction (Nielsen, Th. Van Genuchten and Biggar 1986). In this context, the substrate profile was subdivided into numerous layers with equal thickness (Δz) and the nodes

were allocated at the layer interface. The nodes were arranged in order from the top surface (i=1) to the drainage layer (i=N), so-called positive downwards, and *N-1* elemental layers are created.

To simulate the heterogeneous substrate profile in the VFCW, each node can be characterized by different soil hydraulic properties, and thus the interface between two different types of the porous medium was allocated at the middle of the layer, which is as demonstrated in Figure 4.4. A fully implicit Euler backward method was used to discretize the time step (Δt) (de Vasconcellos and Amorim 2001) in the equation 4.5 and the final finite difference scheme at a given point i is described as:

$$\frac{\theta_{i.Mobile}{}^{j+1,k+1} - \theta_{i,Mobile}{}^{j}}{\Delta t} = \frac{1}{\Delta z}\left[K_{i+\frac{1}{2}}^{j+1,k}\frac{\left(h_{i+1}^{j+1,k+1} - h_{i}^{j+1,k+1}\right)}{\Delta z}\right] - \frac{1}{\Delta z}\left[K_{i-\frac{1}{2}}^{j+1,k}\frac{\left(h_{i}^{j+1,k+1} - h_{i-1}^{j+1,k+1}\right)}{\Delta z}\right] - \frac{\left(K_{i+\frac{1}{2}}^{j+1,k} - K_{i-\frac{1}{2}}^{j+1,k}\right)}{\Delta z} - S - \Gamma_w \tag{4.19}$$

where subscripts i denotes the spatial discretization from the top surface layer, j demonstrates the temporal level and k indicates the iteration levels. The $K_{i+\frac{1}{2}}^{j+1,k}$ and $K_{i-\frac{1}{2}}^{j+1,k}$ are the inter-block hydraulic conductivity between two spatial level. A simple arithmetic mean was used and the inter-block hydraulic conductivity is expressed as:

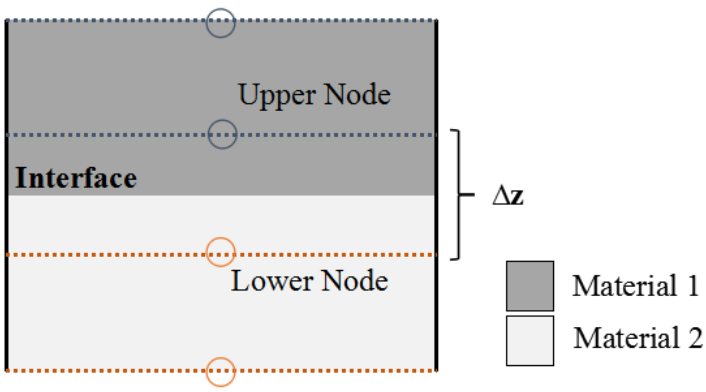

Figure 4.4: Heterogenous interface allocated between two nodes

$$K_{i+\frac{1}{2}}^{j+1,k} = \frac{K_{i+1}^{j+1,k} + K_{i}^{j+1,k}}{2} \qquad K_{i-\frac{1}{2}}^{j+1,k} = \frac{K_{i}^{j+1,k} + K_{i-1}^{j+1,k}}{2} \tag{4.20}$$

A mass conservative numerical method that solves the Richards equation using modified Picard iteration approach (Celia, Bouloutas and Zarba 1990) was used in this study. This method approximates the ${\theta_i}^{j+1,k+1}$ by expanding it in a truncated Taylor series, and thus it is expressed as a function with respect to $h^{j+1,k}$:

$${\theta_i}^{j+1,k+1} = {\theta_i}^{j+1,k} + \left.\frac{d\theta}{dh}\right|^{j+1,k} \left(h^{j+1,k+1} - h^{j+1,k}\right) \tag{4.21}$$

where $\left.\frac{d\theta}{dh}\right|^{j+1,k}$ is known as the soil water capacity $C_i^{j+1,k}$ [L^{-1}]. The $C_i^{j+1,k}$ is obtained from the differentiation of equation 4.2 (van Genuchten 1980):

$$C = \frac{d\theta}{dh} = \left(\frac{1}{h}\right)\left[\frac{-m(\theta_s - \theta_r)}{1-m}\right]\left(\frac{\theta - \theta_r}{\theta_s - \theta_r}\right)\left[1 - \left(\frac{\theta - \theta_r}{\theta_s - \theta_r}\right)^{\frac{1}{m}}\right] \tag{4.22}$$

By substituting equation 4.22 to equation 4.19, it gives:

$$\begin{aligned} C_i^{j+1,k}\,\frac{h_i^{j+1,k+1} - h_i^{j+1,k}}{\Delta t} + \frac{(\theta_{i,Mobile}^{j+1,k} - \theta_{i.Mobile}^{j})}{\Delta t} \\ = \frac{K_{i-\frac{1}{2}}^{j+1,k}}{(\Delta z)^2}\left[(h_{i-1}^{j+1,k+1}) - (h_i^{j+1,k+1})\right] \\ + \frac{K_{i+\frac{1}{2}}^{j+1,k}}{(\Delta z)^2}\left[(h_{i+1}^{j+1,k+1}) - (h_i^{j+1,k+1})\right] \\ - \frac{\left(K_{i+\frac{1}{2}}^{j+1,k} - K_{i-\frac{1}{2}}^{j+1,k}\right)}{\Delta z} - S_i - \Gamma_{w_i} \end{aligned} \tag{4.23}$$

In order to simplify the iterative computation, $\delta_i^{\,k+1}$ was used to represent the dependent variables that denotes the "increment of the variables *h* for passing from the iteration level *k* to the iteration level *k+1*" at every time step (de Vasconcellos and Amorim 2001):

$$\delta_i^{j+1,k} = h_i^{j+1,k+1} - h_i^{j+1,k} \tag{4.24}$$

Equation 4.23 was then modified to accommodate equation 4.24, which gives:

$$\begin{aligned} -\frac{K_{i-\frac{1}{2}}^{j+1,k}}{(\Delta z)^2}\left(\delta_{i-1}^{j+1,k}\right) + \left(\frac{C_i^{j+1,k}}{\Delta t} + \frac{K_{i-\frac{1}{2}}^{j+1,k}}{(\Delta z)^2} + \frac{K_{i+\frac{1}{2}}^{j+1,k}}{(\Delta z)^2}\right)\left(\delta_i^{j+1,k}\right) \\ - \frac{K_{i+\frac{1}{2}}^{j+1,k}}{(\Delta z)^2}\left(\delta_{i+1}^{j+1,k}\right) \\ = \frac{K_{i-1/2}^{j+1,k}}{(\Delta z)^2}\left(h_{i-1}^{j+1,k} - h_i^{j+1,k}\right) + \frac{K_{i+1/2}^{j+1,k}}{(\Delta z)^2}\left(h_{i+1}^{j+1,k} - h_i^{j+1,k}\right) \\ - \frac{\left(K_{i+\frac{1}{2}}^{j+1,k} - K_{i-\frac{1}{2}}^{j+1,k}\right)}{\Delta z} - \frac{\left(\theta_{i,Mobile}^{j+1,k} - \theta_{i.Mobile}^{j}\right)}{\Delta t} - S_i \\ - \Gamma_{w_i} \end{aligned} \tag{4.25}$$

The water exchange between the mobile and immobile region was derived from the mobile and immobile water content of previous temporal level using equation 4.7:

$$\Gamma_w = \omega\left[\left(\frac{\theta_{Mobile}^{j} - \theta_{r,Mobile}}{\theta_{s,Mobile} - \theta_{r,Mobile}}\right) - \left(\frac{\theta_{Immobile}^{j} - \theta_{r,Immobile}}{\theta_{s,Immobile} - \theta_{r,Immobile}}\right)\right] \tag{4.26}$$

This equation was input to the MATLAB ® as a tri-diagonal nonlinear matrix for each time step and solved by the tridiagonal matrix algorithm:

$$\begin{bmatrix} \beta_1^k & \gamma_1^k & 0 & 0 & 0 & \cdots & \cdots & 0 & 0 & 0 \\ \alpha_2^k & \beta_2^k & \gamma_2^k & 0 & 0 & \cdots & \cdots & 0 & 0 & 0 \\ 0 & \alpha_3^k & \beta_3^k & \gamma_3^k & 0 & \cdots & \cdots & 0 & 0 & 0 \\ 0 & 0 & \alpha_4^k & \beta_4^k & \gamma_4^k & \cdots & \cdots & 0 & 0 & 0 \\ 0 & 0 & 0 & \alpha_5^k & \beta_5^k & \cdots & \cdots & 0 & 0 & 0 \\ \vdots & \vdots & \vdots & \vdots & \vdots & \ddots & \ddots & \vdots & \vdots & \vdots \\ \vdots & \vdots & \vdots & \vdots & \vdots & \ddots & \ddots & \vdots & \vdots & \vdots \\ 0 & 0 & 0 & 0 & 0 & \cdots & \cdots & \beta_{N-2}^k & \gamma_{N-2}^k & 0 \\ 0 & 0 & 0 & 0 & 0 & \cdots & \cdots & \alpha_{N-1}^k & \beta_{N-1}^k & \gamma_{N-1}^k \\ 0 & 0 & 0 & 0 & 0 & \cdots & \cdots & 0 & \alpha_N^k & \beta_N^k \end{bmatrix} \begin{bmatrix} \delta_1^{k+1} \\ \delta_2^{k+1} \\ \delta_3^{k+1} \\ \delta_4^{k+1} \\ \delta_5^{k+1} \\ \vdots \\ \vdots \\ \delta_{N-2}^{k+1} \\ \delta_{N-1}^{k+1} \\ \delta_N^{k+1} \end{bmatrix} = \begin{bmatrix} R_1^k \\ R_2^k \\ R_3^k \\ R_4^k \\ R_5^k \\ \vdots \\ \vdots \\ R_{N-2}^k \\ R_{N-1}^k \\ R_N^k \end{bmatrix} \tag{4.27}$$

The coefficient α_i^j, β_i^j, γ_i^j and R_i^j (i = 1, 2, 3… N-1, N; where N represents the total number of nodes) are nonlinear functions and expressed as (de Vasconcellos and Amorim 2001):

$$\alpha_i^{j+1,k} = -\frac{K_{i-\frac{1}{2}}^{j+1,k}}{(\Delta z)^2} \tag{4.28}$$

$$\beta_i^{j+1,k} = \frac{C_i^{j+1,k}}{\Delta t} + \frac{K_{i-\frac{1}{2}}^{j+1,k}}{(\Delta z)^2} + \frac{K_{i+\frac{1}{2}}^{j+1,k}}{(\Delta z)^2} \tag{4.29}$$

$$\gamma_i^{j+1,k} = -\frac{K_{i+\frac{1}{2}}^{j+1,k}}{(\Delta z)^2} \tag{4.30}$$

$$\begin{aligned} R_i^{j+1,k} = {} & \frac{K_{i-\frac{1}{2}}^{j+1,k}}{(\Delta z)^2}\left(h_{i-1}^{j+1,k} - h_i^{j+1,k}\right) + \frac{K_{i+\frac{1}{2}}^{j+1,k}}{(\Delta z)^2}\left(h_{i+1}^{j+1,k} - h_i^{j+1,k}\right) \\ & - \frac{\left(K_{i+\frac{1}{2}}^{j+1,k} - K_{i-\frac{1}{2}}^{j+1,k}\right)}{\Delta z} - \frac{\left(\theta_{i,Mobile}^{j+1,k} - \theta_{i,Mobile}^{j}\right)}{\Delta t} - S_{i,Mobile} \\ & - \Gamma_{w_i} \end{aligned} \tag{4.31}$$

The iterative process is stopped while the difference pressure head computed between two iterative levels at each spatial node for a specific temporal step is smaller than the prescribed tolerance (δ_a):

$$\delta_i^{j+1,k} = \left|h^{j+1,k+1} - h^{j+1,k}\right| \leq \delta_a \tag{4.32}$$

In VF_Sep, two values were introduced as the tolerance, which is represented as maximum tolerance (max. δ_a) and minimum tolerance (min. δ_a). In the iteration process, a small value of acceptable tolerance typically improves the precision of simulation but it also burden on the computational efficiency since the convergence might not be achieved. On the other hand, a wider tolerance has been found to be instable in the prediction of flow. To overcome this potential drawback, VF_Sep took the minimum tolerance as the primary tolerance in the iteration. When the convergence cannot be reached within a limited number of iteration, then the subsequent

computation will compare the residual of the solution to the maximum tolerance. This approach effectively reduces the risk of poor simulation and divergence in the model.

The numerical expression of immobile water content mass balance equation is derived as:

$$\theta_{i.Immobile}{}^{j+1} = \Delta t\left(-S_{i,Immobile} + \Gamma_{w_i}\right) + \theta_{i,Immobile}{}^{j} \tag{4.33}$$

The water exchange between mobile and immobile region is estimated as follows.

$$\Gamma_{w_i}{}^{j+1} = \omega_i \left[\left(\frac{\theta_{Mobile_i}{}^{j} - \theta_{r,Mobile_i}}{\theta_{s,Mobile_i} - \theta_{r,Mobile_i}}\right) - \left(\frac{\theta_{Immobile_i}{}^{j} - \theta_{r,Immobile_i}}{\theta_{s,Immobile_i} - \theta_{r,Immobile_i}}\right)\right] \tag{4.34}$$

4.1.3. Initial and boundary condition

The steady-state initial condition can be input using either initial distribution of pressure potential or water content in the substrate.

$$h(z,t) = h_i(z) \quad t = t_0 \tag{4.35}$$

$$\theta(z,t) = \theta_i(z) \quad t = t_0 \tag{4.36}$$

where h_i [L] is prescribed pressure head at elevation z and initial time t_0.

Due to the intermittent loading mode and the occurrence of temporary surface ponding, the upper boundary condition is capable of switching between the prescribed head-controlled (Dirichlet type) and flux-controlled (Neumann type) boundary condition. The increasing thickness of new-forming sludge deposit was considered in the upper boundary by summing it into the spatial discretization at the top layer ($\Delta z_1 = \Delta z_{top}$), as shown in Figure 4.5.

In order to find the thickness of new-forming sludge deposit layer, the equation 4.17 was discretized according to the temporal step, which is expressed as:

$$\frac{L_S^{j+1} - L_S^{j}}{\Delta t} = \sigma \frac{q_1^{j}}{n_s(1-\bar{n})} - K_y L_S^{j} \tag{4.37}$$

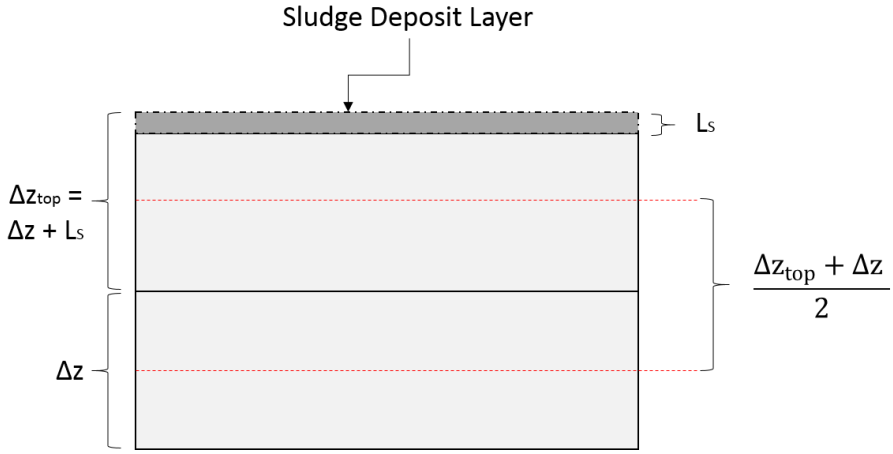

Figure 4.5: Variation of Δz_{top} in the simulation due to the sludge accumulation

where superscript j denotes the temporal level, L_S is the thickness of sludge deposit and the q_1 is the surface infiltration [$L^3 L^{-2} T^{-1}$]. The initial thickness was set to be zero. Accordingly, the thickness of the spatial discretization of the top surface layer is:

$$\Delta z_{top} = \Delta z + L_S^j \tag{4.38}$$

It should be highlighted that the HLR [$L^3 T^{-1}$] applied to the wetland bed is an extremely important parameter in the modelling of hydraulic flow processes of VFCW. The HLR was converted to a prescribed unit surface flux, q_{sur} [$L^3 L^{-2} T^{-1}$] and was applied to the top nodal mass balance equation (Figure 4.6). As a result, the coefficients

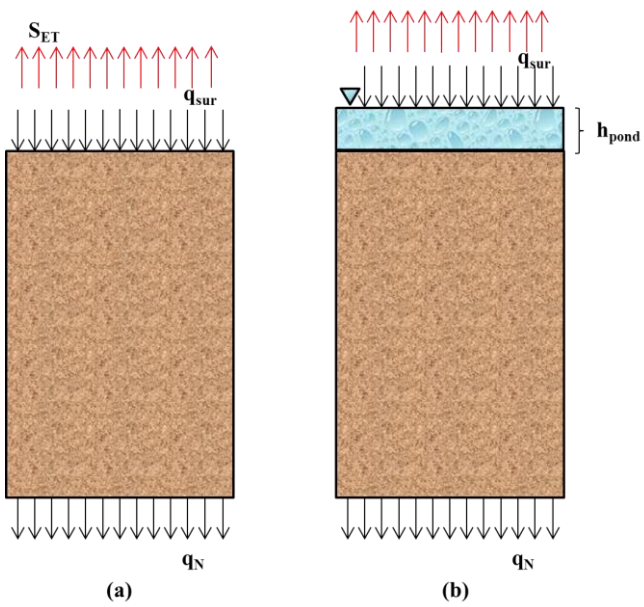

Figure 4.6: Boundary conditions of hydraulic module

of the top node were rearranged with regards to the Neumann type boundary condition and the inclusion of sludge deposit thickness, which are shown as follows.

$$\begin{cases} \alpha_1^{j+1,k} = 0 & (4.39) \\ \beta_1^{j+1,k} = \dfrac{C_1^{j+1,k}}{2\Delta t} + \dfrac{K_{1+\frac{1}{2}}^{j+1,k}}{\Delta z_{top}{}^2} & (4.40) \\ \gamma_1^{j+1,k} = -\dfrac{K_{1+\frac{1}{2}}^{j+1,k}}{\Delta z_{top}{}^2} & (4.41) \end{cases}$$

$$R_1^{j+1,k} = \frac{K_{1+\frac{1}{2}}^{j+1,k}}{\Delta z_{top}{}^2}\left(h_2^{j+1,k} - h_1^{j+1,k}\right) - \frac{K_{1+\frac{1}{2}}^{j+1,k}}{\Delta z_{4top}{}^2} - \frac{\left(\theta_{1,Mobile}^{j+1,k} - \theta_{1,Mobile}^{j}\right)}{2\Delta t} - \frac{q_{sur}}{\Delta z_{top}} - \frac{S_{1,Mobile}}{2\Delta t} - \Gamma_{w_1} \quad (4.42)$$

In this study, it should be highlighted that the loading was not constant along the operation. Therefore, the loading flux is separated into two cases:

$$\begin{cases} q_{sur} = q_0, \quad t_0 \le t \le t_q & (4.43) \\ q_{sur} = 0, \quad t_q < t \le t_{sp} & (4.44) \end{cases}$$

where q_0 is the prescribed surface flux, t_0 is the initial time, t_q is the end of loading period and t_{sp} is the total simulation time.

Due to the continuity in the numerical solution, the coefficient of the second node from the top surface was required to be modified according to the thickness of sludge deposit:

$$\alpha_2^{j+1,k} = -\frac{K_{2-\frac{1}{2}}^{j+1,k}}{\Delta z_{top} \cdot \left(\frac{\Delta z_{top} + \Delta z}{2}\right)} \quad (4.45)$$

$$\beta_2^{j+1,k} = \frac{C_2^{j+1,k}}{\Delta t} + \frac{K_{2-\frac{1}{2}}^{j+1,k}}{\Delta z_{top} \cdot \left(\frac{\Delta z_{top} + \Delta z}{2}\right)} + \frac{K_{2+\frac{1}{2}}^{j+1,k}}{\Delta z \cdot \left(\frac{\Delta z_{top} + \Delta z}{2}\right)} \quad (4.46)$$

$$\gamma_2^{j+1,k} = -\frac{K_{2+\frac{1}{2}}^{j+1,k}}{\Delta z \cdot \left(\frac{\Delta z_{top} + \Delta z}{2}\right)} \tag{4.47}$$

$$\begin{aligned} R_2^{j+1,k} = & \frac{K_{i-\frac{1}{2}}^{j+1,k}}{\Delta z_{top} \cdot \left(\frac{\Delta z_{top} + \Delta z}{2}\right)} \left(h_{i-1}^{j+1,k} - h_i^{j+1,k}\right) \\ & + \frac{K_{i+\frac{1}{2}}^{j+1,k}}{\Delta z \cdot \left(\frac{\Delta z_{top} + \Delta z}{2}\right)} \left(h_{i+1}^{j+1,k} - h_i^{j+1,k}\right) \\ & - \frac{\left(K_{i+\frac{1}{2}}^{j+1,k} - K_{i-\frac{1}{2}}^{j+1,k}\right)}{\left(\frac{\Delta z_{top} + \Delta z}{2}\right)} - \frac{\left(\theta_{i,Mobile}^{j+1,k} - \theta_{i,Mobile}^{j}\right)}{\Delta t} - S_{i,Mobile} \\ & - \Gamma_{w_i} \end{aligned} \tag{4.48}$$

The wetland bed has a specific infiltration capacity to receive loading. While the HLR exceeds the infiltration capacity, the top surface layer of wetland bed is completely saturated ($h_1=0$, $\theta_1= \theta_s$, $K_1=K_S$). Consequently, the extra amount of influent accumulates at the top surface layer and eventually forms a temporary pond. In the case of ponding, the top boundary condition is automatically changed from being flux-controlled to head-controlled, where a prescribed pressure head $h_1(t)$ is equal to the depth of the ponded water (Figure 4.6(b)). Therefore, the upper boundary condition becomes a function of time relating to surface flux q_{sur} and infiltration flux q_1:

$$\begin{cases} h_1 = h_{pond} + q_{sur} - q_1 - L_D^j, & t_0 \le t \le t_q \quad (4.49) \\ h_1 = h_{pond} - q_1 - L_D^j, & t_q < t \le t_{sp} \quad (4.50) \end{cases}$$

where the h_{pond} is the h_1 at previous time step (j-1) [L]. The head-controlled boundary condition will switch back to being flux-controlled at the instance when the h_1 returns to zero due to infiltration. The infiltration flux q_1 is calculated as follows.

$$q_1 = K_{1+\frac{1}{2}}^{j+1}\left(\frac{h_2^{j+1} - h_1^{j+1}}{\Delta z} - 1\right) - \frac{\Delta z}{2}\frac{\left(\theta_{1,Mobile}^{j+1,k} - \theta_{1,Mobile}^{j}\right)}{\Delta t} \tag{4.51}$$

As for the lower boundary condition, both free drainage and seepage face were simulated. The free drainage is also known as a zero-gradient flux boundary condition, which is expressed as:

$$\frac{dh}{dz} = 0 \; at \; z = Z \tag{4.52}$$

Then, the bottom flux q_Z is calculated as:

$$q_N^{j+1} = K_{N-\frac{1}{2}}^{j+1}\left(\frac{h_N^{j+1} - h_{N-1}^{j+1}}{\Delta z} + 1\right) - \frac{\Delta z}{2}\frac{\left(\theta_{N,Mobile}^{j+1,k} - \theta_{N,Mobile}^{j}\right)}{\Delta t} \tag{4.53}$$

4.1.4. Nodal fluxes

The nodal flux is calculated according to time steps using the following formulas:

$$q_1^{j+1} = -\left[K_{1+\frac{1}{2}}^{j+1}\left(\frac{h_2^{j+1} - h_1^{j+1}}{\Delta z_{top}} - 1\right) - \frac{\Delta z}{2}\left(\frac{\theta_1^{j+1} - \theta_1^{j}}{\Delta t}\right)\right] \tag{4.54}$$

$$q_i^{j+1} = -\left\{\frac{\left[K_{i+\frac{1}{2}}^{j+1}\left(\frac{h_{i+1}^{j+1} - h_i^{j+1}}{\Delta z} - 1\right)\Delta z\right] + \left[K_{i-\frac{1}{2}}^{j+1}\left(\frac{h_i^{j+1} - h_{i-1}^{j+1}}{\Delta z} - 1\right)\Delta z\right]}{2\Delta z}\right\} \tag{4.55}$$

$$q_N^{j+1} = -\left[K_{N-\frac{1}{2}}^{j+1}\left(\frac{h_N^{j+1} - h_{N-1}^{j+1}}{\Delta z} + 1\right) - \frac{\Delta z}{2}\left(\frac{\theta_N^{j+1} - \theta_N^{j}}{\Delta t}\right)\right] \tag{4.56}$$

On the other hand, the cumulative infiltration and discharge flux were computed by means of trapezoidal numerical integration. Due to the limitation of inherent memory in MATLAB, the integration was only capable of estimating the cumulative flux with a time step of 1 minute.

4.1.5. Mass balance conservation

The ability of the model to conserve global mass over the domain, which is defined as the mass balance conservation, was evaluated. Although such evaluation is crucial to determine the efficiency of the model, it is incapable of indicating the accuracy of VF_Sep. In this study, the mass balance was computed based on the “total additional mass in the domain” and the “total net flux into the domain”. The additional mass was

calculated with respect to the difference between the initial volume of water content in the sample and the total volume at a specific time. Then, the net flux was estimated according to the flux applied on the top layer of the porous medium and the cumulative flux collected from the bottom layer. The equation of mass balance (MB) measurement can be written as follows.

$$MB\left(t^{j+1}\right) = \frac{\sum_{i=1}^{N-1}\left(\theta_i^{j+1} - \theta_i^0\right)(\Delta z)}{\sum_1^{j+1}\left\{K_{\frac{1}{2}}^{j+1}\left[\frac{h_2^{j+1} - h_1^{j+1}}{\Delta z} + 1\right] - K_{N-\frac{1}{2}}^{j+1}\left[\frac{h_N^{j+1} - h_{N-1}^{j+1}}{\Delta z} + 1\right]\right\}} \quad (4.57)$$

where subscript 0 is the initial time step, $j+1$ is the final time step and N is the bottom node.

4.2. Transport module

In the pilot-scale VFCW-based septage treatment system, most of the treatment processes occur in the substrate. Therefore, a reactive transport module developed based on the advection-dispersion equation (ADE) is essential in reproducing the transformation and degradation of contaminants throughout the wetland bed. The ADE is a common approach to model the transport of solute within a porous medium, where the advection describes the solute displacement caused by the fluid flow and the dispersion represents the divergence due to the effect of molecular diffusion and mechanical dispersion (Fetter and Fetter Jr 1999). This approach has been widely used to investigate the mass transport of contaminants from the surface infiltration to the vadose zone or water table caused by the application of fertilizer, pesticide, waste disposal and accidental oil spills (Kresic 2006). The simulated results from the hydraulic simulation including the volumetric water content (θ) and water flux (q) are required in the transport module. Nevertheless, the modelling of biodegradation demands a bio-kinetics sub-module to estimate a source/ sink term in the dynamics of particular contaminants. In this section, the governing equations, numerical implementation, and limitation of the transport module were introduced.

4.2.1. Governing equations

4.2.1.1. Advection-dispersion equation (ADE)

The solute moving with the flowing water is known as advection. In one-dimensional model, the quantity of water flow used to describe the advection is equal to the average linear flux rate (Fetter and Fetter Jr 1999). Nevertheless, the water flow within the porous medium more or less diverges from the average velocity, which potentially alternates the mixing in the porous medium. This phenomenon is known as the hydraulic dispersion, which is generally described as a combined effect of mechanical dispersion and molecular diffusion in the simulation (Kresic 2006).

The mechanical dispersion is a spreading process caused by the variability of flux rate in the porous medium. This can be explained macroscopically by three phenomena: (a) the effect of the boundary layer of overall water flow in a porous medium, (b) the flow paths with different distances and (c) the flow paths with different pore spaces (Bear and Braester 1972). The irregular velocity of solute-containing water across the medium creates a continuous mixing process along the flow path, which could be greater than the average flux rate to result in a front-mixing in the solute transport profile. In a one-dimensional model, the direction of mixing was assumed to be parallel to the direction of the flow, so-called longitudinal dispersion and is modelled as a function of average linear flow rate.

The molecular diffusion is the solute movement driven by the concentration gradient, which is independent of the water flow. Nevertheless, the solid boundaries of porous medium might hinder the diffusion, and thus it was always factorized with the tortuosity of the porous medium (Fetter and Fetter Jr 1999). Then, the ADE is expressed as (Bresler 1973):

$$\frac{\partial \theta c}{\partial t} = \frac{\partial}{\partial z}\left[D_T \frac{\partial c}{\partial z} - qc\right] \tag{4.58}$$

where θ is the water content [$L^3\ L^{-3}$], c is the solute concentration in aqueous [$M\ L^{-3}$], t is the time [T], z is the vertical distance [L] q is the unit flux rate [$L^1\ T^{-1}$] and D_T is the hydraulic dispersion coefficient [$L^2\ T^{-1}$]. The D_T is estimated as follows (Fetter and Fetter Jr 1999):

$$D_T = D_L|q| + \theta D_D \tag{4.59}$$

where D_L is the empirical longitudinal dispersivity [$L^2 T^{-1}$] and D_D is the molecular diffusion coefficient [$L^2 T^{-1}$]. Equation 4.63 describes the fundamental solute transport in a variably-saturated porous medium. Nevertheless, a variety of processes occurs simultaneously during the percolation. The contaminants could be adsorbed on the surface of the porous medium or degraded by the biochemical processes, and thus these processes were considered in this reactive transport model.

4.2.1.2. Adsorption

During percolation, some contaminants are potentially adsorbed on the surface of the porous medium due to the physical and chemical attraction. This process was always lumped as a total amount of solute deposited from aqueous state to the solid phase. In literature, adsorption was generally considered in two ways (Fetter and Fetter Jr 1999). If the adsorption is rapid compared to the flow velocity, the adsorbed compounds instantaneously reach an equilibrium state with the compounds in the aqueous phase. When the adsorption process is slow, the adsorption is no longer equilibrium-controlled, but a kinetic sorption approach is required, where the adsorbed compounds could be desorbed and returned to the aqueous phase throughout the percolation.

The rate of adsorption is determined as a function of the concentration, which is experimentally derived by measuring the removal rate of a particular contaminant in a specific porous medium. The experimental results are then plotted as an “isotherm” that illustrates the correlation between the influent concentration and the amount of solute adsorbed by the porous medium (Fetter and Fetter Jr 1999). The adsorption isotherm can be presented as a linear or non-linear equation.

In the linear adsorption isotherm, the mass of compound adsorbed on the solid phase is presented as a first-order equation of the concentration in the aqueous phase (Nielsen, Th. Van Genuchten and Biggar 1986):

$$s_e{}^* = K_d c \tag{4.60}$$

where s_e* is the rate of change of adsorbed solute per unit weight of solid [$M\ M^{-1}$] and K_d is the first order coefficient [$L^3\ M^{-1}$]. In the linear adsorption isotherm, the K_d is directly obtained from the slope of the isotherm.

The non-linear isotherms can be presented either in Freundlich and Langmuir isotherm. The Freundlich isotherm correlates the adsorbed solute and solute concentration using a curvilinear relationship, which is given by (Fetter and Fetter Jr 1999):

$$s_e{}^* = K_d C^N \tag{4.61}$$

where N is the Freundlich exponent [-]. In general, The K_d and N in the Freundlich isotherm are determined by empirically fitting the measured data. Both linear and Freundlich isotherms assume that the capacity of the adsorption site is unlimited. However, it is not true in some applications. As a result, the Langmuir adsorption isotherm is developed to implement an upper limit of the adsorption site in the equation, which is presented as (Healy 1990):

$$s_e{}^* = \frac{K_d C}{1 + \eta_k C} \tag{4.62}$$

where η_k is the Langmuir adsorption constant [L^3M^{-1}]. It should be noted that the ADE implemented with the non-linear isotherm requires further mathematical effort to obtain the concentration in the solid phase, and thus VF_Sep only considered the linear isotherm in the modelling of adsorption.

By including the consideration of equilibrium adsorption, the ADE is rewritten as (Nielsen, Th. Van Genuchten and Biggar 1986):

$$\frac{\partial(\theta + \rho_b K_d)c}{\partial t} = \frac{\partial}{\partial z}\left[D_T \frac{\partial c}{\partial z} - qc\right] \tag{4.63}$$

where ρ_b is the bulk density [M L^{-3}]. The equation 4.66 can be solved directly using the given information since the relationship remains linear. The linear adsorption isotherm is widely applied in the simulation of solute transport due to its simple application (Healy 1990).

The kinetic adsorption can be presented as a first-order kinetic rate process with respect to the concentration in the solid phase and aqueous phase. The change of concentration in the solid phase of kinetic site with linear isotherm is obtained using the following equation (Nielsen, Th. Van Genuchten and Biggar 1986):

$$\frac{\partial s_k}{\partial t} = \omega_k (K_d c - s_k) \tag{4.64}$$

where s_k is the mass of adsorbed compound in kinetic site [M M^{-1}] and ω_k is the first-order rate constant for the kinetic adsorbed compound [-].

In most cases, the instantaneous equilibrium adsorption and kinetic adsorption occur simultaneously. Therefore, a two-site adsorption model was introduced to combine both adsorption sites. The total adsorbed mass-based concentration is given by:

$$s = s_e + s_k \tag{4.65}$$

where s is the total concentration in solid phase [M M^{-1}]. Accordingly, the equation 4.64 was added with a fractional coefficient f_E [-] to separate the instantaneous and kinetic adsorption process. Then, the modified transport equation with two-site adsorption to describe the transport of compounds in aqueous and solid phase, respectively, are presented as follows (Nielsen, Th. Van Genuchten and Biggar 1986):

$$\frac{\partial(\theta + f_E \rho_b K_d)c}{\partial t} = \frac{\partial}{\partial z}\left[D_T \frac{\partial c}{\partial z} - qc\right] - \rho_b \omega_k [(1 - f_E) K_d c - s_k] \tag{4.66}$$

$$\rho_b \frac{\partial s_k}{\partial t} = \rho_b \omega_k [(1 - f_E) K_d c - s_k] \tag{4.67}$$

It should be noted that if the model only considers the equilibrium adsorption in the transport mechanism, the f_E can be set to be 1 in the equation, while it is set to be 0 when the adsorption is dominated by the kinetic sorption site.

4.2.1.3. Dual-Porosity transport model with two-site adsorption in mobile phase

In the dual-porosity model, the domain of the transport has to be divided into the mobile and immobile regions:

$$\theta c = \theta_{Mobile} c_{Mobile} + \theta_{Immobile} c_{Immobile} \tag{4.68}$$

where θ is the total water content [L^3 L^{-3}], θ_{Mobile} is the mobile water content [L^3 L^{-3}], $\theta_{Immobile}$ is the immobile water content [L^3 L^{-3}], c is the total concentration [M L^{-3}], c_{Mobile} is the solute concentration in mobile region [M L^{-3}] and $c_{Immobile}$ is the solute concentration in immobile region [M L^{-3}]. In the mobile regions, the transport of

contaminants was simulated using the ADE. Then, the contaminants in the immobile regions were assumed to be stagnant and are only affected by the exchange term between mobile and immobile region. Therefore, the governing equation of dual-porosity transport can be expressed as follows:

$$\frac{\partial(\theta_{Mobile}c_{Mobile})}{\partial t} = \frac{\partial}{\partial z}\left[D_{T,Mobile}\frac{\partial c_{Mobile}}{\partial z} - q_{Mobile}c_{Mobile}\right] - \Gamma_s \tag{4.69}$$

$$\frac{\partial(\theta_{Immobile}c_{Immobile})}{\partial t} = \Gamma_s \tag{4.70}$$

where Γ_s is the exchange rate of contaminants between the mobile and immobile regions [M L^{-3} T^{-1}]. The exchange rate is determined by:

$$\Gamma_s = \alpha_{ph}(c_{Mobile} - c_{Immobile}) + \Gamma_w c^* \tag{4.71}$$

$$\begin{cases} c^* = c_{Mobile} & if\ \Gamma_w > 0 \\ c^* = c_{Immobile} & if\ \Gamma_w < 0 \end{cases} \tag{4.72}$$

where α_{ph} and Γ_w are the solute transfer coefficient [T^{-1}] and water exchange rate between the mobile and immobile region [$L^3L^{-3}T^{-1}$], respectively.

As mentioned in the last section, the adsorption was described in the equilibrium state and kinetic state. The adsorption in the immobile region was assumed to be under an instantaneous equilibrium condition. As for the mobile region, the two-site adsorption is implemented. The total adsorbed concentration *s* is then described as:

$$s = f_{Mobile}\left(s_{e,Mobile} + s_{k,Mobile}\right) + (1 - f_{Mobile})s_{Immobile} \tag{4.73}$$

where f_{Mobile} is the fraction of adsorption sites exposed to mobile water [-], $s_{e,Mobile}$ is the adsorbed concentration in equilibrium with the solution concentration in the mobile zone [M M^{-3}] and $s_{k,Mobile}$ is the adsorbed concentration of the kinetic sites exposed to the mobile water at equilibrium [M M^{-3}]. As a result, the complete dual-porosity solute transport module with two-site adsorption in mobile region is expressed as (Šimůnek et al. 2003):

$$\frac{\partial(\theta_{Mobile} + f_{Mobile}\rho_b f_E K_d)}{\partial t} c_{Mobile} = \frac{\partial}{\partial z}\left[D_{T,Mobile}\frac{\partial c_{Mobile}}{\partial z} - q_{Mobile}c_{Mobile}\right] - \Gamma_{s1} - \Gamma_{s2} - \emptyset_{Mobile} \quad (4.74)$$

where Φ_{Mobile} is the sink/ source term in the mobile regions [M L^{-3} T^{-1}]. Γ_{s1} represents the transfer rate between the mobile and immobile region [$ML^{-3}T^{-1}$]:

$$\Gamma_{s1} = \alpha_{ph}(c_{Mobile} - c_{Immobile}) + \Gamma_w c^* \quad (4.75)$$

Γ_{s2} stands for the mass transfer rate to the kinetic adsorption sites in the mobile region [M L^{-3} T^{-1}], which is given as:

$$\Gamma_{s2} = \omega_k \rho_i\left[(1 - f_E)K_d c_{Mobile} - s_{k,Mobile}\right] \quad (4.76)$$

The rate of change for concentration in the kinetic adsorption sites contacting with the mobile water is presented as:

$$\frac{\partial \rho_b s_k}{\partial t} = \Gamma_{s2} - \emptyset_{k,Mobile} \quad (4.77)$$

where $\emptyset_{k,Mobile}$ is the sink/source term for the adsorbed solute in kinetic adsorption site [M L^{-3} T^{-1}]. As for the immobile solute, the adsorption was only considered at equilibrium condition and, which is given by:

$$\frac{\partial[\theta_{Immobile} + (1 - f_{Mobile})\rho_b K_d]}{\partial t} c_{Immobile} = \Gamma_{s1} - \emptyset_{Immobile} \quad (4.78)$$

where $\emptyset_{Immobile}$ is the sink/source term in immobile regions [M L^{-3} T^{-1}].

4.2.2. Numerical implementation

Similar to the flow module, the one-dimensional reactive solute transport under the variably-saturated condition was numerically formulated using the finite difference method. The nodal discretization used in the proposed solute transport module was the same as that described for the flow module. By neglecting the adsorption term, the basic idea of the derivation was based on the mass balance approach, which is presented as:

$$\frac{\partial \theta_i c_i}{\partial t} = J_i|^+ - J_i|^- \tag{4.79}$$

where subscript i is the spatial node (positive downwards) and J is the total flux of solute (+ for outlet and – for inlet) [M L^{-3} T^{-1}], which is described as:

$$J_i|^+ = D_T \frac{\partial c}{\partial z}|^+ + qc|^+ \tag{4.80}$$

The Crank-Nicolson method were applied to approximate the ADE in terms of time-centred scheme, which is expressed as:

$$\frac{\partial \theta c}{\partial t} = \frac{1}{2}\frac{\partial}{\partial z}\left[D_T(\theta, q)\frac{\partial c}{\partial z} + qc\right]_i^{j+1} + \frac{1}{2}\frac{\partial}{\partial z}\left[D_T(\theta, q)\frac{\partial c}{\partial z} + qc\right]_i^{j} \tag{4.81}$$

A second-order finite difference approximation developed by Bresler (1973) for an ADE of non-reactive component under a variably-saturated condition showed that the temporal approximation was derived as follows:

$$\frac{\partial \theta c}{\partial t} = \theta_i^{j+\frac{1}{2}}\left(\frac{\partial c}{\partial t}\right)_i^{j+\frac{1}{2}} + c_i^{j+\frac{1}{2}}\left(\frac{\partial \theta}{\partial t}\right)_i^{j+\frac{1}{2}} \tag{4.82}$$

By using Taylor's series theorem, the approximation is obtained as:

$$\begin{aligned}\left[\frac{\partial \theta c}{\partial t}\right]_i^{j+\frac{1}{2}} = {} & \frac{\theta_i^{j+1}c_i^{j+1} - \theta_i^{j}c_i^{j}}{\Delta t} \\ & - \left\{\left[\frac{\Delta t}{8}\left(\theta_i^{j+1} - \theta_i^{j}\right)\right] V_i^{j+\frac{1}{2}}\left[V_{i+\frac{1}{2}}^{j+\frac{1}{2}}\left(\frac{c_{i+1}^{j+\frac{1}{2}} - c_i^{j+\frac{1}{2}}}{\Delta z^2}\right)\right.\right. \\ & \left.\left. - V_{i-\frac{1}{2}}^{j+\frac{1}{2}}\left(\frac{c_i^{j+\frac{1}{2}} - c_{i-1}^{j+\frac{1}{2}}}{\Delta z^2}\right)\right]\right\}\end{aligned} \tag{4.83}$$

where Δt is the temporal step, Δz is the spatial step (positive downwards), subscripts i denotes the spatial discretization from top surface layer and superscripts j demonstrates the temporal level. The V denotes the average interstitial flow velocity, which is computed as follow.

$$V_i^{j+\frac{1}{2}} = \frac{q_i^{j+\frac{1}{2}}}{\theta_i^{j+\frac{1}{2}}} \tag{4.84}$$

The second term on the right side of equation 4.83 is a correction term of truncation error from Taylor's series derivation up to second-order. As the term $\theta_i^{j+1} - \theta_i^j$ equals to zero when the porous medium is saturated, the correction term is only visible under unsaturated condition and the flux is relatively rapid. In addition, it appeared to be negligibly small when a fine temporal step was allocated in the numerical solution.

The dispersion term in ADE, which is a second-order derivative, is approximated as follows:

$$\begin{aligned}\frac{\partial}{\partial z}\left(D_T \frac{\partial c}{\partial z}\right)_i^{j+\frac{1}{2}} = \frac{1}{2}&\left[\frac{D_{T_{i+\frac{1}{2}}}^{j+1}}{\Delta z^2}\left(c_{i+1}^{j+1} - c_i^{j+1}\right) - \frac{D_{T_{i-\frac{1}{2}}}^{j+1}}{\Delta z^2}\left(c_i^{j+1} - c_{i-1}^{j+1}\right)\right] \\ &+ \frac{1}{2}\left[\frac{D_{T_{i+\frac{1}{2}}}^{j}}{\Delta z^2}\left(c_{i+1}^{j} - c_i^{j}\right) - \frac{D_{T_{i-\frac{1}{2}}}^{j}}{\Delta z^2}\left(c_i^{j} - c_{i-1}^{j}\right)\right]\end{aligned} \tag{4.85}$$

In order to develop an upper boundary condition for the infiltration case in ADE, a Cauchy (third-type) boundary condition was necessitated at the top of the domain. In Bresler (1973), a first space derivation was applied to the advection term and it has been found to be difficult to partition the inlet flux and outlet flux. This problem was due to the derivation of advection term in this numerical scheme, where a first space derivation was applied. Therefore, a modified second-order finite difference scheme was proposed to derive the advection term in the ADE. The detail derivation is presented in **Appendix B**. The time discretization was derived using Crank-Nicolsen scheme. The final equation is presented as follow.

$$\frac{\theta_i^{j+1}c_i^{j+1}-\theta_i^j c_i^j}{\Delta t} = \frac{1}{2}\left[\frac{D_{T_{i+\frac{1}{2}}}^{j+1}}{\Delta z^2}\left(c_{i+1}^{j+1}-c_i^{j+1}\right)-\frac{D_{T_{i-\frac{1}{2}}}^{j+1}}{\Delta z^2}\left(c_i^{j+1}-c_{i-1}^{j+1}\right)\right] + \frac{1}{2}\left[\frac{D_{T_{i+\frac{1}{2}}}^{j}}{\Delta z^2}\left(c_{i+1}^{j}-c_i^{j}\right)-\frac{D_{T_{i-\frac{1}{2}}}^{j}}{\Delta z^2}\left(c_i^{j}-c_{i-1}^{j}\right)\right] - \frac{1}{2}\left[\frac{q_{i+\frac{1}{2}}^{j+1}c_{i+\frac{1}{2}}^{j+1}-q_{i-\frac{1}{2}}^{j+1}c_{i-\frac{1}{2}}^{j+1}}{\Delta z}\right]-\frac{1}{2}\left[\frac{q_{i+\frac{1}{2}}^{j}c_{i+\frac{1}{2}}^{j}-q_{i-\frac{1}{2}}^{j}c_{i-\frac{1}{2}}^{j}}{\Delta z}\right] \tag{4.86}$$

The modified equation has to be expanded to include the mass transfer term, adsorption and sink/source term. The mass transfer between mobile region and immobile region is expressed as:

$$\Gamma_{i,S1} = \alpha_{ph,i}\left(c_{Mobile_i}^{j} - c_{Immobile_i}^{j}\right) + \Gamma_w c^{*j}_i \tag{4.87}$$

$$\begin{cases} c^* = c_{Mobile} & if\ \Gamma_w > 0 \\ c^* = c_{Immobile} & if\ \Gamma_w < 0 \end{cases} \tag{4.88}$$

It should be noted that this mass transfer term is a function of the concentration in the mobile and immobile regions at the previous temporal step. Therefore, this term was solved at the first place and was independent of the solution of mobile concentration. The derivation of the equilibrium adsorbed solute in the mobile phase is presented as:

$$\left(\rho_{b_i}K_{d_i}f_{Mobile_i}f_{E_i}\frac{\partial c_{Mobile_i}}{\partial t}\right)^{j+\frac{1}{2}} = \rho_{b_i}K_{d_i}f_{Mobile_i}f_{E_i}\frac{\left(c_{Mobile_i}^{j+1}-c_{Mobile_i}^{j}\right)}{\Delta t} \tag{4.89}$$

where the bulk density and distribution coefficient remain constant between temporal step. As for the solute adsorbed by kinetic site, the mass transfer term is given by:

$$\Gamma_{is2} = \omega_{k_i}\rho_{b_i}\left[\left(1 - f_{E_i}\right)K_{d_i}c_{Mobile_i}^{j+1} - s_{k,Mobile_i}^{j}\right] \tag{4.90}$$

The sink/source term in the equation was described as:

$$\left(\emptyset_{Mobile_i}\right)^{j+\frac{1}{2}} = \frac{1}{2}\left(k_i^{j+1}\theta_{Mobile,i}^{j+1} + k_i^{j}\theta_{Mobile,i}^{j}\right) \tag{4.91}$$

where *k* is the zero-order kinetic term (positive for source term and negative for sink term) [T^{-1}]. The similar derivation was applied to the sink/ source term in the immobile region. In the following derivation, the sink term was retained in the following equation to facilitate the presentation. The complete solute transport scheme for the mobile region is rearranged as:

$$\begin{aligned}
c_{Mobile_i}^{j+1}&\left[\frac{\theta_{Mobile_i}^{j+1}}{\Delta t} + \frac{\rho_i K_{d_i} f_{Mobile_i} f_{E_i}}{\Delta t} + \frac{D_{T_{i+\frac{1}{2}}}^{j+1}}{2\Delta z^2} + \frac{D_{T_{i-\frac{1}{2}}}^{j+1}}{\Delta z^2} - \frac{q_{i+\frac{1}{2}}^{j+1}}{4\Delta z} + \frac{q_{i-\frac{1}{2}}^{j+1}}{4\Delta z}\right.\\
&\left. + \omega_{k_i}\rho_{b_i}\left(1 - f_{E_i}\right)K_{d_i}\right] + c_{Mobile_{i+1}}^{j+1}\left(-\frac{D_{T_{i+\frac{1}{2}}}^{j+1}}{2\Delta z^2} + \frac{q_{i+\frac{1}{2}}^{j+1}}{4\Delta z}\right)\\
&+ c_{Mobile_{i-1}}^{j+1}\left(-\frac{D_{T_{i-\frac{1}{2}}}^{j+1}}{\Delta z^2} - \frac{q_{i-\frac{1}{2}}^{j+1}}{4\Delta z}\right)\\
&= c_{Mobile_i}^{j}\left(\frac{\theta_{Mobile_i}^{j}}{\Delta t} + \frac{\rho_i K_{d_i} f_{Mobile_i} f_{E_i}}{\Delta t} - \frac{D_{T_{i+\frac{1}{2}}}^{j}}{2\Delta z^2} - \frac{D_{T_{i-\frac{1}{2}}}^{j}}{\Delta z^2} + \frac{q_{i+\frac{1}{2}}^{j}}{4\Delta z} - \frac{q_{i-\frac{1}{2}}^{j}}{4\Delta z}\right)\\
&+ c_{Mobile_{i+1}}^{j}\left(\frac{D_{T_{i+\frac{1}{2}}}^{j}}{2\Delta z^2} - \frac{q_{i+\frac{1}{2}}^{j}}{4\Delta z}\right) + c_{Mobile_{i-1}}^{j}\left(\frac{D_{T_{i-\frac{1}{2}}}^{j}}{2\Delta z^2} + \frac{q_{i-\frac{1}{2}}^{j}}{4\Delta z}\right) - \Gamma_{i,S1}\\
&+ \omega_{k_i}\rho_{b_i}s_{k,Mobile_i}^{j} + \left(\emptyset_{Mobile_i}\right)^{j+\frac{1}{2}}
\end{aligned} \tag{4.92}$$

Similar to the flow module, the equation was implemented in MATLAB ® as a tri-diagonal matrix for each time step. The concentration in the mobile region at the latest temporal time step (*j+1*) was obtained using the tridiagonal matrix algorithm:

$$\begin{bmatrix} M_1 & U_1 & 0 & 0 & 0 & \cdots & \cdots & 0 & 0 & 0 \\ L_2 & M_2 & U_2 & 0 & 0 & \cdots & \cdots & 0 & 0 & 0 \\ 0 & L_3 & M_3 & U_3 & 0 & \cdots & \cdots & 0 & 0 & 0 \\ 0 & 0 & L_4 & M_4 & U_4 & \cdots & \cdots & 0 & 0 & 0 \\ 0 & 0 & 0 & L_5 & M_5 & \cdots & \cdots & 0 & 0 & 0 \\ \vdots & \vdots & \vdots & \vdots & \vdots & \ddots & \ddots & \vdots & \vdots & \vdots \\ \vdots & \vdots & \vdots & \vdots & \vdots & \ddots & \ddots & \vdots & \vdots & \vdots \\ 0 & 0 & 0 & 0 & 0 & \cdots & \cdots & M_{N-2} & U_{N-2} & 0 \\ 0 & 0 & 0 & 0 & 0 & \cdots & \cdots & L_{N-1} & M_{N-1} & U_{N-1} \\ 0 & 0 & 0 & 0 & 0 & \cdots & \cdots & 0 & L_N & M_N \end{bmatrix} \begin{bmatrix} c_{Mobile_1}^{j+1} \\ c_{Mobile_2}^{j+1} \\ c_{Mobile_3}^{j+1} \\ c_{Mobile_4}^{j+1} \\ c_{Mobile_5}^{j+1} \\ \vdots \\ \vdots \\ c_{Mobile_{N-2}}^{j+1} \\ c_{Mobile_{N-1}}^{j+1} \\ c_{Mobile_N}^{j+1} \end{bmatrix} = \begin{bmatrix} R_1 \\ R_2 \\ R_3 \\ R_4 \\ R_5 \\ \vdots \\ \vdots \\ R_{N-2} \\ R_{N-1} \\ R_N \end{bmatrix} \tag{4.93}$$

where

$$M_i = \frac{\theta_{Mobile_i}^{j+1}}{\Delta t} + \frac{\rho_i K_{d_i} f_{Mobile_i} f_{E_i}}{\Delta t} + \frac{D_{T_{i+\frac{1}{2}}}^{j+1}}{2\Delta z^2} + \frac{D_{T_{i-\frac{1}{2}}}^{j+1}}{\Delta z^2} - \frac{q_{i+\frac{1}{2}}^{j+1}}{4\Delta z} + \frac{q_{i-\frac{1}{2}}^{j+1}}{4\Delta z} + \omega_{k_i}\rho_{b_i}\left(1 - f_{E_i}\right)K_{d_i} \tag{4.94}$$

$$U_i = -\frac{D_{T_{i+\frac{1}{2}}}^{j+1}}{2\Delta z^2} + \frac{q_{i+\frac{1}{2}}^{j+1}}{4\Delta z} \tag{4.95}$$

$$L_i = -\frac{D_{T_{i-\frac{1}{2}}}^{j+1}}{\Delta z^2} - \frac{q_{i-\frac{1}{2}}^{j+1}}{4\Delta z} \tag{4.96}$$

$$\begin{aligned} R_i = c_{Mobile_i}^{j} \Bigg(& \frac{\theta_{Mobile_i}^{j}}{\Delta t} + \frac{\rho_i K_{d_i} f_{Mobile_i} f_{E_i}}{\Delta t} - \frac{D_{T_{i+\frac{1}{2}}}^{j}}{2\Delta z^2} - \frac{D_{T_{i-\frac{1}{2}}}^{j}}{\Delta z^2} + \frac{q_{i+\frac{1}{2}}^{j}}{4\Delta z} \\ & - \frac{q_{i-\frac{1}{2}}^{j}}{4\Delta z} \Bigg) + c_{Mobile_{i+1}}^{j} \left(\frac{D_{T_{i+\frac{1}{2}}}^{j}}{2\Delta z^2} - \frac{q_{i+\frac{1}{2}}^{j}}{4\Delta z} \right) \\ & + c_{Mobile_{i-1}}^{j} \left(\frac{D_{T_{i-\frac{1}{2}}}^{j}}{2\Delta z^2} + \frac{q_{i-\frac{1}{2}}^{j}}{4\Delta z} \right) - \Gamma_{i,S1} + \omega_{k_i}\rho_{b_i} s_{k,Mobile_i}^{j} \\ & + \left(\emptyset_{Mobile_i}\right)^{j+\frac{1}{2}} \end{aligned} \tag{4.97}$$

As for the concentration of solute in the immobile regions, the derivation was similar to ADE, but the movement was neglected since the water was assumed to be stagnant.

The concentration of contaminant in the immobile region is solved using the following transport equation:

$$c_{Immobile_i}^{j+1}\left[\frac{\theta_{Immobile_i}^{j+1}+\left(1-f_{Mobile_i}\right)\rho_{b_i}K_{d_i}}{\Delta t}\right] = c_{Immobile_i}^{j}\left[\frac{\theta_{Immobile,i}^{j}+\left(1-f_{Mobile_i}\right)\rho_{b_i}K_{d_i}}{\Delta t}-\alpha_{ph,i}\right] + \alpha_{ph,i}c_{Mobile_i}^{j}+\Gamma_w c^{*j}_i+\left(\emptyset_{Immobile_i}\right)^{j+\frac{1}{2}} \quad (4.98)$$

where the sink term $\emptyset_{Immobile}$ is similar to equation 4.91.

As for the solid phase in the immobile region, only the equilibrium adsorption was considered, which is presented as:

$$\rho_{b_i}\left(\frac{s_{k_i}^{j+1}-s_{k_i}^{j}}{\Delta t}\right)=\omega_{k_i}\rho_{b_i}\left[\left(1-f_{E_i}\right)K_{d_i}c_{Mobile_i}^{j+1}-s_{k_i}^{j}\right]-\left(\emptyset_{sorbed}\right)_i^{j+\frac{1}{2}} \quad (4.99)$$

where the $c_{Mobile_i}^{j+1}$ was obtained from the result of 4.93. On the other hand, the sink term in the equation is described as:

$$\left(\emptyset_{sorbed}\right)^{j+\frac{1}{2}}=\frac{\rho_{b_i}\left(k_i^{j+1}s_{k_i}^{j+1}+k_i^{j}s_{k_i}^{j}\right)}{2} \quad (4.100)$$

4.2.3. Initial and boundary conditions

The initial conditions of the concentrations of solute in the mobile and immobile regions, as well as the adsorbed solute within the boundaries is self-defined as:

$$c_{Mobile}(i,t)=c_{Mobile_0}(i)\,,\quad i=0\ldots N, t=t_0 \quad (4.101)$$

$$c_{Immobile}(i,t)=c_{Immobile_0}(i)\,,\quad i=0\ldots N, t=t_0 \quad (4.102)$$

$$s_k(i,t)=s_{k_0}(i)\,,\quad i=0\ldots N, t=t_0 \quad (4.103)$$

For the top boundary conditions, the wetland surface (*z=0*) is under infiltration, and thus a Cauchy boundary condition was employed:

$$q_{i=0}^{j} c_{i=0}^{j} - D_{T}{}_{i=0}^{j} \left(\frac{\Delta c_{i=0}^{j}}{\frac{\Delta z}{2}} \right) = q_{i=0}^{j} C_{0}^{j} \tag{4.104}$$

where C_0 is the concentration of the contaminant in the inlet water applied to the wetland bed [M L^{-3}]. The term at the right-hand side is regarded as the inlet flux. Accordingly, equation 4.94 – 4.97 at $i=0$ was modified as follows.

$$M_{i=0} = \frac{\theta_{Mobile}{}_{i}^{j+1}}{2\Delta t} + \frac{\rho_{b_i} K_{d_i} f_{Mobile_i} f_{E_i}}{2\Delta t} + \frac{D_{T}{}_{i+\frac{1}{2}}^{j+1}}{2\Delta z_{top}{}^{2}} - \frac{q_{i+\frac{1}{2}}^{j+1}}{4\Delta z_{top}} + \frac{\omega_{k_i}(1 - f_{E_i}) K_{d_i}}{2} \tag{4.105}$$

$$U_{i=0} = -\frac{D_{T}{}_{i+\frac{1}{2}}^{j+1}}{2\Delta z_{top}{}^{2}} + \frac{q_{i+\frac{1}{2}}^{j+1}}{4\Delta z_{top}} \tag{4.106}$$

$$\begin{aligned} R_{i=0} = {} & c_{Mobile}{}_{1}^{j} \left(\frac{\theta_{Mobile}{}_{i}^{j}}{\Delta t} + \frac{\rho_{b_i} K_{d_i} f_{Mobile_i} f_{E_i}}{\Delta t} - \frac{D_{T}{}_{i+\frac{1}{2}}^{j}}{2\Delta z_{top}{}^{2}} + \frac{q_{i+\frac{1}{2}}^{j}}{4\Delta z_{top}} \right) \\ & + c_{Mobile}{}_{i+1}^{j} \left(\frac{D_{T}{}_{i+\frac{1}{2}}^{j}}{2\Delta z_{top}{}^{2}} - \frac{q_{i+\frac{1}{2}}^{j}}{4\Delta z_{top}} \right) \\ & - \left(\frac{q_{i=o}^{j+1} c_{i=o}^{j+1}}{2} + \frac{q_{i=o}^{j} c_{i=o}^{j}}{2} \right) - \Gamma_{i,S1} + \omega_{k_i} \rho_{b_i} s_{k,Mobile}{}_{i}^{j} \\ & + \frac{1}{2} \left(\emptyset_{Mobile_{i=0}} \right)^{j+\frac{1}{2}} \end{aligned} \tag{4.107}$$

The boundary condition at the bottom of the domain was set to be freely-drained. Therefore, the following condition must be satisfied:

$$\frac{\partial c}{\partial z} = 0 \tag{4.108}$$

Accordingly, the associated equation is presented as:

$$c_{N+1}^{j} = c_{N}^{j} \tag{4.109}$$

The equation 4.94 – 4.97 at *i*=N was then modified to become:

$$M_{i=N} = \frac{\theta_{Mobile_i}^{j+1}}{2\Delta t} + \frac{\rho_{b_i} K_{d_i} f_{Mobile_i} f_{E_i}}{2\Delta t} + \frac{D_{T_{i-\frac{1}{2}}}^{j+1}}{2\Delta z^2} + \frac{q_{i-\frac{1}{2}}^{j+1}}{4\Delta z} - \frac{q_{i=N}^{j+1}}{2\Delta z} + \frac{\omega_{k_i}\rho_{b_i}(1 - f_{E_i})K_{d_i}}{2} \tag{4.110}$$

$$L_{i=N} = -\frac{D_{T_{i-\frac{1}{2}}}^{j+1}}{2\Delta z^2} - \frac{q_{i-\frac{1}{2}}^{j+1}}{4\Delta z} \tag{4.111}$$

$$R_{i=N} = c_{Mobile_i}^{j}\left[\frac{\theta_{Mobile,i}^{j}}{2\Delta t} + \frac{\rho_i K_{d_i} f_{Mobile_i} f_{E_i}}{2\Delta t} - \frac{D_{T_{i-\frac{1}{2}}}^{j}}{2\Delta z^2} - \frac{q_{i-\frac{1}{2}}^{j}}{4\Delta z} + \frac{q_{i=N}^{j}}{2\Delta z}\right] + c_{Mobile_{i-1}}^{j}\left(-\frac{D_{T_{i-\frac{1}{2}}}^{j}}{2\Delta z^2} - \frac{q_{i-\frac{1}{2}}^{j}}{4\Delta z}\right) - \Gamma_{i,S1} + \omega_{k_i} s_{k,Mobile_i}^{j} + \frac{1}{2}\left(\emptyset_{Mobile_{i=N}}\right)^{j+\frac{1}{2}} \tag{4.112}$$

4.2.4. Stability constraints

One of the drawbacks of the numerical solutions of the transport equations is the numerical dispersion, which is also known as oscillatory behaviour in the simulation (Šimunek, van Genuchten and Sejna). The problem could be significant when the transport mechanism is dominated by the advection and the effect of dispersion is minor. The undesired numerical dispersion can be prevented by optimizing the space and time discretization. In order to ensure a robust simulation, a set of stability criterion was implemented in the model to evaluate the level of numerical dispersion with the prescribed discretization.

Two dimensionless criteria were used to determine the level of numerical dispersion of the solution. The first criterion is the Courant number (*Cr*), which determines whether the space between two spatial coordinates is sufficient to describe the

maximum magnitude of velocity with the prescribed temporal discretization (Courant, Friedrichs and Lewy 1928). The equation is presented as:

$$Cr = \frac{q\Delta t}{\Delta z} \tag{4.113}$$

where q denotes the water flux [LT^{-1}], Δt is the duration of temporal discretization [T] and Δz is the size of spatial discretization [L]. The maximum value of Cr should be below 1 to eliminate numerical dispersion.

The second criterion is the Peclet number (Pe). Pe is the ratio between advection and dispersion, which is a useful indicator to illustrate the principal transport mechanisms in the simulation. The governing equation is expressed as:

$$Pe = \frac{q\Delta z}{\theta D} \tag{4.114}$$

where θ is the water content [-] and D is the dispersivity [LT^{-2}]. A higher Pe means that the transport is dominated by the dispersion. To ensure a stable simulation, the Pe should be maintained at a low value, and thus a finer spatial discretization should be adopted to control the number. In this study, the allowable Pe is limited to be below 5.

4.3. Kinetics module

In VF_Sep, the kinetics of particular contaminants were compiled with the transport module to predict its fate throughout the substrate. This kinetics module was linked to the solute transport module as a sink/source term ($\emptyset$). In the pilot-scale VFCW system, the treatment was achieved by a number of physical and biochemical processes that occurs simultaneously during percolation. The major transformation and degradation processes of nitrogenous compounds have been introduced in section 2.3. As these processes generally exhibit a non-linear characteristic and interact with each other, the first-order reaction rate might be oversimplified to simulate the treatment performance (Zhang et al. 2015). On the other hand, the physical filtration is the main mechanism for the deposition of particulate contaminants. A simple first-order coefficient was used to account the removal rate with influent flux. The nitrogen uptake by vegetation was considered in the proposed system, where such removal is described as a function of water uptake.

4.3.1. Bio-kinetic module

The biochemical processes are the main mechanisms in the VFCW to remove organic carbon and nitrogen constituted in the raw septage. These processes are accomplished by the growth and metabolism of active biomass, which is categorized into heterotrophic and autotrophic biomass (Gujer et al. 1999). In general, the biological activity is categorized into aerobic, anoxic and anaerobic processes. The aerobic environment is the most favourable condition to stimulate biological activity (Tchobanoglous et al. 2003; Von Sperling 2007).

The VFCW is globally accepted as an aerobic reactor that efficiently carries out the aerobic decomposition of organic matter and nitrification of NH_4^+-N (Kadlec and Wallace 2008; Vymazal 2007). According to the preliminary study with regards to the oxygen content in a laboratory-scale VFCW, the amount of DO content and the level of oxidation-reduction potential (ORP) in the effluent revealed a similar outcome as it characterized a promising aeration capacity in the system.

The growth of heterotrophic biomass is a naturally-occurring process that decomposes the biodegradable organic compounds to obtain carbon and energy. The organic compound consumed by the biomass is known as the substrate in the process. Its fraction of the amount of biomass in the treatment unit is a crucial parameter for the treatment performance. As an electron acceptor is essential in the process, the development of heterotrophic biomass is sensitive to the oxygen condition in the reactor (Guan et al. 2015; Zhou et al. 2009). Under aerobic conditions, oxygen serves as the terminal electron acceptor. At the time that the oxygen content is low in the system, NO_3^--N plays as the electron acceptor. It is converted into dinitrogen at the end of the process, and thus the decomposition of organic compounds under anoxic conditions is commonly known as denitrification process. When the electron acceptor is absent in the system, anaerobic fermentation will take place and the energy is obtained from the formation of methane (Tchobanoglous et al. 2003). As the VFCW has an excellent re-aeration capacity, anoxic and anaerobic conditions are seldom observed during treatment (Tan et al. 2015).

Autotrophic biomass obtains the energy and carbon source from the oxidation of NH_4^+-N and the reduction of carbon dioxide, respectively (Tchobanoglous et al. 2003). Due to the absence of a substrate in the process, the activity of autotrophic biomass is

generally slow compared to heterotrophic biomass. Its growth, which is commonly known as nitrification, only occurs with sufficient supply of oxygen and alkalinity.

The growth of heterotrophic and autotrophic biomass require NH_4^+-N as a complementary nutrient source to deliver cell synthesis. On the other hand, the biomass debris is produced simultaneously due to the lysis of active biomass. Such accumulation of biomass debris in the treatment unit potentially reduces the viability of treatment.

Due to the complexity of interactive biochemical processes in the VFCWs, a Gujer matrix (Gujer et al. 1999) was employed to develop the bio-kinetics module. This method coupled the stoichiometric relationship, Monod kinetics and composition parameter to correlate the total amount of products to the total mass of reactants in the biological wastewater treatment. This method provided a comprehensive relation of conversion between the components that subjects to the processes including biomass growth and decay, nitrification and denitrification, and hydrolysis. The proposed bio-kinetics module is a simplified version of ASM2D (Henze et al. 1999) and ASM3 (Gujer et al. 1999). As the latest version of ASM, ASM3 is referred as the standard bio-kinetics module in this study, which consists of thirteen components and twelve processes to predict oxygen consumption, sludge production, nitrification and denitrification in the activated sludge system. In VF_Sep, the number of components and processes were reduced to eleven and six, respectively.

4.3.1.1. Components

The components in the bio-kinetic modules were categorized into soluble (S_X) and particulate (X_X) components. The particulate components are defined as the compounds that will be trapped on 0.45μm membrane filters (Gujer et al. 1999). A total of eleven components were included in VF_Sep, encompassing seven soluble components and four particulate components. In order to reduce individual requirements, cell internal storage products of heterotrophic organisms and total suspended solids (TSS) as in the ASM3 were excluded in the proposed bio-kinetics module. The transport of S_X and X_X were simulated using the ADE as described in section 4.2. Nevertheless, the heterotrophic and autotrophic biomass were assumed to be stationary biofilm in the wetland bed. Table 4.1 presents the summary of the descriptions of each component.

Table 4.1: Components in bio-kinetics module

Components	Description
	Soluble components
C1-S_O [M(O_2) L^{-3}]	Dissolved oxygen, which governs all the aerobic processes in the controlled volume.
C2- S_I [M(COD) L^{-3}]	Inert soluble organic matter, which mainly represents the organic matter that cannot be further degraded by any biochemical process in the system. S_I enters the system with influent and is also the product of hydrolysis of particulate biodegradable organic matter (X_S).
C3-Ss [M(COD) L^{-3}]	Readily biodegradable organic matter is the organic matter (carbon and nitrogen) that can be directly consumed by the heterotrophic biomass for their growth.
C4- S_{NH} [M(N) L^{-3}]	Ammonium plus ammonia nitrogen (NH_4^+-N and NH_3-N, respectively) acts as the nitrogen source in both aerobic and anoxic microbial processes. To ease the balance of ionic charges, the module assumed that the NH_4^+-N dominates in the processes. The breakdown of biodegradable organic matter and the decay of microorganisms release a certain amount of S_{NH} to the system. In the microbial processes, the existence of ammonium is important as it serves as the complementary nutrient.
C5- S_{N2} [M(N) L^{-3}]	Dinitrogen (N_2) is the product of denitrification.
C6- S_{NO} [M(N) L^{-3}]	Nitrate nitrogen (NO_3^--N) is the product of nitrification. Under the anoxic condition, S_{NO} acts as the electron acceptor in the growth of heterotrophic biomass.
C7- S_{HCO} [mole(HCO_3^-) L^{-3}]	In the modelling of wastewater treatment, alkalinity is a parameter to identify the ability to adsorb hydrogen ions.

Table 4.1: Components in bio-kinetics module (cont.)

Components	Description
	Particulate components
C8- X_I [M(COD) L^{-3}]	The inert particulate organic matter is incapable of being degraded by any microbial process in the system. Such particulate components are the product from the lysis of active biomass, which accumulates in the system and ultimately reduce the viability of treatment.
C9- X_S [M(COD) L^{-3}]	Slowly biodegradable particulate organic matter is converted to the soluble form by hydrolysis, where the soluble inert and biodegradable organic matter (S_I and S_S, respectively) are the final products in the process.
C10- X_H [M(COD) L^{-3}]	Heterotrophic biomass consumes biodegradable organic compounds to obtain energy and carbon for the growing process. The oxygen serves as the terminal electron acceptor under aerobic environment while the nitrate
C11 X_A [M(COD) L^{-3}]	Autotrophic biomass uses the inorganic compounds as an energy source and carbon dioxide as a carbon source for cell synthesis.

The unit used to present the components in the proposed bio-kinetics module is the same as ASM3 (Gujer et al. 1999). It should be noted that chemical oxygen demand (COD), which is a parameter that quantifies the available electrons in a sample, is used to represent the organic matter and biomass in the system. When the decomposition of organic matter takes place, these electrons are consumed by biomass formation or combined by the terminal electron acceptor. As a result, it is practical to express the concentration of organic matter and biomass using COD. On the other hand, the content of nitrogenous compounds is expressed using nitrogen (N), while the unit of alkalinity is the molar concentration of bicarbonate (HCO_3^-).

The proposed bio-kinetics module lumped the content of Org-N under the category of organic matter [M(COD) L^{-3}]. In organic matter (S_S, S_I, X_S and X_I) and biomass (X_H, and X_N), a composition parameter was used to quantify the amount of nitrogen content in per unit of organic matter, which serves as a conversion factor in the following stoichiometry calculation. The same concept was applied to identify the total suspended solids content in organic matter and biomass. Table 4.2 presents the composition parameters of nitrogen and suspended solids in organic matter and biomass.

4.3.1.2. Reactions

The proposed module consists of six aerobic and anoxic biological processes. The processes in the module are categorized into (a) hydrolysis, (b) heterotrophic processes (denitrification), and (c) autotrophic processes (nitrification). As the cell internal storage was not considered in the proposed module, four processes including the storage of COD and decay of cell internal storage were removed. In addition, the decay of biomass was described as a lysis process, which was not affected by the electron acceptor in the process. Accordingly, the proposed bio-kinetics provides a simple platform to predict the oxygen consumption, decomposition of organic matter, nitrification, and denitrification in VFCW. All of these processes were expressed using Monod-type rate equations. The definition and unit of kinetic parameters used in this module are stated in Table 4.3.

- **Hydrolysis**: Hydrolysis is the solubilisation of slowly particulate biodegradable substrates (X_S) (Grady Jr et al. 2011). Ammonification, where ammonium (S_{NH}) is released from the decomposition of organic matter containing nitrogen, is lumped in this reaction. The occurrence of hydrolysis is

Table 4.2: Composition parameters

	Composition Parameters	Unit
i_{NSI}	**Nitrogen Content in S_I**	$mg_N\ mg_{SI}^{-1}$
i_{NSS}	**Nitrogen Content in S_S**	$mg_N\ mg_{SS}^{-1}$
i_{NXS}	**Nitrogen Content in X_S**	$mg_N\ mg_{XS}^{-1}$
i_{NXI}	**Nitrogen Content in X_I**	$mg_N\ mg_{XI}^{-1}$
i_{NBM}	**Nitrogen Content in Biomass**	$mg_N\ mg_{BM}^{-1}$

Table 4.3: Kinetic parameters

Parameter	Description	Unit
k_H	Hydrolysis rate constant	d^{-1}
K_X	Saturation coefficient for hydrolysis	$mg_{XS}\ mg_{BM}^{-1}$
	Heterotrophic Organisms, Denitrification	
μ_H	Maximum growth rate on substrate	d^{-1}
η_{NO}	Anoxic reduction Factor	-
$K_{H,O}$	Saturation/ Inhibition coefficient for DO	$mg_{SO}\ l^{-1}$
$K_{H,S}$	Saturation coefficient for substrate	$mg_{SS}\ l^{-1}$
$K_{H,NO}$	Saturation coefficient for NO_3^--N	$mg_{SNO}\ l^{-1}$
$K_{H,NH}$	Saturation coefficient for NH_4^+-N	$mg_{SNH}\ l^{-1}$
$K_{H,HCO}$	Saturation coefficient for alkalinity	$mole_{SHCO}\ l^{-1}$
b_H	Rate constant for lysis	d^{-1}
	Autotrophic Organisms, Nitrification	
μ_A	Maximum growth rate on NH_4^+-N	d^{-1}
$K_{A,O}$	Saturation/ Inhibition coefficient for DO	$mg_{SO}\ l^{-1}$
$K_{A,NH}$	Saturation coefficient for NH_4^+-N	$mg_{SNH}\ l^{-1}$
$K_{A,HCO}$	Saturation coefficient for alkalinity	$mole_{SHCO}\ l^{-1}$
b_A	Rate constant for lysis	d^{-1}

assumed to be independent of the availability of oxygen and electron donors. The rate expression of hydrolysis is a modified Monod equation, where the rate is controlled by the ratio of particulate biodegradable substrates to heterotrophic biomass instead of the concentration of particulate substrate concentration:

$$P_1 = k_H \left(\frac{\frac{X_S}{X_H}}{K_X + \frac{X_S}{X_H}} \right) X_H \tag{4.115}$$

- **Aerobic growth of heterotrophic biomass**: The aerobic synthesis of X_H relies on the digestion of the soluble biodegradable organic matter (S_S) for the carbon sources. Meanwhile, dissolved oxygen (S_O) is consumed as the terminal electron acceptor in the process. As the development of heterotrophic bacteria depends on binary fission (Water Environment Federation, Federation and Institute 2005), the rate of growth is correlated to the concentration of active

biomass in the existing active biomass. Thus, the maximum growth rate coefficient, $\widehat{\mu_H}$ is a first-order rate coefficient. The growth rate is influenced by the concentration of readily biodegradable organic matter (S_S), dissolved oxygen (S_O) and ammonium (S_{NH}). S_{NH} is the complementary nutrient in the process to stimulate protein synthesis. Furthermore, alkalinity (S_{HCO}) is included as an effect of pH to the efficiency of biological activity. The Monod-type rate expression with iterative multiple limiting reagent of this process is presented as:

$$P_2 = \widehat{\mu_H}\left(\frac{S_O}{K_{H,O}+S_O}\right)\left(\frac{S_S}{K_{H,S}+S_s}\right)\left(\frac{S_{NH}}{K_{H,NH}+S_{NH}}\right)\left(\frac{S_{HCO}}{K_{H,HCO}+S_{HCO}}\right)X_H \quad (4.116)$$

- **Anoxic growth of heterotrophic biomass**: The anoxic growth of heterotrophic biomass is similar to the circumstances under aerobic condition, except that the nitrate (S_{NO}) replaces the dissolved oxygen (S_O) to act as the terminal electron acceptor. Such heterotrophic growth leads to nitrate reduction and thus it is also known as the denitrification. An inhibition term of dissolved oxygen was added to the rate expression to ensure that the rate is only significant under the condition of low S_O concentration. The rate of anoxic growth is relatively slow compared to aerobic growth, where an anoxic reduction factor η_{NO} was involved in the rate expression to diminish $\widehat{\mu_H}$:

$$P_3 = \widehat{\mu_H}\eta_{NO}\left(\frac{K_{H,O}}{K_{H,O}+S_O}\right)\left(\frac{S_{NO}}{K_{H,NO}+S_{NO}}\right)\left(\frac{S_S}{K_{H,S}+S_s}\right)\left(\frac{S_{NH}}{K_{H,NH}+S_{NH}}\right)X_H \quad (4.117)$$

- **Lysis of heterotrophic biomass**: The lysis considers all the losses of heterotrophs and the associated energy requirement. A traditional decay approach was used to describe the loss of active biomass as it was fully ultimately decomposed into a certain amount of biomass debris, including slowly biodegradable and inert organic matter. Ammonium (S_{NH}) is released during the decomposition. The specific rate is presented as a first-order equation

$$P_4 = b_{H,O2}X_H \quad (4.118)$$

- **Growth of autotrophic biomass**: The autotrophic biomass (X_A) was assumed to incorporate all nitrifying bacteria (*Nitrosomonas* and *Nitrobacter*) to ease the modelling. Nitrifying bacteria consumes carbon dioxide to obtain the carbon for cell synthesis and oxidizes ammonium (S_{NH}) to nitrite (S_{NO}) in order to gain the required energy for the microbial activity, where the process is also known as nitrification. Due to the energy restriction in metabolism as well as the usage of carbon dioxide as a carbon source for cell synthesis, the specific growth rate of autotrophic bacteria is commonly slower than heterotrophic bacteria (Grady Jr et al. 2011). This study considered the nitrification as a single step reaction. As mentioned in the previous section, autotrophs are the obligate aerobic bacteria, which use oxygen as the terminal electron acceptor. The rate expression was presented as:

$$P_5 = \widehat{\mu_A}\left(\frac{S_O}{K_{A,O} + S_O}\right)\left(\frac{S_{NH}}{K_{A,NH} + S_{NH}}\right)\left(\frac{S_{HCO}}{K_{A,\ HCO} + S_{HCO}}\right)X_A \qquad (4.119)$$

- **Lysis of autotrophic biomass:** The circumstances of aerobic endogenous respiration of autotrophic biomass is similar to the description as in **Lysis of heterotrophic biomass**.

$$P_6 = b_{A,O}X_A \qquad (4.120)$$

4.3.1.3. Stoichiometry matrix

The stoichiometry matrix was used to quantify the relation between each component and the associated processes. The coefficients in the matrix were determined by means of mass conservation approach, where a positive sign indicated “production of component” in the process and negative sign means “consumption of component”. Figure 4.7 illustrates a general relationship between the components concerned in this bio-kinetics module. Table 4.4 introduces the stoichiometric parameters used in the module.

The hydrolysis decomposes X_S into S_S and S_I. In the stoichiometry matrix, the variation between components was described as the production of S_S and S_I from per unit of X_S decomposed, where a fraction parameter f_{SI} is utilized to quantify the amount of two products in hydrolysis. The coefficient of S_{NH} is proportional to the production and consumption in the process, where the S_{NH} is released from the decomposition of

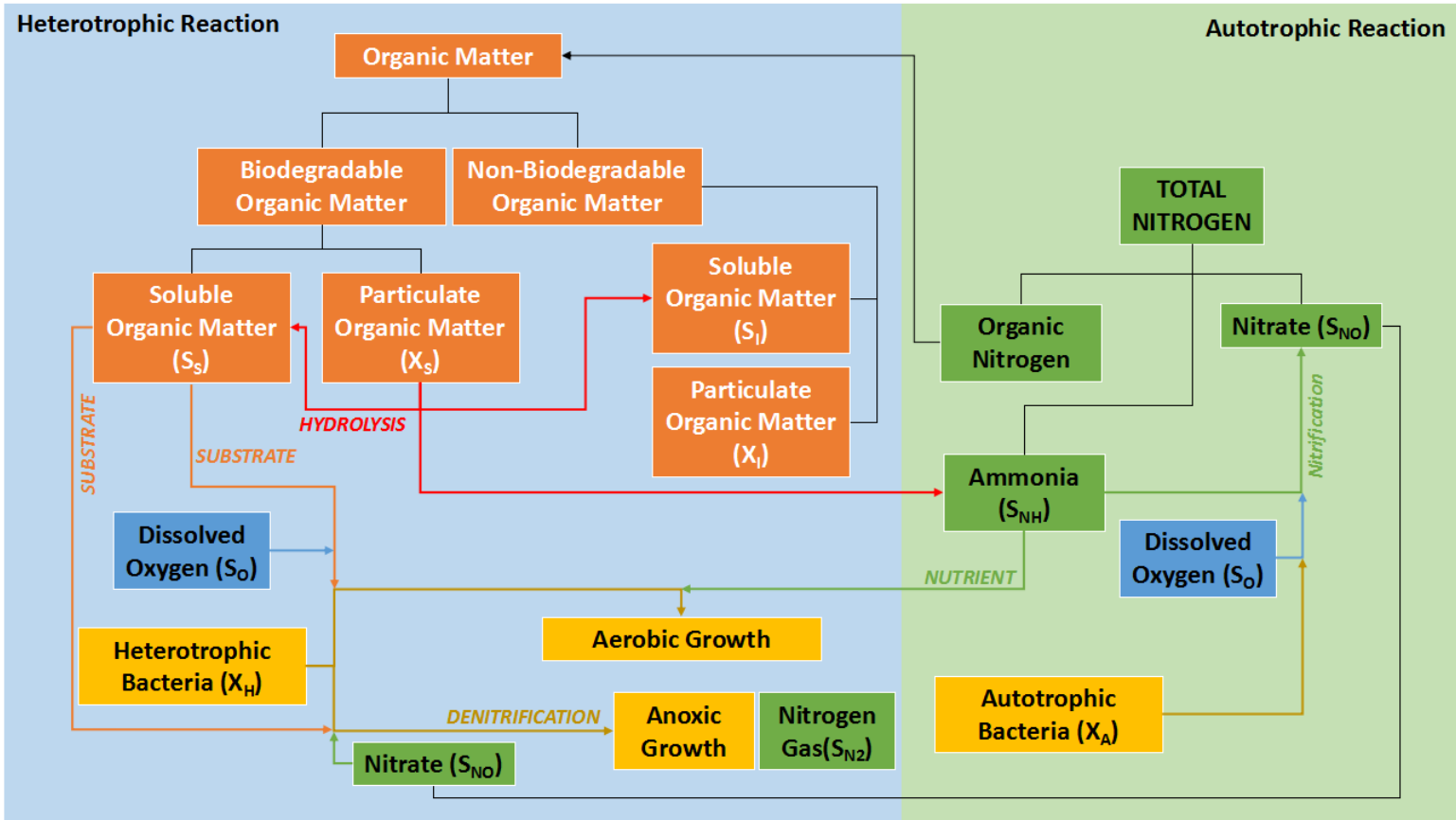

Figure 4.7: The conceptual relationship between the components

Table 4.4: Stoichiometric parameters

	Stoichiometric Parameters	**Unit**
f_{SI}	Fraction of S_I in hydrolysis	$mg_{SI}\ mg_{XS}^{-1}$
f_{XI}	Production of X_I in lysis	$mg_{XI}\ mg_{BM}^{-1}$
$Y_{H,O}$	Aerobic Yield of Heterotrophic Biomass	$mg_{XH}\ mg_{SS}^{-1}$
$Y_{H,NO}$	Anoxic Yield of Heterotrophic Biomass	$mg_{XH}\ mg_{SS}^{-1}$
Y_A	Yield of Autotrophic Biomass	$mg_{XA}\ mg_{NH}^{-1}$

X_S and is subsequently used in the formation of S_S and S_I. The composition parameters as introduced in Table 4.2 are subjected to the matrix to determine the coefficient of S_{NH}.

In general case, the rate of biomass growth is proportion to the amount of substrate decomposed. The process was expressed using a true growth yield factor *Y* to estimate the production of biomass from per unit of substrate consumed. In this bio-kinetics module, three true yield factors were involved, including the aerobic yield of heterotrophic biomass ($Y_{H,O}$), the anoxic yield of heterotrophic biomass ($Y_{H,NO}$), and the yield of autotrophic biomass (Y_A). The substrate consumed by the heterotrophic biomass and autotrophic biomass are S_S and S_{NH}, respectively.

The relation between the production of biomass and the consumption of substrate and electron acceptor was described based on per unit of biomass produced. For an example, the stoichiometric coefficient of heterotrophic biomass in the process of aerobic growth was set to be 1. Then, the coefficient for the consumption of S_S and terminal electron acceptor (S_O) were described as the inverse of yield factor, which were $-\frac{1}{Y_{H,O}}$ and $1-\frac{1}{Y_{H,O}}$, respectively.

Under anoxic conditions, S_{NO} serves as the terminal electron acceptor. The common approach to present the stoichiometric coefficient of the nitrogenous component is by using oxygen equivalence. Therefore, it has a conversion factor of 2.86 mg O_2/ mg N as the oxidation state changed from –III to 0 (Tchobanoglous et al. 2003). The stoichiometric coefficient of S_{NO} was expressed using negative sign to describe the consumption. S_{NH} plays as a nutrient source in the formation of new X_H. Nevertheless, a certain amount of S_{NH} is released from the decomposition of S_S.

The value of yield factors of heterotrophic biomass relies on the substrate, biomass population, and environmental factors. The range of true yield values used in the biological treatment model is wide. The maximum fraction of X_H (COD) produced from per unit of S_S (COD) digested is commonly 0.75, where the remaining Ss is used as the energy source for synthesis (Grady Jr et al. 2011). In addition, the energy used for the metabolism and lysis of biomass might result in the features of biological treatment, where the first is that the observed yield is always lower compared to the true yield and the second is that not all the biomass is active and viable in the treatment mechanisms (Grady Jr et al. 2011).

In the nitrification process, S_{NH} serves as an energy source. On the other hand, the carbon source (CO_2) was assumed to be plentiful in the environment. The change of oxidation state in nitrification is from +V to –III, which resulted in a reduction factor of 4.57 mg to the stoichiometric coefficient of S_O. The yield factor of autotrophic biomass is typically low compared to the heterotrophic biomass.

The lysis of biomass was expressed on the basis of the first-order equation. A production factor f_{XI} was implemented to quantify the production of X_I from per unit of biomass decayed. Then, the remaining of organic matter released from the decomposition was considered as X_S. Meanwhile, a small amount of S_{NH} is released during the process.

The alkalinity is essential in the nitrification process. In this bio-kinetic module, the coefficient of production and consumption of alkalinity was determined from the dynamics of nitrogenous components, S_{NH}, S_{N2} and S_{NO}, based on the unit of ionic charge mole. Hydroxides, carbonates, and bicarbonates of various inorganic matter are the common measure of the alkalinity in wastewater treatment. An equivalence of calcium carbonate ($CaCO_3$) is a typical unit for the alkalinity in wastewater treatment. Accordingly, a stoichiometry matrix is structured and described in Table 4.5. The numerical implementation of bio-kinetics module to the transport module is described in section 4.3.4.

4.3.2. Surface filtration

The excellent solid deposition in the pilot-scale VFCW-based septage treatment system shows its remarkable ability of surface filtration. Such physical filtration is a rapid mechanism to remove particles from the liquid phase when the influent passes

Table 4.5: Stoichiometry matrix of bio-kinetics module

	C1 S_O (mg O_2)	C2 S_I (mg COD)	C3 S_S (mg COD)	C4 S_{NH} (mg N)	C5 S_{N2} (mg N)	C 6 S_{NO} (mg N)	C7 S_{HCO} (Mole)	C8 X_I (mg COD)	C9 X_S (mg COD)	C10 X_H (mg COD)	C11 X_A (mg COD)
P1: Hydrolysis	-	f_{SI}	$1-f_{SI}$	$i_{NXS}-f_{SI}\cdot i_{NSI}-(1-f_{SI})\cdot i_{NSS}$	-	-	z_1	-	-1	-	-
Heterotrophic Organisms, Denitrification											
P2: Aerobic Growth	$1-\frac{1}{Y_{H,O2}}$	-	$-\frac{1}{Y_{H,O2}}$	$\frac{1}{Y_{H,O2}}\cdot i_{NSS}-i_{NBM}$	-	-	z_2	-	-	1	-
P3: Anoxic Growth	-	-	$-\frac{1}{Y_{H,NO}}$	$\frac{1}{Y_{H,NO}}\cdot i_{NSS}-i_{NBM}$	$\frac{1-Y_{H,NO}}{2.86\cdot Y_{H,NO}}$	$\frac{Y_{H,NO}-1}{2.86\cdot Y_{H,NO}}$	z_3	-	-	1	-
P4: Lysis	-	-	-	$i_{NBM}-f_{XI}\cdot i_{NXI}$	-	-	z_4	f_{XI}	-	-1	-
Autotrophic Organisms, Nitrification											
P5: Nitrification	$1-\frac{4.57}{Y_A}$	-	-	$-\frac{1}{Y_A}-i_{NBM}$	-	$\frac{1}{Y_A}$	z_6	-	-	-	1
P6: Lysis	$f_{XI}-1$	-	-	$i_{NBM}-f_{XI}\cdot i_{NXI}$	-	-	z_7	f_{XI}	-	-	-1
Composition Matrix											
COD (mg COD)	-1	1	1	-	-1.71	-4.57	-	1	1	1	1
Nitrogen (mg N)	-	i_{NSI}	i_{NSS}	1	1	1	-	i_{NXI}	i_{NXS}	i_{NBM}	i_{NBM}
Ion Charge (Mole+)	-	-	-	$\frac{1}{14}$	-	$-\frac{1}{14}$	-1	-	-	-	-

Table 4.6: Stoichiometry coefficient of alkalinity

Stoichiometric Coefficient for Alkalinity	
z_1	$\frac{1}{14}\left[i_{NXS} - f_{SI} \cdot i_{NSI} - (1 - f_{SI}) \cdot i_{NSS}\right]$
z_2	$\frac{1}{14}\left[\frac{1}{Y_{H,O2}} \cdot i_{NSS} - i_{NBM}\right]$
z_3	$\frac{1}{14}\left[\frac{1}{Y_{H,NO}} \cdot i_{NSS} - i_{NBM} - \frac{Y_{H,NO} - 1}{2.86 \cdot Y_{H,NO}}\right]$
z_4	$\frac{1}{14}\left[i_{NBM} - f_{XI} \cdot i_{NXI} - (1 - f_{XI}) \cdot i_{NXS}\right]$
z_5	$\frac{1}{14}\left[-\frac{2}{Y_A} - i_{NBM}\right]$
z_6	$\frac{1}{14}\left[i_{NBM} - f_{XI} \cdot i_{NXI} - (1 - f_{XI}) \cdot i_{NXS}\right]$

through the medium that is only permeable to fluid flow. As explained in section 4.1.1.5, the accumulation of sludge deposit layer was estimated using a mass balance approach, which was fundamental for the amount of influent solute flux and a retention parameter of the wetland bed. In a similar way, the simplest way to numerically describe the removal of particulate component at the surface layer was using the first order kinetics proposed by Iwasaki, Slade, and Stanley (1937):

$$\emptyset_f(0,t) = \sigma q_{sur}(0,t) C_0(0,t) \tag{4.121}$$

where $\emptyset_f$ is the sink term for filtration, σ is the retention parameter, q_{sur} is the influent flux and C_0 is the solute concentration of influent.

4.3.3. Nutrient uptake by vegetation

The nutrients and minerals are adsorbed by the vegetation for growing process, and thus the uptake of NH_4^+-N, NO_3^--N and phosphorus are generally considered in the wetland ecosystem. In this study, the extraction of nutrient by vegetation emerged exclusively to the rate of root water uptake using an uncompensated method:

$$\emptyset_v(z,t) = ST(z,t) \cdot c(z,t) \tag{4.122}$$

where $\emptyset_v$ is the sink term of passive nutrient uptake [M L^{-2} T^{-1}], ST is the root water uptake [L T^{-1}] and c is the concentration in the aqueous phase in mobile region [M L^{-3}].

4.3.4. Numerical implementation

In VF_Sep, the bio-kinetics module was developed independently in a style of Gujer matrix (Gujer et al. 1999), which is a combination of stoichiometry, composition and reaction kinetics (Langergraber and Šimůnek 2012). In the bio-kinetics module, the components are subdivided into five groups. First, S_O, S_S, S_{HCO}, S_I and S_{N2} is only affected by the biochemical reactions. S_{NH} is involved in the bio-kinetics, adsorption and plant uptake, while S_{NO} is free from the influence of adsorption. The surface filtration is imposed to the particulate components including X_S and X_I. The heterotrophic and autotrophic biomass, X_H and X_A, was assumed to be fixed biomass at a particular layer.

The stoichiometry matrix requires the concentration of each component in the computation of the process rate. The proposed model confines the node with the prescribed thickness $\left(\frac{z_{upper}}{2} + \frac{z_{lower}}{2}\right)$ as a layer and assumes the particular layer as a CSTR. In the dual-porosity model, the transport of components is divided into mobile region and immobile region and the estimation of the associated biodegradation are carried out separately. A term of mass transfer is allocated between the regions, which is estimated with respect to the water transfer rate. All concentrations in the bio-kinetics module are necessary to be in the form of the liquid phase [M L^{-3}]. The mass-based concentration in the solid phase, s_i [M M^{-1}] is converted according to the water content, θ [-] and bulk density ρ [M L^{-3}] as follow:

$$c_i = \frac{\rho}{\theta} s_i \tag{4.123}$$

The summation of the concentration [M L^{-3}] of the liquid and solid phase in the mobile and immobile regions, which is represented by the C_{mobile} and $C_{immobile}$, respectively, are then transferred to the bio-kinetics module to obtain the kinetic rate. In the stoichiometric matrix, the interactions between components are jointed and a simultaneous computation at each iteration step is essential (Langergraber and Šimůnek 2006). Figure 4.8 demonstrates the flow to estimate the rate of biochemical reaction at a random node *i*. To find the reaction rate at the current time step *j+1*, the concentrations of all eleven components ($C1^j_i$ ~ $C11^j_i$) at the time step *j* are extracted as the input to obtain the corresponded reaction kinetics ($k1^{j+1}_i$ ~ $k11^{j+1}_i$). Then, the

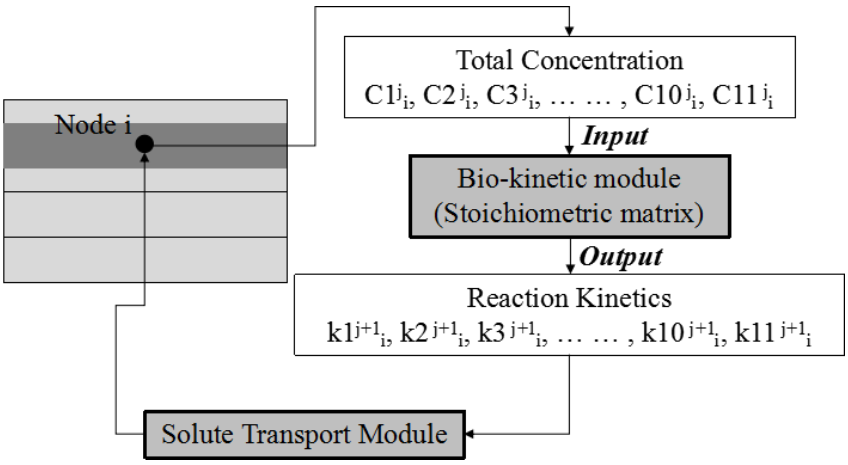

Figure 4.8: The procedure to estimate the biochemical reaction rate at node i

outputs are returned to the solute transport module to merge with the transport equation of the particular component at time step *j+1*.

It should be noted that only three components, S_{NH}, X_H and X_A, were assumed to be involved in the adsorption. Therefore, the total concentration of S_O, S_S, S_I, S_{NO}, S_{N2}, S_{HCO}, X_S and X_I in both mobile and immobile regions are only determined in the aqueous phase, as illustrated in Figure 4.9.

The S_{NH} is the only component simulated with adsorption capability. The adsorption of the S_{NH} in the mobile region is separated in the equilibrium and kinetic state. In the immobile region, only the equilibrium state is considered. Figure 4.10 illustrates the relation of S_{NH} between the solid phase and liquid phase in the mobile and immobile region. The heterotrophic and autotrophic biomass are assumed as a homogenous biofilm attached uniformly on the surface of the porous medium. Therefore, all biomass were assumed to be stationary and is considered under solid phase only. The portion of biomass in the mobile and immobile region are determined according to the fraction of mobile phase (f_{MO}). Then, the associated concentration of biomass is determined using equation 4.123, which involved the bulk density of the substrate material and the water content in particular region in the equation.

The reaction terms of each component are identified by coupling the stoichiometry matrix (Table 4.7) and the equations of reaction processes (equation 4.115 – 4.120). The overall reaction term *R* for component *m* can be obtained as follows:

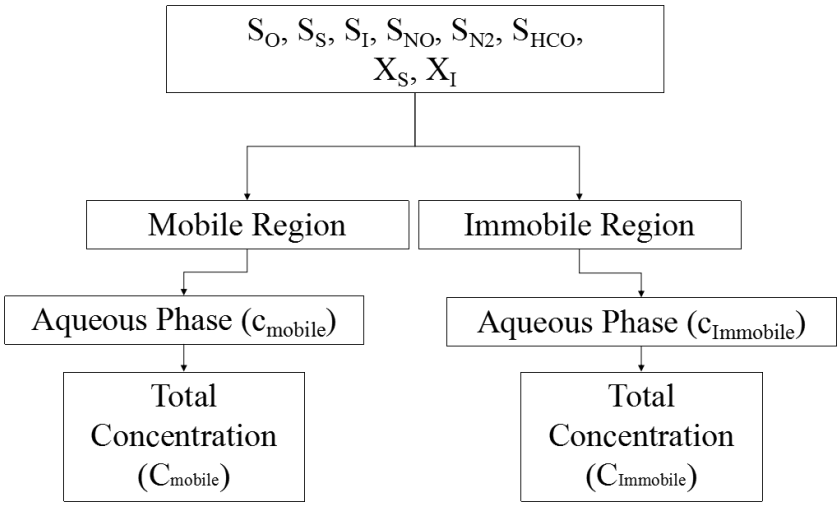

Figure 4.9: Determination of the total concentration of S_O, S_S, S_I, S_{NO}, S_{N2}, S_{HCO}, X_S, and X_I

$$R_m = \sum_{n=1}^{m} v_{n,m} P_n \tag{4.124}$$

where m denotes the components 1 – 11, n denotes the processes 1-6, R_m is the reaction term for component m [M L^{-3} T^{-1}], $v_{n,m}$ is stoichiometric factor for component m and process n [M M^{-1}], Pn is the zero-order reaction rate for process n [M L^{-3} T^{-1}]. The R_m was used as the zero-order kinetic term to describe the gain or removal via the biochemical process.

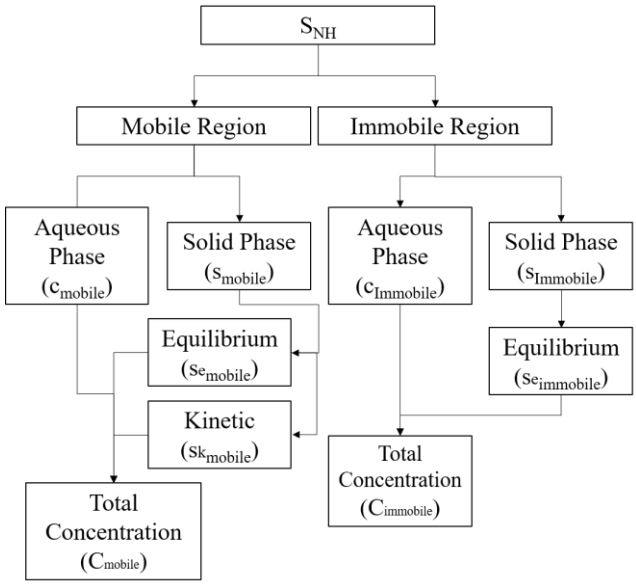

Figure 4.10: Determination of the total concentration of S_{NH}

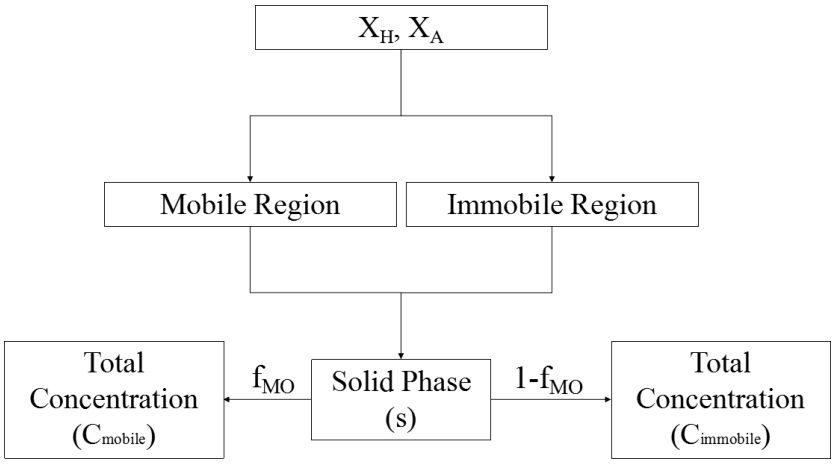

Figure 4.11: Determination of the total concentration of X_H and X_A

The surface filtration was modelled using a simple first-order approach in the top node. It is a sink term to estimate the local removal in the transport of particulate compounds. On the other hand, the sink term for nutrient uptake is dependent on the transpiration rate in the hydraulic simulation, which is a first-order rate coefficient in the transport. When the water uptake is zero, the nutrient uptake by vegetation has no effect on the fate of nitrogenous constituents.

4.4. Summary of program code in MATLAB®

The coding of VF_Sep was developed using simulation software MATLAB® 2013b. Figure 4.12 demonstrates the flow chart of the proposed model. The program code involved the main transport module and three sub-modules for van-Genuchtent Mualem model (VGM model), evapotranspiration (ET module) and bio-kinetics module, which are represented in grey boxes in the flow chart. The main transport module was divided into two parts, which were a hydraulic simulation and a reactive transport simulation.

The first step of the principle concept is to read the input files to initialize the various variables in the simulation. These parameters include the information of geometry, time, iteration criteria, hydraulic properties, transport parameters, influent quality, boundary conditions and initial condition. Except for the initial condition that is imported from a xlsx file, the remaining information is input directly in the main transport module. The simulation starts with the computation of hydraulic behaviour and then to the reactive transport. The sub-modules VGM and ET were used in the simulation of hydraulic behaviour, while the bio-kinetics sub-module was employed

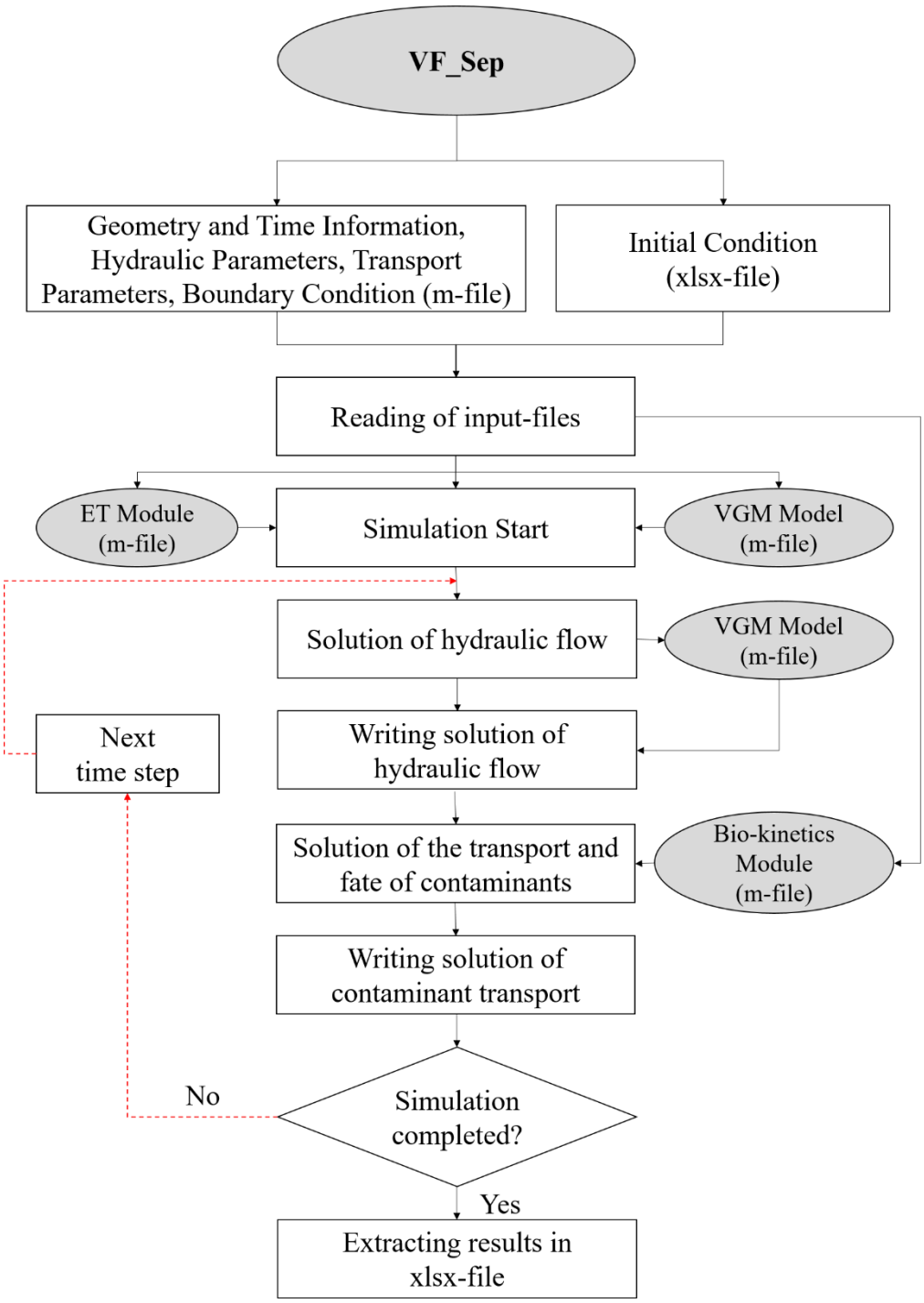

Figure 4.12: Flow chart of the VF_Sep

in the reactive transport. The simulation repeats the same procedure in every time step until the prescribed final simulation time is reached. Then, the simulated results are saved in a xlsx file.

The modelling of hydraulic behaviour and reactive transport were coded in the same m-file and this part could not be individually executed. The detailed flow chart of the hydraulic simulation is illustrated in Figure 4.13. The inputs required in the hydraulic simulation are listed in the same figure. When the simulation is initialised, several matrices are created to accommodate the simulated data of hydraulic behaviour and contaminant transport with regards to the information of geometry and time. The VGM model was employed to compute the initial water content and hydraulic conductivity according to the initial pressure head distribution and the prescribed hydraulic characteristics. The ET module estimates the rate of water loss to the atmosphere. This rate is further derived into evaporation and transpiration in the m-file. Subsequently, the iterative computation of hydraulic behaviour is then executed with these initialized variables.

The pressure head (h) from the non-linear Richards equation was solved using the modified Picard iteration method. The convergence of the solution is obtained by comparing the residual of the solution to the prescribed minimum tolerance. Then, the solution from the simulation, which is in term of h, is then used to calculate the water content and water flux in both mobile and immobile regions. As for case that the convergence fails to be obtained within the maximum number of iterations, the residual is then compared to the prescribed maximum tolerance. If the solution is incapable of converging to the tolerance, the simulation will be terminated and considered as failure. The simulated data are temporarily stored in the matrices created previously, and the simulation is continued until the end of the prescribed duration. When the simulation is completed, all the simulated data are output in a xlsx file.

The routine of the simulation for contaminants transport is described in Figure 4.14. The simulated water content and water flux are exported from hydraulic module to the transport module. Then, they are coupled with the transport parameters, influent concentration, initial concentration, and boundary condition to deliver the simulation of transport. As the adsorption was considered as a linear kinetics in the proposed

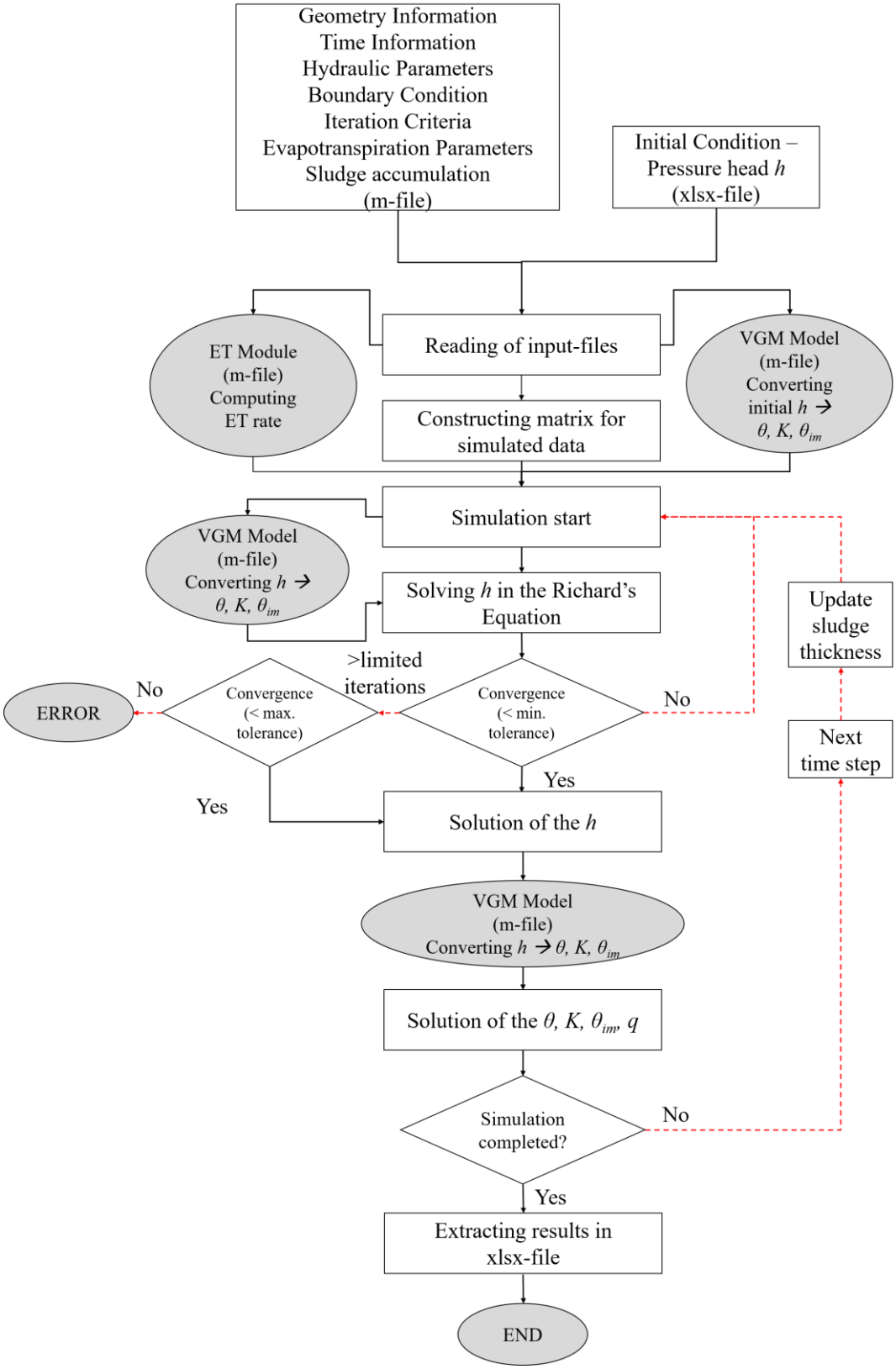

Figure 4.13: Flow chart of hydraulic module

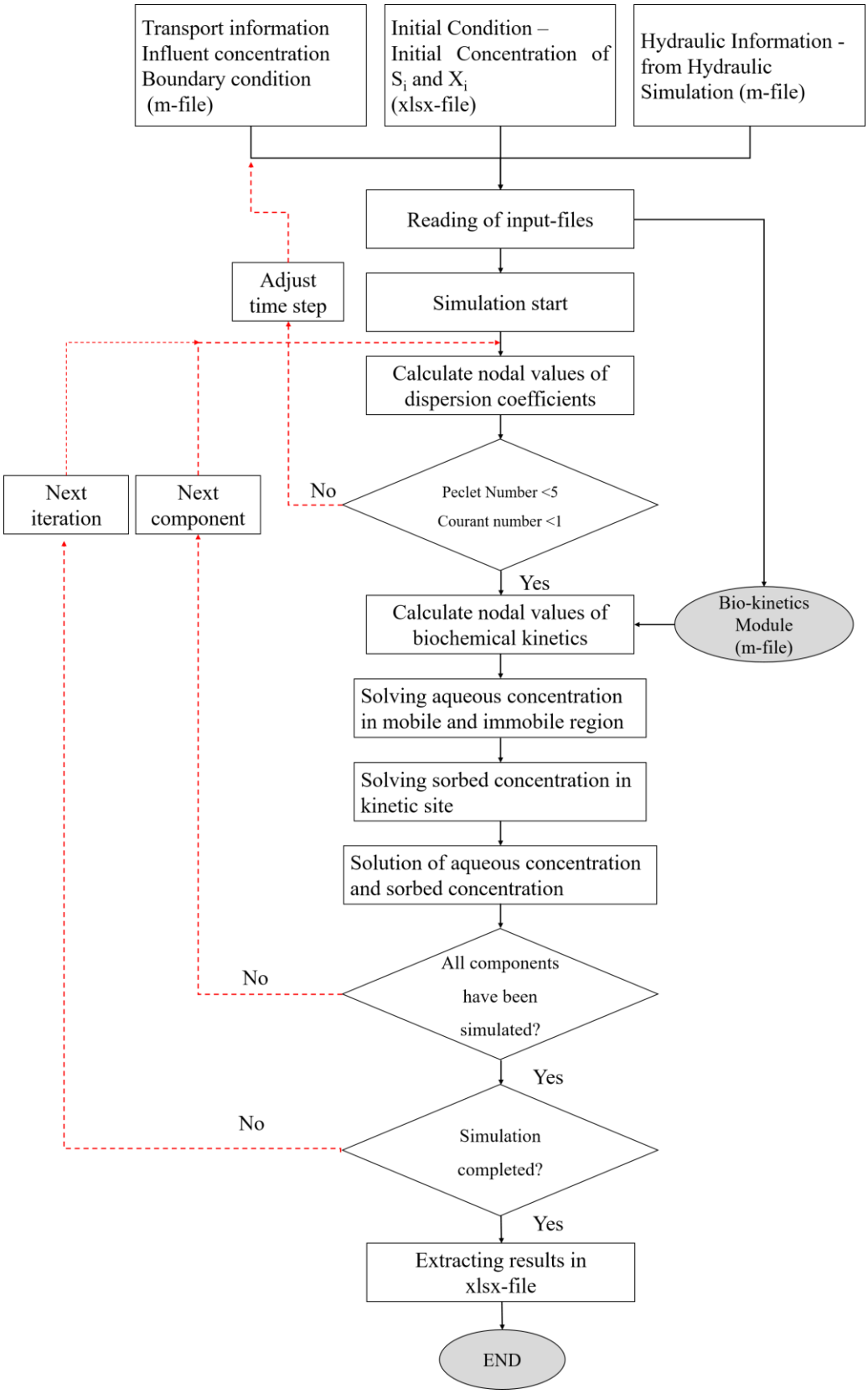

Figure 4.14: Flow chart of transport module

model, the computation of ADE is carried out directly without the necessity of iterative algorithm.

The first step in the transport module is to obtain the values of dispersion coefficient in each node from the prescribed transport parameters and simulated water flux. Then, the dispersion coefficient is evaluated with the spatial and temporal size to determine the level of numerical dispersion. If the undesired *Cr* (>1) or *Pe* (>5) is observed, the simulation will be stopped and the discretization of space and time have to be corrected to prevent numerical dispersion.

The simulation of transport has to be repeated for all components considered in the model. The computations of bio-kinetics for each component has been explained in section 4.3.4, where the coefficients of degradation are obtained simultaneously based on the concentrations of all components at the previous time step. Therefore, the simulation of reactive transport of particular component is independently carried out with the associated bio-kinetics coefficient at each iteration step. The calculation of the next component is started only after the solution of the aqueous concentration and sorbed concentration of a particular component has been obtained. After the simulation of all components considered in the model is finished, the iterative procedure is repeated until the end of the prescribed simulation time. The simulated data, which are stored temporarily in the matrices as mentioned in Figure 4.14, are converted to a xlsx file at the end of simulation. At this stage, the simulation process in the proposed multi-component reactive transport model is considered to be complete.

Chapter 5 Laboratory Experimental Results

The current understanding has established an overview of the potential factors in the wetland system designed for septage treatment, including the influence of the vegetation, loading regime, and the alternation of impounding. To date, the following conclusions have been made for the first-stage treatment of the two-stage VFCW-based septage treatment system (Jong 2014):

- The wetland bed operated weekly using a solids loading rate up to 350 kg total solids (TS) m^{-2} yr^{-1} produced a removal approximately 98 %, 99 % and 93 % for total suspended solids (TSS), chemical oxygen demand (COD) and ammonia nitrogen (NH_3-N), respectively;
- The presence of vegetation enhanced the removal of organic matter and nitrogenous constituents, as well as the dewatering efficiency;
- The aeration capability was high with the installation of ventilation pipes;
- The excessive development of sludge deposit layer was the main reason of clogging phenomenon and this can be prevented through the appropriate resting regime.

A wetland bed was built as described in Chapter 3 and was modelled to investigate the hydraulic and treatment performance. In order to ensure the system was ready to operate, a preliminary experiment was undertaken to gain insights into the overall treatment efficiency of TS, organic matter and nitrogenous constituents, and the results are presented in section 5.1. Then, the flow of the wetland bed was continuously monitored to plot the hydraulic and treatment dynamics throughout the feeding-draining cycle. Twenty-five operations have been carried out with varying hydraulic loads in this study. In this chapter, the experimental results are presented in terms of hydraulic behaviour (section 5.2) and treatment performance (section 5.3). As for the statistical analysis, the minimum, maximum, mean, and standard deviation are determined to evaluate the collected data. It should be noted that the mean and standard deviation of particular set of data is presented as mean ± standard deviation to simplify the presentation.

5.1. Preliminary experiment

A 3-month preliminary experiment was carried out to determine the maturity of the newly-built pilot-scaled VFCW-based septage treatment system. Prior to the preliminary test, the wetland beds were acclimatized for two months to stimulate the development of active biomass. A layer of sludge deposit was formed, while the vegetation grew well. Figure 5.1 and Figure 5.2 demonstrate the wetland bed before and after acclimatization, respectively.

The acclimatized bed was initially loaded according to solids loading rate (SLR), where the concentration of TSS was measured in-situ using Hach® DR2800 spectrophotometer. The operation was designed with an SLR of 100 kg TSS m^{-2} yr^{-1}. The raw septage contained an abundance of solids, organic matter, and nitrogen compounds, however, the concentration of dissolved oxygen (DO) was always low. The water quality parameters monitored in the preliminary test included electrical conductivity (EC), pH, DO, TSS, total nitrogen (TN), NH_3-N and nitrate nitrogen (NO_3^--N). Figure 5.3 shows the comparison between the samples of influent raw septage (left 1) and the effluent. The turbidity in the effluent demonstrated a significant reduction.

Figure 5.4 - Figure 5.6 presents the overall performance of the two planted wetland beds (A1 and B1) and the unplanted wetland bed (C1). In general, the EC in the effluent remained the same or slightly increased from the influent. The variation between the planted and unplanted beds is insignificant. The high DO concentration in the effluent indicated that the VFCW aerated the influent well. Nevertheless, the insufficiently thick sludge accumulation in the first two tests resulted in a low DO concentration in the effluent. In the following runs, the hydraulic retention time was significantly extended due to the adequate sludge accumulation and subsequently the average DO concentration in the effluent rose to approximately 6 mg l^{-1}. The presence of vegetation did not bring an impact to the DO in the effluent. This observation implies that the contribution of vegetation is minor to the oxygen transport.

The comparisons between the influent and effluent concentrations show that the removal of TSS and COD widely distributed between 30 % and 95 %. It was found that the removal rates of these parameters are proportional to the sludge accumulation. The unplanted bed displayed a lower treatment efficiency compared to the planted bed

at the beginning stage, but the performance improved rapidly when the sludge deposit has accumulated to a certain thickness. Accordingly, the removal of TSS and COD improved to 95 % and 80 %, respectively. In addition, the clogging phenomenon due to the excessive sludge deposit was observed in the last few operation.

Figure 5.1: The wetland bed before acclimatization

Figure 5.2: The wetland bed after acclimatization

Figure 5.3: Comparison between raw septage (left 1) and effluent

.

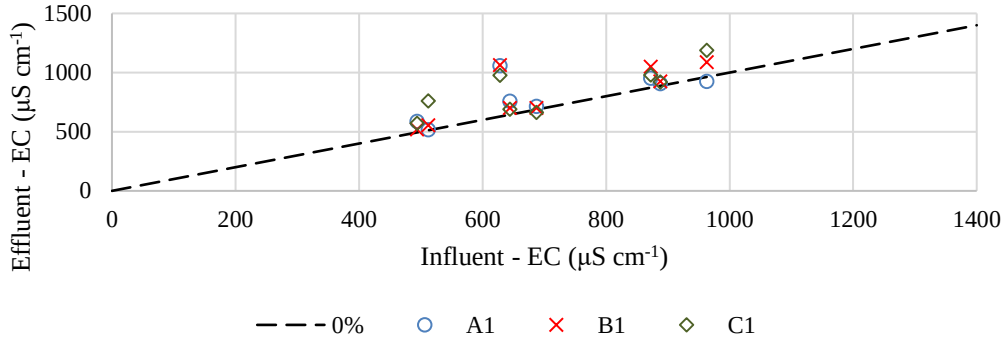

(a)

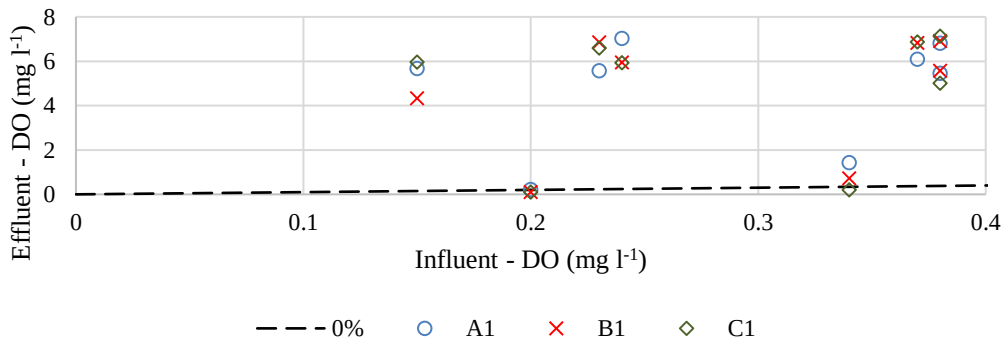

(b)

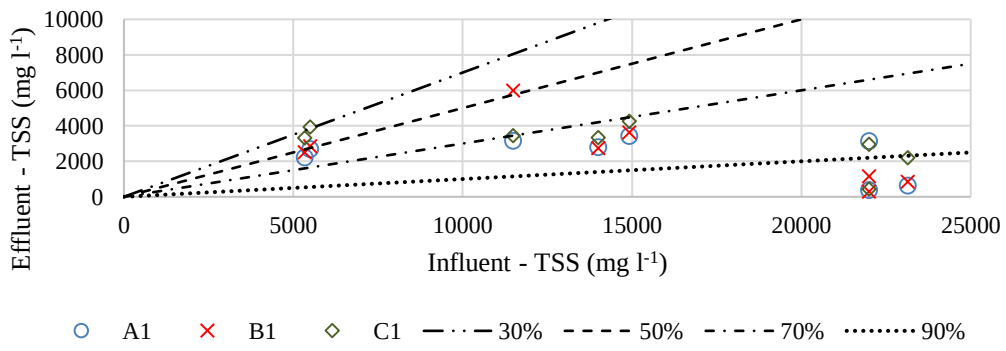

(c)

Figure 5.4: Comparison of (a) electrical conductivity (EC), (b) dissolved oxygen (DO) and (c) total suspended solids (TSS) between influent and effluent. The percentages in the diagram indicate the removal efficiency throughout the treatment.

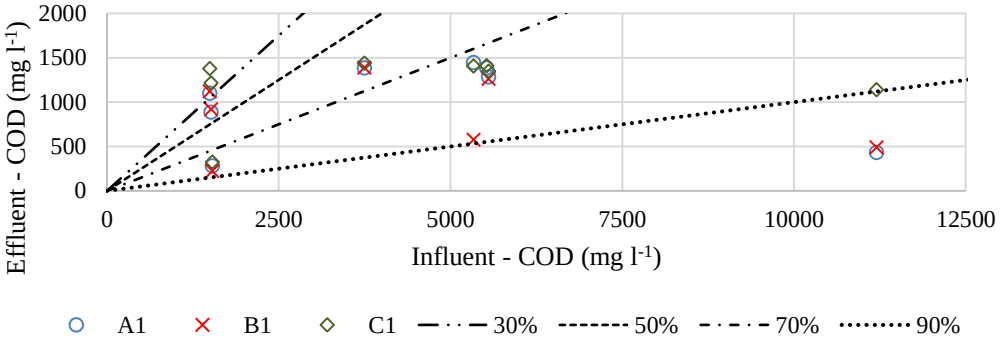

(a)

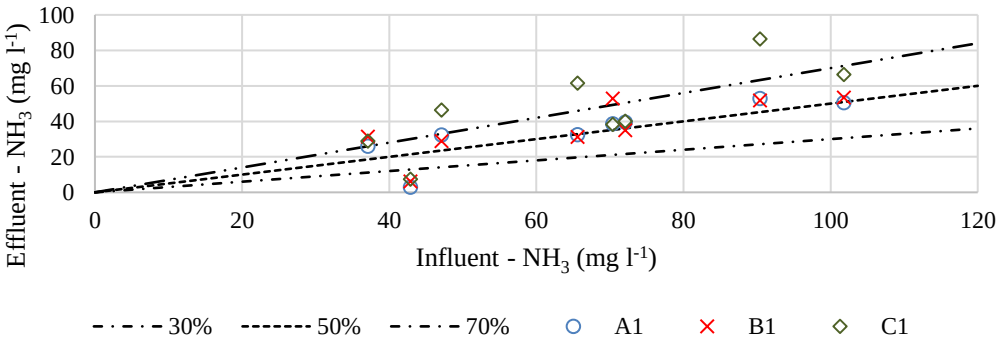

(b)

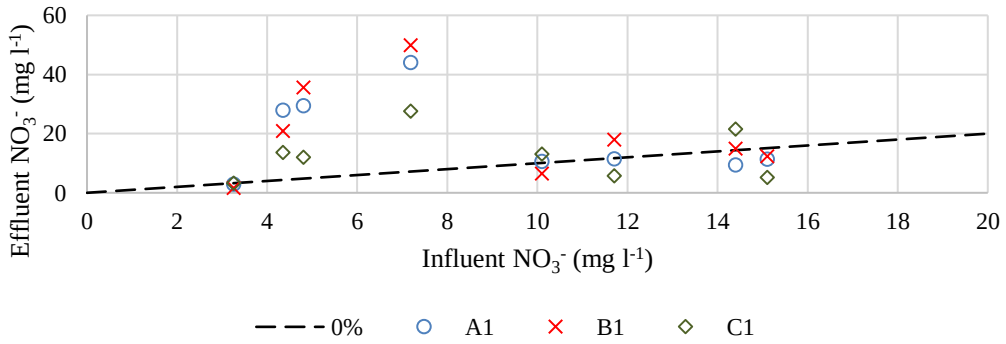

(c)

Figure 5.5: Comparison of (a) chemical oxygen demand (COD), (b) ammonia (NH_3) and (c) nitrate (NO_3^-) between influent and effluent. The percentages in the diagram indicate the removal efficiency throughout the treatment.

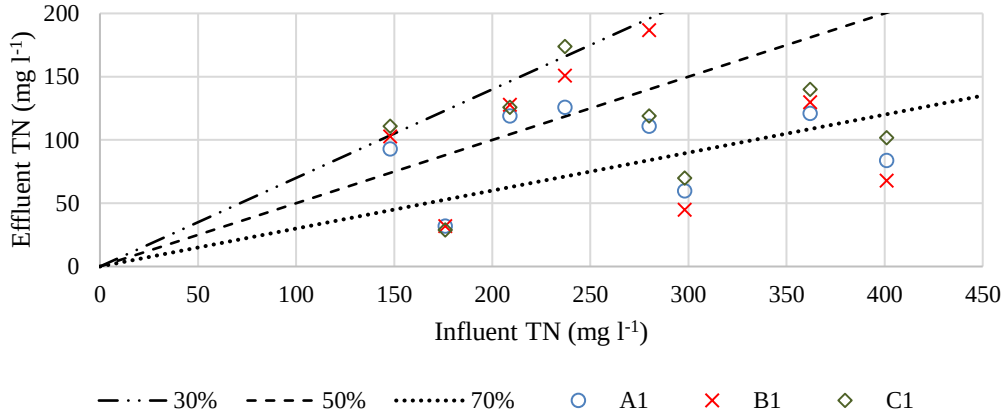

Figure 5.6: The comparison of total nitrogen (TN) between influent and effluent. The percentages in the diagram indicate the removal efficiency throughout the treatment.

The treatment efficiency of nitrogenous constituents varied significantly. The experimental result shows that the reduction of NH_3 was between 30 % and 50 %. This average was much lower than the previous study (Jong 2014). In addition, the unplanted bed was found to be poor in removing NH_3-N. This highlights the importance of vegetation upon nitrogen uptake and microbial development. The high concentration of NO_3^--N in the effluent reflects that the pilot-scale VFCW is favourable for nitrification. Nevertheless, the relatively high concentration of NH_3-N in the effluent implies that the efficiency of nitrification in the current system is still limited by the rapid percolation rate and high organic content. As the contribution of nitrite (NO_2^--N) was negligibly small in the raw septage and effluent, the nitrogen balance between TN, NH_3-N, and NO_3^--N can be used to describe the content of organic nitrogen (Org-N). The excellent treatment of TN indicated that the majority of Org-N exists in the particulate form and they are removed instantaneously via surface filtration.

In summary, the treatment of TSS and organic matter in the pilot-scale VFCW treating septage were excellent. Nitrification was observed throughout the preliminary test. These outcomes have demonstrated that the first stage wetland beds were ready to run the experiment. Furthermore, the influence of vegetation was found to be insignificant to the treatment of TSS and COD; however, it greatly affected the nitrogen removal and minimized the clogging problem. The sludge deposit layer acted as a low hydraulic

retention time of influent in the wetland bed. However, the excessive accumulation might reduce the infiltration capacity of the wetland bed and ultimately lead to clogging. A continuous sampling approach was further carried out in this study to merge the effect of hydraulic behaviour to the nitrogen dynamics, subsequently providing a better insight towards the performance of the VFCW-based septage treatment system.

5.2. Hydraulic behaviour

A total of twenty-five sets of data were collected from two vegetated first stage wetland beds in between November 2015 to February 2016. The complete results of effluent flux are presented in Appendix C. Since the system configuration, macrophytes condition, and operating regime of both beds were similar, the results were analysed and presented together. The experiments were run on the basis of “feed-and-drain”. The raw septage was loaded in batches with specific volumes, and the effluent was collected and measured for its quantity and quality. It should be noted that the maximum monitoring duration in this study is up to 12 hrs (600 mins) due to the instrumental limitation.

Due to the limitation of a rapid and accurate method to identify the concentration of TS, the experiments were run according to the hydraulic loading rate (HLR). In this study, five HLRs were employed, which were 50 l d^{-1}, 75 l d^{-1}, 100 l d^{-1}, 125 l d^{-1} and 150 l d^{-1}. As mentioned in section 5.1, the influence of the sludge thickness is vital to the hydraulic behaviour and treatment performance. In the entire experiment, the maximum and minimum sludge thicknesses were 12 cm and 3 cm, respectively. The thickness of the accumulated sludge appeared to be proportional to the total amount of solids loaded to the wetland bed. It was observed that the excessive accumulation of sludge deposit led to permanent ponding at the wetland surface. Therefore, the sludge layer was excavated to “recover” the infiltration capacity of the wetland bed, resulting in a decrease in the sludge thickness in the following cases (i.e. 14A to 16A, 15B to 17B).

Since the solids loading rate (SLR) has been recommended as the loading regime in the literature, the solids content, which is calculated from the hydraulic load (l) and TS concentration (mg l^{-1}), is considered as a factor to the hydraulic behaviour. Due to the varying TS concentration in the raw septage, the solids load is highly dynamic, ranging

from 105 g to 2325 g while the average is 727.40 ± 590.73 g. Table 5.1 summarizes all the operating conditions.

5.2.1. Water recovery

In the first part of the analysis, the water recovery percentage is used as a simplified indicator of hydraulic productivity in the VFCW resulting from the system configuration, operation, and influent quality. The total volume of collected effluent and the calculated water recovery percentage are presented in Table 5.1. The mean water recovery was 58.78 %. The standard deviation of the water recovery was ± 25.71 %, which revealed that it was highly variable throughout the experiment. The maximum and minimum percentage were observed in case 18A (24th January 2016) and case 13B (7th January 2016), respectively, where the highest percentage reached 90.00 % on and the lowest was 9.72 %. Both cases were loaded with 125 l of influent, and the solids load with the maximum recovery was higher than the case with the lowest recovery. This outcome implied that neither hydraulic load nor solids load appeared to significantly impact the water recovery during treatment. On the other hand, the sludge thickness of the maximum water recovery was 4 cm, which was much thinner compared to the 9 cm in the minimum case.

The associated water recovery percentage from the varying hydraulic loads, solids loads and sludge thicknesses are plotted in Figure 5.7, Figure 5.8 and Figure 5.9, respectively. These correlations further support the key role of the sludge deposit layer in the water recovery. Figure 5.7 and Figure 5.8 indicate that the recovery percentages were highly variable with regards to the hydraulic loads and solids load. Meanwhile, Figure 5.9 shows that the hydraulic performance was significantly influenced by the build-up of solid deposition, where the water recovery was inversely proportional to the sludge thickness. For those cases where the sludge thickness was more than 8 cm, the recovery percentage were generally below 25 %. The thick sludge deposit layer created a significant resistance against the infiltration capacity, which resulted in a slow effluent flux and decreased the efficiency of water recovery.

5.2.2. Delay of flow occurrence

Figure 5.10 illustrates the effluent fluxes for twenty-five operational runs. Figure 5.11Figure 5.11 to Figure 5.13 present the three patterns of effluent flux development.

Table 5.1: Hydraulic loading rate (HLR), sludge thickness, solids loading rate (SLR), collected effluent and water recovery percentage of the experiment

No. of test A = Wetland A B= Wetland B		HLR (l)	Sludge thickness (cm)	TS (g l^{-1})	SLR (g)	Collected effluent (L)	Water recovery (%)
1A	18/11/2015	75	5	3.40	255.00	63.81	85.08%
2A	24/11/2015	75	5	10.60	795.00	60.41	80.55%
3A	01/12/2015	75	6	4.80	360.00	53.94	71.92%
4B	4/12/2015	75	7	1.40	105.00	64.40	85.87%
5A	08/12/2015	75	7	-*	-*	62.83	83.77%
6A	12/12/2015	75	5	1.60	120.00	54.03	68.14%
7B	13/12/2015	75	5	1.40	105.00	52.11	69.48%
8A	16/12/2015	100	6	12.80	1280.00	73.41	73.41%
9B	17/12/2015	100	5	4.60	460.00	70.10	70.10%
10B	24/12/2015	100	12	10.70	1070.00	22.75	22.75%
11A	27/12/2015	100	8	12.60	1260.00	47.34	46.94%
12B	31/12/2015	125	7	9.50	1187.50	18.22	14.58%
13B	7/1/2016	125	9	4.20	525.00	12.15	9.72%
14A	10/01/2016	125	12	9.60	1200.00	13.81	11.04%
15B	14/01/2016	50	10	24.00	1200.00	12.25	24.49%
16A	21/01/2016	100	3	1.70	170.00	45.32	45.32%
17B	21/01/2016	100	3	19.50	1950.00	47.59	47.59%
18A	24/01/2016	125	3	2.20	275.00	112.50	90.00%
19B	24/01/2016	125	4	2.70	337.50	110.76	88.61%
20A	28/01/2016	150	3	3.20	480.00	122.06	81.37%
21B	28/1/2016	150	4	1.50	225.00	53.31	35.67%
22A	16/02/2016	50	3	7.80	390.00	31.24	62.48%
23B	16/02/2016	50	4	8.90	445.00	33.12	67.43%
24B	21/2/2016	125	5	18.60	2325.00	70.54	56.43%
25B	27/2/2016	50	6	14.70	735.00	38.39	76.77%
	Max.	150	12	24.00	2325.00	122.06	90.00%
	Min.	50	3	1.40	105.00	12.15	9.72%
	Mean	95	5.88	8.00	718.96	54.27	58.78%
	Standard Deviation	30.62	2.64	6.46	597.23	29.81	25.92%

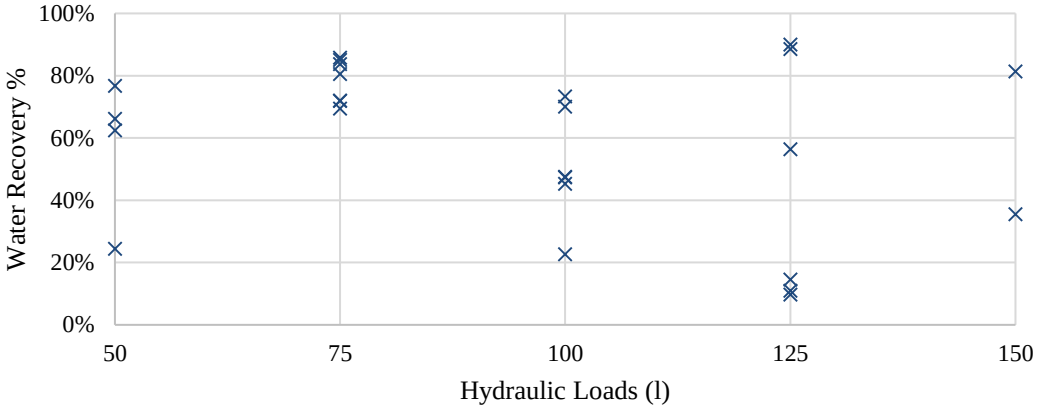

Figure 5.7: Water recovery percentage versus hydraulic load

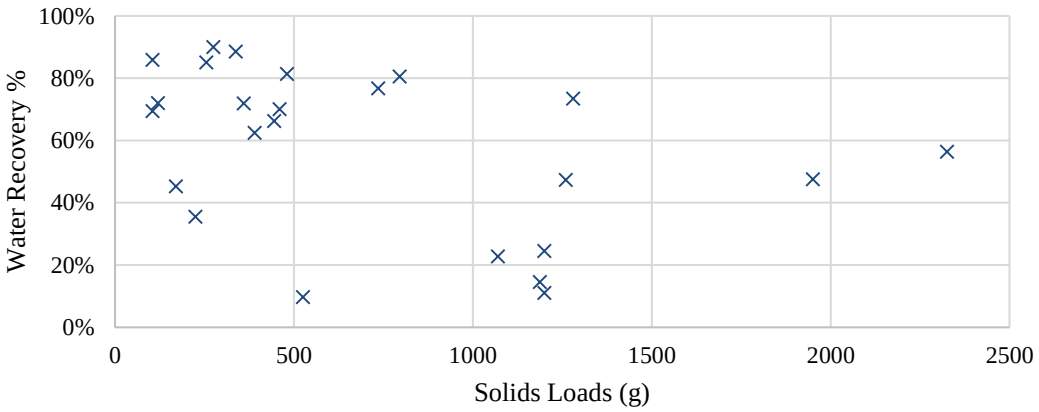

Figure 5.8: Water recovery percentage versus solids load

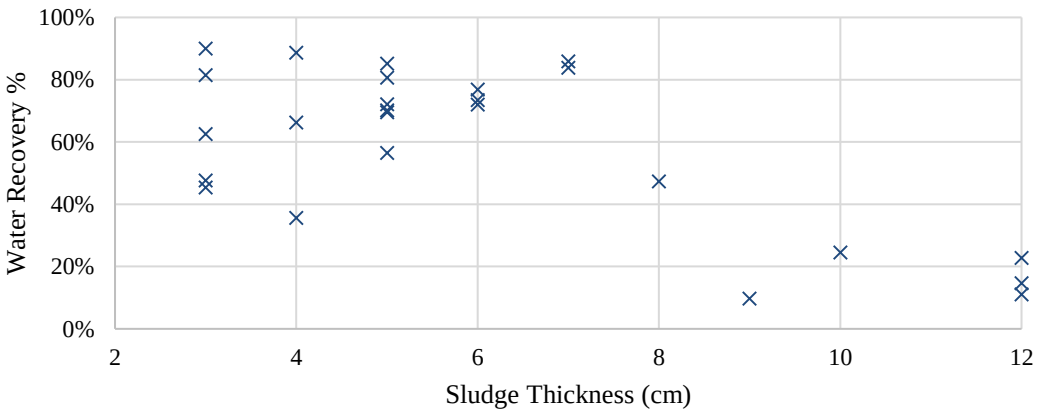

Figure 5.9: Water recovery percentage versus sludge thickness

Since the VF_Sep assumed the direction of flow as positive upwards, the results of effluent fluxes are presented with a negative sign. Figure 5.11 presents the case of "typical flow", where the discharge was smooth and unhindered. Its effluent flux reached the maximum rate immediately upon the observed start of discharge, and then followed by a gradual reduction. This pattern indicated that the peak effluent flux was generated by the largest head difference due to the maximum depth of ponding when the discharge started. Then, the continuous outflow reduced the head difference and decelerated the percolation rate throughout the wetland bed.

Nevertheless, some cases demonstrated an acceleration of effluent flux after the discharge had occurred. The flow pattern showed a V-shaped development as displayed in Figure 5.12, which was due to the "bypass" phenomenon. During some experimental runs, the experimental site experienced a strong wind that mechanically created a number of flow paths due to the movement of reed stems. Accordingly, the infiltration rate was accelerated, subsequently creating a sudden rise in the volume of effluent.

As for the "clogged" cases, the peak effluent flux was determined to be slower than the two previous cases, and it reduced to an insignificant rate within a short period as illustrated in Figure 5.13. The peak effluent flux in the "clogged" case was generally below 0.01 cm min^{-1}.

In a feeding-draining cycle, the discharge did not start immediately after loading. There was a delay between the time of loading and the start of discharge, and this duration can be taken as an indicator of the infiltration capacity of the wetland bed. Table 5.2 presents the delay of the flow occurrence in each case. The measured outflow dynamics were then compared to the hydraulic load, solids load and sludge thickness as shown in Figure 5.14, Figure 5.15 and Figure 5.16, respectively. The delay of flow varied within 3 to 70 minutes after loading, subsequently resulting in a high standard deviation (mean = 26.66 ± 20.66 minutes after loading). There was no direct link observed between the flow delay and the hydraulic load, solids load and sludge thickness. Therefore, the flow delay can be seen to be more sensitive to the systematic factor.

In the hydraulic simulation, the time of flow occurrence was calibrated with respect to the initial condition of pore water pressure in the substrate. The value of initial

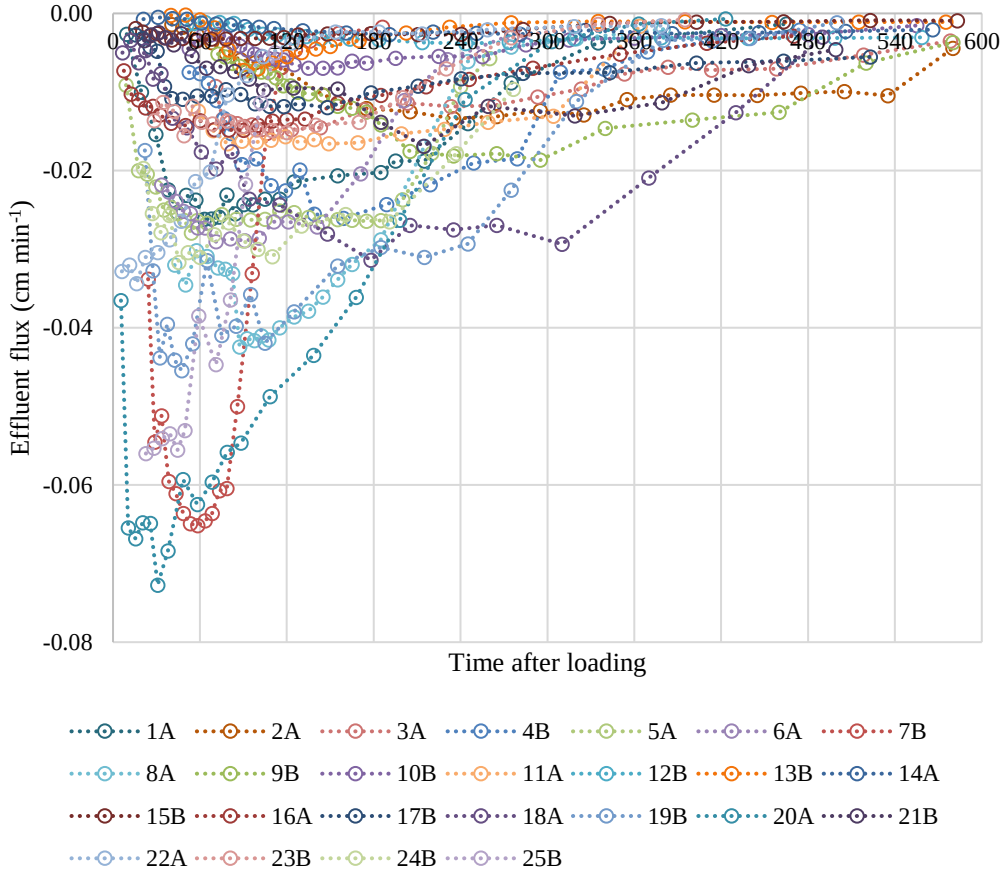

Figure 5.10: Twenty-five batches of effluent flux measured from the first stage treatment of a pilot-scale VFCW

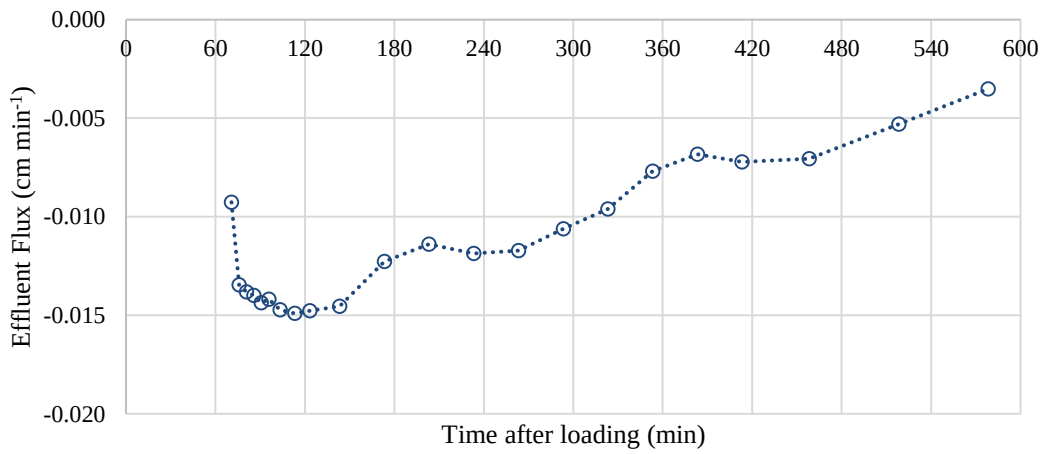

Figure 5.11: "Typical flow" case (case 3A)

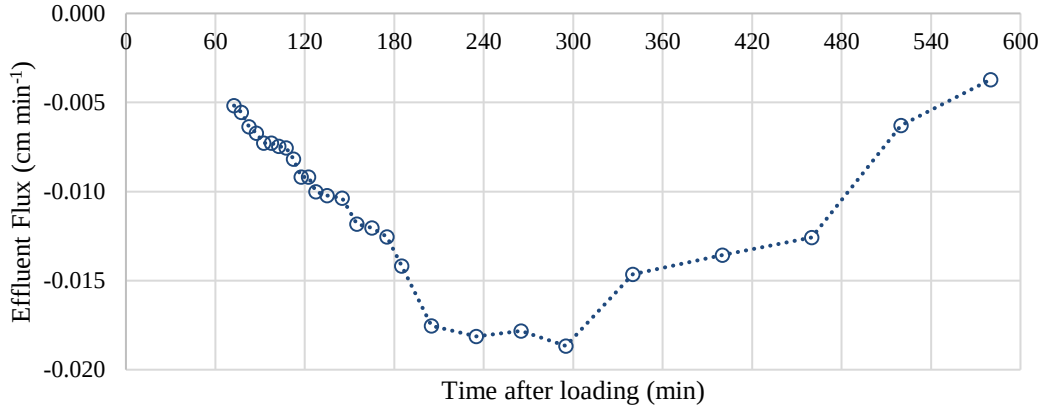

Figure 5.12: "Bypass" case - V-shaped development of effluent flux (Case 9B)

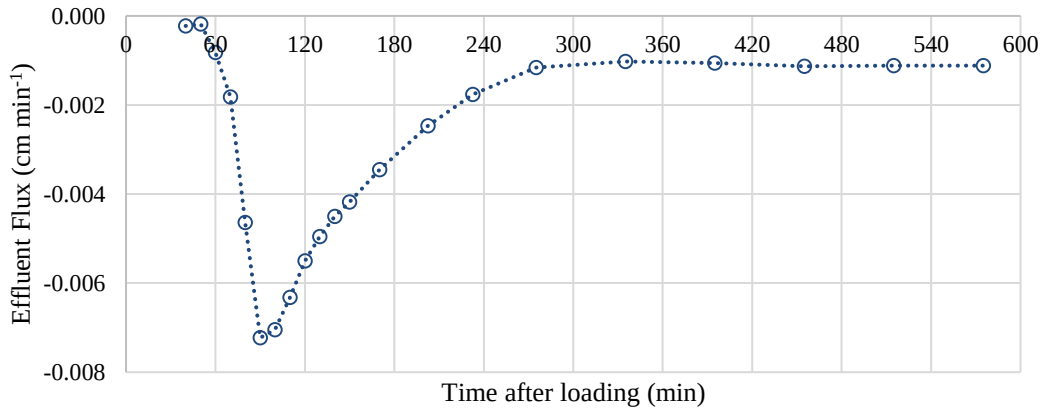

Figure 5.13: "Clogged" case - a low peak flux with rapid reduction (Case 13B)

condition was calibrated from the pattern of effluent flow, which will be introduced in the next chapter. The inherent water pressure is a parameter to quantify the water content in a porous medium before loading. A lower water pressure indicates a lower residual water content in the substrate. This parameter is sensitive to the duration of resting.

It should be noted that the fluid motion in the substrate is not only dominated by the gravity. The capillary effect is also significant as it might retain a certain amount of water in the pore spaces. Theoretically, a higher inherent water content within the gravel layer promotes the formation of water path under the unsaturated condition, and thus a lower pressure head potentially delays the start of effluent discharge.

Table 5.2: Hydraulic loading rate (HLR), sludge thickness, solids loading rate (SLR), flow occurring delay and peak flow of the experiments

No. of test A = Wetland A B= Wetland B		HLR (l)	Sludge thickness (cm)	TS (g l^{-1})	SLR (g)	Flow occurring delay (min)	Peak effluent flux (cm min^{-1})
1A	18/11/2015	75	5	3.40	255.00	4.50	0.0262
2A	24/11/2015	75	5	10.60	795.00	38.00	0.0134
3A	01/12/2015	75	6	4.80	360.00	68.25	0.0149
4B	4/12/2015	75	7	1.40	105.00	47.50	0.0261
5A	08/12/2015	75	7	-*	-*	3.00	0.0280
6A	12/12/2015	75	5	1.60	120.00	6.55	0.0290
7B	13/12/2015	75	5	1.40	105.00	21.75	0.0652
8A	16/12/2015	100	6	12.80	1280.00	40.00	0.0425
9B	17/12/2015	100	5	4.60	460.00	70.00	0.0187
10B	24/12/2015	100	12	10.70	1070.00	50.00	0.0070
11A	27/12/2015	100	8	12.60	1260.00	44.00	0.0166
12B	31/12/2015	125	12	9.50	1187.50	48.50	0.0038
13B	7/1/2016	125	9	4.20	525.00	35.00	0.0072
14A	10/01/2016	125	12	9.60	1200.00	16.00	0.0027
15B	14/01/2016	50	10	24.00	1200.00	13.00	0.0035
16A	21/01/2016	100	3	1.70	170.00	5.00	0.0149
17B	21/01/2016	100	3	19.50	1950.00	8.00	0.0120
18A	24/01/2016	125	3	2.20	275.00	4.00	0.0314
19B	24/01/2016	125	4	2.70	337.50	19.00	0.0455
20A	28/01/2016	150	3	3.20	480.00	3.00	0.0727
21B	28/1/2016	150	4	1.50	225.00	19.00	0.0222
22A	16/02/2016	50	3	7.80	390.00	3.33	0.0344
23B	16/02/2016	50	4	8.90	445.00	26.00	0.0155
24B	21/2/2016	125	5	18.60	2325.00	18.50	0.0317
25B	27/2/2016	50	6	14.70	735.00	20.17	0.0560
	Max.	150	12	24.00	2325.00	70.00	0.0727
	Min.	50	3	1.40	105.00	3.00	0.0027
	Mean	95	5.88	8.00	718.96	26.66	0.0256
	Standard Deviation	30.62	2.64	6.46	597.23	20.66	0.0189

**experimental error*

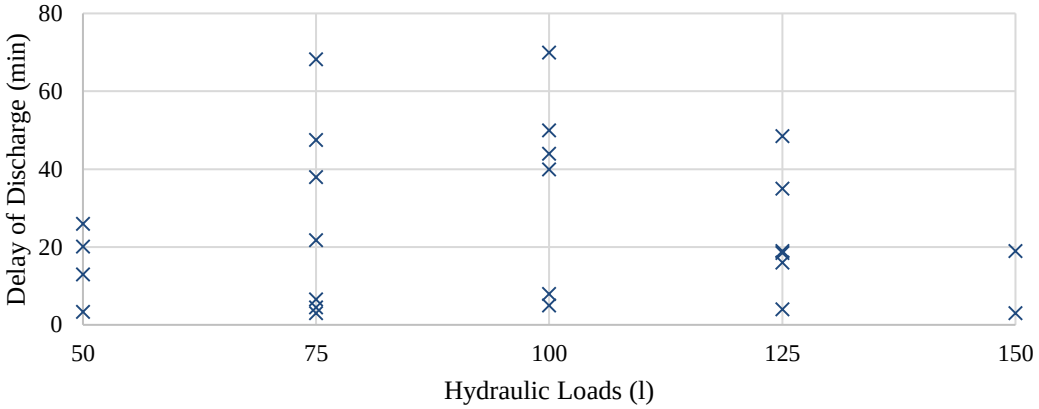

Figure 5.14: Flow occurring delay versus hydraulic load

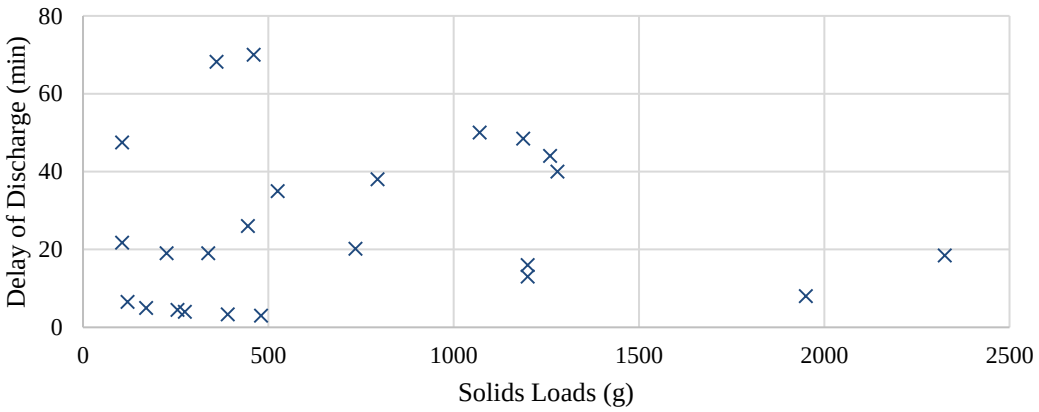

Figure 5.15: Flow occuring delay versus solids load

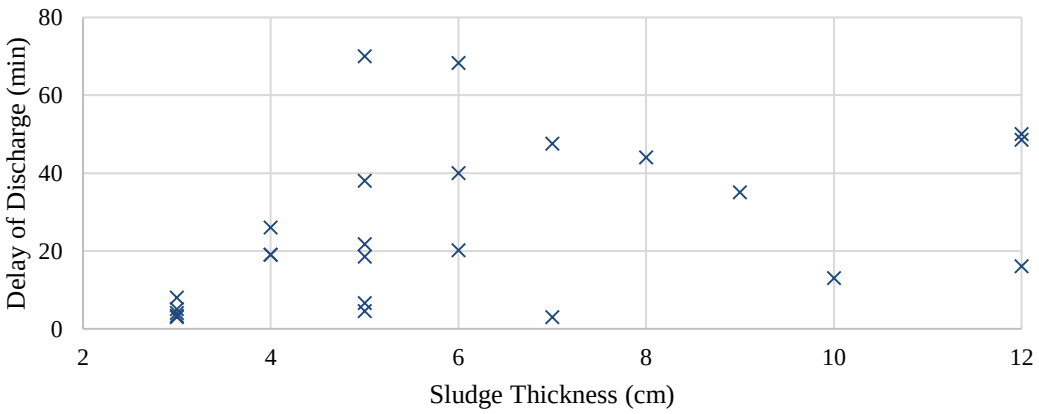

Figure 5.16: Flow occurring delay versus sludge thickness

Although evaporation is incapable of reaching the deeper layer of the wetland bed, the root water uptake by the vegetation and the convection via the ventilation system potentially remove the water content in the substrate during the resting period. This can be visualized in the sludge deposit accumulated at the wetland surface. The sludge deposit right after the loading looked like slurry as shown in Figure 5.17 (left). At the late stage of loading, the ponding depth was generally low and the effluent flow was insignificant. Therefore, the dewatering through the drainage was assumed to be negligible. The high water content in the sludge deposit layer, which was mainly attributed to the capillary effect, is considered to be stagnant.

During the resting period, evaporation extracted the water from the sludge deposit. The residual slurry was then dried and became a "mud-like" sludge deposit as displayed in Figure 5.17 (middle). This progression required approximately 1 – 2 days to form cracks on the top surface. However, the water content at this stage was still high. When the resting period was extended, the sludge deposit became a hard and fragile sludge cake. The water content was low at this stage and the cracks reached the gravel layer, which is shown in Figure 5.17 (right). Therefore, a longer resting period is helpful in preventing the substrate clogging (Tan et al. 2015).

The progressive drying process of sludge deposit layer demonstrated a significant change in its hydraulic properties. The undesirable cracks potentially allowed the influent to bypass the layer and accelerate the effluent flow. Therefore, it is necessary to assume that the hydraulic properties of gravel are not affected by this kind of water

Figure 5.17: (Left) The slurry with high water content accumulated on the surface of the wetland bed right after loading. (Center) Some cracks formed on the top surface of sludge deposit layer during resting period. (Right) The large cracks exposed the gravel layer after the extended resting period

loss throughout the resting period. On the other hand, the sludge layer was sensitive to this drying process and the formation of cracking should be considered in the analysis of hydraulic performance. It is generally accepted that the resting period is vital towards creating a permeable sludge layer to improve the hydraulic efficiency.

5.2.3. Peak effluent flux

According to Table 5.2, the peak effluent fluxes among twenty-five runs of the experiment were highly variable. Figure 5.18 and Figure 5.19 demonstrate that no significant trend is observed in the comparisons of flow intensity to the hydraulic load and solids load, respectively. Meanwhile, the peak effluent flux shows a dependency on the sludge thickness as shown in Figure 5.20.

The low permeability of the sludge deposit layer acts as a flow regulator that controls the infiltration rate. The measured data revealed that the peak effluent fluxes were generally below 0.01 cm min^{-1} for the cases with sludge thickness exceeding 9 cm. Nevertheless, a thin sludge layer did not promise a high effluent flow rate, where the flow intensity was still affected by the hydraulic and solids load, as well as the condition of sludge layer.

In the literature, the importance of hydraulic and solids load on pollutant removal has been highlighted (Torrens et al. 2009; Stefanakis and Tsihrintzis 2012). Theoretically, a high hydraulic load generates a greater head difference, and thus the associated effluent flow is accelerated (Richards 1931). On the other hand, high solids and organic load enhance the formation of a “clogging mat” that slows down the infiltration flow (Xu et al. 2013). However, these effects were concealed by the dominant parameter, which is the sludge thickness in this study.

Although a low hydraulic and solids load has been recommended as the optimal loading regime to improve the effluent quality, it does result in a low productivity and is inefficient from the view of the operation. Winter and Goetz (2003) and Xu et al. (2013) indicated that a high hydraulic load with high solids and organic content in the influent significantly reduced the hydraulic capacity because of the rapid sludge accumulation. Therefore, although the influence of hydraulic and solids load do not reflect directly on the associated effluent flow, they are still important to the development of the sludge deposit layer and treatment performance in long-term operation.

Previous studies have revealed that the influence of vegetation is significant in CW system (Langergraber 2005; Gagnon et al. 2012). Stefanakis and Tsihrintzis (2011) claimed that evapotranspiration (ET) is the primary dewatering mechanism in reed beds treating sludge. Nevertheless, this outcome is invalid in this study, as the average water recovery from drainage is more than 50 %. Białowiec, Albuquerque, and Randerson (2014) indicated that a wetland bed planted with willow contributed ET ranging from 0.01 to 0.46 cm d^{-1} and the performance revealed a dependency on the maturity of the bed. On the other hand, Borin et al. (2011) suggested a range of ET rate up to 3.09 cm d^{-1} for the bed planted with *Phragmites australis* during summer (average temperature = 23.5˚C, relative humidity = 60.1 %). However, the proposed ET rate is only valid to the specific wetland configuration and surrounding environment, where the differences in the system such as the condition of surface layer and vegetation could alter the efficiency and thus these literature data may not be referred directly. As the wetland beds were operated at a feeding-draining cycle, the hydraulic retention time was relatively short and thus the influence of ET was limited. However, the current outcomes were insufficient to conclude that such an effect is negligible in the treatment, as this water loss could be vital during the resting period, especially for the drying of sludge deposit layer.

The presence of vegetation such as common reeds in the wetland bed was promising in clogging prevention. The stem and the new shoot of vegetation could prevent the clogging in the sludge deposit layer, subsequently improving the overall hydraulic

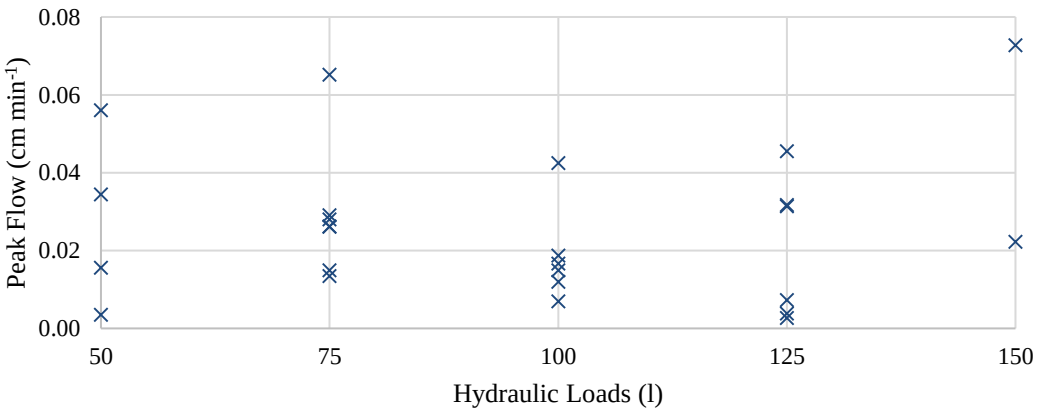

Figure 5.18: Peak effluent flux versus hydraulic load

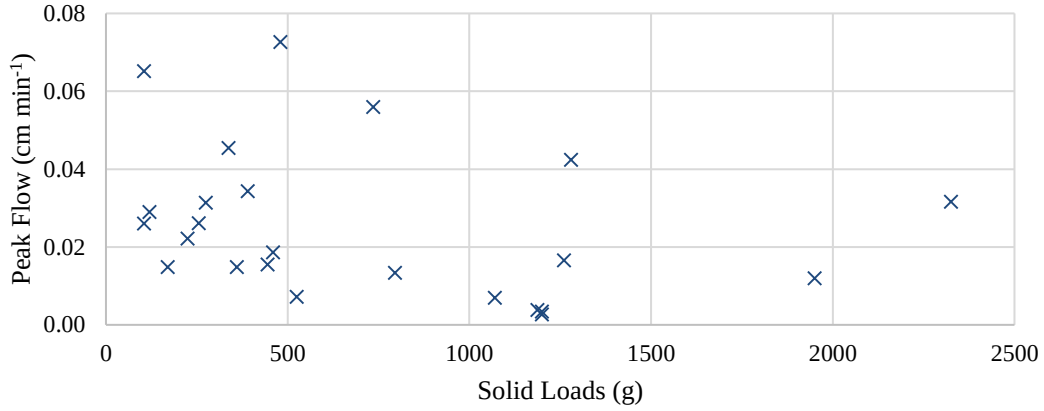

Figure 5.19: Peak effluent flux versus solid load

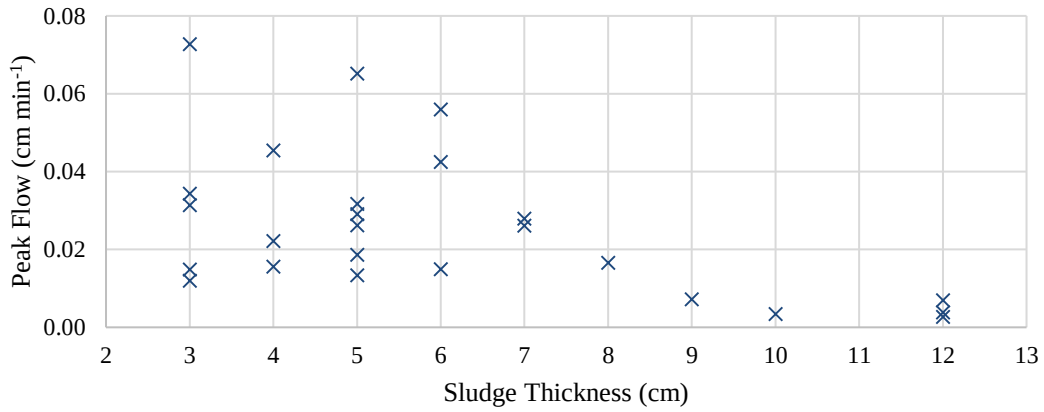

Figure 5.20: Peak effluent flux versus sludge thickness

conductivity of the wetland beds. Figure 5.21 shows the cracks formed via the mechanical vibration of the reed stem caused by the strong wind, which allowed the influent to bypass the layer and caused a high effluent flux. It should be noted that the common reeds were transplanted to the gravel bed when their root systems has attained a fair level of development, and thus the root distribution did not influence the water balance and the hydraulic conductivity in the sludge deposit layer. However, the absence of vegetation does not prohibit the formation of cracks, which is as displayed in Figure 5.22. This drying progression tended to be dominated by environmental factors such as the temperature and humidity, rather than the effect of vegetation.

5.2.4. Summary

In summary, the experimental outcomes showed the dominant role of the sludge deposit layer in the hydraulic behaviour of the pilot-scale VFCW designed for septage treatment. This observation agrees with the outcomes in Giraldi et al. (2009) and Molle (2014), where the accumulation of this low permeable layer drastically changed the hydraulic performance of the VFCW. Although the influence of hydraulic load and solids load were insignificant to the water recovery and effluent flow rate, they are crucial factors to the sludge accumulation and cannot be ignored in the long-term operation. The flow pattern in twenty-five set of measured data could be categorized into “typical flow”, “bypass”, and “clogged” cases, which characterized different hydraulic behaviour in the system. During the experimental runs, the effect of ET was limited due to the relatively short hydraulic retention time. However, this drying process could be vital during the resting period. As the excessive sludge accumulation was the main reason for clogging, such water loss dried the sludge deposit and caused cracks. This process increased the overall hydraulic conductivity and accelerated the effluent flow from the bed. The presence of vegetation ensured a better infiltration capacity of the wetland bed, however, the effect was not statistically quantified with the hydraulic efficiency in this study.

Figure 5.21: Cracks formed via the mechanical vibration of the reed stem caused by the strong wind

Figure 5.22: Cracks formed in the controlled bed during resting period

5.3. Treatment performance

5.3.1. The quality of raw septage

The raw septage used in this study was collected from the households near the Curtin University Malaysia Campus. The collected septage was screened and storedin two 400-gallon storage tanks. The raw septage was screened again before entering the distribution tank to eliminate the gross solids that might damage the centrifugal pumps. The raw septage was homogenized mechanically during the feeding and was sampled from the distribution device and stored in a 300 ml Hach© disposable BOD bottle. Figure 5.23 shows the sample of raw septage, which displayed an extremely high turbidity. The quality of the twenty-five batches of raw septage is presented in Table 5.3. It should be noted that the concentration of Org-N was estimated from the nitrogen balance between TN, NH_4^+-N, and NO_3^--N, as the concentration of NO_2^- -N is negligibly small.

In general, the raw septage was slightly alkaline, ranging from 7.34 to 7.89. The mean pH was 7.58 $\pm$ 0.15, which was similar to the data in the literature as presented in Table 5.4. The oxygen content in the raw septage was extremely low, where only two samples had a DO concentration higher than 1 mg l^{-1}. The DO content in raw septage was fluctuating throughout the experiments, and the mean concentration was 0.39 $\pm$ 0.32 mg l^{-1}. The temperature of the raw septage was 27.65 $\pm$ 1.33 ˚C on average. These results revealed that the raw septage was slightly alkaline and typically anaerobic.

Figure 5.23: Sample of raw septage.

The concentration of TS in twenty-four samples was highly variable, ranging from 1,400 to 24,000 mg l^{-1}, with only eight samples constituting TS of more than 10,000 mg l^{-1}. The mean concentration of TS was only 8,000 $\pm$ 6,465.96 mg l^{-1}. This mean concentration was much lower compared to the data from the literature as shown in Table 5.4. Due to the lower TS concentration, the mean concentration of TCOD appeared to be low compared to the literature data. The maximum concentration of TCOD was only 8,606 mg l^{-1} and was much lower than the literature data. The mean concentration of TCOD was 3,847.79 $\pm$ 2,587.61 mg l^{-1}.

The concentration of TCOD was compared to the solids content, which is demonstrated in Figure 5.24. It shows a linear relation between organic matter and solids content in raw septage. The concentration of TCOD was about half of the TS concentration. Nevertheless, this study did not further include the analysis of the fraction of particulate to total COD in the raw septage, and thus it was impossible to quantify a factor to correlate the organic matter and the solids content.

The nitrogenous constituents in the raw septage, including TN, NH_4^+-N and NO_3^--N, were highly variable between various batches of the collection. The concentration of TN varied from 44 mg l^{-1} to 371 mg l^{-1}. The mean TN concentration from twenty-three samples was 165.97 $\pm$ 105.09 mg l^{-1}, which was much lower compared to the concentration of total Kjeldahl nitrogen (TKN) in the literature. Figure 5.25 illustrates a linear relationship between the concentration of TN and TS, highlighting the contribution of solids content to the amount of nitrogen in raw septage.

The concentrations of NH_4^+-N ranged from 32 to 84 mg l^{-1} throughout the experiments, and the mean concentration was 52.06 $\pm$ 13.39 mg l^{-1}. The lower standard deviation indicates that the amount of NH_4^+-N was relatively consistent in the raw septage. However, this concentration was much lower compared to the literature data as stated in Table 5.4. Meanwhile, the range of NO_3^--N concentration was between 2.63 to 28.50 mg l^{-1} and the mean concentration was 9.40 $\pm$ 5.97 mg l^{-1}, which was comparable to the literature data. As for the Org-N, there were two cases showing negative values since its concentration was estimated from the nitrogen balance among TN, NH_4^+-N and NO_3^--N. The minimum and maximum concentration of Org-N were 2.53 and 307.27 mg l^{-1}, respectively, while the mean concentration was 116.02 $\pm$ 99.48 mg l^{-1}. Figure 5.26 shows that the total concentrations of NH_4^+-N and NO_3^--N were

Table 5.3: Quality of raw septage for twenty-five batches of treatment

No. of test A = Wetland A B= Wetland B		pH	DO (mg l^{-1})	Temp (°C)	TS (mg l^{-1})	TCOD (mg l^{-1})	TN (mg l^{-1})	NH_4^+-N (mg l^{-1})	NO_3^--N (mg l^{-1})	Org-N (mg l^{-1})
1A	18/11/2015	7.39	0.35	26.90	3,400.00	1,383.00	51.00	54.90	10.20	-**
2A	24/11/2015	7.34	0.25	26.80	10,600.00	4,578.00	176.00	47.00	10.00	119.00
3A	01/12/2015	7.45	0.48	26.90	4,800.00	1,411.00	120.00	47.90	11.00	61.10
4B	4/12/2015	7.61	0.26	28.70	1,400.00	1,019.00	80.00	44.50	7.75	27.80
5A	08/12/2015	7.68	0.45	29.70	-*	-*	-*	41.80	14.10	-*
6A	12/12/2015	7.59	1.46	29.60	1,600.00	1,583.00	44.00	35.20	17.40	-**
7B	13/12/2015	7.41	0.30	30.90	1,400.00	997.00	78.00	36.40	28.50	13.10
8A	16/12/2015	7.37	0.38	28.50	12,800.00	7,485.00	242.00	61.90	17.50	162.60
9B	17/12/2015	7.47	0.72	26.70	4,600.00	4,203.00	150.00	49.10	9.54	91.40
10B	24/12/2015	7.41	1.14	28.60	10,700.00	5,162.00	-*	74.50	2.75	-*
11A	27/12/2015	7.53	0.05	24.10	12,600.00	8,606.00	203.00	84.00	2.69	116.30
12B	31/12/2015	7.61	0.10	27.60	9,500.00	6,471.00	151.00	58.00	8.09	84.90
13B	7/1/2016	7.72	0.68	29.00	4,200.00	2,698.00	125.00	74.30	8.97	41.70
14A	10/01/2016	7.66	0.26	27.90	9,600.00	3,888.00	318.00	65.50	8.63	243.90
15B	14/01/2016	7.55	0.19	27.80	24,000.00	7,753.00	368.00	58.10	2.63	307.30
16A	21/01/2016	7.61	0.11	26.80	1,700.00	850.00	72.00	32.00	5.23	34.80
17B	21/1/2016	7.46	0.25	26.70	19,500.00	6,846.00	335.00	35.60	8.66	290.70
18A	24/01/2016	7.86	0.50	26.80	2,200.00	904.00	56.00	48.30	5.17	2.50
19B	24/1/2016	7.89	0.35	27.30	2,700.00	1,162.00	99.00	48.40	5.44	45.20
20A	28/01/2016	7.62	0.25	27.80	3,200.00	3,049.00	121.00	44.10	4.58	72.30
21B	28/1/2016	7.66	0.22	27.30	1,500.00	1,162.00	49.00	40.50	4.21	4.30
22A	16/02/2016	7.71	0.28	27.70	7,800.00	3,415.00	169.00	55.40	6.14	107.50
23B	16/02/2016	7.68	0.24	26.70	8,900.00	4,232.00	161.00	60.10	8.78	92.10
24B	21/2/2016	7.64	0.21	27.50	18,600.00	7,052.00	371.00	62.30	8.53	300.20
25B	27/2/2016	7.47	0.18	26.90	14,700.00	6,438.00	278.00	41.80	18.40	217.80
	Max.	7.89	1.46	30.90	24,000.00	86,06.00	371.00	84.00	28.50	307.27
	Min.	7.34	0.05	24.10	1,400.00	850.00	44.00	32.00	2.63	2.53
	Mean	7.58	0.39	27.65	8,000.00	3,847.79	165.96	52.06	9.40	116.02
	Standard Deviation	0.15	0.32	1.33	6,465.96	2,587.61	105.09	13.39	5.97	99.48

**experimental error*

***TN < NH_4^+-N + NO_3^--N*

Table 5.4: Average concentration of quality parameters in the literature

	Country	pH	TS (mg l^{-1})	TCOD (mg l^{-1})	TKN (mg l^{-1})	NH_4^+-N (mg l^{-1})	NO_3^--N (mg l^{-1})
Koottatep et al. (2004)	Thailand	7.50	15,350	15,700	1,100	415**	7
Paing and Voisin (2005)	France	-	27,887*	32,954	1,142	-	13
Cofie et al. (2006)	Ghana	8.10	<20,000	<20,000	-	<1000**	-
Kengne et al. (2009)	Ghana	7.50	27,600*	31,100	1,100	600	-
Troesch, Lienard, et al. (2009)	France	7.30	33,675	46,255	1,546	308	-
Vincent et al. (2011)	France	-	23,000*	42,000	1,423	287	-

**measured as total suspended solids*

***measured as NH_3-N*

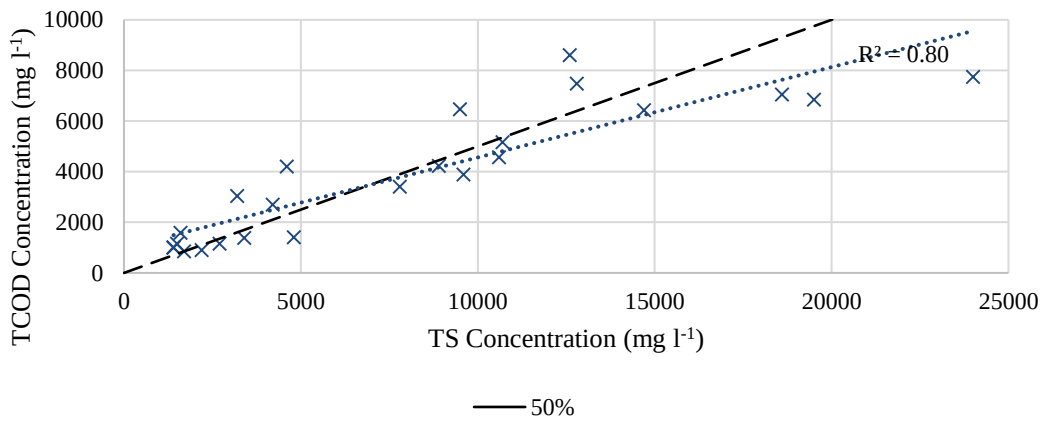

Figure 5.24: TCOD concentration versus TS concentration

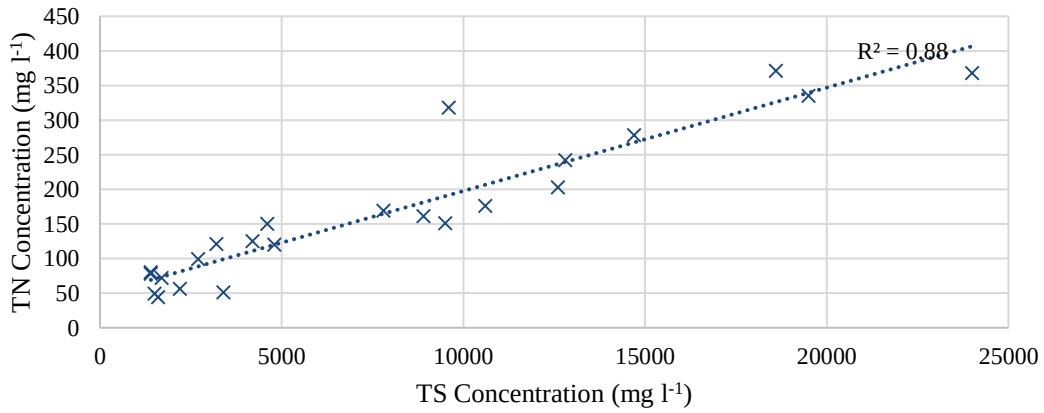

Figure 5.25: TN concentration versus TS concentration

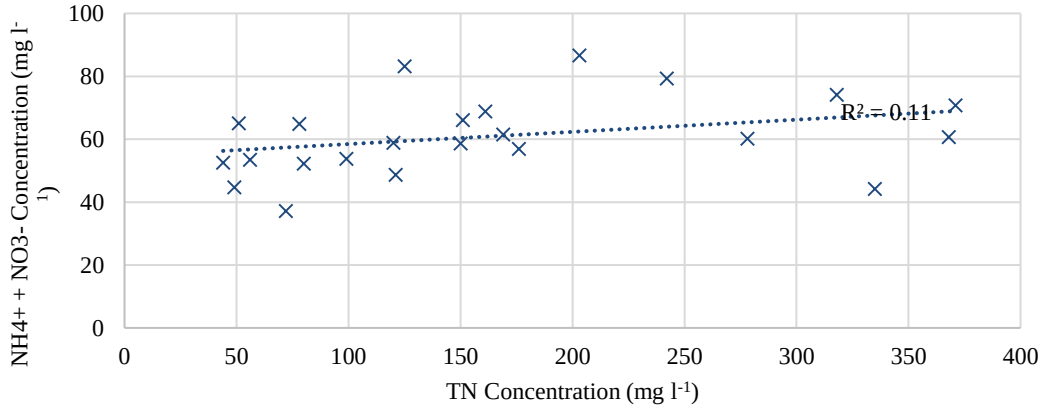

Figure 5.26: TN concentration versus NH_4^+-N + NO_3^--N concentration

considerably consistent with regards to the varying TN concentration. The concentration ranged from 40 to 80 mg l^{-1} for twenty-three samples. On the other hand, the linear regression line presented in Figure 5.27 indicates the dependency of Org-N on the concentration of TN. As mentioned previously, this study excluded the extraction of solid constituents, and thus the portion of particulate and dissolved organic components was unable to be evaluated. In Figure 5.28, a relationship was observed between the concentration of Org-N and TS, indicating that the majority of Org-N existed in particulate form. However, the comparison between the TCOD and Org-N as illustrated in Figure 5.29 shows no significant relationship, and the ratio of Org-N/TCOD varied from 0.28 % to 6.27 %. The low fraction showed the minor portion of Org-N in the overall organic matter. As a result, it can be concluded that that the concentration of dissolved nitrogenous constituents in raw septage, which mainly existed in the form of NH_4^+-N and NO_3^--N, were relatively consistent and independent from the concentration of TN and TS. Meanwhile, the Org-N, which mainly existed in particulate form, potentially dominated the nitrogen sources in the raw septage when the solids content was high.

5.3.2. Overall analysis of effluent quality

The pilot-scale, two-stage VFCW has been proven to provide a reliable efficiency on solids, organic matter, and ammonia removals. Nevertheless, the analysis of the removal efficiency remained at a “black-box” approach, where the treatment performance was evaluated based on the total mass removal rate from the influent (Jong 2014; Jong and Tang 2014, 2015). This approach provided a simple

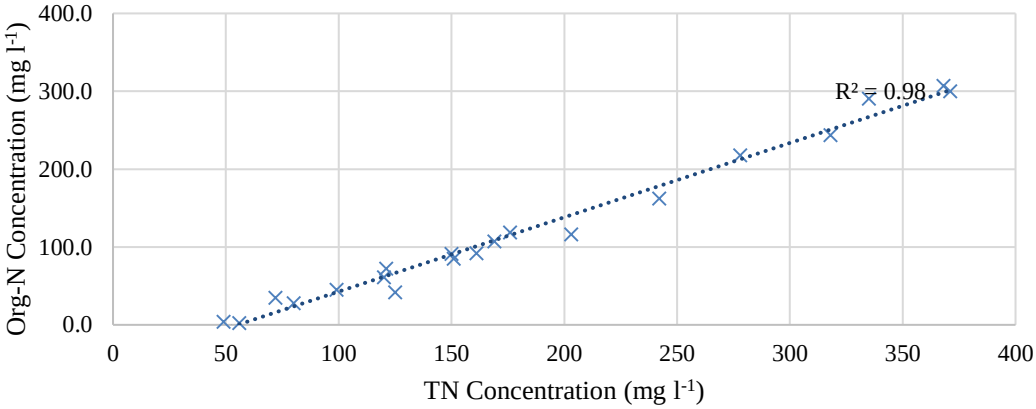

Figure 5.27: TN concentration versus Org-N concentration

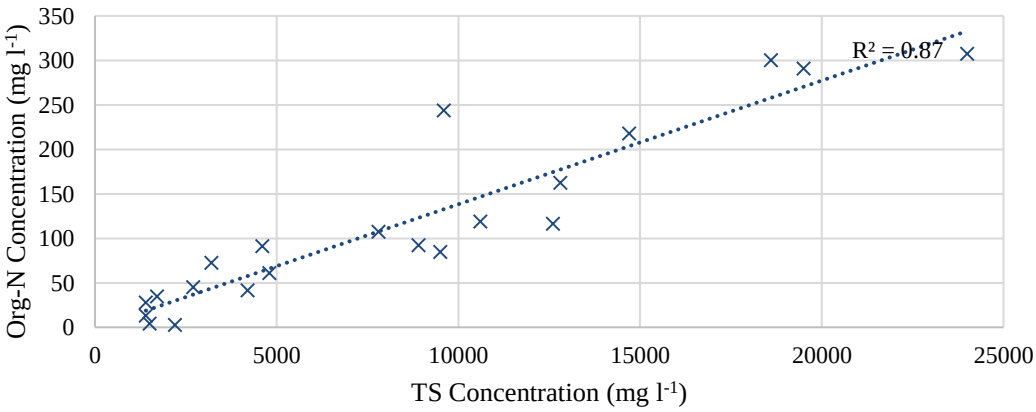

Figure 5.28: TS concentration versus Org-N concentration

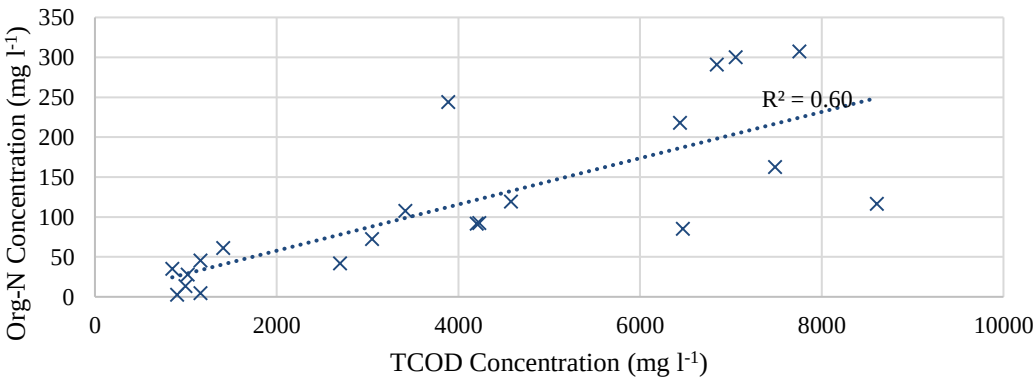

Figure 5.29: TCOD concentration versus Org-N concentration

methodology to quantify the treatment efficiency with respect to varying influent quality; however, the lack of information with regards to the correlation between the dynamics of outflow and the concentration of contaminants potentially overestimated the treatment performance.

In order to provide a more reliable analysis on the impact of hydraulic behaviour, a continuous sampling method was carried out to simultaneously measure the quantity and quality of effluent. Accordingly, the relationship between the hydraulic and treatment efficiency could be subsequently used for the numerical modelling or optimization of operation. The complete results of effluent quality are presented in Appendix C. Figure 5.30 shows an example of the sample collection, where the effluent demonstrated a gradient of cleanliness with regards to time. Twenty -five sets of data have been collected with regard to the varying hydraulic load, and the quality parameters measured included DO, pH, temperature, TS, TCOD, TN, NH_4^+-N and NO_3^--N. It should be noted that the concentration of TS, TCOD and TN were not tracked in detail due to the time constraint.

5.3.2.1. Dissolved oxygen (DO)

Figure 5.31 demonstrates the temporal concentration of effluent for twenty-five loading events. Compared to the anoxic influent, the effluent was significantly aerated and the DO concentrations were mostly within the range of 5.00 to 7.00 mg l^{-1}. The maximum DO concentration in the effluent could reach up to 7.50 mg l^{-1}. This value was close to the saturated DO concentration in the water under 25˚C (8.30 mg l^{-1} as stated in American Public Health et al. (1915)).

Figure 5.30: The samples of effluent showed a gradient of cleanliness with regards to time (Case 3A)

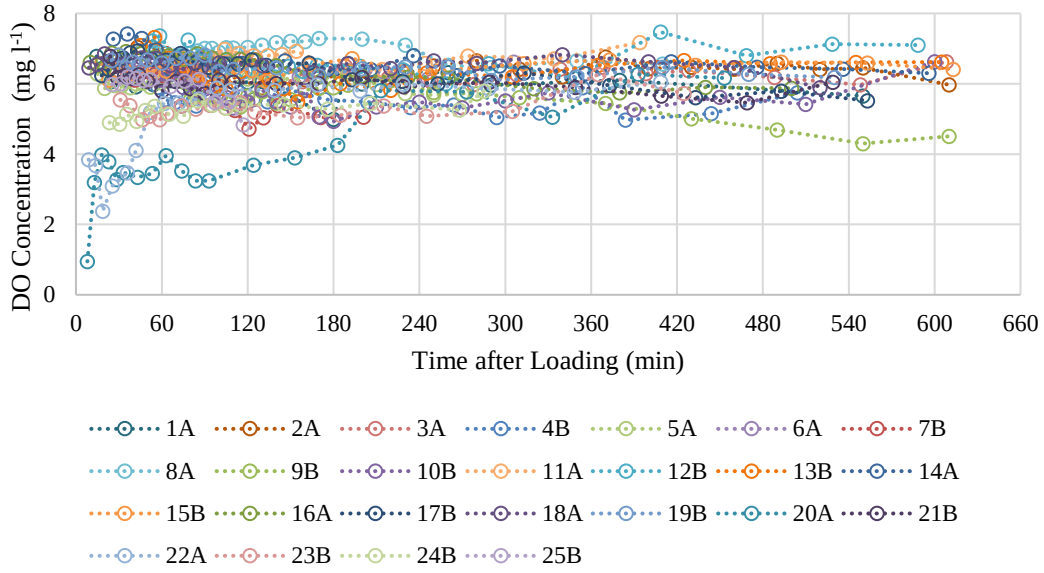

Figure 5.31: Temporal plots of DO concentration in the effluent for twenty-five batches of treatment

According to a study about the oxygen transport in a down-flow VFCW (Fuchs 2009), the unsaturated condition in the substrate ensured a sufficient aeration capacity to meet the oxygen demand for biodegradation. The high DO concentration measured in the effluent highlights the great oxygen restoration in the pilot plant. Nevertheless, the DO concentration in the early effluent of case 20A and 22A were relatively low (below 4.00 mg l^{-1}). This phenomenon was attributed to the rapid infiltration rate caused by the thin sludge deposit layer, which was 3 cm in both cases. The thin sludge layer led to insufficient retention time for aeration. This correlation will be further discussed in section 5.3.3.

5.3.2.2. pH

The dynamics of pH in the effluent is stable in the entire experiment. The average pH in the influent was 7.58 ± 0.15, and Figure 5.32 shows that the pH in the effluent ranged between 7.50 and 8.30. The rise of pH is attributed to the biodegradation in the wetland bed, where the nitrification consumes the alkalinity in the process. The relationship between pH and outflow dynamics is insignificant.

5.3.2.3. Temperature

The temperature of the effluent was greatly affected by the surrounding environment. In a loading event, the temperature generally reached the maximum after 180 – 240

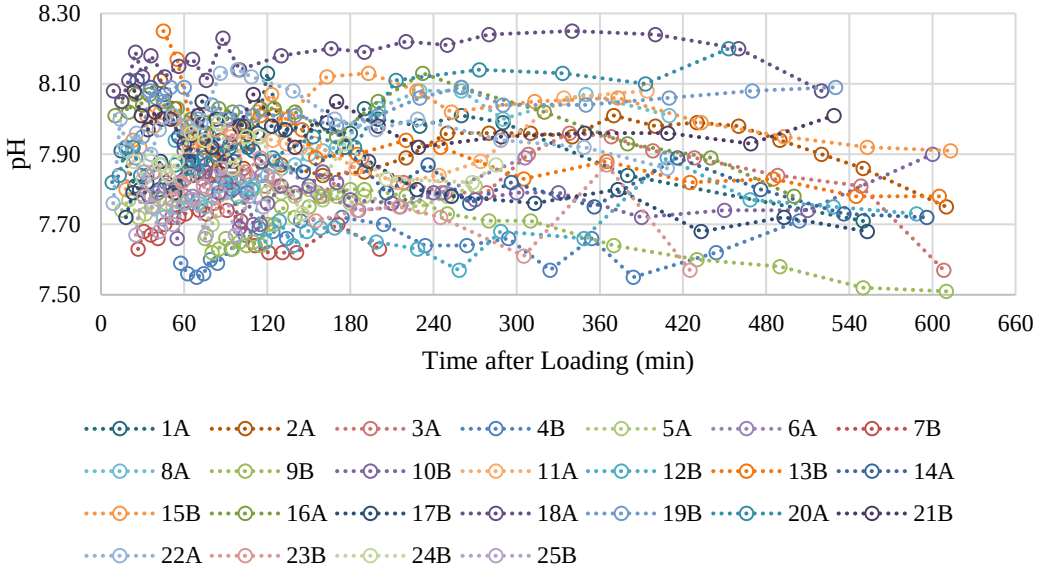

Figure 5.32: Temporal plots of pH in the effluent for twenty-five batches of treatment

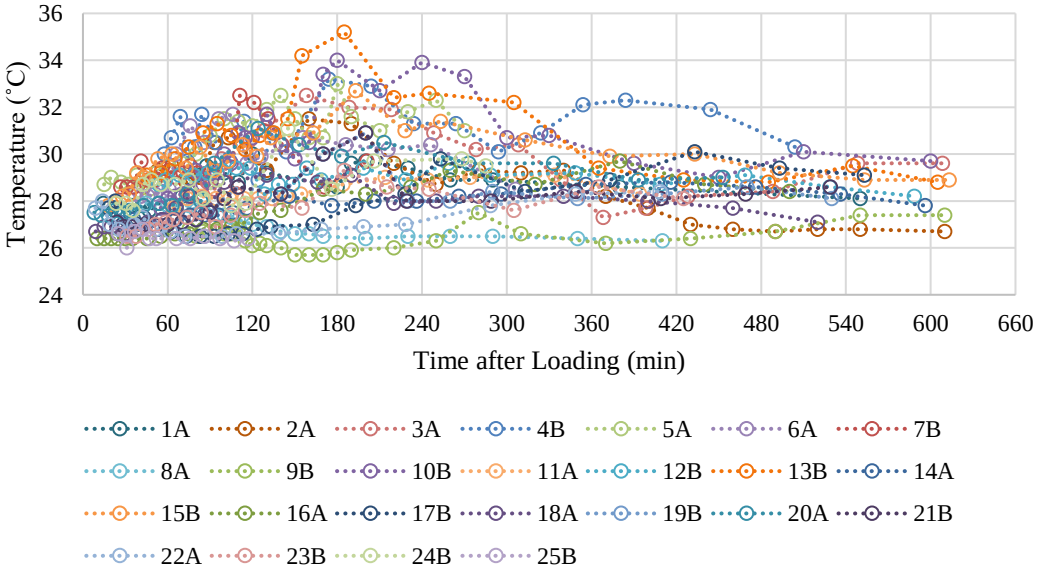

Figure 5.33: Temporal plots of temperature in the effluent for twenty-five batches of treatment

minutes from loading as illustrated in Figure 5.33. It was because the loading typically started at 7.00 am and the temperature reached the maximum at approximately 10.00 am – 12.00 pm. Then, the sunlight imposed on the wetland bed gradually reduced after 12.00 pm (due to the orientation of the experiment site and wetland beds), and thus the

temperature of the effluent was observed with a decline. The temporal temperatures widely distributed between 26˚C and 35˚C and the influence of outflow dynamics is insignificant. This range of temperature is favourable for bioactivity, where the optimum temperature is between 25˚C and 35˚C as stated in Water Environment Federation, Federation, and Institute (2005).

5.3.2.4. Total solids (TS)

As mentioned previously, the TS in the effluent was not completely tracked as the parameters above. The lack of data resulted in a poor resolution in the temporal plots as demonstrated in Figure 5.34. There was no general trend observed in the entire experiment. Nevertheless, Figure 5.30 shows that the turbidity of the effluent sample gradually reduced due to a reduction in the solids content. It should be noted that this phenomenon was only applied to the case with "typical flow" pattern. As for the "bypass" case, the turbidity was always fluctuating, which is displayed in Figure 5.35.

The overall removal of TS in the pilot plant is promising, where the TS concentration in the effluent was reduced to under 3,500 mg l^{-1} from the mean influent concentration of 8,000 mg l^{-1}. The main mechanism to remove TS in the VFCW is the physical filtration at the wetland surface. The excellent performance of the proposed system indicates that the sand layer is unnecessary to enhance the efficiency of filtration. The

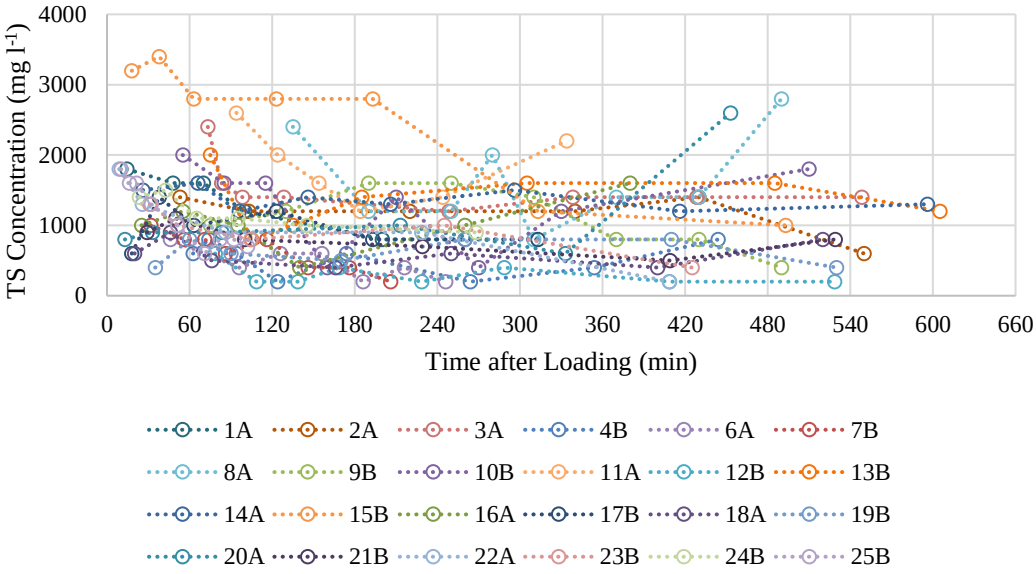

Figure 5.34: Temporal plots of TS concentration in the effluent for twenty-four batches of treatment

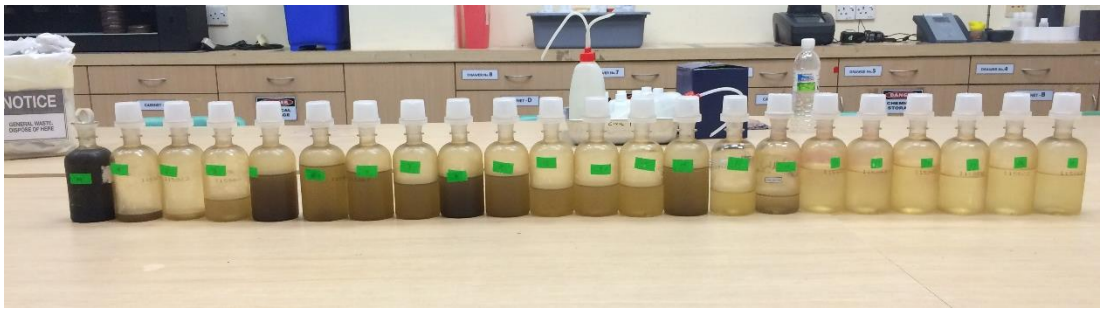

Figure 5.35: Samples of effluent for case 13B (7th January 2016 – clogging)

natural formation of sludge deposit layer at the wetland surface is capable of delivering a substantial removal for TS.

Table 5.5 summarizes the removal efficiency of TS. The average removal rate of TS was 77.74 ± 15.95 %. There were only four cases showing removal efficiency less than 60%, highlighting the great ability of TS removal in the proposed system. Nevertheless, the average removal rate was lower than the data from the literature, where the efficiency could reach up to 80 – 90 % (Lienard and Payrastre 1996; Koottatep et al. 2001; Paing and Voisin 2005; Kengne et al. 2008; Troesch, Lienard, et al. 2009; Jong and Tang 2013). There was no direct correlation between the hydraulic efficiency and TS removal; however, a higher solids load tends to result in a higher TS removal rate as demonstrated in Figure 5.36.

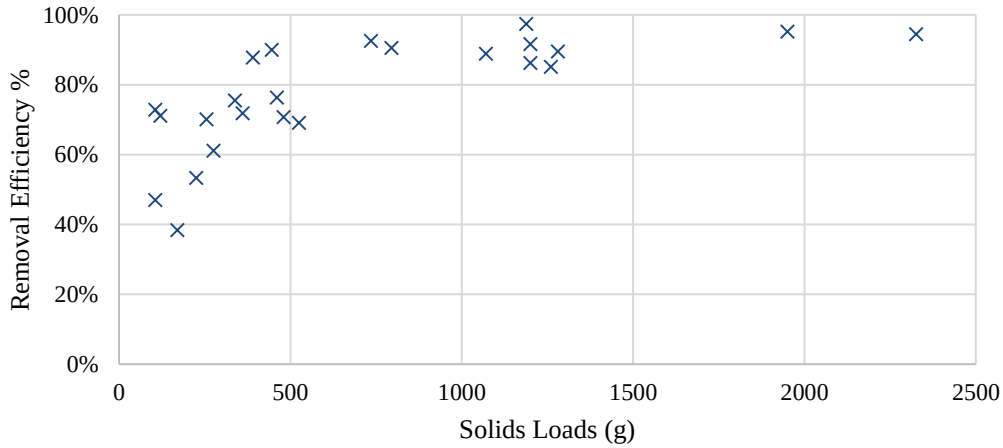

Figure 5.36: Solid loads versus TS removal

Table 5.5: Removal efficiency of TS

No. of test A = Wetland A B= Wetland B		HLR (L)	Sludge thickness (cm)	SLR (g)	Water recovery (%)	Peak effluent flux (cm min^{-1})	TS removal efficiency (%)
1A	18/11/2015	75	5	255	85.08%	0.026182	70.07%
2A	24/11/2015	75	5	795	80.55%	0.013394	90.51%
3A	01/12/2015	75	6	360	71.92%	0.014909	71.80%
4B	4/12/2015	75	7	105	85.87%	0.026076	72.82%
5A	08/12/2015	75	7	-*	83.77%	0.027955	-*
6A	12/12/2015	75	5	120	68.14%	0.029045	71.06%
7B	13/12/2015	75	5	105	69.48%	0.065182	46.97%
8A	16/12/2015	100	6	1280	73.41%	0.042455	89.49%
9B	17/12/2015	100	5	460	70.10%	0.018667	76.32%
10B	24/12/2015	100	12	1070	22.75%	0.006955	88.89%
11A	27/12/2015	100	8	1260	47.34%	0.016591	85.09%
12B	31/12/2015	125	12	1187.5	14.58%	0.003833	97.33%
13B	7/1/2016	125	9	525	9.72%	0.007227	69.05%
14A	10/01/2016	125	12	1200	11.04%	0.002682	86.18%
15B	14/01/2016	50	10	1200	24.49%	0.003455	91.57%
16A	21/01/2016	100	3	170	45.32%	0.014864	38.33%
17B	21/1/2016	100	3	1950	47.59%	0.011975	95.13%
18A	24/01/2016	125	3	275	90.00%	0.031383	61.04%
19B	24/1/2016	125	4	337.5	88.61%	0.045455	75.47%
20A	28/01/2016	150	3	480	81.37%	0.072727	70.72%
21B	28/1/2016	150	4	225	42.44%	0.022182	53.26%
22A	16/02/2016	50	3	390	62.48%	0.034364	87.76%
23B	16/02/2016	50	4	445	67.43%	0.015545	89.94%
24B	21/2/2016	125	5	2325	56.43%	0.031667	94.48%
25B	27/2/2016	50	6	735	76.77%	0.056000	92.49%
	Max.	150	12	2325	90.00%	0.072727	97.33%
	Min.	50	3	105	9.72%	0.002682	38.33%
	Average	95	5.88	718.96	59.07%	0.025631	77.74%
	Standard Deviation	30.62	2.64	597.23	25.70%	0.018859	15.95%

**experimental error*

5.3.2.5. Total chemical oxygen demand (TCOD)

Figure 5.37 shows that the concentration of TCOD in the effluent reduced gradually. Compared to the average concentration of influent (3,847.49 ± 2,587.61 mg l^{-1}), the removal of TCOD is impressive as most of the concentrations remained below 800 mg l^{-1} in the effluent. Table 5.6 indicates that the average TCOD removal could reach up to 89.11 ± 9.10 % and it was comparable to the literature data (Lienard and Payrastre 1996; Koottatep et al. 2001; Paing and Voisin 2005; Kengne et al. 2008; Troesch, Lienard, et al. 2009; Jong and Tang 2013). There were only three cases demonstrating a removal efficiency below 80 %, and thus the removal of TCOD was considered to be more consistent than the removal of TS.

The concentrations of TCOD in the effluent showed a dependency on the TS concentration. Therefore, the substantial removal of TCOD could be attributed to the physical filtration. The residual biodegradable organic matter was then decayed by the hydrolysis process and was ultimately consumed by the heterotrophs. The aerobic condition in the VFCW is favourable for the removal of organic matter (Vymazal 2010a). The consistent removal of TCOD showed no dependency on the system configuration and operating regime. Nevertheless, the concentration of TCOD in the effluent showed a similar trend with the typical outflow dynamics. A slower

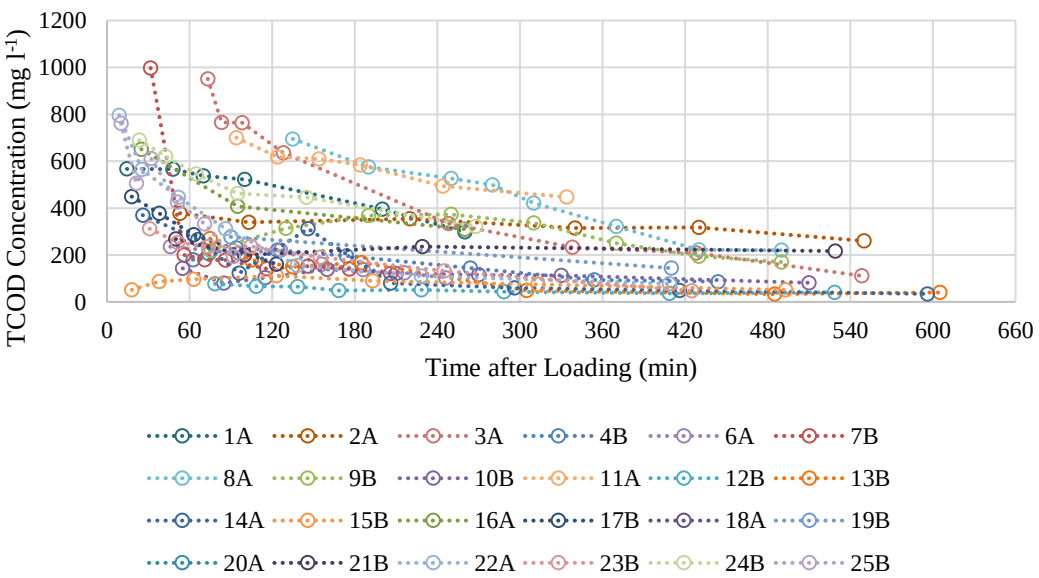

Figure 5.37: Temporal plots of TCOD concentration in the effluent for twenty-four batches of treatment

Table 5.6: Removal efficiency of TCOD

No. of test A = Wetland A B= Wetland B		HLR (L)	Sludge thickness (cm)	SLR (g)	Water recovery (%)	Peak effluent flux (cm min^{-1})	TCOD removal efficiency (%)
1A	18/11/2015	75	5	255	85.08%	0.026182	69.85%
2A	24/11/2015	75	5	795	80.55%	0.013394	93.19%
3A	01/12/2015	75	6	360	71.92%	0.014909	77.45%
4B	4/12/2015	75	7	105	85.87%	0.026076	84.11%
5A	08/12/2015	75	7	-*	83.77%	0.027955	-*
6A	12/12/2015	75	5	120	68.14%	0.029045	90.04%
7B	13/12/2015	75	5	105	69.48%	0.065182	83.56%
8A	16/12/2015	100	6	1280	73.41%	0.042455	93.16%
9B	17/12/2015	100	5	460	70.10%	0.018667	98.89%
10B	24/12/2015	100	12	1070	22.75%	0.006955	97.90%
11A	27/12/2015	100	8	1260	47.34%	0.016591	93.61%
12B	31/12/2015	125	12	1187.5	14.58%	0.003833	99.30%
13B	7/1/2016	125	9	525	9.72%	0.007227	95.96%
14A	10/01/2016	125	12	1200	11.04%	0.002682	97.91%
15B	14/01/2016	50	10	1200	24.49%	0.003455	95.48%
16A	21/01/2016	100	3	170	45.32%	0.014864	65.55%
17B	21/1/2016	100	3	1950	47.59%	0.011975	96.41%
18A	24/01/2016	125	3	275	90.00%	0.031383	81.44%
19B	24/1/2016	125	4	337.5	88.61%	0.045455	84.49%
20A	28/01/2016	150	3	480	81.37%	0.072727	87.73%
21B	28/1/2016	150	4	225	42.44%	0.022182	80.59%
22A	16/02/2016	50	3	390	62.48%	0.034364	89.18%
23B	16/02/2016	50	4	445	67.43%	0.015545	95.83%
24B	21/2/2016	125	5	2325	56.43%	0.031667	94.00%
25B	27/2/2016	50	6	735	76.77%	0.056000	92.96%
	Max.	150	12	2325	90.00%	0.072727	99.30%
	Min.	50	3	105	9.72%	0.002682	65.55%
	Average	95	5.88	718.96	59.07%	0.025631	89.11%
	Standard Deviation	30.62	2.64	597.23	25.70%	0.018859	9.10%

**experimental error*

percolation in the wetland bed was positive to the treatment process as it extended the retention time of influent in the wetland bed.

5.3.2.6. Nitrogen dynamics

The nitrogen dynamics in the pilot-scale VFCW was a complex cycle. The nitrogenous constituents mainly existed in the form of Org-N, NH_4^+-N and NO_3^-- N, and the concentration of NO_2^-- N was negligibly low throughout the experiment. Figure 5.38 illustrates the temporal concentration of TN in the effluent for twenty-four sets of loading event. Table 5.7 presents the treatment efficiency of the TN. The concentration of TN were highly dynamic in the effluent and an average removal efficiency of 68.81 $\pm$ 16.45 % was achieved. It should be noted that the TN concentration in the effluent was always less than the summation of the concentration of NH_4^+-N and NO_3^-- N, and thus the temporal concentration of Org-N was unable to be identified in this part of analysis. The TN removal rate compared to the treatment efficiency of TKN. As the literature indicated that the removal of TKN generally exceeded 80% (Lienard and Payrastre 1996; Koottatep et al. 2001; Paing and Voisin 2005; Kengne et al. 2008; Troesch, Lienard, et al. 2009), the removal of TN in the proposed system was underperforming. However, it should be noted that the contribution of NO_3^-- N was significant in the effluent, implying that the removal efficiency of TN was generally lower than TKN.

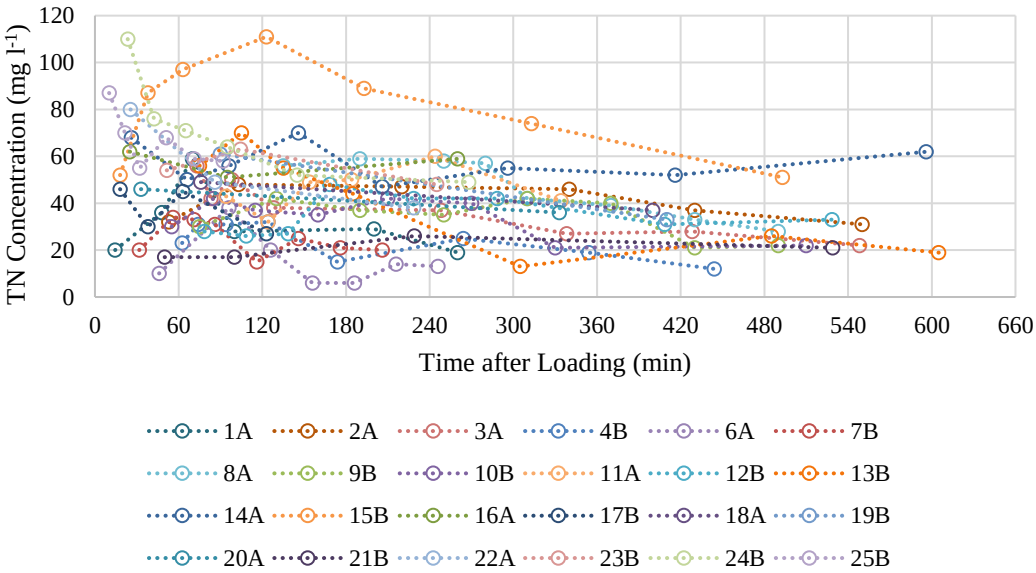

Figure 5.38: Temporal plots of TN concentration in the effluent for twenty-four batches of treatment

Table 5.7: Removal efficiency of TN

No. of test A = Wetland A B= Wetland B		HLR (L)	Sludge thickness (cm)	SLR (g)	Water recovery (%)	Peak effluent flux (cm min^{-1})	TN removal efficiency (%)
1A	18/11/2015	75	5	255	85.08%	0.026182	41.70%
2A	24/11/2015	75	5	795	80.55%	0.013394	77.17%
3A	01/12/2015	75	6	360	71.92%	0.014909	73.41%
4B	4/12/2015	75	7	105	85.87%	0.026076	71.59%
5A	08/12/2015	75	7	-*	83.77%	0.027955	-*
6A	12/12/2015	75	5	120	68.14%	0.029045	79.55%
7B	13/12/2015	75	5	105	69.48%	0.065182	63.95%
8A	16/12/2015	100	6	1280	73.41%	0.042455	77.35%
9B	17/12/2015	100	5	460	70.10%	0.018667	96.37%
10B	24/12/2015	100	12	1070	22.75%	0.006955	-
11A	27/12/2015	100	8	1260	47.34%	0.016591	77.17%
12B	31/12/2015	125	12	1187.5	14.58%	0.003833	76.57%
13B	7/1/2016	125	9	525	9.72%	0.007227	69.06%
14A	10/01/2016	125	12	1200	11.04%	0.002682	82.13%
15B	14/01/2016	50	10	1200	24.49%	0.003455	77.87%
16A	21/01/2016	100	3	170	45.32%	0.014864	43.10%
17B	21/1/2016	100	3	1950	47.59%	0.011975	89.96%
18A	24/01/2016	125	3	275	90.00%	0.031383	31.99%
19B	24/1/2016	125	4	337.5	88.61%	0.045455	58.95%
20A	28/01/2016	150	3	480	81.37%	0.072727	68.73%
21B	28/1/2016	150	4	225	42.44%	0.022182	55.94%
22A	16/02/2016	50	3	390	62.48%	0.034364	42.72%
23B	16/02/2016	50	4	445	67.43%	0.015545	67.25%
24B	21/2/2016	125	5	2325	56.43%	0.031667	84.56%
25B	27/2/2016	50	6	735	76.77%	0.056000	76.77%
	Max.	150	12	2325	90.00%	0.072727	96.37%
	Min.	50	3	105	9.72%	0.002682	31.99%
	Average	95	5.88	718.96	59.07%	0.025631	68.81%
	Standard Deviation	30.62	2.64	597.23	25.70%	0.018859	16.45%

**experimental error*

To have a better understanding with regards to the nitrogen dynamics in the proposed VFCW, the analysis of the overall nitrogen removal has to be split into specific constituents, which include NH_4^+-N and NO_3^--N. The average NH_4^+-N concentration in the influent was 52.06 ± 13.39 mg l^{-1}, while the concentration in the effluent was reduced to 50 mg l^{-1}. Figure 5.39 displays that the concentration of NH_4^+-N in the effluent distributed between 0.93 mg l^{-1} and 70.00 mg l^{-1}. Typically, the concentration of NH_4^+-N rapidly rose at the early phase. Then, it was followed by a gradual reduction.

Table 5.8 shows that thirteen cases were obtained with removal efficiency below 50 % and the average removal efficiency was only 48.86 ± 21.37%. The removal efficiency was comparable to the performance observed by Lienard and Payrastre (1996) and Troesch, Lienard, et al. (2009), but it was significantly lower than Koottatep et al. (2004), Kengne et al. (2009) and Jong and Tang (2013). The dynamics of NH_4^+-N and removal efficiency revealed that the proposed system is still incapable of delivering a consistent and effective treatment upon NH_4^+-N.

In the VFCW, the removal of NH_4^+-N is dependent on the nitrification and adsorption. As the nitrification is a biochemical mechanism, it is sensitive to the percolation rate through the substrate. The same concept can be applied to the adsorption, which is a surface-based process that occurs when the contaminants passing by the available adsorbent site. Figure 5.40 illustrates a dependency of NH_4^+-N removal on peak

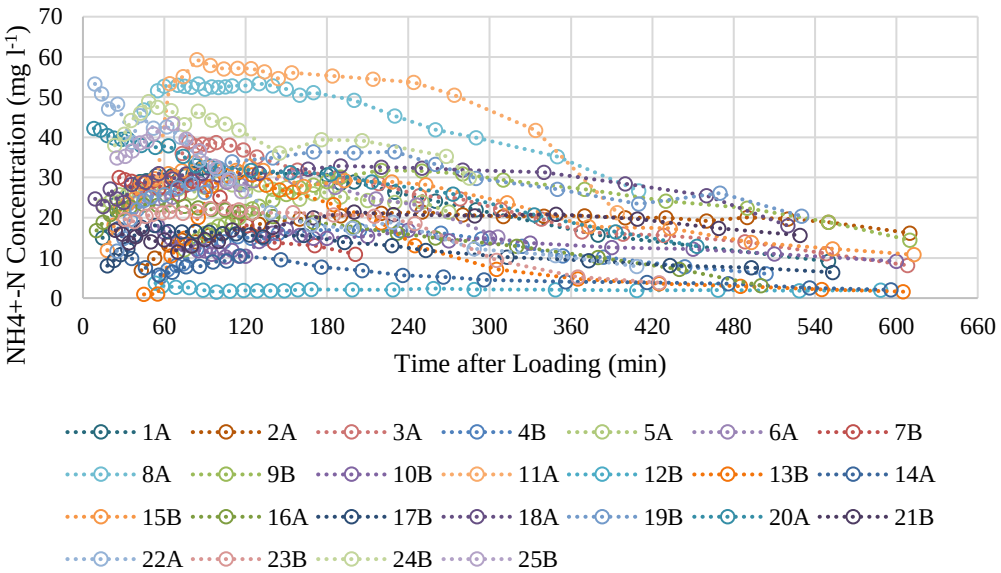

Figure 5.39: Temporal plots of NH_4^+-N concentration in the effluent for twenty-five batches of treatment

Table 5.8: Removal efficiency of NH_4^+-N

No. of test A = Wetland A B= Wetland B		HLR (L)	Sludge thickness (cm)	SLR (g)	Water recovery (%)	Peak effluent flux (cm min^{-1})	NH_4^+-N removal efficiency (%)
1A	18/11/2015	75	5	255	85.08%	0.026182	50.51%
2A	24/11/2015	75	5	795	80.55%	0.013394	58.09%
3A	01/12/2015	75	6	360	71.92%	0.014909	49.70%
4B	4/12/2015	75	7	105	85.87%	0.026076	67.36%
5A	08/12/2015	75	7	-*	83.77%	0.027955	37.55%
6A	12/12/2015	75	5	120	68.14%	0.029045	23.70%
7B	13/12/2015	75	5	105	69.48%	0.065182	25.52%
8A	16/12/2015	100	6	1280	73.41%	0.042455	19.56%
9B	17/12/2015	100	5	460	70.10%	0.018667	47.08%
10B	24/12/2015	100	12	1070	22.75%	0.006955	81.70%
11A	27/12/2015	100	8	1260	47.34%	0.016591	38.40%
12B	31/12/2015	125	12	1187.5	14.58%	0.003833	96.51%
13B	7/1/2016	125	9	525	9.72%	0.007227	76.94%
14A	10/01/2016	125	12	1200	11.04%	0.002682	79.36%
15B	14/01/2016	50	10	1200	24.49%	0.003455	57.73%
16A	21/01/2016	100	3	170	45.32%	0.014864	46.50%
17B	21/1/2016	100	3	1950	47.59%	0.011975	66.41%
18A	24/01/2016	125	3	275	90.00%	0.031383	36.86%
19B	24/1/2016	125	4	337.5	88.61%	0.045455	36.29%
20A	28/01/2016	150	3	480	81.37%	0.072727	24.09%
21B	28/1/2016	150	4	225	42.44%	0.022182	55.11%
22A	16/02/2016	50	3	390	62.48%	0.034364	33.95%
23B	16/02/2016	50	4	445	67.43%	0.015545	67.55%
24B	21/2/2016	125	5	2325	56.43%	0.031667	35.51%
25B	27/2/2016	50	6	735	76.77%	0.056000	9.53%
	Max.	150	12	2325	90.00%	0.072727	96.51%
	Min.	50	3	105	9.72%	0.002682	9.53%
	Average	95	5.88	718.96	59.07%	0.025631	48.86%
	Standard Deviation	30.62	2.64	597.23	25.70%	0.018859	21.37%

**experimental error*

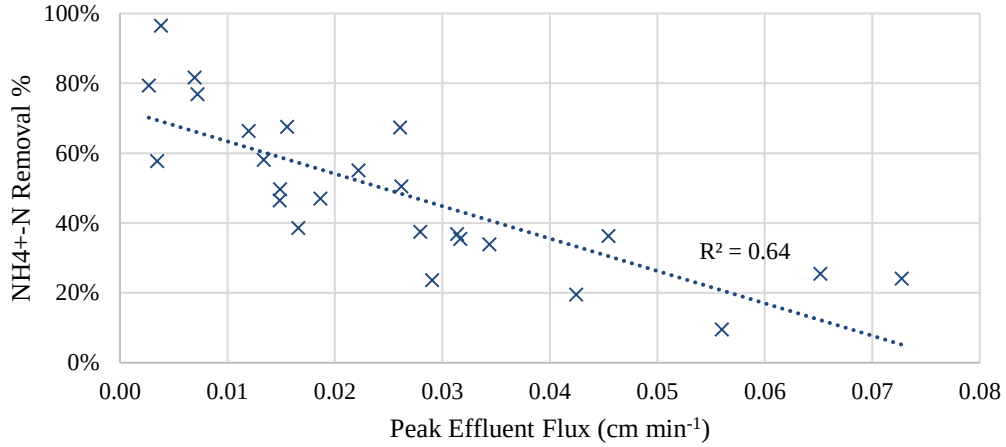

Figure 5.40: Peak effluent flux versus removal efficiency of NH_4^+-N

effluent flux. A rapid effluent flow typically led to a poor treatment performance. For those cases with peak effluent above 0.03 cm min^{-1}, the removal efficiencies of NH_4^+-N were always below 40 %.

The last concern in NH_4^+-N dynamics is the ammonification process. According to the influent quality, the fraction of Org-N was high in TN. The breakdown of Org-N potentially increased the concentration of NH_4^+-N. Nevertheless, the degradable and inert Org-N was not determined, and thus the ammonification rate was unable to be quantified in this study. However, this could be partially visualized by a further analysis of the balance between NH_4^+-N and NO_3^--N throughout the experiment.

In general, the concentration of NO_3^--N in the effluent was inversely proportional to the concentration of NH_4^+-N. A rise of NH_4^+-N was generally accompanied by a drop of NO_3^--N. The concentration of NO_3^--N declined at the early phase of effluent, and it only increased when the effluent flow started to decelerate as described in Figure 5.41. The high concentration in the effluent at the beginning of discharge is believed to be the NO_3^--N retained in the substrate before loading, and flushed out during the next draining. The concentration of NO_3^--N significantly increased from the average influent concentration of 9.40 $\pm$ 5.97 mg l^{-1} to at least 10 mg l^{-1}at the late stage of effluent. In addition to the source from influent, the rise of NO_3^--N was attributed to the nitrification of NH_4^+-N. This finding was supported by the drop of NH_4^+-N as shown in Figure 5.41. As a result, NO_3^--N was greatly affected by the outflow dynamics. There was only a case measured with a removal of NO_3^--N. In addition,

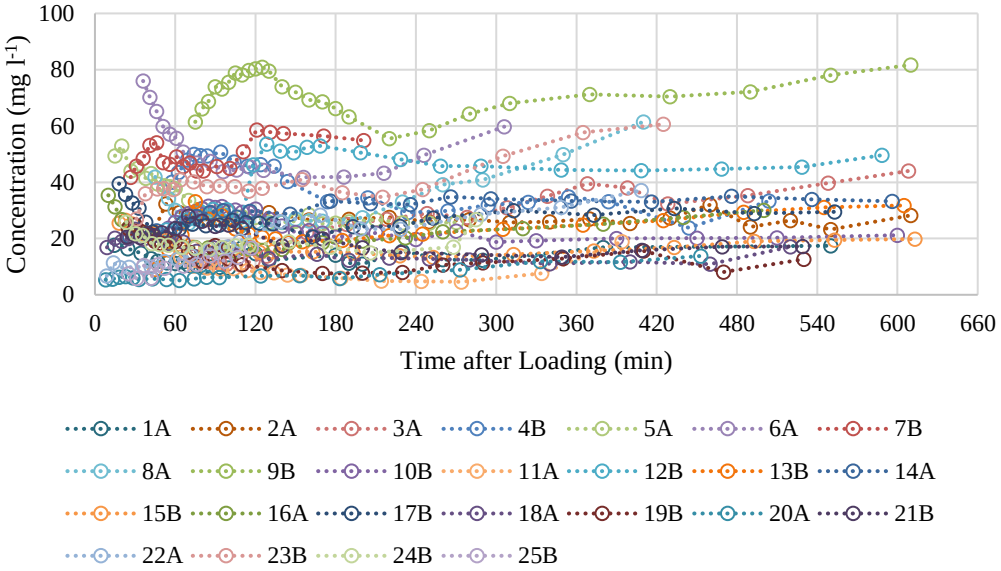

Figure 5.41: Temporal plots of NO_3^--N concentration in the effluent for twenty-five batches of treatment

the high DO concentration in the effluent indicated that the pilot-scale VFCW was unfavourable for the anoxic denitrification.

To have a better overview for the relation between NH_4^+-N and NO_3^--N, the dynamics of the combined concentration were evaluated. Figure 5.42 shows that the dynamics of NH_4^+-N and NO_3^--N were relatively stable, indicating that the ultimate removal of

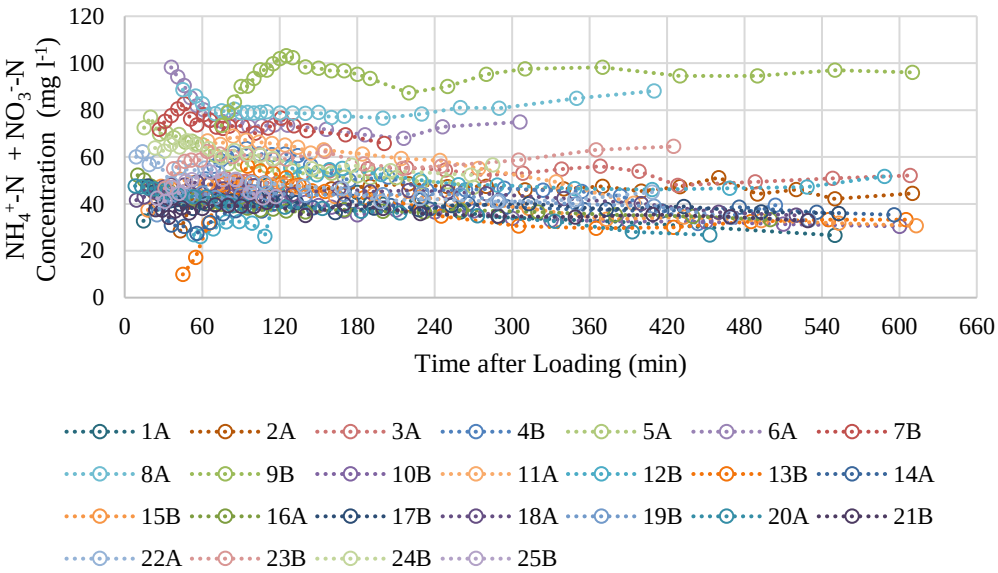

Figure 5.42: Temporal plots of NH_4^+-N + NO_3^--N in the effluent for twenty-five batches of treatment

Table 5.9: Removal efficiency of NH_4^+-N + NO_3^--N

No. of Test A = Wetland A B= Wetland B		HLR (L)	Sludge Thickness (cm)	Total Solid Loads (g)	Water Recovery %	Peak flow (cm min^{-1})	NH_4^+-N+ NO_3^--N Removal Efficiency (%)
1A	18/11/2015	75	5	255	85.08%	0.026182	37.72%
2A	24/11/2015	75	5	795	80.55%	0.013394	18.59%
3A	01/12/2015	75	6	360	71.92%	0.014909	11.05%
4B	4/12/2015	75	7	105	85.87%	0.026076	3.81%
5A	08/12/2015	75	7	-*	83.77%	0.027955	-1.37%
6A	12/12/2015	75	5	120	68.14%	0.029045	-42.27%
7B	13/12/2015	75	5	105	69.48%	0.065182	-15.31%
8A	16/12/2015	100	6	1280	73.41%	0.042455	-0.14%
9B	17/12/2015	100	5	460	70.10%	0.018667	-61.56%
10B	24/12/2015	100	12	1070	22.75%	0.006955	53.47%
11A	27/12/2015	100	8	1260	47.34%	0.016591	31.92%
12B	31/12/2015	125	12	1187.5	14.58%	0.003833	27.85%
13B	7/1/2016	125	9	525	9.72%	0.007227	50.44%
14A	10/01/2016	125	12	1200	11.04%	0.002682	49.18%
15B	14/01/2016	50	10	1200	24.49%	0.003455	32.26%
16A	21/01/2016	100	3	170	45.32%	0.014864	-2.21%
17B	21/1/2016	100	3	1950	47.59%	0.011975	12.53%
18A	24/01/2016	125	3	275	90.00%	0.031383	13.82%
19B	24/1/2016	125	4	337.5	88.61%	0.045455	20.50%
20A	28/01/2016	150	3	480	81.37%	0.072727	17.85%
21B	28/1/2016	150	4	225	42.44%	0.022182	18.67%
22A	16/02/2016	50	3	390	62.48%	0.034364	15.45%
23B	16/02/2016	50	4	445	67.43%	0.015545	14.70%
24B	21/2/2016	125	5	2325	56.43%	0.031667	18.36%
25B	27/2/2016	50	6	735	76.77%	0.056000	20.59%
	Max.	150	12	2325	90.00%	0.072727	53.47%
	Min.	50	3	105	9.72%	0.002682	-61.56%
	Average	95	5.88	718.96	59.07%	0.025631	13.84%
	Standard Deviation	30.62	2.64	597.23	25.70%	0.018859	25.49%

**experimental error*

nitrogen was still limited by the absence of denitrification in the pilot-scale system.

Based on the overall removal efficiency presented in Table 5.9, only six cases show a removal efficiency above 30 % and five cases were measured with increment. By neglecting the cases with increasing effluent concentrations, the average removal efficiency of combined NH_4^+-N and NO_3^--N was only 24.67 $\pm$ 13.86 %. All of these outcomes indicated that the current system configuration and operating regime were insufficiently effective to treat the dissolved nitrogenous constituents. Therefore, the majority of TN removal was attributed to the filtration of particulate Org-N. Furthermore, the rise of the combined concentration of NH_4^+-N and NO_3^--N showed that the ammonification of Org-N potentially recharged the amount of NH_4^+-N throughout the treatment.

In summary, the nitrogen dynamics in the pilot-scale VFCW designed for septage treatment was highly inconsistent. The overall treatment performance of TN was promising, which achieved an average removal efficiency of 68 %. Nevertheless, the average removal efficiency of NH_4^+-N was below 50 %. In addition, the increase of NO_3^--N in the effluent reflected that the pilot plant was incapable of delivering a complete removal pathway for the nitrogen. In the pilot-scale VFCW, ammonification and nitrification were the major biochemical mechanisms; however, denitrification was less likely to occur due to the dominant aerobic condition. The physical filtration of particulate Org-N at the wetland surface contributed remarkable nitrogen removal. The proposed system is necessary to be adapted with a secondary treatment, particularly an anoxic system to enhance the treatment of excessive NO_3^--N. Both the dynamics of NH_4^+-N and NO_3^--N exhibited a dependency on the hydraulic behaviour.

5.3.3. The correlation between hydraulic behaviour and nitrogen dynamic

In last section, the temporal plots of TS, TCOD, TN, NH_4^+-N and NO_3^-- N revealed that the hydraulic behaviour plays a key role in the treatment performance of the pilot-scale VFCW designed for septage treatment. However, its influence was only briefly explained since the analysis was hindered by the varying influent quality and operating condition. Therefore, case 22A and 23B, which were loaded with the same volume of septage under the same condition, were evaluated to highlight the correlation between outflow dynamics and treatment performance.

5.3.3.1. A direct comparison between 22A (Wetland A) versus 23 B (Wetland B)

Table 5.10 summarizes the initial thickness of sludge deposit and the influent quality of case 22A (Wetland A) and case 23B (Wetland B). The pH and the concentration of DO and TN of two cases were similar. The TS, NH_4^+-N, NO_3^--N and COD were slightly higher in the Wetland B. Except for the thickness of sludge, both cases characterized the same substrate profile and were loaded with 50 l (4.45 cm) of raw septage at the same time. Figure 5.43 displays the effluent collected in wetland A and wetland B, respectively. The sample collected from both cases showed a similar trend in colour change. The effluent contained high particulate constituents at the early phase. Then, the effluent gradually turned clear with the time. At the late phase, the effluent from wetland A was clearer than the effluent from wetland B.

The effluent flow rate and the cumulative flow of both beds are illustrated in Figure 5.44. Due to the thinner deposit layer in bed A, the effluent was instantaneously collected after feeding. Then, the effluent flux demonstrated a rapid drop and stabilized at a slow rate at 150 minutes after feeding. As for the wetland B, the effluent was only observed at half an hour after feeding. The effluent flux remained constant for about 150 minutes. After that, the effluent flux gradually decelerated and became insignificant at 400th minutes after feeding. Table 5.11 summarizes the hydraulic performance of both beds. The maximum effluent flux of wetland A and wetland B were 0.034 cm min^{-1} and 0.016 cm min^{-1}, respectively. Although both cases demonstrated different patterns of effluent flow, the overall recoveries of water were similar. Wetland A obtained a water recovery of 62.48 % and wetland B recovered 67.43 % of influent.

Table 5.10: Sludge thickness and influent quality of bed A and bed B

	Sludge Thickness (cm)	pH	DO (mg l^{-1})	NH_4^+-N (mg l^{-1})	NO_3^--N (mg l^{-1})	TN (mg l^{-1})	TS (mg l^{-1})	COD (mg l^{-1})
Wetland A	3	7.71	0.28	55.40	6.14	169.00	7800.00	3415.00
Wetland B	4	7.68	0.24	60.10	8.78	161.00	8900.00	4232.00

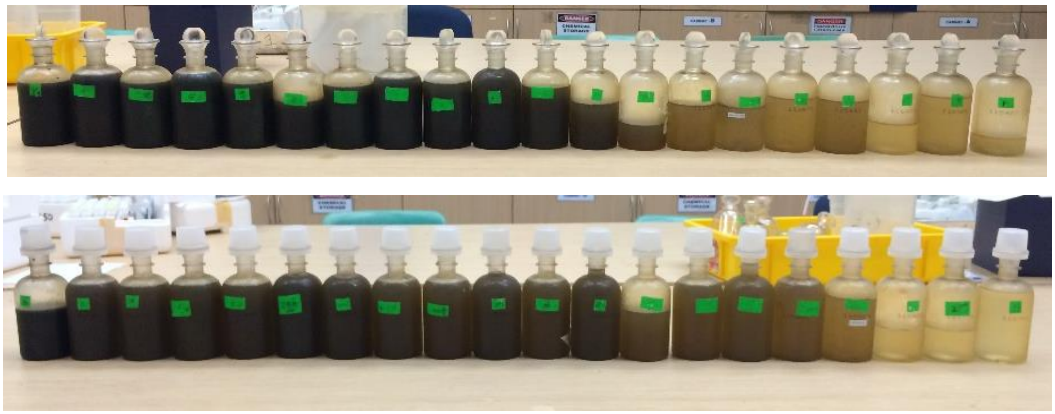

Figure 5.43: (Top) Effluent samples collected in 22A (Wetland A) (Bottom) Effluent samples collected in 23B (Wetland B)

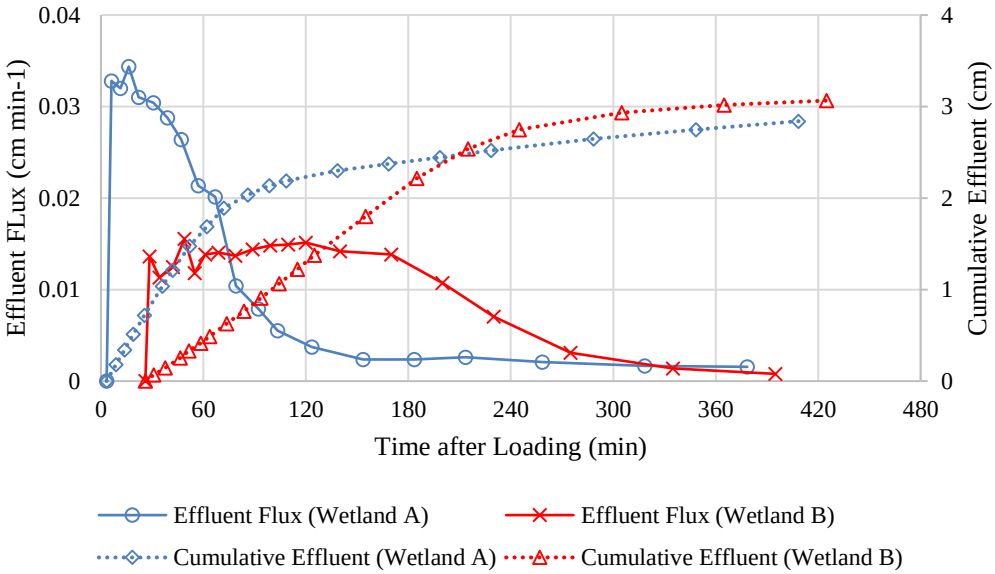

Figure 5.44: Effluent flux and cumulative effluent

Table 5.11: Comparisons of hydraulic performance and treatment efficiency

	Water Recovery (%)	Peak effluent flux (cm min^{-1})	NH_4^+-N	NH_4^+-N + NO_3^--N	TN	TS	TCOD
Wetland A	62.48%	0.034	33.95%	15.45%	42.72%	87.76%	89.18%
Wetland B	67.43%	0.016	67.55%	14.70%	67.25%	89.94%	95.83%

Figure 5.45 illustrates the relation between DO concentration and effluent flux. In wetland A, the rapid flow at the early phase resulted in a low oxygen content. Then, the DO gradually increased and remained approximately 6 mg l^{-1} until the end of the experiment. This observation indicated that the influence of the percolation rate was vital to the aeration efficiency in the VFCW. An adequate retention time was compulsory to effectively dissolve the gaseous oxygen retained in the pores of the substrate. As the effluent flow in wetland B was slower and more consistent, the DO concentrations were above 5 mg l^{-1} throughout the collection.

Figure 5.46 shows that the pH dynamic has no remarkable dependency on the hydraulic behaviour. The overall pH in the effluent from wetland A was higher than wetland B. Since there was no external alkaline or chemical added during the operation, the variation of pH was expected to be the result of biochemical reactions. As mentioned in section 2.5.1, the alkalinity is an essential component in the nitrification. The better removal of NH_4^+-N in wetland B implied that the lower pH was probably because of the higher consumption of alkalinity by nitrification.

Both wetlands demonstrated excellent treatment performance to TS and TCOD, where the removal rates were generally higher than 85 %. Figure 5.47 and Figure 5.48 illustrate that the concentrations of TS and TCOD in the effluent showed similar trends with the outflow dynamics. A more rapid effluent flux was observed with a higher

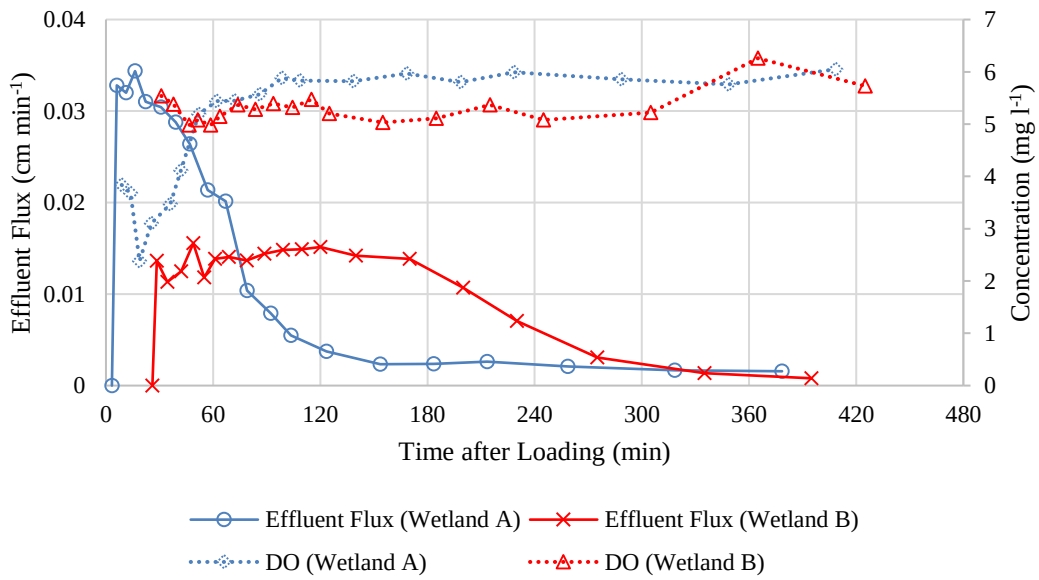

Figure 5.45: Relation between DO and outflow dynamics

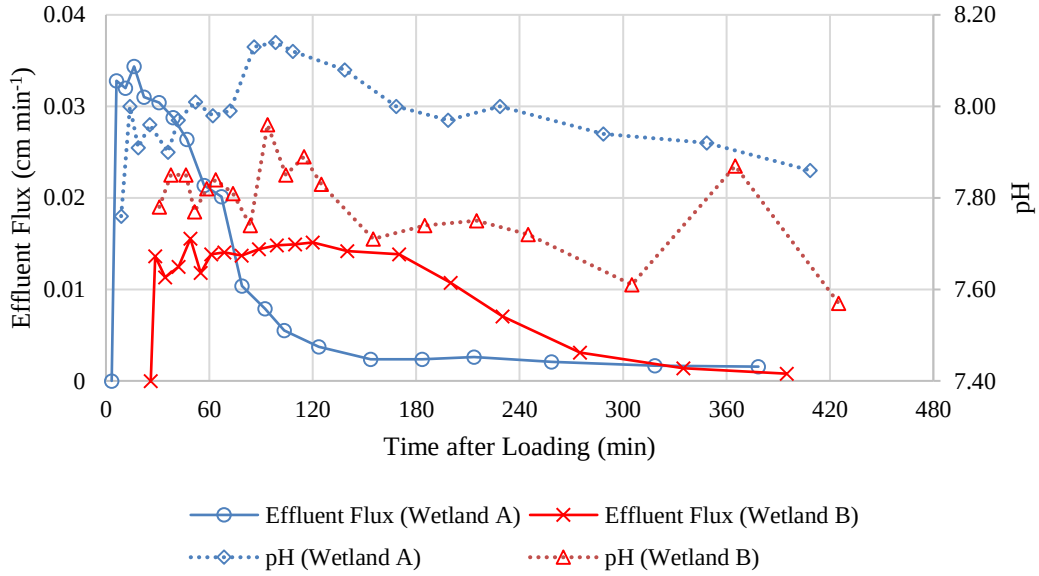

Figure 5.46: Relation between pH and outflow dynamics

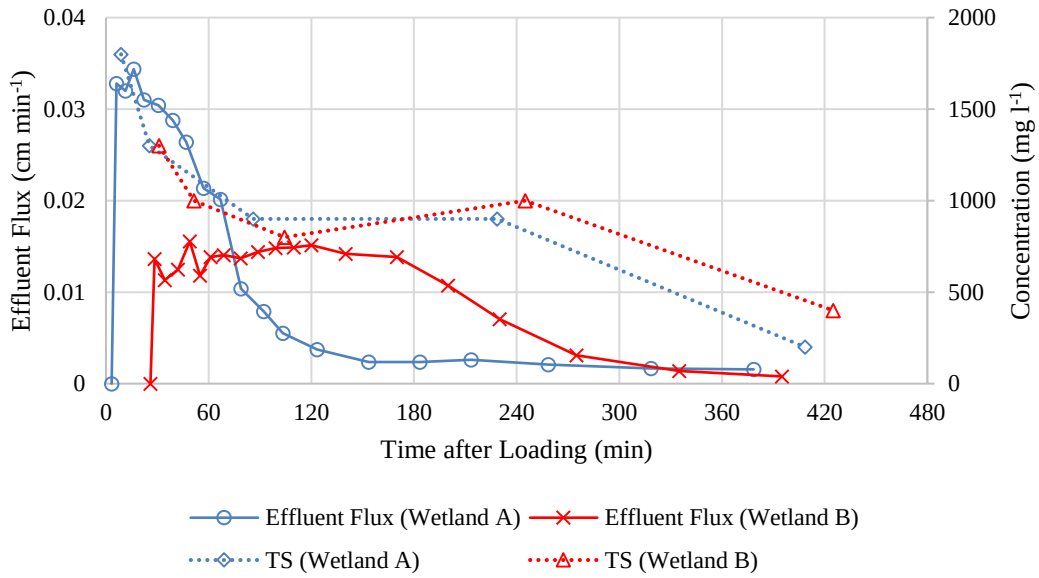

Figure 5.47: Relation between TS and outflow dynamics

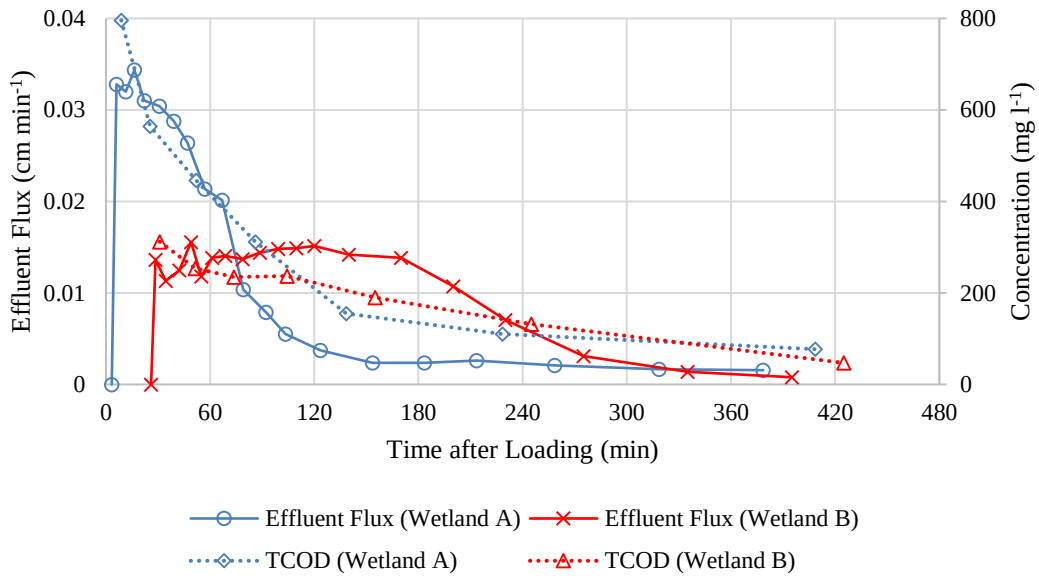

Figure 5.48: Relation between TCOD and outflow dynamics

concentration in the effluent. The treatment efficiency of TS and TCOD reflected that the slower percolation rate in wetland B resulted in a better treatment compared to wetland A. However, the difference was only 2% for TS and 6% for TCOD.

In general, the removal of TS is dependent on the surface filtration. Its efficiency is governed by the pore size of the porous medium used in the substrate, where the coarse gravel used in the first stage wetland bed is incapable of performing an outstanding filtration compared to the one topped with sand. Nevertheless, the formation of sludge deposit at the wetland surface built up an effective filter layer to separate the solids from the liquid, which has been identified as an important factor in the VFCW.

Cracks were observed in the sludge deposit layer during the resting period. At the beginning of the operation, these cracks allowed the influent to bypass the sludge deposit layer and thus the effluent was only partially filtered. It subsequently resulted in a higher TS concentration in the effluent at the early phase. Meanwhile, the incoming solids were then retained in the sludge deposit layer and "sealed" the cracks, and thus the effluent flux was decelerated and the efficiency of filtration was recovered. Troesch, Lienard, et al. (2009) observed the similar phenomenon, where the filtration was deficient while the sludge deposit layer was either too thin or cracked. Accordingly, it is presumed that the hydraulic behaviour was dependent on the rate of solid deposition. Nevertheless, this correlation requires a further study with regards to the formation of cracks and the rate of solids retention. In addition, the excessive

accumulation of sludge deposit might lead to the substantial reduction of the hydraulic efficiency in the wetland bed, which has been discussed in section 5.2.

Apart from the rapid surface filtration, the TCOD is removed biochemically in the substrate. The contact time between the organic matter and active biomass is determined by the percolation rate of influent. Figure 5.48 clearly demonstrates this relationship. In wetland A, the high concentration of TCOD was accompanied with a rapid effluent flux at the early phase and the reduction. Then, the following drop of concentration responded well to the deceleration of effluent flow. The slower effluent flux in wetland B was observed with low TCOD in the effluent, which remained below 350 mg l^{-1} throughout the experiment.

The concentration of TN displayed a correlation to the outflow dynamics. However, the dynamics of TN were poorly identified since there are only three measurements in each wetland bed as illustrated in Figure 5.49. The removal efficiency showed that the slow effluent flux in wetland B was advantageous to the removal of TN, where a removal efficiency of 67.25 % was achieved. Meanwhile, only 42.72 % of TN was eliminated in wetland A.

Figure 5.50 illustrates that the pattern of concentration NH_4^+-N in the effluent fairly matched with the outflow dynamics. In wetland A, the concentration of NH_4^+-N in the early flow had no significant change compared to the influent, implying that the percolation rate could be too fast for NH_4^+-N to be nitrified. The concentrations rapidly reduced with the deceleration of effluent. The NH_4^+-N was greatly removed in the early effluent of wetland B. Then, the concentration of NH_4^+-N declined when the effluent flux started to slow down at the late phase of the experiment. Wetland A only achieved a removal of 33.95 %. Meanwhile, the removal of NH_4^+-N reached 67.55 % in wetland B. This comparison highlighted that the removal of NH_4^+-N, either through nitrification or adsorption in the substrate, was governed by the percolation rate. This finding agreed with a column study, in which the duration of percolation was controlled using a throttle outflow (Henrichs, Welker and Uhl 2009). The study indicated that the treatment efficiency was proportional to the retention time of influent within the wetland beds.

As the nitrification is the main removal mechanism of NH_4^+-N, the increment of the concentration of NO_3^--N tended to be inversely proportional to the percolation rate as

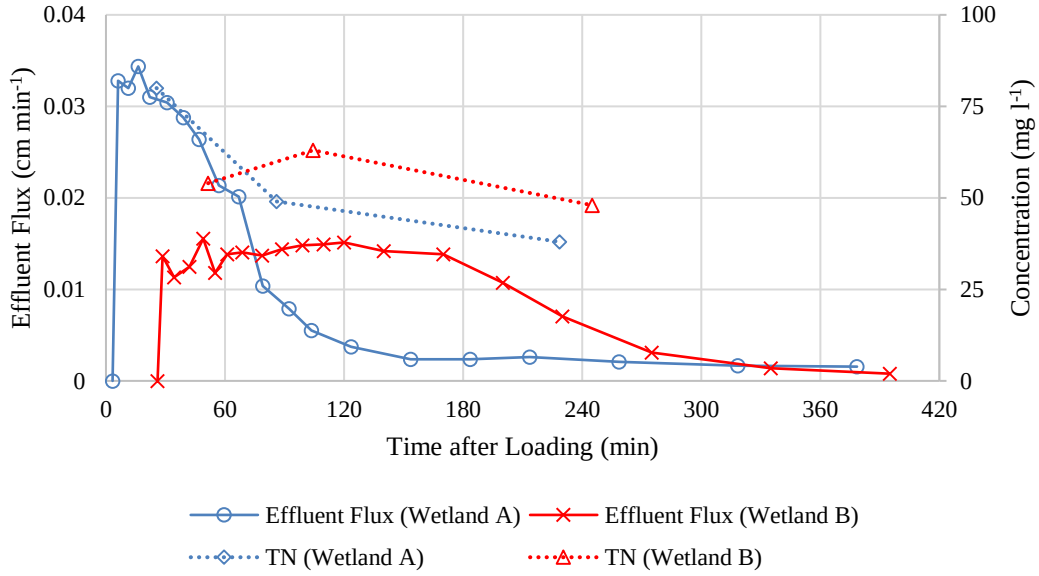

Figure 5.49: Relation between TN and outflow dynamics

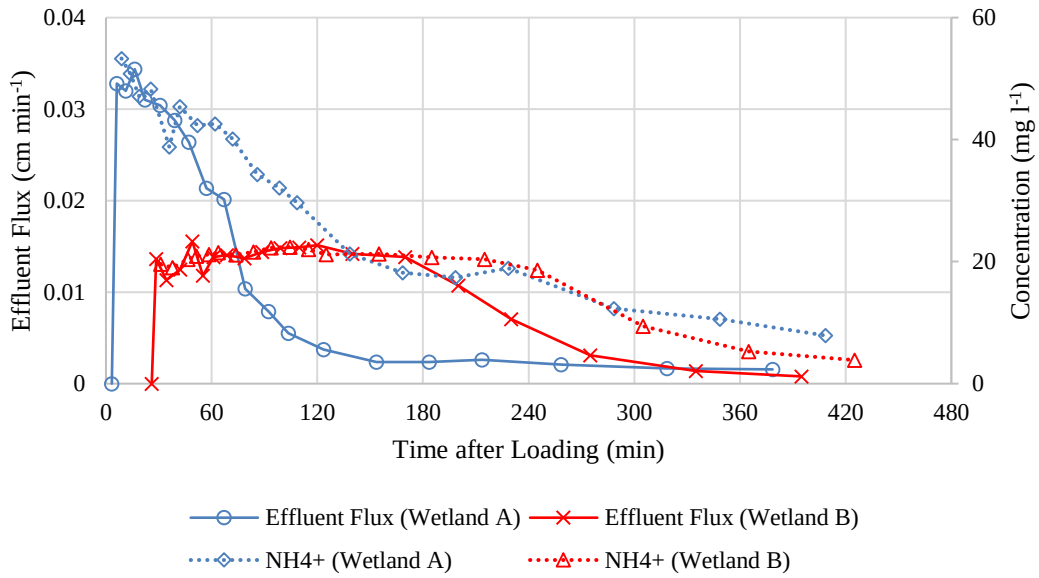

Figure 5.50: Relation between NH_4^+-N and outflow dynamics

demonstrated in Figure 5.51. The concentration of NO_3^--N was low in the early discharge from the wetland A. Meanwhile, the first NO_3^--N measurement in wetland B was much higher compared to the influent, indicating that the nitrification had been stimulated when the first flush occurred. The lower nitrification rate in wetland A highlighted that an adequate hydraulic retention time was complementary to the VFCW. Furthermore, this observation agreed with the relationship between aeration capacity and percolation rate in the pilot plant as mentioned earlier.

Figure 5.52 shows that the dynamics of the combined NH_4^+-N and NO_3^--N were relatively consistent compared to the dynamics of the individual nitrogenous constituent. In wetland A, the concentration appeared to be reduced slightly. Wetland B exhibited an increase in the early phase and remained stable for the remaining effluent. The overall concentrations of combined NH_4^+-N and NO_3^--N were lower in wetland A. However, the removal efficiency in both beds were similar, where 15.45 % and 14.70 % were obtained in wetland A and wetland B respectively. This similar removal rate implied that the ammonification of Org-N should be considered in this aspect. The slower percolation rate potentially recharged the amount of NH_4^+-N from the hydrolysis of organic matter. Simultaneously, the TN removal could be enhanced by the occurrence of ammonification. This hypothesis is agreed by the better TN removal in wetland B.

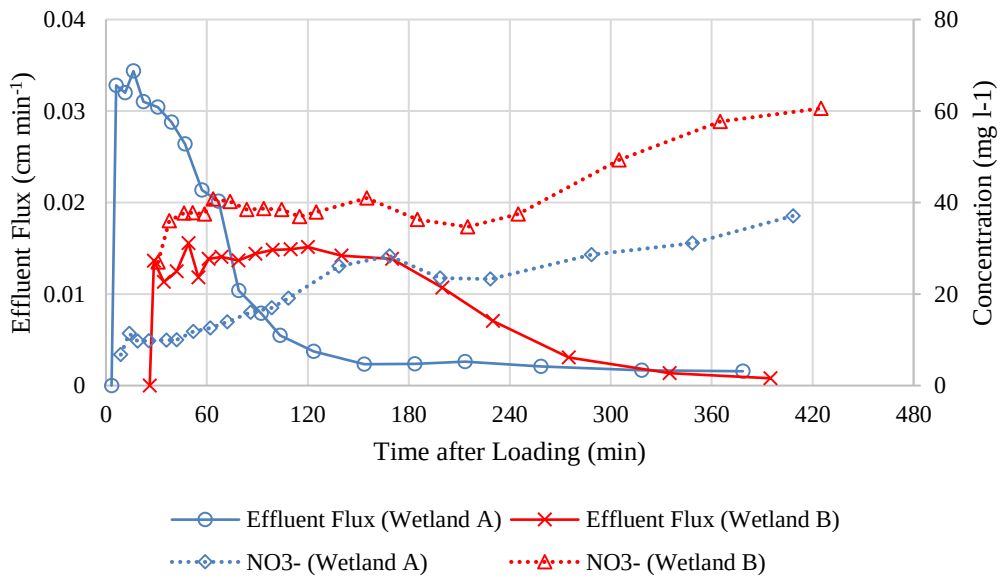

Figure 5.51: Relation between NO_3^--N and outflow dynamics

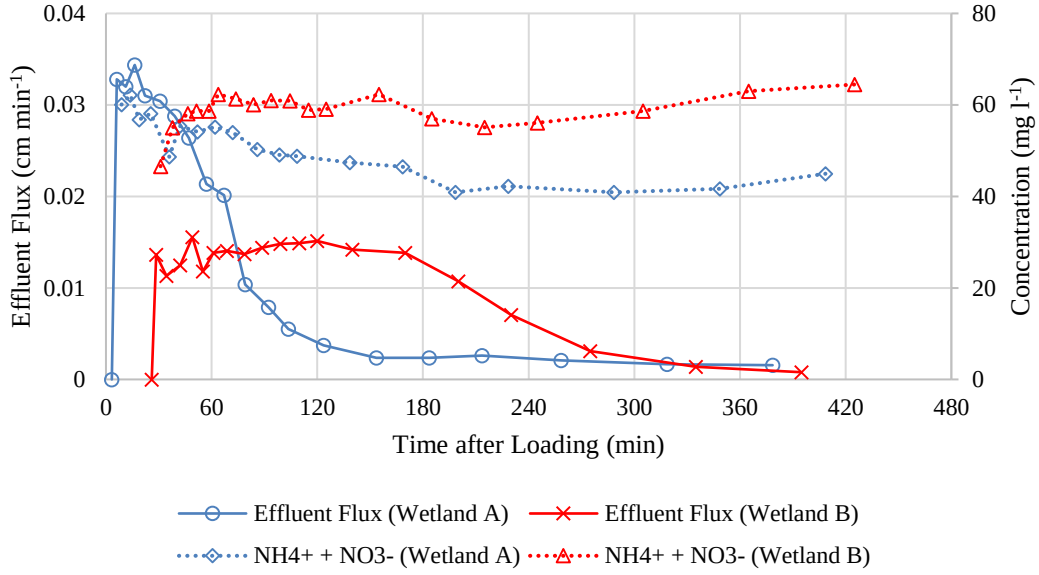

Figure 5.52: Relation between NH_4^+-N + NO_3^--N and outflow dynamics

5.3.3.2. Overall analysis of the influence of hydraulic behaviour on nitrogen dynamic

The influence of outflow dynamics on the treatment performance was significant from the direct comparison between cases 22A and 23B. The dependency of the dynamics of NH_4^+-N and NO_3^--N on the effluent flux were highlighted. Nevertheless, this analysis was statically insufficient to justify the correlation between the hydraulic behaviour and nitrogen removal. Therefore, the following section compared the patterns of nitrogen dynamics for all twenty-five cases to the associated outflow dynamics using linear regression analysis.

Section 5.2.2 has indicated that the flow pattern could be subdivided into three categories, which are “typical flow”, “bypass” and “clogged”. The “typical flow” case demonstrated that the effluent flux reached the maximum rate right after or soon after the effluent had been observed. In the cases with “bypass”, the flow rate tended to accelerate gradually after the start of effluent discharge, and thus the temporal plot of the effluent flux demonstrated a “V-shape” or “U-shape”. The peak effluent flux in the “clogged cases” was generally below 0.01 cm min^{-1} and the developments of flow were highly variable. The number of cases of “typical flow”, “bypass” and “clogged” cases is fifteen, five, and five, respectively.

Figure 5.53 illustrates the comparison between outflow dynamics and nitrogen dynamics for the selected cases exhibiting a "typical flow". In general, the trends of temporal NH_4^+-N dynamics fitted well with the outflow dynamics. Theoretically, a slow percolation rate is advantageous to the treatment, where the extended retention time enhances the efficiency of aeration and nitrification. Therefore, the rapid effluent flux at the early phase generally contained a high NH_4^+-N concentration. This phenomenon can be observed in the cases of 1A, 3A, 7B, 20A, and 22A. Figure 5.54 demonstrates the comparison for the "bypass" cases.

The values of coefficient of determination (R^2) in each case are summarized in Table 5.12: For the cases with "typical flow", there were ten cases with R^2 values higher than 0.80. The mean R^2 was approximately 0.74. Meanwhile, the cases with "bypass" indicated a mean R^2 of 0.73, which illustrated a linear correlation between the dynamics of outflow and NH_4^+-N concentration.

It should be noted that the concentration of NH_4^+-N in the first sample of the effluent was more or less reduced compared to the influent concentration. This indicated that the removal of NH_4^+-N could be instantaneous in the VFCW. In general, the concentrations of NO_3^--N appeared to be inversely proportional to the concentrations of NH_4^+-N, where the rise of one component was typically accompanied with the drop of the other.

Accordingly, nitrification can be recognized as the major mechanism to treat NH_4^+-N in the pilot-scale VFCW designed for septage treatment. However, the overall production of NO_3^--N was not equivalent to the substantial removal of NH_4^+-N, implying that other pathways such as adsorption took place simultaneously with nitrification.

The role of plant uptake is always minor in the nitrogen removal. Besides, the nitrogen volatilization is less likely to happen due to the neutral pH throughout the treatment (Vymazal 2007; Tunçsiper 2009). Therefore, the adsorption of NH_4^+-N is hypothesized as the second major mechanism in the treatment of NH_4^+-N. However, the quantification of the adsorption capacity of the pilot plant was not carried out to the granular porous medium. It was because the measurement of adsorbed NH_4^+-N in the substrate potentially damages the substrate and interferes with the following performance.

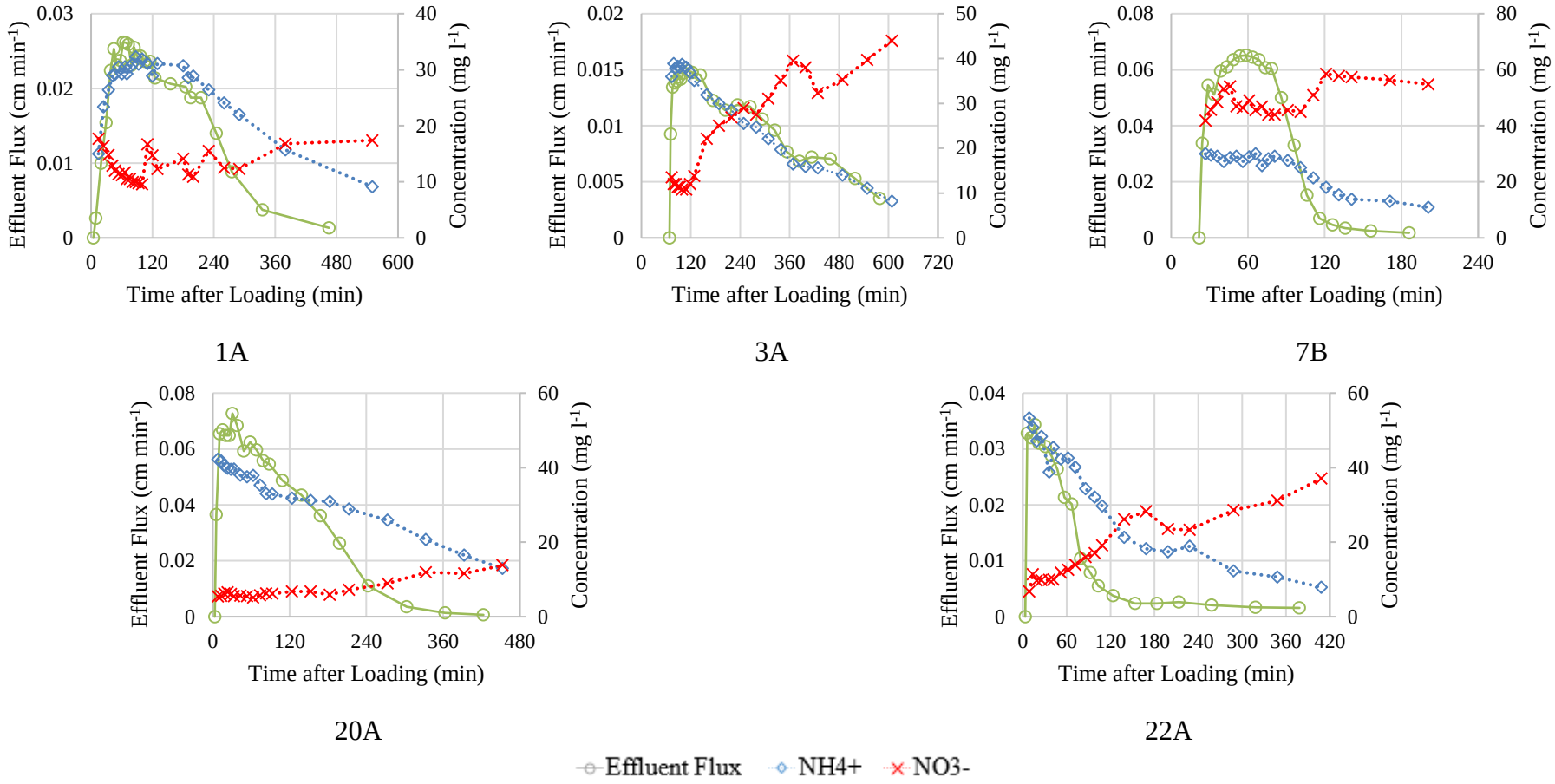

Figure 5.53: Relation between outflow dynamics and nitrogen dynamics for "typical flow" cases

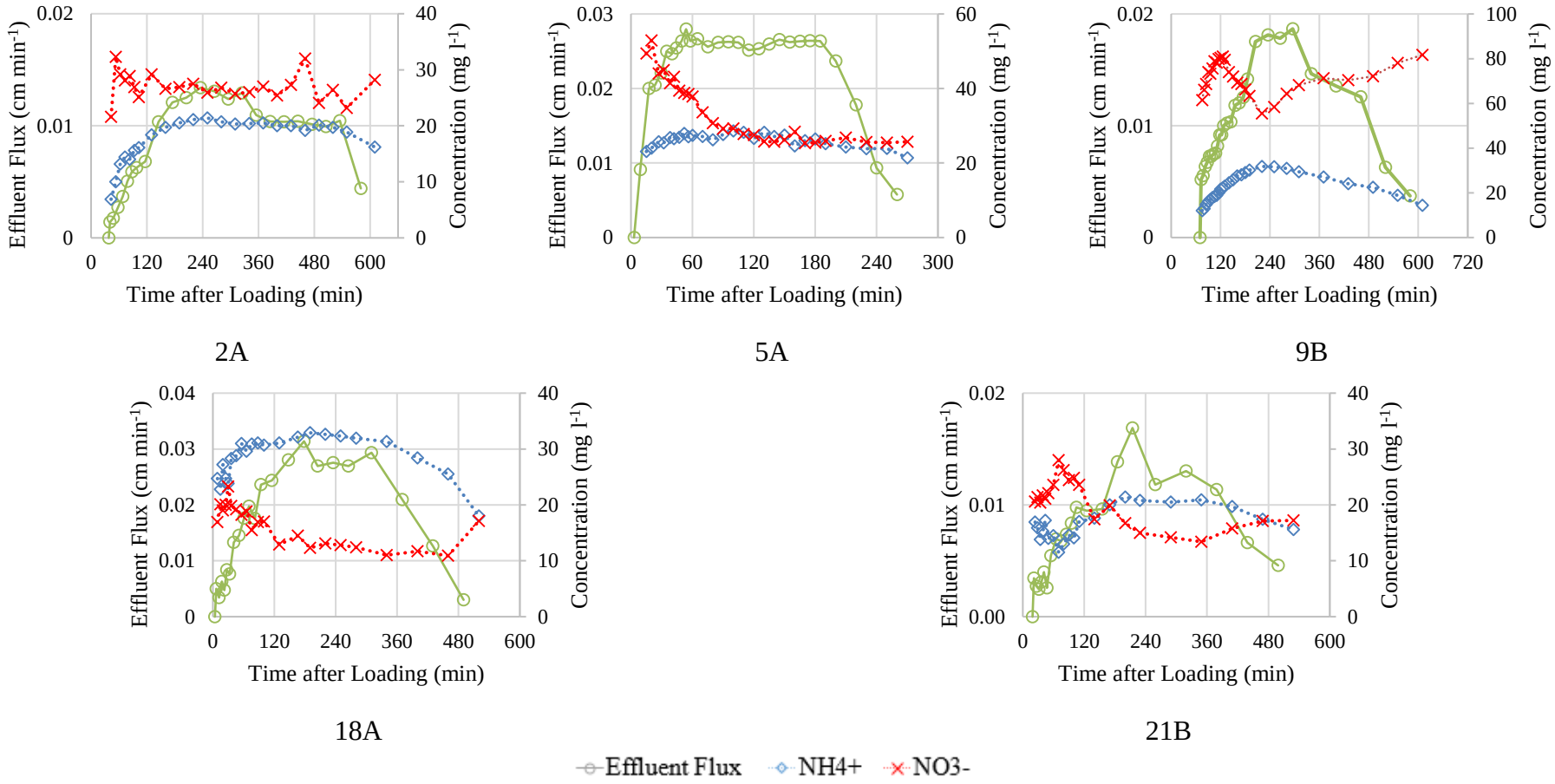

Figure 5.54: Relation between outflow dynamics and nitrogen dynamic for "bypass" case

Table 5.12: Coefficient of determination (R^2) of each case

Typical Case		Bypass		Clogging	
Case	R^2	Case	R^2	Case	R^2
1A	0.85	2A	0.87	10B	0.11
3A	0.85	5A	0.66	12B	0.30
4B	0.80	9B	0.86	13B	0.87
6A	0.58	18A	0.75	14A	0.29
7B	0.83	21B	0.53	15B	0.79
8A	0.81	-	-	-	-
11A	0.91	-	-	-	-
16A	0.91	-	-	-	-
17B	0.71	-	-	-	-
19B	0.04	-	-	-	-
20A	0.81	-	-	-	-
22A	0.87	-	-	-	-
23B	0.90	-	-	-	-
24B	0.69	-	-	-	-
25B	0.60	-	-	-	-
Mean	0.74	**Mean**	0.73	**Mean**	0.47

Instead of the gravel in the substrate, Molle (2014) indicated that the adsorption of the NH_4^+-N was more likely to occur in the organic matter in the sludge deposit layer. The sludge deposit layer removed from the top of the wetland bed as shown in Figure 5.55 was then tested for the content of NH_4^+-N and NO_3^--N by employing the 2.0 M KCl extraction method (Maynard and Kalra 1993). Ten 20 g samples of sludge deposit were obtained from different locations on the wetland surface and were mixed with 50 mL of 2.0 M KCl in a beaker. The mixture was then placed on the laboratory shaker for an hour. Subsequently, the mixture was filtered using filter paper and 50 mL of 2.0 M KCl was added to wash the filtered solid. The HACH HQ40d portable multi-parameter meter with specific probes was used to measure the concentration of NH_4^+-N and NO_3^--N in the mixture. Then, the measured concentration was converted to mass-based using following equation:

$$NO_3^-/NH_4^+\left(\frac{mg}{g}\right) = NO_3^-/NH_4^+\left(\frac{mg}{L}\right) \times \frac{0.1}{20}\left(\frac{L}{g}\right) \tag{5.5}$$

Figure 5.55: Sample of sludge deposit layer removed from the wetland surface

The results showed that the sludge deposit contained a remarkable amount of NH_4^+-N, ranging from 6 to 8.95 mg g^{-1}. The concentration of NO_3^--N was relatively low, which ranged between 1.52 and 2.27 mg g^{-1}. This finding supported the adsorption as an important mechanism to remove NH_4^+-N, and it explained the disequilibrium between the NH_4^+-N and NO_3^--N. Nevertheless, this analysis was only performed to examine the presence of adsorbed nitrogenous constituents in the sludge deposit layer, but its contribution to the overall nitrogen removal was not clearly quantified, and thus the potential capacity remained unknown in this study.

Another remarkable observation in this section was the high NO_3^--N concentration in the first flush of the effluent such as cases 4B, 5A, 6A, 16A, and 17B. As a certain amount of NH_4^+-N was adsorbed in the wetland bed after a feeding-draining cycle, nitrification took place and produced NO_3^--N during the resting period (Molle et al. 2006). The NO_3^--N was retained in the substrate with the residual water content at the late stage of loading event due to the absence of transport movement. When the wetland bed was loaded again, the NO_3^--N retained at the previous batch of treatment was washed out by the invaded influent and caused a high concentration at the early phase of effluent.

As for the clogging case as displayed in Figure 5.56, the relations between outflow dynamics and nitrogen dynamic were highly variable compared to the previous cases. Only case 13B and 15B demonstrated that the concentration of NH_4^+-N exhibited the same trend with outflow dynamics. The low mean R^2 value shown in the Table 5.12 revealed that the correlation between effluent flux and NH_4^+-N was insignificant in the clogging case. The most important feature in the clogging cases was the slow effluent

flux throughout the feeding-draining cycle. As mentioned previously, a slow effluent flow enhances the efficiency of nitrification due to the longer contact time between NH_4^+-N and microorganisms. However, this presumption was only observed in case 12B and 14A, while other cases still contained a significant amount of NH_4^+-N in the effluent. The short circuit of percolation in the clogging cases was believed to be the main reason for the unstable hydraulic behaviour.

5.3.4. Summary

In summary, the raw septage used in this study was slightly alkaline and the oxygen content was extremely low throughout twenty-five set of loading events. The solids content and the concentrations of organic matter and nitrogenous constituents were highly variable. Although the average concentration of TS, TCOD, TN and NH_4^+-N in the raw septage were much lower compared to the literature data, the quality was still highly hazardous to the environment. The analysis showed that the concentrations of TCOD and Org-N were dependent on the solids content. This correlation indicated that the majority of organic matter existed in the particulate form. As for the nitrogenous constituents, the concentration of NH_4^+-N and NO_3^--N were generally consistent and independent from the TS and TN. The portion of the Org-N in the TN proportionally correlated to the TS concentration.

The overall performance of the pilot-scale VFCW-based septage treatment system was satisfactory. The high DO concentration in the effluent showed that the proposed configurations and operating regimes delivered an excellent aeration capacity. The pH of the effluent was slightly increased compared to the raw septage. On average, the removal efficiency of TS and TCOD achieved 78 % and 89 %, respectively. The treatment performance was comparable to the performance of other existing systems. Nevertheless, the removal of nitrogen was less desirable. The mean removal efficiency of TN was approximately 68 % and the performance was up-and-down throughout the time. The treatment of NH_4^+-N was poor and the mean removal rate was less than 50 %. The increase of NO_3^--N in the effluent indicated that the nitrification was favourable in the pilot plant. The temporal plots of the effluent quality illustrate that most quality parameters were dependent on the hydraulic behaviour. An excellent aeration and solid deposition were usually accompanied with a slow effluent, subsequently resulting in a better removal for TCOD, TN, NH_4^+-N in the pilot-scale VFCW.

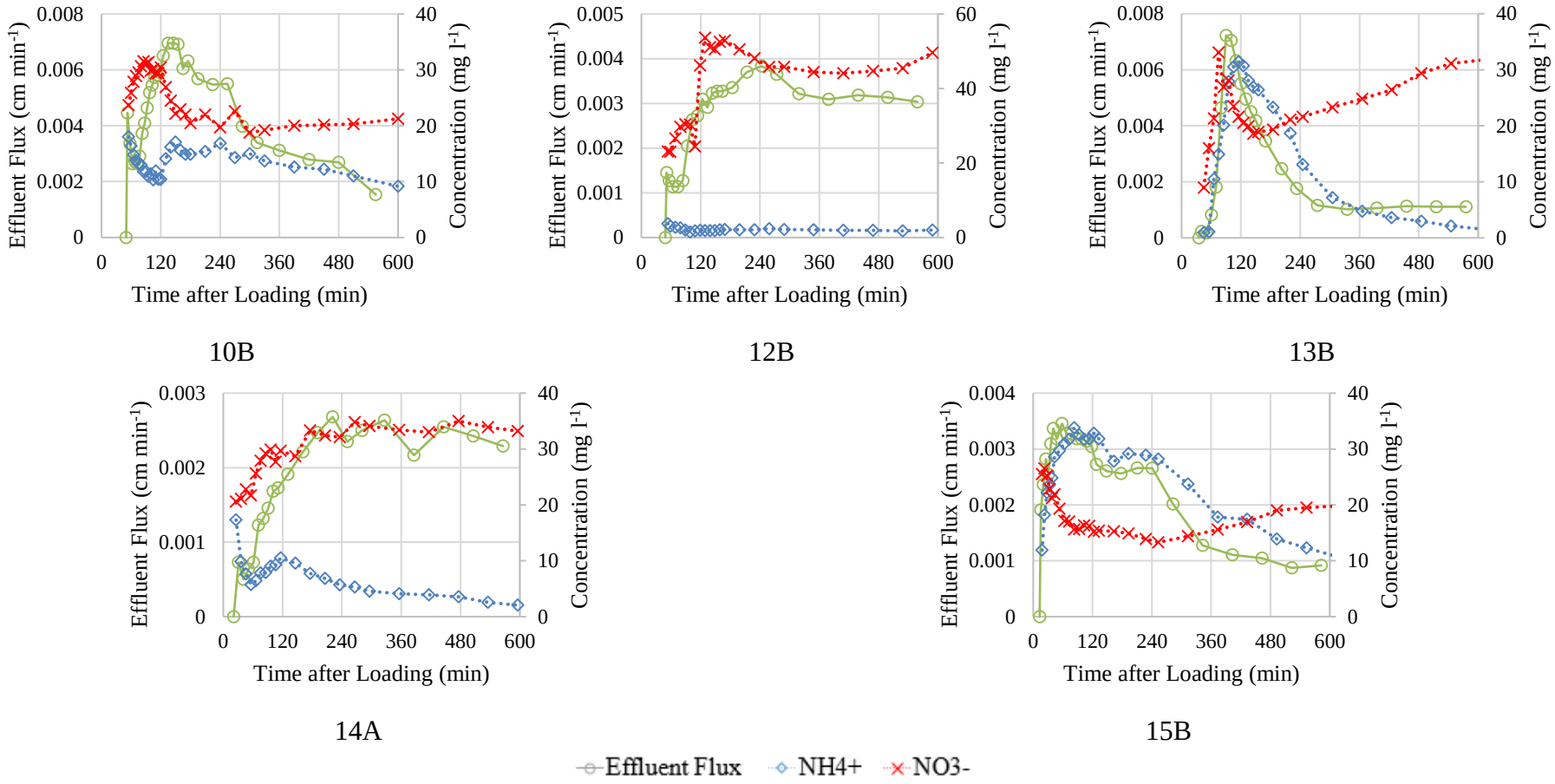

Figure 5.56: Relation between outflow dynamics and nitrogen dynamics for "clogged" cases

The hydraulic behaviour is key to the nitrogen dynamics. In the cases with the "typical flow", the concentration of NH_4^+-N showed a dependency on outflow dynamics. Besides, the rise of NO_3^--N was always observed with a drop of NH_4^+-N. This observation showed that nitrification was the main mechanism to remove NH_4^+-N in the pilots-scale VFCW. A slower percolation rate returned to a longer contact time between NH_4^+-N and the attached biofilm in the substrate, subsequently enhancing the efficiency of nitrification. In most cases, NO_3^--N was produced due to the favourable aerobic condition. By extracting the nitrogen content in the sludge deposit, the adsorption of NH_4^+-N in this layer was noteworthy. The adsorbed NH_4^+-N could be nitrified during resting period and subsequently resulted in a flushing-out of NO_3^--N in the early effluent. Nevertheless, the overall removal of combined NH_4^+-N and NO_3^--N was less than expectation.

The relation between the outflow dynamics and the concentration of NH_4^+-N and NO_3^--N in the pilot-scale VFCW designed for septage treatment was identified using linear regression analysis. Ten cases with "typical flow" characterized R^2 higher than 0.80, where the average R^2 of fifteen cases was found to be 0.74, which evidently supported the hypothesis that the hydraulic behaviour eventually governed the treatment of nitrogenous constituents. In addition, the cases with "bypass" also obtained an average R^2 of 0.73. From the perspective of the treatment efficiency, the current removals of TN and NH_4^+-N were considered to be poor. This was mainly due to the rapid percolation rate throughout the substrate. As a recommendation to improve the system, an additional stage of treatment should be added to remove residual NH_4^+-N and excessive NO_3^--N production in the percolate from the first stage treatment.

5.4. Tracer experiments

Twelve sets of tracer experiment (3A – 14A) have been carried out with the assessment of hydraulics and water quality to investigate the transport mechanism of non-reactive solute throughout the wetland bed. The raw septage was mixed with a specific amount of KBr (1 mole) as described in section 3.2.3 to attain the influent Br^- concentration of 0.001 mole l^{-1}. Nevertheless, Table 5.13 shows that the measured concentration of Br^- in influent failed to reach the designed concentration, where the average of the measured tracer concentration in the influent was only 0.00033 ± 0.00009 mole l^{-1}. As the radiometer and Br^- electrode probe has been properly calibrated and it accurately

measured the Br^- concentration in KBr with various dilution factors, the discrepancies were attributable to the raw sample. One of the reasons was the low concentration in the influent that resulted in a low volume ratio of the mixture (1:1000) and it could be too low to be evenly distributed within the raw septage. In addition, the high solids content in the raw septage might influence the sensitivity of the radiometer in detecting the tracer. Consequently, the outcome of the tracer experiment was only taken as a reference for the general trend of solute transport, but not for the calibration of transport parameters.

Figure 5.57 demonstrated the dynamics of tracer concentrations in the effluent. In cases 4B, 5A, 6A and 7B, the tracer concentration rose at the early stage, while in cases 8A, 10B, 12B, 13B, and 14A, a drop in the tracer concentration was observed. The first measurements of tracer concentration ranged between 0.000 08 mole l^{-1} and 0.000 48 mole l^{-1}. Then, the tracer concentration generally stabilized within the range of 0.000 14 mole l^{-1} to 0.000 22 mole l^{-1} at the late phase of the experiment.

This observation showed that the transport of contaminant was sensitive to the background concentration in the wetland bed. Although section 3.2.3 has highlighted that the Br^- is theoretically absent in the wetland system, the tracer retained in the residual water content from the previous loading possibly affected the overall trend of tracer transport. When the wetland bed was free from tracer, the early rise of the concentration indicated that the tracer gradually mixed with the inherent water content until the equilibrium state was reached. As the tracer experiment was continuously carried out, the residual tracer in the wetland bed increased with the time of loading. Therefore, the last few sets of the experiment (12B, 13B, 14A) illustrated a first flush of tracer when the effluent had been formed.

Due to the highly variable tracer concentration in the effluent, its overall trend had no correlation to the effluent flux. According to Table 5.13, the average percentage of tracer recovery was 62.15 $\pm$ 20.82% and there was no remarkable relation to the hydraulic loads, sludge thickness, TS loads and even water recovery. This implied that the tracer experiment carried out with Br^- in this study was highly unstable, and thus the results were unreliable in terms of the verification of the simulation.

In summary, although the calibration of transport parameters using the results of this experiment was not successful, some important insights have been gained towards the

Table 5.13: Results of tracer experiment

No. of test A = Wetland A B= Wetland B		HLR (L)	Sludge Thickness (cm)	SLR (g)	Water recovery (%)	Influent tracer concentration (mole l^{-1})	Tracer recovery (%)
3A	01/12/2015	75	6	360	71.92%	0.00040	49.40%
4B	4/12/2015	75	7	105	85.87%	0.00040	41.95%
5A	08/12/2015	75	7	-	83.77%	0.00020	93.05%
6A	12/12/2015	75	5	120	68.14%	0.00021	87.57%
7B	13/12/2015	75	5	105	69.48%	0.00040	40.65%
8A	16/12/2015	100	6	1280	73.41%	0.00038	58.36%
9B	17/12/2015	100	5	460	70.10%	0.00039	50.65%
10B	24/12/2015	100	12	1070	22.75%	0.00034	56.93%
11A	27/12/2015	100	8	1260	47.34%	0.00037	64.86%
12B	31/12/2015	125	12	1187.5	14.58%	0.00032	70.42%
13B	7/1/2016	125	9	525	9.72%	0.00017	96.43%
14A	10/01/2016	125	12	1200	11.04%	0.00037	35.50%
	Max.	125.00	12.00	1280.00	85.87%	0.00040	96.43%
	Min.	75.00	5.00	105.00	9.72%	0.00017	35.50%
	Average	95.83	7.83	697.50	52.31%	0.00033	62.15%
Standard Deviation		20.87	2.79	502.27	29.62%	0.00009	20.82%

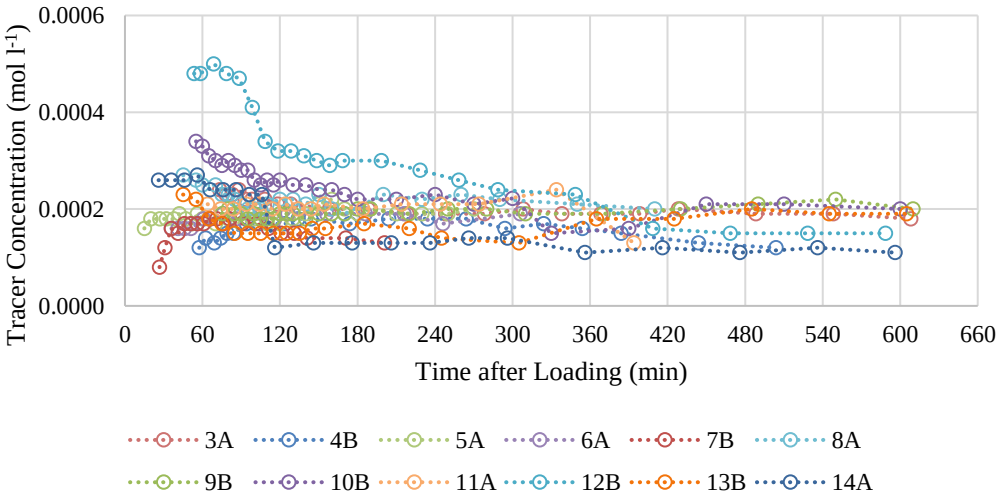

Figure 5.57: Temporal plots of Br^- concentration in the effluent for twelve batches of treatment

pattern of solute transport. The first observation was the influence of background concentration on the tracer concentration at the early phase. Besides, the stable tracer concentration level at the late phase of the feeding-draining cycle demonstrated dissimilar pattern compared to the results in Langergraber and Šimůnek (2006) and Giraldi, de Michieli Vitturi, and Iannelli (2010), where the tracer in the effluent generally demonstrated a rise-and-drop within a feeding cycle. This can be attributed to the different methodology of the tracer experiment, where a pulse input was generally employed during feeding. In this study, the tracer was pre-mixed with the influent and was loaded in batch, and thus it was reasonable to observe an equilibrium state at the end of the experiment.

Chapter 6 Simulation of Hydraulic Behaviour

A feasible hydraulic simulation is essential to predict the transport and fate of nitrogenous constituents in the system. The proposed model, VF_Sep, which includes a variably-saturated flow module and an ET sub-module, was calibrated with the measured outflow dynamics of the first stage treatment in a pilot-scale, two-stage VFCW. In summary, the inputs of the hydraulic module consist of time, geometry, boundary condition, iteration criteria, and initial pressure head. The expected outcomes include the profiles of pressure head, water content, flux, and plant water uptake. In this chapter, the calibration procedure is discussed, including the set-up of simulation, assumption, and limitation in hydraulic simulation, calibration of parameters and error analysis. In addition, the significance of the evapotranspiration (ET) and sludge accumulation are evaluated, and the future improvement of the hydraulic module is suggested.

6.1. Review of the calibration procedure and established hydraulic parameters

In this study, the main challenge in the calibration was the lack of standard hydraulic parameters for the granular porous medium. There are two general methods to determine the variably-saturated hydraulic properties of the porous medium in the wetland bed, which are the direct laboratory method and the indirect modelling method. Direct laboratory measurement was attempted as a preliminary study of the calibration. The porosity, saturated hydraulic conductivity (K_S), and hydraulic retention curve (HRC) of the porous medium used in the wetland bed was measured by means of porosity test, constant head tests (Figure 6.1) and hanging column tests (Figure 6.2), respectively. Then, the VGM parameters were estimated with regards to the HRC using the software RETC (Van Genuchten, Leij and Yates 1991).

However, these data, which are presented in Table 6.1, were considered to be instrumentally constrained and statistically insufficient to provide reliable results. Another concern was that the sample for laboratory quantification was grabbed from the clean bed, where the sampling of the porous medium from the wetland bed that is in operation, will potentially destroy the bed and interfere with the treatment performance.

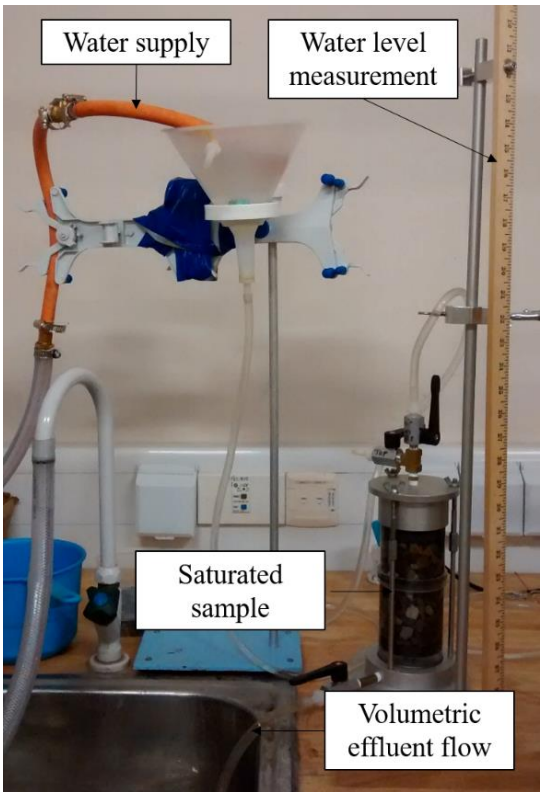

Figure 6.1: Constant head test to measure the saturated hydraulic conductivity of porous medium

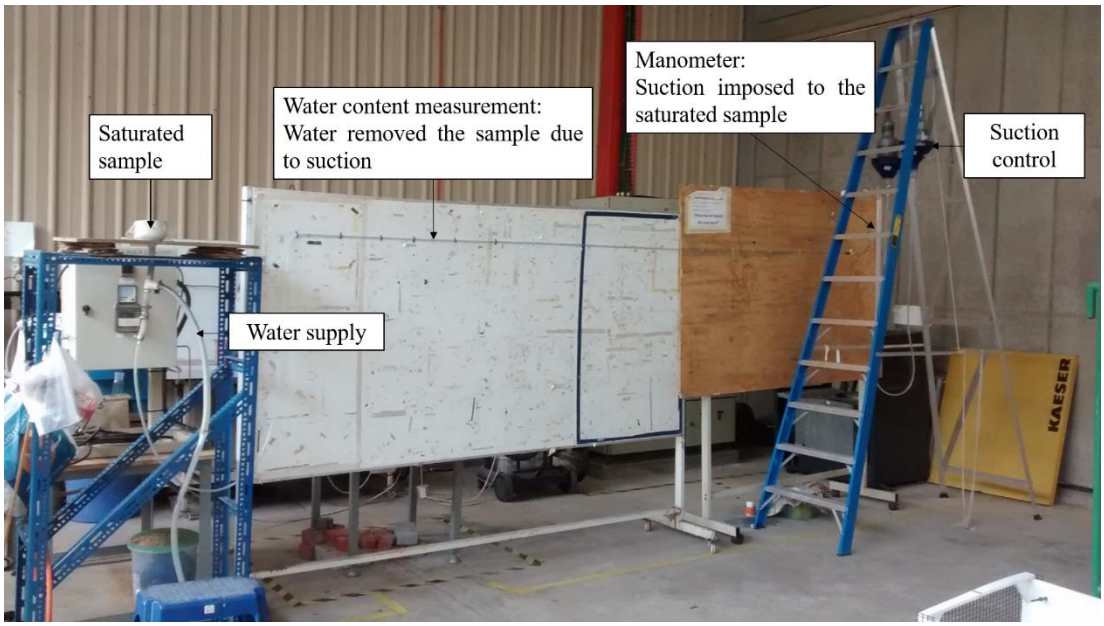

Figure 6.2: Hanging column test to measure the amount of water removed from the saturated porous medium caused by the suction

Table 6.1: Laboratory measurement of hydraulic parameters

	Porosity (-)	K_S (cm min-1)	α (cm^{-1})	n (-)
Sludge deposit	0.75	0.0002	0.69	2.71
Gravel (10 mm)	0.46	15.3000	1.04	2.08
Gravel (37.5mm)	0.67	17.2600	-	-

Moreover, Khaleel and Relyea (1997) highlighted that the laboratory-measured hydraulic retention curve (HRC) of gravel required further correction in order to be applied in the field. This has been supported by Morvannou et al. (2013a), which indicated that the direct laboratory method produced reasonable measurements for the particular soil sample. However, these measurements generally failed to reproduce the scenario in the field due to factors such as the vegetation and the hysteresis effect. Therefore, the outcome of direct measurement was not reported in detail here. This set of data was only referred to as the initial parameters for calibration. In addition, there is no standard method to optimize the laboratory data for the application of a field-scale system, and thus an indirect method is often carried out.

The indirect method determines the hydraulic parameters of the wetland bed through the inverse modelling of measured data, or by calibrating the hydraulic parameters using a mathematical model to fit the measured data. In inverse modelling, the concern is the insufficiency of data to conduct reasonable analysis, especially in the event-based simulation (Dittmer, Meyer and Langergraber 2005). The collection of enormous data could be time-consuming and costly to satisfy the requirement of inverse modelling. A more budget-friendly alternative is to calibrate the hydraulic parameters by fitting the simulated results obtained from the mathematical model with the measured data, which is proposed by Dittmer, Meyer, and Langergraber (2005). Toscano et al. (2009) applied the same procedure to calibrate the hydraulic parameters of a pilot-scale, two-stage hybrid (HF + VF) subsurface-flow constructed wetland. The calibration by fitting generally combines the visual evaluation and statistical analysis to match the outflow dynamics with simulated results.

Table 6.2 presents the hydraulic parameters of gravel used in the literature to simulate the hydraulic behaviour of VFCW as an equilibrium flow. The standard hydraulic parameters of sand specified in Carsel and Parrish (1988) are presented as the benchmark in the calibration procedure. It is found that even though the particle size

Table 6.2: Hydraulic parameters of gravel used in the literature for hydraulic simulation of VFCW (equilibrium flow)

Reference	Particle size (mm)	θ_r (-)	θ_s (-)	α (cm^{-1})	n (-)	K_s ($cm\ min^{-1}$)
Carsel and Parrish (1988)	-	0.045	0.430	0.145	2.68	0.50
Langergraber and Šimůnek (2005)	4-8	0.045	0.410	0.145	5.00	1000.00
	16-32	0.056	0.150	0.145	1.92	1000.00
Langergraber and Šimůnek (2006)	2-8	0.050	0.370	0.050	2.80	600.00
Toscano et al. (2009)	16-32	0.050	0.190	0.028	4.00	8.30
Maier et al. (2009)	4-8	-	0.350	0.085	9.80	7.80
	8-16	-	-	0.097	8.60	258.00
Giraldi, de Michieli Vitturi, and Iannelli (2010)	5-10	0.036	0.483	0.145	2.68	23.88
	20-30	0.035	0.480	0.145	2.68	120.00
	50-60	0.035	0.480	0.145	2.68	120.00
Morvannou et al. (2013a)	-	0.310	0.406	2.860	1.35	6.60
	-	0.220	0.406	2.770	1.30	6.60
	30-60	0.230	0.440	2.720	1.47	71.40
Fournel et al. (2013)	10-20	0.040	0.430	0.180	3.30	70.00

was similar, the hydraulic parameters vary from case to case and no general trend were observed. Such deviations are attributed to the difference in the purpose and calibrating procedure of the studies. Morvannou et al. (2013b) proposed the only set of calibrated hydraulic parameters for the dual-porosity model, which is summarized in Table 6.3. As mentioned in the previous section, Morvannou et al. (2013a) inversely modelled the hydraulic parameters using an in-situ assessment with regards to the water content along the wetland bed. Maier et al. (2009) delivered a similar approach to calibrate the hydraulic parameters of a full-scale VFCW using the data of discharge. Although these

Table 6.3: Hydraulic parameters of gravel used in the literature for hydraulic simulation of VFCW (preferential flow)

Reference	θ_r^m (-)	θ_s^m (-)	α (cm^{-1})	n (-)	K_s ($cm\ min^{-1}$)	θ_r^{im} (-)	θ_s^{im} (-)	ω (min^{-1})
Morvannou et al. (2013b)	0.0	0.02	0.145	5.00	1500.00	0.38	0.39	0.30
	0.0	0.05	0.145	1.92	1500.00	0.34	0.36	0.30

studies showed that these parameters successfully fitted the experimental measurement, some of them were "unreasonable" compared to the typical values. For example, the calibrated value of n in Maier et al. (2009) is extremely high compared to other studies. Besides, the value of residual water content (θ_r) and α are much higher than the typical value in Morvannou et al. (2013a). Therefore, these hydraulic parameters were only reliable in the specific condition and were unable to be used as global parameters. The same outcome was observed in the study of the dual-porosity model (Morvannou et al. 2013b), where most of the pore spaces were assumed to be within the immobile region of the substrate.

In most cases, the gravel was seldom used as the main layer, while it acted as the intermediate layer or drainage layer in the substrate profile (Langergraber and Šimůnek 2005; Morvannou et al. 2013b; Langergraber and Šimůnek 2006; Toscano et al. 2009; Fournel et al. 2013). In general, the drainage layer was assumed to be saturated in the simulation, and hence its effect to the overall calibration was minor. In this case, the values of VGM parameters were always referred to the standard of sand (Langergraber and Šimůnek 2005). Giraldi, de Michieli Vitturi, and Iannelli (2010) calibrated the dispersity of the gravel bed to fit the results of the tracer experiment by using the VGM parameters of sand. Although such an approach simplified the calibration of VGM parameters, it was difficult to match the measured data by calibrating the value of the saturated hydraulic conductivity (K_s) only. In general, K_s was the most variable parameter, ranging from 6.60 to 1000 cm min^{-1}, and thus the current literature was unable to justify a set of standard hydraulic parameters for coarse gravel.

Fournel et al. (2013) proposed a guideline to elaborate the hydraulic parameters of gravel from the standard hydraulic parameter. First, the θ_s is higher for the coarser gravel due to the higher porosity, but it is vice versa for θ_r. The values of α, n and Ks are proportional to the grain size. This concept is employed to range the values for calibration. The typical value of θ_r is between 0.03 and 0.05 and the value of θ_s is between 0.4 and 0.5. The initial value of α is generally higher than 0.15 cm^{-1} but lower than 0.4 cm^{-1}, and n ranges from 3 to 5. The K_s was assumed to be higher than 1000 cm min^{-1}. It should be noted that the ratio between the mobile and immobile region was calibrated according to the measured data.

The previous chapter has highlighted the key role of the sludge deposit layer in the hydraulic performance. Nevertheless, only Morvannou et al. (2013a) established a set of hydraulic parameters for the sludge deposit, which is presented in Table 6.4. The θ_r and θ_s used in this study were extremely high compared to the standard hydraulic parameters of loam and silt showed in Table 6.5. In terms of the VGM parameters, α and K_s were similar to the standard value of sand and the value of n was close to the standard value of loam. Therefore, the range of the hydraulic parameters of sludge deposit was interpolated between the standard parameters of sand and loam.

In summary, the calibration of the optimal hydraulic parameters was performed using the visual evaluation and the error analysis (mean absolute percentage error, MAE (%)) to fit the measured effluent flux in the experiments. According to the hydraulic parameters for gravel and sludge deposit, the hydraulic parameters of gravel was elaborated from the standard parameters of sand and the hydraulic parameters of sludge deposit was interpolated between the standard parameters of sand and loam. Further investigation with regards to the portion between mobile and immobile region is required in the calibration.

6.2. Assumptions

The aim of the hydraulic simulation is to match the simulated results with the measured data of effluent flux (cm min^{-1}) obtained from the pilot-scale VFCW treating septage. As not all factors were able to be measured in this study, several assumptions were made in the simulations:

Table 6.4: Hydraulic parameters of sludge deposit used in the literature for hydraulic simulation of VFCW (equilibrium flow)

Reference	θ_r (-)	θ_s (-)	α (cm^{-1})	n (-)	K_s (cm min^{-1})
Morvannou et al. (2013a)	0.65	0.84	0.15	1.80	0.45

Table 6.5: Standard Hydraulic parameters of loam and silt (equilibrium flow)

Reference	Soil Catalogue	θ_r (-)	θ_s (-)	α (cm^{-1})	n (-)	K_s (cm min^{-1})
Carsel and Parrish (1988)	Loam	0.078	0.43	0.036	1.56	0.017
	Silt	0.034	0.46	0.016	1.37	0.004

- The hydraulic properties of the wetland bed and the associated hydraulic behaviour (infiltration rate, water flux, ET, etc.) were assumed to be horizontally homogenous over the wetland bed. All the simulated results were presented as per unit area [L^{-2}].
- The initial pressure distribution was assumed to be under the equilibrium state, where the initial pressure is equivalent along the substrate profile before the operation.
- The effect of vegetation was only considered in terms of root water uptake, while its influence on the hydraulic performance (cracking around the stem, root penetration, etc) was assumed to be lumped with the hydraulic properties of the substrate profile.
- The ET rate was assumed to be constant throughout the simulation
- The hydraulic properties of the newly formed sludge deposit were assumed to be equal to the existing sludge deposit.
- The hysteresis effect was not considered in the hydraulic simulation.
- The sink term considered in the proposed model only included the water loss from ET and the water content retained in the immobile region. Therefore, the associated water recovery was theoretically conservative with the amount of influent.

6.3. Simulation set-up

The substrate profile in the pilot-scale first stage wetland bed consists of three layers, which include the small-size gravel layer, the medium-size gravel layer, and the drainage layer. The sludge deposit at the wetland surface, which has been evidently identified as a crucial factor in the hydraulic performance, was included as the top layer in the simulation. On the other hand, since the drainage layer only acted as a drain and its influence on the overall hydraulic retention time was negligibly minor in the system, this layer was excluded from the profile of simulation.

The substrate profile in the simulation is illustrated in Figure 6.3. Apart from the particulate constituents retained at the surface that formed the sludge deposit layer, a certain amount of solid passed through the surface and was deposited at the upper zone of the main layer. As a result, the hydraulic properties of this zone was changed with

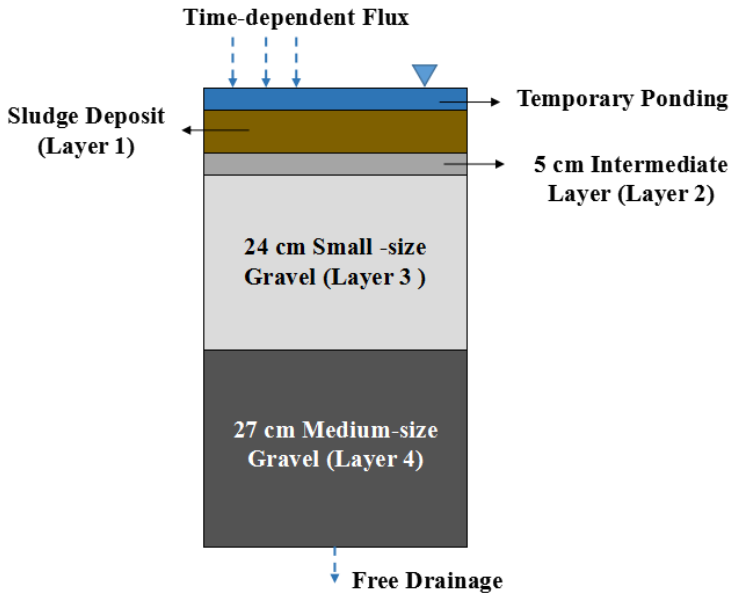

Figure 6.3: Substrate profile in the simulation

time as the porosity was greatly reduced (Kim and Forquet 2016). A 5 cm intermediate layer was implemented to describe this transition interface at the top of the main layer. Consequently, the thickness of the small-size gravel layer was reduced to 22 cm. The thickness of medium-size gravel layer remained as 27 cm.

The spatial discretization (*dz*) in the hydraulic simulation was set to be 1 cm. Although a finer discretization hypothetically improves the resolution and the accuracy of results, the duration for computation may substantially increase at the same time. The preliminary simulation of pressure head, water content and flux as illustrated in Figure 6.4 show that the finer discretization did not result in a significant difference from the default discretization. Therefore, the spatial discretization of 1 cm was reasonable in the proposed model. Another potential drawback of the finer mesh was its instability in countering the high K_s of gravel bed, which ranged from 120 to 1000 cm min^{-1} in the literature (Langergraber and Šimůnek 2005; Giraldi, de Michieli Vitturi and Iannelli 2010). When this range of K_s was adopted in the simulation, the simulated results tended to be unstable since the water movement was too fast to be predicted within the small discretization.

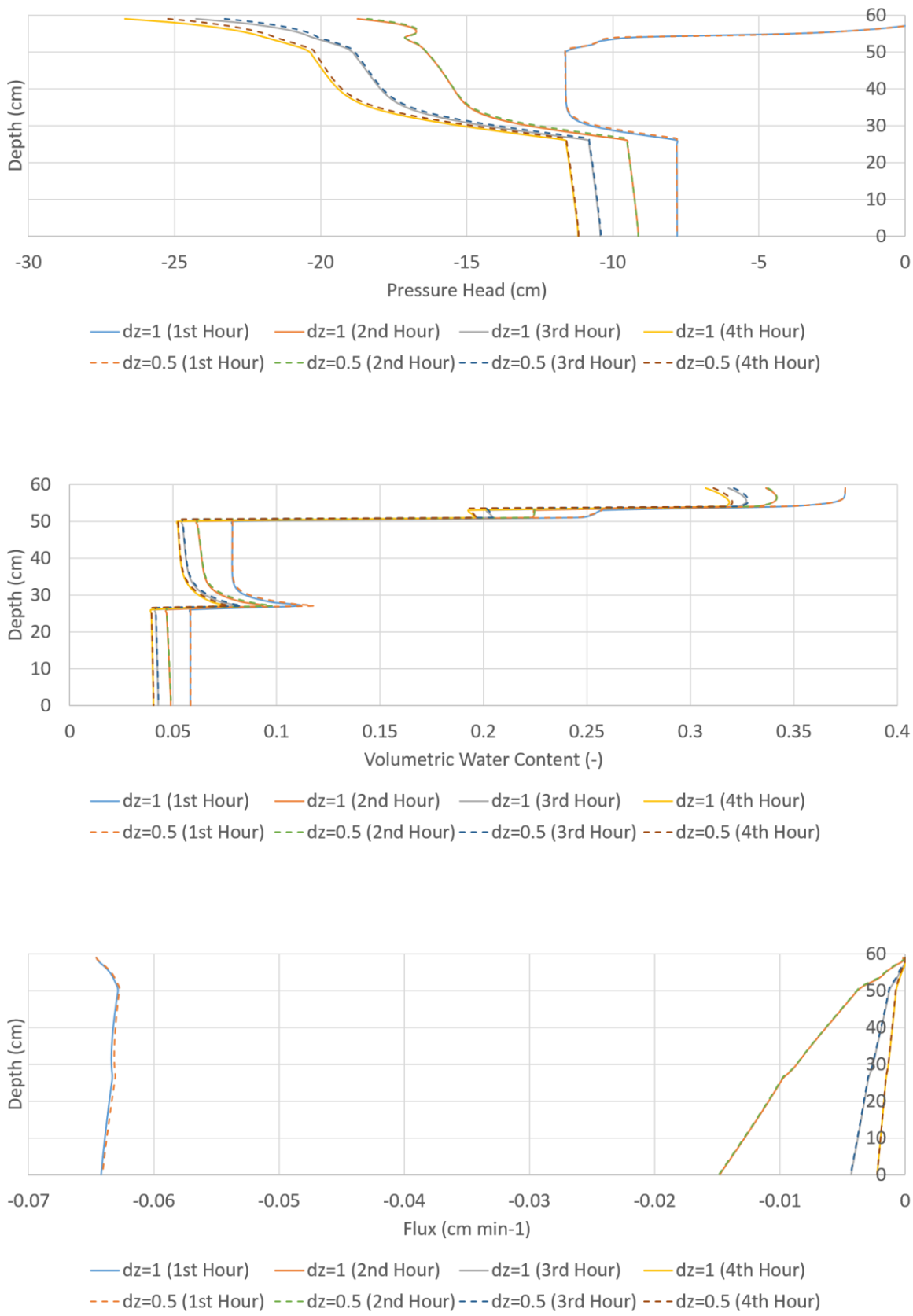

Figure 6.4: The comparison between a default spatial discretization (1.00 cm) and a finer spatial discretization (0.50 cm).

The time frame for the hydraulic simulation was determined from the measured data. The standard time unit in the simulation was in terms of minutes. The default temporal discretization was set to be 1/360 minute to guarantee a stable simulation. The maximum time frame was suggested to be 1 day (1440 minutes) due to the limitation of data storage in the simulation software.

The minimum and maximum tolerance for pressure head in the iterative computation were 0.01 and 1 cm, respectively. The reliability of these tolerances has been verified, as cited in Huang, Mohanty, and van Genuchten (1996). The maximum allowable number of iterations was prescribed to be 30. The reliability of the time discretization and iteration criteria in the hydraulic simulation was evaluated using the mass balance analysis.

As for the upper boundary condition, the loading time was fixed to be three minutes. Then, the feeding flux was converted by dividing the hydraulic loading rate (HLR) [L^3] to the wetland surface area [L^2]. The rate for case 50 l, 75 l, 100 l, 125 l, and 150 l were 1.50 cm min^{-1}, 2.30 cm min^{-1}, 3.00 cm min^{-1}, 3.80 cm min^{-1}, and 4.50 cm min^{-1}, respectively. Free drainage was used as the lower boundary condition in the simulation. Table 6.6 summarizes the information for geometry, time, and iteration criteria in the1 hydraulic simulation.

6.4. Inputs for ET and sludge accumulation

The weather data input to the ET module was obtained from the historical data in the website Weather Underground (2016), which is presented in Table 6.7. The experiments have been carried out in between November 2015 and February 2016. As the measurement of solar radiation was absent, the Julian day was used to determine

Table 6.6: The information for geometry, time, and iteration criteria in the hydraulic simulation.

Information in hydraulic simulation	Values
Spatial discretization [L]	1.00 cm
Temporal discretization [T]	1/360 minutes
Minimum tolerance for pressure head [L]	0.01 cm
Maximum tolerance for pressure head [L]	1.00 cm
Maximum allowable number of iteration [-]	30.00

Table 6.7: Weather data (Weather Underground 2016)

Date	Julian day (-)	Maximum temperature (˚C)	Minimum temperature (˚C)	Maximum humidity (%)	Minimum humidity (%)	Average wind velocity (m s^{-1})
2015-11-18	322	29	24	100	71	2.22
2015-11-24	328	30	24	100	70	1.67
2015-12-01	335	31	25	100	66	1.94
2015-12-04	338	32	24	100	63	1.67
2015-12-08	342	35	25	100	56	2.22
2015-12-12	346	31	25	100	70	1.67
2015-12-13	347	31	25	100	69	1.39
2015-12-16	350	28	24	100	69	1.39
2015-12-17	351	28	24	97	78	2.22
2015-12-24	358	33	23	100	53	1.39
2015-12-27	361	32	24	100	62	2.22
2015-12-31	365	32	26	94	57	3.61
2016-01-07	7	31	24	97	63	1.94
2016-01-10	10	31	26	94	74	1.67
2016-01-14	14	32	24	100	59	1.67
2016-01-21	21	30	25	100	70	1.39
2016-01-24	24	32	24	94	37	3.61
2016-01-28	28	31	24	100	66	1.67
2016-02-16	47	31	24	94	51	2.50
2016-02-21	52	31	25	89	55	4.17
2016-02-27	58	32	26	89	54	3.89
	Maximum	35	26	100	78	4.17
	Minimum	28	23	89	37	1.39
	Mean	31.10	24.52	97.52	62.52	2.20
	Standard Deviation	1.54	0.79	3.62	9.28	0.85

the potential solar radiation as shown in Appendix A. The maximum daily temperatures ranged from 28 to 35˚C, while the minimum temperatures were between 23˚C and 26 ˚C. Due to the frequent rains, the maximum daily humidity remained high throughout the entire experimental period (89 % - 100 %). The minimum daily humidity could be as low as 37% and its average is 62.52 $\pm$ 9.28 %. In most cases, the wind velocities were between 1.39 m s^{-1} to 2.50 m s^{-1}. There were only two days recorded with the wind velocity that exceeded 3 m s^{-1}.

The continuous growth of the common reeds altered its height over the wetland beds throughout the experimental period. Figure 6.5 shows the growth of common reeds at the end of experimental period. In the simulation, the height used in the ET module was assumed to be 1 m. The height of wind and humidity measurement was standardized as 2 m. The coefficient of active left area index (LAI_{active}) was referred to the standard value in Zotarelli et al. (2010) as 0.5. Figure 6.6 shows that the maximum root length of the common reeds in the pilot plant reached approximately 30 cm. The fraction of root length density at the top 10 % of the root zone was assumed to be 0.40. The wilting point of the vegetation was set to be 0.10 and the functional parameters for water stress distribution was fixed as 0.23. The root length density was estimated to be 0.05. The values of all parameters used in the ET module is presented in Table 6.8.

The rate of sludge accumulation was estimated from the fraction of particles retained at the wetland surface. According to the average removal rate of solids removal as shown in section 5.3, the retention coefficient of solids was approximately 0.80. The erosion of sludge deposit was neglected in the model because of the gravel bed that provided a strong structural support against the corrosion during loading. The porosity of the sludge deposit, which is the summation of the mobile region and immobile region, was assumed to be constant throughout the operation. The density of water was standardized as 1 g cm^{-3} while the density of the sludge deposit was assumed to be 1.10 g cm^{-3}. The values of these parameters are summarized in Table 6.9.

Table 6.8: Inputs for ET

Parameters	Values
Height of crop, h_c (m)	1.00
Height of wind measurement, z_w (m)	2.00
Height of humidity measurement, z_h (m)	2.00
LAI_{active} coefficient, *a* (-)	0.50
Empirical coefficient in Beer-lambert law, a_{b1} (-)	0.50
Maximum root depth, z_R (cm)	30.00
Fraction of the root length density in the top 10% of the root zone, F_{10} (-)	0.40
Wilting point, Θ_{wiltn} (-)	0.10
Functional parameter for water stress distribution, γ_α (-)	0.23
Root length density, g_0 (g cm^{-3})	0.01

Figure 6.5: Common reeds at the end of experiment

Figure 6.6: The root length of common reeds reached up to 30 cm

Table 6.9: Inputs for sludge accumulation

Parameters	Values
Erosion rate (cm min^{-1})	0
Retention parameters (-)	0.80
Porosity (-)	0.42
Density of water (g cm^{-3})	1.00
Density of sludge deposit (g cm^{-3})	1.10

6.5. Procedure for calibration of hydraulic parameters to fit measured data

The application of VF_Sep was only limited to the typical flow cases obtained from the laboratory experiment as shown in Figure 6.7. It is because the theoretical variably-saturated flow model simulates an effluent flux that is proportional to the level of surface ponding. As a result, the cases of “bypass” and “clogged” were not considered in the scope of simulation. According to the temporal plots of effluent flux, two main criteria were necessary to be satisfied in the calibration of hydraulic parameters, namely: peak effluent flux and the start of effluent discharge. These criteria are shown in Figure 6.7. In this calibration, one of the goals was to fit all sets of the measured effluent flux with the same set of hydraulic parameters to verify its reliability. However, the hydraulic properties of the heterogeneous substrate were inconsistent in each case.

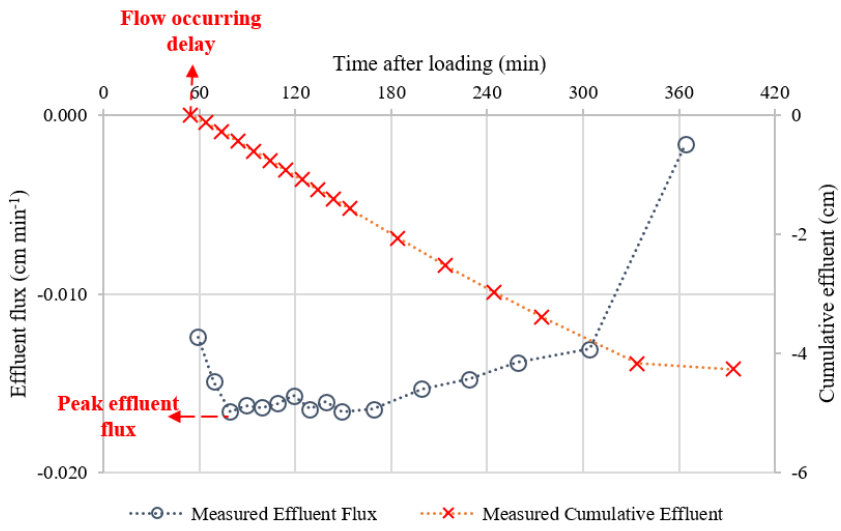

Figure 6.7: Effluent flux of "typical flow"

Although the multi-layered substrate profile provided more degrees of freedom to improve the accuracy, it simultaneously over-parameterized the simulation. It was important to identify the relative influence of each layer in the overall hydraulic performance, and thus the sensitivity of the prescribed hydraulic parameters could be evaluated to control the number of degree of freedom to be as low as possible.

In the substrate profile, the sludge deposit at the wetland surface was a low permeability mat that "regulates" the infiltration rate of the system. In chapter 5, the assessment of hydraulic behaviour revealed that the water recovery and peak effluent flux were dependent on the thickness of sludge deposit, highlighting its dominant role in the VFCW. Accordingly, the percolation throughout the gravel layer, which was characterized with a high water conductivity, was generally under the unsaturated condition and the associated hydraulic retention time was relatively short. The filtration of solid particles and the growth of biofilm potentially reduced the pore spaces at the upper fragment of the gravel bed. This circumstance was described by placing a 5 cm intermediate layer that resulted in a longer duration of percolation. Nevertheless, its permeability was still high and the effect was constrained by the top sludge deposit layer.

Section 5.1 has discussed the influence of cracks in the sludge deposit layer formed during resting period upon the delay of flow occurrence and peak effluent flux. This phenomenon was the main obstacle to obtain a set of optimal hydraulic parameters to fit all measured data. The influence of the resting period upon the hydraulic properties

of the intermediate layer and gravel layer was relatively minor, but it was vital to the distribution of initial pressure.

As the variably-saturated flow is a function of water content, the portion between the mobile region and immobile region is important to the hydraulic simulation. Giraldi et al. (2009) reported that the majority of the dead zones was found in the upper layers of bed. This assumption was used in VF_Sep, where the immobile regions in the sludge deposit and intermediate layer were more significant than in the gravel layers due to the presence of micropores that retains the stagnant water.

Accordingly, it could be postulated that the influence of the sludge deposit layer is most crucial in the substrate profile. It should be noted that nine inputs are required by each layer in the hydraulic simulation. The hydraulic parameter l was assumed to be 0.50 (Giraldi, de Michieli Vitturi and Iannelli 2010) for different grain sizes. As the influence of intermediate layer and gravel layer was minor, the hydraulic properties of these layers were fixed as constant in the calibration. Some guidelines have been found in the calibration process:

- In general, the intermediate layer and gravel layer were unsaturated due to the limited amount of percolation through the sludge deposit layer.
- The effective saturation in the mobile region was a function of the saturated water content (θ_s^m). In the unsaturated flow, the unsaturated hydraulic conductivity was greatly reduced by the low effective saturation due to the high θ_s^m. Therefore, the values of both parameters were necessary to be weighted carefully in the calibration.
- The VGM parameters, α and n, typically governed the amount of water retained in the substrate corresponded to the pressure head. If the values of both parameters used in the gravel layer were as low as the parameters for sand or silt, the inherent water content and water flux estimated from the initial pressure distribution were unreasonable and eventually failed to converge during the iterative computation.
- The amount of water exchanged between the mobile and immobile region was insignificant due to the low effective saturation in both regions.

The sludge deposit layer was assumed to consist mostly of the immobile region. Therefore, the layer was generally saturated throughout the operation. In this study,

the values of the VGM parameters were generally too low to describe a high inherent water content before the wetland bed was loaded. Besides, the water migration between the mobile and immobile regions always reached the equilibrium state in the simulation. The saturated hydraulic conductivity was revealed as the most sensitive parameter to match the maximum effluent flux, which dominated the flux across this low permeable layer. Table 6.10 presents the hydraulic parameters fixed in the hydraulic simulation to match the measured effluent flux obtained from the pilot-scale system.

Another important factor in the hydraulic simulation was the initial water content in the wetland bed. When the bed was dry, the flow of water was less smooth than in the wet condition. Therefore, the initial water content, which was implemented as initial pressure head in the proposed model, was optimized to match the flow occurring delay. The influence of the drying process during resting period has been discussed in section 5.2.2.

6.6. Results and Discussions

The hydraulic module was unable to match all twenty-five sets of data obtained throughout the experiment. In the last section, it has been highlighted that only the "typical flow" cases complied with the theoretical concept established in VF_Sep. Among the measured data, five cases were categorized as "bypass" and five cases were categorized as "clogged", thus there were only fifteen cases satisfying the requirement for calibration. As the K_s of sludge deposit layer and initial pressure distribution were selected as the degree of freedom in the calibration, a set of calibrated parameters was proposed. To verify the accuracy of the proposed model, the simulated results were analysed based on the mean absolute percentage error (MAE (%)) and regression analysis. The MAE is a statistical calculation to quantify the deviation between the actual data and predicted data, where a lower percentage means a better performance of simulation:

$$MAE\% = \frac{1}{n}\sum_{i=1}^{n}\left|\frac{A_t - P_t}{A_t}\right| \times 100\% \qquad (6.1)$$

Table 6.10: The values of hydraulic parameters used in the hydraulic simulation

Hydraulic parameters	Layer 1 – Sludge deposit layer	Layer 2 – Intermediate layer (5 cm)	Layer 3 – Small-size gravel layer (22 cm)	Layer 4 – Medium-size gravel layer (27 cm)
θ_r^m (-)	0.08	0.06	0.04	0.04
θ_s^m (-)	0.22	0.28	0.32	0.36
α (cm^{-1})	0.07	0.18	0.29	0.36
n (-)	1.80	2.70	3.50	4.00
K_s ($cm\ min^{-1}$)	*	10.00	1300.00	1500.00
l (-)	0.50	0.50	0.50	0.50
θ_r^{im} (-)	0.10	0.03	0	0
θ_s^{im} (-)	0.20	0.18	0.14	0.12
ω (min^{-1})	0.002	0.007	0.02	0.04

A_t is the actual flow rate in the experiment, P_t is the predicted value of the simulation and n is the number of data.

On the other hand, the linear regression analysis was conducted between the measured and simulated flux to determine the coefficient of determination (R^2). The R^2, which ranges from 0 to 1, describes the similarity of overall flow trends between actual and predicted data. It should be noted that the value of R^2 is unable to be referred to as an indicator of accuracy in the hydraulic simulation, and thus this parameter only represents the consistency of variation between the measured and simulated data. The R^2 was obtained from the function of regression analysis in Microsoft Excel.

In order to simplify the review upon the efficiency of the model, the simulated results were divided into three categories with respect to the MAE (%); which were below 15 %, between 15 % and 25 %, and over 25 %. The cases with MAE (%) exceeding 25 % (4B, 16A, and 20A) were considered as modelling failure and were not presented in this section. The non-conservative water recovery (average percentage < 60 %) significantly impacted on the precision of the simulation. A correction factor derived from the ratio of the volume of influent to the effluent was proposed to improve the accuracy of the model. Furthermore, the influence of ET and sludge accumulation on the overall hydraulic simulation were evaluated.

6.6.1. Simulated results

The calibration with two degrees of freedom delivered a simple approach to match the measured data. The K_s was calibrated in advance to match the maximum effluent flux. Then, the initial pressure head was adjusted to fit the flow occurring delay. Both criteria have to be weighted simultaneously, where the K_s also impacted on the flow occurring time but the initial pressure head had a minor influence on the maximum effluent flux.

There were eight calibrated simulations with MAE (%) below 15 %. Figure 6.8 - Figure 6.15 illustrate the simulated results of the effluent flux and cumulative effluent. The calibrated initial pressure head (h_{init}) and saturated hydraulic conductivity of sludge layer (K_s), as well as the mean absolute percentage error (MAE(%)) and coefficient of determination (R^2) of simulated results, are summarized in Table 6.11. Furthermore, the relatively high average R^2 in the regression analysis (0.81) revealed that VF_Sep is promising in simulating the effluent flow.

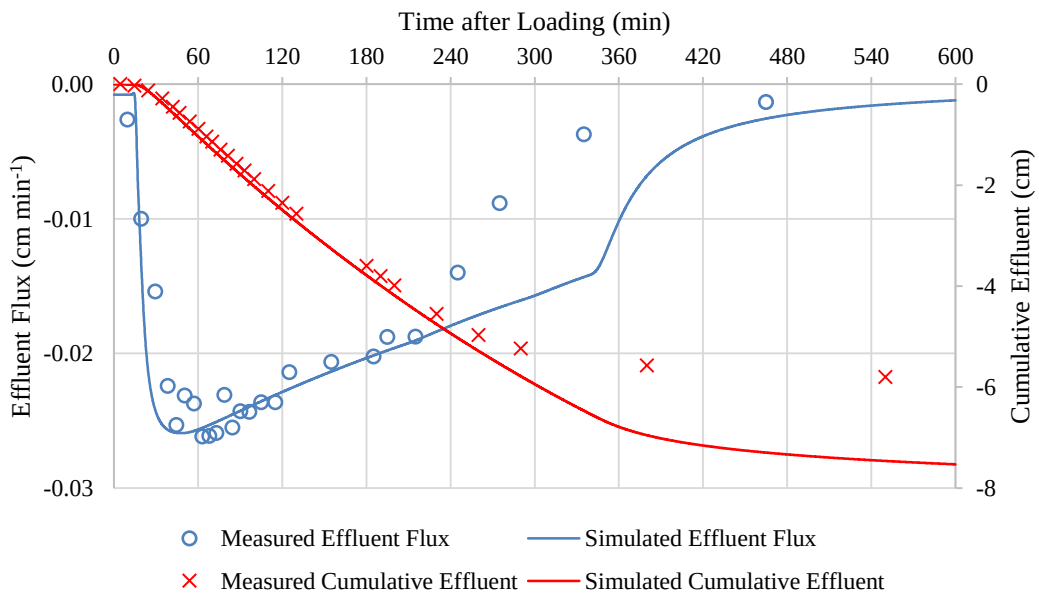

Figure 6.8: Simulated results of case 1A (18-11-2015: 75 l)

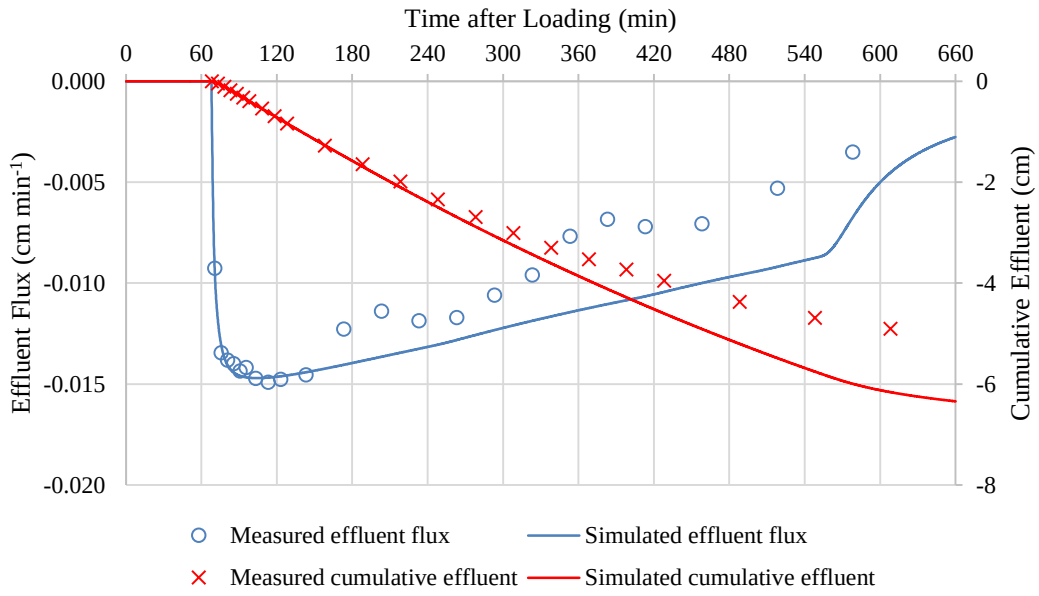

Figure 6.9: Simulated results of case 3A (1-12-2015: 75 l)

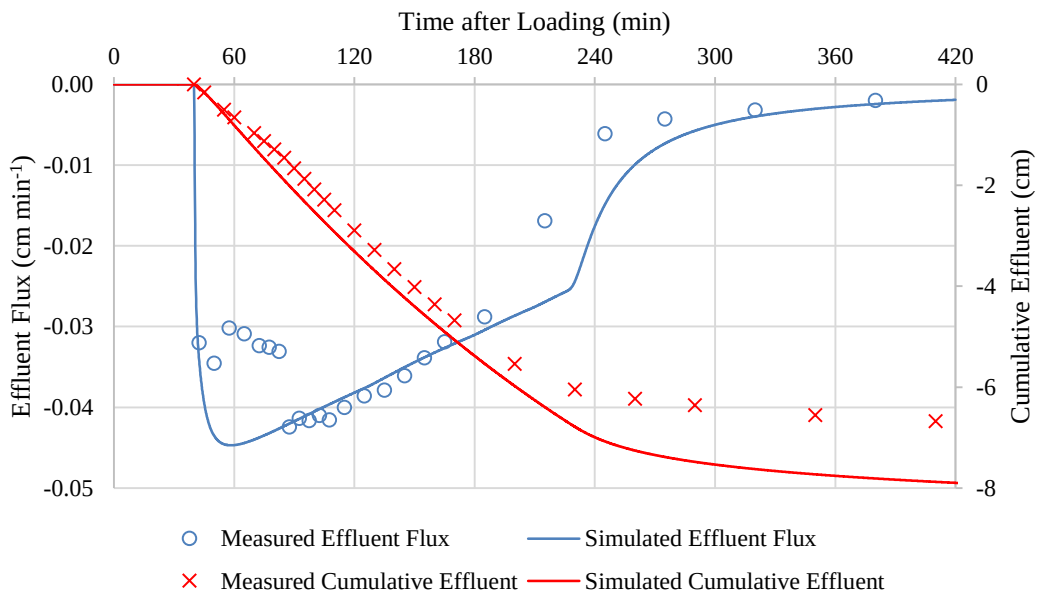

Figure 6.10: Simulated results of case 8A (16-12-2015: 100 l)

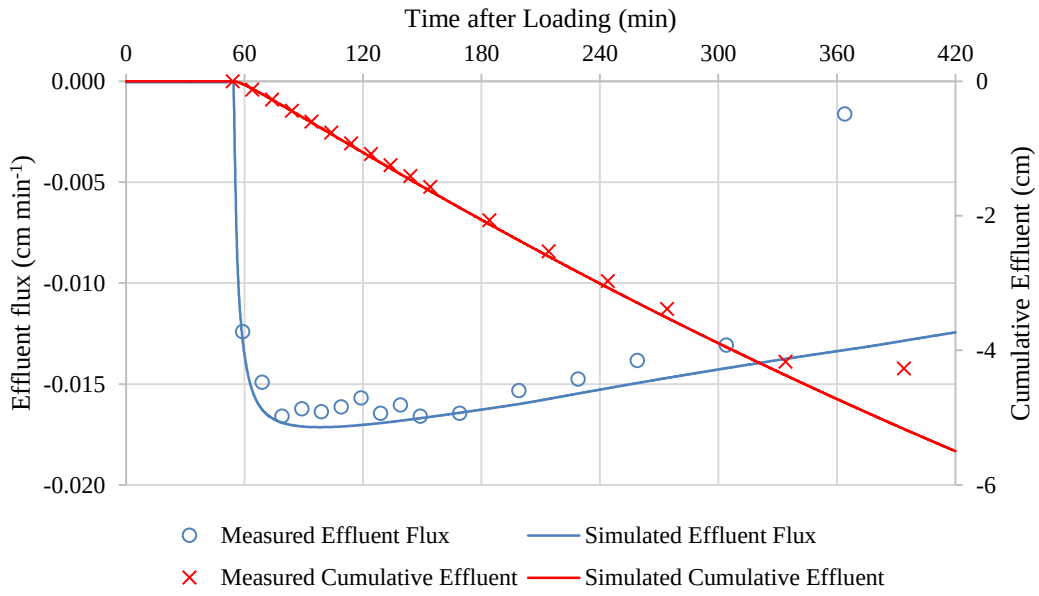

Figure 6.11: Simulated results of case 11A (27-12-2015: 100 l)

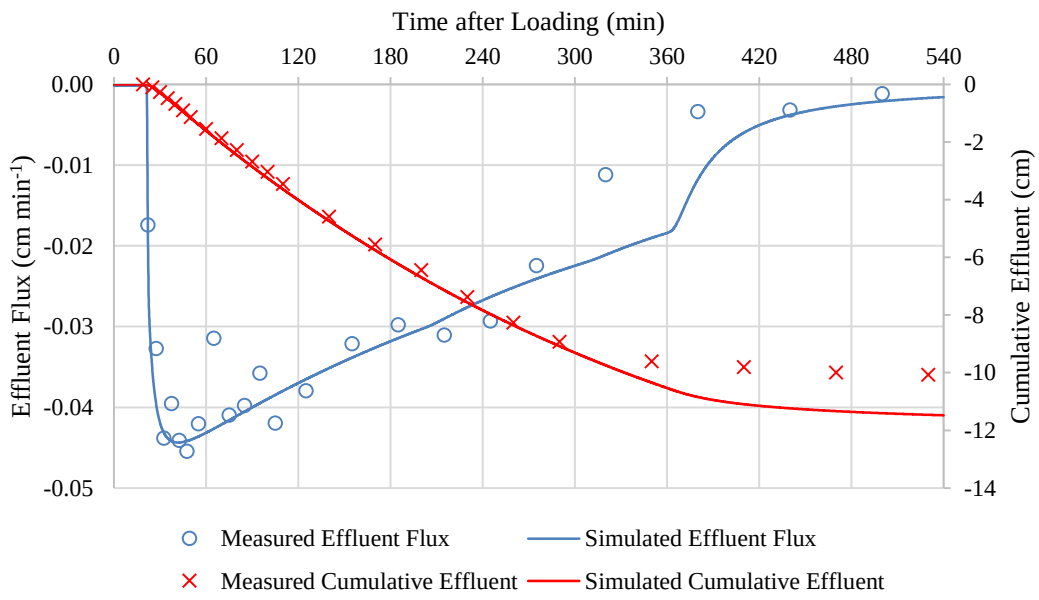

Figure 6.12: Simulated results of case 19B (24-1-2016: 125 l)

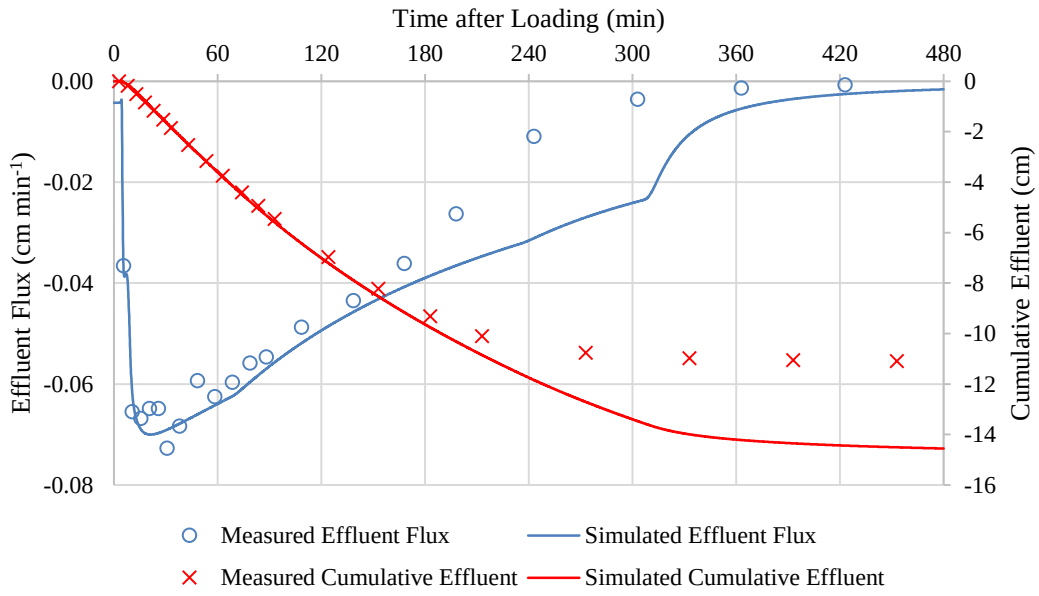

Figure 6.13: Simulated results of case 20A (28-1-2016: 150 l)

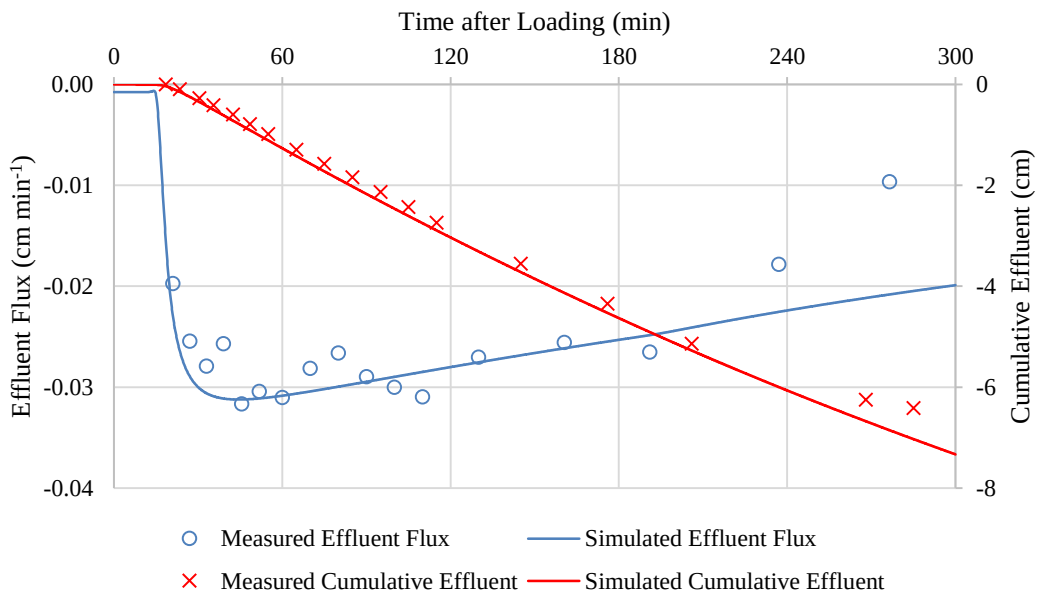

Figure 6.14: Simulated results of case 24B (21-2-2016: 125 l)

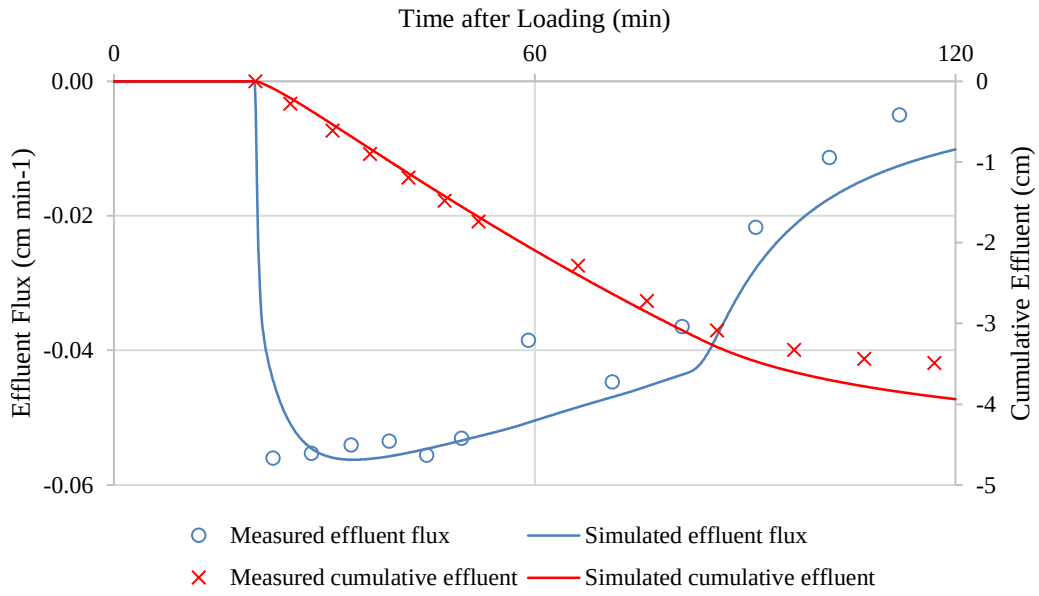

Figure 6.15: Simulated results of case 25B (27-2-2016: 50 l)

Table 6.11: Summary of calibrated parameters and error analysis

No. of test A = Wetland A B= Wetland B		HLR (l)	Sludge thickness (cm)	Water recovery (%)	Calibrated h_{int} (cm)	Calibrated K_s (cm min^{-1})	MAE (%)	R^2
1A	**18/11/2015**	75	5.00	85.08%	-12.00	0.0092	11.63%	0.84
3A	**1/12/2015**	75	6.00	71.92%	-18.00	0.0062	14.25%	0.80
8A	**16/12/2015**	100	6.00	73.41%	-34.00	0.0186	14.57%	0.83
11A	**27/12/2015**	100	8.00	46.94%	-16.00	0.0077	9.76%	0.57
19B	**24/1/2016**	125	4.00	88.61%	-15.00	0.0105	10.23%	0.87
20A	**28/1/2016**	150	3.00	81.37%	-10.00	0.0112	11.58%	0.94
24B	**21/2/2016**	125	5.00	56.43%	-12.00	0.0086	9.99%	0.74
25B	**27/2/2016**	50	6.00	76.77%	-15.00	0.0323	12.17%	0.92
		Maximum	8.00	88.61%	-10.00	0.0323	14.57%	0.94
		Minimum	3.00	46.94%	-34.00	0.0062	9.76%	0.57
		Mean	5.38	72.57%	-16.50	0.0130	11.77%	0.81
		Standard deviation	1.41	13.36%	7.04	0.0081	1.72%	0.11

The calibration of the proposed hydraulic module successfully reproduced the measured effluent flux with respect to varying HLR and sludge thickness. Table 6.11 shows that the calibrated h_{int} ranged from -10 to -21 cm, reflecting that the water content in the pilot-scale wetland bed remained high after the resting period. On the other hand, the deviation of calibrated values of K_s in sludge deposit layer was significant from cases to case, ranging from 0.0062 to 0.0323 cm min^{-1}. This highlighted that the hydraulic conductivity of this layer could be greatly affected by its thickness, water content and the formation of cracks during resting period.

By calibrating the K_s and h_{init}, the simulated effluent flux and cumulative effluent effectively matched the experimental measurements at the early phase. However, there were two exceptions throughout the experiment. In case 8A, the maximum flux was only observed after a constant effluent discharge has been observed for 30 minutes, and thus the flux during this period was over-predicted since the K_s was calibrated to fit the maximum flux. As for case 25B, the simulated result underestimated the first effluent flux, but the following simulated results fitted the measured data well.

The effluent flux at the late stage was generally over-predicted by the proposed model and contributed to the majority of the deviations in the error analysis. In the simulation, a rapid reduction of effluent flux was illustrated when the surface ponding has completely infiltrated. The measured data showed that such deceleration occurred earlier than the simulated effluent flux, and led to an over-prediction of approximately 2 cm in the cumulative effluent. This difference was similar to the water loss from the measurements of water balance in the experiments. As mentioned in the previous section, the proposed hydraulic module is theoretically conservative. Although the water exchange in the immobile regions and the influence of ET had been employed to account for the water balance, the simulated results still over-predicted the overall cumulative effluent.

In general, the cases with a high water recovery tended to result in a lower MAE (%) in the hydraulic simulation. Nevertheless, two exceptions were observed. In case 11A and 24B, the effluent flux was stable at the early phase of treatment, but it unpredictably decelerated and instantaneously became insignificant at the late phase of treatment. On the other hand, the simulated results illustrated a continuous effluent, and thus the major deviations were distributed at the last two points, as shown in Figure

6.11 and Figure 6.14. As a result, their MAE (%) were still desirable. However, these discrepancies led to poor R^2 value, highlighting that low MAE (%) did not deserve a desirable R^2.

Figure 6.16 - Figure 6.19 show four cases with calibrated parameters that displayed a MAE (%) between 15 and 25 %. The information of operation, values of calibrated parameters and error analysis are presented in Table 6.12. Similar to the cases explained above, the low water recovery was the main reason for the relatively high MAE (%) in the hydraulic simulation. In general, the water recovery obtained in these cases were below 70 %, subsequently contributing to significant discrepancies in terms of the overall cumulative effluent. These comparisons between laboratory measurement and simulated results revealed that the influence of water recovery was vital in the modelling of hydraulic behaviour in the VFCW, and thus a correction coefficient for the water balance was essential to improve the accuracy of the simulation.

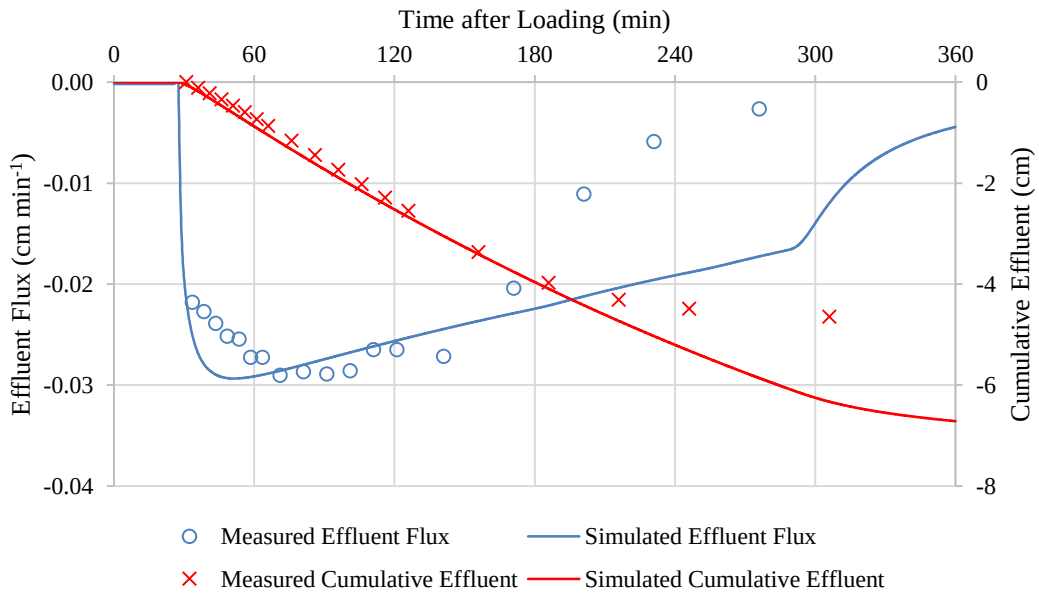

Figure 6.16: Simulated results of case 6A (12-12-2015: 75 L)

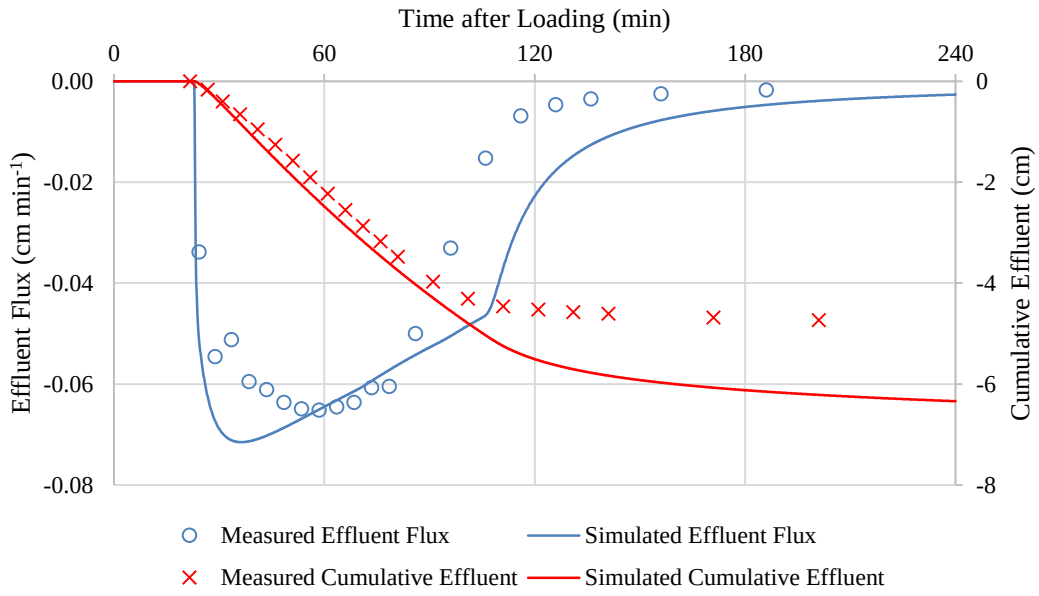

Figure 6.17: Simulated results of case 7B (13-12-2015: 75 L)

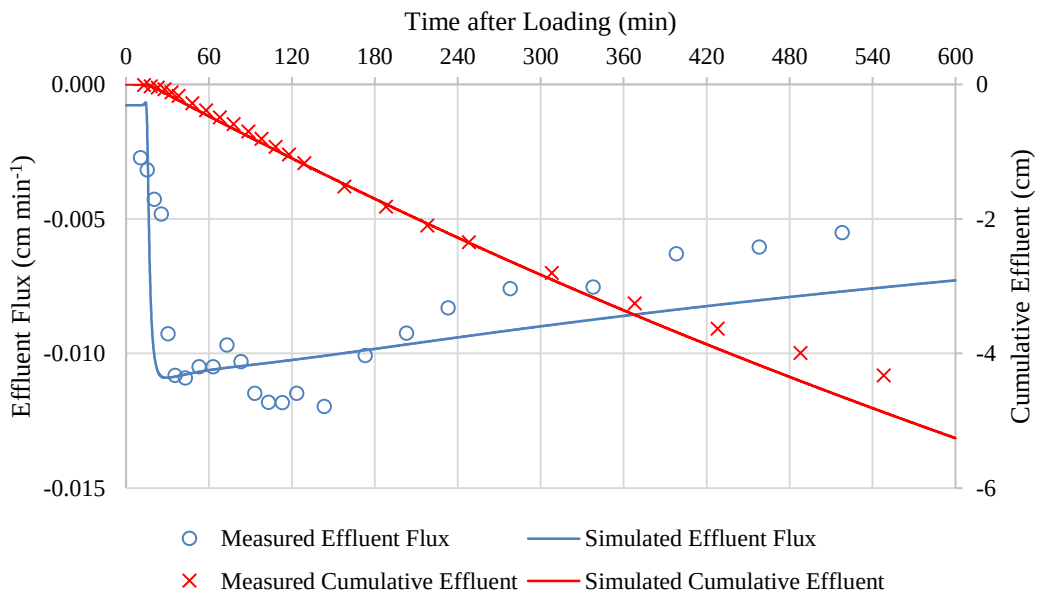

Figure 6.18: Simulated results of case 17B (21-1-2015: 100 L)

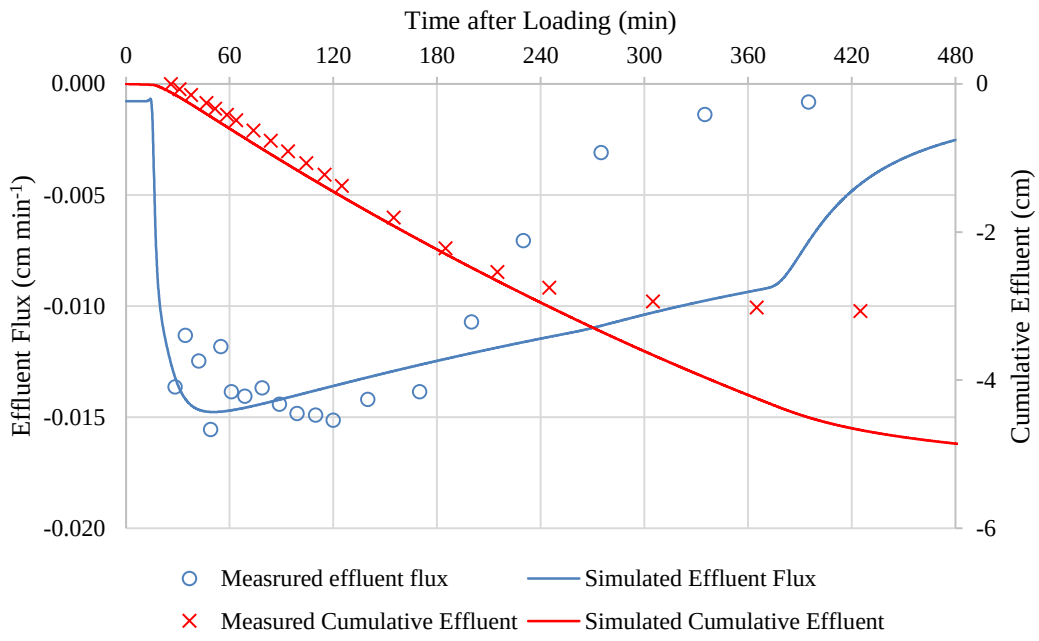

Figure 6.19: Simulated results of case 23B (16-2-2016: 50 L)

Table 6.12: Summary of calibrated parameters and error analysis

No. of test A = Wetland A B= Wetland B		HLR (l)	Sludge thickness (cm)	Water recovery %	Calibrated h_{int} (cm)	Calibrated K_s (cm min^{-1})	MAE (%)	R^2
6A	**12/12/2015**	75	5.00	68.14%	-14.00	0.0108	18.26%	0.78
7B	**13/12/2015**	75	5.00	69.48%	-21.00	0.0310	23.21%	0.87
17B	**21/1/2016**	100	3.00	47.59%	-12.00	0.0020	17.05%	0.52
23B	**16/2/2016**	50	4.00	67.43%	-12.00	0.0052	21.05%	0.78
		Maximum	5.00	69.48%	-12.00	0.0310	23.21%	0.87
		Minimum	3.00	47.59%	-21.00	0.0020	17.05%	0.52
		Mean	4.25	63.16%	-15.00	0.0124	19.89%	0.74
		Standard deviation	0.83	9.02%	4.12	0.0112	2.40%	0.13

In most cases, the water loss via ET to the atmosphere was too small to influence the outflow dynamics, and thus the high volumetric difference between influent and effluent was unable to be individually attributed to this mechanism. As the water exchange rate between the mobile and immobile region was proportional with respect to the gradient of saturation, the stagnant water retained in the substrate brought a

minor effect towards the water recovery under the unsaturated condition. In fact, stagnant surface water was always found in the late phase of the feeding-drainage cycle, which generally appeared with a depth of about 1-2 cm as shown in Figure 6.20. This observation implied that the wetland bed might have a limitation of water level that induced an effective infiltration and discharge. Such an unforeseen situation alternated the prescribed boundary condition, which presumed that the total amount of infiltration was ideally equivalent to the hydraulic load. Therefore, a modification to the boundary condition, particularly the HLR, was adopted to improve the efficiency of VF_Sep.

This approach was found in Giraldi and Iannelli (2009), which aimed to calibrate a solute transport model with the tracer experiment in a VFCW while the recovery of tracer was non-conservative in the laboratory experiment. The authors estimated a new influent rate according to the tracer recovery in the effluent and obtained a significant improvement in terms of accuracy. In this study, a correction coefficient (CR) was derived from the water recovery percentage and was implemented in the boundary condition to refine the rate of influent flux. It should be noted that the CR had a limited effect upon the cases with a precise prediction for cumulative effluent such as case 17B, 24B, and 25B. A total of seven cases (1A, 3A, 6A, 7B, 19B, 20A, and 23B) were recalibrated with the updated boundary condition that included the CR.

Figure 6.20: Stagnant raw septage at the wetland surface during later stage of treatment

Figure 6.21 - Figure 6.34 display the comparisons between the simulated effluent flux with and without CR, as well as the comparisons between the simulated cumulative effluent with and without CR. Table 6.13 shows the comparison between MAE (%) and R^2 of the simulated results with and without CR. In the recalibration, the initial pressure distribution remained the same as the calibrated value in the original simulation, but the K_s was increased due to the lower loading rate. The calibrated values are presented in Table 6.14.

According to the temporal plots of effluent flux, the effluent flux at the early phase was not affected by the inclusion of CR. Nevertheless, the prediction at the later phase was improved significantly compared to the original simulation. Therefore, the deviation between the measured and simulated cumulative effluent was greatly reduced. Table 6.13 shows that the associated MAE (%) and R^2 were significantly minimized. The mean of MAE (%) was reduced from 15.74 % $\pm$ 4.74 % to 11.06 % $\pm$ 3.17 % and the mean R^2 was increased from 0.84 $\pm$ 0.05 to 0.89 $\pm$ 0.04. The improvement is proportional to the water recovery percentage. The cases with low water recovery such as case 6A, 7B, and 23B showed remarkable minimization of error, while the effect on cases 1A and 19B were relatively minor.

Table 6.13: MAE (%) and R^2 of the simulated results with and without CR

No. of test		**Water recovery (%)**	**CR**	**MAE (%)**		**R^2**	
A = Wetland A				Without CR	With CR	Without CR	With CR
B= Wetland B							
1A	**18/11/2015**	85.08%	0.85	11.63%	9.55%	0.84	0.89
3A	**1/12/2015**	71.92%	0.72	14.25%	10.48%	0.80	0.82
6A	**12/12/2015**	68.14%	0.68	18.26%	10.17%	0.78	0.88
7B	**13/12/2015**	69.48%	0.69	23.21%	17.95%	0.87	0.88
19B	**24/1/2016**	88.61%	0.89	10.23%	9.83%	0.87	0.93
20A	**28/1/2016**	81.37%	0.81	11.58%	7.08%	0.94	0.97
23B	**16/2/2016**	67.43%	0.67	21.05%	12.46%	0.78	0.88
	Maximum	88.61%	0.89	23.21%	17.95%	0.94	0.97
	Minimum	67.43%	0.67	10.23%	7.08%	0.78	0.82
	Mean	75.90%	0.76	15.74%	11.07%	0.84	0.89
	Standard deviation	8.25%	0.08	4.74%	3.17%	0.05	0.04

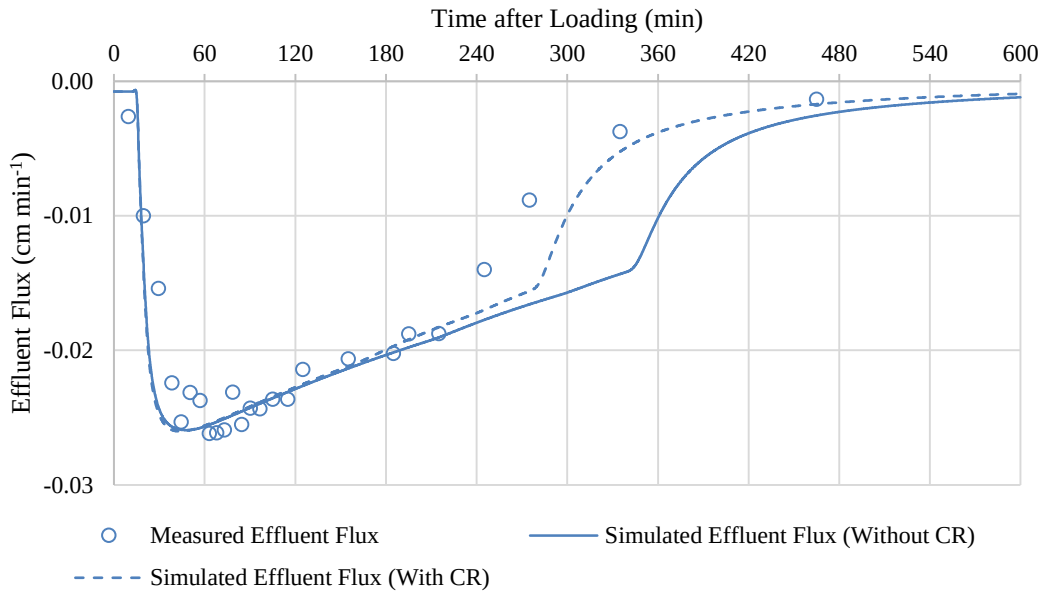

Figure 6.21: Simulated effluent flux with and without correction coefficient of case 1A (18-11-2015: 75 L)

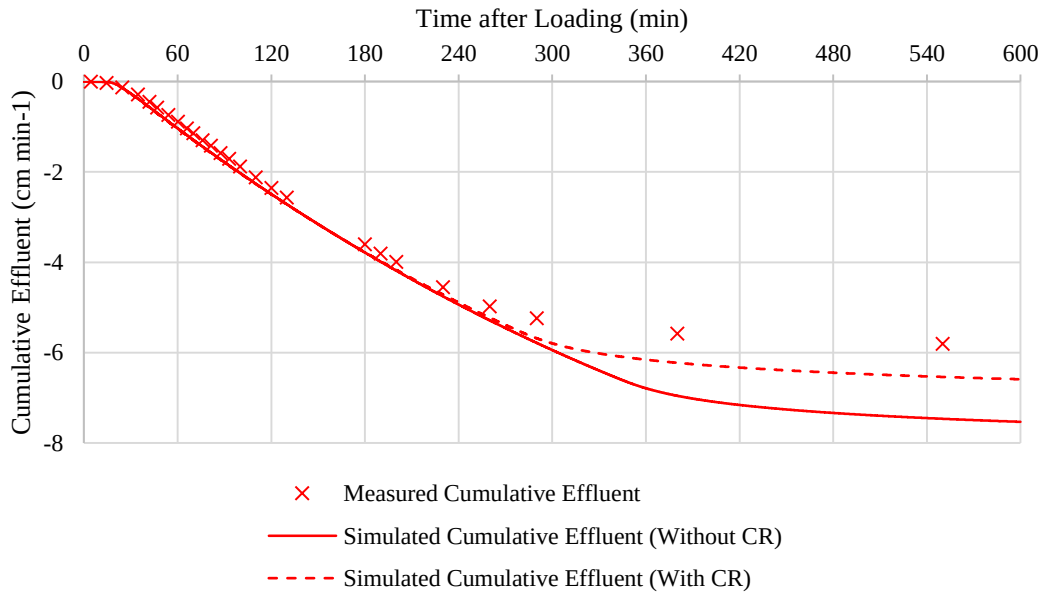

Figure 6.22: Simulated cumulative effluent with and without correction coefficient of case 1A (18-11-2015: 75 L)

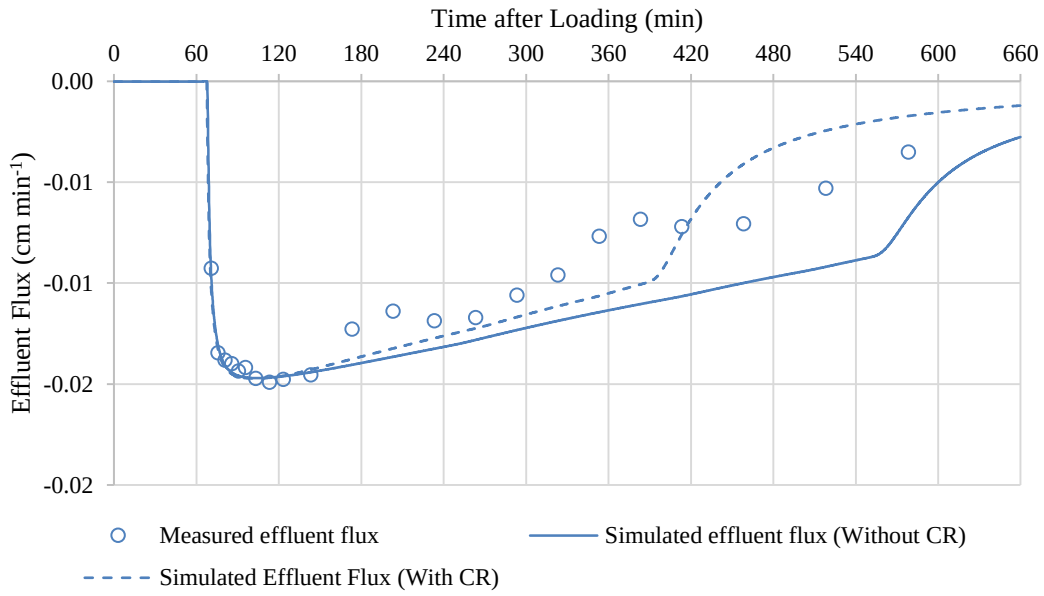

Figure 6.23: Simulated effluent flux with and without correction coefficient of case 3A (1-12-2015: 75 L)

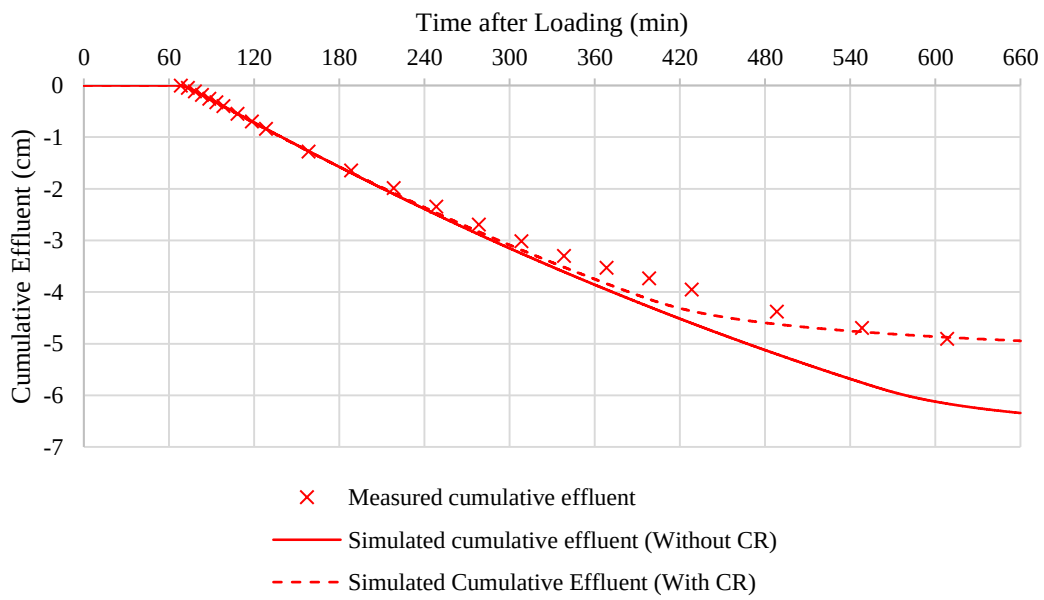

Figure 6.24: Simulated cumulative effluent with and without correction coefficient of case 3A (1-12-2015: 75 L)

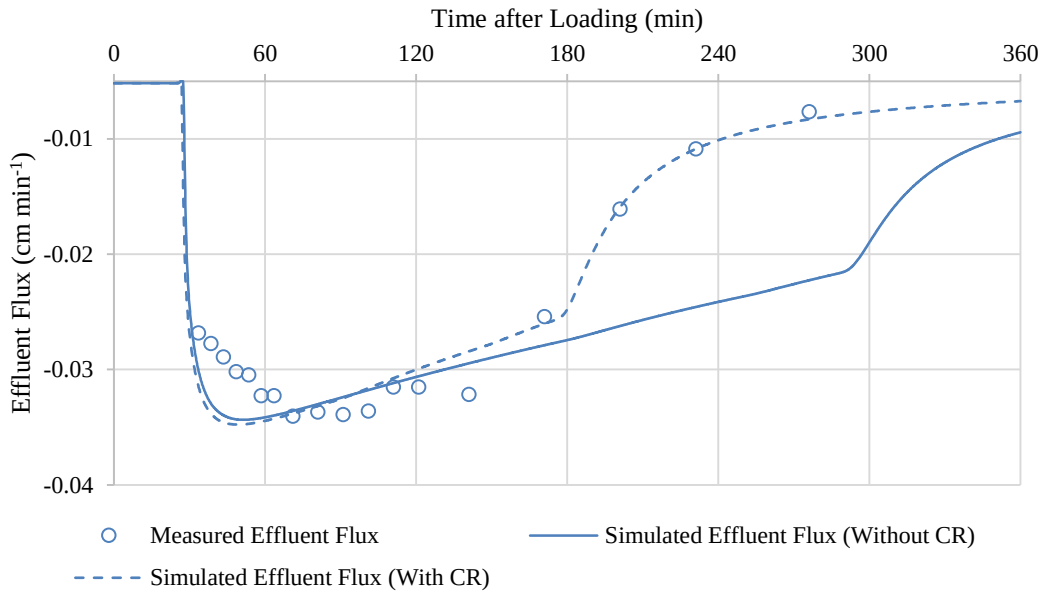

Figure 6.25: Simulated effluent flux with and without correction coefficient of case 6A (12-12-2015: 75 L)

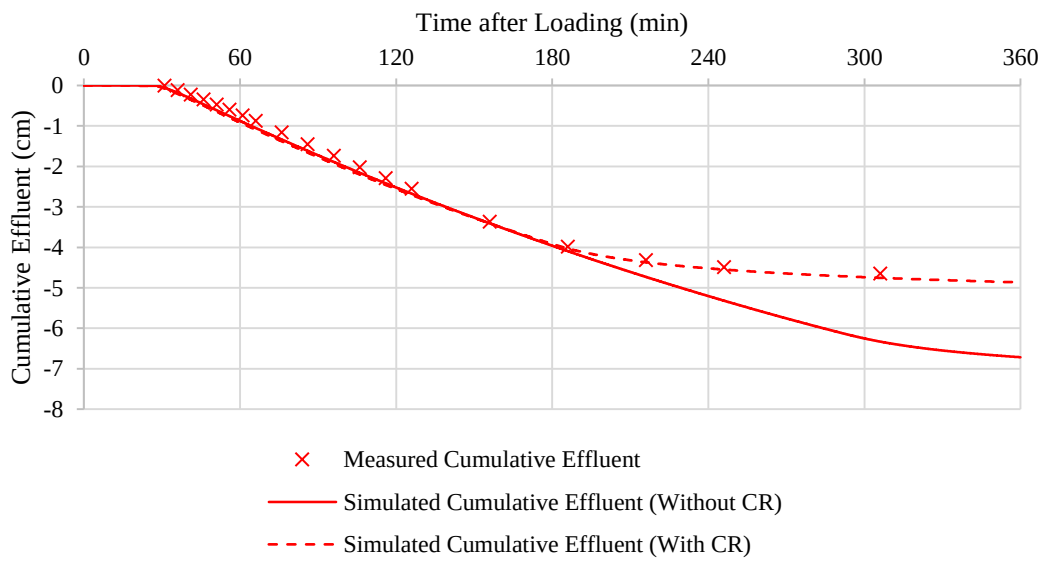

Figure 6.26: Simulated cumulative effluent with and without correction coefficient of case 6A (12-12-2015: 75 L)

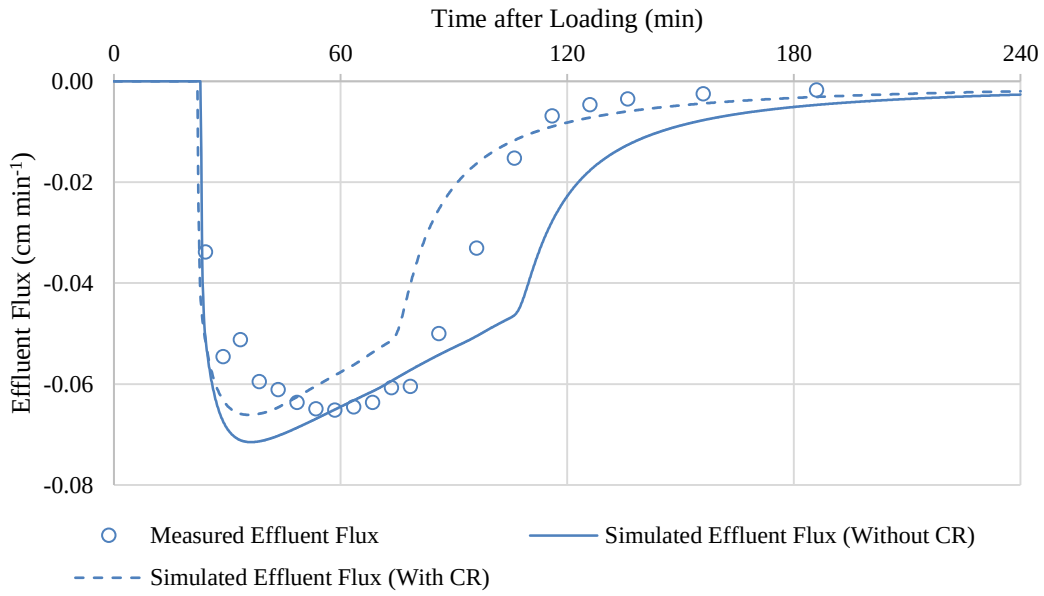

Figure 6.27: Simulated effluent flux with and without correction coefficient of case 7B (13-12-2015: 75 L)

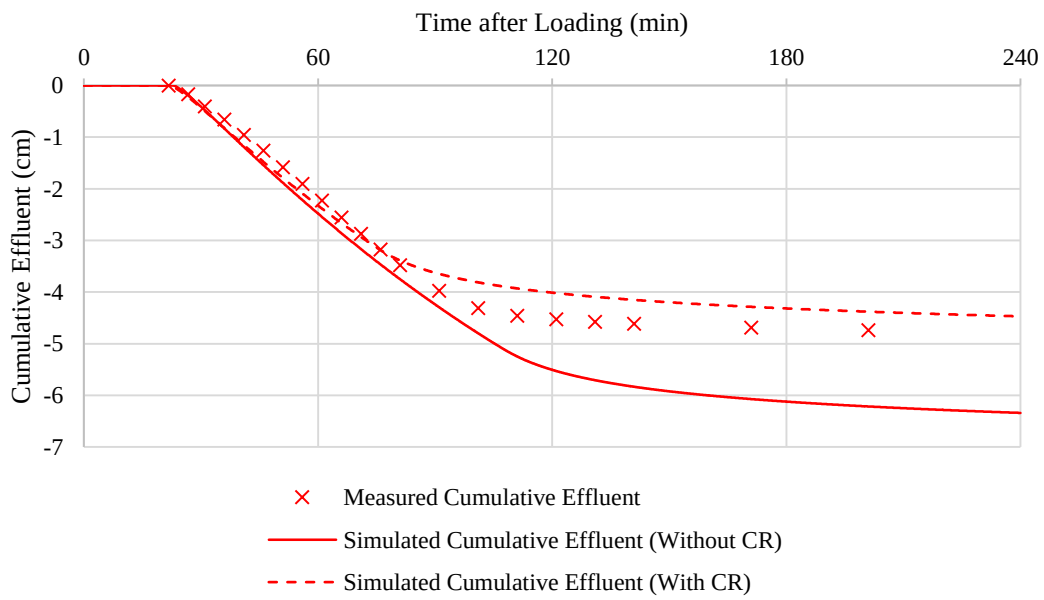

Figure 6.28: Simulated cumulative effluent with CR of case 7B (13-12-2015: 75 L)

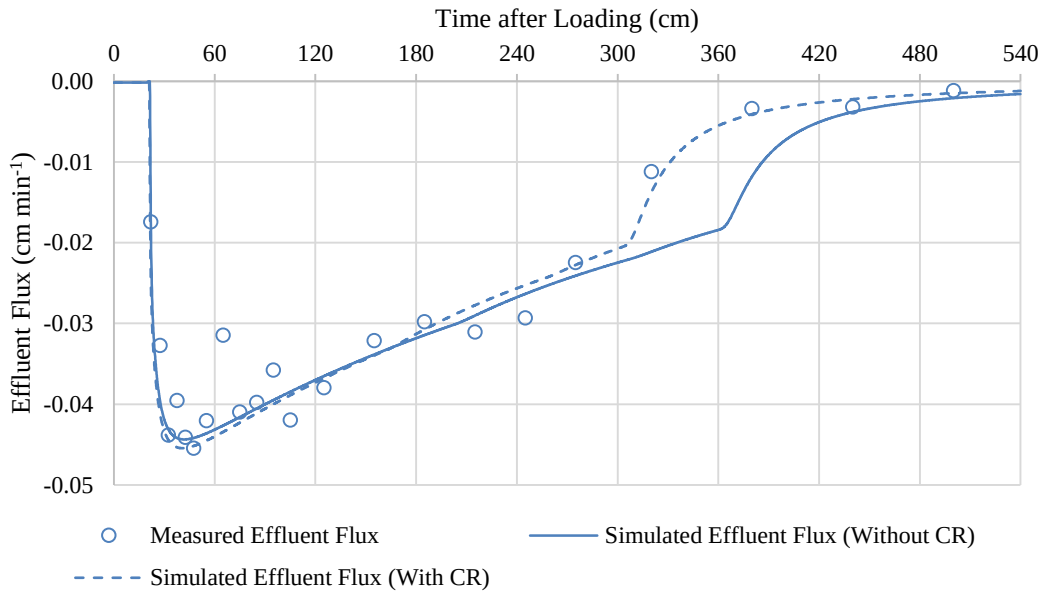

Figure 6.29: Simulated effluent flux with and without correction coefficient of case 19B (24-1-2016: 125 L)

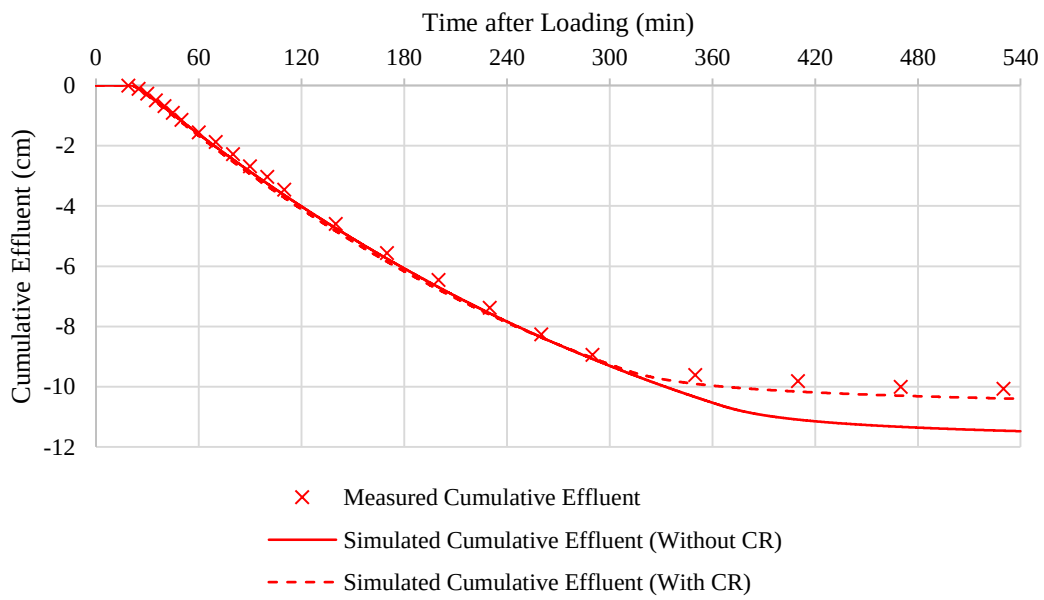

Figure 6.30: Simulated cumulative effluent with and without correction coefficient of case 19B (24-1-2016: 125 L)

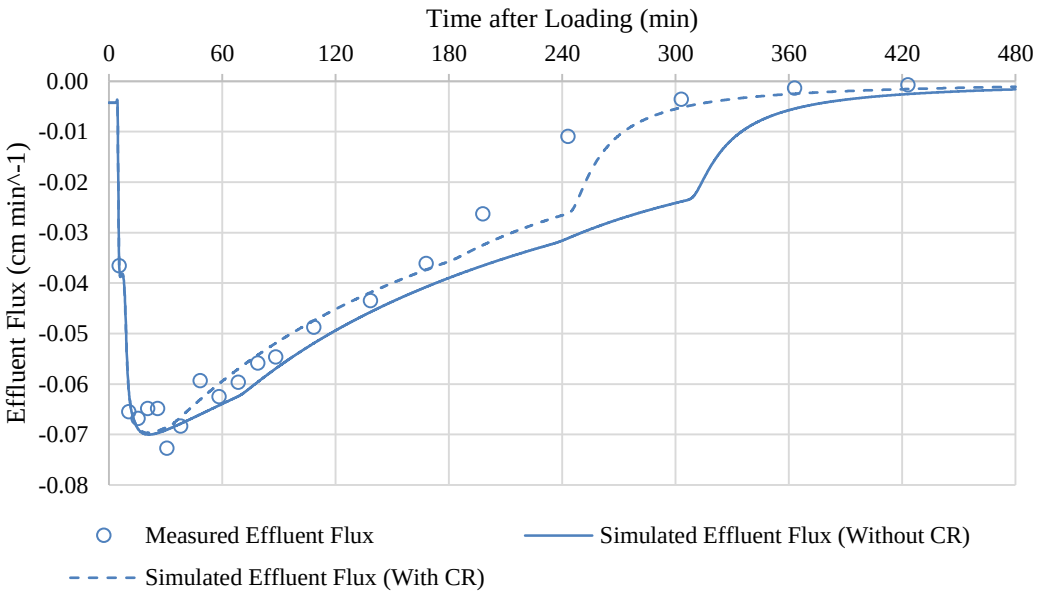

Figure 6.31: Simulated effluent flux with and without correction coefficient of case 20A (28-1-2016: 150 L)

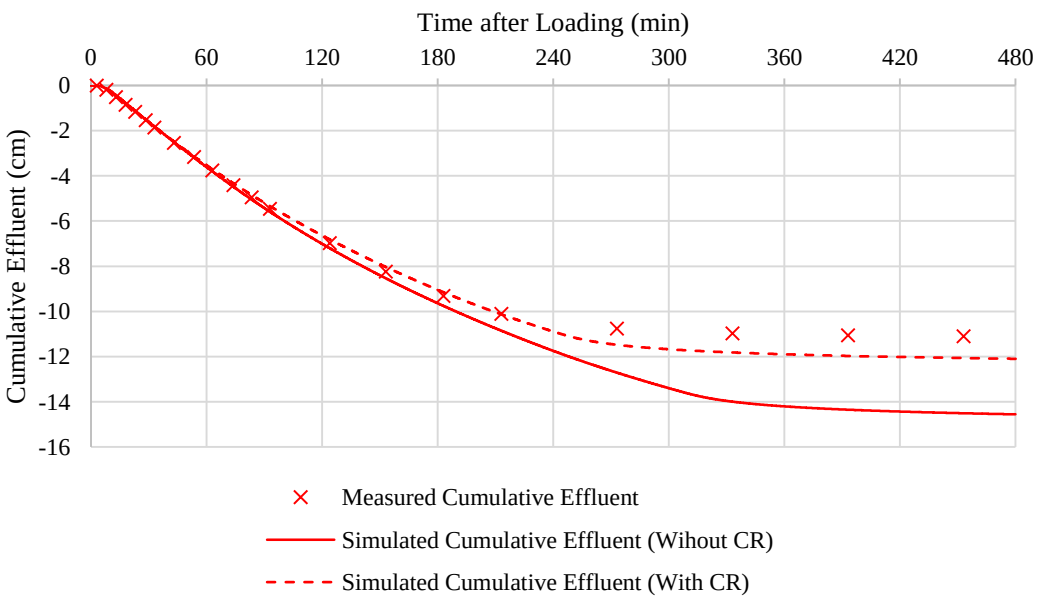

Figure 6.32: Simulated cumulative effluent with and without correction coefficient of case 20A (28-1-2016: 150 L)

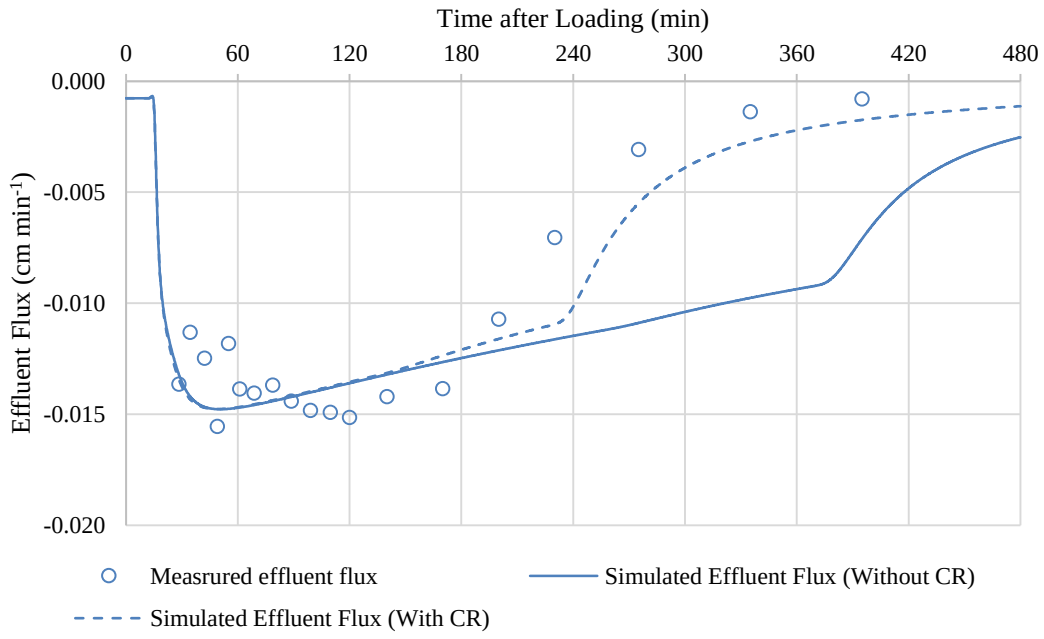

Figure 6.33: Simulated effluent flux with and without correction coefficient of case 23B (16-2-2015: 50 l)

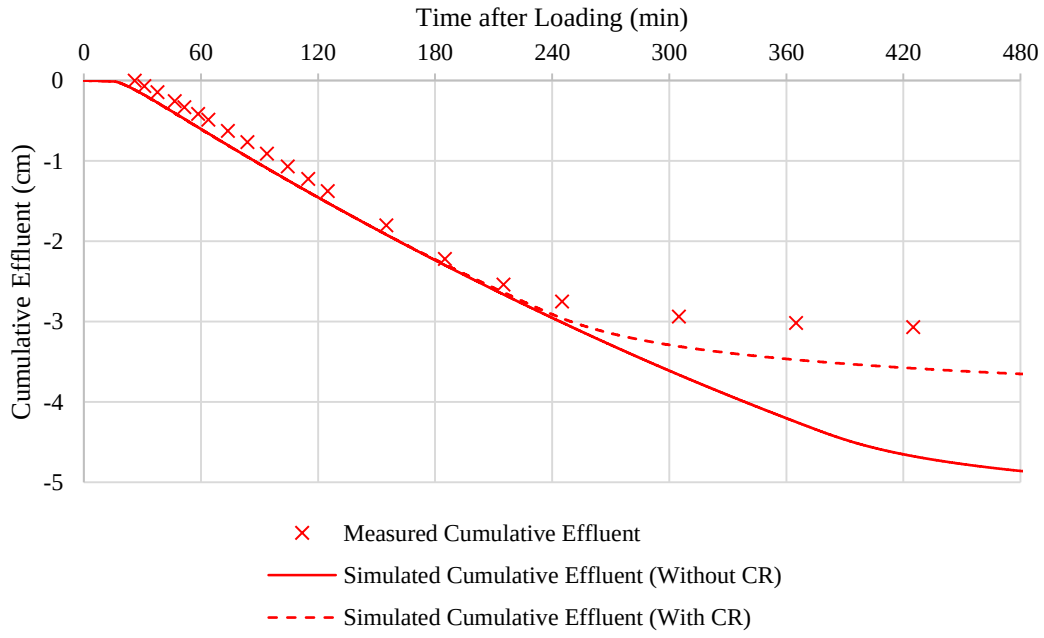

Figure 6.34: Simulated cumulative effluent with and without correction coefficient of case 23B (16-2-2015: 50 l)

Table 6.14: Summary of calibrated K_s

No. of test A = Wetland A B= Wetland B		Water recovery (%)	CR	K_s (cm min^{-1}) Without CR	With CR
1A	**18/11/2015**	85.08%	0.85	0.0092	0.0101
3A	**1/12/2015**	71.92%	0.72	0.0062	0.0072
6A	**12/12/2015**	68.14%	0.68	0.0108	0.0135
7B	**13/12/2015**	69.48%	0.69	0.0310	0.0331
19B	**24/1/2016**	88.61%	0.89	0.0105	0.0117
20A	**28/1/2016**	81.37%	0.81	0.0112	0.0125
23B	**16/2/2016**	67.43%	0.67	0.0052	0.0062
	Maximum	88.61%	0.89	0.0310	0.0331
	Minimum	67.43%	0.67	0.0052	0.0062
	Mean	75.90%	0.76	0.0120	0.0135
	Standard deviation	8.25%	0.08	0.0080	0.0084

The CR in the simulation effectively compensates the error caused by the difference of water balance. Nevertheless, the current experimental outcome was insufficient to derive a global factor to tolerate the discrepancies in terms of water recovery between cases. In order to identify a minimum level of surface water that stimulates the effluent, a systematic investigation with regards to the residual of influent throughout the experiment is necessary for the future research.

6.6.2. Sensitivity Analysis: ET and Sludge Accumulation

The simulated results without CR overestimated the exact effluent flux from the pilot-scale VFCW. From the perspective of water budget, the excellent dewatering performance of sewage sludge in the VFCWs depends on the draining through the substrate and the ET through the vegetation (De Maeseneer 1997; Edwards et al. 2001). Therefore, the consideration of water loss via the atmosphere is able to improve the accuracy of the hydraulic simulation (Galvão et al. 2010).

Although ET was estimated using the Penman-Monteith equation (Zotarelli et al. 2010) with the climatic data (temperature, humidity and wind speed), the comparison showed that its influence was minor to the overall hydraulic behaviour. In fact, most of the advanced mechanistic models considered this influence in the hydraulic module (Giraldi, de Michieli Vitturi and Iannelli 2010; Ouyang, Luo and Cui 2011), but the

discussion with regards to its contribution was always limited in the literature. This gap of knowledge is due to the difficulty in quantifying the rate of ET in the VFCW (Borin et al. 2011). In this study, such a specific measurement was not carried out. The lack of data subsequently led to the controversial assumption with regards to the relative contribution between the ET and draining in terms of dewatering mechanism. Stefanakis and Tsihrintzis (2011) claimed that the ET was the main dewatering mechanism in the sludge treatment wetland, and the rate of such water loss showed a relation with the loading rate. However, the water recovery obtained from the proposed system treating septage was found to be relatively high, subsequently highlighting the dominant role of drainage.

ET is a slow dewatering process. Its efficiency is dependent on the weather and vegetation conditions, as well as the saturation level of the wetland bed. The high temperature and windy weather in Malaysia are favourable for this dewatering mechanism. However, the humid air potentially limits the efficiency. The common reeds used in the pilot system is one of the most common vegetation used for the CW system because of its remarkable transpiration ability, rapid growth rate, and impressive tolerance to the contaminants and ponding (Białowiec, Wojnowska-Baryła and Agopsowicz 2007). However, the coverage of common reeds was less dense in the pilot-scale VFCW. The initial density was nine clumps per bed and the new shoots were only observed around the original clump. Figure 6.35 displays the growth condition of the common reeds in the pilot system. The common reeds reached up to 1.50 m tall in the few original clumps, but the overall growth was less desirable due to the relatively short period of acclimatization. As the ET rate showed a dependency on the growth of vegetation (Białowiec, Wojnowska-Baryła and Agopsowicz 2007), the index used to represent the vegetation in the hydraulic simulation, which is the *LAI* in the Penman-Monteith equation, was necessary to be properly calibrated.

In this study, the average height of crops was assumed to be 1 m and the empirical factor for *LAI* was assumed to be 4. The PET rate was then estimated according to the weather data and parameters as listed in Table 6.7 and Table 6.8, respectively. The estimated values are presented in Table 6.15. The PET rate was between 0.55 and 1.00 cm d^{-1} and the average rate was 0.70 ± 0.17 cm d^{-1}. There was no specific study carried out to measure the ET rate in a wetland bed with common reeds in Malaysia.

Figure 6.35: The growth condition of common reeds during experiment

Table 6.15: Potential evapotranspiration rate (PET) in each case

Date	Julian Day (-)	Maximum Temperature (˚C)	Minimum Temperature (˚C)	Maximum Humidity (%)	Minimum Humidity (%)	Average wind velocity (m s^{-1})	Potential ET (cm d^{-1})
2015-11-18	322	29.00	24.00	100.00	71.00	2.22	0.56
2015-12-01	335	31.00	25.00	100.00	66.00	1.94	0.62
2015-12-12	346	31.00	25.00	100.00	70.00	1.67	0.58
2015-12-13	347	31.00	25.00	100.00	69.00	1.39	0.57
2015-12-16	350	28.00	24.00	100.00	69.00	1.39	0.55
2015-12-27	361	32.00	24.00	100.00	62.00	2.22	0.67
2016-01-21	21	30.00	25.00	100.00	70.00	1.39	0.58
2016-01-24	24	32.00	24.00	94.00	37.00	3.61	1.00
2016-01-28	28	31.00	24.00	100.00	66.00	1.67	0.57
2016-02-16	47	31.00	24.00	94.00	51.00	2.50	0.81
2016-02-21	52	31.00	25.00	89.00	55.00	4.17	0.93
2016-02-27	58	32.00	26.00	89.00	54.00	3.89	0.97
Maximum		32.00	26.00	100.00	71.00	4.17	1.00
Minimum		28.00	24.00	89.00	37.00	1.39	0.55
Mean		30.75	24.58	97.17	61.67	2.34	0.70
Standard Deviation		1.16	0.79	4.26	9.99	0.97	0.17

However, the estimated rate was comparable to a study of ET in a irrigated rice field in Malaysia (*Oryza sativa*) (Abdullahi et al. 2013), which obtained a maximum rate of 0.73 cm d^{-1}. Białowiec, Wojnowska-Baryła, and Agopsowicz (2007) found a maximum ET rate up to 0.49 cm d^{-1} in a CW vegetated with common reeds during summer. Stefanakis and Tsihrintzis (2011) measured a cumulative ET of 243.35 cm throughout a year (October 2008 to October 2009, daily average ET rate = 0.67 cm d^{-1}) in a sludge drying reed bed. Borin et al. (2011) and Milani and Toscano (2013) reviewed the available data of ET rate of common reeds in literature and indicated that the range was between 0.02 and 5.70 cm d^{-1}, and most cases showed a maximum rate below 1 cm d^{-1}. In addition, the same study revealed that the ET rate in a pilot-scale CW system can be up to 5.40 cm d^{-1} in Mediterranean region due to the massive growth of common reeds (plant coefficient can be up to 8.5). As a result, the measurement of ET rate in the literature reflected that the simulated results in this study were within a reasonable range and the plant coefficient of 1 was a reasonable assumption.

VF_Sep considered the influence of sludge accumulation by accounting the flow delay caused by the accumulation of sludge deposit during infiltration. The current approach simulated the sludge accumulation as a function of time and the resistance was estimated from the variation of thickness in the top spatial layer, while its hydraulic properties remained constant in the simulation. The accumulation rate of sludge deposit was estimated according to the concentration of total solids (TS) constituted in the raw septage and infiltration rate, which has been described in section 4.1.3. The simulated thickness of sludge accumulation ranged between 0.01 cm and 0.29 cm, however, such a thin layer was difficult to be physically measured and thus the verification of these results was excluded.

The effect of ET and sludge accumulation (SA) upon the hydraulic simulation were simultaneously evaluated by the comparison to the simulated result as displayed in Figure 6.36 - Figure 6.47. In most cases, the combined effect was negligible due to the low ET rate and thin sludge accumulation throughout the simulation. Cases 11A, 23B, and 24B showed a visible reduction in the effluent flux and cumulative effluent due to the relatively high ET rate and sludge accumulation, but the associated improvement of accuracy were still insignificant.

Table 6.16: Simulated sludge accumulation in each case

No. of test A = Wetland A B= Wetland B		HLR (l)	CR (-)	Sludge thickness (cm)	TS (g l^{-1})	SLR (g)	Sludge Accumulation (cm)
1A	18/11/2015	75	0.85	5	3.40	255.00	0.03
3A	01/12/2015	75	0.72	6	4.80	360.00	0.02
6A	12/12/2015	75	0.68	5	1.60	120.00	0.02
7B	13/12/2015	75	0.69	5	1.40	105.00	0.01
8A	16/12/2015	100	-	6	12.80	1280.00	0.16
11A	27/12/2015	100	-	8	12.60	1260.00	0.13
17B	21/01/2016	100	-	3	19.50	1950.00	0.14
19B	24/01/2016	125	0.89	4	2.70	337.50	0.02
20A	28/01/2016	150	0.81	3	3.20	480.00	0.05
23B	16/02/2016	50	0.67	4	8.90	445.00	0.04
24B	21/2/2016	125	-	5	18.60	2325.00	0.29
25B	27/2/2016	50	-	6	14.70	735.00	0.09
			Max.	8	19.5	2325.00	0.29
			Min.	3	1.40	105.00	0.01
			Mean	5	8.68	804.38	0.08
			Standard deviation	1.35	6.43	705.48	0.08

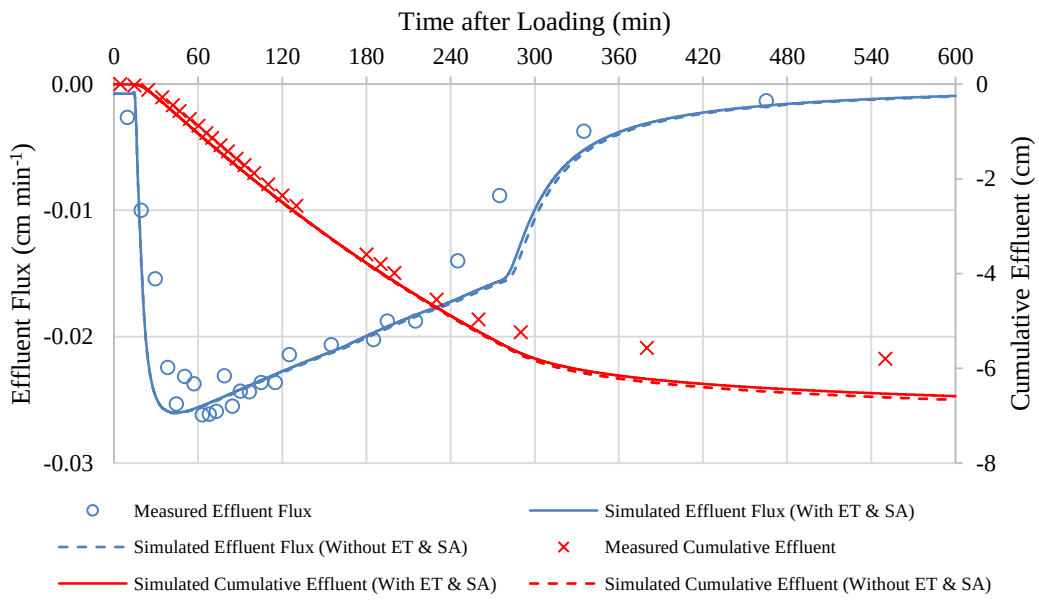

Figure 6.36: Comparison between simulation with- and without evapotranspiration and sludge accumulation for case 1A (18-11-2015: 75 L)

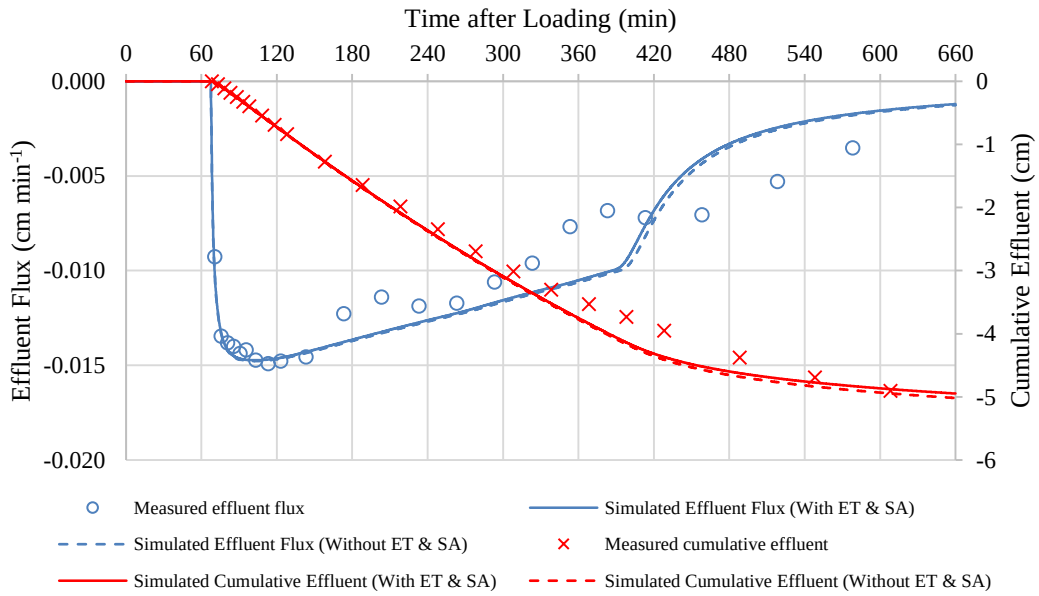

Figure 6.37: Comparison between simulation with- and without evapotranspiration and sludge accumulation for case 3A (1-12-2015: 75 L)

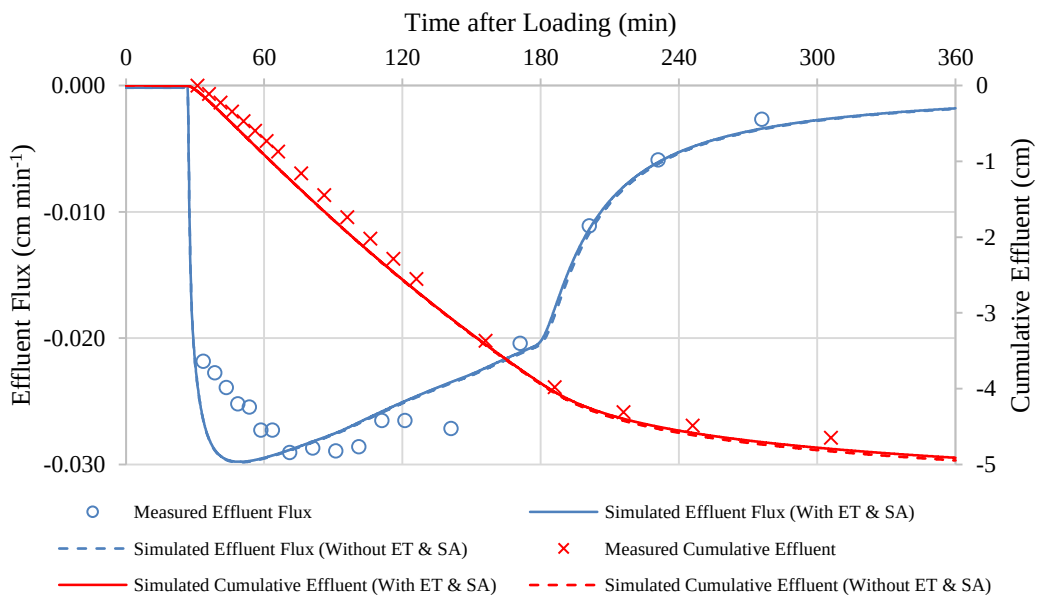

Figure 6.38: Comparison between simulation with- and without evapotranspiration and sludge accumulation for case 6A (12-12-2015: 75 L)

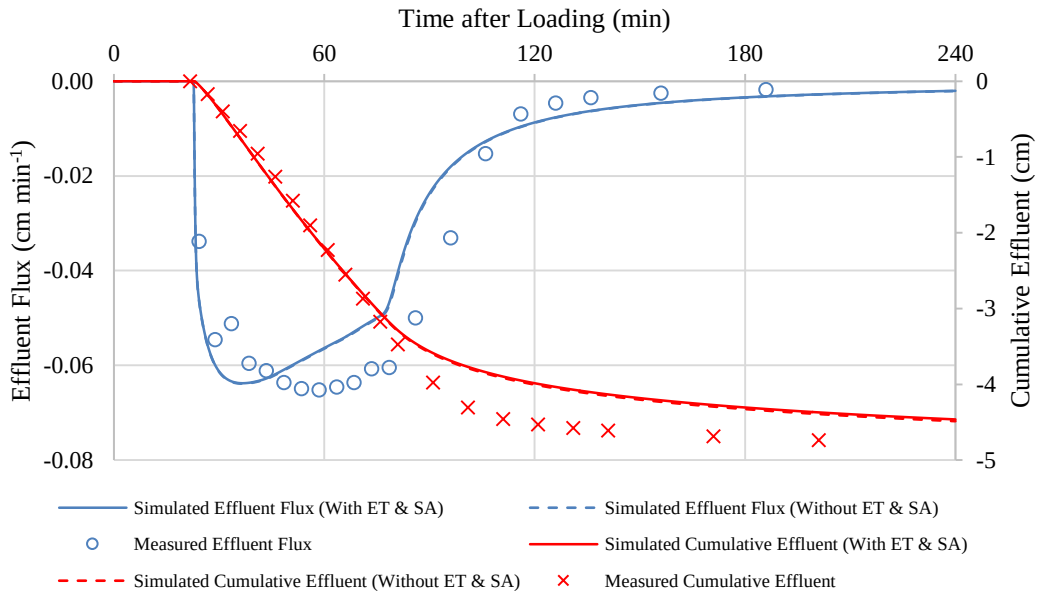

Figure 6.39: Comparison between simulation with- and without evapotranspiration and sludge accumulation for case 7B (13-12-2015: 75 L)

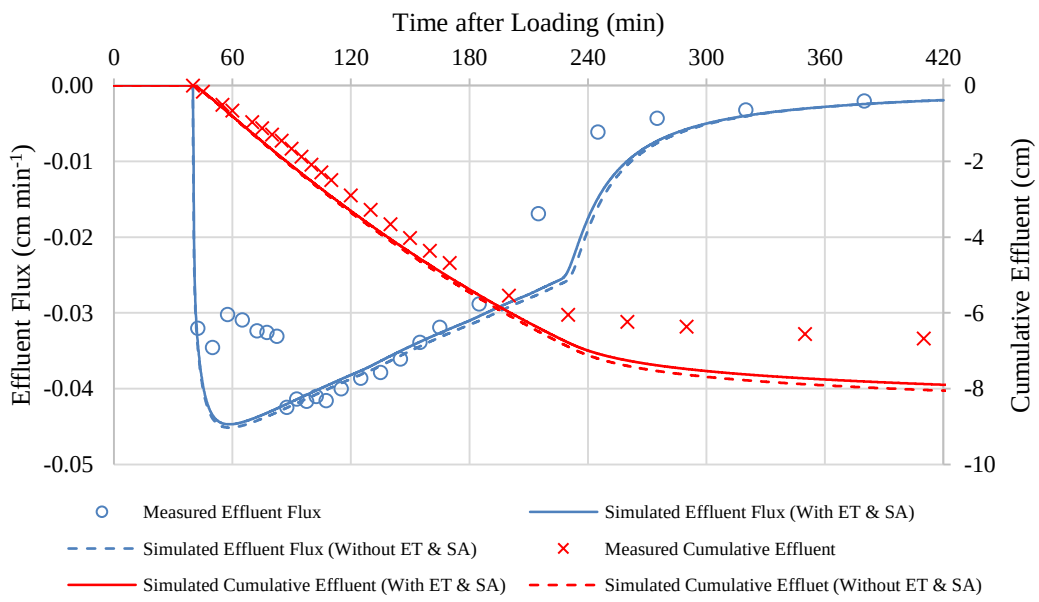

Figure 6.40: Comparison between simulation with- and without evapotranspiration and sludge accumulation for case 8A (16-12-2015: 100 L)

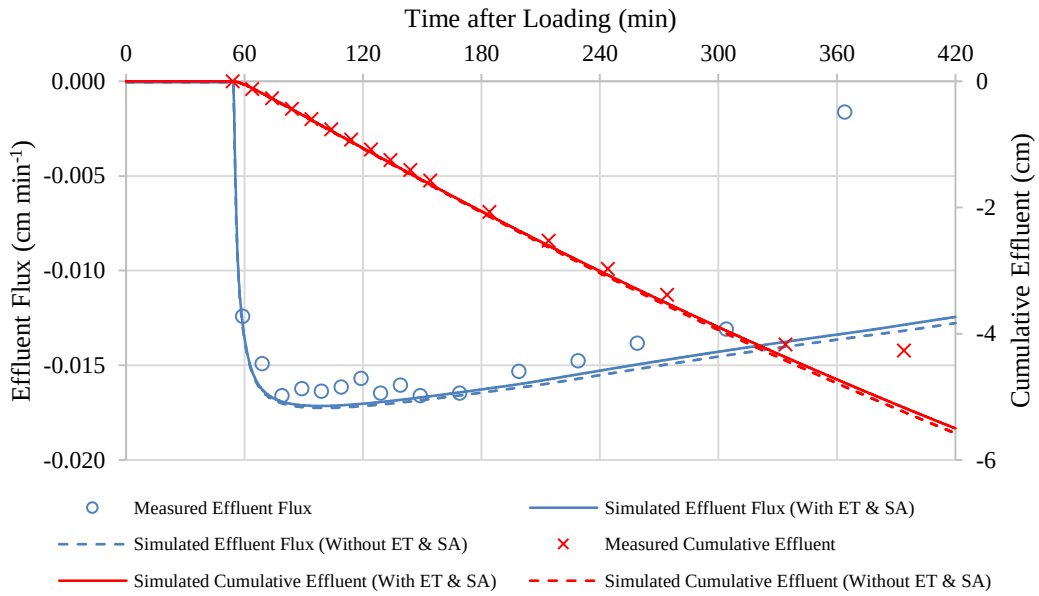

Figure 6.41: Comparison between simulation with- and without evapotranspiration and sludge accumulation for case 11A (27-12-2015: 100 L)

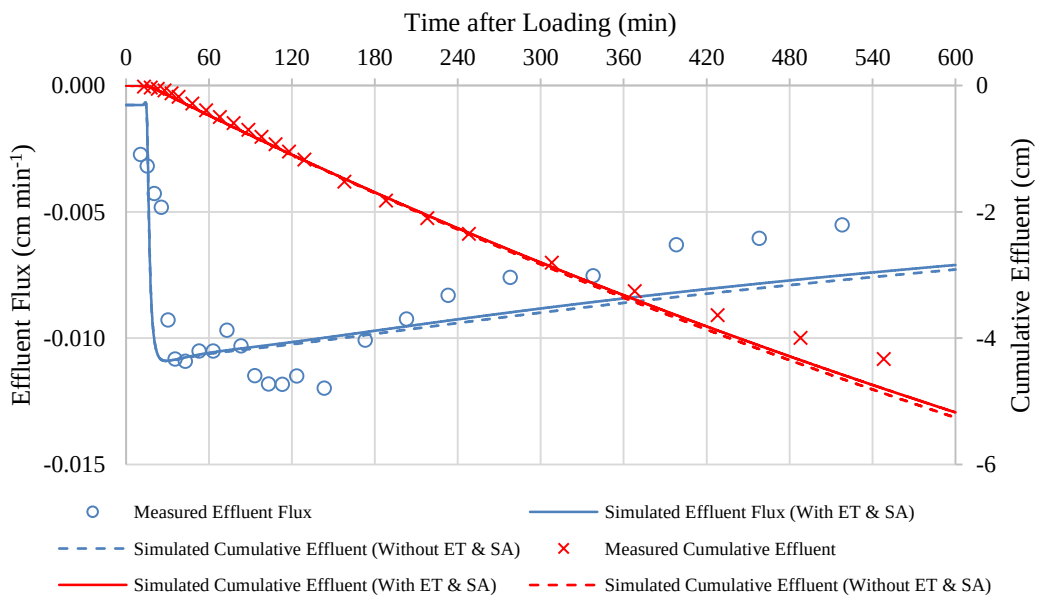

Figure 6.42: Comparison between simulation with- and without evapotranspiration and sludge accumulation for case 17B (21-1-2016: 100 L)

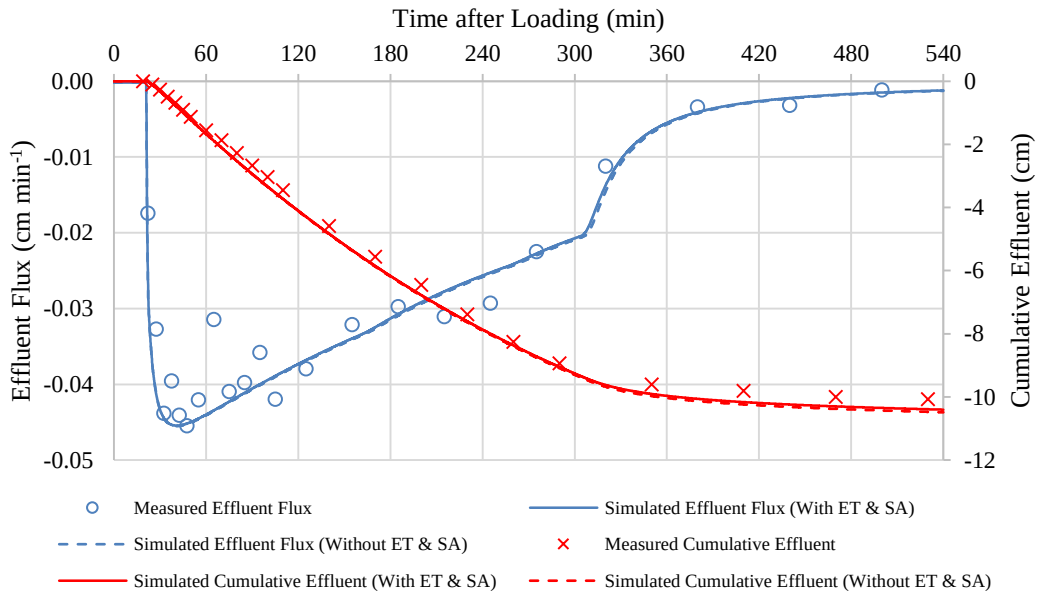

Figure 6.43: Comparison between simulation with- and without evapotranspiration and sludge accumulation for case 19B (24-1-2016: 125 L)

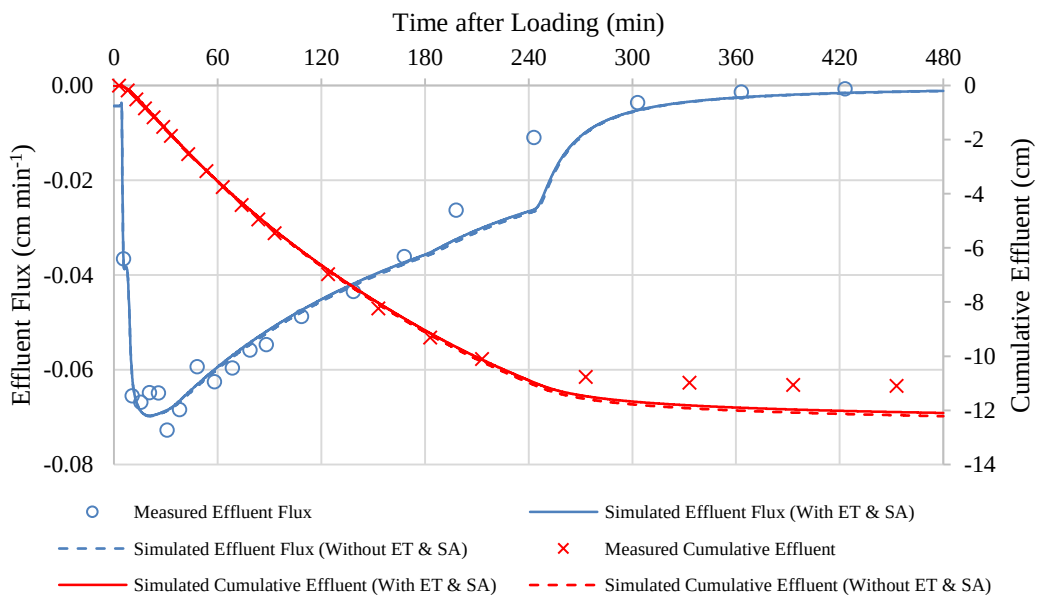

Figure 6.44: Comparison between simulation with- and without evapotranspiration and sludge accumulation for case 20A (28-1-2016: 150 L)

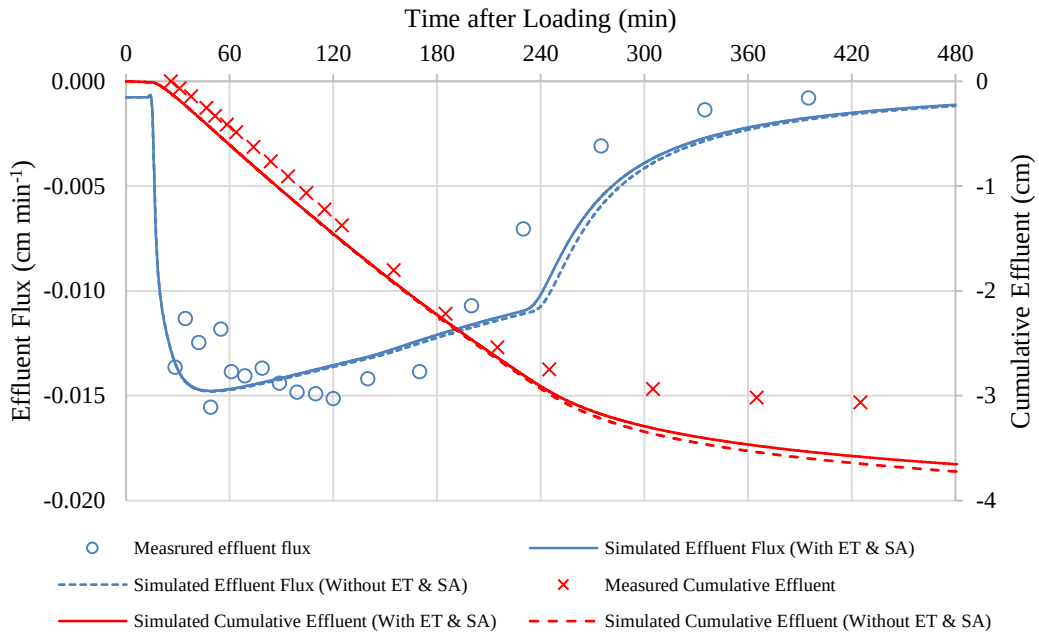

Figure 6.45: Comparison between simulation with- and without evapotranspiration and sludge accumulation for case 23B (16-2-2016: 50 L)

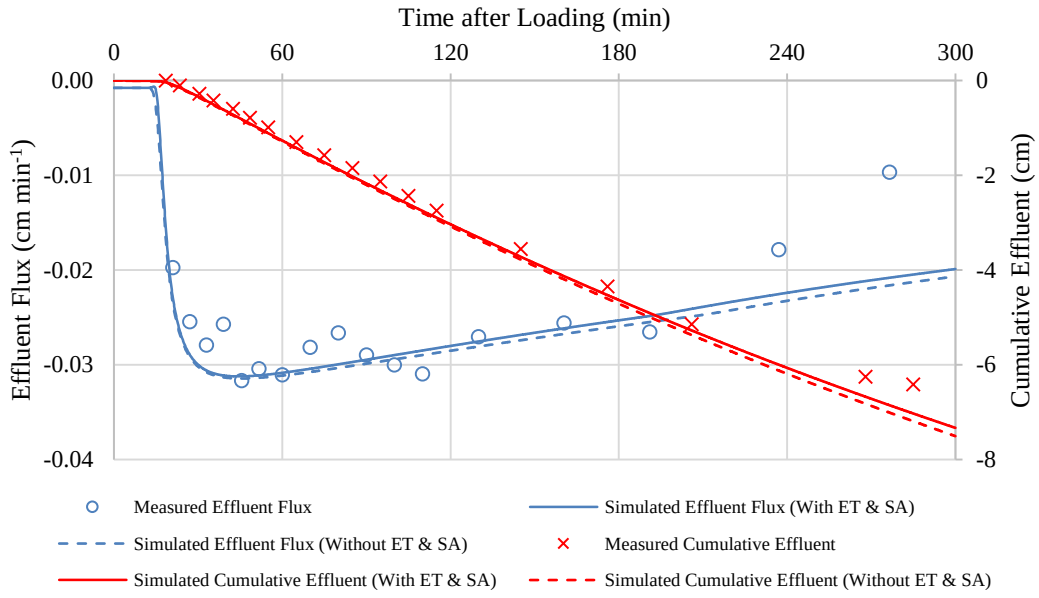

Figure 6.46: Comparison between simulation with- and without evapotranspiration and sludge accumulation for case 24B (21-2-2016: 125 L)

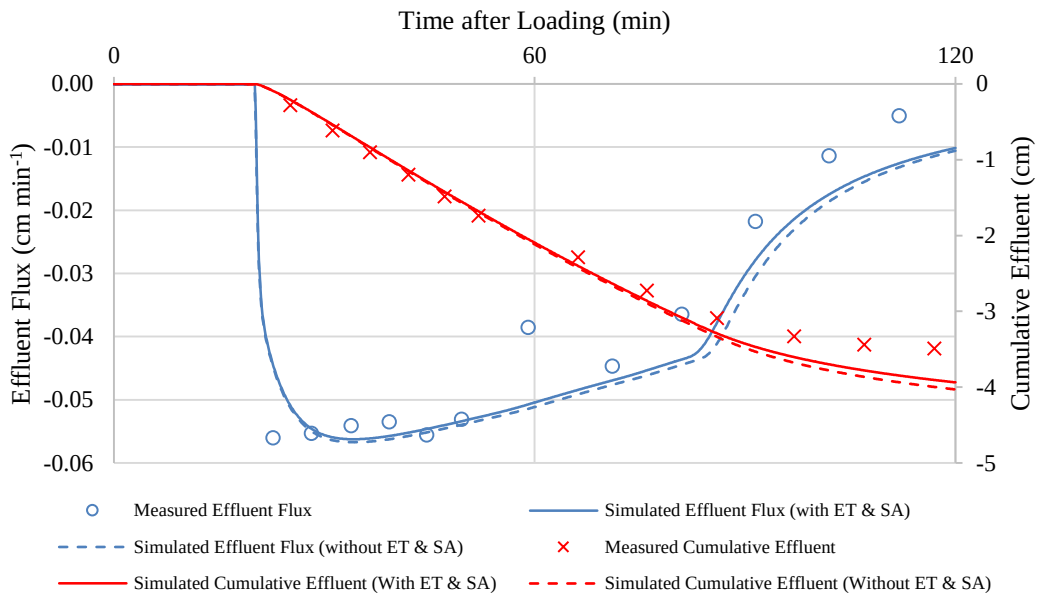

Figure 6.47: Comparison between simulation with- and without evapotranspiration and sludge accumulation for case 25B (21-2-2016: 50 l)

In general, the ET rate is extremely low compared to the rapid effluent flux in the pilot-scale VFCW. Since the evapotranspiration is a function of time, its role could be noteworthy when the simulation time is extended to a feeding-draining-feeding cycle (e.g. the resting period is included in the hydraulic simulation). This can be observed from the comparison between the simulated results of cumulative effluent, where the difference was more significant at the end of simulation time. Moreover, the ET becomes the dominant dewatering mechanism when the wetland bed is fully covered by well-grown common reeds, and thus it is an essential module in the simulation of VFCW. In future research, a laboratory quantification of ET should be carried out with the measurement of water content in the top layers to verify the values.

The modelling of flow delay due to the sludge accumulation was less affected by the simulation time because of its instantaneous formation. This could be observed in cases 24B and 25B, where the cumulative ET was only accounted for a relatively short simulation time, but the sludge accumulation imposed a visible reduction in the cumulative effluent. In general, TS concentration was low in influent, and thus the new-forming sludge layer was predicted to be thin. Consequently, the influence of sludge accumulation on the overall hydraulic simulation was insignificant. As the proposed module for the simulation of sludge accumulation was still at the

fundamental stage, it was only aimed to deliver a simultaneous sludge accumulation during the infiltration.

In fact, the hydraulic conductivity in sludge deposit layer was reduced due to the incoming solids that block the water flow path, and thus a stagnant water pond was always observed at the end of the experiment. Therefore, the estimation of pressure drop due to the gradual clogging using the Kozeny-Carmen equation (Giraldi, de Michieli Vitturi and Iannelli 2010) is suggested to be incorporated with the current module of sludge accumulation to improve the accuracy of the hydraulic simulation. Nevertheless, the current knowledge with regards to the swelling and shrinkage in the sludge deposit layer and the mechanism of sludge accumulation were lacking in the literature (Molle 2014). Accordingly, a further investigation towards the relation between the hydraulic properties of sludge deposit layer, the accumulation rate of the sludge thickness, and the physical and chemical characteristics of raw septage is required to empirically simulate the sludge accumulation during loading.

6.6.3. Validation with HYDRUS-1D

In order to validate the capability of VF_Sep, the simulation of the outflow dynamics was compared to a commercially available hydraulic simulator, HYDRUS-1D. The same hydraulic parameters and initial conditions were implemented in HYDRUS-1D, but the effect of ET and sludge accumulation were not available in the simulation. Figure 6.48 - Figure 6.51 present the selected cases for the comparison.

In general, the simulated outflow dynamics obtained from both models are comparable, especially the peak flux and deceleration. The main difference between the simulations was found to be the delay of the flow occurrence, where HYRDRUS-1D showed a more rapid flow compared to the VF_Sep. This deviation appeared to be dependent on the flux rate. A slower flux tended to result in a more significant difference as shown in Figure 6.49, while a rapid flux illustrated a minor deviation (Figure 6.48 and Figure 6.51). As indicated in section 6.6.2, the influence of ET and sludge accumulation was insignificant towards the outflow at the early stage, and thus the deviation was attributed to the different assumption and numerical method used to develop the model.

The results obtained from HYDRUS-1D displayed numerical dispersion in certain cases. Figure 6.50 showed that the performance of HYDRUS-1D was unstable when a relatively wet condition was implemented, where significant numerical dispersion

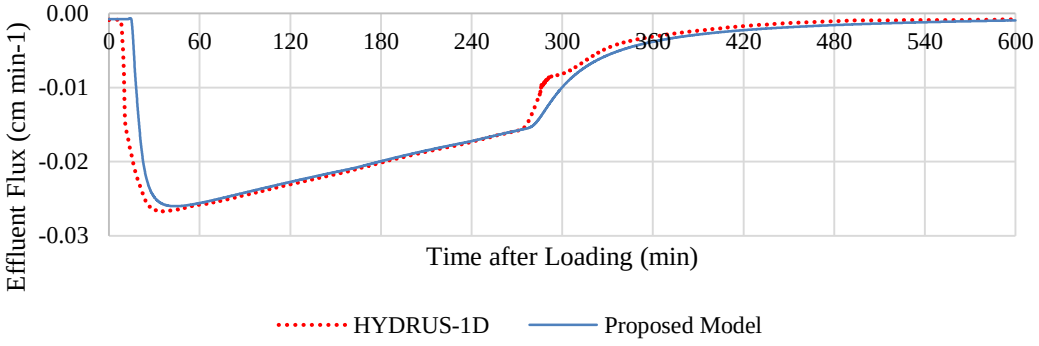

Figure 6.48: Comparison between HYDRUS-1D and VF_Sep for case 1A (18-11-2016: 75 L)

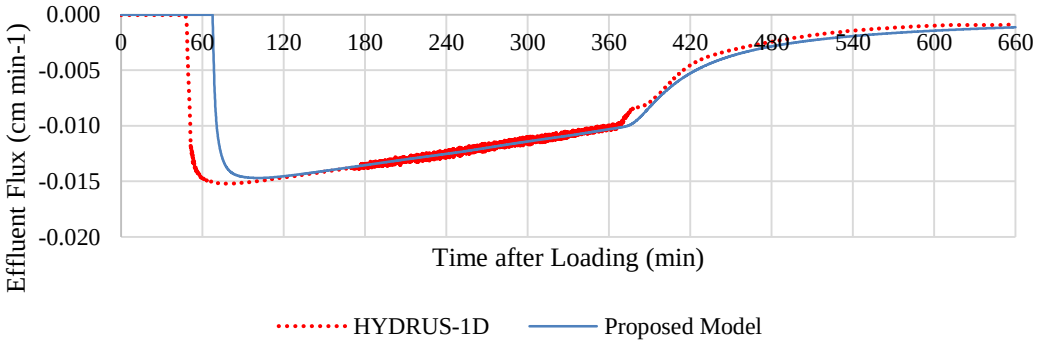

Figure 6.49: Comparison between HYDRUS-1D and VF_Sep for case 3A (1-12-2016: 75 L)

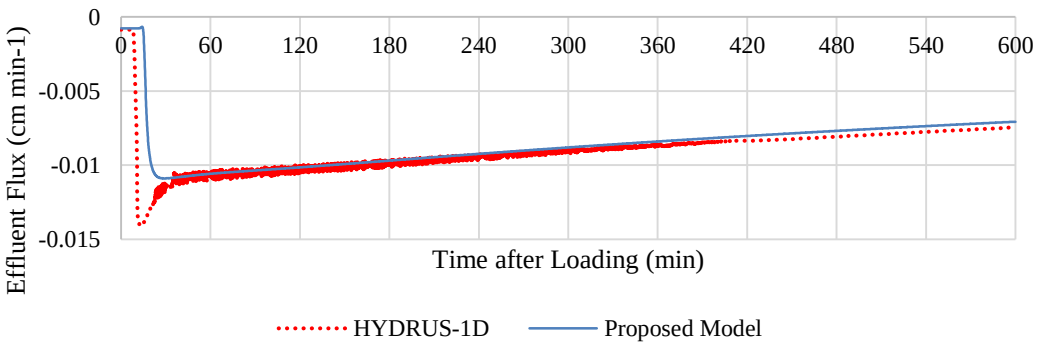

Figure 6.50: Comparison between HYDRUS-1D and VF_Sep for case 17B (21-1-2015: 100 L)

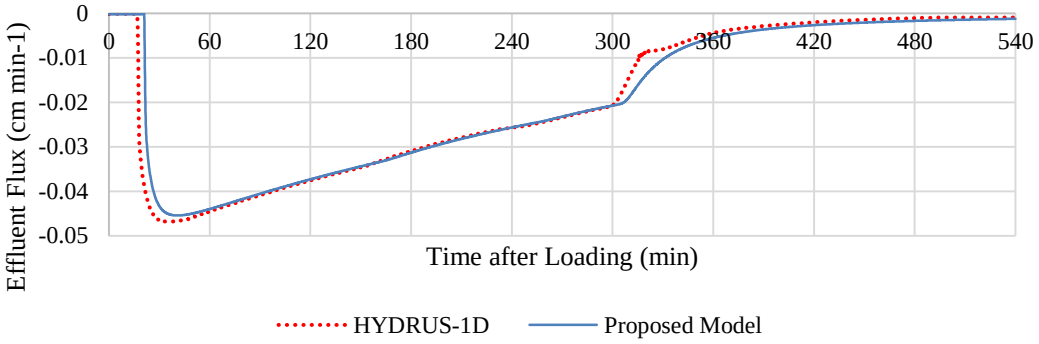

Figure 6.51: Comparison between HYDRUS-1D and VF_Sep for case 19B (24-1-2016: 125 L)

was observed throughout the simulation. Besides, the numerical dispersion was also observed in case 3A (Figure 6.49) at a certain period of simulation. Meanwhile, the VF_Sep performed steadily under varying conditions.

The good match between the VF_Sep and HYDRUS-1D indicated that the proposed model is a reliable and robust simulator, which is capable of handling various parameters and conditions. Case 3A showed that significant discrepancy was observed in the early stage of outflow. However, it was unable to justify which model provided a more accurate simulation at the current stage, where a comprehensive mathematical study was required to analyse their computational capacity. The overall performance of VF_Sep was considered to be satisfactory to describe the hydraulic behaviour in a VFCW.

6.7. Summary

In summary, the proposed hydraulic module in VF_Sep works well in reproducing the effluent flux in the pilot-scale VFCW. The substrate profile was subdivided into the top sludge deposit layer (thickness was obtained from physical measurement), intermediate layer (5 cm), small-sized gravel layer (22 cm) and medium-sized gravel layer (27 cm), and the drainage layer was excluded in the domain of simulation due to its short retention time. The upper boundary condition was set to be switchable between temporal flux-controlled and head-controlled to describe the loading and temporary ponding. The lower boundary condition was set to be free drainage.

The hydraulic parameters of the substrate material were calibrated to match the measured data of flow occurring delay and peak flux based on visual evaluation and

error analysis. To achieve this, a preliminary sensitivity analysis was carried out to evaluate the influence of hydraulic parameters in the simulation. It was found that the hydraulic conductivity of sludge deposit layer and the initial pressure distribution are the most significant parameters in calibrating the peak flux and flow occurring time, respectively. Other hydraulic parameters were postulated to be constant in all cases.

In general, VF_sep promisingly simulated the effluent flux in the pilot-scale VFCW with respect to the varying HLR and sludge thickness. In this study, the MAE (%) and regression analysis (R^2) were used to evaluate the accuracy of the simulated results. The proposed model was calibrated to fit fifteen cases with the "typical flow" pattern, but three cases showed MAE (%) exceeding 25 % and were considered as modelling failure. In the remaining cases, eight cases showed MAE (%) below 15 % and four cases showed MAE (%) between 15 % and 25 %. The average value of R^2 was above 0.75, indicating the good ability of hydraulic module in reproducing the trends of effluent flux in VFCW system.

The analysis of the simulated result showed that the majority of the error can be attributed to the low water recovery in the laboratory experiment. In fact, a stagnant water pond was always observed throughout the experiment, which implied that the wetland bed characterized a minimum depth of surface water to discharge the percolate. This phenomenon caused a significant level of discrepancies to the prescribed loading rate in the hydraulic simulation. Therefore, a correction factor (CR) was derived from the water recovery and was implemented in the upper boundary condition to optimize the hydraulic load. Accordingly, the simulated results showed a great improvement in MAE (%) and R^2, but this approach required further validation by investigating the mechanism causing the stagnant surface water in the pilot system.

The simulated result revealed that the effect of ET and sludge accumulation were relatively minor towards the hydraulic behaviour. In VF_Sep, the water loss via ET was estimated using the Penman-Monteith equation with the weather data and the rate was reasonable compared to the literature data. However, the estimated rate was generally much slower than the rapid effluent flux, and thus its influence was only significant when the simulation time was extended. As a fundamental study to account the sludge accumulation in the hydraulic simulation, the current approach only estimated the flow delay caused by the thickness of the sludge deposit during

infiltration. The variation of hydraulic properties in sludge deposit layer should be incorporated with the current approach by implementing a clean bed theory such as the Kozeny-Carman equation to describe the influence of instantaneous sludge accumulation. Overall, the good match between VF_Sep and HYDRUS-1D indicates that the proposed model is a reliable and robust simulator, and is capable of encountering various parameters and conditions in the VFCW.

Chapter 7 Simulation of Nitrogen Dynamics

According to the measured data, the first stage treatment of the pilot-scale, two-stage VFCW-based septage treatment system demonstrated an excellent aeration capacity and removed solids content and organic matter effectively. Nevertheless, the overall nitrogen removal was less effective, as excessive NH_4^+-N and NO_3^--N were always observed in the effluent. In addition, the fluctuating quality of effluent within a short-term, feeding-draining cycle highlighted the dynamic behaviour of treatment processes in the pilot-scale VFCW.

The VFCW can be regarded as a combination of physical filter and aerobic fixed biofilm reactor. Since the influent was not impounded in the wetland bed, the treatment of nitrogenous compounds occurred along the percolation pathway as a result of physical, biological and chemical processes. In the proposed model, the advection-dispersion equation (ADE) was used to numerically simulate the transport of contaminants throughout the wetland bed. Due to the variable saturation in the wetland bed, the degree of mixing of contaminants could be highly dynamic along the profile.

The particulate nitrogen only exists in Org-N form, and its removal is mainly attributed to the physical filtration of solids. On the other hand, the removal of dissolved nitrogen is by means of a number of biochemical mechanisms including ammonification, nitrification, and adsorption. The associated removal rate is highly dependent on the transport pattern and limiting factors such as the distribution of biofilm, oxygen content, alkalinity, and others. The complexity of the interaction between these factors is the main challenge to numerically reproduce the nitrogen dynamics in the VFCWs.

The batch loading of septage through the variably-saturated substrate is an extensive operating strategy aimed at stimulating the aerobic process. Nevertheless, such an irregular load pattern results in a random alteration of loading and resting phases. Since the percolate from the wetland bed is the major risk to the public, the simulation of the treatment processes was focused on the loading phase and the following resting period is excluded. The hydraulic simulation mentioned in Chapter 6 was used to reproduce the transport and fate of contaminants throughout the substrate by coupling with ADE and bio-kinetics sub-module. In this chapter, the dynamics of NH_4^+-N and NO_3^--N

were modelled by calibrating the relevant parameters and initial condition according to the data obtained from the laboratory experiments.

7.1. Simulation setup

7.1.1. Fundamental concepts

As the VF_Sep is a 1D reactive transport model, it describes the processes in the VFCW as a series of continuous stirred tank reactors (CSTRs). The wetland bed was discretized into multiple horizontally-homogenous layers, and each layer can be described as a CSTR. Eleven components were considered in the proposed model, including oxygen, alkalinity, organic matter, nitrogenous constituents, and active biomass. This study focused on the simulation of nitrogen dynamics, and thus the simulated results of the dynamics of ammonium (S_{NH}) and nitrate (S_{NO}) were expected to match with the data obtained from the pilot-scale VFCW.

The surface filtration, adsorption, vegetation uptake and biological processes are the mechanisms involved in the modelling of contaminant removals. The surface filtration describes the straining of particulate matter at the wetland surface, including the slowly biodegradable organic matter (X_S) and the particulate inert organic matter (X_I). The adsorption was only implemented in the transport of S_{NH}. In addition to this, both S_{NH} and S_{NO} are potentially extracted by the vegetation as the nutrient source. All of these removal mechanisms were simulated as sink terms in the transport module. However, their contributions are limited to the nitrogen removal, where the biological process is still the dominant mechanism in removing nitrogenous constituents.

The basic concept of the biological process is to quantitatively express the substrate consumption by the biomass growth (Grady Jr et al. 2011). According to the measured data, the ammonification of Org-N and nitrification of NH_4^+-N were the major process in the pilot-scale VFCW-based septage treatment system. Denitrification was not observed throughout the experiment due to the aerated wetland bed. Therefore, the autotrophic biomass (X_A), which is the essential bacteria in the decomposition of S_{NH}, plays a major role compared to the heterotrophic biomass (X_H) in the calibration of the proposed model.

The ammonification process was included in the hydrolysis of slowly biodegradable organic matter (X_S). Although this process is independent from oxygen content, it is

constrained by the population of X_H. Nitrification was simulated as a one-step process in the bio-kinetics module. Although the dynamics of S_S was not the main concern in this study, the competition between aerobic degradation process and nitrification for DO potentially influences the nitrogen dynamics. Nevertheless, the high DO concentration in the effluent revealed that this component was not limited throughout the treatment, and thus this effect was assumed to be negligible. Additionally, the S_{NH} and S_{NO} was set to be extracted along with the water uptake by the vegetation. The active uptake of nutrient was excluded in VF_Sep.

The roles of X_S in the nitrogen dynamics is only the release of S_{NH} in the process of hydrolysis. Therefore, the trapped X_S at the top layer theoretically increases the concentration of S_{NH}. S_{NH} is consumed as a nutrient in the development of X_H. Due to the high organic load in the septage treatment, this effect could be significant towards the nitrogen balance in the wetland bed. VF_Sep simplified the decay of biomass as a lysis process, which is a first-order reaction and is free from the limiting reagent in the system. The lysis of biomass generates inert organic matter (S_I and X_I) in the treatment unit, which has no effect on the stoichiometric coefficient of other components. The dinitrogen (S_{N2}) is the final product of denitrification, and thus its concentration is independent from the stoichiometric coefficient and Monod kinetics of other components.

In addition to S_O, the alkalinity (S_{HCO}) is a limiting factor in the biological treatment process. In the experiments, pH remained at a favourable range for biochemical process, where Grady Jr et al. (2011) highlighted that a pH below 6.6 might inhibit the efficiency of nitrification. There was no remarkable pH drop observed in the effluent, which implies that the demand of alkalinity is sufficient throughout the treatment. Accordingly, it was assumed that the alkalinity is not limited in the system, and thus its term in the reactions was set to be 1 to simplify the calibration.

Accordingly, the presence of active biomass is essential to stimulate the biological process. In the VFCW, the active biomass was simulated as biofilms that attached on the surface of porous medium, which is stationary in the wetland bed. Therefore, the contaminants are treated when contacting with the attached-growth biofilm during percolation. Consequently, the transport of contaminants eventually governs the residence time in the treatment unit to stimulate the biofilm-mediated processes.

The proposed model investigates the biodegradation at a macroscopic level. The biofilm-mediated processes were assumed to occur under a full contact condition, where the concentration of active biomass is the key in the simulation. The variation of biofilm thickness, diffusion efficiency between the liquid-biofilm interface and other microscopic parameters were excluded from the scope of study.

Another important criteria in the biological treatment is the saturation level in the wetland bed. It should be noted that the occurrence of biological processes was assumed to be in the liquid phase. Therefore, the kinetics rates of biological processes were implemented as functions of water content. As the batch loading creates an unsaturated condition, the variability of water content along the depth of wetland bed greatly affects the efficiency of treatment. The precision of the simulation of hydraulic behaviour and transport of contaminants is vital to accurately predict the nitrogen dynamics in the pilot-scale VFCW.

7.1.2. Transport parameters

The transport of contaminants was modelled using the ADE approach. In the proposed model, the ADE was coupled with the volumetric water content to describe the degree of mixing of particular contaminants under a variably-saturated condition. The advection term is derived based on the nodal flux simulated in the hydraulic module and no external parameter is required. Besides, the hydraulic dispersion is a combined effect of mechanical dispersion and molecular diffusion. Giraldi, de Michieli Vitturi, and Iannelli (2010) indicated that the effect of molecular diffusion can be negligible in the liquid phase, and thus it is excluded to simplify the simulation.

Mechanical dispersion refers to the acceleration or deceleration of contaminant transport from the average flux rate. It is mainly caused by the mixing along the non-uniform water flow paths in a homogenous porous medium. In the proposed one-dimensional model, this effect was described as a product of average flux rate and longitudinal dispersity (D_L). The D_L was assumed as a constant in a homogenous porous medium. Nevertheless, there is limited information about the dispersivity of the coarse porous medium, especially for gravel bed.

The typical values of D_L used in Langergraber and Šimůnek (2006) were low, ranging from 1.25 cm to 3.00 cm for the sand bed. On the other hand, Toscano et al. (2009) employed a D_L of 15 cm in modelling a pilot-scale VFCW constructed by fine gravel

(0.06 – 4.00 mm). Fuchs (2009) used a D_L of 3 cm for a sand bed. Giraldi et al. (2009) highlighted the close correlation between the D_L and saturation degree in a gravel-based VFCW, and a set of tracer experiment was carried out to calibrate the D_L. The authors concluded that the D_L for the completely saturated, partially saturated, and draining condition were 4.50 cm, 10 cm, and 14 cm, respectively. As the proposed model has described the flux as a function of water content, the variation of D_L with regards to the saturation degree was assumed to be negligible.

Similar to the hydraulic parameters, the literature data showed that the D_L of wetland bed is variable from case to case. In fact, Delgado (2007) highlighted that it was "basically impossible" to determine its exact characteristic of transport mechanism due to the highly irregular structure of a porous medium. Therefore, the current transport equation is developed based on the method of spatial averaging to obtain the average concentration in the porous medium. From the aspect of porous medium, the D_L is dependent on the distance travelled, flux rate, particle diameter, distribution of particle size, and particle shape (Delgado 2006). The influence of the viscosity, density and temperature on D_L was neglected in this study. This study assumed that the irregularity in the porous medium with coarser grain size is higher, which results in a more significant dispersion. In general, the D_L is calibrated according to the non-reactive tracer experiment. However, the tracer experiment carried out in this study demonstrated a poor mass recovery, and thus it was not suitable to be referred to calibrate the parameters. As a result, the D_L of the wetland beds (sludge deposit layer, intermediate layer, small size gravel layer, and medium size gravel layer) was directly calibrated to fit the concentration of NH_4^+-N in the effluent.

The contaminants such as organic carbon and NH_4^+-N are potentially adsorbed onto the surface of the porous medium. As the concept of dual-porosity was adopted in this study, the adsorption capacity was dependent on the water content in the mobile and immobile region. In this study, the adsorption was considered as a kinetic process in the transport of NH_4^+-N only, which is similar to CW2D (Langergraber and Šimůnek 2006). Therefore, the fraction of mobile site (f_{mo}) was set to be 1 and the fraction of equilibrium site (f_E) was set to be 0.

The biological process in the VFCW is generally described as an attached-growth wastewater treatment. Thus, the active biofilm was only defined in the solid phase.

There is no mass transport term included in its dynamics and the growth is only affected by the bio-kinetics. As the detachment of attached biofilm was excluded in the proposed model, the washout of active biomass was described based on the lysis process. The degradation of biomass releases X_I, S_I and a certain amount of S_{NH} back to the percolate and is eventually drained from the system. The physical filtration was implemented to describe the transport of particulate organic matter. This mechanism was simulated as a function of the solids retention coefficient, and the deep bed filtration was not considered in the proposed model. The value of coefficient was estimated from the average removal rate of total solids throughout the experiment, where 0.80 was employed in all simulation.

7.1.3. Bio-kinetics parameters

The level of parameterization is an important measurement for the applicability of the mechanistic model. Although the increment of the model complexity results in a better simulation of the reality, Meyer et al. (2015) highlighted that it is required to be weighted for its practicability in handling. As the proposed model generally consists of the bio-kinetics module inspired by the ASM (Henze et al. 1999), a number of parameters were involved as the inputs to perform the simulation. The simplification of the bio-kinetics module requires fifteen parameters, which consist of two parameters for hydrolysis, eight parameters for the decomposition of organic matter (aerobic decomposition and denitrification) and five parameters for nitrification.

Due to the concern of model complexity, it is impractical to experimentally identify or calibrate every parameter in the bio-kinetics module to match the data from an experiment or full-scale system. Therefore, this study aims to employ a set of reference parameters to simulate the nitrogen dynamics of all experiments. The measurement of the bio-kinetics parameters was not included in the scope of the study, and thus the values were obtained from the literature.

There was limited information with regards to the kinetics and stoichiometric parameters in reproducing the biochemical processes in the VFCW. Five set of kinetics parameters, including McBride and Tanner (1999), Langergraber and Šimůnek (2005), Fuchs (2009), Petitjean et al. (2012) and Pálfy et al. (2016), were reviewed and compared to the typical values used in the ASM2D (Henze et al. 1999).

McBride and Tanner (1999) proposed a model to predict the development of biofilm in a subsurface CW, which is regarded as the fundamental study to describe the biochemical processes in the CW-based wastewater treatment system. CW2D (Langergraber and Šimůnek 2005) is one of the most comprehensively established model for VFCWs, which has been successfully applied to the treatment of sewage (Langergraber and Šimůnek 2005; Toscano et al. 2009; Fuchs 2009; Morvannou et al. 2014) and combined sewer overflow (CSO) (Dittmer, Meyer and Langergraber 2005; Henrichs, Welker and Uhl 2009; Pálfy et al. 2016). These studies proposed different approaches to calibrate the model, however, most of the parameters were directly referred to the standard values proposed in Langergraber and Šimůnek (2005) excepted for Fuchs (2009) and Pálfy et al. (2016). Petitjean et al. (2012) proposed a simplified module of CW1M (Langergraber, Rousseau, et al. 2009a), which excluded the anoxic denitrification in the bio-kinetics.

Table 7.1 summarizes the kinetics parameters used in these studies (at 20˚C). These parameters consist of process rate constants and saturation coefficients of limiting substrates. As the alkalinity term in the Monod-type rate expression was assumed to be unlimited in this study, its relevant parameter was not included in this review. In brief, the process rates varied among the studies, but the typical values of saturation coefficient are similar.

Due to the favourable aerobic condition in the VFCW treating septage, the most important process in the nitrogen removal is nitrification. In this study, the nitrification was simulated as a single-step process and the limiting components include oxygen and NH_4^+-N. In CW2D, nitrification was a two-step process. The autotrophic biomass was subdivided into two groups, where *Nitrosomonas* oxidizes NH_4^+-N to NO_2^-- N, and then it is further oxidized by *Nitrobacter* to NO_3^-- N. Therefore, there were two sets of rate constants and saturation coefficients to describe the complete nitrification in the VFCW.

In general, the rate of maximum growth and lysis of the X_A were low compared to the X_H. In ASM2D, the maximum growth rate of autotrophic biomass (μ_A) was 1 d^{-1}. The same value was used in Petitjean et al. (2012), while the values used in McBride and Tanner (1999) was only 0.50 d^{-1}. The μ_A of *Nitrosomonas* and *Nitrobacter* in Langergraber and Šimůnek (2005) were 0.90 d^{-1} and 1.00 d^{-1}, respectively.

Table 7.1: Review on kinetics parameters used in previous studies (20˚C)

Parameter	Unit	ASM2D (Henze et al. 1999)	McBride and Tanner (1999)	CW2D (Langergraber and Šimůnek 2006)	CW2D (Fuchs 2009)	Petitjean et al. (2012)	CW2D (Pálfy et al. 2016)
				Hydrolysis			
k_H	d^{-1}	3.00	5.00	3.00	0.05	3.00	0.20
K_X	$mg_{SS}\ mg_{XS}^{-1}$	0.10	0.20*	0.10	0.10	0.10	-
				Heterotrophic Biomass			
μ_H	d^{-1}	6.00	5.00	6.00	0.70	6.00	0.04
b_H	d^{-1}	0.40	0.02	0.40	0.10	0.09	-
η_H	-	0.80	0.80	0.80	0.00	-	-
$K_{H,O}$	$mg_{SO}\ l^{-1}$	0.20	0.20	0.20	0.20	0.20	-
$K_{H,S}$	$mg_{SS}\ l^{-1}$	2.00	4.00*	2.00	2.00	2.00	-
$K_{H,NO}$	$mg_{NO}\ l^{-1}$	0.50	0.50	0.50**	0.50**	-	-
$K_{H,NH}$	$mg_{NH}\ l^{-1}$	0.01	0.05	0.05	0.05	0.05	-
				Autotrophic Biomass			
μ_A	d^{-1}	1.00	0.50	0.90^{NH4} / 1.00^{NO}**	0.40**	1.00	0.03^{NH4}/ 0.04^{NO}**
b_A	d^{-1}	0.15	0.02	0.15**	0.28^{NH}/ 0.30^{NO}**	0.15	-
$K_{A,O}$	$mg_{SO}\ l^{-1}$	0.50	0.50	0.10^{NH}/ 1.00^{NO}**	0.10^{NH}/ 1.00^{NO}**	0.50	0.07**
$K_{A,NH}$	$mg_{NH}\ l^{-1}$	1.00	1.00	0.50**	0.50**	0.50	-

**on fermentable substrate*

***CW2D described the nitrification and denitrification as a two-step process. The saturation constants for reduction of NO_2^-- N and NO_3^- -N were same in the model. The maximum growth rate and saturation constants for oxidation of NH_4^+-N and NO_2^-- N were varying in the model. The superscript NH indicates the values used for first step nitrification, and the superscript NO indicates the values for second step nitrification.*

Fuchs (2009) estimated a μ_A of 0.40 d^{-1} for both nitrifying bacteria, where the author indicated that the rate constants used in the long-term simulation (30-day) could be significantly different from the simulation of a single hydraulic load. The μ_A employed in Pálfy et al. (2016) were extremely low compared to other studies, which were 0.03 d^{-1} and 0.04 d^{-1} for *Nitrosomonas* and *Nitrobacter*, respectively.

The decay rate of autotrophic biomass (b_A) used in the ASM2D, Langergraber and Šimůnek (2005) and Petitjean et al. (2012) were 0.15 d^{-1}, while McBride and Tanner (1999) implemented a low b_A of 0.02 d^{-1}. On the other hand, the value of b_A used in Fuchs (2009) for *Nitrosomonas* and *Nitrobacter* were 0.28 d^{-1} and 0.30 d^{-1}, respectively. Accordingly, the net growth rate of *Nitrosomonas* and *Nitrobacter* were 0.12 d^{-1} and 0.10 d^{-1}, respectively, which were much lower than other typical values.

In the Monod-kinetics expression, the saturation coefficient, which is also known as the half-velocity constant, denotes "the substrate concentration at one-half the maximum specific substrate utilization rate" (Tchobanoglous et al. 2003). In general, this parameter describes the degree of influence for limiting substrate in the biological process. In the proposed model, the nitrification is limited by the concentrations of S_O and S_{NH}.

The value of saturation coefficient of S_O ($K_{A,O}$) was same in ASM2D, McBride and Tanner (1999) and Petitjean et al. (2012), where a typical value of 0.50 mg l^{-1} was employed. However, the $K_{A,O}$ implemented in the Langergraber and Šimůnek (2005) and Fuchs (2009) was 0.10 mg l^{-1} and 1.00 mg l^{-1} for first step and second step nitrification respectively. The higher value highlighted that the oxygen demand in the second step nitrification was higher. Pálfy et al. (2016) proposed a low $K_{A,O}$, which was only 0.07 mg l^{-1}. The saturation coefficient of S_{NH} ($K_{A,NH}$) was 1 mg l^{-1} in ASM2D and McBride and Tanner (1999), while its value was 0.50 mg l^{-1} in Langergraber and Šimůnek (2005), Fuchs (2009) and Petitjean et al. (2012).

The hydrolysis rate constant (k_H) ranged from 3 to 5 d^{-1}. However, Fuchs (2009) and Pálfy et al. (2016) proposed a low hydrolysis rate constant, which were 0.05 d^{-1} and 0.20 d^{-1}. The typical value of the saturation coefficient of slowly degradable organic matter (K_X) was 0.10 mg_{SS} mg_{XS}^{-1}.

As for the growth of X_H, the typical maximum growth rate (μ_H) ranged from 5 d^{-1} to 6 d^{-1}. However, the values proposed by Fuchs (2009) and Pálfy et al. (2016) were only 0.70 d^{-1} and 0.04 d^{-1}, respectively. The decay rate (b_H) was highly fluctuating, where the ASM2D and Langergraber and Šimůnek (2005) employed a value of 0.40 d^{-1}, while other studies used a value below 0.10 d^{-1}. The typical anoxic coefficient (η_H) and saturation coefficient ($K_{H,O}$, $K_{H,S}$, $K_{H,NH}$, $K_{H,NO}$) for heterotrophic growth were similar in the literature.

Table 7.2 summarizes the stoichiometric parameters used in the literature. In general, the fraction of S_I produced in the hydrolysis of X_S (f_{SI}) was assumed to be 0 mg_{SI} mg_{XS}^{-1}. The production of X_I in the biomass lysis (f_{XI}) was 0.1 mg_{XI} mg_{BM}^{-1} in ASM2D and McBride and Tanner (1999), and 0.15 was used in Langergraber and Šimůnek (2005) and Fuchs (2009). Due to the lack of information with regards to the dynamics of active biomass during loading and inter-event, Pálfy et al. (2016) assumed that the biomass lysis produces nearly 100% of X_I to individually observe the influence of parameters.

The yield coefficient of heterotrophic biomass under aerobic and anoxic condition ($Y_{H,O}$ and $Y_{H,NO}$, respectively) was 0.63 mg_{XH} mg_{SS}^{-1} in most of the simulations. On the other hand, the typical value of yield coefficient of autotrophic biomass (Y_A) in the literature was 0.24 mg_{XA} mg_{NH}^{-1}. Pálfy et al. (2016) proposed relatively low $Y_{H,NO}$ and Y_A, which were 0.07 mg_{XH} $mg_{SS}^{-1}$and 0.06 mg_{XA} mg_{NH}^{-1} respectively.

Table 7.3 summarizes the composition parameters in the literature. In the proposed model, the nitrogen content in five categories of organics matter was considered. The value of nitrogen in S_S (i_{NSS}), S_I (i_{NSI}), X_S (i_{NXS}), and biomass (i_{NBM}) were the same in the existing modelling, which were 0.03 mg_N mg_{SS}^{-1}, 0.01 mg_N mg_{SI}^{-1}, 0.04 mg_N $mg_{XS}^{-1}$and 0.07 mg_N mg_{BM}^{-1}, respectively. The composition parameter of X_I was only included in ASM2D and McBride and Tanner (1999), which ranged from 0.02 to 0.03 mg_N mg_{XI}^{-1}.

Table 7.2: Review of stoichiometric parameters used in previous studies (20˚C)

Parameter	Unit	ASM2D (Henze et al. 1999)	McBride and Tanner (1999)	CW2D (Langergraber and Šimůnek 2006)	Fuchs (2009)	Petitjean et al. (2012)	Pálfy et al. (2016)
f_{SI}	mg_{SI} mg_{XS}^{-1}	0	0	0	0	0	-
f_{XI}	mg_{XI} mg_{BM}^{-1}	0.1	0.1	0.1	0.1	-	0.999
$Y_{H,O}$	mg_{XH} mg_{SS}^{-1}	0.63	0.63	0.63	0.63	0.63	0.065
$Y_{H,NO}$	mg_{XH} mg_{SS}^{-1}	0.63	0.63	0.63	0.63	-	0.065
Y_A	mg_{XA} mg_{NH}^{-1}	0.24	0.24	0.24*	0.24*	0.24*	0.06*

**Considered as two-step nitrification. The yield coefficients used in both processes are the same.*

Table 7.3: Review of composition parameters used in previous studies (20˚C)

Parameter	Unit	ASM2D (Henze et al. 1999)	McBride and Tanner (1999)	CW2D (Langergraber and Šimůnek 2006)	Fuchs (2009)
i_{NSS}	$mg_N\ mg_{SS}^{-1}$	0.03	0.03	0.03	0.03
i_{NSI}	$mg_N\ mg_{SI}^{-1}$	0.01	0.01	0.01	0.01
i_{NXS}	$mg_N\ mg_{XS}^{-1}$	0.04	0.04	0.04*	0.04*
i_{NXI}	$mg_N\ mg_{XI}^{-1}$	0.02	0.03	-	-
i_{NBM}	$mg_N\ mg_{BM}^{-1}$	0.07	0.07	0.07	0.07

**The value is referred to the nitrogen content in slowly degradable organic matter.*

According to the literature review, the range of the kinetics parameters in the VFCW has been briefly identified. In summary, the saturation coefficient, stoichiometric and composite parameters were consistent in the literature and can be directly applied to the proposed model. On the other hand, the reaction rate constant calibrated in Fuchs (2009) and Pálfy et al. (2016) were much lower compared to the typical values proposed in ASM2D and Langergraber and Šimůnek (2005). However, these parameters are only valid to the specific configuration and operating condition. Therefore, the values of the rate constants in the proposed bio-kinetics module were obtained from Langergraber and Šimůnek (2005) and Petitjean et al. (2012). The values of all parameters employed in the proposed model are listed in Table 7.4.

The effect of temperature is remarkable to the biological process. The low temperature leads to an ineffective treatment, which eventually leads to effluent with poor quality. Grady Jr et al. (2011) highlighted that it is particularly important to the nitrification as the μ_A is extremely sensitive to the temperature. Therefore, it is commonly accepted that the efficiency of the biological process is better in the tropical region. As most of the kinetic and stoichiometry parameters in the literature were only valid at the specific reference temperature, the adjustment of kinetics and stoichiometry parameters with regards to the temperature is implemented in the bio-kinetics module as follow (Grady Jr et al. 2011):

$$k_T = k_{20} \cdot \theta_T{}^{(T-20)} \tag{7.1}$$

where k_{20} is the value of the parameter at the reference temperature (20˚C), θ_T is the temperature coefficient, and T is the temperature.

Table 7.4: Proposed values for the parameters in bio-kinetics module

Parameter	Unit	Values
k_H	d^{-1}	3.00
K_X	$mg_{SS}\ mg_{XS}^{-1}$	0.10
μ_H	d^{-1}	6.00
b_H	d^{-1}	0.40
η_H	-	0.80
$K_{H,O}$	$mg_{SO}\ l^{-1}$	0.20
$K_{H,S}$	$mg_{SS}\ l^{-1}$	2.00
$K_{H,NO}$	$mg_{NO}\ l^{-1}$	0.50
$K_{H,NH}$	$mg_{NH}\ l^{-1}$	0.05
μ_A	d^{-1}	1.00
b_A	d^{-1}	0.15
$K_{A,O}$	$mg_{SO}\ l^{-1}$	0.50
$K_{A,NH}$	$mg_{NH}\ l^{-1}$	0.50
f_{SI}	$mg_{SI}\ mg_{XS}^{-1}$	0.00
f_{XI}	$mg_{XI}\ mg_{BM}^{-1}$	0.10
$Y_{H,O2}$	$mg_{XH}\ mg_{SS}^{-1}$	0.63
$Y_{H,NO}$	$mg_{XH}\ mg_{SS}^{-1}$	0.63
Y_A	$mg_{XA}\ mg_{NH}^{-1}$	0.24
i_{NSS}	$mg_N\ mg_{SS}^{-1}$	0.03
i_{NSI}	$mg_N\ mg_{SI}^{-1}$	0.01
i_{NXS}	$mg_N\ mg_{XS}^{-1}$	0.04
i_{NXI}	$mg_N\ mg_{XI}^{-1}$	0.02
i_{NBM}	$mg_N\ mg_{BM}^{-1}$	0.07

The coefficient θ_T is estimated by plotting the rate versus temperature, which demonstrates a slope equal to the coefficient. In this study, the θ_T of the bio-kinetics parameters are obtained from Grady Jr et al. (2011) and are summarized in Table 7.5. In general, the yield coefficients are assumed to be independent of temperature. The maximum growth rate, lysis rate and saturation coefficient of the substrate are significantly affected by the temperature, especially for the parameters describing the nitrification. In Table 7.5, the comparisons of the parameters at different temperature show that the μ_A and $K_{A,NH}$ are doubled from 20˚C to 28 ˚C. In this study, the bio-kinetics parameters are factorized with respect to the average temperature of the effluent due to the absence of heat transport module.

Table 7.5: Temperature coefficient of bio-kinetics parameters

Parameter	θ_T	Value at 20˚C	Value at 28˚C
k_H	1.06	3.00	4.78
μ_H	1.09	6.00	11.96
b_H	1.03	0.40	0.51
$K_{H,S}$	1.00	2.00	2.00
$K_{H,NH}$	1.14	0.05	0.14
μ_A	1.11	1.00	2.30
b_A	1.03	0.15	0.19
$K_{A,NH}$	1.14	0.50	1.43
$Y_{H,O2}$	1.00	0.63	0.63
$Y_{H,NO}$	1.00	0.63	0.63
Y_A	1.00	0.24	0.24

7.1.4. Initial conditions and boundary conditions

Intermittence of feeding and rest periods alternates the inherent population of active biomass and the concentration of residual contaminants in the wetland bed. The initial concentration of all quality parameters at each node become the major uncertainty in the simulation, and the associated determination was rarely discussed in the literature. As mentioned in section 7.1.1, the transport of contaminants can be divided into the solid and liquid phases, and the liquid phase can be further subdivided into the mobile and immobile region. Therefore, twenty-one sets of initial conditions (nine sets for the mobile region, nine sets for the immobile region, and three sets for the solid phase) were required in the proposed model. The conventional method to determine the initial condition is to measure the concentration of quality parameters along the depth of the wetland bed. However, such a measurement is difficult in the relatively large surface area of the pilot-scale system. Therefore, the initial condition is generally calibrated according to the measured data collected from the pilot plant (Morvannou et al. 2014).

Since the main objective of this study is to simulate the nitrogen dynamics in the pilot-scale VFCW, the residual organic matter (S_S, S_I, X_S, and X_I) was assumed to be absent in the wetland bed. In this study, the biological process was implemented in the mobile region only, and thus the initial conditions in the immobile region were neglected. In order to simplify the calibration, the oxygen content was assumed to be constantly supplied throughout the experiment, where the concentration was set to be under the

quasi-steady state. The laboratory experiment showed that the concentration of DO in the effluent ranged within 5 to 6 mg l^{-1}. Accordingly, the constant concentration of S_O was fixed as 5 mg l^{-1} in the simulation. Besides, the results obtained from the pilot-scale system indicated that the pH of the effluent remained at an optimal range throughout the treatment, and thus the limitation of alkalinity to the biodegradation was assumed to be negligible in the simulation. Additionally, S_{N2} is the final product of the biological process, and thus it has no effect on the overall performance of the VFCW and the associated initial concentration was assumed to be zero. Accordingly, the calibration of initial conditions was reduced to four components, which are S_{NH}, S_{NO}, X_H, and X_A. Similar to the transport parameters, this section aims to deliver a standard of initial conditions to reproduce the nitrogen dynamics for all cases.

In the transport module, the upper boundary condition takes into account the influent quality, including oxygen content, nitrogenous constituents, and organic matter. The values of parameters S_O, S_{NH}, S_{NO}, and TS can be obtained directly from the laboratory measurement, while S_{N2}, X_H, and X_A were assumed to be absent in the influent. In addition, the organic matter is required to be subdivided to a different category. The portion of organic matter was assumed to be 0.10, 0.30, 0.10, and 0.50 for S_I, S_S, X_S, and X_I, respectively.

7.1.5. Calibration of transport parameters

This section aims to introduce a calibration method to match the simulation with the measured data of the nitrogen dynamics (NH_4^+-N and NO_3^--N). As explained in section 7.1.3, the bio-kinetics parameters used in this study were assumed as a set of constant. These rates and coefficients, which were empirically determined based on a series of experiments, have been widely applied in various studies (McBride and Tanner 1999; Langergraber and Šimůnek 2005; Toscano et al. 2009). Therefore, the main challenge in the calibration was setting up the transport parameters and the initial conditions of residual nitrogen and active biofilm.

It should be noted that only the cases with adequate hydraulic simulation were carried out with the modelling of nitrogen dynamics. In order to develop a standard procedure for the calibration, the trends of the nitrogen dynamics were preliminarily analyzed. In general, the concentration of NH_4^+-N appeared to increase rapidly in the effluent during the early stage and declined gradually in the late stage of treatment. Meanwhile,

the concentration of NO_3^--N dropped rapidly in the early stage and slightly rose at the late stage.

This observation was explained by the quality of influent, where NH_4^+-N was always high and NO_3^--N was generally low. Besides, it also reflects that certain amount of NH_4^+-N and NO_3^--N were trapped or generated in the wetland bed between the feedings, and hence the invasion of new feeding caused the washout of the residuals and resulted in a noticeable background concentration in the early effluent. This mixing process, which is described by the ADE, is greatly affected by D_L. In addition, the peak concentration of NH_4^+-N illustrated a remarkable reduction from the influent, which is attributed to the instantaneous adsorption in the sludge deposit and intermediate layer. Therefore, the calibration of transport parameters and initial conditions is necessary to be carried out simultaneously. However, such an approach is hindered by a large number of parameters in the calibration, and thus this study aims to establish a set of prescribed transport parameters that can fit all measured data in the pilot-scale VFCW. Then, the proposed model only requires the initial conditions to be calibrated in each case.

The dynamics of NH_4^+-N involves the processes of hydrolysis, adsorption and biodegradation and vegetation uptake. In addition to nitrification, the consumption of NH_4^+-N in the growth of X_H was found to be remarkable in the preliminary calibration. In the meantime, the dynamics of NO_3^--N is relatively simple, where the nitrification is the only governing process since the denitrification was not observed in the pilot system and the effect of vegetation is always negligible. Therefore, the concentration of NO_3^--N was calibrated first to determine the D_L and the distribution of X_A in the wetland bed. Then, the adsorption coefficient and the concentration of X_H was only calibrated.

In order to simplify the calibration, the distribution of NH_4^+-N and NO_3^--N in the gravel layer were initially assumed to be under an equilibrium state and the concentration is identical as the first measurement of the effluent. The initial concentrations of NH_4^+-N in the sludge deposit layer and intermediate layer were anticipated to be higher to match the increase of concentration in the early effluent, and then NO_3^--N was presumed to be absent in these regions to illustrate the drop at the beginning of effluent. Throughout the calibration, the D_L of the sludge deposit layer

and intermediate layer were found to be 1 cm and 5 cm, respectively. Meanwhile, the D_L of the small-size gravel and medium-size gravel layers were 15 cm and 25 cm, respectively. Besides, the coefficient of adsorption in the sludge deposit layer and intermediate layer were set to be 0.03 cm^3 min^{-1} and 0.01 cm^3 min^{-1}, respectively.

The distribution of biofilm is the key parameter in the modelling of biodegradation. Since the direct quantification was no available in this study, the input of initial biofilm distribution was obtained through the calibration and literature data. The rhizosphere zone and porous medium provide a significant surface area for the development of biofilm (Larsen and Greenway 2004). Tietz et al. (2007) highlighted that the 95% of microbial biomass was found in the top 10 cm of the wetland bed, and this could be attributable to the accumulation of fine particulates and sufficient supply of nutrient and oxygen. Besides, Foladori, Bruni, and Tamburini (2015) found that the amount of active biomass decreases with the depth of wetland bed, where the concentration of bacteria within the top 10 cm was 3.7 times higher than the bottom layer. In addition, the saturation level is crucial to the efficiency of biological processes. According to the hydraulic simulation, the water content in the gravel layer was always low, and thus the efficiency of biodegradation could be assumed to be negligible. As a result, the active biomass was assumed to be within the sludge deposit layer and intermediate layer only. A ratio of 1:8 was used with reference to Pálfy et al. (2016) to describe the distribution of X_H in the wetland bed under a self-stabilized condition. To ease the calibration, the initial conditions of biofilm were assumed to be the same in a homogenous porous medium. The calibration showed that a 2 mg kg^{-1} of X_A within the sludge deposit layer (bulk density = 1.70 g cm^{-3}) and 1 mg kg^{-1} of X_A within the intermediate layer (bulk density = 2.30 g cm^{-3}) illustrated a good match with the measured data. Accordingly, the initial concentrations of X_H were set to be 16 mg kg^{-1} and 8 mg kg^{-1} in the sludge deposit layer and the intermediate layer, respectively.

7.1.6. Summary of Assumptions

The assumptions and associated set-up are summarized as follows:

- Due to the rapid water flux throughout the wetland bed, the molecular diffusion was assumed to be negligible in the transport mechanism of the liquid phase.
- The active transport between the mobile and immobile regions was assumed to be negligible. Therefore, the coefficient of active solute transfer (α_{ph}) was set

to be zero and the solute exchange completely depends on the water exchange between two domains.

- As the mechanical dispersion is a function of water flux, the D_L was assumed to be the same in a homogenous porous material. The D_L was calibrated according to the measured data, which obtained 1 cm, 5 cm, 15 cm, and 25 cm for the sludge deposit layer, intermediate layer, small-size gravel layer, and medium-size gravel layer, respectively.
- The adsorption was only considered for component S_{NH}.
- The adsorption was assumed as a kinetic process, which only occurs in the mobile region. Therefore, the f_{MO}, f_E and ω_k are set to be 1, 0, and 1, respectively.
- The adsorption process was simulated using a linear isotherm. The coefficient for adsorption of S_{NH} is dependent on the properties of the porous medium.
- The coefficient of adsorption in the sludge deposit layer and intermediate layer were set to be 0.03 cm^3 min^{-1} and 0.01 cm^3 min^{-1}, respectively. The adsorption was assumed to be negligible in the gravel layer.
- The extraction of S_{NH} and S_{NO} by vegetation uptake was dependent on the water uptake by vegetation.
- It was assumed that the active biomass is stationary in the wetland bed as attached biofilm.
- The coefficient of surface filtration was obtained from the average removal rate of total solids throughout the experiment, where a value of 0.80 was employed in all simulations.
- The deep bed filtration within the granular medium was assumed to be negligible.
- The proposed model simulated the biological process at a macroscopic level, where the contaminants were assumed to be fully contacting with the attached biofilm. The influence of biofilm thickness, diffusion between the liquid-biofilm interface, and other microscopic process was not considered in this study.
- As the heat transfer was not included in the proposed model, the bio-kinetics parameters that are dependent on temperature were factorized with respect to the average temperature of the effluent.

- As the re-aeration rate through the ventilation pipe and the saturation of oxygen at different layer were not measured throughout the experiment, S_O was assumed to be under a quasi-steady state at a concentration of 5 mg l^{-1}.
- According to the measured data, the pH in the effluent remained at a favourable range for the biochemical process. Therefore, the Monod kinetics rate was assumed to be independent of the limitation of alkalinity.
- The degradation of active biofilm was described by the lysis process, which releases X_I and S_I back to the percolate and is eventually discharged from the system.
- The portion of organic matter was assumed to be 0.10, 0.30, 0.10, and 0.50 for S_I, S_S, X_S, and X_I, respectively.
- The active biofilm was assumed to be uniformly distributed over the sludge deposit layer and intermediate layer only.

7.2. Results and Discussions

7.2.1. Simulated Results

The prescribed transport parameters and bio-kinetics parameters presented in the previous section were implemented in the proposed model and the initial conditions were calibrated to fit the simulated result with the measured nitrogen dynamics within a feeding-draining cycle. Figure 7.1 - Figure 7.8 present the simulated results of case 1A, 3A, 8A, 11A, 19B, 20A, 24B, and 25B, respectively. The simulation of case 6A, 7B, 17B, and 23B failed to deliver a reasonable match with the measured data, and thus these cases were not presented in this study. The performance of the VF_Sep was evaluated using the mean absolute percentage error (MAE (%)) as presented in section 6.5. The result of error analysis is summarized in Table 7.6.

VF_Sep is a combination of implicit functions of physical and biochemical characteristics to macroscopically describe the treatment processes in the VFCW. The current simulation setup described the VFCW as a bio-filter, where the development of biofilm was only simulated within the upper layer of the wetland bed. In order to deliver a robust simulation, a set of prescribed transport parameters and bio-kinetics

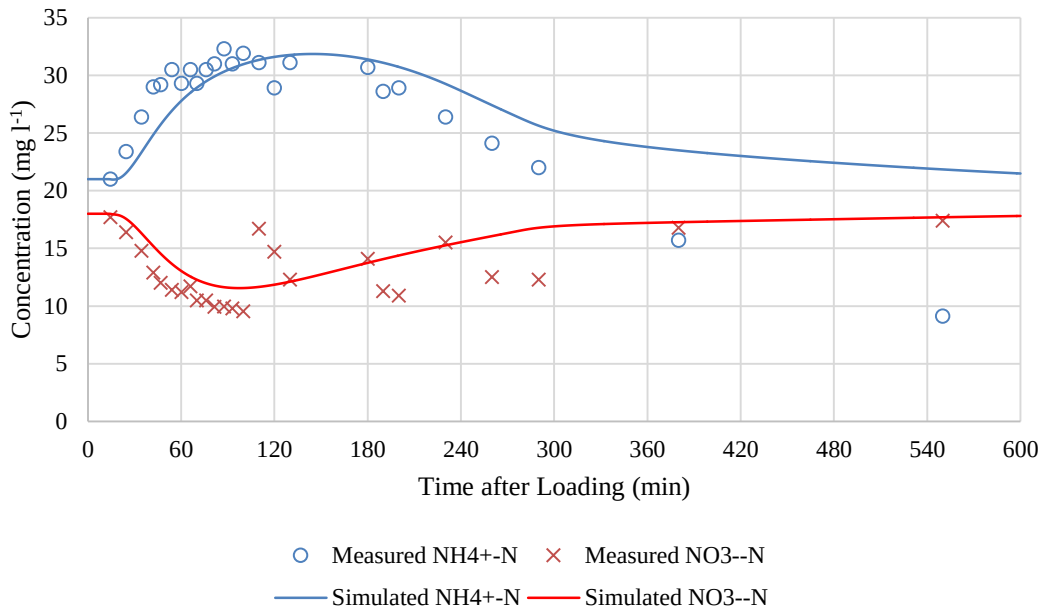

Figure 7.1: Simulated results of case 1A (18-11-2015: 75 l)

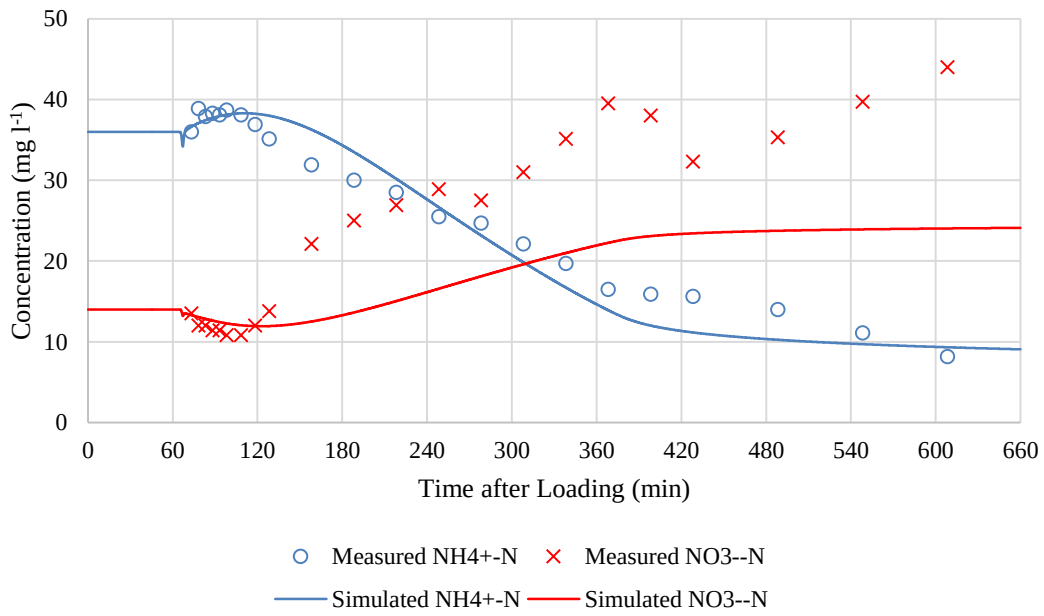

Figure 7.2: Simulated results of case 3A (1-12-2015: 75 l)

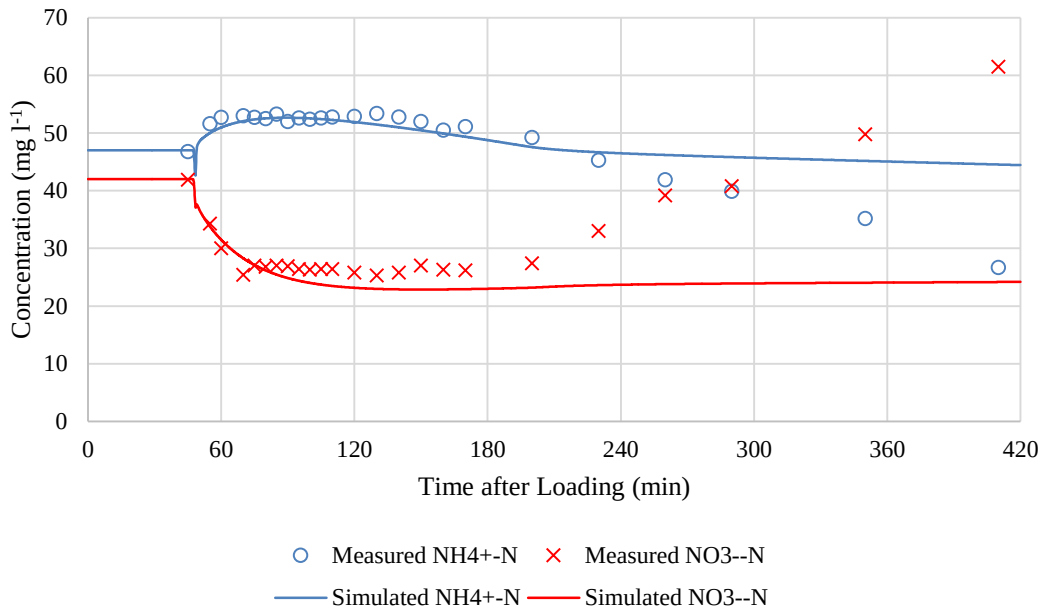

Figure 7.3: Simulated results of case 8A (16-12-2015: 100 l)

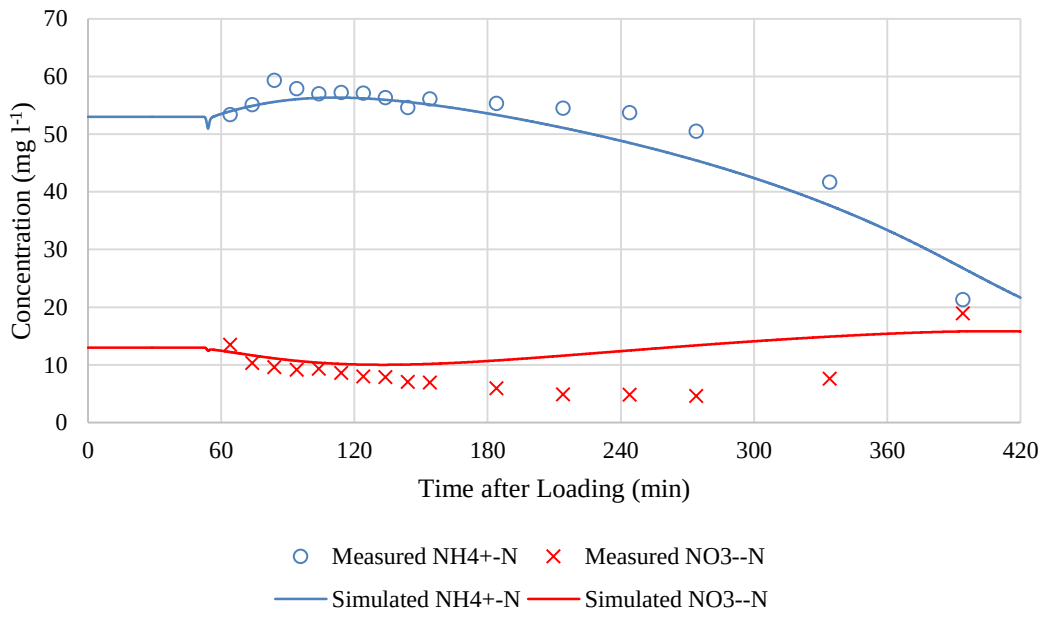

Figure 7.4: Simulated results of case 11A (27-12-2015: 100 l)

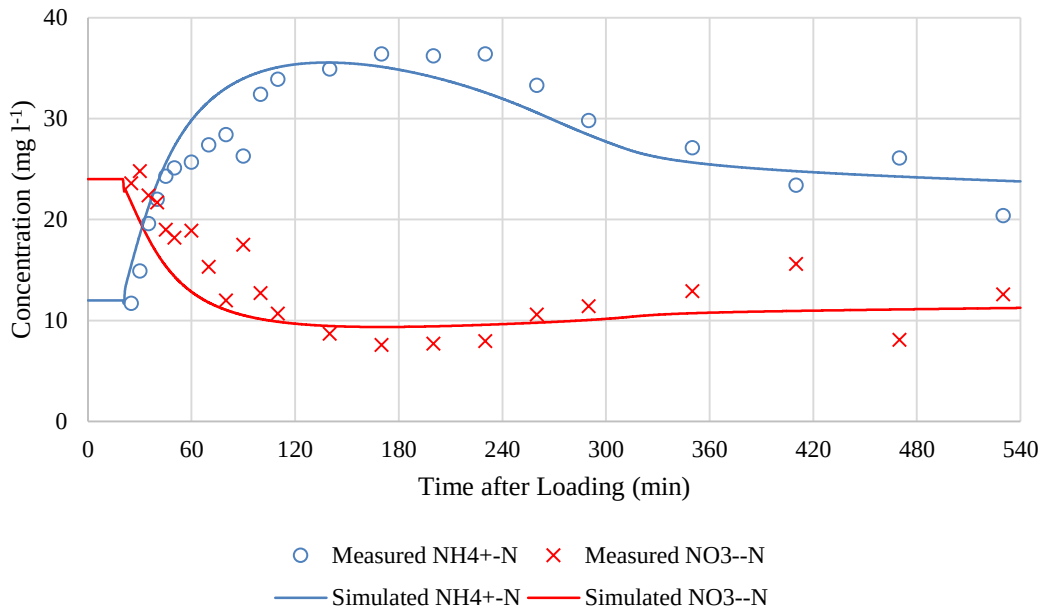

Figure 7.5: Simulated results of case 19B (24-1-2016: 125 l)

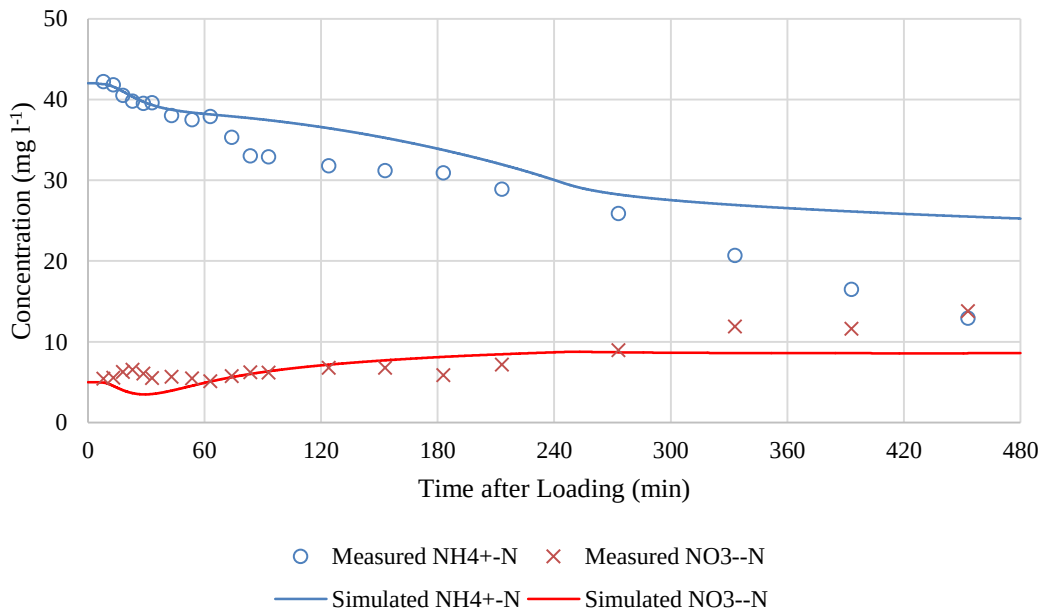

Figure 7.6: Simulated results of case 20A (28-1-2016: 150 l)

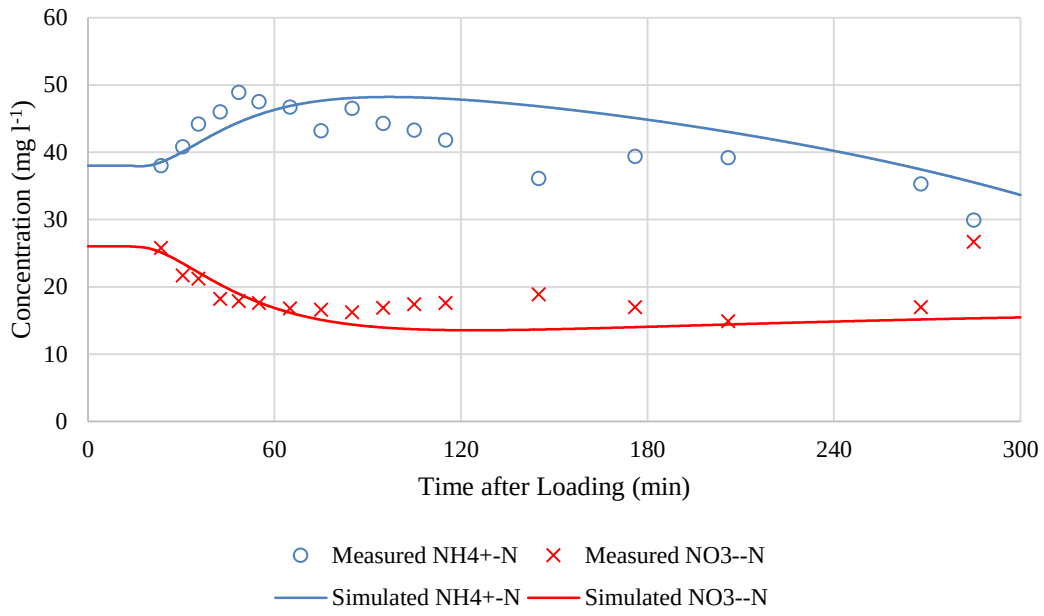

Figure 7.7: Simulated results of case 24B (21-2-2016: 125 l)

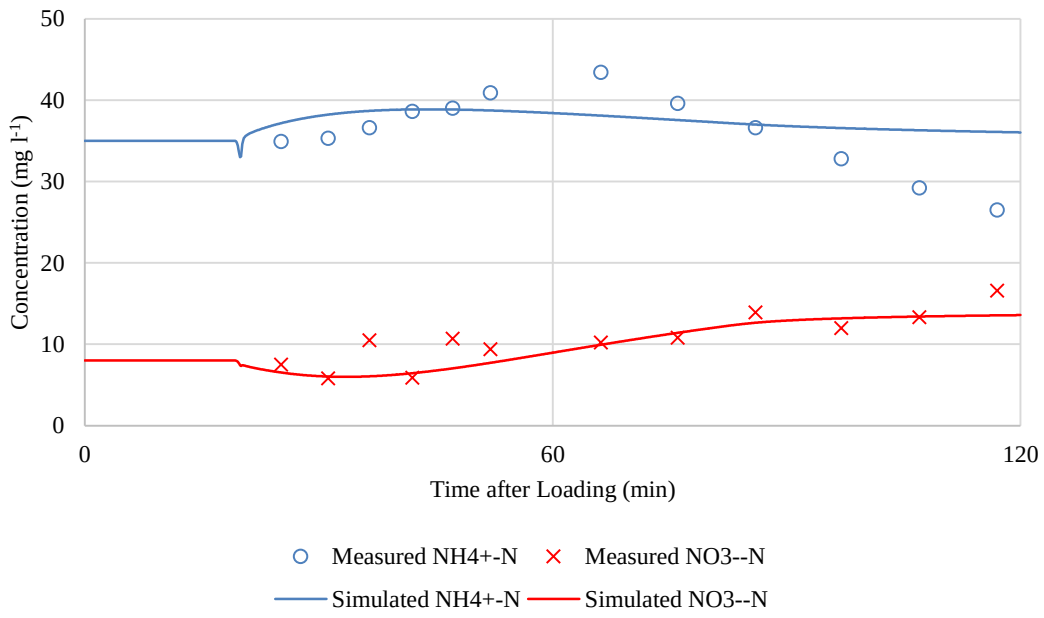

Figure 7.8: Simulated results of case 25B (27-2-2016: 50 l)

Table 7.6: MAE (%) of NH_4^+-N and NO_3^--N

Cases	MAE (%) of NH_4^+-N	MAE (%) of NO_3^--N
1A	9.44 %	14.57 %
3A	7.21 %	33.27 %
8A	4.82 %	19.51 %
11A	4.10 %	41.51 %
19B	7.59 %	10.23 %
20A	9.31 %	20.39 %
24B	7.13 %	12.79 %
25B	8.49 %	14.39 %
Maximum	4.10 %	10.23 %
Minimum	9.44 %	41.51 %
Mean	7.26 %	20.83 %
Standard deviation	1.82 %	10.26 %

parameters were calibrated to fit the available measured data as much as possible. The hydraulic behaviour and influent concentration is the main variable in the simulation of treatment performance. Overall, the general trend of NH_4^+-N in the effluent was well predicted, where the MAE (%) between the simulated results and laboratory measurement are on average below 10 %. This has shown that the prescribed transport and bio-kinetics parameters were capable of delivering a promising simulation. However, the simulation of NO_3^--N was less desirable, where the mean MAE (%) was approximately 10 % and it exceeded 40 % in a particular case.

As mentioned in section 7.1.5, the calibration of NO_3^--N was more direct due to the absence of denitrification in the VFCW. The simulation of NO_3-$^-$N generally demonstrated a good match with the measured data, which is illustrated with cases 1A, 11A, 19B, 20A, 24B, and 25B. However, the discrepancies between the simulated and measured data in cases 3A and 8A were significant. The prescribed transport parameters and calibrated initial conditions successfully reproduced the first stage of NO_3-$^-$N dynamics in most of the simulations, but nitrification was generally under-predicted in the late phase of discharge. In fact, the simulation of NO_3-$^-$N dynamics was reasonable from the visible evaluation. The high MAE (%) in case 11A and 20A was attributable to the low measured concentration of NO_3-$^-$N in the analysis. Besides, the under-predicted NO_3-$^-$N highlights that the prescribed concentration of biofilm

might not be valid in certain cases, where a detailed investigation for their distribution in the wetland bed is required to improve the efficiency of the proposed model.

According to the measured data and simulated data, the dynamics of NO_3^--N could be discussed in two stages. A certain amount of NO_3^--N was yielded in the wetland bed due to the residual NH_4^+-N nitrified during the resting period, and thus the first measurement of effluent was generally high. Then, the low influent concentration and poor nitrification at the early phase resulted in a drop in concentration, and this period was recognized as the first stage of NO_3^--N dynamics. The proposed model promisingly simulated the concentration of NO_3^--N at this stage, subsequently indicating the poor nitrification in the early operation.

As for the second stage, NO_3^--N was gradually yielded by nitrification in the following percolation. Theoretically, nitrification depends on the saturation level, oxygen content, and population of active biomass. Since the upper layer was always saturated and oxygen was sufficiently supplied, the active biomass is considered as the rate-limiting factor in the process. The simulation illustrated that the increase of NO_3^--N is proportional to the growth of X_A. Figure 7.9 displays an example of biomass development in the sludge deposit layer and intermediate layer throughout the operation. The incoming NH_4^+-N in the new feeding led to a constant development of X_A until the temporary ponding was completely infiltrated, and then the following growth was insignificant. The growth of biofilm in the sludge deposit layer was more rapid due to a higher saturation level and initial concentration, highlighting its vital role in the removal of NH_4^+-N.

Accordingly, the nitrification rate was more rapid when the active biofilm had been extensively developed. This was observed from the concentration of NO_3-$^-$N in the effluent that stabilized after the descending in the early phase, and gradually rose for the remaining time. However, the simulated concentration of NO_3^--N was much lower than the measured data in case 3A and 18A, which implied that the concentration of inherent biofilm in these cases might be underestimated. Another possible reason for these discrepancies could be due to the bio-kinetics parameter used in the simulation, but it required further laboratory data to calibrate a new set of parameters. In addition, the discharge at the late phase of the feeding-draining cycle was greatly reduced, and thus a significant amount of NH_4^+-N was trapped within the bed and was further

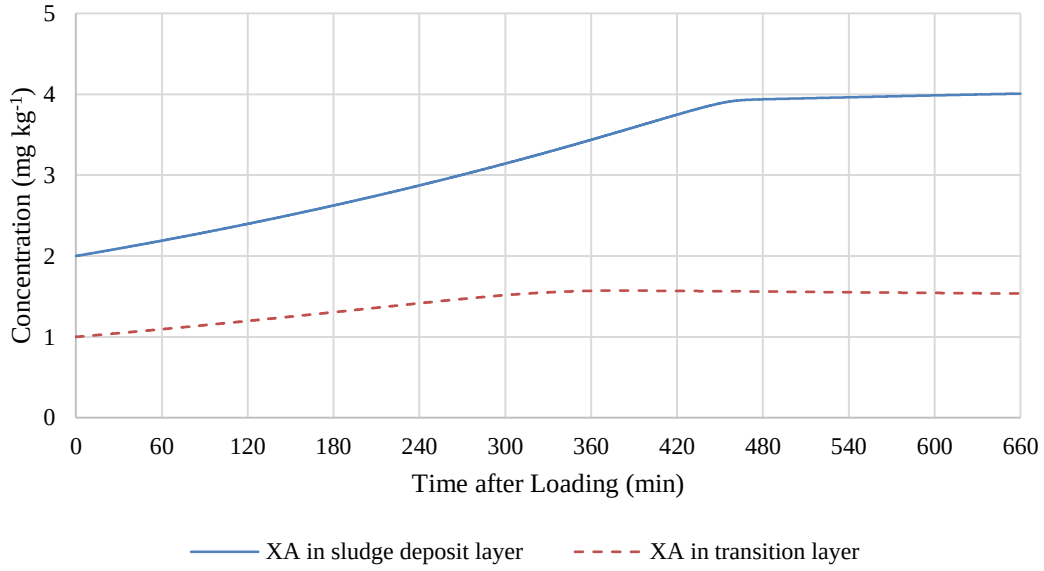

Figure 7.9: Development of X_A of case 3A (1-12-2015: 75 l)

nitrified in the resting period, which explained the high background concentration in the next feeding cycle.

The error analysis indicated that the modelling of NH_4^+-N dynamics was excellent, where the MAE (%) are below 10 % in all cases. Similar to NO_3^--N, the dynamics of NH_4^+-N can be separated into two phases. In general, a rise of NH_4^+-N was observed in the early effluent. The prescribed transport parameter and the calibrated initial conditions successfully predicted the concentration of NH_4^+-N in this phase. In addition to the influent, a large amount of NH_4^+-N was found to be accumulated in the upper layer and subsequently created the rise. This can be explained by the retained X_S at the top surface of wetland bed, which were hydrolysed and released NH_4^+-N during the inter-event period. At the early stage of treatment, the development of active biofilm was still low, and thus the removal of NH_4^+-N was generally ineffective.

In the late phase of NH_4^+-N dynamics, the concentration was gradually reduced due to the continuous growth of active biofilm. The substantial decline at this stage was not accurately predicted in several cases, especially in case 1A, 20A, and 25B. As the removal of NH_4^+-N is a complex process, the discrepancy is essential to be analysed with respect to each removal pathway. In addition to nitrification, the effect of adsorption and aerobic respiration were noticeable in the pilot-scale VFCW in terms of NH_4^+-N removal. In the context that the efficiency of nitrification can be assessed according to the dynamics of NO_3^--N, the simulation of the nitrification rate was

hypothesized to be reasonable. Therefore, the imbalance between the reduction of NH_4^+-N and the production of NO_3^--N was then presumed to be dependent on the adsorption and aerobic respiration.

7.2.2. Discussion

VF_Sep is aimed to be a research-oriented numerical scheme to study the nitrogen dynamics in a pilot-scale VFCW treating septage, which is capable of evaluating the contribution of each mechanism in the nitrogen dynamics. According to the current outcomes, nitrification, adsorption and aerobic respiration were revealed as the main removal and retention mechanisms in the nitrogen dynamics of the pilot plant. Vymazal (2007) indicated that the highly aerobic condition in the VFCW results in a great treatment of NH_4^+-N, but the potential to remove NO_3^--N is low and thus its concentration commonly increases in the effluent. A similar phenomenon was observed in the laboratory experiment, and this trend has been successfully illustrated by the proposed model. A mass balance analysis of nitrogen removal (Morvannou et al. 2014) demonstrated that majority of NH_4^+-N was nitrified in the VFCW. As a result, the proposed model delivered a promising simulation towards the fate of NH_4^+-N with respect to the current assumption and prescribed parameters.

7.2.2.1. The influence of DO

The saturation level and oxygen content are the governing parameters to determine the extent of nitrification in the VFCW. Accordingly, the proposed model was developed by interlinking the oxygen content, saturation level, and biofilm growth to describe the biodegradation process. As the water content in the porous medium acts as the intervening substance between the contaminants and biofilm in the liquid phase, Henrichs, Welker, and Uhl (2009) indicated that nitrification was provoked during the saturated period. Kayser and Kunst (2005) explained that the rapid infiltration in the VFCW is advantageous for the wetland bed to be aerated via diffusion and convection. A number of studies have highlighted the effect of oxygenation on nitrification. Kayser and Kunst (2005) indicated that the aerobic processes were completed within the top 10 cm of wetland bed due to the diffusion at the wetland surface, and its rate could be deteriorated because of overloads. Woźniak, Dittmer, and Welker (2007) measured that the consumption of oxygen was extremely high in the first 30 cm of the wetland bed, implying that biodegradation was limited in the upper layer. Petitjean et al. (2012)

found that the consumption and restoration of oxygen can be described in four steps in a feeding-draining cycle, which demonstrated a close correlation to the development of biofilm.

The hydraulic simulation has been repeatedly emphasized as a prerequisite in the numerical model for nitrogen dynamics (Langergraber and Šimůnek 2005). The contact time between the influent and attached biofilm was governed by the hydraulic simulation in the proposed model, where the influence of saturation level was described by the water content in the ADE. Therefore, the undesirable nitrification in the pilot-scale VFCW could be attributed to the rapid flux through the wetland bed, which limited a complete nitrification to take place. In this study, the active biomass was assumed to be present in the sludge deposit and intermediate layer only. The sludge deposit is a layer of settlement caused by the particulate constituents in the raw septage, subsequently reducing the infiltration capacity of the upper layer of wetland bed. In this context, the sludge deposit and intermediate layer are more saturated and contain a higher water content throughout the feeding-draining cycle, and thus the biological processes mostly take place in the upper layer of wetland bed. This observation was supported by a study of hydraulic behaviour (Henrichs, Welker and Uhl 2009). Besides, several studies highlighted that most of the biomass was discovered in the first 10 cm of wetland bed (Langergraber, Tietz and Haberl 2007; Tietz et al. 2007; Foladori, Bruni and Tamburini 2015). Accordingly, the biodegradation in the deeper layer of wetland bed is minor due to the low water content and poor biomass development. However, a specific study is necessary to correlate the development of biofilm to the water content at different depths of wetland bed as a future study to strengthen this outcome.

In addition to the initial oxygen content in the wetland bed, re-aeration took place via the ventilation pipes during the feeding to maintain the high oxygenation in the system. However, this rate was difficult to be determined while an oxygen profile of the system was unavailable in this study, and thus the transport of oxygen was assumed to be under the quasi-steady state in the simulation. According to the laboratory experiment, the concentration of DO in the effluent was generally above 5 mg l^{-1}, and thus this conservative value was implemented as a constant concentration in the simulation. DO is a rate-liming substrate in the Monod kinetic of nitrification. As the saturation coefficient of S_O was 0.5 mg l^{-1}, the alteration of its limiting term in the Monod

equation is small when the DO is higher than 5 mg l^{-1}. Thus, this simplified attempt delivered reasonable prediction for NH_4^+-N dynamics.

To remark on the significance of DO in the proposed model, four cases of simulations (3A, 11A, 19B, and 25B) were re-simulated without the condition of constant DO, where the associated source was limited to the initial concentration in the wetland bed. Figure 7.10 - Figure 7.13 show the comparisons between the simulations with constant and inconstant DO. The results indicated that the DO was quickly consumed by aerobic respiration and nitrification due to the high organic and nutrient load in the septage treatment. Consequently, the production of NO_3^--N was almost negligible, which resulted in a gradual drop in the simulation. Meanwhile, the concentration of NH_4^+-N was over-predicted due to the absence of nitrification. Although the assumption of constant DO in the wetland bed reasonably predicted the dynamics of NO_3^--N, a more reliable module is essential to describe the oxygen transport and re-aeration in the VFCW treating septage.

The gap of knowledge between the oxygen profile and nitrogen dynamics in the VFCW treating septage should be further investigated by quantifying the renewal and consumption rate of oxygen at different depths of the wetland bed. This attempt will be useful to regulate an optimal loading regime and resting period to guarantee a robust treatment performance of the system.

7.2.2.2. Adsorption

Similar to Henrichs, Welker, and Uhl (2009) and Morvannou et al. (2014), adsorption was found to be a remarkable removal mechanism of NH_4^+-N in the pilot-scale VFCW system. It should be noted that VF_Sep described the adsorption as a linear kinetic process driven by the difference in concentration between the liquid and solid phase, and thus this process is only prohibited when an equilibrium state is achieved. Overall, this approach delivered a reasonable simulation towards the removal of NH_4^+-N. To evaluate the role of adsorption in the system, case 3A, 11A, 19B, and 25B were re-simulated by removing the adsorption coefficient, where the removal of NH_4^+-N only depends on biodegradation. The simulated results are presented in Figure 7.14 -Figure 7.17. As the adsorption was only applied in the transport module of NH_4^+-N, its influence was negligible in the dynamics of NO_3^--N. The comparisons between the simulated results demonstrated that the concentration of NH_4^+-N was significantly

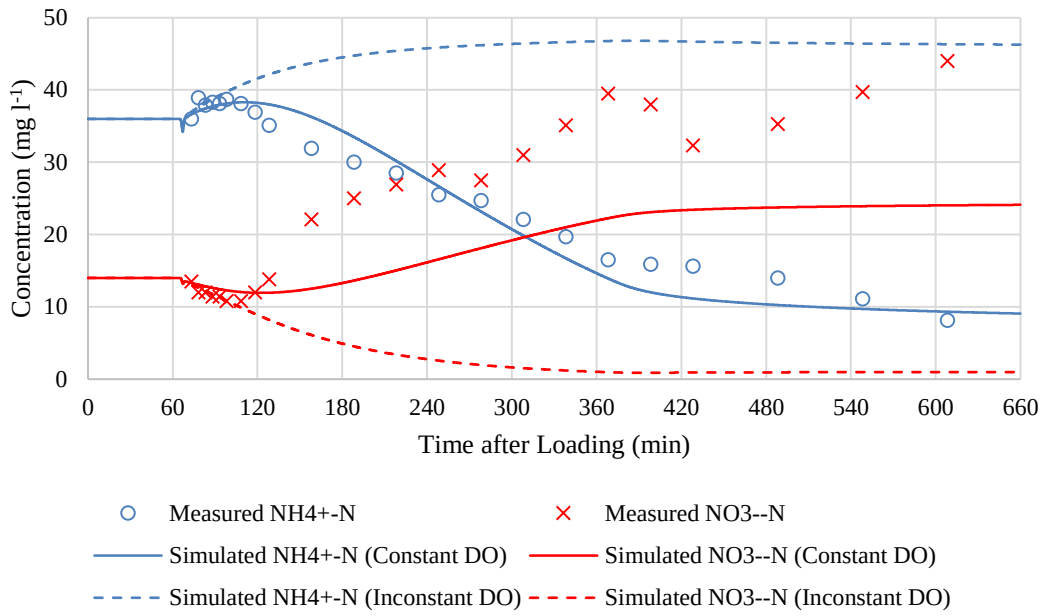

Figure 7.10: Influence of DO on nitrogen dynamics of case 3A (1-12-2015: 75 l)

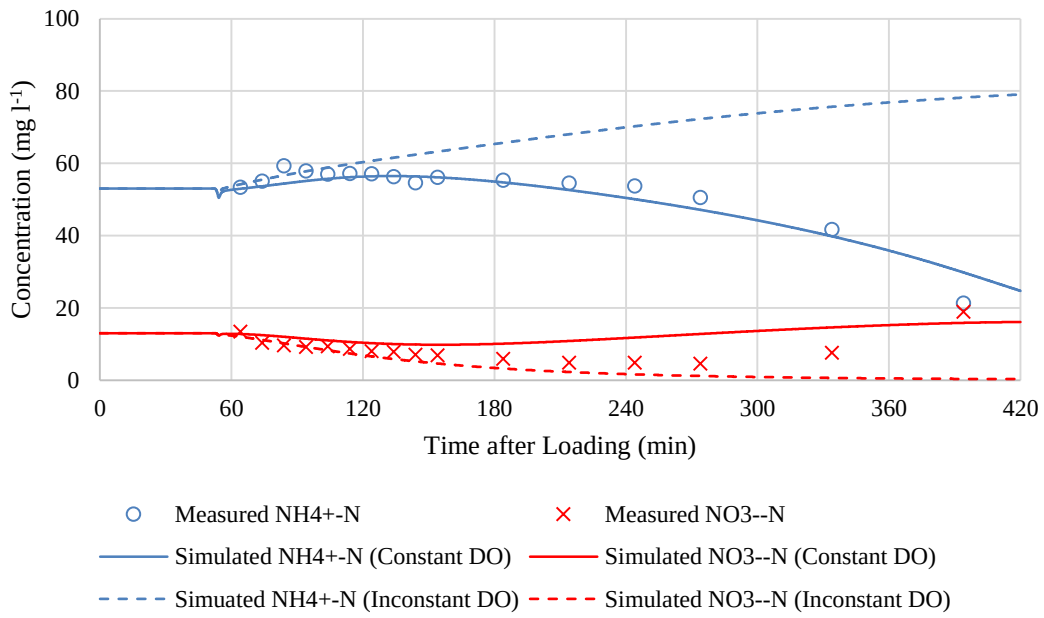

Figure 7.11: Influence of DO on nitrogen dynamics of case 11A (27-12-2015: 100 l)

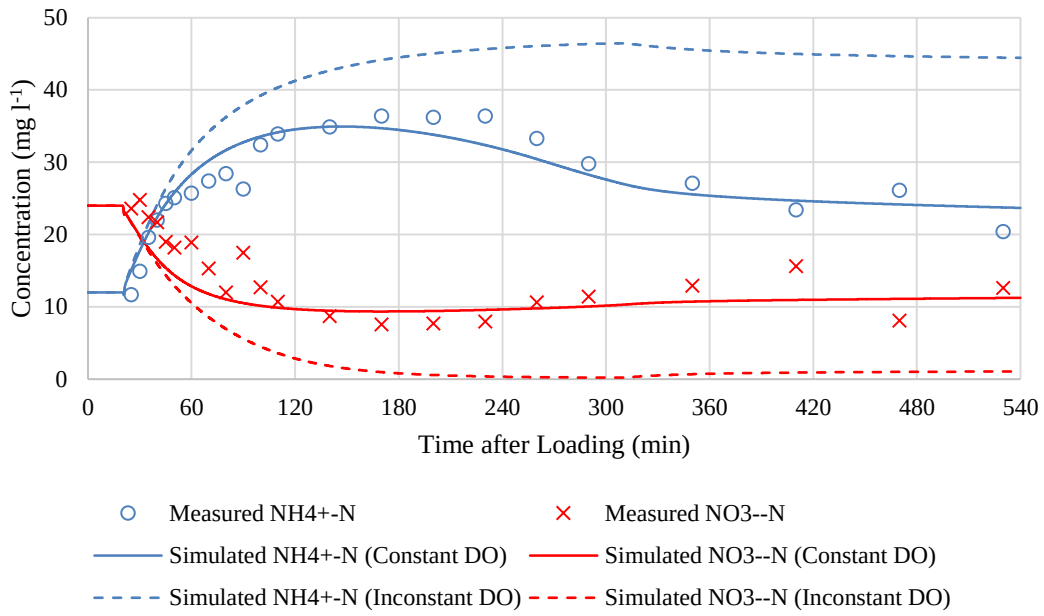

Figure 7.12: Influence of DO on nitrogen dynamics of case 19B (24-1-2016: 125 l)

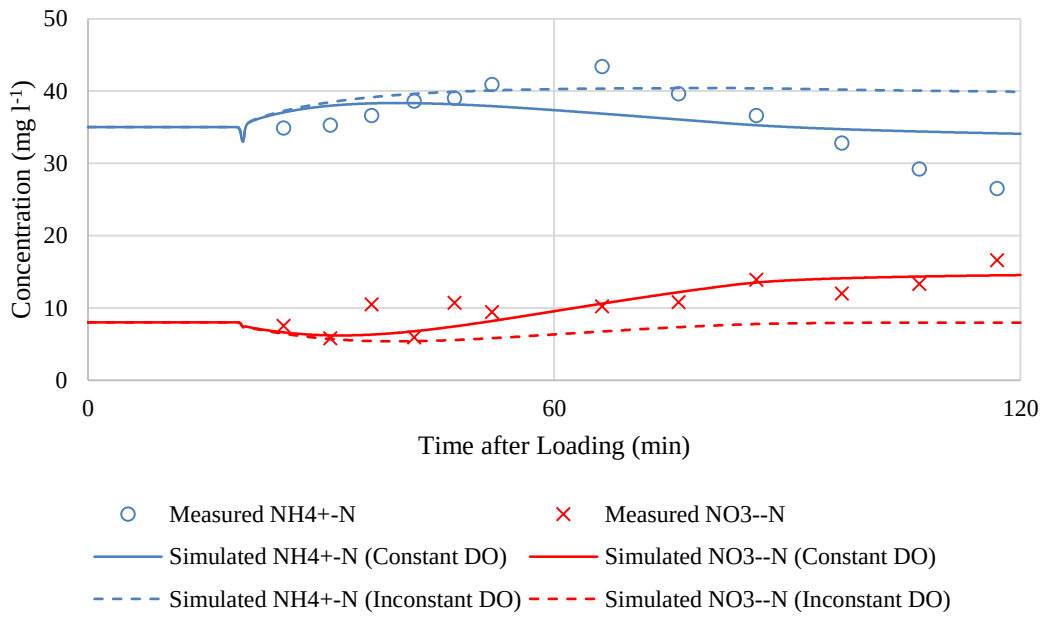

Figure 7.13: Influence of DO on nitrogen dynamics of case 25B (27-2-2016: 50 l)

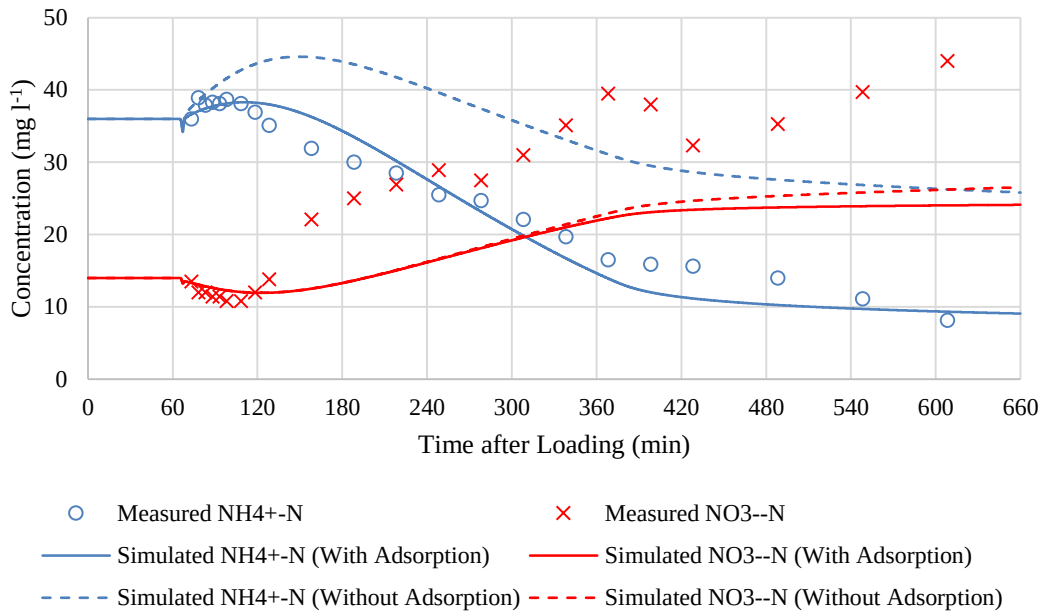

Figure 7.14: Influence of adsorption on nitrogen dynamics of case 3A (1-12-2015: 75 l)

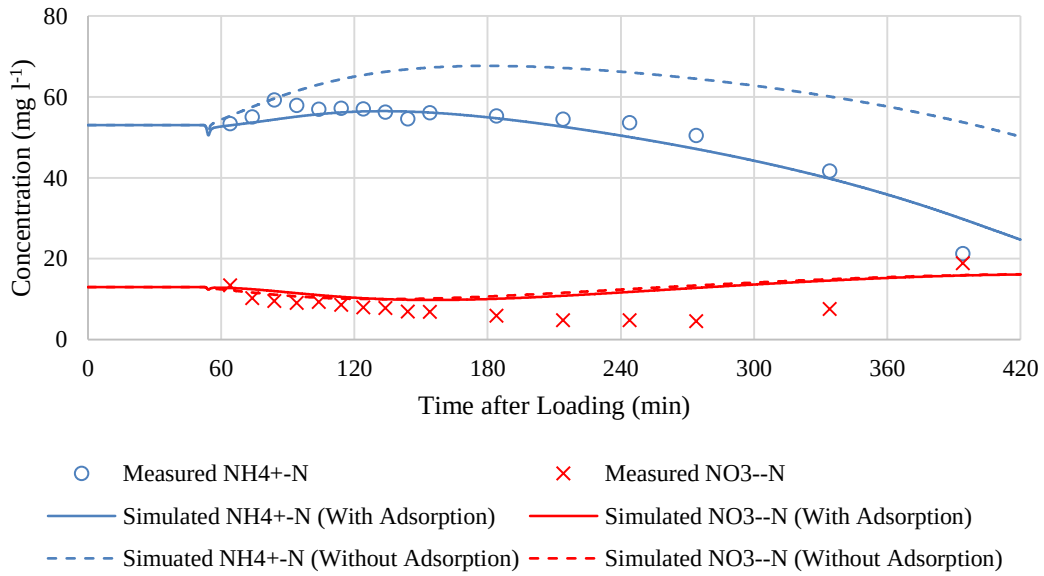

Figure 7.15: Influence of adsorption on nitrogen dynamics of case 11A (27-12-2015: 100 l)

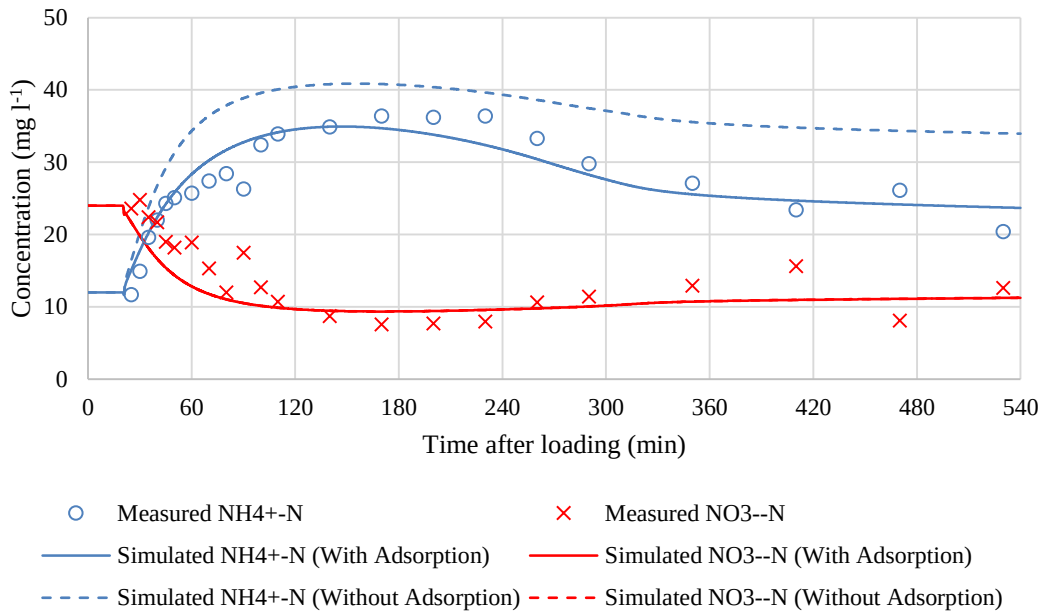

Figure 7.16: Influence of adsorption on nitrogen dynamics of case 19B (24-1-2016: 125 l)

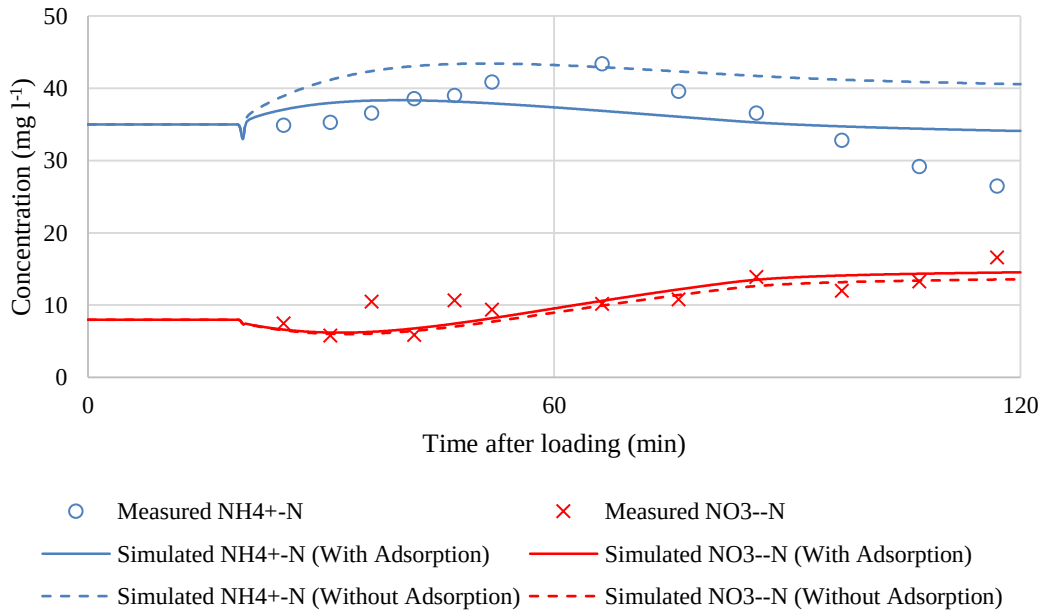

Figure 7.17: Influence of adsorption on nitrogen dynamics of case 25B (27-2-2016: 125 l)

over-predicted when the adsorption was absence in the simulation.

In the proposed model, adsorption was described as a first-order reaction, which instantaneously removed NH_4^+-N and was not affected by the growth of active biofilm in the wetland bed. Accordingly, its rate was consistent throughout the feeding-draining cycle, and this could be regarded as the main pathway of NH_4^+-N removal after nitrification. This finding was similar to Morvannou et al. (2014), which indicated that a certain amount of NH_4^+-N was adsorbed onto the organic matter instead of being nitrified during the feeding period.

The drawback of linear adsorption isotherm is that the adsorbate on the surface of the medium is unlimited, which could be untrue in the reality. Therefore, the use of the Langmuir isotherm may be necessary to "control" the adsorption in the VFCW. However, such an isotherm requires more effort in the numerical development. RSF_Sim (Meyer and Dittmer 2015) proposed a two-stage linear isotherm to describe the adsorption of NH_4^+-N in a VFCW system treating combined sewer overflow (CSO), where a critical concentration of adsorbed NH_4^+-N was implemented to distinguish the rapid and slow adsorption due to the change of concentration. In addition, the coefficient of the isotherm is required to be experimentally measured to validate the values used in the current simulation, especially for the capacity of adsorption in the sludge deposit layer. The similar attempt should be carried out to determine the maximum capacity of biofilm development.

7.2.2.3. Consumption of NH_4^+-N in the growth of X_H

The consumption of NH_4^+-N in the growth of X_H is the less discussed mechanism in the literature. One of the reasons is that the organic content in the sewage or CSO is not as high as septage. Therefore, such an effect is insignificant in the simulation of the treatment of sewage, but the high concentration of chemical oxygen demand (COD) in the raw septage stimulates a great development of X_H in the wetland bed, which simultaneously consumes a certain amount of NH_4^+-N in the process. Case 3A, 19B, 24B and 25B were re-simulated by setting the concentrations of organic matter to zero to assess the effect of aerobic respiration.

Figure 7.18 - Figure 7.21 present the influence of aerobic respiration on the simulation of nitrogen dynamics. Due to the high organic load in the septage treatment, the growth

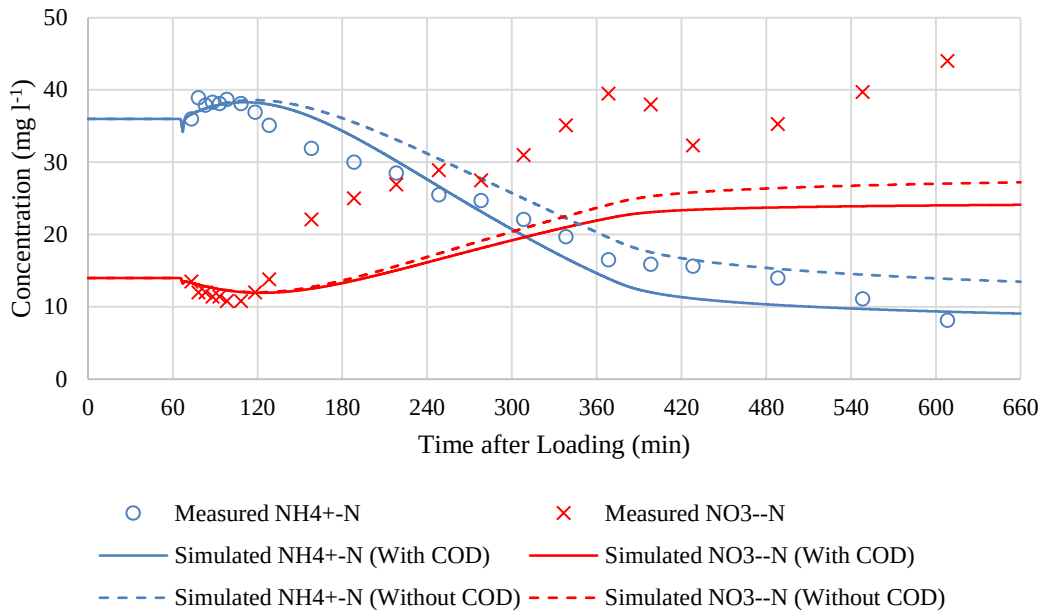

Figure 7.18: Influence of aerobic respiration on nitrogen dynamics of case 3A (1-12-2015: 75 l)

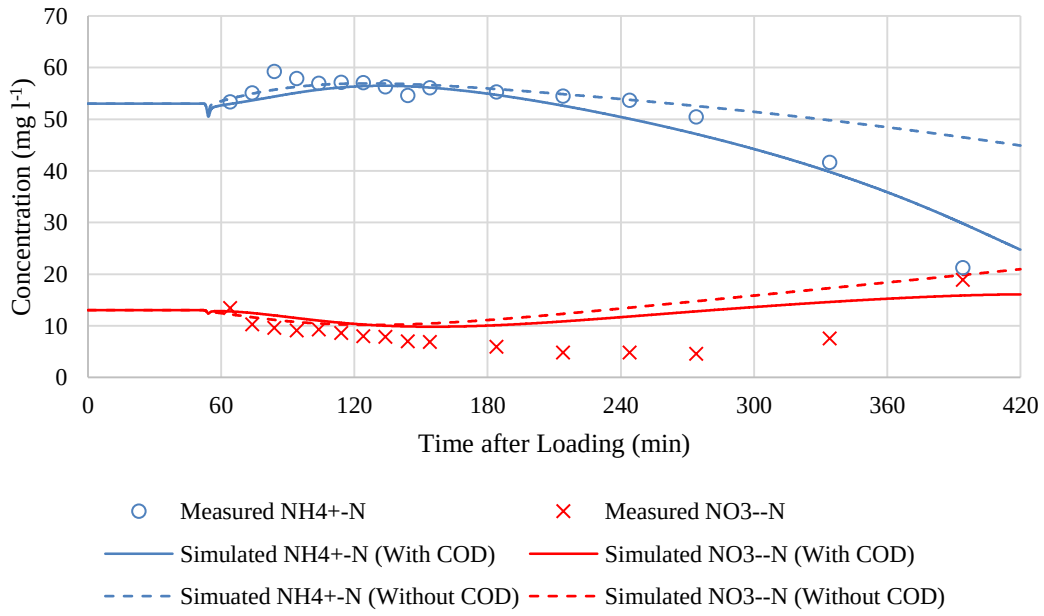

Figure 7.19: Influence of aerobic respiration on nitrogen dynamics of case 11A (27-12-2015: 100 l)

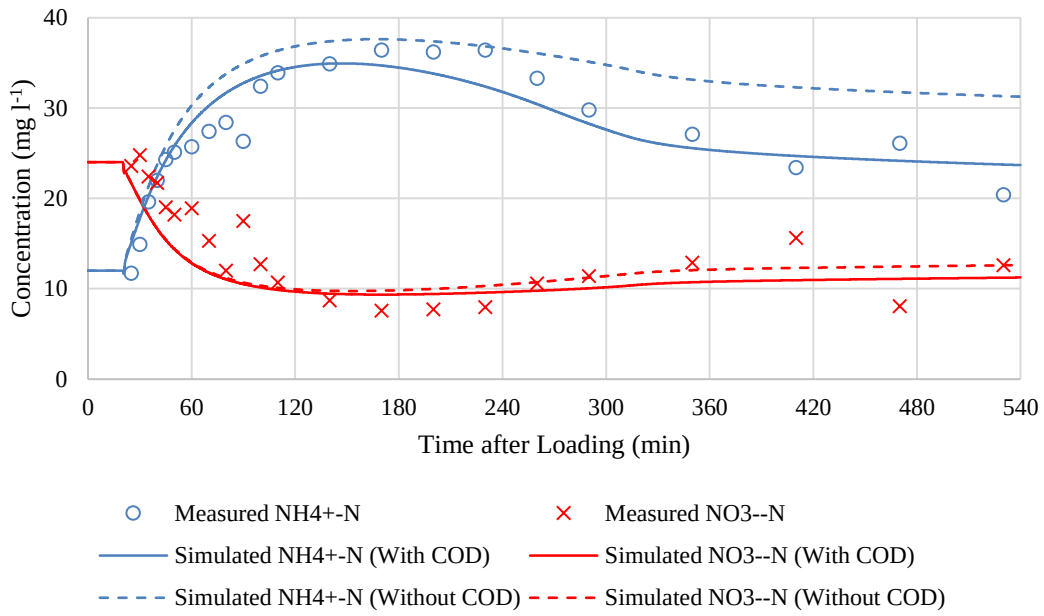

Figure 7.20: Influence of aerobic respiration on nitrogen dynamics of case 19B (24-1-2016: 125 l)

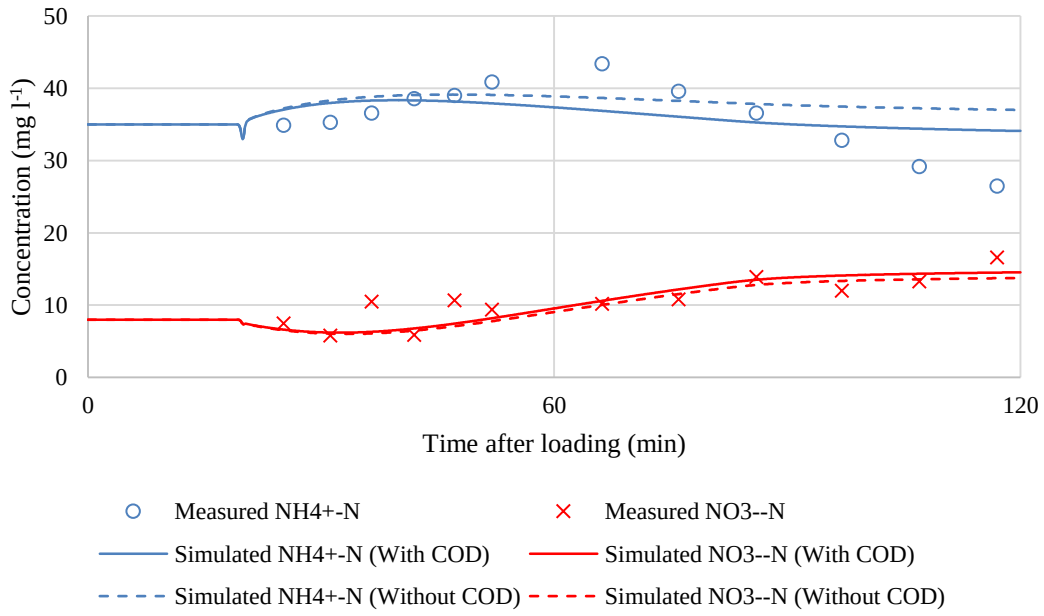

Figure 7.21: Influence of aerobic respiration on nitrogen dynamics of case 25B (27-2-2016: 50 l)

of X_H was dominant in the wetland bed. Accordingly, the demand on NH_4^+-N as a complementary nutrient was significant in the microbial growth. The simulated results demonstrated that the concentration of NH_4^+-N was over-predicted when the consideration of the organic matter was absent in the simulation. The consumption of NH_4^+-N was found to be proportional to the development of X_H, which could be observed from the gaps between the simulated results with and without aerobic respiration. In general, such a difference became more significant in the late phase of the cycle, where the growth of X_H was more notable while the rate of aerobic respiration is relatively high. When the simulation time was short, the growth of X_H was still undesirable. Then, the associated difference between the simulations was insignificant, which is as shown in Figure 7.21.

As higher NH_4^+-N concentrations were found in the simulation without the consideration of carbon cycles, the production of NO_3^--N was greater due to the better efficiency of nitrification. Although the overall contribution of this removal pathway was minor compared to nitrification and adsorption, it was still an important consideration to describe the substantial drop of NH_4^+-N in the late phase of effluent. In the proposed model, the hydrolysis of slowly degradable organic matter and the decay of active biomass potentially restored a certain amount of NH_4^+-N in the wetland bed, however, these mechanisms were insignificant since the consumption of NH_4^+-N was more vital most of the time. The current literature showed that the COD/N ratio potentially influences the overall treatment performance of the VFCWs (Fan et al. 2013). One of the main uncertainties in the simulation of COD is its fractionalization to the particulate and dissolved, as well as the biodegradable and inert matter. The calibration of the dynamics of COD and the measurement of X_H development are required in the future study to quantitatively analyse its contribution in the overall nitrogen dynamics.

Although the fate of organic matter is not the main concern in this study, the hydrolysis of X_S actually represents the ammonification process in the proposed model, subsequently acting as part of nitrogen dynamics. A first-order filtration coefficient was implemented in the transport module, and thus most of the X_S was retained at the surface of the wetland bed. Consequently, the hydrolysis mainly took place at the upper layer of wetland bed, which caused a substantial increase in the early effluent as described above. The high solids content in the raw septage emphasizes the importance

of filtration module in the modelling of VFCWs, particularly, the removal of particulate organic nitrogen (Org-N) in terms of nitrogen dynamics. In addition, the hydraulic properties of the wetland bed are reduced by the filtration, which ultimately alternates the overall treatment performance of the system. The role of plant uptake was considered to be negligibly minor in a feeding-draining cycle due to the low transpiration rate, where its influence could be more significant during the long resting period. However, a laboratory experiment with regards to the nitrogen content is needed to identify this influence in the nitrogen dynamics.

The bio-kinetic parameters used in this study were effective to simulate the nitrogen dynamics of the pilot-scale VFCW. This set of parameters were obtained from the available data in the literature (Henze et al. 1999; McBride and Tanner 1999; Langergraber and Šimůnek 2005; Fuchs 2009; Petitjean et al. 2012), and effect of temperature was considered to suit these parameters in the application under a tropical climate. The current approach only took into account the average temperature to refine the values of bio-kinetics, which could bring a certain level of discrepancy as the temperature was not always constant throughout the feeding-draining cycle. Therefore, a heat transport module should be added in future to precisely quantify the influence of temperature change. In addition, a more detailed analysis on the alkalinity in the wetland bed is necessary to determine the impact of pH change on the treatment performance of the VFCW-based septage treatment system.

7.3. Summary

With the current assumption and prescribed transport and bio-kinetics parameters, the proposed model promisingly simulated the nitrogen dynamics of the pilot-scale VFCW treating septage. The current study calibrated the parameters by matching the simulated results to the concentration of NH_4^+-N and NO_3^--N in the effluent, where the prescribed transport and bio-kinetics parameters reasonably predicted the overall nitrogen dynamics in the pilot-scale VFCW. The transport parameters were found to be 1 cm, 5 cm, 15 cm, and 25 cm for sludge deposit layer, intermediate layer, small size gravel layer, and medium size gravel layer, respectively. The adsorption coefficient was only implemented in the sludge deposit layer and the intermediate layer, which contained a certain amount of organic matter within the medium. The bio-kinetics parameters were calibrated from the available literature data. The influent

quality, hydraulic behaviour, and initial conditions were the main variables in the simulation. The biofilm was assumed to be only present in the sludge deposit layer and the intermediate layer. The simulated results showed that the MAE (%) of NH_4^+-N was generally below 10 %, but the error of NO_3-$^-$N was approximately 20 % and up to 40 % in particular case.

According to the simulation, nitrification was found to be the major removal pathways of NH_4^+-N in the pilot plant, and it was followed by adsorption and consumption by the X_H growth. Meanwhile, the NO_3^--N in the effluent was only affected by the nitrification process. The water content, oxygenation and biofilm distribution are referred to as the main influencing factors in the nitrogen dynamics. In terms of water content, a saturated condition stimulates the biological process as the contact between the contaminants and biofilm is enhanced, while the rapid flux in the VFCW system limits a complete nitrification to take place. Nitrification is a strictly aerobic process, and thus the fluctuation of oxygen content can directly result on its dynamic. As the laboratory experiment showed that DO in the effluent was always high, the proposed model assumed that DO was under a quasi-steady state, where its concentration constantly remained at 5 mg l^{-1} throughout the operation to simplify the simulation. In the proposed model, the influence of oxygen is minor when its concentration is above 5 mg l^{-1} in the expression of Monod kinetic.

The linear adsorption isotherm in VF_Sep successfully minimized the discrepancies between the measured data and simulated results of NH_4^+-N in the effluent. This process is not affected by the biofilm growth and oxygen content in the wetland bed, which generally delivers an instantaneous and consistent removal towards NH_4^+-N. Due to the high organic load in the septage treatment, the consumption of NH_4^+-N by the excessive growth of X_H was noticeable to the overall nitrogen dynamics. This mechanism was vital to accurately predict the substantial drop of NH_4^+-N in the late phase of discharge. The hydrolysis of retained X_S at the wetland surface successfully described the increase of NH_4^+-N in the early effluent. The nitrogen uptake by the vegetation was negligible in the simulation of the VFCW-based septage treatment system.

In summary, a further work is required in future studies to provide better insights to the simulation of the VFCW treating septage:

- The initial concentration of oxygen, nitrogenous constituents, and active biofilm along the wetland bed should be measured to improve the accuracy of simulation;
- An oxygen profile in the wetland bed is essential to investigate the renewal and consumption of DO during the operation and resting period;
- A water content profile should be obtained to link the treatment efficiency with saturation level;
- The distribution of active biofilm along the depth of wetland bed should be measured to validate the current assumptions in the simulation of microbial activities;
- Laboratory experiments should be carried out to determine the adsorption capacity of NH_4^+-N and active biofilm in the sludge deposit and gravel bed, where a rate-limiting adsorption should be implemented instead of linear adsorption to avoid the unlimited adsorption and biomass growth in the simulation;
- The modelling of nitrogen dynamics should be carried out simultaneously with the dynamics of organic matter. Nevertheless, the fraction of organic matter in terms of particulate and dissolved, as well as biodegradable and inert, were unclear in this study;
- The filtration in the wetland bed should be further analysed to accurately simulate the treatment performance.
- The influence of temperature and alkalinity to the bio-kinetics should be further studied to enhance the understanding of their interactions to the bio-kinetics.

Chapter 8 Conclusion and Recommendation

8.1. Summary of work

The analysis of the influence of system configurations and loading regimes in a vertical flow constructed wetland (VFCW) treating septage still remained at a "black-box" level in the literature (Jong 2014). In fact, the hydraulic behaviour of the VFCW-based septage treatment system is inconsistent due to the intermittent batch loading, subsequently leading to a highly variable treatment efficiency. However, the knowledge with regards to this behaviour is lacking in the literature, especially for the nitrogen dynamics throughout the feeding-draining cycle.

In this study, the hydraulic behaviour and the nitrogen dynamics in the first stage treatment of a pilot-scale, two-stage VFCW–based septage treatment system were investigated and simulated. The wetland bed was constructed using three layers of crushed limestone in a polyethylene tank with a surface area of 1.10 m^2 and a depth of 0.74 m. A layer of sludge deposit was formed at the top surface after two months of acclimatization. Twenty-five sets of data were obtained for the analysis of hydraulic behaviour and treatment efficiency with varying hydraulic loading rate (HLR), ranging from 50 l to 150 l per load.

A mechanistic model, which was named as VF_Sep, was developed using the simulation software MATLAB ® to numerically describe the hydraulic performance and the degradation process in the VFCW-based septage treatment system. The proposed model consisted of a variably-saturated flow module, a transport module, and a bio-kinetics module. This study aims to simulate the nitrogen dynamics in a pilot-scale VFCW system, and thus VF_Sep was only calibrated to match the concentration of NH_4^+-N and NO_3^--N in the effluent. In this chapter, the findings and significance of this study are concluded; alongside with several recommendations for further studies are listed.

8.2. Conclusion

8.2.1. Laboratory experiment

The pilot-scale VFCW-based septage treatment system was operated for twenty-five runs to investigate its hydraulic behaviour and treatment efficiency. The experimental

results revealed that the water recovery and peak effluent flux in the pilot-scale VFCW were greatly affected by the thickness of the sludge deposit layer. The retention of solids at the wetland surface forms a low-permeability layer that "regulates" the percolation rate in the wetland bed. Although the influence of hydraulic and solids load was insignificant, both of these parameters govern the accumulation rate of sludge deposit; thereby they are vital in terms of long-term operation.

During the operation, the effect of evapotranspiration (ET) was limited in the VFCW due to the short hydraulic retention time. However, this drying process could be remarkable during the resting period by forming cracks in the sludge deposit layer. Therefore, the resting period is a key feature to avoid substrate clogging, which eventually extends the lifespan of the wetland bed.

In general, the hydraulic behaviour can be categorized into "typical flow", "bypass", and "clogged" cases. The effluent flux of "typical flow" case was proportional to the level of surface ponding, while the "bypass" case showed that the effluent flux accelerated at the early phase of discharge due to the cracks created mechanically by the combined effect of wind and vegetation. The effluent flux in the "clogged" case was always slow and reduced to insignificant rate due to the over-accumulation of sludge deposit.

Overall, the pilot-scale VFCW showed a great potential in delivering a promising treatment performance for septage. According to the laboratory system, the aeration capacity of the system was remarkable, where the dissolved oxygen (DO) concentration was generally above 5 mg l^{-1}. The performance of total solids (TS) and total chemical oxygen demand (TCOD) removal was excellent, achieving an efficiency of 78 % and 89 % respectively. However, the treatment of nitrogenous constituents was relatively poor. The mean removal rate of total nitrogen (TN) was approximately 68%, while the removal of ammonium (NH_4^+-N) was less than 50 %. Nitrification was favourable in the pilot plant, and thus the concentration of nitrate (NO_3-$^-$N) generally increased in the effluent.

The continuous sampling of effluent determined the dynamics of hydraulic behaviour and nitrogen transformations in the pilot-scale VFCW-based septage treatment system. The concentration of NH_4^+-N and NO_3^--N was compared to the associated hydraulic behaviour, and the analysis highlighted that a slower effluent flux generally delivered

a better aeration efficiency and solid deposition. In addition, the treatment efficiency of TCOD, TN, and NH_4^+-N were improved. This relationship was further investigated using linear regression analysis, where the value of the coefficient of determination (R^2) was generally above 0.80 in the cases with "typical flow". Accordingly, this study has revealed the direct relationship between the hydraulic behaviour and nitrogen dynamics in the VFCW-based septage treatment system. These outcomes have filled the gaps in terms of the "black-box" in such a system.

The findings in the laboratory experiment highlight that the hydraulic control is crucial in the optimization of treatment performance in the VFCW-based septage treatment system. The treatment of nitrogenous constituents in the pilot-scale VFCW underperformed due to the rapid percolation rate. A thicker sludge deposit layer could improve the treatment performance by prolonging the hydraulic retention time. However, the consequence of substrate clogging should be considered to sustain the long-term operation of the system. Thus, an additional stage of treatment is suggested to further remove the residual NH_4^+-N and excessive NO_3^--N in the percolate from the first stage treatment.

8.2.2. Modelling of the hydraulic behaviour in the VFCW-based septage treatment system

A dual-porosity transport model was used to simulate the hydraulic behaviour in the VFCW-based septage treatment system. The Richards equation was employed to describe the variably-saturated flow in the mobile region, while the hydraulic parameters were characterized using the van Genuchten-Mualem model. The water content in the immobile region is only affected by the water exchange from the mobile region. The upper boundary condition was set to be flux-controlled to describe the intermittent loading, while it is capable of switching to head-controlled when a pond is formed at the wetland surface. Free drainage was used as the lower boundary condition. The influence of evapotranspiration (ET) and sludge accumulation were considered. The substrate profile of the pilot-scale VFCW was divided into four layers, which were the sludge deposit layer, intermittent layer, small size gravel layer, and medium size gravel layer. The hydraulic parameters were calibrated from the measured data by taking the hydraulic loading rate and thickness of the sludge deposit as variables.

Both laboratory experiment and hydraulic simulation indicated that the sludge deposit was a vital influencing factor to the hydraulic efficiency of the pilot-scale VFCW. The hydraulic conductivity of the sludge deposit layer and the initial pressure distribution showed a great impact on the accuracy of the simulation. The effluent flux was calibrated according to the hydraulic conductivity of the sludge deposit layer, which showed a dependency on the sludge deposit thickness. On the other hand, the initial pressure distribution was adjusted to match the flow occurring delay. The accumulation rate of sludge deposit was computed according to the TS concentration in the influent.

This attempt successfully reproduced the dynamics of effluent flux, where the mean absolute percentage errors (MAE (%)) and R^2 between the simulated and measured data were generally below 15 % and approximately 0.80, respectively. Besides, the majority of error was caused by the rapid deceleration of effluent flux at the late phase of discharge, and thus the cases with poor water recovery were generally accompanied with higher MAE (%).

The laboratory experiment also discovered that a certain level of raw septage was retained at the wetland surface during the late phase of treatment. Accordingly, a correction factor (CR) was added to in the simulation to refine the loading rate. This attempt was feasible to reduce the MAE (%) to approximately 10 % and improve the values of R^2. As a result, the implementation of CR derived from the water recovery percentage effectively improve the accuracy of the simulation.

Due to the short hydraulic retention time, the influence of ET was limited in the simulation. Besides, VF_Sep describes the effect of sludge accumulation by considering the increase of its thickness only, where the estimation showed that the associated effect was minor. The reduction of the porosity in the sludge deposit during loading should be further studied to improve the accuracy of the proposed model. The simulated results were compared to a commercial simulation software HYDRUS-1D, which obtained a good match for the peak effluent flux, but the flow occurring delay was slightly over-predicted.

8.2.3. Modelling of the nitrogen dynamics in the VFCW-based septage treatment system

The transport of contaminant was described using the advection-dispersion equation (ADE). The adsorption was simulated using linear isotherm. The bio-kinetics module was developed using a Gujer matrix method, which combines the stoichiometric relation, composition parameter, Monod kinetics, and temperature coefficient. Eleven components were considered in the proposed model, including DO, alkalinity, four fractions of organic matter, NH_4^+-N, NO_3^--N, nitrogen gas, heterotrophic biomass and autotrophic biomass. The processes involved in the bio-kinetics module are hydrolysis, aerobic growth of X_H, denitrification, nitrification, and lysis of X_H and X_A. The active biomass was assumed to be stationary in the sludge deposit and intermediate layers, while the adsorption was only imposed to NH_4^+-N. The slowly biodegradable and particulate inert organic matter were described to be retained at the wetland surface as a result of surface filtration. NH_4^+-N and NO_3^--N is potential to be extracted by the vegetation as a nutrient source. The influent quality and hydraulic behaviour were the variables in the simulation of contaminant transport.

The proposed model demonstrated that an accurate hydraulic simulation was a prerequisite to the modelling of nitrogen dynamics. The transport parameters and adsorption coefficient were calibrated in advance to deliver a set of prescribed parameters. The bio-kinetics parameters were obtained from the literature and were factorized to the temperature of effluent. The DO was assumed to be under a quasi-steady state at 5 mg l^{-1} throughout the simulation. The distribution of biomass was calibrated according to the measured NO_3^--N to obtain a set of prescribed biomass concentrations, which was applied to every simulation. In this context, the initial concentrations of NH_4^+-N and NO_3^--N in the wetland bed were the only parameters to be adjusted to match the measured data.

VF_Sep has been calibrated according to the measured data of the VFCW-based septage treatment system, and the overall trend of nitrogen dynamics was successfully reproduced. The MAE (%) between the measured and simulated NH_4^+-N concentration were below 10%, while the MAE (%) of NO_3^--N were relatively higher and exceeded 40 % in particular case. The high MAE (%) could be attributed to the low measured NO_3^--N in the laboratory experiment. Besides, the discrepancies of

simulated NH_4^+-N and NO_3^--N concentration were more significant at the late phase of discharge as the efficiency of nitrification was under-predicted.

According to the simulation, nitrification was found to be the most significant removing mechanism of NH_4^+-N. The efficiency of nitrification was dependent on the concentration of biomass, where the removal was more significant when the biofilm had been well-developed at the late phase of treatment. The concentration of DO greatly affected the simulation of the aerobic process, where the implementation of constant DO is feasible in describing the continuous aeration from the ventilation devices throughout the operation.

As the reduction of NH_4^+-N was generally higher than the increase of NO_3^--N in the effluent, the adsorption of NH_4^+-N in the wetland bed was referred as the second most important process in removing NH_4^+-N. The consumption of NH_4^+-N by the aerobic growth of heterotrophic biomass significantly reduced the concentration at the late phase of the discharge due to the well-developed biomass.

The ammonification process, which was lumped in the hydrolysis of slowly biodegradable organic matter, potentially increased the concentration of NH_4^+-N in the simulation. However, a further study is required to determine the nitrogen content in the total chemical oxygen demand.

Conclusively, the objectives of this thesis, including the development and calibration of a mechanistic model for the VFCW-based septage treatment system, VF_Sep, as well as the identification of the relation between hydraulic behaviour and nitrogen dynamics through the laboratory experiment and numerical simulation, have been successfully achieved. VF_Sep is an economical alternative to investigate the governing parameters of the VFCW-based septage treatment system. Several useful insights have been gained to enhance the understanding in the VFCWs treating septage, which could be helpful for its development in terms of the treatment efficiency and sustainability.

8.3. Significance of current work

A lack of design and operation guideline for the VFCW treating septage is the main reason that hindered the development of such a green technology. Koottatep et al. (2004) and Jong (2014) have established a set of basic guidelines for the design and

operation of VFCW-based septage treatment system, including the substrate profile, optimal solids loading rate (SLR) and frequency of loading. However, these assessments focused on the removal rate between the influent and effluent only, while a combined study of hydraulic behaviour and treatment performance was absent in the literature. The direct relationship between the hydraulic behaviour and the nitrogen dynamics revealed in this study has gained important insights towards the hydraulic control of the VFCW-based septage treatment system. Besides, the interactions between the hydraulic behaviour and HLR, SLR, and sludge thickness were studied, which contributes helpful information for the establishment of design and operation guideline in the future.

The development of the mechanistic model, VF_Sep, potentially revealed the "black-box" in the VFCW-based septage treatment system. The proposed model is a starting point for the research to numerically formulate the treatment processes in such a septage treatment system. VF_Sep provides a platform to simulate the hydraulic flow, contaminant transport, microbial activities, and the associated influence factors simultaneously under varying substrate profile and loading regime. The current outcome indicated that VF_Sep has a good potential to be an economical tool in designing and optimizing the configurations and operation to improve the removal of nitrogenous constituents.

In addition, the simulated results could be a set of reference to enhance the sustainability of the VFCW-based septage treatment system. As the substrate clogging is the main drawback that shortens the lifespan of the system, the hydraulic simulation of VF_Sep can be used as a reference to evaluate the hydraulic efficiency of the wetland bed under varying sludge thickness. In summary, a number of useful insights have been gained to the knowledge of the septage treatment using the VFCW, subsequently encouraging the implementation of such a system in the local area.

8.4. Recommendations for Future Work

Due to the limitation of this study, a number of further studies are required to enhance the understanding of this system to improve the efficiency and reliability of the system. These gaps of knowledge are summarized and the recommendations are suggested as follows:

- The microbial activities are the major mechanism for removing the organic matter and nitrogenous constituents. However, the understanding with regards to the amount of active biomass in the pilot-scale VFCW-based septage treatment system was limited. The measurement of attached biofilm along the substrate profile could be carried out to enhance the knowledge of the development of the microbial community throughout the operation and resting period.
- The current laboratory experiment only focused on the outflow dynamics and the associated quality. Although it delivered a simple approach to analyse the efficiency of the pilot-scale system, the interactions between contaminants, porous medium, oxygen, and active biomass along the substrate profile were not measured through the laboratory experiment. Therefore, the percolate could be sampled at a different depth of substrate to develop a profile of particular contaminant in the wetland bed, which will be helpful to understand the activities in the pilot-scale VFCW.
- A great aeration capacity was observed in the pilot-scale VFCW-based septage treatment system. This could be attributed to the intermittent loading regime and the installation of ventilation pipes in the wetland bed. However, the lack of oxygen profile hinders the analysis of the aeration capacity in the system. A further investigation on the consumption and restoration of oxygen content during the loading and resting period is necessary to fill such a research gap.
- ET is a significant dewatering mechanism in the pilot-scale VFCW during the resting period. However, its measurement was absent in this study, and thus its overall contribution to the water loss was unable to be concluded at the moment. A detail investigation on the water loss with respect to the temperature, wind effect and vegetation uptake is suggested to develop better understanding of the effect of ET.
- The accumulation of sludge deposit was found as an effective layer to enhance the hydraulic retention time and remove the particulate constituents from the influent. However, the analysis of this layer was briefly conducted in this study, where the laboratory experiments indicated that significant amount of COD and NH_4^+-N were measured. To highlight the contribution of this layer to the

overall treatment performance, a comprehensive investigation could be carried out with regards to its moisture content, accumulation rate and quality throughout the feeding-resting cycle. The same method could also be conducted to determine the influence of vegetation in the nitrogen cycle.

- A set of tracer test has been carried out by using sodium bromide as tracer in this study. However, the results were considered to be unreliable due to the poor tracer recovery. It has reflected that the salt tracer might be inappropriate to be used in the wetland system. A further study on the tracer test using dye could be carried out to provide more data with regards to the hydraulic behaviour to validate the model.
- The current version of model is only capable of simulating the hydraulic behaviour and nitrogen dynamics with free drainage, and thus it was only applied to the first stage treatment of the pilot-scale system. The application of model to the second stage treatment requires certain modification to the lower boundary condition to describe the impounding condition. In addition, such a loading regime hinders the calibration of hydraulic simulation due to the absence of outflow dynamics, and thus the measurement of moisture content at different depth of wetland bed is essential throughout the operation of second stage treatment.
- In this study, the values of the parameters, including the hydraulic parameters, initial concentration of oxygen, organic matter, nitrogenous constituents, active biofilm and alkalinity along the substrate profile were obtained from the literature or based on the calibration due to the limitation of time and budget. In order to improve the capability of the model in describing the real situations, adequate laboratory testing should be carried out to to determine the values of these parameters. The measurement of oxygen profile is important for the estimation of reaeration rate to enhance the capability of the model. In addition, the adsorption capacity of NH_4^+-N and the concentration of biofilm are necessary to be determined to improve the simulation.
- In this study, the modelling of clogging due to the sludge accumulation was at a macroscopic level. The delay of hydraulic flow was conceptualized to be affected by the sludge thickness only, while the implementation of head loss

theory such as Kozeny-Carman equation could improve the performance of the model.

- Although the cycle of organic matter were considered in the proposed model, its simulation were not carried out due to the lacking of measured data. To model the dynamics of organic matter, a comprehensive laboratory experiment could be conducted to provide sufficient measured data for the calibration.
- The modelling of filtration in the pilot-scale VFCW treating septage could be further studied to improve the simulation of retained solids.
- A heat transport module could be added to the proposed model to gain a better understanding to the influence of temperature.

References

Abboud, Nelly M. 1993. "Formation of Filter Cakes with Particle Penetration at the Filter Septum." *Particulate science and technology* 11 (3-4): 115-131.

Abboud, Nelly M, and M Yavuz Corapcioglu. 1993. "Numerical Solution and Sensitivity Analysis of Filter Cake Permeability and Resistance to Model Parameters." *Transport in porous media* 10 (3): 235-255.

Abdullahi, Abubakar Sadiq, Mohammad AminMohammad Soom, Desa Ahmad, and Abdul RashidMohamed Shariff. 2013. "Characterization of Rice (Oryza Sativa) Evapotranspiration Using Micro Paddy Lysimeter and Class" a" Pan in Tropical Environments." *Australian Journal of Crop Science* 7 (5): 650.

AECOM, SANDEC, and Eawag. 2010. *A Rapid Assessment of Septage Management in Asia : Policies and Practies in India, Indonesia, Malaysia, the Philippines, Sri Lanka, Thailand, and Vietnam*. Bangkok, Thailand: USAID

American Public Health, Association, Association American Water Works, Federation Water Pollution Control, and Federation Water Environment. 1915. *Standard Methods for the Examination of Water and Wastewater*. Vol. 2: American Public Health Association.

Babatunde, A. O., Y. Q. Zhao, M. O'Neill, and B. O'Sullivan. 2008. "Constructed Wetlands for Environmental Pollution Control: A Review of Developments, Research and Practice in Ireland." *Environment International* 34 (1): 116-126. doi: http://dx.doi.org/10.1016/j.envint.2007.06.013.

Baker, L. A. 1998. "Design Considerations and Applications for Wetland Treatment of High-Nitrate Waters." *Water Science and Technology* 38 (1): 389-395. doi: http://dx.doi.org/10.1016/S0273-1223(98)00425-9.

Bear, Jacob, and Carol Braester. 1972. "On the Flow of Two Immiscible Fluids in Fractured Porous Media" *Proc. First Int. Symp. on Fundamentals of Trans. Phen. in Porous Media*,

Białowiec, Andrzej, Antonio Albuquerque, and Peter F. Randerson. 2014. "The Influence of Evapotranspiration on Vertical Flow Subsurface Constructed

Wetland Performance." *Ecological Engineering* 67 (0): 89-94. doi: http://dx.doi.org/10.1016/j.ecoleng.2014.03.032.

Białowiec, Andrzej, Irena Wojnowska-Baryła, and Marek Agopsowicz. 2007. "The Efficiency of Evapotranspiration of Landfill Leachate in the Soil–Plant System with Willow Salix Amygdalina L." *Ecological Engineering* 30 (4): 356-361. doi: http://dx.doi.org/10.1016/j.ecoleng.2007.04.006.

Bigambo, T., and A. W. Mayo. 2005. "Nitrogen Transformation in Horizontal Subsurface Flow Constructed Wetlands Ii: Effect of Biofilm." *Physics and Chemistry of the Earth, Parts A/B/C* 30 (11–16): 668-672. doi: http://dx.doi.org/10.1016/j.pce.2005.08.006.

Boller, M. A., and M. C. Kavanaugh. 1995. "Particle Characteristics and Headloss Increase in Granular Media Filtration." *Water Research* 29 (4): 1139-1149. doi: http://dx.doi.org/10.1016/0043-1354(94)00256-7.

Borin, Maurizio, Mirco Milani, Michela Salvato, and Attilio Toscano. 2011. "Evaluation of Phragmites Australis (Cav.) Trin. Evapotranspiration in Northern and Southern Italy." *Ecological Engineering* 37 (5): 721-728. doi: http://dx.doi.org/10.1016/j.ecoleng.2010.05.003.

Bowmer, Kathleen H. 1987. "Nutrient Removal from Effluents by an Artificial Wetland: Influence of Rhizosphere Aeration and Preferential Flow Studied Using Bromide and Dye Tracers." *Water Research* 21 (5): 591-599.

Bresler, Eshel. 1973. "Simultaneous Transport of Solutes and Water under Transient Unsaturated Flow Conditions." *Water Resources Research* 9 (4): 975-986. doi: 10.1029/WR009i004p00975.

Brix, Hans. 1997. "Do Macrophytes Play a Role in Constructed Treatment Wetlands?" *Water Science and Technology* 35 (5): 11-17. doi: http://dx.doi.org/10.1016/S0273-1223(97)00047-4.

Bustillo-Lecompte, Ciro Fernando, Mehrab Mehrvar, Edgar Quiñones-Bolaños, and Claudia Fernanda Castro-Faccetti. 2016. "Modeling Organic Matter and Nitrogen Removal from Domestic Wastewater in a Pilot-Scale Vertical Subsurface Flow Constructed Wetland." *Journal of Environmental Science and Health, Part A* 51 (5): 414-424. doi: 10.1080/10934529.2015.1120528.

Carsel, Robert F., and Rudolph S. Parrish. 1988. "Developing Joint Probability Distributions of Soil Water Retention Characteristics." *Water Resources Research* 24 (5): 755-769. doi: 10.1029/WR024i005p00755.

Celia, Michael A., Efthimios T. Bouloutas, and Rebecca L. Zarba. 1990. "A General Mass-Conservative Numerical Solution for the Unsaturated Flow Equation." *Water Resources Research* 26 (7): 1483-1496. doi: 10.1029/WR026i007p01483.

Centre for Science and Environment New Delhi. 2011. *Policy Paper on Septage Management in India*. New Delhi.

Cofie, O. O., S. Agbottah, M. Strauss, H. Esseku, A. Montangero, E. Awuah, and D. Kone. 2006. "Solid–Liquid Separation of Faecal Sludge Using Drying Beds in Ghana: Implications for Nutrient Recycling in Urban Agriculture." *Water Research* 40 (1): 75-82. doi: http://dx.doi.org/10.1016/j.watres.2005.10.023.

Cooper, P. 2005. "The Performance of Vertical Flow Constructed Wetland Systems with Special Reference to the Significance of Oxygen Transfer and Hydraulic Loading Rates." *Water Science & Technology* 51 (9): 81-90.

Courant, Richard, Kurt Friedrichs, and Hans Lewy. 1928. "Über Die Partiellen Differenzengleichungen Der Mathematischen Physik." *Mathematische Annalen* 100 (1): 32-74.

Crites, Ron, and George Tchobanoglous. 1998. *Small and Decentralized Wastewater Management Systems*. New York: McGraw-Hill Book Company.

De Maeseneer, Jean L. 1997. "Constructed Wetlands for Sludge Dewatering." *Water Science and Technology* 35 (5): 279-285. doi: http://dx.doi.org/10.1016/S0273-1223(97)00080-2.

de Vasconcellos, Carlos Alexandre Bastos, and José Carlos Cesar Amorim. 2001. "Numerical Simulation of Unsaturated Flow in Porous Media Using a Mass-Conservative Model."

Delgado, J. M. P. Q. 2006. "A Critical Review of Dispersion in Packed Beds." *Heat and Mass Transfer* 42 (4): 279-310. doi: 10.1007/s00231-005-0019-0.

———. 2007. "Longitudinal and Transverse Dispersion in Porous Media." *Chemical Engineering Research and Design* 85 (9): 1245-1252. doi: 10.1205/cherd07017.

Diemont, Stewart A. W. 2006. "Mosquito Larvae Density and Pollutant Removal in Tropical Wetland Treatment Systems in Honduras." *Environment International* 32 (3): 332-341. doi: http://dx.doi.org/10.1016/j.envint.2005.07.001.

Dittmer, U., D. Meyer, and G. Langergraber. 2005. "Simulation of a Subsurface Vertical Flow Constructed Wetland for Cso Treatment." *Water Science & Technology* 51 (9): 8.

Edwards, JK, KR Gray, DJ Cooper, AJ Biddlestone, and N Willoughby. 2001. "Reed Bed Dewatering of Agricultural Sludges and Slurries." *Water science and technology* 44 (11-12): 551-558.

Fan, Jinlin, Bo Zhang, Jian Zhang, Huu Hao Ngo, Wenshan Guo, Feifei Liu, Yeye Guo, and Haiming Wu. 2013. "Intermittent Aeration Strategy to Enhance Organics and Nitrogen Removal in Subsurface Flow Constructed Wetlands." *Bioresource Technology* 141 (0): 117-122. doi: http://dx.doi.org/10.1016/j.biortech.2013.03.077.

Faulwetter, Jennifer L., Vincent Gagnon, Carina Sundberg, Florent Chazarenc, Mark D. Burr, Jacques Brisson, Anne K. Camper, and Otto R. Stein. 2009. "Microbial Processes Influencing Performance of Treatment Wetlands: A Review." *Ecological Engineering* 35 (6): 987-1004. doi: http://dx.doi.org/10.1016/j.ecoleng.2008.12.030.

Fetter, Charles Willard, and C. W. Fetter Jr. 1999. *Contaminant Hydrogeology*. Vol. 500: Prentice hall Upper Saddle River, NJ.

Foladori, P., L. Bruni, and S. Tamburini. 2015. "Bacteria Viability and Decay in Water and Soil of Vertical Subsurface Flow Constructed Wetlands." *Ecological Engineering* 82: 49-56. doi: http://dx.doi.org/10.1016/j.ecoleng.2015.04.058.

Forquet, Nicolas, Adrien Wanko, Robert Mosé, and Antoine-Georges Sadowski. 2009. "Diphasic Modelling of Vertical Flow Filter." *Ecological Engineering* 35 (1): 47-56.

Fournel, Julien, Nicolas Forquet, Pascal Molle, and Alain Grasmick. 2013. "Modeling Constructed Wetlands with Variably Saturated Vertical Subsurface-Flow for Urban Stormwater Treatment." *Ecological Engineering* 55 (0): 1-8. doi: http://dx.doi.org/10.1016/j.ecoleng.2013.02.004.

Fuchs, Valerie J. 2009. *Nitrogen Removal and Sustainability of Vertical Flow Constructed Wetlands for Small Scale Wastewater Treatment*: Michigan Technological University.

Gagnon, Vincent, Florent Chazarenc, Margit Kõiv, and Jacques Brisson. 2012. "Effect of Plant Species on Water Quality at the Outlet of a Sludge Treatment Wetland." *Water research* 46 (16): 5305-5315. http://www.sciencedirect.com/science/article/pii/S0043135412004897.

Galvão, Ana Fonseca, José Saldanha Matos, Filipa Santos Ferreira, and Francisco Nunes Correia. 2010. "Simulating Flows in Horizontal Subsurface Flow Constructed Wetlands Operating in Portugal." *Ecological Engineering* 36 (4): 596-600. doi: http://dx.doi.org/10.1016/j.ecoleng.2009.11.014.

Gerardi, Michael H. 2003. *Nitrification and Denitrification in the Activated Sludge Process*: John Wiley & Sons.

Gerke, HH, and MT van Genuchten. 1993. "A Dual - Porosity Model for Simulating the Preferential Movement of Water and Solutes in Structured Porous Media." *Water Resources Research* 29 (2): 305-319.

Gerke, Sara, Lawrence A Baker, and Ying Xu. 2001. "Nitrogen Transformations in a Wetland Receiving Lagoon Effluent: Sequential Model and Implications for Water Reuse." *Water research* 35 (16): 3857-3866. http://www.sciencedirect.com/science/article/pii/S004313540100121X.

Gersberg, RoM, BV Elkins, and CR Goldman. 1983. "Nitrogen Removal in Artificial Wetlands." *Water Research* 17 (9): 1009-1014.

Giraldi, D., M. de Michieli Vitturi, and R. Iannelli. 2010. "Fitovert: A Dynamic Numerical Model of Subsurface Vertical Flow Constructed Wetlands." *Environmental Modelling & Software* 25 (5): 633-640. doi: http://dx.doi.org/10.1016/j.envsoft.2009.05.007.

Giraldi, David, Mattia de'Michieli Vitturi, Mattia Zaramella, Andrea Marion, and Renato Iannelli. 2009. "Hydrodynamics of Vertical Subsurface Flow Constructed Wetlands: Tracer Tests with Rhodamine Wt and Numerical Modelling." *Ecological Engineering* 35 (2): 265-273. doi: http://dx.doi.org/10.1016/j.ecoleng.2008.06.004.

Giraldi, David, and Renato Iannelli. 2009. "Measurements of Water Content Distribution in Vertical Subsurface Flow Constructed Wetlands Using a Capacitance Probe: Benefits and Limitations." *Desalination* 243 (1–3): 182-194. doi: http://dx.doi.org/10.1016/j.desal.2008.05.012.

Grady Jr, CP Leslie, Glen T Daigger, Nancy G Love, and Carlos DM Filipe. 2011. *Biological Wastewater Treatment*: CRC Press.

Guan, Wei, Min Yin, Tao He, and Shuguang Xie. 2015. "Influence of Substrate Type on Microbial Community Structure in Vertical-Flow Constructed Wetland Treating Polluted River Water." *Environmental Science and Pollution Research* 22 (20): 16202-16209.

Gujer, Willi, Mogens Henze, Takahashi Mino, and Mark van Loosdrecht. 1999. "Activated Sludge Model No. 3." *Water Science and Technology* 39 (1): 183-193. doi: http://dx.doi.org/10.1016/S0273-1223(98)00785-9.

Haberl, R., S. Grego, G. Langergraber, R. H. Kadlec, A. R. Cicalini, S. Martins Dias, J. M. Novais et al. 2003. "Constructed Wetlands for the Treatment of Organic Pollutants." *JSS - J Soils & Sediments* 3 (2): 109-124. http://infoscience.epfl.ch/record/30408.

Hamersley, M. Robert, Brian L. Howes, David S. White, Susan Johnke, Dale Young, Susan B. Peterson, and John M. Teal. 2001. "Nitrogen Balance and Cycling in an Ecologically Engineered Septage Treatment System." *Ecological Engineering* 18 (1): 61-75. doi: http://dx.doi.org/10.1016/S0925-8574(01)00066-0.

Harrison, Ellen Z., and Molly Moffe. 2003. "Septage Quality and Its Effect on Field Life for Land Applications1." *JAWRA Journal of the American Water Resources Association* 39 (1): 87-97. doi: 10.1111/j.1752-1688.2003.tb01563.x.

Healy, R. W. 1990. *Simulation of Solute Transport in Variably Saturated Porous Media with Supplemental Information on Modifications to the Us Geological Survey's Computer Program Vs2d*.

Henrichs, M, A Welker, and M Uhl. 2009. "Modelling of Biofilters for Ammonium Reduction in Combined Sewer Overflow." *Water Science and Technology* 60 (3): 825.

Henze, M., W. Gujer, M. Van Loosdrecht, T. Mino, L. Blackall, Mogens Henze, Willi Gujer et al. 1999. "Modelling and Microbiology of Activated Sludge Processesactivated Sludge Model No.2d, Asm2d." *Water Science and Technology* 39 (1): 165-182. doi: http://dx.doi.org/10.1016/S0273-1223(98)00829-4.

Henze, Mogens, Willi Gujer, Takashi Mino, and M Van Loosedrecht. 2000. *Activated Sludge Models Asm1, Asm2, Asm2d and Asm3*. London.

Herouvim, Elissavet, Christos S. Akratos, Athanasia Tekerlekopoulou, and Dimitrios V. Vayenas. 2011. "Treatment of Olive Mill Wastewater in Pilot-Scale Vertical Flow Constructed Wetlands." *Ecological Engineering* 37 (6): 931-939. doi: http://dx.doi.org/10.1016/j.ecoleng.2011.01.018.

Hua, G.F., W. Zhu, L.F. Zhao, and J.Y. Huang. 2010. "Clogging Pattern in Vertical Flow Constructed Wetlands: Insight from a Laboratory Study." *Journal of Hazardous Materials* 180: 668-674. http://www.sciencedirect.com/science/article/pii/S0304389410005340.

Huang, K., B. P. Mohanty, and M. Th van Genuchten. 1996. "A New Convergence Criterion for the Modified Picard Iteration Method to Solve the Variably Saturated Flow Equation." *Journal of Hydrology* 178 (1–4): 69-91. doi: http://dx.doi.org/10.1016/0022-1694(95)02799-8.

Iwasaki, Tomihisa, JJ Slade, and Wm E Stanley. 1937. "Some Notes on Sand Filtration [with Discussion]." *Journal (American Water Works Association)*: 1591-1602.

Jong, Siaw Wee Valerie. 2014. "An Engineered Wetlands System for Septage Treatment in Malaysia."

Jong, Valerie Siaw Wee, and Fu Ee Tang. 2013. "Septage Treatment by a Two-Stage Pilot-Scale Vertical Flow Engineered Wetlands System: Organic Matters and

Nutrient Removal by Varying Operational Strategies." In *The 11th IWA Conference on Small Water & Wastewater Systems and Sludge Management, Harbin, China: Harbin Institute of Technology,* Oct 27-30.

———. 2014. "Organic Matter and Nitrogen Removal at Planted Wetlands Treating Domestic Septage with Varying Operational Strategies." *Water Science & Technology* 70 (2): 9.

———. 2015. "The Use of Palm Kernel Shell (Pks) as Substrate Material in Vertical-Flow Engineered Wetlands for Septage Treatment in Malaysia." *Water Science and Technology* 72 (1): 84-91.

Kadlec, R. H. 2009. "Comparison of Free Water and Horizontal Subsurface Treatment Wetlands." *Ecological Engineering* 35 (2): 159-174. doi: http://dx.doi.org/10.1016/j.ecoleng.2008.04.008.

Kadlec, R.H., and S. Wallace. 2008. *Treatment Wetlands, Second Edition*: Taylor & Francis.

Kadlec, Robert H. 2000. "The Inadequacy of First-Order Treatment Wetland Models." *Ecological Engineering* 15 (1–2): 105-119. doi: http://dx.doi.org/10.1016/S0925-8574(99)00039-7.

Kayser, K., and S. Kunst. 2005. "Processes in Vertical-Flow Reed Beds: Nitrification, Oxygen Transfer and Soil Clogging." *Water Science and Technology* 51 (9): 177. http://wst.iwaponline.com/content/51/9/177.abstract.

Kengne, I. M., Amougou Akoa, E. K. Soh, V. Tsama, M. M. Ngoutane, P. H. Dodane, and D. Koné. 2008. "Effects of Faecal Sludge Application on Growth Characteristics and Chemical Composition of Echinochloa Pyramidalis (Lam.) Hitch. And Chase and Cyperus Papyrus L." *Ecological Engineering* 34 (3): 233-242. doi: http://dx.doi.org/10.1016/j.ecoleng.2008.08.007.

Kengne, I. M., P. H. Dodane, Amougou Akoa, and D. Koné. 2009. "Vertical-Flow Constructed Wetlands as Sustainable Sanitation Approach for Faecal Sludge Dewatering in Developing Countries." *Desalination* 248 (1–3): 291-297. doi: http://dx.doi.org/10.1016/j.desal.2008.05.068.

Khaleel, R., and J. F. Relyea. 1997. "Correcting Laboratory - Measured Moisture Retention Data for Gravels." *Water resources research* 33 (8): 1875-1878.

Kim, B, M Gautier, P Michel, and R Gourdon. 2013. "Physical-Chemical Characterization of Sludge and Granular Materials from a Vertical Flow Constructed Wetland for Municipal Wastewater Treatment." *Water Science and Technology* 68 (10): 2257-63.

Kim, Boram, and Nicolas Forquet. 2016. "Pore-Scale Observation of Deposit within the Gravel Matrix of a Vertical Flow Constructed Wetland." *Environmental Technology*: 1-5. doi: 10.1080/09593330.2016.1178334.

Kivaisi, Amelia K. 2001. "The Potential for Constructed Wetlands for Wastewater Treatment and Reuse in Developing Countries: A Review." *Ecological Engineering* 16 (4): 545-560. doi: http://dx.doi.org/10.1016/S0925-8574(00)00113-0.

Kone, Doulaye, and Martin Strauss. 2004. "Low-Cost Options for Treating Faecal Sludges (Fs) in Developing Countries - Challenges and Performance." In *9th International IWA Specialist Group Conference on Wetlands Systems for Water Pollution Control, Avignon, France*.

Konnerup, Dennis, Thammarat Koottatep, and Hans Brix. 2009. "Treatment of Domestic Wastewater in Tropical, Subsurface Flow Constructed Wetlands Planted with Canna and Heliconia." *Ecological Engineering* 35 (2): 248-257. doi: http://dx.doi.org/10.1016/j.ecoleng.2008.04.018.

Koottatep, T., C. Polprasert, N.T.K. Oanh, U.Heinss, A. Montangero, and M.Strauss. 2001. "Septage Dewatering in Vertical-Flow Constructed Wetlands Located in the Tropics." *Water Science & Technology* 44 (2-3): 8.

Koottatep, T., N. Surinkul, C. Polprasert, ASM. Kamal, D. Koné, A. Montangero, U. Heinss, and M. Strauss. 2004. "Treatment of Septage in Constructed Wetlands in Tropical Climate–Lessons Learnt after Seven Years of Operation." *Water Science and Technology* 51 (9): 119-126.

Kresic, Neven. 2006. *Hydrogeology and Groundwater Modeling*: CRC press.

Kumar, J. L. G., and Y. Q. Zhao. 2011. "A Review on Numerous Modeling Approaches for Effective, Economical and Ecological Treatment Wetlands." *Journal of Environmental Management* 92 (3): 400-406. doi: http://dx.doi.org/10.1016/j.jenvman.2010.11.012.

Kuschk, P., A. Wießner, U. Kappelmeyer, E. Weißbrodt, M. Kästner, and U. Stottmeister. 2003. "Annual Cycle of Nitrogen Removal by a Pilot-Scale Subsurface Horizontal Flow in a Constructed Wetland under Moderate Climate." *Water Research* 37 (17): 4236-4242. doi: http://dx.doi.org/10.1016/S0043-1354(03)00163-5.

Lai, Chun-Ta, and Gabriel Katul. 2000. "The Dynamic Role of Root-Water Uptake in Coupling Potential to Actual Transpiration." *Advances in Water Resources* 23 (4): 427-439. doi: http://dx.doi.org/10.1016/S0309-1708(99)00023-8.

Langergraber, G. 2005. "The Role of Plant Uptake on the Removal of Organic Matter and Nutrients in Subsurface Flow Constructed Wetlands: A Simulation Study." *Water Science & Technology* 51 (9): 213-223.

———. 2007. "Simulation of the Treatment Performance of Outdoor Subsurface Flow Constructed Wetlands in Temperate Climates." *Science of The Total Environment* 380 (1–3): 210-219. doi: http://dx.doi.org/10.1016/j.scitotenv.2006.10.030.

———. 2008. "Modeling of Processes in Subsurface Flow Constructed Wetlands: A Review " *Vadose Zone J.* 7 (2): 830-842. doi: 10.2136/vzj2007.0054.

Langergraber, G. 2003. "Simulation of Subsurface Flow Constructed Wetlands--Results and Further Research Needs." *Water Science & Technology* 48 (5): 10.

Langergraber, G., A. Tietz, and R. Haberl. 2007. "Comparison of Measured and Simulated Distribution of Microbial Biomass in Subsurface Vertical Flow Constructed Wetlands." *Water Science and Technology* 56 (3): 233. http://wst.iwaponline.com/content/56/3/233.abstract.

Langergraber, Guenter. 2011. "Numerical Modelling: A Tool for Better Constructed Wetland Design?" *Water Science & Technology* 64 (1): 14-21.

Langergraber, Guenter, Diederik P. L. Rousseau, Joan García, and Javier Mena. 2009a. "Cwm1: A General Model to Describe Biokinetic Processes in Subsurface Flow Constructed Wetlands." *Water Science & Technology* 59 (9): 10.

Langergraber, Guenter, Diederik PL Rousseau, Joan García, and Javier Mena. 2009b. "Cwm1: A General Model to Describe Biokinetic Processes in Subsurface Flow Constructed Wetlands."

Langergraber, Günter, David Giraldi, Javier Mena, Daniel Meyer, Miguel Peña, Attilio Toscano, Alessandro Brovelli, and E. Asuman Korkusuz. 2009. "Recent Developments in Numerical Modelling of Subsurface Flow Constructed Wetlands." *Science of The Total Environment* 407 (13): 3931-3943. doi: http://dx.doi.org/10.1016/j.scitotenv.2008.07.057.

Langergraber, Günter, and Elke Muellegger. 2005. "Ecological Sanitation—a Way to Solve Global Sanitation Problems?" *Environment International* 31 (3): 433-444. doi: http://dx.doi.org/10.1016/j.envint.2004.08.006.

Langergraber, Günter, and Jirka Šimůnek. 2005. "Modeling Variably Saturated Water Flow and Multicomponent Reactive Transport in Constructed Wetlands." *Vadose Zone J.* 4 (4): 924-938. doi: 10.2136/vzj2004.0166.

———. 2006. "Cw2d."

———. 2012. "Reactive Transport Modeling of Subsurface Flow Constructed Wetlands Using the Hydrus Wetland Module." *gsvadzone* 11 (2): -. doi: 10.2136/vzj2011.0104.

Larsen, E., and M. Greenway. 2004. "Quantification of Biofilms in a Sub-Surface Flow Wetland and Their Role in Nutrient Removal." *Water Science and Technology* 49 (11-12): 115. http://wst.iwaponline.com/content/49/11-12/115.abstract.

Lau, Hieng Ung. 2012. "Sewerage in Sarawak: The Future Development." Sewerage Services Deaparment Sarawak.

Lavrova, Silviya, and Bogdana Koumanova. 2010. "Influence of Recirculation in a Lab-Scale Vertical Flow Constructed Wetland on the Treatment Efficiency of Landfill Leachate." *Bioresource technology* 101 (6): 1756-1761. http://www.sciencedirect.com/science/article/pii/S0960852409014047.

Lee, Byoung-Hwa, and Miklas Scholz. 2007. "What Is the Role of< I> Phragmites Australis</I> in Experimental Constructed Wetland Filters Treating Urban Runoff?" *Ecological Engineering* 29 (1): 87-95.

Lee, Chang - gyun, Tim D Fletcher, and Guangzhi Sun. 2009. "Nitrogen Removal in Constructed Wetland Systems." *Engineering in Life Sciences* 9 (1): 11-22.

Levy, B. S., and R. M. Chambers. 1987. "Bromide as a Conservative Tracer for Soil-Water Studies." *Hydrological Processes* 1 (4): 385-389. doi: 10.1002/hyp.3360010406.

Li, KY, JB Boisvert, and R De Jong. 1999. "An Exponential Root-Water-Uptake Model." *Canadian Journal of soil science* 79 (2): 333-343.

Liénard, A, Ph Duchène, and D Gorini. 1995. "A Study of Activated Sludge Dewatering in Experimental Reed-Planted or Unplanted Sludge Drying Beds." *Water Science and Technology* 32 (3): 251-261.

Lienard, Alain, and Francois Payrastre. 1996. "Treatment of Sludge from Septic Tanks in a Reed-Bed Filters Pilot Plant." In *5th international conference on wetland systems for water pollution control, Vienna: Austria*.

Liu, Lei, Xinhua Zhao, Nan Zhao, Zheng Shen, Mei Wang, Yuzhang Guo, and Yinbo Xu. 2013. "Effect of Aeration Modes and Influent Cod/N Ratios on the Nitrogen Removal Performance of Vertical Flow Constructed Wetland." *Ecological Engineering* 57: 10-16. doi: http://dx.doi.org/10.1016/j.ecoleng.2013.04.019.

Liu, Wenxin, Mohamed F. Dahad, and Rao Y. Surampali. 2005. "Nitrogen Transformations Modeling in Subsurface-Flow Constructed Wetlands." *Water Environment Research* 77 (3): 13. http://search.proquest.com.dbgw.lis.curtin.edu.au/docview/216067928?accountid=10382.

Llorens, Esther, Maarten W. Saaltink, and Joan García. 2011. "Cwm1 Implementation in Retrasocodebright: First Results Using Horizontal Subsurface Flow Constructed Wetland Data." *Chemical Engineering Journal* 166 (1): 224-232. doi: http://dx.doi.org/10.1016/j.cej.2010.10.065.

Maier, Uli, Cecilia DeBiase, Oliver Baeder-Bederski, and Peter Bayer. 2009. "Calibration of Hydraulic Parameters for Large-Scale Vertical Flow Constructed Wetlands." *Journal of Hydrology* 369 (3–4): 260-273. doi: http://dx.doi.org/10.1016/j.jhydrol.2009.02.032.

Marsili-Libelli, Stefano, and Nicola Checchi. 2005. "Identification of Dynamic Models for Horizontal Subsurface Constructed Wetlands." *Ecological Modelling* 187 (2–3): 201-218. doi: http://dx.doi.org/10.1016/j.ecolmodel.2005.01.043.

Martin, Jay F, and KR Reddy. 1997. "Interaction and Spatial Distribution of Wetland Nitrogen Processes." *Ecological Modelling* 105 (1): 1-21.

Maynard, DG, and YP Kalra. 1993. "Nitrate and Exchangeable Ammonium Nitrogen." *Soil sampling and methods of analysis* 1.

Mayo, A. W., and T. Bigambo. 2005. "Nitrogen Transformation in Horizontal Subsurface Flow Constructed Wetlands I: Model Development." *Physics and Chemistry of the Earth, Parts A/B/C* 30 (11–16): 658-667. doi: http://dx.doi.org/10.1016/j.pce.2005.08.005.

Mburu, Njenga, David Sanchez-Ramos, Diederik P. L. Rousseau, Johan J. A. van Bruggen, George Thumbi, Otto R. Stein, Paul B. Hook, and Piet N. L. Lens. 2012. "Simulation of Carbon, Nitrogen and Sulphur Conversion in Batch-Operated Experimental Wetland Mesocosms." *Ecological Engineering* 42 (0): 304-315. doi: http://dx.doi.org/10.1016/j.ecoleng.2012.02.003.

McBride, Graham B., and Chris C. Tanner. 1999. "Modelling Biofilm Nitrogen Transformations in Constructed Wetland Mesocosms with Fluctuating Water Levels." *Ecological Engineering* 14 (1–2): 93-106. doi: http://dx.doi.org/10.1016/S0925-8574(99)00022-1.

McGechan, M. B., S. E. Moir, K. Castle, and I. P. J. Smit. 2005. "Modelling Oxygen Transport in a Reedbed-Constructed Wetland Purification System for Dilute Effluents." *Biosystems Engineering* 91 (2): 191-200. doi: http://dx.doi.org/10.1016/j.biosystemseng.2004.12.009.

McGechan, M. B., S. E. Moir, G. Sym, and K. Castle. 2005. "Estimating Inorganic and Organic Nitrogen Transformation Rates in a Model of a Constructed

Wetland Purification System for Dilute Farm Effluents." *Biosystems Engineering* 91 (1): 61-75. doi: http://dx.doi.org/10.1016/j.biosystemseng.2004.12.010.

Meiri, David. 1989. "A Tracer Test for Detecting Cross Contamination Along a Monitoring Well Column." *Groundwater Monitoring & Remediation* 9 (2): 78-81.

Method 8163. 2012. HACH COMPANY, U.S.A

Meyer, Daniel, Florent Chazarenc, Dominique Claveau-Mallet, Ulrich Dittmer, Nicolas Forquet, Pascal Molle, Ania Morvannou et al. 2015. "Modelling Constructed Wetlands: Scopes and Aims – a Comparative Review." *Ecological Engineering* 80: 205-213. doi: http://dx.doi.org/10.1016/j.ecoleng.2014.10.031.

Meyer, Daniel, and Ulrich Dittmer. 2015. "Rsf_Sim – a Simulation Tool to Support the Design of Constructed Wetlands for Combined Sewer Overflow Treatment." *Ecological Engineering* 80: 198-204. doi: http://dx.doi.org/10.1016/j.ecoleng.2014.10.032.

Milani, M., and A. Toscano. 2013. "Evapotranspiration from Pilot-Scale Constructed Wetlands Planted with Phragmites Australis in a Mediterranean Environment." *Journal of Environmental Science and Health, Part A* 48 (1532-4117 (Electronic)): 568-580.

Molle, P, A Linard, C Boutin, G Merlin, and A Iwema. 2005. "How to Treat Raw Sewage with Constructed Wetlands: An Overview of the French Systems." *Water Science & Technology* 51 (9): 11-21.

Molle, P. 2014. "French Vertical Flow Constructed Wetlands: A Need of a Better Understanding of the Role of the Deposit Layer." *Water Science & Technology* 69 (1).

Molle, P., A. Liénard, A. Grasmick, and A. Iwema. 2006. "Effect of Reeds and Feeding Operations on Hydraulic Behaviour of Vertical Flow Constructed Wetlands under Hydraulic Overloads." *Water Research* 40 (3): 606-612. doi: http://dx.doi.org/10.1016/j.watres.2005.11.026.

Morvannou, A., N. Forquet, M. Vanclooster, and P. Molle. 2013a. "Characterizing Hydraulic Properties of Filter Material of a Vertical Flow Constructed Wetland." *Ecological Engineering* 60: 325-335. doi: http://dx.doi.org/10.1016/j.ecoleng.2013.06.042.

Morvannou, Ania, Jean-Marc Choubert, Marnik Vanclooster, and Pascal Molle. 2011. "Solid Respirometry to Characterize Nitrification Kinetics: A Better Insight for Modelling Nitrogen Conversion in Vertical Flow Constructed Wetlands." *Water Research* 45 (16): 4995-5004. doi: http://dx.doi.org/10.1016/j.watres.2011.07.004.

———. 2014. "Modeling Nitrogen Removal in a Vertical Flow Constructed Wetland Treating Directly Domestic Wastewater." *Ecological Engineering* 70: 379-386. doi: http://dx.doi.org/10.1016/j.ecoleng.2014.06.034.

Morvannou, Ania, Nicolas Forquet, Marnik Vanclooster, and Pascal Molle. 2013b. "Which Hydraulic Model to Use for Vertical Flow Constructed Wetlands?" In *4th International Conference HYDRUS Software Application to Subsurface Flow and Contaminant Transport Problems, Prague: Czech Republic,* 21-22 March.

Mualem, Yechezkel. 1976. "A New Model for Predicting the Hydraulic Conductivity of Unsaturated Porous Media." *Water Resources Research* 12 (3): 513-522. doi: 10.1029/WR012i003p00513.

Nielsen, D. R., M. Th. Van Genuchten, and J. W. Biggar. 1986. "Water Flow and Solute Transport Processes in the Unsaturated Zone." *Water Resources Research* 22 (9S): 89S-108S. doi: 10.1029/WR022i09Sp0089S.

O'Connor, Donald J, and William E Dobbins. 1958. "Mechanism of Reaeration in Natural Streams." *Transactions of the American Society of Civil Engineers* 123 (1): 641-666.

Ojeda, Esther, Joan Caldentey, Maarten W. Saaltink, and Joan García. 2008. "Evaluation of Relative Importance of Different Microbial Reactions on Organic Matter Removal in Horizontal Subsurface-Flow Constructed Wetlands Using a 2d Simulation Model." *Ecological Engineering* 34 (1): 65-75. doi: http://dx.doi.org/10.1016/j.ecoleng.2008.05.007.

Olivella, Sebastià, A Gens, J Carrera, and EE Alonso. 1996. "Numerical Formulation for a Simulator (Code_Bright) for the Coupled Analysis of Saline Media." *Engineering computations* 13 (7): 87-112.

Ouyang, Y., S. M. Luo, and L. H. Cui. 2011. "Estimation of Nitrogen Dynamics in a Vertical-Flow Constructed Wetland." *Ecological Engineering* 37 (3): 453-459. doi: http://dx.doi.org/10.1016/j.ecoleng.2010.11.008.

Ouyang, Ying, ShiMing Luo, LiHua Cui, YingHu Liu, and Zhong Qin. 2010. "Estimation of Water Dynamics in a Vertical-Flow Constructed Wetland with a Growing Plant Species." *Journal of Soils and Sediments* 10 (7): 1219-1228. doi: 10.1007/s11368-010-0240-4.

Paing, J., and J. Voisin. 2005. "Vertical Flow Constructed Wetlands for Municipal Wastewater and Septage Treatment in French Rural Area." *Water Science & Technology;* 51 (9): 11.

Pálfy, T. G., P. Molle, G. Langergraber, S. Troesch, R. Gourdon, and D. Meyer. 2016. "Simulation of Constructed Wetlands Treating Combined Sewer Overflow Using Hydrus/Cw2d." *Ecological Engineering* 87: 340-347. doi: http://dx.doi.org/10.1016/j.ecoleng.2015.11.048.

Panuvatvanich, Atitaya, Thammarat Koottatep, and Doulaye Koné. 2009. "Hydraulic Behaviour of Vertical - Flow Constructed Wetland under Different Operating Conditions." *Environmental Technology* 30 (10): 1031-1040. doi: 10.1080/09593330903051667.

Petitjean, A., N. Forquet, A. Wanko, J. Laurent, P. Molle, R. Mosé, and A. Sadowski. 2012. "Modelling Aerobic Biodegradation in Vertical Flow Sand Filters: Impact of Operational Considerations on Oxygen Transfer and Bacterial Activity." *Water Research* 46 (7): 2270-2280. doi: http://dx.doi.org/10.1016/j.watres.2012.01.054.

Platzer, Christoph. 1999. "Design Recommendations for Subsurface Flow Constructed Wetlands for Nitrification and Denitrification." *Water Science and Technology* 40 (3): 257-263. doi: http://dx.doi.org/10.1016/S0273-1223(99)00420-5.

Rajabzadeh, Amin Reza, Raymond L. Legge, and Kela P. Weber. 2015. "Multiphysics Modelling of Flow Dynamics, Biofilm Development and Wastewater

Treatment in a Subsurface Vertical Flow Constructed Wetland Mesocosm." *Ecological Engineering* 74: 107-116. doi: http://dx.doi.org/10.1016/j.ecoleng.2014.09.122.

Richards, L. A. 1931. "Capillary Conduction of Liquids through Porous Mediums." *Journal of Applied Physics* 1 (5): 318-333. doi: doi:http://dx.doi.org/10.1063/1.1745010.

Robertson, GP, and PM Groffman. 2007. "Nitrogen Transformations." *Soil microbiology, ecology, and biochemistry*: 341-364.

Rousseau, Diederik. 2005. "Performance of Constructed Treatment Wetlands: Model-Based Evaluation and Impact of Operation and Maintenance." Ghent University.

Saaltink, M.W., F. Batlle, C. Ayora, J. Carrera, and S. Olivella. 2004. "Retraso, a Code for Modelling Reactive Transport in Saturated and Unsaturated Porous Media." *Geologica Acta* 2 (3): 235-251.

Saaltink, Maarten W, Carlos Ayora, Pieter J Stuyfzand, and Harrie Timmer. 2003. "Analysis of a Deep Well Recharge Experiment by Calibrating a Reactive Transport Model with Field Data." *Journal of contaminant hydrology* 65 (1): 1-18.

Saeed, Tanveer, and Guangzhi Sun. 2011a. "A Comparative Study on the Removal of Nutrients and Organic Matter in Wetland Reactors Employing Organic Media." *Chemical Engineering Journal* 171 (2): 439-447. doi: http://dx.doi.org/10.1016/j.cej.2011.03.101.

———. 2011b. "Kinetic Modelling of Nitrogen and Organics Removal in Vertical and Horizontal Flow Wetlands." *Water Research* 45 (10): 3137-3152. doi: http://dx.doi.org/10.1016/j.watres.2011.03.031.

Samsó, Roger, and Joan Garcia. 2013. "Bio_Pore, a Mathematical Model to Simulate Biofilm Growth and Water Quality Improvement in Porous Media: Application and Calibration for Constructed Wetlands." *Ecological Engineering* 54 (0): 116-127. doi: http://dx.doi.org/10.1016/j.ecoleng.2013.01.021.

Samsó, Roger, and Joan García. 2014. "The Cartridge Theory: A Description of the Functioning of Horizontal Subsurface Flow Constructed Wetlands for

Wastewater Treatment, Based on Modelling Results." *Science of The Total Environment* 473–474 (0): 651-658. doi: http://dx.doi.org/10.1016/j.scitotenv.2013.12.070.

Šejna, M, and J Šimůnek. 2007. "Hydrus (2d/3d): Graphical User Interface for the Hydrus Software Package Simulating Two-and Three-Dimensional Movement of Water, Heat, and Multiple Solutes in Variably-Saturated Media." *Available at www. pc-progress. cz (verified 20 Feb. 2008). PC-Progress, Prague, Czech Republic*.

Shutes, R. B. E. 2001. "Artificial Wetlands and Water Quality Improvement." *Environment International* 26 (5–6): 441-447. doi: http://dx.doi.org/10.1016/S0160-4120(01)00025-3.

Sim, Cheng Hua. 2003. *The Use of Constructed Wetlands for Wastewater Treatment*. Selangor, Malaysia: Wetlands International - Malaysia Office.

Simunek, J, M Th Van Genuchten, and M Sejna. 2005. "The Hydrus-1d Software Package for Simulating the One-Dimensional Movement of Water, Heat, and Multiple Solutes in Variably-Saturated Media." *University of California-Riverside Research Reports* 3: 1-240.

Šimunek, J, M Th van Genuchten, and M Sejna. 1997. "The Hydrus-1d Software Package for Simulating the Movement of Water." *Heat, and Multiple Solutes in Variably Saturated Media, Version* 3.

Šimůnek, Jirka. 2005. "Models of Water Flow and Solute Transport in the Unsaturated Zone." *Encyclopedia of hydrological sciences*.

Šimůnek, Jirka, Nick J Jarvis, M Th Van Genuchten, and Annemieke Gärdenäs. 2003. "Review and Comparison of Models for Describing Non-Equilibrium and Preferential Flow and Transport in the Vadose Zone." *Journal of Hydrology* 272 (1): 14-35.

Šimůnek, Jirka, and Martinus Th van Genuchten. 2008. "Modeling Nonequilibrium Flow and Transport Processes Using Hydrus." *Vadose Zone Journal* 7 (2): 782-797.

Siracusa, G, and AD La Rosa. 2006. "Design of a Constructed Wetland for Wastewater Treatment in a Sicilian Town and Environmental Evaluation Using the Emergy Analysis." *ecological modelling* 197 (3): 490-497.

Stefanakis, Alexandros I., and Vassilios A. Tsihrintzis. 2011. "Dewatering Mechanisms in Pilot-Scale Sludge Drying Reed Beds: Effect of Design and Operational Parameters." *Chemical Engineering Journal* 172 (1): 430-443. doi: http://dx.doi.org/10.1016/j.cej.2011.05.111.

———. 2012. "Effects of Loading, Resting Period, Temperature, Porous Media, Vegetation and Aeration on Performance of Pilot-Scale Vertical Flow Constructed Wetlands." *Chemical engineering journal* 181: 416-430.

Stottmeister, U., A. Wießner, P. Kuschk, U. Kappelmeyer, M. Kästner, O. Bederski, R. A. Müller, and H. Moormann. 2003. "Effects of Plants and Microorganisms in Constructed Wetlands for Wastewater Treatment." *Biotechnology Advances* 22 (1–2): 93-117. doi: http://dx.doi.org/10.1016/j.biotechadv.2003.08.010.

Strauss, M., S. A. Larmie, and U. Heinss. 1997. "Treatment of Sludges from on-Site Sanitation — Low-Cost Options." *Water Science and Technology* 35 (6): 129-136. doi: http://dx.doi.org/10.1016/S0273-1223(97)00103-0.

Strauss, Martin. 2006. "Urban Excreta Management-Situation, Challenges, and Promising Solutions" *IWA Asia-Pacific Regional Conference, Dakar: Senagal,*

Tan, Yee Yong, Fu Ee Tang, Agus Saptoro, and Ee Huey Khor. 2015. "Septage Treatment Using Vertical-Flow Engineered Wetland: A Critical Review." *Chemical Engineering Transaction* 45.

Tchobanoglous, G., F.L. Burton, H.D. Stensel, Metcalf, and Eddy. 2003. *Wastewater Engineering: Treatment and Reuse*: McGraw-Hill Education.

Tietz, Alexandra, Alexander Kirschner, Günter Langergraber, Kirsten Sleytr, and Raimund Haberl. 2007. "Characterisation of Microbial Biocoenosis in Vertical Subsurface Flow Constructed Wetlands." *Science of The Total Environment* 380 (1–3): 163-172. doi: http://dx.doi.org/10.1016/j.scitotenv.2006.11.034.

Torrens, Antonina, Pascal Molle, Catherine Boutin, and Miquel Salgot. 2009. "Impact of Design and Operation Variables on the Performance of Vertical-Flow Constructed Wetlands and Intermittent Sand Filters Treating Pond Effluent."

Water Research 43 (7): 1851-1858. doi: http://dx.doi.org/10.1016/j.watres.2009.01.023.

Toscano, Attilio, Günter Langergraber, Simona Consoli, and Giuseppe L. Cirelli. 2009. "Modelling Pollutant Removal in a Pilot-Scale Two-Stage Subsurface Flow Constructed Wetlands." *Ecological Engineering* 35 (2): 281-289. doi: http://dx.doi.org/10.1016/j.ecoleng.2008.07.011.

Troesch, S., A. Liénard, P. Molle, G. Merlin, and D. Esser. 2009. "Treatment of Septage in Sludge Drying Reed Beds: A Case Study on Pilot-Scale Beds." *Water Science & Technology* 60 (3): 11. doi: 10.2166/wst.2009.389.

Troesch, S., A. Lienard, P. Molle, G. Merlin, and D. Esser. 2009. "Treatment of Septage in Sludge Drying Reed Beds: A Case Study on Pilot-Scale Beds." *Water Science and Technology* 60 (3): 643-653.

Tunçsiper, B. 2009. "Nitrogen Removal in a Combined Vertical and Horizontal Subsurface-Flow Constructed Wetland System." *Desalination* 247 (1–3): 466-475. doi: http://dx.doi.org/10.1016/j.desal.2009.03.003.

United States Environmental Protection Agency. 1999a. *Manual: Constructed Wetlands Treatment of Municipal Wastewater*. Cincinnati, Ohio 45268: National Risk Management Research Laboratory, Office of Research and Development, U. S. Environmental Protection Agency.

———. 1999b. *Septage Treatment/Disposal*. Washington, D.C., United States.

Van Cappellen, Philippe, and Jean-Francois Gaillard. 1996. "Biogeochemical Dynamics in Aquatic Sediments." *Reviews in mineralogy and geochemistry* 34 (1): 335-376.

Van Genuchten, M. Th, F. J. Leij, and S. R. Yates. 1991. *The Retc Code for Quantifying the Hydraulic Functions of Unsaturated Soils*: Citeseer.

van Genuchten, M. Th. 1980. "A Closed-Form Equation for Predicting the Hydraulic Conductivity of Unsaturated Soils1." *Soil Sci. Soc. Am. J.* 44 (5): 892-898. doi: 10.2136/sssaj1980.03615995004400050002x.

Varado, N., I. Braud, and P. J. Ross. 2006. "Development and Assessment of an Efficient Vadose Zone Module Solving the 1d Richards' Equation and

Including Root Extraction by Plants." *Journal of Hydrology* 323 (1–4): 258-275. doi: http://dx.doi.org/10.1016/j.jhydrol.2005.09.015.

Verhoeven, Jos T. A., and Arthur F. M. Meuleman. 1999. "Wetlands for Wastewater Treatment: Opportunities and Limitations." *Ecological Engineering* 12 (1–2): 5-12. doi: http://dx.doi.org/10.1016/S0925-8574(98)00050-0.

Vincent, J., P. Molle, C. Wisniewski, and A. Liénard. 2011. "Sludge Drying Reed Beds for Septage Treatment: Towards Design and Operation Recommendations." *Bioresource Technology* 102 (17): 8327-8330. doi: http://dx.doi.org/10.1016/j.biortech.2011.06.019.

Von Sperling, Marcos. 2007. "Activated Sludge and Aerobic Biofilm Reactors." *Water Intelligence Online* 6: 9781780402123.

Vymazal, Jan. 2007. "Removal of Nutrients in Various Types of Constructed Wetlands." *Science of The Total Environment* 380 (1–3): 48-65. doi: http://dx.doi.org/10.1016/j.scitotenv.2006.09.014.

———. 2010a. "Constructed Wetlands for Wastewater Treatment." *Water* 2 (3): 530-549. http://www.mdpi.com/2073-4441/2/3/530.

———. 2010b. "Constructed Wetlands for Wastewater Treatment: Five Decades of Experience†." *Environmental Science & Technology* 45 (1): 61-69. doi: 10.1021/es101403q.

Vymazal, Jan, and Lenka Kröpfelová. 2009. "Removal of Organics in Constructed Wetlands with Horizontal Sub-Surface Flow: A Review of the Field Experience." *Science of The Total Environment* 407 (13): 3911-3922. doi: http://dx.doi.org/10.1016/j.scitotenv.2008.08.032.

Wallace, Scott, and David Austin. 2008. "Emerging Models for Nitrogen Removal in Treatment Wetlands." *Journal of environmental health* 71 (4): 10-16.

Wang, Yanhua, Jixiang Zhang, Hainan Kong, Yuhei Inamori, Kaiqin Xu, Ryuhei Inamori, and Takashi Kondo. 2009. "A Simulation Model of Nitrogen Transformation in Reed Constructed Wetlands." *Desalination* 235 (1–3): 93-101. doi: http://dx.doi.org/10.1016/j.desal.2008.01.012.

Wanko, A., R. Mose, J. Carrayrou, and A. G. Sadowski. 2006. "Simulation of Biodegradation in Infiltration Seepage— Model Development and Hydrodynamic Calibration." *Water, Air, and Soil Pollution* 177 (1-4): 19-43. doi: 10.1007/s11270-005-9046-1.

Water Environment Federation, Biological Nutrient Removal Operation in Wastewater Treatment Plants Task Force, Water Environment Federation, and Environmental and Water Resources Institute. 2005. *Biological Nutrient Removal (Bnr) Operation in Wastewater Treatment Plants : Wef Manual of Practice No. 30: Wef Manual of Practice*: McGraw-Hill Education.

Weather Underground. 2016. Historical Weather. Accessed 3rd June, https://www.wunderground.com/history/.

WHO. 2006. *Guidelines for the Safe Use of Wastewater, Excreta and Greywater: Policy and Regulatory Aspects*. Vol. 1: World Health Organization.

Winter, K-J, and D Goetz. 2003. "The Impact of Sewage Composition on the Soil Clogging Phenomena of Vertical Flow Constructed Wetlands." *Water Science and Technology* 48 (5): 9-14.

Woźniak, R., U. Dittmer, and A. Welker. 2007. "Interaction of Oxygen Concentration and Retention of Pollutants in Vertical Flow Constructed Wetlands for Cso Treatment." *Water Science and Technology* 56 (3): 31-38. http://wst.iwaponline.com/content/56/3/31.abstract.

Wynn, Theresa Maria, and Sarah K. Liehr. 2001. "Development of a Constructed Subsurface-Flow Wetland Simulation Model." *Ecological Engineering* 16 (4): 519-536. doi: http://dx.doi.org/10.1016/S0925-8574(00)00115-4.

Xu, Qiaoling, Lihua Cui, Ling Zhang, Zixia Li, and Guangwei Yu. 2013. "The Effect of Two Factor Combination of Three Kinds of Loading on the Soil Clogging in Vertical Flow Constructed Wetland." *Frontier of Environmental Science* 2 (4).

Yalcuk, Arda, and Aysenur Ugurlu. 2009. "Comparison of Horizontal and Vertical Constructed Wetland Systems for Landfill Leachate Treatment." *Bioresource Technology* 100 (9): 2521-2526. doi: http://dx.doi.org/10.1016/j.biortech.2008.11.029.

Yang, Lei, Hui-Ting Chang, and Mong-Na Lo Huang. 2001. "Nutrient Removal in Gravel- and Soil-Based Wetland Microcosms with and without Vegetation." *Ecological Engineering* 18 (1): 91-105. doi: http://dx.doi.org/10.1016/S0925-8574(01)00068-4.

Zhang, Dong Qing, Soon Keat Tan, Richard M. Gersberg, Junfei Zhu, Sara Sadreddini, and Yifei Li. 2012. "Nutrient Removal in Tropical Subsurface Flow Constructed Wetlands under Batch and Continuous Flow Conditions." *Journal of Environmental Management* 96 (1): 1-6. doi: http://dx.doi.org/10.1016/j.jenvman.2011.10.009.

Zhang, Shiyang, Gu Li, Xiaoli Li, and Ling Tao. 2015. "Multiple Linear Modeling of Outflow Nitrogen Dynamics in Vertical-Flow Constructed Wetlands under Two Different Operating States." *Ecological Engineering* 81: 53-61. doi: http://dx.doi.org/10.1016/j.ecoleng.2015.04.028.

Zhang, Ting, Dong Xu, Feng He, Yongyuan Zhang, and Zhenbin Wu. 2012. "Application of Constructed Wetland for Water Pollution Control in China During 1990–2010." *Ecological Engineering* 47 (0): 189-197. doi: http://dx.doi.org/10.1016/j.ecoleng.2012.06.022.

Zhao, YQ, Guangzhi Sun, and SJ Allen. 2004. "Anti-Sized Reed Bed System for Animal Wastewater Treatment: A Comparative Study." *Water Research* 38 (12): 2907-2917. http://www.sciencedirect.com/science/article/pii/S0043135404001745.

Zhou, Qiaohong, Feng He, Zhang Liping, Yanfen Wang, and Zhenbin Wu. 2009. "Characteristics of the Microbial Communities in the Integrated Vertical-Flow Constructed Wetlands." *Journal of Environmental Sciences* 21 (9): 1261-1267. doi: http://dx.doi.org/10.1016/S1001-0742(08)62413-4.

Zotarelli, Lincoln, Michael D Dukes, Consuelo C Romero, Kati W Migliaccio, and Kelly T Morgan. 2010. "Step by Step Calculation of the Penman-Monteith Evapotranspiration (Fao-56 Method)." *Institute of Food and Agricultural Sciences. University of Florida (2010).*

Zurita, F., J. De Anda, and M. A. Belmont. 2009. "Treatment of Domestic Wastewater and Production of Commercial Flowers in Vertical and Horizontal Subsurface-

Flow Constructed Wetlands." *Ecological Engineering* 35 (5): 861-869. doi: http://dx.doi.org/10.1016/j.ecoleng.2008.12.026.

Appendices

Appendix A: Penman-Monteith Equation – Detail Calculation (Zotarelli et al. 2010)

$$ET_o = \frac{1}{\lambda}\left[\frac{\Delta \cdot (R_n - G) + \rho_a \cdot C_p \cdot \left(\frac{e_s - e_a}{r_a}\right)}{\Delta + \gamma\left(1 + \frac{r_c}{r_a}\right)}\right] \quad \text{(A.1)}$$

where ET = potential evapotranspiration rate (mm d^{-1})

ET_{rad} = radiation term (mm d^{-1})

ET_{aero} = aerodynamic term (mm d^{-1})

λ = latent heat of vaporization (=2.45 MJ kg^{-1})

R_n = net radiation at surface (MJ m^{-2} d^{-1}) [refer to equation A.2]

G = soil heat flux (MJ m-2 d^{-1}) [refer to equation A.3]

ρ_a = atmospheric density (kg m^{-3}) [refer to equation A.4]

Cp = specific heat of moist air (=1.013 × MJ kg^{-1} ˚C^{-1})

e_s = the saturation vapour pressure at particular temperature (kPa) [refer to equation A.5]

e_a = the actual vapour pressure [refer to equation A.2i]

r_c = crop canopy resistance (s m^{-1}) [refer to equation A.6]

r_a = aerodynamic resistance (s m^{-1}) [refer to equation A.7]

γ = psychrometric constant (kPa ˚C^{-1}) [refer to equation A.8]

Δ = slope of the vapour pressure curve (kPa ˚C^{-1}) [refer to equation A.9]

$$R_n = R_{ns} - R_{nl} \quad \text{(A.2)}$$

Where R_{ns} = net solar or short-wave radiation (MJ m^{-2} d^{-1}) [refer to equation A.2a]

R_{nl} = net outgoing long-wave radiation (MJ m^{-2} d^{-1}) [refer to equation A.2i]

$$R_{ns} = (1 - \alpha)R_s \quad \text{(A.2a)}$$

where α = albedo or the canopy reflection coefficient (=0.23)

R_S = incoming solar radiation (MJ m^{-2} d^{-1}) [refer to equation A.2b]

$$R_s = \left(a_s + \frac{b_s n}{N}\right) R_a \tag{A.2b}$$

where a_s & b_s = parameters for the fraction of radiation (a_s = 0.25 and b_s -0.5)

n = daylight hour (= 12 hours)

N = maximum possible duration of sunshine or daylight hours [refer to equation A.2c]

Ra = extraterrestrial radiation (MJ m^{-2} d^{-1}) [refer to equation A.2d]

$$N = \frac{24}{\pi}\,\omega_s \tag{A.2c}$$

where π = pi (=3.1416)

ω_s = sunset hour angle (rad) [refer to equation A.2e]

$$R_a = \frac{G_{sc}}{\pi} d_r(\omega_s \sin\varphi \sin\delta + \cos\varphi \cos\delta \sin\omega_s) \tag{A.2d}$$

where G_{SC} = solar constant (=0.0820 MJ m-2 min-1)

d_r = relative distance between Earth and Sun (-)[refer to equation A.2f]

φ = site latitude (rad) (Miri=4.33˚)

δ = solar declination (rad) [refer to equation A.2g]

$$\omega_s = \cos^{-1}(-\tan\varphi \tan\delta) \tag{A.2e}$$

$$d_r = 1 + 0.033\ \cos\left(\frac{2\pi}{365}J\right) \tag{A.2f}$$

where J = Julian day, number of the day in the year (-)

$$\delta = 0.409\ \sin\left(\frac{2\pi}{365}J - 1.39\right) \tag{A.2g}$$

$$R_{nl} = \sigma \left[\frac{T_{max,k}^4 + T_{min,k}^4}{2}\right]\left(0.34 - 0.14\sqrt{e_a}\right)\left(1.35\ \frac{R_s}{R_{SO}} - 0.35\right) \qquad \text{(A.2h)}$$

where σ = Stefan-Boltzmann constant (=4.903×10-9 MJ K^{-4} m^{-2} day^{-1})

$T_{max,k}$ = maximum absolute temperature during the 24-hour period (=˚C+273.16)

$T_{min,k}$ = minimum absolute temperature during the 24-hour period (=˚C+273.16)

e_a = actual vapour pressure (KPa) [refer to equation A.2i]

R_S = incoming solar radiation (MJ m^{-2} day^{-1}) [refer to equation A.2b]

R_{SO} = calculated clear sky radiation (MJ m^{-2} day^{-1}) [refer to equation A.2l]

R_S/ R_{SO} = relative short-wave radiation (≤ 1)

$$e_a = \frac{e^o(T_{min})\frac{RH_{max}}{100} + e^o(T_{max})\frac{RH_{min}}{100}}{2} \qquad \text{(A.2i)}$$

Where $e^o(T_{max})$ = saturation vapour pressure at maximum temperature (kPa) [refer to equation A.2j]

$e^o(T_{min})$ = saturation vapour pressure at minimum temperature (kPa) [refer to equation A.2k]

RH_{max} = maximum relative humidity (%)

RH_{min} = minimum relative humidity (%)

$$e^o(T_{max}) = 0.6108e^{\left[\frac{17.27T_{max}}{T_{max}+237.3}\right]} \qquad \text{(A.2j)}$$

$$e^o(T_{min}) = 0.6108e^{\left[\frac{17.27T_{min}}{T_{max}+237.3}\right]} \qquad \text{(A.2k)}$$

where T_{max} = maximum temperature during the 24-hour period (˚C)

T_{min} = minimum temperature during the 24-hour period (˚C)

$$R_{sO} = (a_s + b_s)R_a \qquad \text{(A.2l)}$$

where a_s & b_s = parameters for the fraction of radiation (a_s = 0.25 and b_s -0.5)

Ra = extraterrestrial radiation (MJ m^{-2} d^{-1}) [refer to equation A.2d]

$$\begin{cases} For\ day\ and\ 10-ten\ periods, & G_{day} \approx 0 \\ For\ hourly\ or\ shorter\ periods, & G_{hr} = 0.1R_n \end{cases} \quad (A.3)$$

where R_n = net radiation at surface (MJ m^{-2} d^{-1}) [refer to equation A.2]

$$\rho_a = \frac{1000P}{287.058(273.15 + T_{mean})} \quad (A.4)$$

where P = actual pressure (kPa) [refer to equation A.4a]

T_{mean} = mean temperature (˚C) [refer to equation A.4b]

$$P = 101.3\left[\frac{293 - 0.0065z}{293}\right]^{5.26} \quad (A.4a)$$

where z = elevation above sea level (m) (Miri=18 m)

$$T_{mean} = \frac{T_{min} + T_{max}}{2} \quad (A.4b)$$

where T_{min} = minimum temperature (˚C)

T_{max} = maximum temperature (˚C)

$$e_s = \frac{e_{T_{min}} + e_{T_{max}}}{2} \quad (A.5)$$

where e_{Tmin} = saturation vapour pressure at the minimum temperature (kPa) [refer to equation A.5a]

e_{Tmax} = saturation vapour pressure at the maximum temperature (kPa) [refer to equation A.5b]

$$e_{min} = 0.6108e^{\left[\frac{17.27T_{min}}{T_{min}+237.3}\right]} \quad (A.5a)$$

$$e_{max} = 0.6108e^{\left[\frac{17.27T_{max}}{T_{max}+237.3}\right]} \quad \text{(A.5b)}$$

where T_{min} = minimum temperature (˚C)

T_{max} = maximum temperature (˚C)

$$r_c = \frac{r_l}{LAI_{active}} \quad \text{(A.6)}$$

where r_l = bulk stomatal resistance of the well-illuminated leaf (=100s m-1)

LAI_{active} = active leaf area index (leaf area/ soil surface)

[refer to equation A.6a]

$$r_a = \frac{\ln\left[\frac{z_m - d}{z_{om}}\right]\ln\left[\frac{z_h - d}{z_{oh}}\right]}{k^2 u_z} \quad \text{(A.7)}$$

Where z_m = height of wind measurement (m)

z_h = height of humidity measurement (m)

d = zero plane displacement height (m) [refer to equation A.7a]

z_{om} = roughness length governing momentum transfer (m) (=0.123 h)

[refer to equation A.7b]

z_{oh} = roughness length governing transfer of heat and vapour

[refer to equation A.7c]

k = von Karman's constant (=0.41)

u_z = wind speed at height z (m s^{-1})

$$d = \frac{2}{3}\,h \quad \text{(A.7a)}$$

$$z_{om} = 0.123\,h \quad \text{(A.7b)}$$

$$zoh = 0.1\,z_{om} \quad \text{(A.7c)}$$

where h = height of crop (m)

$$\gamma = \frac{C_p P}{\epsilon \lambda} \tag{A.8}$$

where P = atmospheric pressure (kPa) [refer to equation A.4a]

λ = latent heat of vaporization (=2.45 MJ kg^{-1})

C_p = specific heat of moist air (=1.013 × MJ kg^{-1} ˚C^{-1})

ε = ratio molecular weight of water vapour/ dry air (=0.622)

$$\Delta = \frac{4098\left[0.6108e^{\left(\frac{17.27T_{mean}}{T_{mean}+237.3}\right)}\right]}{(T_{mean}+237.3)^2} \tag{A.9}$$

Where T_{mean} = mean temperature (˚C) [refer to equation A.4b]

Appendix B: Derivation of Advective term in the Advective-Dispersion equation using Second-order Finite Difference Scheme

$$\frac{\partial \theta c}{\partial t} = \frac{\partial}{\partial z}\left[D_T \frac{\partial c}{\partial z} - qc\right] \tag{B.1}$$

Firstly, the advection term was differentiated using the chain rule to become:

$$\frac{\partial qc}{\partial z} = q\frac{\partial c}{\partial z} + c\frac{\partial q}{\partial z} \tag{B.2}$$

Similar to Bresler (1973), the numerical derivation of the advection term accounted on Taylor's series up to second-order truncation error, but an average concentration between two nodes was used instead of the nodal concentrations:

$$q_{i-\frac{1}{2}} = q_i - \frac{\Delta z}{2}\frac{\partial q_i}{\partial z} + O(\Delta z^3) \tag{B.3}$$

$$q_{i+\frac{1}{2}} = q_i + \frac{\Delta z}{2}\frac{\partial q_i}{\partial z} + O(\Delta z^3) \tag{B.4}$$

$$c_{i-\frac{1}{2}} = c_i - \frac{\Delta z}{2}\frac{\partial c_i}{\partial z} + O(\Delta z^3) \tag{B.5}$$

$$c_{i+\frac{1}{2}} = c_i + \frac{\Delta z}{2}\frac{\partial c_i}{\partial z} + O(\Delta z^3) \tag{B.6}$$

By neglecting the higher order truncation error, the product of $q_{i-\frac{1}{2}}c_{i-\frac{1}{2}}$ was subtracted by $q_{i+\frac{1}{2}}c_{i+\frac{1}{2}}$ and this yields:

$$c_i\frac{\partial q_i}{\partial z} + q_i\frac{\partial c_i}{\partial z} = \frac{q_{i+\frac{1}{2}}c_{i+\frac{1}{2}} - q_{i-\frac{1}{2}}c_{i-\frac{1}{2}}}{\Delta z} \tag{B.7}$$

where the terms at the left side is equivalent to $\frac{\partial qc}{\partial z}$ in equation B.2, and thus the finalized advection term can be expressed as:

$$\frac{\partial q_i c_i}{\partial z} = \frac{q_{i+\frac{1}{2}}c_{i+\frac{1}{2}} - q_{i-\frac{1}{2}}c_{i-\frac{1}{2}}}{\Delta z} \tag{B.8}$$

Using the Crank-Nicolsen scheme, the advection term is presented as:

$$\left(\frac{\partial}{\partial z} q_i c_i\right)_i^{j+\frac{1}{2}} = \frac{1}{2}\left[\frac{q_{i+\frac{1}{2}}^{j+1}\left(\frac{c_{i+1}^{j+1} + c_i^{j+1}}{2}\right) - q_{i-\frac{1}{2}}^{j+1}\left(\frac{c_i^{j+1} + c_{i-1}^{j+1}}{2}\right)}{\Delta z}\right] + \frac{1}{2}\left[\frac{q_{i+\frac{1}{2}}^{j}\left(\frac{c_{i+1}^{j} + c_i^{j}}{2}\right) - q_{i-\frac{1}{2}}^{j}\left(\frac{c_i^{j} + c_{i-1}^{j}}{2}\right)}{\Delta z}\right] \quad \text{(B.9)}$$

Appendix C: Experimental Results of Hydraulic Behaviour and Treatment Performance

Appendix C1: Case 1A (18-11-2015: 75 l)

Time After Loading (min)	Collected Volume (ml)	Effluent Flux (cm min^{-1})	Acc. Effluent (cm)	pH	DO (mg l^{-1})	NH_4^+ (mg l^{-1})	NO_3^- (mg l^{-1})	Temp (ºC)	COD (mg l^{-1})	TS (mg l^{-1})	TN (mg l^{-1})
Influent	-	-	-	7.39	0.35	54.90	10.20	26.90	1383	3400	51
4.50	-	0.0000	0.0000	-	-	-	-	-	-	-	-
14.50	290	-0.0026	-0.0264	7.91	6.78	21.00	17.70	27.90	567	1800	20
24.50	1100	-0.0100	-0.1264	7.81	6.06	23.40	16.40	27.40	-	-	-
34.50	1695	-0.0154	-0.2805	7.78	6.11	26.40	14.80	27.80	-	-	-
42.00	1850	-0.0224	-0.4486	7.80	5.92	29.00	12.90	27.80	-	-	-
46.83	1345	-0.0253	-0.5709	7.82	6.14	29.20	12.00	27.60	566	1600	36
54.00	1825	-0.0231	-0.7368	7.81	5.98	30.50	11.40	27.90	-	-	-
60.17	1610	-0.0237	-0.8832	7.83	6.17	29.30	11.20	27.80	-	-	-
66.00	1680	-0.0262	-1.0359	7.84	6.09	30.50	11.70	27.80	-	-	-
70.00	1150	-0.0261	-1.1405	7.85	6.10	29.30	10.50	28.20	538	1600	59
76.00	1710	-0.0259	-1.2959	7.87	6.04	30.50	10.50	29.00	-	-	-
81.33	1355	-0.0231	-1.4191	7.88	6.09	31.00	9.94	29.10	-	-	-
87.50	1730	-0.0255	-1.5764	7.90	5.99	32.30	9.96	29.50	-	-	-
93.00	1470	-0.0243	-1.7100	7.92	6.27	31.00	9.78	29.30	-	-	-
100.00	1875	-0.0244	-1.8805	7.93	6.07	31.90	9.55	29.20	523	1200	28
110.00	2600	-0.0236	-2.1168	7.91	6.04	31.10	16.70	28.80	-	-	-
120.00	2600	-0.0236	-2.3532	8.13	6.04	28.90	14.70	30.00	-	-	-
130.00	2355	-0.0214	-2.5673	7.97	6.07	31.10	12.30	29.20	-	-	-
180.00	11350	-0.0206	-3.5991	7.96	4.99	30.70	14.10	28.60	-	-	-
190.00	2225	-0.0202	-3.8014	8.03	6.58	28.60	11.30	29.60	-	-	-
200.00	2065	-0.0188	-3.9891	8.00	6.00	28.90	10.90	29.70	396	800	29
230.00	6190	-0.0188	-4.5518	7.98	6.35	26.40	15.50	29.40	-	-	-
260.00	4622	-0.0140	-4.9720	8.01	6.32	24.10	12.50	28.90	298	800	19
290.00	2915	-0.0088	-5.2370	7.99	5.96	22.00	12.30	28.90	-	-	-
380.00	3700	-0.0037	-5.5734	7.84	6.10	15.70	16.80	28.60	-	-	-
550.00	2500	-0.0013	-5.8006	7.71	5.65	9.14	17.40	28.10	-	-	-

Appendix C2: Case 2A (24-11-2015: 75 l)

Time After Loading (min)	Collected Volume (ml)	Effluent Flux (cm min^{-1})	Acc. Effluent (cm)	pH	DO (mg l^{-1})	NH_4^+ (mg l^{-1})	NO_3^- (mg l^{-1})	Temp (ºC)	COD (mg l^{-1})	TS (mg l^{-1})	TN (mg l^{-1})
Influent	-	-	-	7.34	0.25	47.00	10.00	26.80	4578	10600	176
38.00	-	0.0000	0.0000	-	-	-	-	-	-	-	-
43.00	78	-0.0014	-0.0071	8.11	7.04	6.89	21.60	28.60	-	-	-
53.00	194	-0.0018	-0.0247	8.03	7.04	10.00	32.30	29.30	378	1400	32
63.00	300	-0.0027	-0.0520	7.94	6.86	13.20	29.20	29.50	-	-	-
73.00	406	-0.0037	-0.0889	7.94	6.77	14.40	28.10	28.80	-	-	-
83.00	556	-0.0051	-0.1395	7.85	6.33	14.00	28.90	29.00	-	-	-
93.00	648	-0.0059	-0.1984	7.82	6.43	15.60	26.90	30.50	-	-	-
103.00	690	-0.0063	-0.2611	7.86	6.29	16.10	25.10	30.70	340	1200	48
130.00	2025	-0.0068	-0.4452	7.87	5.89	18.40	29.20	29.30	-	-	-
160.00	3420	-0.0104	-0.7561	7.84	6.12	19.70	26.60	31.50	-	-	-
190.00	3990	-0.0121	-1.1188	7.85	6.26	20.50	26.90	31.30	-	-	-
220.00	4130	-0.0125	-1.4943	7.89	6.11	21.10	27.50	29.60	354	1200	47
250.00	4420	-0.0134	-1.8961	7.96	6.51	21.40	25.90	28.70	-	-	-
280.00	4320	-0.0131	-2.2888	7.96	6.65	20.70	26.80	29.30	-	-	-
310.00	4085	-0.0124	-2.6602	7.96	6.42	20.30	25.70	29.20	-	-	-
340.00	4265	-0.0129	-3.0479	7.95	6.20	20.40	26.00	29.30	315	1200	46
370.00	3615	-0.0110	-3.3765	8.01	6.76	20.50	27.00	28.20	-	-	-
400.00	3425	-0.0104	-3.6879	7.98	6.43	20.00	25.40	27.70	-	-	-
430.00	3420	-0.0104	-3.9988	7.99	6.47	20.00	27.30	27.00	317	1400	37
460.00	3435	-0.0104	-4.3111	7.98	6.42	19.20	32.00	26.80	-	-	-
490.00	3345	-0.0101	-4.6152	7.94	6.58	20.10	24.10	26.70	-	-	-
520.00	3280	-0.0099	-4.9134	7.90	6.41	19.70	26.40	26.80	-	-	-
550.00	3450	-0.0105	-5.2270	7.86	6.45	18.90	23.20	26.80	260	600	31
610.00	2915	-0.0044	-5.4920	7.75	5.97	16.20	28.20	26.70	-	-	-

Appendix C3: Case 3A (1-12-2015: 75 l)

Time After Loading (min)	Collected Volume (ml)	Effluent Flux (cm min^{-1})	Acc. Effluent (cm)	pH	DO (mg l^{-1})	NH_4^+ (mg l^{-1})	NO_3^- (mg l^{-1})	Temp (ºC)	COD (mg l^{-1})	TS (mg l^{-1})	TN (mg l^{-1})
Influent	-	-	-	7.45	0.48	47.90	11.00	26.90	1411	4800	120
68.25	-	0.0000	0.0000	-	-	-	-	-	-	-	-
73.25	510	-0.0093	-0.0464	7.83	6.70	36.00	13.50	28.30	951	2400	56
78.25	740	-0.0135	-0.1136	7.84	6.74	38.90	12.00	27.90	-	-	-
83.25	760	-0.0138	-0.1827	7.84	6.68	37.90	12.00	28.70	766	1600	42
88.25	770	-0.0140	-0.2527	7.83	6.74	38.30	11.40	28.80	-	-	-
93.25	790	-0.0144	-0.3245	7.83	6.63	38.10	11.40	28.50	-	-	-
98.25	780	-0.0142	-0.3955	7.83	6.72	38.70	10.80	29.80	764	1400	50
108.25	1620	-0.0147	-0.5427	7.83	6.66	38.10	10.80	28.30	-	-	-
118.25	1640	-0.0149	-0.6918	7.81	6.74	36.90	12.00	30.60	-	-	-
128.25	1625	-0.0148	-0.8395	7.81	6.13	35.10	13.80	31.00	635	1400	38
38158.25	4800	-0.0145	-1.2759	7.78	6.06	31.90	22.10	32.50	-	-	-
188.25	4050	-0.0123	-1.6441	7.89	6.50	30.00	25.00	32.00	-	-	-
218.25	3760	-0.0114	-1.9859	7.82	6.16	28.50	26.90	31.90	-	-	-
248.25	3915	-0.0119	-2.3418	7.79	6.06	25.50	28.90	30.90	334	1200	37
278.25	3865	-0.0117	-2.6932	7.79	5.98	24.70	27.50	30.20	-	-	-
308.25	3500	-0.0106	-3.0114	7.90	6.25	22.10	31.00	30.40	-	-	-
338.25	3170	-0.0096	-3.2995	7.96	6.42	19.70	35.10	28.90	233	1400	27
368.25	2535	-0.0077	-3.5300	7.95	6.47	16.50	39.50	27.30	-	-	-
398.25	2255	-0.0068	-3.7350	7.91	6.29	15.90	38.00	27.70	-	-	-
428.25	2380	-0.0072	-3.9514	7.89	6.37	15.60	32.30	28.20	209	1400	28
488.25	4660	-0.0071	-4.3750	7.84	6.18	14.00	35.30	28.40	-	-	-
548.25	3495	-0.0053	-4.6927	7.81	5.97	11.10	39.70	29.60	111	1400	22
608.25	2320	-0.0035	-4.9036	7.57	6.63	8.15	44.00	29.60	-	-	-

Appendix C4: Case 4B (4-12-2015: 75 l)

Time After Loading (min)	Collected Volume (ml)	Effluent Flux (cm min^{-1})	Acc. Effluent (cm)	pH	DO (mg l^{-1})	NH_4^+ (mg l^{-1})	NO_3^- (mg l^{-1})	Temp (ºC)	COD (mg l^{-1})	TS (mg l^{-1})	TN (mg l^{-1})
Influent	-	-	-	7.61	0.26	44.50	7.75	28.70	1019	1400	80
47.50	-	0.0000	0.0000	-	-	-	-	-	-	-	-
57.50	825	-0.0075	-0.0750	7.59	5.90	5.32	40.10	30.00	-	-	-
62.50	420	-0.0076	-0.1132	7.56	5.55	7.13	43.50	30.70	180	600	23
69.00	635	-0.0089	-0.1709	7.55	5.46	8.13	47.90	31.60	-	-	-
74.00	610	-0.0111	-0.2264	7.56	5.37	8.56	50.00	29.70	205	800	31
79.00	735	-0.0134	-0.2932	7.60	5.62	10.60	49.50	30.30	-	-	-
84.00	840	-0.0153	-0.3695	7.59	5.37	12.30	49.40	31.70	-	-	-
94.00	2115	-0.0192	-0.5618	7.63	5.59	12.80	50.70	30.50	230	600	31
104.00	2035	-0.0185	-0.7468	7.67	5.55	14.00	47.20	29.70	-	-	-
114.00	2410	-0.0219	-0.9659	7.69	5.75	15.30	45.70	31.40	-	-	-
124.00	2480	-0.0225	-1.1914	7.68	5.55	14.90	46.30	28.90	220	200	32
134.00	2190	-0.0199	-1.3905	7.66	5.49	14.80	45.70	30.90	-	-	-
144.00	2810	-0.0255	-1.6459	7.71	5.89	16.10	40.30	30.10	-	-	-
174.00	8605	-0.0261	-2.4282	7.72	5.55	16.90	33.10	33.20	196	600	15
204.00	8025	-0.0243	-3.1577	7.70	5.48	16.90	34.50	32.90	-	-	-
234.00	7190	-0.0218	-3.8114	7.64	5.33	16.80	29.20	31.30	-	-	-
264.00	6280	-0.0190	-4.3823	7.64	5.40	16.20	29.80	31.30	144	200	25
294.00	6095	-0.0185	-4.9364	7.66	5.04	14.70	31.90	30.10	-	-	-
324.00	2460	-0.0075	-5.1600	7.57	5.17	12.90	32.90	30.90	-	-	-
354.00	2335	-0.0071	-5.3723	7.66	5.89	10.50	34.80	32.10	93	400	19
384.00	1610	-0.0049	-5.5186	7.55	4.97	10.20	33.10	32.30	-	-	-
444.00	2310	-0.0035	-5.7286	7.62	5.15	7.82	23.80	31.90	86	800	12
504.00	1385	-0.0021	-5.8545	7.71	5.74	6.08	33.30	30.30	-	-	-

Appendix C5: Case 5A (8-12-2015: 75 l)

Time After Loading (min)	Collected Volume (ml)	Effluent Flux (cm min^{-1})	Acc. Effluent (cm)	pH	DO (mg l^{-1})	NH_4^+ (mg l^{-1})	NO_3^- (mg l^{-1})	Temp (ºC)	COD (mg l^{-1})	TS (mg l^{-1})	TN (mg l^{-1})
Influent	-	-	-	7.68	0.45	41.80	14.10	29.70	-	-	-
3.00	-	0.0000	0.0000	-	-	-	-	-	-	-	-
15.00	1205	-0.0091	-0.1095	7.74	6.28	23.10	49.40	28.70	-	-	-
20.00	1100	-0.0200	-0.2095	7.77	5.87	24.00	52.90	29.00	-	-	-
27.00	1575	-0.0205	-0.3527	7.72	5.95	25.70	44.00	28.80	-	-	-
32.00	1215	-0.0221	-0.4632	7.73	5.94	25.40	44.90	28.70	-	-	-
38.00	1650	-0.0250	-0.6132	7.75	5.89	26.80	41.40	29.10	-	-	-
42.00	1085	-0.0247	-0.7118	7.77	6.00	26.50	43.10	28.90	-	-	-
47.00	1400	-0.0255	-0.8391	7.76	6.02	26.90	39.40	28.50	-	-	-
52.00	1450	-0.0264	-0.9709	7.75	5.91	27.90	38.80	29.20	-	-	-
56.00	1230	-0.0280	-1.0827	7.78	6.14	27.00	38.50	29.10	-	-	-
60.00	1160	-0.0264	-1.1882	7.76	6.03	27.40	37.80	29.50	-	-	-
70.00	2935	-0.0267	-1.4550	7.77	6.15	27.10	33.60	29.60	-	-	-
80.00	2815	-0.0256	-1.7109	7.70	6.17	26.20	30.70	30.00	-	-	-
90.00	2880	-0.0262	-1.9727	7.79	6.22	27.60	29.20	30.80	-	-	-
100.00	2890	-0.0263	-2.2355	7.75	6.02	28.60	29.30	31.50	-	-	-
110.00	2880	-0.0262	-2.4973	7.80	6.23	28.20	27.80	31.40	-	-	-
120.00	2765	-0.0251	-2.7486	7.79	6.14	26.60	27.50	31.20	-	-	-
130.00	2785	-0.0253	-3.0018	7.79	6.33	28.20	25.80	31.90	-	-	-
140.00	2855	-0.0260	-3.2614	7.78	6.09	27.10	25.70	32.50	-	-	-
150.00	2920	-0.0265	-3.5268	7.80	6.15	27.50	26.20	31.50	-	-	-
160.00	2885	-0.0262	-3.7891	7.77	6.18	24.60	28.40	30.70	-	-	-
170.00	2895	-0.0263	-4.0523	7.78	6.26	26.00	25.30	30.70	-	-	-
180.00	2905	-0.0264	-4.3164	7.76	6.12	26.40	25.50	33.00	-	-	-
190.00	2900	-0.0264	-4.5800	7.78	6.27	25.20	25.90	31.60	-	-	-
210.00	5210	-0.0237	-5.0536	7.76	5.98	24.30	26.80	31.00	-	-	-
230.00	3915	-0.0178	-5.4095	7.75	5.73	23.80	25.60	31.80	-	-	-
250.00	2055	-0.0093	-5.5964	7.78	5.68	23.90	25.50	32.30	-	-	-
270.00	1265	-0.0058	-5.7114	7.81	5.71	21.40	25.70	31.00	-	-	-

Appendix C6: Case 6A (12-12-2015: 75 l)

Time After Loading (min)	Collected Volume (ml)	Effluent Flux (cm min^{-1})	Acc. Effluent (cm)	pH	DO (mg l^{-1})	NH_4^+ (mg l^{-1})	NO_3^- (mg l^{-1})	Temp (ºC)	COD (mg l^{-1})	TS (mg l^{-1})	TN (mg l^{-1})
Influent	-	-	-	7.59	1.46	35.20	17.40	29.6	1583	1600	44
31.00	-	0.0000	0.0000	-	-	-	-	-	-	-	-
36.00	1200	-0.0218	-0.1091	7.78	6.17	22.20	76.00	28.30	-	-	-
41.00	1250	-0.0227	-0.2227	7.79	6.32	24.00	70.20	28.20	-	-	-
46.00	1315	-0.0239	-0.3423	7.81	6.53	25.20	65.20	28.20	235	800	10
51.00	1385	-0.0252	-0.4682	7.80	6.59	25.50	59.80	28.30	-	-	-
56.00	1400	-0.0255	-0.5955	7.82	6.57	24.80	57.10	28.40	-	-	-
61.00	1500	-0.0273	-0.7318	7.78	6.43	24.40	55.70	28.50	-	-	-
66.00	1500	-0.0273	-0.8682	7.78	6.51	25.10	50.80	30.00	-	-	-
76.00	3195	-0.0290	-1.1586	7.80	6.57	28.10	46.90	31.20	-	-	-
86.00	3155	-0.0287	-1.4455	7.79	6.25	28.50	47.40	30.50	-	-	-
96.00	3180	-0.0289	-1.7345	7.83	6.70	29.20	43.80	31.50	207	400	38
106.00	3145	-0.0286	-2.0205	7.84	6.62	28.80	44.40	31.70	-	-	-
116.00	2915	-0.0265	-2.2855	7.84	6.33	28.20	45.40	29.60	-	-	-
126.00	2915	-0.0265	-2.5505	7.88	6.68	29.20	44.30	29.90	220	600	20
156.00	8960	-0.0272	-3.3650	7.79	6.20	30.00	41.80	30.70	161	600	6
186.00	6735	-0.0204	-3.9773	7.74	6.37	27.60	41.90	30.40	138	200	6
216.00	3660	-0.0111	-4.3100	7.75	6.33	24.70	43.30	30.20	124	400	14
246.00	1940	-0.0059	-4.4864	7.79	6.14	23.20	49.60	30.40	102	200	13
306.00	1755	-0.0027	-4.6459	7.89	6.62	15.20	59.70	28.50	-	-	-

Appendix C7: Case 7B (13-12-2015: 75 l)

Time After Loading (min)	Collected Volume (ml)	Effluent Flux (cm min^{-1})	Acc. Effluent (cm)	pH	DO (mg l^{-1})	NH_4^+ (mg l^{-1})	NO_3^- (mg l^{-1})	Temp (ºC)	COD (mg l^{-1})	TS (mg l^{-1})	TN (mg l^{-1})
Influent	-	-	-	7.41	0.30	36.40	28.50	30.90	997	1400	78
21.75	-	0.0000	0.0000	-	-	-	-	-	-	-	-
26.75	1860	-0.0338	-0.1691	7.63	6.63	30.00	41.80	28.60	200	1000	20
31.00	2550	-0.0545	-0.4009	7.68	6.55	29.50	45.70	28.60	-	-	-
36.00	2815	-0.0512	-0.6568	7.67	6.35	29.10	48.50	28.60	-	-	-
41.00	3275	-0.0595	-0.9545	7.66	6.11	27.30	53.20	29.70	-	-	-
46.00	3360	-0.0611	-1.2600	7.70	6.35	28.60	54.10	28.90	-	-	-
51.00	3500	-0.0636	-1.5782	7.72	6.34	29.10	47.00	28.90	180	800	34
56.00	3570	-0.0649	-1.9027	7.72	6.30	27.30	46.40	29.40	-	-	-
61.00	3585	-0.0652	-2.2286	7.73	6.24	28.90	49.10	29.30	-	-	-
66.00	3550	-0.0645	-2.5514	7.77	6.44	30.00	45.60	29.00	178	800	33
71.00	3500	-0.0636	-2.8695	7.74	6.29	25.80	46.90	29.20	-	-	-
76.00	3340	-0.0607	-3.1732	7.73	6.28	28.20	44.00	29.50	-	-	-
81.00	3325	-0.0605	-3.4755	7.76	6.41	29.10	44.00	29.20	142	600	31
91.00	5500	-0.0500	-3.9755	7.74	6.04	27.70	45.60	29.30	-	-	-
101.00	3640	-0.0331	-4.3064	7.71	5.89	25.10	45.00	26.90	-	-	-
111.00	1680	-0.0153	-4.4591	7.64	5.24	21.40	50.90	32.50	153	800	15
121.00	760	-0.0069	-4.5282	7.62	4.72	18.00	58.60	32.20	-	-	-
131.00	510	-0.0046	-4.5745	7.62	5.03	15.40	57.80	31.50	-	-	-
141.00	385	-0.0035	-4.6095	7.62	5.38	13.80	57.40	30.40	140	400	25
171.00	825	-0.0025	-4.6845	7.70	5.04	13.10	56.40	28.60	121	400	21
201.00	580	-0.0018	-4.7373	7.63	5.05	10.90	54.80	29.70	75	200	20

Appendix C8: Case 8A (16-12-2015: 100 l)

Time After Loading (min)	Collected Volume (ml)	Effluent Flux (cm min^{-1})	Acc. Effluent (cm)	pH	DO (mg l^{-1})	NH_4^+ (mg l^{-1})	NO_3^- (mg l^{-1})	Temp (ºC)	COD (mg l^{-1})	TS (mg l^{-1})	TN (mg l^{-1})
Influent	-	-	-	7.37	0.38	61.90	17.50	28.50	7485	12800	242
40.00	-	0.0000	0.0000	-	-	-	-	-	-	-	-
45.00	1760	-0.0320	-0.1600	7.72	6.89	46.80	41.90	27.90	695	2400	56
55.00	3800	-0.0345	-0.5055	7.75	6.90	51.60	34.30	27.70	-	-	-
60.00	1660	-0.0302	-0.6564	7.76	6.89	52.70	30.00	27.80	-	-	-
70.00	3400	-0.0309	-0.9655	7.76	6.80	53.00	25.40	27.80	-	-	-
75.00	1780	-0.0324	-1.1273	7.75	6.83	52.70	27.00	27.80	-	-	-
80.00	1790	-0.0325	-1.2900	7.78	6.86	52.50	26.80	27.60	-	-	-
85.00	1820	-0.0331	-1.4555	7.81	6.94	53.30	27.00	27.60	-	-	-
90.00	2335	-0.0425	-1.6677	7.83	7.01	52.00	26.90	27.60	-	-	-
95.00	2275	-0.0414	-1.8745	7.81	7.01	52.60	26.40	27.40	-	-	-
100.00	2290	-0.0416	-2.0827	7.82	6.90	52.40	26.30	27.40	-	-	-
105.00	2255	-0.0410	-2.2877	7.80	7.03	52.60	26.40	27.30	-	-	-
110.00	2285	-0.0415	-2.4955	7.81	7.02	52.80	26.40	27.20	575	1200	59
120.00	4400	-0.0400	-2.8955	7.84	7.04	52.90	25.80	27.00	-	-	-
130.00	4245	-0.0386	-3.2814	7.86	7.10	53.40	25.30	26.90	-	-	-
140.00	4165	-0.0379	-3.6600	7.87	7.17	52.80	25.80	26.70	-	-	-
150.00	3970	-0.0361	-4.0209	7.90	7.21	52.00	27.00	26.60	-	-	-
160.00	3725	-0.0339	-4.3595	7.91	7.20	50.50	26.30	26.60	-	-	-
170.00	3510	-0.0319	-4.6786	7.92	7.29	51.10	26.20	26.50	526	1200	58
200.00	9500	-0.0288	-5.5423	8.03	7.27	49.20	27.40	26.40	499	2000	57
230.00	5580	-0.0169	-6.0495	8.08	7.10	45.30	33.00	26.50	421	800	42
260.00	2015	-0.0061	-6.2327	8.08	6.53	41.90	39.20	26.50	-	-	-
290.00	1415	-0.0043	-6.3614	8.00	6.46	39.90	40.80	26.50	322	1400	39
350.00	2110	-0.0032	-6.5532	8.07	6.65	35.20	49.80	26.40	222	1400	33
410.00	1325	-0.0020	-6.6736	8.01	6.56	26.70	61.50	26.30	220	2800	28

Appendix C9: Case 9B (17-12-2015: 100 l)

Time After Loading (min)	Collected Volume (ml)	Effluent Flux (cm min^{-1})	Acc. Effluent (cm)	pH	DO (mg l^{-1})	NH_4^+ (mg l^{-1})	NO_3^- (mg l^{-1})	Temp (ºC)	COD (mg l^{-1})	TS (mg l^{-1})	TN (mg l^{-1})
Influent	-	-	-	7.47	0.72	49.10	9.54	26.70	4203	4600	150
70.00	-	0.0000	0.0000	-	-	-	-	-	-	-	-
75.00	285	-0.0052	-0.0259	7.66	6.06	12.00	61.40	26.80	219	1000	30
80.00	305	-0.0055	-0.0536	7.62	5.54	12.90	66.10	26.50	-	-	-
85.00	350	-0.0064	-0.0855	7.63	5.64	14.70	68.70	26.70	-	-	-
90.00	370	-0.0067	-0.1191	7.66	5.61	16.10	74.00	26.70	-	-	-
95.00	400	-0.0073	-0.1555	7.63	5.39	17.00	73.20	26.70	-	-	-
100.00	400	-0.0073	-0.1918	7.65	5.58	17.90	75.60	26.60	-	-	-
105.00	410	-0.0075	-0.2291	7.64	5.44	18.40	78.80	26.60	-	-	-
110.00	415	-0.0075	-0.2668	7.65	5.54	18.80	78.20	26.80	-	-	-
115.00	450	-0.0082	-0.3077	7.64	5.34	20.00	79.80	26.30	-	-	-
120.00	505	-0.0092	-0.3536	7.70	5.65	21.60	80.30	26.10	-	-	-
125.00	505	-0.0092	-0.3995	7.70	5.59	22.20	80.90	26.20	-	-	-
130.00	550	-0.0100	-0.4495	7.75	5.77	22.90	79.50	26.10	314	1200	42
140.00	1125	-0.0102	-0.5518	7.72	5.45	24.40	74.00	26.00	-	-	-
150.00	1140	-0.0104	-0.6555	7.75	5.55	25.80	72.00	25.70	-	-	-
160.00	1300	-0.0118	-0.7736	7.78	5.83	27.50	69.30	25.70	-	-	-
170.00	1325	-0.0120	-0.8941	7.79	5.87	28.10	68.60	25.70	-	-	-
180.00	1380	-0.0125	-1.0195	7.80	5.89	29.00	66.20	25.80	-	-	-
190.00	1560	-0.0142	-1.1614	7.80	5.96	30.10	63.30	25.90	368	1600	37
220.00	5785	-0.0175	-1.6873	7.78	6.09	31.80	55.50	26.00	-	-	-
250.00	5985	-0.0181	-2.2314	7.73	5.75	31.60	58.40	26.30	373	1600	35
280.00	5880	-0.0178	-2.7659	7.71	5.72	30.90	64.30	27.50	-	-	-
310.00	6160	-0.0187	-3.3259	7.71	5.61	29.40	68.10	26.60	336	1400	42
370.00	9660	-0.0146	-4.2041	7.64	5.44	27.10	71.20	26.20	250	800	40
430.00	8950	-0.0136	-5.0177	7.60	5.01	24.10	70.40	26.40	195	800	21
490.00	8305	-0.0126	-5.7727	7.58	4.69	22.40	72.10	26.70	170	400	22
550.00	4150	-0.0063	-6.1500	7.52	4.30	18.90	78.10	27.40	-	-	-
610.00	2450	-0.0037	-6.3727	7.51	4.51	14.40	81.70	27.40	-	-	-

Appendix C10: Case 10B (24-12-2015: 100 l)

Time After Loading (min)	Collected Volume (ml)	Effluent Flux (cm min^{-1})	Acc. Effluent (cm)	pH	DO (mg l^{-1})	NH_4^+ (mg l^{-1})	NO_3^- (mg l^{-1})	Temp (ºC)	COD (mg l^{-1})	TS (mg l^{-1})	TN (mg l^{-1})
Influent	-	-	-	7.41	1.14	74.50	2.75	28.60	5162	10700	-
50.00	-	0.0000	0.0000	-	-	-	-	-	-	-	-
55.00	245	-0.0045	-0.0223	7.66	6.23	18.00	23.69	27.70	143	2000	-
60.00	185	-0.0034	-0.0391	7.91	6.11	16.40	25.85	28.10	-	-	-
65.00	145	-0.0026	-0.0523	7.90	6.26	14.80	27.85	28.20	-	-	-
70.00	150	-0.0027	-0.0659	7.88	6.39	13.80	28.92	28.30	-	-	-
75.00	145	-0.0026	-0.0791	7.85	5.90	13.20	29.54	28.40	-	-	-
80.00	160	-0.0029	-0.0936	7.84	6.03	13.00	30.62	29.30	-	-	-
85.00	205	-0.0037	-0.1123	7.79	5.80	11.80	31.54	28.70	80	1600	-
90.00	225	-0.0041	-0.1327	7.82	5.85	11.80	31.08	28.80	-	-	-
95.00	255	-0.0046	-0.1559	7.80	5.90	10.90	31.38	29.20	-	-	-
100.00	285	-0.0052	-0.1818	7.69	5.51	11.40	29.85	30.00	-	-	-
105.00	300	-0.0055	-0.2091	7.79	5.62	10.30	30.15	29.60	-	-	-
110.00	315	-0.0057	-0.2377	7.70	5.32	11.90	29.38	30.90	-	-	-
115.00	320	-0.0058	-0.2668	7.70	5.63	10.40	29.38	30.70	103	1600	-
120.00	325	-0.0059	-0.2964	7.76	5.48	10.40	30.46	30.70	-	-	-
130.00	715	-0.0065	-0.3614	7.81	5.83	14.10	26.92	31.70	-	-	-
140.00	765	-0.0070	-0.4309	7.79	5.49	16.20	24.46	30.40	-	-	-
150.00	765	-0.0070	-0.5005	7.81	5.34	17.10	22.15	29.80	-	-	-
160.00	760	-0.0069	-0.5695	7.85	5.81	15.60	22.92	30.50	139	400	-
170.00	665	-0.0060	-0.6300	7.82	5.06	14.90	22.00	33.40	-	-	-
180.00	695	-0.0063	-0.6932	7.77	4.93	14.90	20.46	34.00	-	-	-
210.00	1875	-0.0057	-0.8636	7.76	5.34	15.40	22.00	32.70	121	1400	-
240.00	1805	-0.0055	-1.0277	7.79	5.48	16.90	19.69	33.90	-	-	-
270.00	1815	-0.0055	-1.1927	7.77	5.32	14.30	22.62	33.30	115	400	-
300.00	1315	-0.0040	-1.3123	7.79	5.52	15.00	18.77	30.70	-	-	-
330.00	1120	-0.0034	-1.4141	7.79	5.74	13.70	19.23	30.80	113	1200	-
390.00	2055	-0.0031	-1.6009	7.72	5.26	12.60	20.00	29.60	-	-	-
450.00	1840	-0.0028	-1.7682	7.74	5.62	12.20	20.15	29.00	-	-	-
510.00	1775	-0.0027	-1.9295	7.74	5.42	11.00	20.31	30.10	82	1800	-
600.00	1525	-0.0015	-2.0682	7.90	6.63	9.16	21.23	29.70	-	-	-

Appendix C11: Case 11A (27-12-2015: 100 l)

Time After Loading (min)	Collected Volume (ml)	Effluent Flux (cm min^{-1})	Acc. Effluent (cm)	pH	DO (mg l^{-1})	NH_4^+ (mg l^{-1})	NO_3^- (mg l^{-1})	Temp (ºC)	COD (mg l^{-1})	TS (mg l^{-1})	TN (mg l^{-1})
Influent	-	-	-	7.53	0.05	84.00	2.69	24.10	8606	12600	203
54.00	-	0.0000	0.0000	-	-	-	-	-	-	-	-
64.00	1365	-0.0124	-0.1241	7.92	6.73	53.40	13.46	27.70	-	-	-
74.00	1640	-0.0149	-0.2732	7.93	6.74	55.10	10.29	28.10	-	-	-
84.00	1825	-0.0166	-0.4391	7.91	6.67	59.30	9.60	28.20	-	-	-
94.00	1785	-0.0162	-0.6014	7.95	6.74	57.90	9.15	28.10	700	2600	43
104.00	1800	-0.0164	-0.7650	7.97	6.98	57.00	9.34	28.10	-	-	-
114.00	1775	-0.0161	-0.9264	7.95	6.86	57.20	8.62	28.10	-	-	-
124.00	1725	-0.0157	-1.0832	7.94	6.80	57.10	8.00	28.10	618	2000	32
134.00	1810	-0.0165	-1.2477	7.93	6.80	56.30	7.88	28.10	-	-	-
144.00	1765	-0.0160	-1.4082	7.92	6.84	54.60	7.02	28.20	-	-	-
154.00	1825	-0.0166	-1.5741	7.93	6.93	56.10	6.92	28.30	610	1600	49
184.00	5430	-0.0165	-2.0677	7.86	6.36	55.30	5.94	28.70	584	1200	50
214.00	5055	-0.0153	-2.5273	7.82	6.41	54.50	4.88	29.00	-	-	-
244.00	4870	-0.0148	-2.9700	7.84	6.58	53.70	4.83	28.90	493	1400	60
274.00	4565	-0.0138	-3.3850	7.88	6.79	50.50	4.60	29.00	-	-	-
334.00	8630	-0.0131	-4.1695	8.06	6.71	41.70	7.60	29.10	447	2200	41
394.00	1075	-0.0016	-4.2673	8.08	7.17	21.30	18.92	28.30	-	-	-

Appendix C12: Case 12B (31-12-2015: 100 l)

Time After Loading (min)	Collected Volume (ml)	Effluent Flux (cm min^{-1})	Acc. Effluent (cm)	pH	DO (mg l^{-1})	NH_4^+ (mg l^{-1})	NO_3^- (mg l^{-1})	Temp (ºC)	COD (mg l^{-1})	TS (mg l^{-1})	TN (mg l^{-1})
Influent	-	-	-	7.61	0.10	58.00	8.09	27.60	6471	9500	151
48.50	-	0.0000	0.0000	-	-	-	-	-	-	-	-
53.50	80	-0.0015	-0.0073	7.94	7.22	3.73	23.10	28.70	-	-	-
58.50	70	-0.0013	-0.0136	7.98	7.36	3.04	23.00	28.90	-	-	-
68.50	125	-0.0011	-0.0250	7.86	6.78	2.73	26.60	29.10	-	-	-
78.50	125	-0.0011	-0.0364	7.95	7.25	2.63	29.70	29.10	77	600	28
88.50	140	-0.0013	-0.0491	7.83	6.80	2.03	30.40	29.20	-	-	-
98.50	225	-0.0020	-0.0695	7.78	6.45	1.50	30.30	29.30	-	-	-
108.50	290	-0.0026	-0.0959	7.80	6.48	1.75	24.40	29.40	67	200	26
118.50	300	-0.0027	-0.1232	7.65	6.37	1.90	46.20	29.40	-	-	-
128.50	340	-0.0031	-0.1541	7.71	6.47	1.82	53.60	28.30	-	-	-
138.50	320	-0.0029	-0.1832	7.64	6.20	1.82	51.10	28.70	65	200	27
148.50	355	-0.0032	-0.2155	7.68	6.50	1.84	50.50	28.70	-	-	-
158.50	360	-0.0033	-0.2482	7.69	6.35	2.04	52.50	29.40	-	-	-
168.50	360	-0.0033	-0.2809	7.69	6.53	2.15	52.90	28.90	49	400	48
198.50	1105	-0.0033	-0.3814	7.65	6.50	2.04	50.50	29.40	-	-	-
228.50	1220	-0.0037	-0.4923	7.63	6.40	2.08	48.10	28.90	52	200	42
258.50	1265	-0.0038	-0.6073	7.57	6.00	2.36	45.80	29.60	-	-	-
288.50	1205	-0.0037	-0.7168	7.68	6.57	2.14	45.80	29.10	43	400	42
348.50	2120	-0.0032	-0.9095	7.66	6.15	2.08	44.40	29.20	-	-	-
408.50	2040	-0.0031	-1.0950	7.89	7.47	1.94	44.10	28.70	36	200	31
468.50	2100	-0.0032	-1.2859	7.77	6.80	1.96	44.70	29.10	-	-	-
528.50	2070	-0.0031	-1.4741	7.75	7.13	1.81	45.40	28.60	41	200	33
588.50	2005	-0.0030	-1.6564	7.73	7.10	2.02	49.60	28.20	-	-	-

Appendix C13: Case 13B (7-1-2016: 125 l)

Time After Loading (min)	Collected Volume (ml)	Effluent Flux (cm min^{-1})	Acc. Effluent (cm)	pH	DO (mg l^{-1})	NH_4^+ (mg l^{-1})	NO_3^- (mg l^{-1})	Temp (ºC)	COD (mg l^{-1})	TS (mg l^{-1})	TN (mg l^{-1})
Influent	-	-	-	7.72	0.68	74.30	8.97	29.00	2698	4200	125
35.00	-	0.0000	0.0000	-	-	-	-	-	-	-	-
45.00	25	-0.0002	-0.0023	8.25	7.09	0.93	8.97	29.10	-	-	-
55.00	20	-0.0002	-0.0041	8.17	7.32	1.08	16.00	29.20	-	-	-
65.00	90	-0.0008	-0.0123	7.98	6.73	10.50	21.30	29.80	-	-	-
75.00	200	-0.0018	-0.0305	7.92	6.52	14.90	33.10	30.30	270	2000	56
85.00	510	-0.0046	-0.0768	7.89	6.25	20.10	26.90	30.90	-	-	-
95.00	795	-0.0072	-0.1491	7.86	5.92	27.90	28.10	31.30	-	-	-
105.00	775	-0.0070	-0.2195	7.93	5.84	30.50	23.50	30.80	178	800	70
115.00	695	-0.0063	-0.2827	8.01	6.35	31.40	21.60	30.20	-	-	-
125.00	605	-0.0055	-0.3377	8.01	6.68	30.70	20.50	30.80	-	-	-
135.00	545	-0.0050	-0.3873	8.00	6.12	28.10	19.90	30.90	150	1000	55
145.00	495	-0.0045	-0.4323	7.97	5.86	26.90	18.60	31.50	-	-	-
155.00	460	-0.0042	-0.4741	7.89	5.49	26.40	18.90	34.20	-	-	-
185.00	1140	-0.0035	-0.5777	7.90	6.01	23.30	19.30	35.20	167	1400	44
220.00	950	-0.0025	-0.6641	7.94	5.82	18.70	21.10	32.40	-	-	-
245.00	485	-0.0018	-0.7082	7.92	6.31	13.10	21.60	32.60	-	-	-
305.00	765	-0.0012	-0.7777	7.83	6.20	7.18	23.30	32.20	49	1600	13
365.00	675	-0.0010	-0.8391	7.88	6.53	4.75	24.80	29.40	-	-	-
425.00	700	-0.0011	-0.9027	7.82	6.66	3.60	26.40	28.90	-	-	-
485.00	745	-0.0011	-0.9705	7.83	6.57	2.99	29.40	28.80	33	1600	26
545.00	735	-0.0011	-1.0373	7.78	6.61	2.13	31.10	29.50	-	-	-
605.00	735	-0.0011	-1.1041	7.78	6.62	1.57	31.70	28.80	41	1200	19

Appendix C14: Case 14A (10-1-2016: 125 l)

Time After Loading (min)	Collected Volume (ml)	Effluent Flux (cm min^{-1})	Acc. Effluent (cm)	pH	DO (mg l^{-1})	NH_4^+ (mg l^{-1})	NO_3^- (mg l^{-1})	Temp (ºC)	COD (mg l^{-1})	TS (mg l^{-1})	TN (mg l^{-1})
Influent	-	-	-	7.72	0.68	74.30	8.97	29.00	3888	9600	318
16.00	-	0.0000	0.0000	-	-	-	-	-	-	-	-
26.00	80	-0.0007	-0.0073	8.11	7.27	17.30	20.60	27.10	370	1500	68
36.00	55	-0.0005	-0.0123	8.09	7.42	9.85	21.08	27.20	-	-	-
46.00	70	-0.0006	-0.0186	8.07	7.29	7.61	22.80	27.10	-	-	-
56.00	80	-0.0007	-0.0259	7.95	6.96	5.73	21.70	27.20	-	-	-
66.00	135	-0.0012	-0.0382	7.88	6.42	6.42	25.60	27.20	265	1600	50
76.00	145	-0.0013	-0.0514	7.96	6.79	7.83	27.90	27.40	-	-	-
86.00	160	-0.0015	-0.0659	7.94	6.71	7.88	29.20	27.40	-	-	-
96.00	185	-0.0017	-0.0827	7.88	6.33	9.03	29.90	27.40	122	1200	56
106.00	190	-0.0017	-0.1000	7.92	6.56	9.26	27.70	27.50	-	-	-
116.00	210	-0.0019	-0.1191	7.88	6.58	10.50	29.70	27.70	-	-	-
146.00	730	-0.0022	-0.1855	7.85	6.65	9.59	28.70	28.20	312	1400	70
176.00	815	-0.0025	-0.2595	7.92	6.41	7.72	33.30	27.80	-	-	-
206.00	885	-0.0027	-0.3400	7.79	6.41	6.82	32.40	28.00	80	1300	47
236.00	775	-0.0023	-0.4105	7.87	6.80	5.67	32.10	28.00	-	-	-
266.00	825	-0.0025	-0.4855	7.76	6.24	5.30	34.80	28.20	-	-	-
296.00	870	-0.0026	-0.5645	7.82	6.51	4.56	34.10	28.30	60	1500	55
356.00	1430	-0.0022	-0.6945	7.75	6.29	4.10	33.40	28.70	-	-	-
416.00	1680	-0.0025	-0.8473	7.89	6.63	3.90	33.00	28.80	49	1200	52
476.00	1600	-0.0024	-0.9927	7.80	6.47	3.56	35.00	28.60	-	-	-
536.00	1510	-0.0023	-1.1300	7.73	6.42	2.55	33.90	28.30	-	-	-
596.00	1375	-0.0021	-1.2550	7.72	6.30	2.06	33.20	27.80	34	1300	62

Appendix C15: Case 15B (14-1-2016: 125 l)

Time After Loading (min)	Collected Volume (ml)	Effluent Flux (cm min^{-1})	Acc. Effluent (cm)	pH	DO (mg l^{-1})	NH_4^+ (mg l^{-1})	NO_3^- (mg l^{-1})	Temp (ºC)	COD (mg l^{-1})	TS (mg l^{-1})	TN (mg l^{-1})
Influent	-	-	-	7.55	0.19	58.10	2.63	27.80	7753	24000	368
13.00	-	0.0000	0.0000	-	-	-	-	-	-	-	-
18.00	105	-0.0019	-0.0095	7.80	6.57	11.90	25.50	27.80	418	3200	52
23.00	130	-0.0024	-0.0214	7.94	6.11	18.20	26.50	27.90	-	-	-
28.00	155	-0.0028	-0.0355	7.92	6.38	22.20	25.20	28.20	-	-	-
33.00	140	-0.0025	-0.0482	8.01	6.58	23.60	22.90	28.30	-	-	-
38.00	170	-0.0031	-0.0636	7.98	6.28	24.80	21.20	29.20	566	3400	87
43.00	185	-0.0034	-0.0805	8.02	6.26	28.60	21.90	29.00	-	-	-
53.00	350	-0.0032	-0.1123	8.00	6.54	29.70	19.30	29.80	-	-	-
63.00	380	-0.0035	-0.1468	7.96	6.36	31.00	17.10	30.00	507	2800	97
73.00	360	-0.0033	-0.1795	8.05	6.68	31.70	17.00	29.40	-	-	-
83.00	360	-0.0033	-0.2123	7.97	6.34	33.80	15.60	30.30	-	-	-
93.00	350	-0.0032	-0.2441	7.97	6.17	32.50	15.70	29.30	-	-	-
103.00	350	-0.0032	-0.2759	7.97	6.05	31.70	16.30	29.70	-	-	-
113.00	345	-0.0031	-0.3073	8.02	6.48	31.80	16.20	30.40	-	-	-
123.00	335	-0.0030	-0.3377	8.07	6.38	32.80	15.20	29.90	423	2800	111
133.00	300	-0.0027	-0.3650	8.00	6.07	31.80	15.40	30.70	-	-	-
163.00	860	-0.0026	-0.4432	8.12	6.54	27.80	15.30	30.90	-	-	-
193.00	845	-0.0026	-0.5200	8.13	6.72	29.20	14.90	32.70	362	2800	89
228.00	1025	-0.0027	-0.6132	8.08	6.34	28.90	13.90	31.00	-	-	-
253.00	730	-0.0027	-0.6795	8.02	6.36	28.20	13.30	31.40	-	-	-
313.00	1330	-0.0020	-0.8005	8.05	6.57	23.70	14.40	30.60	321	1200	74
373.00	840	-0.0013	-0.8768	8.06	6.68	17.80	15.60	29.90	-	-	-
433.00	730	-0.0011	-0.9432	7.99	6.53	17.40	16.90	30.00	-	-	-
493.00	690	-0.0010	-1.0059	7.95	6.62	13.90	19.00	29.20	190	1000	51
553.00	575	-0.0009	-1.0582	7.92	6.59	12.30	19.50	28.90	-	-	-
613.00	605	-0.0009	-1.1132	7.91	6.41	10.80	19.80	28.90	-	-	-

Appendix C16: Case 16A (21-1-2016: 100 l)

Time After Loading (min)	Collected Volume (ml)	Effluent Flux (cm min^{-1})	Acc. Effluent (cm)	pH	DO (mg l^{-1})	NH_4^+ (mg l^{-1})	NO_3^- (mg l^{-1})	Temp (ºC)	COD (mg l^{-1})	TS (mg l^{-1})	TN (mg l^{-1})
Influent	-	-	-	7.61	0.11	32.00	5.23	26.80	850	1700	72
10.00	-	0.0000	0.0000	-	-	-	-	-	-	-	-
15.00	400	-0.0073	-0.0364	8.01	6.61	16.80	35.40	26.40	-	-	-
20.00	565	-0.0103	-0.0877	8.05	6.54	18.90	31.30	26.40	-	-	-
25.00	605	-0.0110	-0.1427	8.02	6.45	20.80	26.80	26.40	651	1000	62
30.00	660	-0.0120	-0.2027	8.07	6.87	21.90	23.80	26.40	-	-	-
35.00	650	-0.0118	-0.2618	8.04	6.70	22.30	22.10	26.40	-	-	-
45.25	710	-0.0129	-0.3264	8.07	6.92	22.70	22.20	26.40	-	-	-
55.00	1575	-0.0140	-0.4695	8.04	6.85	23.20	19.80	26.40	-	1200	-
65.00	1530	-0.0143	-0.6086	8.03	6.75	23.10	18.60	26.50	-	-	-
75.00	1500	-0.0136	-0.7450	8.00	6.80	23.00	17.10	26.60	-	-	-
85.00	1625	-0.0148	-0.8927	7.99	6.70	22.90	16.90	26.60	-	-	-
95.00	1630	-0.0148	-1.0409	8.03	6.85	22.50	16.70	26.80	408	1000	51
105.00	1635	-0.0149	-1.1895	8.02	6.74	22.10	16.10	26.80	-	-	-
115.00	1565	-0.0142	-1.3318	7.98	6.69	21.90	15.50	26.90	-	-	-
125.00	1505	-0.0137	-1.4686	8.03	6.70	21.40	16.40	27.10	-	-	-
140.00	1485	-0.0135	-1.6036	8.03	6.67	21.20	15.80	27.50	-	400	59
170.00	2215	-0.0134	-1.8050	8.02	6.52	20.30	16.20	27.60	310	-	-
200.00	3755	-0.0114	-2.1464	7.95	6.20	18.90	18.60	28.50	-	-	-
232.00	3445	-0.0104	-2.4595	8.05	6.22	17.70	19.10	28.30	-	-	-
260.00	3280	-0.0093	-2.7577	8.13	6.19	16.20	20.30	28.60	-	1000	-
320.00	2580	-0.0084	-2.9923	8.09	6.16	15.00	22.40	29.30	-	-	-
380.00	4600	-0.0070	-3.4105	8.02	5.86	12.90	23.60	28.70	164	1600	21
440.00	3405	-0.0052	-3.7200	7.93	5.74	10.10	25.20	29.70	-	-	-
500.00	2500	-0.0038	-3.9473	7.89	5.90	7.16	27.50	28.70	-	-	-

Appendix C17: Case 17B (21-1-2016: 100 l)

Time After Loading (min)	Collected Volume (ml)	Effluent Flux (cm min^{-1})	Acc. Effluent (cm)	pH	DO (mg l^{-1})	NH_4^+ (mg l^{-1})	NO_3^- (mg l^{-1})	Temp (ºC)	COD (mg l^{-1})	TS (mg l^{-1})	TN (mg l^{-1})
Influent	-	-	-	7.46	0.25	35.60	8.66	26.70	6846	19500	335
8.00	-	0.0000	0.0000	-	-	-	-	-	-	-	-
13.00	150	-0.0027	-0.0136	7.72	6.24	8.03	39.50	27.70	-	-	-
18.00	175	-0.0032	-0.0295	7.79	6.41	9.42	35.70	28.00	-	-	-
23.00	235	-0.0043	-0.0509	7.80	6.69	10.80	32.70	27.00	449	-	46
28.00	265	-0.0048	-0.0750	7.82	6.74	12.20	30.80	26.80	-	600	-
33.00	510	-0.0093	-0.1214	7.85	6.88	15.60	25.80	27.00	-	-	-
38.00	595	-0.0108	-0.1755	7.88	6.94	17.70	22.30	27.30	-	-	-
48.00	1200	-0.0109	-0.2845	7.79	6.70	18.10	20.00	26.80	-	-	-
58.00	1155	-0.0105	-0.3895	7.88	6.67	16.60	23.40	26.70	-	1400	-
68.00	1155	-0.0105	-0.4945	8.05	6.86	16.50	25.20	26.50	-	-	-
78.00	1065	-0.0097	-0.5914	8.00	6.59	16.60	24.60	26.50	-	-	-
88.50	1190	-0.0103	-0.6995	8.00	6.47	16.40	24.80	26.50	-	-	-
98.00	1200	-0.0115	-0.8086	7.98	6.57	16.00	26.50	26.60	377	1000	30
108.20	1325	-0.0118	-0.9291	7.96	6.57	16.00	25.70	26.60	-	-	-
118.00	1275	-0.0118	-1.0450	7.98	6.68	15.70	25.50	26.80	-	-	-
129.00	1390	-0.0115	-1.1714	7.97	6.53	15.20	25.30	26.90	-	-	-
158.00	3820	-0.0120	-1.5186	7.99	6.59	15.60	20.60	27.00	-	1200	-
188.00	3325	-0.0101	-1.8209	7.88	6.12	13.90	24.30	27.80	-	-	-
218.00	3050	-0.0092	-2.0982	7.80	6.07	13.10	24.40	28.30	286	-	45
248.00	2740	-0.0083	-2.3473	7.78	6.00	11.90	27.30	29.80	-	-	-
308.00	5010	-0.0076	-2.8027	7.76	6.31	10.20	29.90	28.40	-	800	-
368.00	4970	-0.0075	-3.2545	7.80	5.95	9.33	28.30	28.90	-	-	-
428.00	4155	-0.0063	-3.6323	7.68	5.61	8.10	30.70	30.10	-	800	-
488.00	3990	-0.0060	-3.9950	7.72	5.79	7.61	28.90	29.40	161	-	27
548.00	3640	-0.0055	-4.3259	7.68	5.52	6.41	29.50	29.10	-	-	-

Appendix C18: Case 18A (24-1-2016: 125 l)

Time After Loading (min)	Collected Volume (ml)	Effluent Flux (cm min^{-1})	Acc. Effluent (cm)	pH	DO (mg l^{-1})	NH_4^+ (mg l^{-1})	NO_3^- (mg l^{-1})	Temp (ºC)	COD (mg l^{-1})	TS (mg l^{-1})	TN (mg l^{-1})
Influent	-	-	-	7.86	0.50	48.30	5.17	26.80	904	2200	56
4.00	-	0.0000	0.0000	-	-	-	-	-	-	-	-
9.00	275	-0.0050	-0.0250	8.08	6.45	24.70	16.90	26.70	-	-	-
15.00	225	-0.0034	-0.0455	8.05	6.55	22.80	20.10	26.90	-	-	-
20.00	345	-0.0063	-0.0768	8.11	6.85	27.20	19.00	26.90	-	600	-
25.00	260	-0.0047	-0.1005	8.19	6.67	24.70	20.00	26.60	-	-	-
30.00	460	-0.0084	-0.1423	8.12	6.54	23.80	23.30	26.60	-	-	-
36.00	505	-0.0077	-0.1882	8.18	6.59	28.30	19.80	27.00	-	-	-
46.00	1465	-0.0133	-0.3214	8.12	6.74	28.80	19.20	27.10	-	900	-
56.00	1600	-0.0145	-0.4668	8.15	6.73	31.00	18.20	27.20	-	-	-
66.00	1940	-0.0176	-0.6432	8.17	6.53	29.60	18.80	27.70	-	-	-
76.00	2175	-0.0198	-0.8409	8.11	6.42	30.90	15.50	28.20	226	500	49
88.00	2320	-0.0176	-1.0518	8.23	6.49	31.10	16.90	27.60	-	-	-
100.00	3120	-0.0236	-1.3355	8.14	6.59	30.70	17.00	28.80	-	-	-
130.00	8035	-0.0243	-2.0659	8.18	6.52	31.10	12.90	29.10	-	-	-
166.00	11115	-0.0281	-3.0764	8.20	6.33	32.10	14.50	28.80	-	400	-
190.00	8285	-0.0314	-3.8295	8.19	6.57	32.90	12.30	29.10	-	-	-
220.00	8890	-0.0269	-4.6377	8.22	6.44	32.60	13.10	27.90	-	-	-
250.00	9090	-0.0275	-5.4641	8.21	6.65	32.30	12.80	28.00	-	600	-
280.00	8895	-0.03	-6.2727	8.24	6.58	31.90	12.40	28.20	-	-	-
340.00	19375	-0.03	-8.0341	8.25	6.83	31.30	11.00	28.20	-	-	-
400.00	13810	-0.0209	-9.2895	8.24	6.63	28.40	11.70	28.00	162	400	37
460.00	8335	-0.0126	-10.0473	8.20	6.46	25.50	10.90	27.70	-	-	-
520.00	1975	-0.0030	-10.2268	8.08	5.89	18.00	17.10	27.10	-	800	-

Appendix C19: Case 19B (24-1-2016: 125 l)

Time After Loading (min)	Collected Volume (ml)	Effluent Flux (cm min^{-1})	Acc. Effluent (cm)	pH	DO (mg l^{-1})	NH_4^+ (mg l^{-1})	NO_3^- (mg l^{-1})	Temp (ºC)	COD (mg l^{-1})	TS (mg l^{-1})	TN (mg l^{-1})
Influent	-	-	-	7.89	0.35	48.40	5.44	27.30	1162	2700	99
19.00	-	0.0000	0.0000	-	-	-	-	-	-	-	-
25.00	1150	-0.0174	-0.1045	7.89	6.66	11.70	23.60	27.10	-	-	-
30.00	1800	-0.0327	-0.2682	7.95	6.82	14.90	24.80	26.90	-	-	-
35.00	2410	-0.0438	-0.4873	8.08	6.45	19.60	22.40	26.90	-	400	-
40.00	2175	-0.0395	-0.6850	8.06	6.62	22.00	21.70	26.80	-	-	-
45.00	2425	-0.0441	-0.9055	8.05	6.55	24.30	19.00	27.00	-	-	-
50.00	2500	-0.0455	-1.1327	8.09	6.68	25.10	18.20	27.00	-	-	-
60.00	4625	-0.0420	-1.5532	8.09	6.59	25.70	18.90	27.00	-	800	-
70.00	3460	-0.0315	-1.8677	8.00	6.73	27.40	15.30	27.10	-	-	-
80.00	4505	-0.0410	-2.2773	8.04	6.73	28.40	12.00	27.20	-	-	-
90.00	4375	-0.0398	-2.6750	8.00	6.82	26.30	17.50	27.50	277	600	61
100.00	3935	-0.0358	-3.0327	8.02	6.35	32.40	12.70	28.10	-	-	-
110.00	4615	-0.0420	-3.4523	8.01	6.41	33.90	10.70	28.60	-	-	-
140.00	12525	-0.0380	-4.5909	8.01	6.45	34.90	8.70	28.30	-	-	-
170.00	10605	-0.0321	-5.5550	7.98	6.23	36.40	7.58	30.00	-	500	-
200.00	9825	-0.0298	-6.4482	8.01	6.43	36.20	7.70	30.90	-	-	-
230.00	10245	-0.0310	-7.3795	8.06	6.48	36.40	7.96	28.00	-	-	-
260.00	9670	-0.0293	-8.2586	8.09	6.48	33.30	10.60	28.00	-	800	-
290.00	7415	-0.0225	-8.9327	8.04	6.10	29.80	11.40	28.40	-	-	-
350.00	7390	-0.0112	-9.6045	8.04	6.20	27.10	12.90	28.10	-	-	-
410.00	2245	-0.0034	-9.8086	8.06	6.47	23.40	15.60	28.30	144	800	33
470.00	2100	-0.0032	-9.9995	8.08	6.27	26.10	8.07	28.60	-	-	-
530.00	765	-0.0012	-10.0691	8.09	6.18	20.40	12.60	28.10	-	400	-

Appendix C20: Case 20A (28-1-2016: 150 l)

Time After Loading (min)	Collected Volume (ml)	Effluent Flux (cm min^{-1})	Acc. Effluent (cm)	pH	DO (mg l^{-1})	NH_4^+ (mg l^{-1})	NO_3^- (mg l^{-1})	Temp (ºC)	COD (mg l^{-1})	TS (mg l^{-1})	TN (mg l^{-1})
Influent	-	-	-	7.62	0.25	44.10	4.58	27.80	3049	3200	121
3.00	-	0.0000	0.0000	-	-	-	-	-	-	-	-
8.00	2010	-0.0365	-0.1827	7.82	0.95	42.20	5.41	27.50	-	-	-
13.00	3600	-0.0655	-0.5100	7.84	3.20	41.80	5.54	27.40	-	800	-
18.00	3675	-0.0668	-0.8441	7.92	3.98	40.50	6.26	27.40	-	-	-
23.00	3565	-0.0648	-1.1682	7.92	3.79	39.80	6.54	27.60	-	-	-
28.50	3925	-0.0649	-1.5250	7.84	3.28	39.50	6.06	27.50	-	-	-
33.00	3600	-0.0727	-1.8523	7.84	3.48	39.60	5.51	27.60	730	900	46
43.00	7520	-0.0684	-2.5359	7.87	3.34	38.00	5.67	27.80	-	-	-
53.50	6850	-0.0593	-3.1586	7.87	3.45	37.50	5.45	27.90	-	-	-
63.00	6530	-0.0625	-3.7523	7.86	3.96	37.90	5.11	27.80	-	-	-
74.00	7215	-0.0596	-4.4082	7.89	3.52	35.30	5.74	28.30	-	-	-
83.50	5835	-0.0558	-4.9386	7.90	3.24	33.00	6.23	28.00	452	900	-
93.00	5710	-0.0546	-5.4577	7.93	3.24	32.90	6.19	29.60	-	-	-
124.00	16620	-0.0487	-6.9686	7.89	3.69	31.80	6.76	31.10	-	-	-
153.00	13870	-0.0435	-8.2295	7.95	3.90	31.20	6.79	30.40	-	-	-
183.00	11915	-0.0361	-9.3127	7.92	4.25	30.90	5.86	29.90	-	-	-
213.00	8680	-0.0263	-10.1018	8.11	5.81	28.90	7.19	30.50	-	1000	-
273.00	7230	-0.0110	-10.7591	8.14	5.77	25.90	8.94	29.60	-	-	-
333.00	2360	-0.0036	-10.9736	8.13	5.05	20.70	11.90	29.60	-	600	36
393.00	880	-0.0013	-11.0536	8.10	6.27	16.50	11.60	28.90	-	-	-
453.00	465	-0.0007	-11.0959	8.20	6.16	12.90	13.80	29.00	228	2600	-

Appendix C21: Case 21B (28-1-2016: 150 l)

Time After Loading (min)	Collected Volume (ml)	Effluent Flux (cm min^{-1})	Acc. Effluent (cm)	pH	DO (mg l^{-1})	NH_4^+ (mg l^{-1})	NO_3^- (mg l^{-1})	Temp (ºC)	COD (mg l^{-1})	TS (mg l^{-1})	TN (mg l^{-1})
Influent	-	-	-	7.66	0.22	40.50	4.21	27.30	1162	1500	49
19.00	-	0.0000	0.0000	-	-	-	-	-	-	-	-
24.00	190	-0.0035	-0.0173	8.08	6.78	16.90	20.60	27.10	-	-	-
29.00	150	-0.0027	-0.0309	8.01	6.18	15.90	21.40	26.90	-	900	-
34.00	135	-0.0025	-0.0432	7.97	6.23	13.80	20.40	26.90	-	-	-
39.00	170	-0.0031	-0.0586	8.02	6.15	15.30	21.70	26.80	-	-	-
44.00	220	-0.0040	-0.0786	8.00	6.25	17.20	21.10	27.00	-	-	-
50.00	170	-0.0026	-0.0941	8.00	6.07	14.00	22.10	27.00	268	1100	17
60.00	600	-0.0055	-0.1486	7.93	5.79	14.50	23.60	27.00	-	-	-
70.00	765	-0.0070	-0.2182	8.01	6.06	11.50	28.00	27.10	-	-	-
80.00	745	-0.0068	-0.2859	7.92	5.86	13.00	26.20	27.20	-	-	-
90.00	810	-0.0074	-0.3595	7.88	5.73	14.60	24.40	27.50	-	-	-
100.00	920	-0.0084	-0.4432	7.98	6.11	14.10	24.80	28.10	200	800	17
110.00	1075	-0.0098	-0.5409	8.07	6.04	17.00	23.60	28.60	-	-	-
140.00	3130	-0.0095	-0.8255	7.92	6.01	17.60	17.40	28.30	-	-	-
170.00	3175	-0.0096	-1.1141	8.05	6.00	20.00	19.90	30.00	-	-	-
200.00	4570	-0.0138	-1.5295	7.98	6.18	21.40	16.70	30.90	-	-	-
229.00	5385	-0.0169	-2.0191	7.92	5.92	20.80	15.00	28.00	235	700	26
289.00	7790	-0.0118	-2.7273	7.95	6.04	20.50	14.20	28.00	-	-	-
349.00	8605	-0.0130	-3.5095	7.96	5.90	20.90	13.40	28.40	-	-	-
409.00	7500	-0.0114	-4.1914	7.96	5.65	19.70	15.80	28.10	-	500	-
469.00	4375	-0.0066	-4.5891	7.93	5.46	17.40	17.10	28.30	-	-	-
529.00	3030	50.50	-0.0046	8.01	6.04	15.60	17.20	28.60	216	800	21

Appendix C22: Case 22A (16-2-2016: 50 l)

Time After Loading (min)	Collected Volume (ml)	Effluent Flux (cm min^{-1})	Acc. Effluent (cm)	pH	DO (mg l^{-1})	NH_4^+ (mg l^{-1})	NO_3^- (mg l^{-1})	Temp (ºC)	COD (mg l^{-1})	TS (mg l^{-1})	TN (mg l^{-1})
Influent	-	-	-	7.66	0.22	40.50	4.21	27.30	1162	1500	49
19.00	-	0.0000	0.0000	-	-	-	-	-	-	-	-
24.00	190	-0.0035	-0.0173	8.08	6.78	16.90	20.60	27.10	-	-	-
29.00	150	-0.0027	-0.0309	8.01	6.18	15.90	21.40	26.90	-	900	-
34.00	135	-0.0025	-0.0432	7.97	6.23	13.80	20.40	26.90	-	-	-
39.00	170	-0.0031	-0.0586	8.02	6.15	15.30	21.70	26.80	-	-	-
44.00	220	-0.0040	-0.0786	8.00	6.25	17.20	21.10	27.00	-	-	-
50.00	170	-0.0026	-0.0941	8.00	6.07	14.00	22.10	27.00	268	1100	17
60.00	600	-0.0055	-0.1486	7.93	5.79	14.50	23.60	27.00	-	-	-
70.00	765	-0.0070	-0.2182	8.01	6.06	11.50	28.00	27.10	-	-	-
80.00	745	-0.0068	-0.2859	7.92	5.86	13.00	26.20	27.20	-	-	-
90.00	810	-0.0074	-0.3595	7.88	5.73	14.60	24.40	27.50	-	-	-
100.00	920	-0.0084	-0.4432	7.98	6.11	14.10	24.80	28.10	200	800	17
110.00	1075	-0.0098	-0.5409	8.07	6.04	17.00	23.60	28.60	-	-	-
140.00	3130	-0.0095	-0.8255	7.92	6.01	17.60	17.40	28.30	-	-	-
170.00	3175	-0.0096	-1.1141	8.05	6.00	20.00	19.90	30.00	-	-	-
200.00	4570	-0.0138	-1.5295	7.98	6.18	21.40	16.70	30.90	-	-	-
229.00	5385	-0.0169	-2.0191	7.92	5.92	20.80	15.00	28.00	235	700	26
289.00	7790	-0.0118	-2.7273	7.95	6.04	20.50	14.20	28.00	-	-	-
349.00	8605	-0.0130	-3.5095	7.96	5.90	20.90	13.40	28.40	-	-	-
409.00	7500	-0.0114	-4.1914	7.96	5.65	19.70	15.80	28.10	-	500	-
469.00	4375	-0.0066	-4.5891	7.93	5.46	17.40	17.10	28.30	-	-	-
529.00	3030	50.50	-0.0046	8.01	6.04	15.60	17.20	28.60	216	800	21

Appendix C23: Case 23B (16-2-2016: 50 l)

Time After Loading (min)	Collected Volume (ml)	Effluent Flux (cm min^{-1})	Acc. Effluent (cm)	pH	DO (mg l^{-1})	NH_4^+ (mg l^{-1})	NO_3^- (mg l^{-1})	Temp (ºC)	COD (mg l^{-1})	TS (mg l^{-1})	TN (mg l^{-1})
Influent	-	-	-	7.68	0.24	60.10	8.78	26.70	4232	8900	161
26.00	-	0.0000	0.0000	-	-	-	-	-	-	-	-
31.00	750	-0.0136	-0.0682	7.78	5.54	19.60	27.00	26.50	312	1300	-
37.75	840	-0.0113	-0.1445	7.85	5.38	19.00	36.00	26.50	-	-	-
46.50	1200	-0.0125	-0.2536	7.85	4.98	20.40	37.70	26.80	-	-	-
51.50	855	-0.0155	-0.3314	7.77	5.08	20.90	37.80	27.00	254	1000	54
58.50	910	-0.0118	-0.4141	7.82	4.98	21.20	37.50	27.10	-	-	-
63.75	800	-0.0139	-0.4868	7.84	5.15	21.50	40.80	27.20	-	-	-
73.75	1545	-0.0140	-0.6273	7.81	5.37	21.10	40.20	27.30	235	-	-
83.75	1505	-0.0137	-0.7641	7.74	5.28	21.60	38.50	27.50	-	-	-
93.75	1585	-0.0144	-0.9082	7.96	5.39	22.30	38.70	26.90	-	-	-
104.42	1740	-0.0148	-1.0664	7.85	5.32	22.40	38.50	27.40	237	800	63
115.00	1735	-0.0149	-1.2241	7.89	5.47	22.00	36.90	27.60	-	-	-
125.00	1665	-0.0151	-1.3755	7.83	5.20	21.20	37.90	27.90	-	-	-
155.00	4685	-0.0142	-1.8014	7.71	5.03	21.30	41.00	27.70	190	-	-
185.00	4570	-0.0138	-2.2168	7.74	5.11	20.70	36.30	29.30	-	-	-
215.00	3535	-0.0107	-2.5382	7.75	5.37	20.40	34.70	28.60	-	-	-
245.00	2325	-0.0070	-2.7495	7.72	5.08	18.60	37.50	28.50	132	1000	48
305.00	2035	-0.0031	-2.9345	7.61	5.22	9.40	49.30	27.60	-	-	-
365.00	905	-0.0014	-3.0168	7.87	6.26	5.30	57.70	28.60	-	-	-
425.00	530	-0.0008	-3.0650	7.57	5.73	3.86	60.60	28.10	47	400	-

Appendix C24: Case 24B (21-2-2016: 125 l)

Time After Loading (min)	Collected Volume (ml)	Effluent Flux (cm min^{-1})	Acc. Effluent (cm)	pH	DO (mg l^{-1})	NH_4^+ (mg l^{-1})	NO_3^- (mg l^{-1})	Temp (ºC)	COD (mg l^{-1})	TS (mg l^{-1})	TN (mg l^{-1})
Influent	-	-	-	7.64	0.21	62.30	8.53	27.50	7052	18600	371
18.50	-	0.0000	0.0000	-	-	-	-	-	-	-	-
23.50	1085	-0.0197	-0.0986	7.88	4.90	38.00	25.80	27.90	690	1400	110
30.50	1960	-0.0255	-0.2768	7.83	4.85	40.80	21.70	27.90	-	-	-
35.50	1535	-0.0279	-0.4164	7.88	5.13	44.20	21.20	27.60	-	-	-
42.50	1980	-0.0257	-0.5964	7.87	4.93	46.00	18.20	28.70	621	1500	76
48.50	2090	-0.0317	-0.7864	7.84	5.24	48.90	17.90	28.90	-	-	-
55.00	2175	-0.0304	-0.9841	7.88	5.36	47.50	17.60	28.70	-	-	-
65.00	3415	-0.0310	-1.2945	7.96	5.13	46.70	16.80	28.70	545	1100	71
75.00	3095	-0.0281	-1.5759	7.94	5.08	43.20	16.60	28.90	-	-	-
85.00	2930	-0.0266	-1.8423	7.99	5.52	46.50	16.20	28.10	-	-	-
95.00	3185	-0.0290	-2.1318	7.86	5.40	44.30	16.90	28.90	462	1100	64
105.00	3300	-0.0300	-2.4318	7.95	5.31	43.30	17.40	27.80	-	-	-
115.00	3405	-0.0310	-2.7414	7.95	5.40	41.80	17.60	27.90	-	-	-
145.00	8925	-0.0270	-3.5527	7.73	5.41	36.10	18.90	31.10	446	1000	52
176.00	8725	-0.0256	-4.3459	7.93	5.28	39.40	17.00	28.50	-	-	-
206.00	8750	-0.0265	-5.1414	7.83	5.44	39.20	14.90	29.70	-	-	-
268.00	12175	-0.0179	-6.2482	7.82	5.25	35.30	17.00	29.80	321	900	49
285.00	1805	-0.0097	-6.4123	7.87	5.79	29.90	26.70	29.50	-	-	-

Appendix C25: Case 25B (27-2-2016: 50 l)

Time After Loading (min)	Collected Volume (ml)	Effluent Flux (cm min^{-1})	Acc. Effluent (cm)	pH	DO (mg l^{-1})	NH_4^+ (mg l^{-1})	NO_3^- (mg l^{-1})	Temp (ºC)	COD (mg l^{-1})	TS (mg l^{-1})	TN (mg l^{-1})
Influent	-	-	-	7.47	0.18	41.80	18.40	26.90	7052	18600	371
20.17	-	0.0000	0.0000	-	-	-	-	-	-	-	-
25.17	3080	-0.0560	-0.2800	7.67	5.98	34.90	7.50	26.60	761	1800	87
31.17	3650	-0.0553	-0.6118	7.85	6.00	35.30	5.80	26.00	-	1600	-
36.50	3170	-0.0541	-0.9000	7.75	6.20	36.60	10.50	26.70	506	1600	70
42.00	3235	-0.0535	-1.1941	7.68	6.15	38.60	5.90	26.80	-	-	-
47.17	3160	-0.0556	-1.4814	7.74	6.10	39.00	10.70	26.40	611	1300	55
52.00	2820	-0.0531	-1.7377	7.70	6.12	40.90	9.40	26.40	-	-	-
66.17	6000	-0.0385	-2.2832	7.77	5.93	43.40	10.20	26.40	425	1000	68
76.00	4830	-0.0447	-2.7223	7.67	6.08	39.60	10.80	26.40	-	-	-
86.00	4010	-0.0365	-3.0868	7.86	6.13	36.60	13.90	26.50	333	600	59
97.00	2630	-0.0217	-3.3259	7.67	5.47	32.80	12.00	26.40	-	800	-
107.00	1250	-0.0114	-3.4395	7.78	5.49	29.20	13.30	26.30	193	800	58
117.00	550	-0.0050	-3.4895	7.75	4.83	26.50	16.60	26.40	-	700	-